Transactions of the ASME

TRANSACTIONS OF THE AMERICAN SOCIETY OF MECHANICAL ENGINEERS

VOLUME 80 OCTOBER 1958 NUMBER 7

Transactions

of The American Society of Mechanical Engineers

Published on the tenth of every month, except March, June, September, and December

Published monthly by The American Society of Mechanical Engineers. Publication office at 20th and Northampton Streets, Easton, Pa. The editorial department is located at the headquarters of the Society, 29 West Thirty-Ninth Street, New York 18, N. Y. Cable address, "Mechanees," New York. Price $1.50 a copy, $12.00 annually for Transactions and the *Journal of Applied Mechanics;* to members, $1.00 a copy, $6.00 annually. Add $1.50 for postage to all countries outside the United States, Canada, and Pan American Union. Changes of address must be received at Society headquarters seven weeks before they are to be effective on the mailing list. Please send old as well as new address. . . . By-Law: The Society shall not be responsible for statements or opinions advanced in papers or . . . printed in its publications (B13, Par. 4). . . . Entered as second-class matter March 2, 1928, at the Post Office at Easton, Pa., under the Act of August 24, 1912. . .

Analysis of the Effect of Pulsations on the Response of Mercurial-Type Differential-Pressure Recorders

By R. J. MARTIN[1] and D. S. MOSELEY,[2] SAN ANTONIO, TEXAS

Low-frequency periodic pressure pulsations are sometimes encountered in gas pipelines. These pulsations may cause oscillation of the recording pens of orifice meters, making a true reading of gas flow difficult. In this paper, general equations describing the response of the mercurial-type differential-pressure recorder to such pulsations are developed. For the purpose of this paper the system of equations is then linearized and a specific solution is presented.

Introduction

When pressure pulsations are present in a flowing gas stream whose flow rate is being measured by an orifice meter, the recording differential pen may be agitated severely if the frequency of the periodic pressure difference at the pressure taps is near the resonant frequency of some element of the meter system. When combined with the low resolution of the 24-hr, 7-day, or 31-day chart drive, results may often appear not as a line but as a ribbon of ink, called "paint." The term painting is familiar to most gas-measurement engineers. It is possible, however, to have pressure pulsations at higher frequencies than those of the meter system and the recordings will appear as a smooth line and appreciable errors due to pulsation still may result.

Where paint occurs, one can only estimate the quantity of gas passing through the meter. Therefore, in meter design, it is desirable to prevent pipeline pulsations from affecting the pen motion, and heavy damping of the flow of the mercury in the meter is often provided by the presence of a valve restriction in the mercury flow channel. Fig. 1 shows a sketch of an idealized but typical mercurial-type differential-pressure recorder.

This paper is restricted to an analysis of the behavior of the pneumatic and mechanical system which transforms a differential pressure at the inlet and outlet pressure taps to a pen motion suitable for recording. The paper represents an effort to study the frequency response of a mercurial-type differential-pressure recorder resembling those used in commercial practice, and in such purpose differs from the work of Williams (1)[3] on manometer gages.

It is thought that the analysis presented might be of assistance to the instrument designer. By using the equations and results of this analysis as a guide, he could select design parameters so that his instrument would have no natural resonances in the region of probable exciting frequencies.

It is not the purpose of this paper to deal with the orifice and the origins of a periodic pressure difference at the taps, nor to discuss the origin of erroneous flow reading even where pulsations are not transmitted to the pen. These matters are treated elsewhere in the literature (2, 3, 4) and, in addition, a program of research in this area is now under way at the authors' institution. It is important, however, to know something of the order of magnitude of each of the static and dynamic pressures as it might appear in an actual meter installation. Data published by Baird and Bechtold (5) have indicated the relative change in amplitude and phase of the instantaneous pressures at the taps, and measurements made in conjunction with the program of pulsation suppression at Southwest Research Institute have indicated that line pulsation pressures near compressors range downward from ±5 per cent of line static pressures in extreme cases. Guided by these data, the analysis which follows presumes the pulsations to be describable in acoustic terms, and acoustic development is employed wherever applicable.

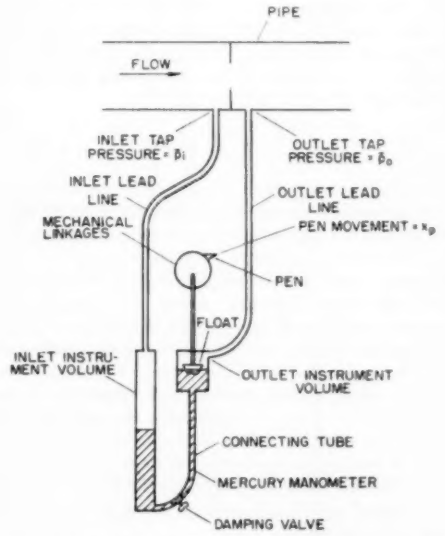

Fig. 1 Essentials of a mercurial-type differential-pressure recorder

Analysis

The general conditions of the analysis presume that gas is passing through a pipeline orifice with constant net flow rate. The pressure drop caused by the orifice is a small fraction of the base pressure. On this steady flow is superposed a disturbance which manifests itself as harmonic pressure variations at the meter taps. The amplitude of the pressure fluctuations in the pipe is of acoustic magnitude in reference to base pressure in the pipe.

These pressure fluctuations generate compressional waves

---

[1] Research Engineer, Southwest Research Institute.

[2] Senior Research Physicist, Southwest Research Institute.

[3] Numbers in parentheses refer to the Bibliography at the end of the paper.

Contributed by the Research Committee on Fluid Meters and presented at the Annual Meeting, New York, N. Y., December 1–6, 1957, of The American Society of Mechanical Engineers.

Note: Statements and opinions advanced in papers are to be understood as individual expressions of their authors and not those of the Society. Manuscript received at ASME Headquarters, July 29, 1957. Paper No. 57—A-82.

which propagate in both directions in the lead lines between the taps and the mercury surfaces, the latter serving as reflectors of waves originating at the near tap and as radiators of acoustic energy derived from the remote tap.[4] It is assumed that the acoustic waves in the lead lines are plane. The validity of the plane-wave assumption for small tubes, regardless of how the tubes are bent, is discussed by Rayleigh (6), for the case of undamped waves.

Since damping of the waves due to resistance at the tube walls is not ignored here, the waves could not actually be plane, because the wall resistance would cause a peaked velocity profile. However, the plane-wave assumption can be used if the acoustic parameters, considered constant at any cross section, are really the averages at that section. The partial differential equation for damped waves propagated in tubes, using the idea of averages, is given by Kinsler and Frey (7) as

$$c'^2 \frac{\partial^2 \xi}{\partial x^2} = \frac{\partial^2 \xi}{\partial t^2} + 2\alpha c' \frac{\partial \xi}{\partial t} \quad \ldots\ldots\ldots\ldots [1]$$

where c' is the damped wave velocity, α is the damping factor, ξ is acoustic-particle displacement, and t is time. From Equation [1], the gas volume influxes to the mercury chambers, v_o and v_i, may be developed (see Section 2 of the Appendix).

The pressure variations in the gas volumes within the mercury chambers will be determined by v_o and v_i. The volume of gas in a mercury chamber, if the acoustic disturbance were absent, may be regarded as a constant mass of gas that suffers an adiabatic pressure cycle due to the acoustic waves in the lead lines. The mercury chambers are so small, with respect to the acoustic wave lengths of interest here, that they are treated as lumped elements. By continuity, then, if the pressure variation in the lead lines is everywhere harmonic, it must be harmonic in the mercury chambers. The expression for the adiabatic cycle of the base volumes of gas in the mercury chambers is developed in Section 3 of the Appendix.

The pressure cycles in the gas in the mercury chambers provide the driving forces that oscillate the mercury column. Other forces which determine the character of this motion are the restoring force of gravity, the reactive force on the mercury due to accelerating the float and float stem, and resistance to the mercury flow. The equation of motion of the mercury, in terms of the motion of the mercury surface in the float chamber, is presented in Section 4 of the Appendix.

Gravity, buoyancy, velocity damping between the float and the mercury, and the motion of the mercury level in the float chamber, determine the equation of motion for the float which is given in Section 5 of the Appendix.

The pen motion is assumed to be determined by a frictionless proportional linkage between the float stem and the pen. Friction and pen mass will certainly be small in such a linkage so that any motion of the float will be unaffected by the presence of a pen.

The system of equations developed to define the pen motion may be linearized, as shown in Section 6 of the Appendix, without seriously affecting the calculation of the resonant frequencies in the orifice meter. The neglect of the nonlinear terms which do come into play in cases of extreme values of applied pressures will chiefly suppress the nonlinear distortion frequencies.

A major problem in an actual solution is the establishment of criteria for the damping of the mercury flow. No general expression for the resistance to the mercury flow has been developed because of the wide variety of instrument configurations. However, for any given instrument, one simple test would yield information for computing the resistance coefficient in the linearized mercury-motion equation. A differential pressure, adequate to produce full-scale deflection of the recording pen, is applied to the instrument. The pressure is withdrawn abruptly, and the deflection-time relation that follows is recorded. From this information the damping coefficient D_m may be found. For the usual case, which is that of an overdamped instrument, the method for computing D_m is given in Section 7 of the Appendix.

For the flow resistance between the float and the mercury, Stoke's law applied to a sphere of the same diameter as the float is suggested as an approximation. Stoke's law for the sphere moving in a homogeneous medium is

$$\text{Drag force} = 3\pi\mu W u \quad \ldots\ldots\ldots\ldots [2]$$

where μ is the viscosity of the medium, W is the diameter of the sphere, and u is the velocity of the sphere. Correspondingly, the resistance coefficient of velocity for the float would be

$$D_f = 3\pi\mu_m W \quad \ldots\ldots\ldots\ldots [3]$$

where W is now the effective diameter of the float.

Numerical Example and Discussion

Methane gas at a system pressure on the upstream side of the orifice of 1000 psia and a temperature of 100 F was assumed. It was supposed that a base flow such as to produce a differential head across the orifice of 50 in. of water existed. A harmonic pressure pulsation having an amplitude of 1 psi at the upstream tap was considered superposed on the steady-state pressures. The amplitude at the downstream tap was defined to be $^9/_{10}$ of that at the upstream tap. A phase shift of 30 deg was assumed across the orifice. Combining these conditions with a set of arbitrary geometrical specifications for an idealized instrument, the constants tabulated in Table 1 were derived. The mercury-flow damping coefficient D_m was computed from results of a typical test, as explained in the preceding section.

Table 1 Values for numerical example

A_i = 3.168 sq in.	p_{om} = 0.8 psi
A_n = 0.196 sq in.	R_f = 2.04 in.
A_o = 19.6 sq in.	S = 0.196 sq in.
c = 1386 fps	V_i = 43.2 cu in.
D_m = 5074 lb/sec	V_o = 26.0 cu in.
d_i = 3.96 in.	W = 2.63 in.
d_o = 2.04 in.	γ = 1.113
g = 32.2 ft/sec^2	θ = 0.785 radian
K = 0.3	μ = 7.4 10^{-6} lb/ft sec
L_i = 45.0 ft	μ_m = 0.001 lb/ft sec
L_n = 1.3 ft	ρ_i = 2.68 pcf
L_o = 50.0 ft	ρ_m = 849 pcf
m_f = 5.0 lb	ρ_o = 2.675 pcf
P_i = 1000 psia	ϕ_i = 0 radian
P_o = 998.2 psia	ϕ_o = 0.524 radian
p_{im} = 1.0 psi	

Using these quantities, the pen motion was calculated at various values of driving frequency, and the resulting amplitude of motion as a function of frequency is shown in Fig. 2, for both damped and undamped motions.

The undamped case has three resonance peaks: The first, at $\omega = 1$ radian per sec, is due to natural resonance of the mercury column. The second, at $\omega = 28.75$, is due to resonance of the float with respect to the mercury. The third, at $\omega = 35$, is due to resonance in the lead lines. This is actually a double peak, but the difference assigned, and usually encountered for the lead-line lengths, was not sufficient to resolve this peak into its two components. Theoretically, if the scale were explored to infinity, an infinite number of pairs of lead-line resonance cases would be found; in this example the next pair of lead-line resonances is at $\omega = 100$ and $\omega = 112$. The latter pair and all pairs

[4] Abrupt changes in the cross section of the flow lines will cause additional wave reflections to occur.

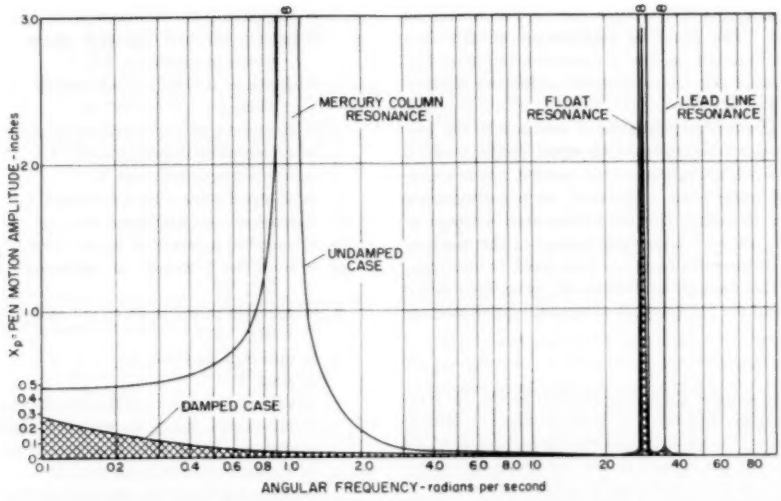

Fig. 2 Predicted frequency response of meter of Fig. 1. Input excitation is oscillatory differential pressure of constant amplitude.

of higher order have been omitted from Fig. 2 in the interest of clarity.

The presence of damping eliminated the infinite peaks. The resonant peak at $\omega = 1$ was removed completely, as the mercury column flow is overdamped. The amplitude at $\omega = 0$ corresponds to the static deflection of the system in the usual meaning of the term, and this is over and above the static 50 in. of water which was assumed.

The amplitude peak at $\omega = 28.75$ is still high. In fact, for the quantities used it probably would exceed the limit imposed by the chart range. This peak could be a source of real trouble and, as the calculation plainly shows, it is not eliminated by putting resistance in the mercury flow path.

However, this amplitude peak can be shifted to above the range of probable disturbances by reducing the float mass, all other factors being maintained the same. This can be done by going to a lighter material, or by using a hollow float. Reduction of the mass in the example here, from 5 lb to 1 lb, would shift this peak to $\omega = 53.3$.

The damping in the lead lines and in the mercury column reduced the third peak to a low, but not negligible value. The sure way to avoid paint from lead-line resonances is to reduce the length of the lead lines. This increases the ω-value at resonance, roughly in the inverse ratio to the reduction in lead-line length.

The base line in Fig. 2 can be thought of as representing a condition of steady flow with a head difference across the orifice plate of 50 in. of water. This would be at mid-chart on a 0 to 100 in. of water meter. Fig. 3 shows the results against the background of a chart. For pictorial clarity, only the realistic damped case is shown. Regions of appreciable disturbance are shaded. For any given frequency, the width of paint on the meter chart is given by the total vertical extent of the shaded zone, above and below the line.

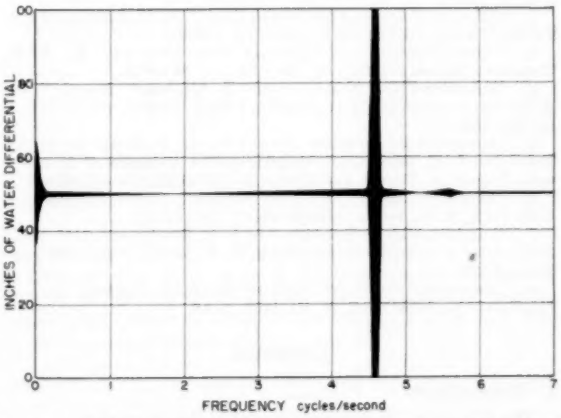

Fig. 3 Predicted paint on special chart of 100-in. range. Input excitation is a differential of 50 in. plus a pulsative differential pressure of variable frequency and constant amplitude of 14 in.

Summary and Conclusions

A mercurial-type differential-pressure recorder, including lead lines, mercury column, float, and pen has been analyzed with respect to pen displacement as a function of harmonic pressure disturbances at the pressure taps. After linearization of equations, three basic resonances are found. The lowest of these is the mercury column resonance which is removed by overdamping, according to present design practice. The second is the float-on-mercury resonance which can be controlled in frequency. The third is lead-line resonance which, with usual lead-line size and length, is of small importance.

Although this instrument as used commercially is intended to record only net flow, it occasionally must be used where there are pulsations. This analysis has attempted to show the performance of such an instrument in response to pulsation pressures of a periodic nature. It assumes that the amplitudes of disturbance are small enough in practice to permit linearization of the equations or that counter measures, apart from the instrument adjustments, would be employed to reduce the amplitudes of pulsation to tractable levels.

The shape of the resonance peaks shown in Figs. 2 and 3 are typical of a linear oscillating system. The analysis of the present paper accounts for certain nonlinearities, but these were omitted in the computations for simplicity by the linearization procedure described. Had the computations been based on nonlinear analysis, not only would the amplitudes be everywhere frequency

dependent, but the resonant frequencies themselves would be amplitude dependent. The practical implication of this fact is not of importance, however, as meter operation in this range of large amplitudes would not be permissible under any circumstances.

The analysis also shows that, because of resonance, the pen will not display different frequencies with equal facility, which means that even fast clock operation cannot present a true reproduction of the input wave form. However, as a consequence of the assumption of linearity, the time-integrated average of the motion of the pen will be a true reproduction of the mean or time average of the differential pressure presented to the taps. Thus a chart speed fast enough to resolve all wave-form detail is the maximum needed for the purpose of obtaining the average differential pressure.

Acknowledgment

The authors wish to express their appreciation to Dr. H. Norman Abramson, Manager, Engineering Analysis Section, Southwest Research Institute, for valuable comments and suggestions in the preparation of this paper, and to the American Gas Association for partial support and permission to publish this work.

Bibliography

1 "Pulsation Errors in Manometer Gages," by T. J. Williams, TRANS. ASME, vol. 78, 1956, pp. 1461–1469.
2 "Effect of Pulsations on Flow of Gases," by H. Judd and D. B. Pheley, TRANS. ASME, vol. 44, 1922, pp. 853–918.
3 "Basic Difficulties in Pulsating Flow Metering," by A. R. Deschere, TRANS. ASME, vol. 74, 1952, pp. 919–924.
4 "Pulsating-Flow Measurement—A Literature Survey," by A. K. Oppenheim and E. G. Chilton, TRANS. ASME, vol. 77, 1955, pp. 225–248.
5 "Dynamics of Pulsative Flow Through Orifices," by R. C. Baird and I. C. Bechtold, *Instruments—The Magazine of Measurement, Inspection, Testing, and Control*, vol. 25, 1952, pp. 481–486.
6 "Theory of Sound," by Lord Rayleigh, Dover Publications, New York, N. Y., second edition, vol. 2, 1945, p. 62.
7 "Fundamentals of Acoustics," by L. E. Kinsler and A. R. Frey, John Wiley & Sons, Inc., New York, N. Y., first edition, 1950, pp. 242 and 128.
8 "Acoustics," by G. W. Stewart and R. B. Lindsay, D. Van Nostrand Co., New York, N. Y., 1930, p. 68.

APPENDIX

1 Nomenclature

The following nomenclature is used in the Appendix:

A = cross-sectional areas of mercury chambers or connecting tube, L^2
B, C = coefficients in lead-line equations, L
D_f = drag coefficient for resistance between float and mercury, MT^{-1}
D_m = coefficient of resistance offered to mercury flow in manometer, MT^{-1}
K = motion transfer ratio between float and pen
L = lead-line length, L
L_n = length of connecting tube between mercury chambers, L
M, N = moduli of complex numbers as defined in Section 2
P = absolute pressure in gas—no pulsations, $ML^{-1}T^{-2}$
R_f = radius of float at its base, L
R_{fs} = radius of float at mercury surface—no pulsations, L
S = cross-sectional area of lead line, L^2
V = volume of gas in mercury chamber—no pulsations, L^3
V_f = volume of the float submerged at time t, L^3
W = effective diameter of float, and diameter of sphere in Stokes' law, L
X = displacement of mercury in chambers or connecting tube, L
a, b = angles in polar representation of complex numbers
c, c' = undamped and damped phase velocities of acoustic waves in lead lines, LT^{-1}
d = depth of mercury in chambers at no pulsation condition, L
f = frequency of impressed oscillations, T^{-1}
g = acceleration of gravity, LT^{-2}
k = wave-length constant, L^{-1}
k' = damped wave-length constant, L^{-1}
m_f = mass of float and stem, M
p = acoustic pressure at tap at time t, $ML^{-1}T^{-2}$
p_v = acoustic pressure in mercury chamber at time t, $ML^{-1}T^{-2}$
p_x = acoustic pressure at time t and any station in lead line, $ML^{-1}T^{-2}$
r = radius of lead line, L
t = time, T
u = velocity of sphere in fluid in Stokes' law, LT^{-1}
v = volumetric influx to mercury chambers, L^3
x = distance along lead line, measured from tap, L
y_f, y_p = displacement of float, pen, L
α = damping factor for acoustic waves in lead lines, L^{-1}
γ = specific heat ratio for gas
θ = angle between side of float and vertical
μ, μ_m = viscosity of gas, mercury, $ML^{-1}T^{-1}$
ξ = acoustic particle displacement, L
ρ, ρ_m = density of gas, mercury, ML^{-3}
σ = phase angle of pressure variation in mercury chamber relative to reference pressure
ϕ = phase angle of pressure fluctuation at tap
ω = angular frequency of impressed vibrations = $2\pi f$, T^{-1}

Subscripts

i, o = lead line and instrument volume connected to up-stream, downstream side of orifice
m = amplitude or mercury
n = connecting tube

NOTE: Bar over quantity denotes complex quantity, and dot over quantity denotes derivative with respect to time.

2 Acoustic Waves in Lead Lines

The general solution for Equation [1], see Kinsler and Frey (7), is

$$\bar{\xi} = \bar{C}e^{-\alpha x}e^{j(\omega t - k'x)} + \bar{B}e^{\alpha x}e^{j(\omega t + k'x)} \quad [4]$$

By making the definition $\bar{k} = k' - j\alpha$, Equation [4] may be written as

$$\bar{\xi} = \bar{C}e^{j(\omega t - \bar{k}x)} + \bar{B}e^{j(\omega t + \bar{k}x)} \quad [5]$$

Pressure may be obtained from particle displacement by

$$p_x = -\frac{\omega c' \rho}{\bar{k}} \frac{\partial \bar{\xi}}{\partial x} \quad [6]$$

From Equations [5] and [6] it follows that

$$p_x = j\omega c' \rho e^{j\omega t} [\bar{C}e^{-j\bar{k}x} - \bar{B}e^{j\bar{k}x}] \quad [7]$$

$\bar{C}$ and $\bar{B}$ can be expressed in terms of the applied tap pressure and the pressure in the near mercury chamber by writing Equation [7] for $x = 0$ and $x = L$. These pressures are $\bar{p} = p_m e^{j\omega t}$ and $\bar{p}_v = p_{vm}e^{j\omega t}$, respectively. $\bar{C}$ and $\bar{B}$ are found to be

$$\bar{C} = \frac{\bar{p}_{vm} - \bar{p}_m e^{j\bar{k}L}}{2\omega c' \rho(\sin \bar{k}L)} \quad \text{and} \quad \bar{B} = \frac{\bar{p}_{vm} - \bar{p}_m e^{-j\bar{k}L}}{2\omega c' \rho(\sin \bar{k}L)} \quad [8]$$

The particle displacement, Equation [5], times the cross-

sectional area of the tube, yields volume displacement. Writing this for $x = L$, and using the coefficients from Equation [8]

$$\bar{v} = \frac{S(p_{v_m} \cos kL - p_m)e^{j\omega t}}{\rho c'\omega(\sin kL)} \quad \ldots\ldots [9]$$

But the real volume inflow to the mercury chambers is desired. For convenience, the definitions in Equation [10] are made

$$\left.\begin{aligned} \sin kL &\equiv Me^{ja} \qquad \cos kL \equiv Ne^{jb} \\ \bar{p}_m &\equiv p_m e^{j\phi} \qquad \bar{p}_{v_m} \equiv p_{v_m} e^{j\sigma} \end{aligned}\right\} \quad \ldots\ldots [10]$$

From Equations [9] and [10], the real volume inflow, as expressed in Equation [11], may be derived

$$v = \frac{S[Np_{v_m} \cos(\omega t + \sigma + b - a) - p_m \cos(\omega t + \phi - a)]}{\rho c'\omega M} \quad \ldots\ldots [11]$$

where

$$\begin{aligned} M &= [(\sin k'L \cosh \alpha L)^2 + (\cos k'L \sinh \alpha L)^2]^{1/2} \\ N &= [(\cos k'L \cosh \alpha L)^2 + (\sin k'L \sinh \alpha L)^2]^{1/2} \\ a &= \arctan\left(\frac{-\tanh \alpha L}{\tan k'L}\right) \\ b &= \arctan[(\tan k'L)(\tanh \alpha L)] \end{aligned}$$

With appropriate subscripts, i.e., o or i, the expressions just derived are applicable to either lead line. Note that either ϕ_o or ϕ_i may be set equal to zero, thus establishing a phase reference.

It must be stated how k', the damped wave-length constant, and α, the damping factor, may be computed. They are given by Stewart and Lindsay (8) as

$$k' = \omega/c', \quad \text{where} \quad c' = c\left[1 - \frac{1}{2r}\left(\frac{2\mu}{\rho\omega}\right)^{1/2}\right] \quad \ldots [12]$$

$$\alpha = \frac{1}{rc}\left(\frac{\mu\omega}{2\rho}\right)^{1/2} \quad \ldots\ldots [13]$$

3 Pressure Cycles in Mercury-Chamber Gas Volumes

The periodic flow of gas in the lead lines imposes a pressure cycle, assumed to be adiabatic, on the base volume of gas that would be in the mercury chamber if there were no pulsations. The pressure in a mercury-chamber gas volume is composed of a steady base pressure and a harmonic component, whose sum is

$$P + p_{v_m} \cos(\omega t + \sigma) \quad \ldots\ldots [14]$$

The chamber volume available to the gas at any time is $V + AX$, and the volume of gas (referred to base density) that is in the chamber is $V + v$, where v may be negative, as in the case of efflux from the chamber. That proportion of the chamber occupied by the base volume of gas is

$$\frac{V}{V + v} \quad \ldots\ldots [15]$$

The volume occupied by the base volume is then

$$\frac{V(V + AX)}{V + v} \quad \ldots\ldots [16]$$

For the adiabatic process on the base volume, it follows that

$$PV^\gamma = [P + p_{v_m} \cos(\omega t + \sigma)]\left[\frac{V(V + AX)}{V + v}\right]^\gamma \quad \ldots [17]$$

Simplifying and rearranging yields

$$\left(\frac{V + v}{V + AX}\right)^\gamma = 1 + \frac{p_{v_m} \cos(\omega t + \sigma)}{P} \quad \ldots\ldots [18]$$

With appropriate subscripts, i.e., o or i, the foregoing expressions are applicable to either chamber. The mercury-level displacements for the two chambers are related to each other by the cross-sectional areas of the chambers. Thus

$$X_i = -\frac{A_o}{A_i} X_o \quad \ldots\ldots [19]$$

where downward displacement is defined as positive in both cases.

4 Motion of Mercury

Only forces and motions parallel to the instrument axis shall be considered. At any time, the velocities of the mercury in the two instrument volumes and in the connecting tube are different, because of the different cross sections involved. The difficulty this presents in writing the equation of motion is overcome by writing it for a volume of liquid of constant cross section, composed of the mercury in the tube and in vertical cylindrical volumes in the mercury chambers directly above the ends of the tube.

At any time t the pressure difference causes a force

$$(P_o - P_i)A_n + [p_{v_{om}} \cos(\omega t + \sigma_o) - p_{v_{im}} \cos(\omega t + \sigma_i)]\, A_n \quad \ldots [20]$$

Gravity acting on the unbalanced head of mercury exerts a force

$$\left[\frac{P_i - P_o}{\rho_m g} - X_o + X_i\right] \rho_m g A_n \quad \ldots\ldots [21]$$

The reactive force on the mercury resulting from acceleration of the float and stem is

$$-m_f \ddot{y}_f (A_n/A_o) \quad \ldots\ldots [22]$$

A resistance force $D_m \dot{X}_o$ also will be involved.

Using the four forces given in the foregoing, the equation of motion for the mercury is written. After simplifying, and expressing all motions in terms of the motion of the mercury level in the float side, Equation [23] is obtained

$$\begin{aligned} &[p_{v_{om}} \cos(\omega t + \sigma_o) - p_{v_{im}} \cos(\omega t + \sigma_i)]\, A_n \\ &\quad - \rho_m g A_n \left(\frac{A_o}{A_i} + 1\right) X_o - m_f \ddot{y}_f \frac{A_n}{A_o} \\ &- D_m \dot{X}_o - A_o \rho_m (L_n + d_o + d_i)\ddot{X}_o + A_o \rho_m \left(1 - \frac{A_o}{A_i}\right) X_o \ddot{X}_o = 0 \end{aligned} \quad \ldots\ldots [23]$$

5 Motion of Float and Pen

The float was assumed to be a truncated cone, wider at the top than at the bottom, and coupled to the mercury through its buoyancy and drag forces. It can be shown that the volume of mercury displaced by the float at any time is given by

$$\begin{aligned} V_f = \frac{\pi}{3}(y_f - X_o + R_{f_o} \cot\theta)[(y_f - X_o) \tan\theta + R_{f_o}]^3 \\ - \frac{\pi}{3}(\cot\theta) R_f^3 \end{aligned} \quad \ldots\ldots [24]$$

where

$$R_{f_o} = \left(\frac{3m_f(\tan\theta)}{\pi\rho_m} + R_f^3\right)^{1/3}$$

Considering the forces of buoyancy, gravity, and resistance

$$m_f g - V_f \rho_m g - D_f(\dot{y}_f - \dot{X}_o) - m_f \ddot{y}_f = 0 \quad [25]$$

where V_f is a rather involved function of y_f and X_o.

Float and pen motions are related by

$$y_f = K y_p \quad [26]$$

6 Linearized System

Equation [11] for both lead lines, Equation [18] for both gas volumes, Equation [23] for the mercury motion, and Equation [25] for the float, form a set of six basic equations that define the system. These may be linearized, and a summary algebraic equation expressing amplitude as a function of frequency may be obtained. The real amplitude of pen motion is

$$y_{pm} = \{[\mathrm{Re}\bar{y}_{pm}]^2 + [\mathrm{Im}\bar{y}_{pm}]^2\}^{1/2} \quad [27]$$

where

$$\bar{y}_{pm} = \frac{(\pi g \rho_m R_{fo}^2 + j\omega D_f)\bar{X}_{om}}{\pi g \rho_m K R_{fo}^2 - K m_f \omega^2 + D_f K j\omega}$$

and

$$\bar{X}_{om} = \frac{A_n\left[\frac{\bar{q}_{o1}\bar{q}_{o3}\bar{p}_{om}}{A_o \cos \bar{k}L_o} - \frac{\bar{q}_{i1}\bar{q}_{i3}\bar{p}_{im}}{A_i \cos \bar{k}L_i}\right]}{A_n \rho_m g\left(1 + \frac{A_o}{A_i}\right) - A_n\left(\bar{q}_{o3} + \frac{A_o}{A_i}\bar{q}_{i3}\right) + j\omega D_m - A_n \rho_m (L_n + d_o + d_i)\omega^2}$$

and the $\bar{q}$'s are given by

$$\bar{q}_{o1} = \frac{S_o \cos \bar{k}L_o}{\rho_o c' \omega \sin \bar{k}L_o}, \quad \bar{q}_{i1} = \frac{S_i \cos \bar{k}L_i}{\rho_i c' \omega \sin \bar{k}L_i}$$

$$\bar{q}_{o3} = \frac{P_o \gamma A_o}{\gamma \bar{q}_{o1} P_o - V_o}, \quad \bar{q}_{i3} = \frac{P_i \gamma A_i}{\gamma \bar{q}_{i1} P_i - V_i}$$

7 Mercury Motion-Damping Coefficient

The motion of the mercury in the test for determining the damping coefficient is free. Equation [23], when appropriately linearized, and written without the forcing function, will apply to this type of test. Thus

$$A_n \rho_m (L_n + d_o + d_i)\ddot{X}_o + D_m \dot{X}_o + \rho_m g A_n\left(\frac{A_o}{A_i} + 1\right) X_o = 0 \quad [28]$$

For a given instrument, and a set of displacement-time values taken from a test, D_m is evidently determinate. The general expression for D_m is found to be

$$D_m = \frac{2\rho_m g A_n\left(\frac{A_o}{A_i} + 1\right) t}{\ln X_{o(\max)} - \ln X_o} \quad [29]$$

where $X_{o(\max)}$ is the displacement of the mercury corresponding to maximum pen motion, and X_o and t are any pair of values from a test. Since the test is not exactly a linear phenomenon, D_m is best determined as a mean of several values found from Equation [29], by using a series of X_o and t data from the test result.

Discussion

L. K. Spink.[5] This paper should go far to correct one of the misunderstandings which probably has caused more poor measurements and unreadable charts than any other. The statement that damping a meter will not eliminate the familiar square-root error inherent in pulsating flow has been warped to imply that a meter on pulsating or fluctuating flow should never be damped.

Every commercially successful meter has certain inherent damping characteristics even if the damping adjustment is wide open. Attempts to use totally undamped designs always have resulted in unreadable chart records. Measurements on the steadiest flows we could produce at our laboratory have shown high-frequency pulses of differential upward of 5 per cent.

Measurement of flow with high-amplitude pulsation is out of the question with our present techniques, so let us eliminate that from our consideration of the problem. Measurement of flow with moderate amplitude pulsation is a compromise, but can be done within reasonable limits. Understanding that it is a compromise, which alternative is better—to try to average a chart with a painted line extending 20 to 40 per cent of the chart scale, with no time spacing to show how long the differential was high and how long it was low; or to damp the meter to give a linear average of the differential as it exists at the recording element? It is believed the answer can be read from the last paragraph of this paper.

It is the writer's belief that all industries owe a debt of gratitude to the authors, and to the American Gas Association which sponsored the work behind it, for a realistic approach to the problem, with figures representative of an actual commercial meter.

Authors' Closure

The comments by Mr. Spink are certainly in order and are much appreciated. His statement of alternatives leaves small room for doubt of his recommendation for the user. We would only emphasize the point that the applied damping must be of a kind which will result in the desired linear average of the differential.

The authors would like to call the attention of careful readers to an ambiguous arrangement of the expression for $\bar{X}_{om}$ in Equation [27]. The line of type beginning $+ j\omega D_m \ldots$ is part of the denominator of the expression immediately above it.

---

[5] Engineer, Charge of Flow Measurement, The Foxboro Company, Foxboro, Mass. Mem. ASME. (Deceased, December 23, 1957.)

Subcritical and Critical Flow Through Straight-Through, Elbow, and Tee A-N Fittings and Sharp-Edged Orifices at Elevated Temperatures[1]

By A. L. DUCOFFE,[2] J. R. BENNETT,[3] AND C. G. RAY,[3] ATLANTA, GA.

This paper presents the results of an investigation of the flow through straight-through, elbow, and tee A-N standard fittings at negligible approach velocity with approach temperatures up to 1100 F and head pressures up to 60 psia. The element pressure ratio, i.e., the ratio of downstream to upstream static pressure across the test element, was varied between 1.0 and approximately 0.25. Empirical equations for the subcritical and critical flow regimes are derived for the rate of weight flow as a function of element pressure ratio, flow area, and approach temperature and pressure. Empirical equations for a given geometry are derived for a flow factor which is shown to be a function of pressure ratio only in both the subcritical and critical regions. In addition, previous work at room temperature on the flow through sharp-edged orifices in the subcritical and critical regimes has been extended to include a variation of approach temperature up to 1100 F.

Nomenclature

THE following nomenclature is used in the paper:

A = flow area through orifice or fitting
D_1 = pipe inside diameter
D_2 = fitting or orifice-flow diameter
E = correction for thermal expansion
f = function
F = degrees Fahrenheit
g = gravitational acceleration (32.17 ft/sec^2)
K = incompressible flow coefficient
K_c = compressible flow coefficient = KY
p_1 = static pressure upstream of test specimen
p_2 = static pressure downstream of test specimen
Δp = static pressure drop across test specimen
r = pressure ratio, p_2/p_1
R = gas constant for air (53.34 ft/deg R)
R = degrees Rankine
RN = Reynolds number = $\dfrac{\rho V_1 D_2}{g\mu}$
T_1 = temperature upstream of test specimen, deg Rankine
V_1 = velocity upstream of test specimen
W = flow rate, lb/sec
Y = compressibility correction factor
β = diameter ratio, D_2/D_1
μ = viscosity, lb-sec/ft^2
π = 3.1416
ρ = density of air, pcf
Ω = flow factor, (deg R)$^{1/2}$/sec

Introduction

The rapid increase in velocities of airplanes, missiles, and test vehicles has brought about the necessity of more accurate lag predictions for pressure instrumentation during high-speed maneuvers, climbing, and diving. The pressure lag, in some instances, causes large errors in the measured pressure.

Until recently linear theory (1–3)[4] was considered adequate for predicting the lag of pressure-sensing instrumentation. The linear theory describes the response of a resistance-capitance electrical system. The differential equation is transformed into a pressure equation where the electrical resistance is a function of viscosity, diameter, and length of plumbing leading to the chamber of the measuring instrument, and the electrical capitance is represented as a function of the internal pressure and the volume of the instrument. The solution of this equation using a step input in pressure makes it possible to determine a time constant for the system. However, recent tests (4) show that the time constant determined is dependent on the size of pressure step being applied. The derivation of a nonlinear, quasi-steady, empirical theory (4) shows good agreement with experiment. In the nonlinear theory development (4), the plumbing variables such as fitting diameter, line length, and diameter, and so on, are included as constants for a given system but are modified by empirical constants. In addition, the effect of temperature has not been verified experimentally.

The purpose of the present work, being conducted in the Aeronautics Department at the Georgia Institute of Technology (under consultant contract with the Sandia Corporation, Albuquerque, N. M.), is to gain some understanding into the mechanism which contributes to the pressure lag in a pneumatic sensing system. It appears that the over-all problem could be attacked by isolating the various types of hardware which constitute the system. Each part of the system such as fittings, lines, instrument volume, and so forth, will be analyzed separately over a range of temperature and pressure, and the characteristics of each determined. Once the individual characteristics are known, complete systems will be analyzed and tested; the end point of the research will consist of an attempt to correlate typical system constants with individual hardware properties.

[1] This research was sponsored by the Sandia Corporation of Albuquerque, N. M., under consultant contract with the senior author and was the subject of two Masters' theses submitted by Messrs. Bennett and Ray in partial fulfillment of the requirements for the degree of Master of Science in Aeronautical Engineering in the Graduate School of the Georgia Institute of Technology.

[2] Professor of Aeronautical Engineering, Georgia Institute of Technology, and Consultant to the Aerodynamics Department of the Sandia Corporation.

[3] Graduate Student, Georgia Institute of Technology.

Contributed by the Research Committee on Fluid Meters and presented at the Annual Meeting, New York, N. Y., December 1–6, 1957, of THE AMERICAN SOCIETY OF MECHANICAL ENGINEERS.

NOTE: Statements and opinions advanced in papers are to be understood as individual expressions of their authors and not those of the Society. Manuscript received at ASME Headquarters, July 26, 1957 Paper No. 57—A-60.

[4] Numbers in parentheses refer to the Bibliography at the end of the paper.

The present analysis, i.e., the initial phase of the project, consists of the measurement of flow constants for typical standard A-N fittings, such as straight-through, tees, and elbows which are usually found in pressure-sensing systems. The A-N designation refers to Air Force-Navy standards for tube fittings used in the aircraft and missile industries. The parameters varied were the fitting inside diameter, approach temperature, and pressure ratio across the fitting.

In addition, the work of Perry (5) on sharp-edged orifices is extended from approach temperatures of approximately 70 up to 1100 F.

Experimental Apparatus

A general layout of the equipment used for the present series of tests is shown schematically in Fig. 1. The air supply, not shown in Fig. 1, consisted of a 75-hp compressor delivering air to a 600-cu-ft tank, then through a pressure regulator to a 110-cu-ft surge tank which then leads to the test equipment. The delivery capacity of the compressor was sufficient to maintain constant regulated pressure in the surge tank for the duration of each run. Double extra heavy, 4-in. steel pipe (ID = 3.15 in.) was used from the elbow downstream of the quick-acting gate valve to the 1-in. gate valve at the exit end. A standard ASME metering orifice (shown in Fig. 2) was located between the first set of flanges. The pressure drop across the metering orifice was measured by the use of flange taps and read from a cistern-type alcohol manometer with a reading accuracy of $\pm 1/2$ mm. The ratio of metering-orifice diameter to inside pipe diameter was chosen at $\beta = 0.20$. The pressure and temperature upstream of the metering orifice were measured by means of a pipe tap connected to a cistern-type mercury manometer and a chromel-alumel thermocouple (0.032-in-diam wire) connected to a potentiometer, respectively. The heater section is represented schematically in Figs. 3 and 4. Heat was supplied by eight Inconel strip heaters with a rating of 1200 watts each at 220 volts. The heaters were divided into three banks containing two heaters in the first bank and three heaters in each of the other two banks. In each bank the heaters were wired in parallel, and mounted in-

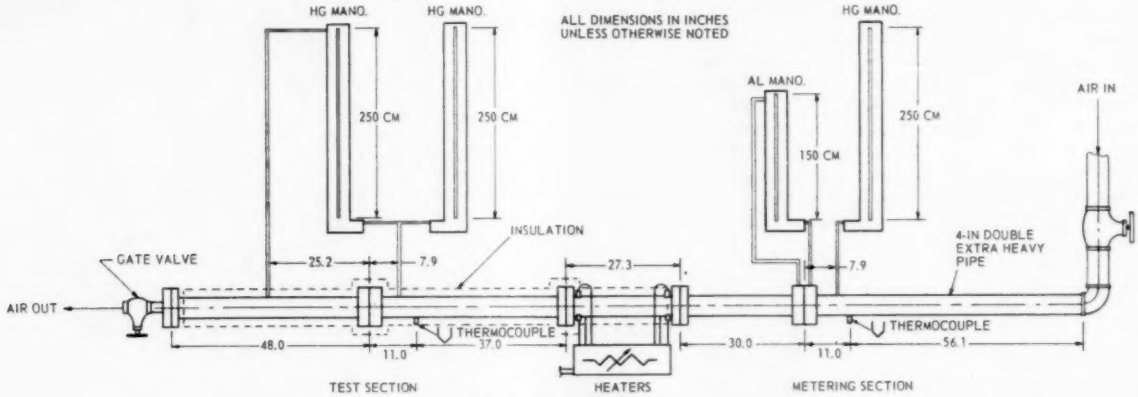

Fig. 1 Test apparatus

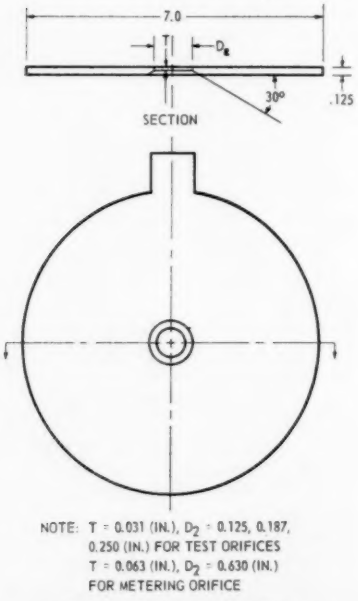

Fig. 2 Orifice construction

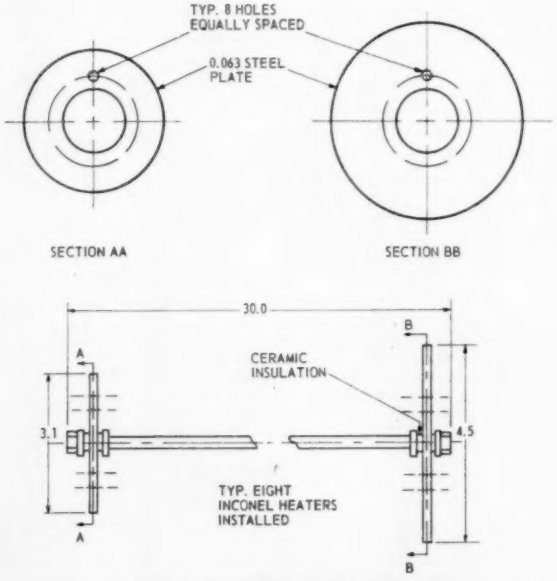

Fig. 3 Inconel heater installation

side the pipe on sheet-steel end plates as shown in Fig. 3. The downstream end plate was free to move inside the pipe to allow for expansion while the upstream plate was fixed between the flanges. Power was conducted through the pipe by means of jet-engine igniter plugs screwed into the pipe as shown in Fig. 4. Copper leads carried current from the plug electrodes to the heater terminals. Current to each bank of heaters was controlled by an autotransformer having continuous control from zero to 100 per cent power. The heater section and all sections downstream of this section were insulated with 4 in. of high-temperature calcium-silicate insulation wrapped externally around the pipe. The test specimen was located between the flanges in the middle of the test section as shown in Fig. 1. The upstream pressure and temperature in front of the test specimen were measured by means of a cistern-type mercury manometer and a chromel-alumel thermocouple, respectively. The pressure drop across the test specimen was measured by the use of pipe taps located according to ASME standards reported in reference (6) and recorded on a cistern-type manometer. The back pressure on the test specimen was controlled by adjustment of the 1-in. gate valve located at the extreme downstream end of the test apparatus, Fig. 1.

The steel A-N fittings were installed between the test-section flanges by brazing them in steel plates as shown in Fig. 5. The sharp-edged orifices were machined from stainless-steel plates according to ASME standards (6) and were positioned between the flanges by means of two locating pins. The fittings and sharp-edged orifices tested are listed in Table 1.

Test Procedure

With the test specimen placed in the test section, surge-tank pressures (absolute) were adjusted to 30, 45, or 60 psi by means of the pressure regulator. The upstream and downstream gate valves were then opened and the heaters activated by adjustment of the autotransformers. The downstream gate valve was adjusted to give the desired value of pressure drop Δp across the test specimen. Simultaneously, the autotransformers were manipulated to give flow temperatures which varied between room temperature and 1100 F. Several minutes were required before stabilization of the temperature at a given Δp was realized. For a given temperature the gate-valve position was changed in steps which yielded almost uniform increments in Δp until the gate valve was wide open. Because of the time required for each run the program was run extensively at surge-tank pressures of 30 and 60 psi, temperatures of 250, 500, and 1100 F for the −4

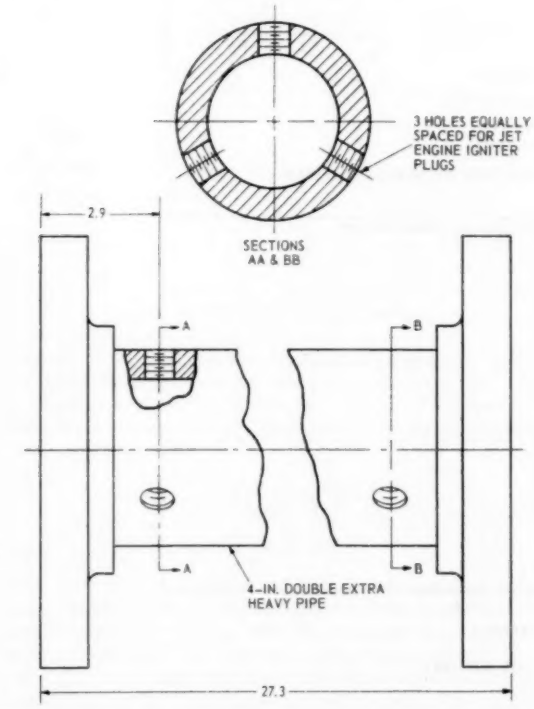

Fig. 4 Jet-engine igniter-plug installation

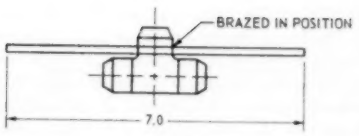

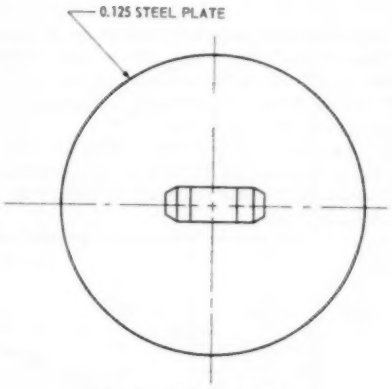

Fig. 5 Fitting installation

Table 1 Test specimens

Identification		Diameter, D_2	Diameter ratio, D_2/D_1
		Sharp-Edged Orifices	
A		0.125	0.0397
B		0.187	0.0593
C		0.250	0.0793
		A-N Fittings	
A–N-815-3[a]	Straight through	0.122	0.0387
A–N-815-4		0.169	0.0537
A–N-815-5		0.235	0.0747
A–N-815-6		0.296	0.0940
A–N-821-3	Elbow	0.119	0.0378
A–N-821-4		0.169	0.0537
A–N-821-5		0.235	0.0747
A–N-821-6		0.294	0.0933
A–N-824-3	Tee	0.124	0.0394
A–N-824-4		0.169	0.0537
A–N-824-5		0.234	0.0743
A–N-824-6		0.295	0.0937

[a] The designation A–N-815-3, for example, is broken down as follows: The three numbers following the letters A-N identify the fitting geometry such as tee, elbow, etc., and the number following the third dash is associated with the size of the fitting; i.e., size of tubing which can be connected and the inside diameter of the flow area through the fitting.

Note: D_1 is the pipe inside diameter and D_2 is the fitting or orifice inside diameter.

and −6 A-N fitting sizes and the 0.187-in. and 0.250-in-diam orifices. The intermediate pressure and temperatures were used as checks on the data for the fitting and orifice sizes outlined in Table 1. The smaller inside diameter orifice and the remaining fittings were tested to the extent of determining their characteristics only at the extremities of the temperature range for a lesser number of pressure ratios at surge-tank pressures of 30 and 60 psi.

The rate of weight flow for the system was computed (7) from the measured pressure and temperature upstream of the metering orifice and the pressure drop across the metering orifice. The characteristics of the test specimen were obtained by the measurement of the upstream temperature and pressure, and the pressure drop across the test specimen.

The choice of a metering orifice with a diameter ratio β equal to 0.2 resulted in Reynolds numbers such that standard ASME methods (7) and discharge coefficients (7) could be used to evaluate all flow rates except for a small number of low flow rates which resulted in Reynolds numbers below 10,000. For the runs with RN < 10,000 the flow rates were computed using discharge coefficients determined by Ambrosius and Spink (8).

Theory

The determination of the form of the flow equations can be obtained by assuming a perfect, incompressible flow through the fitting or orifice. The resulting equation (7) is given as

$$W = \frac{A}{(1 - \beta^4)^{1/2}} \left(\frac{2gp_1\Delta p}{RT_1} \right)^{1/2} \quad \ldots\ldots\ldots\ldots [1]$$

where W is the rate of weight flow, lb/sec, A is the orifice or fitting flow area, $(\pi D_2^2/4)$, β is the diameter ratio, (D_2/D_1), g is the gravitational acceleration, p_1 is the static pressure upstream of the test element, Δp is the static pressure drop across the test element, R is the gas constant, and T_1 is the absolute static temperature

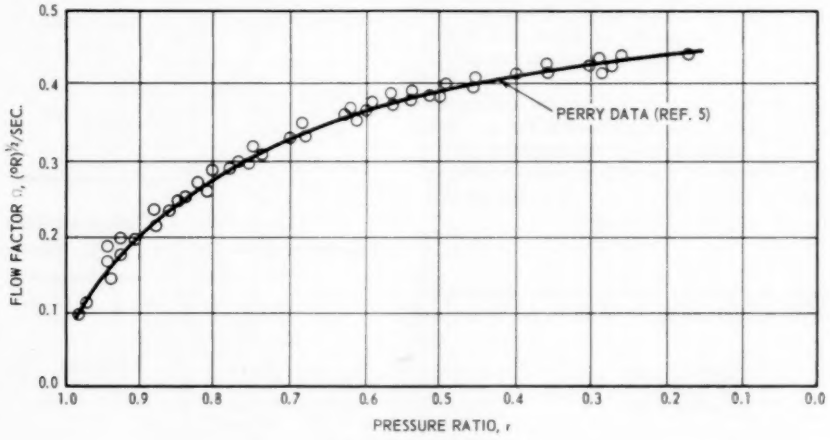

D_2 = 0.125, 0.187, 0.250 (IN.)
530°R < T_1 < 1560°R
p_1 = 30, 45, AND 60 PSIA.

Fig. 6 Flow factor as a function of pressure ratio for sharp-edged orifices

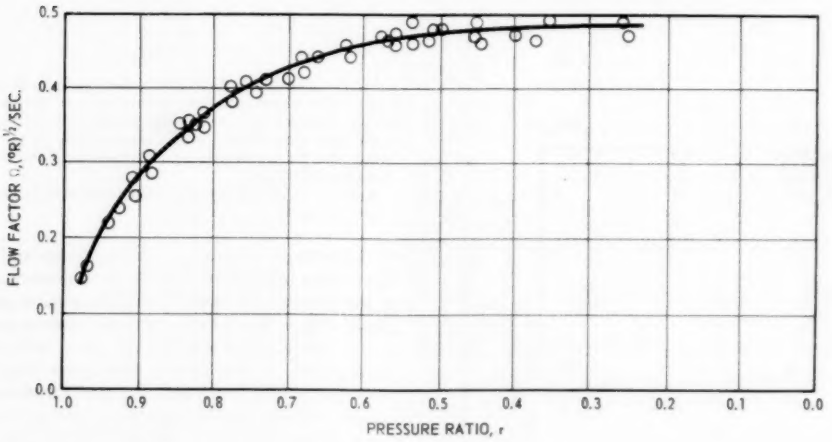

D_2 = 0.122, 0.169, 0.235, 0.296 (IN.)
530°R < T_1 < 1560°R
p_1 = 30, 45, AND 60 PSIA.

Fig. 7 Flow factor as a function of pressure ratio for straight-through (A–N-815) fittings

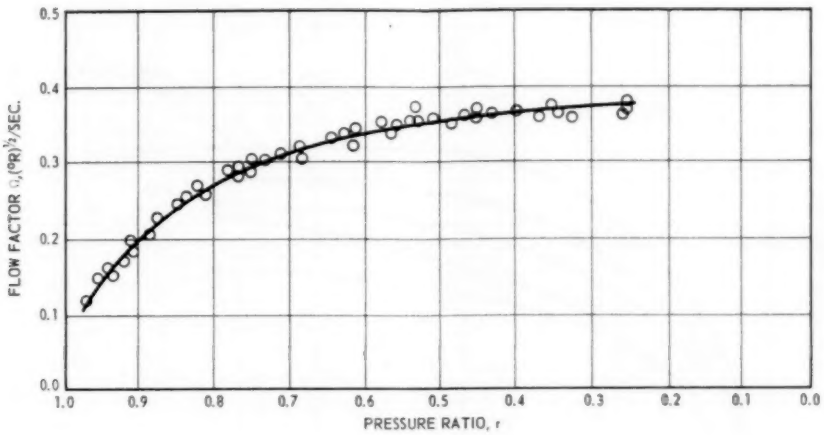

D_2 = 0.119, 0.169, 0.235, 0.294 (IN.)
530°R < T_1 < 1560°R
p_1 = 30, 45, AND 60 PSIA.

Fig. 8 Flow factor as a function of pressure ratio for elbow (A–N-821) fittings

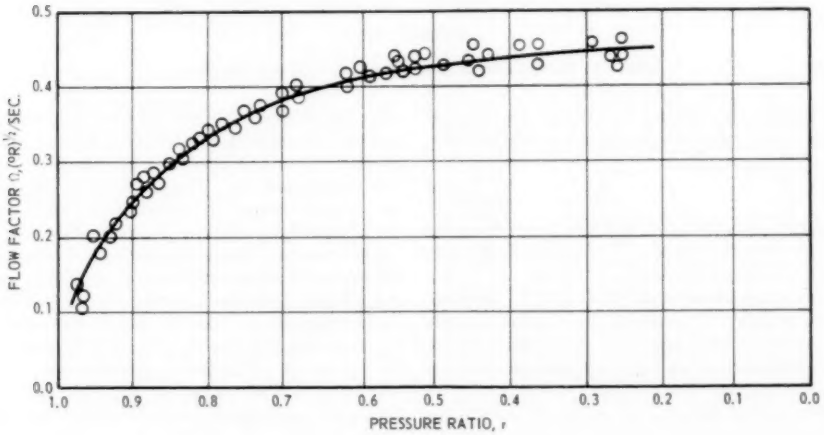

D_2 = 0.214, 0.169, 0.234, 0.295 (IN.)
530°R < T_1 < 1560°R
p_1 =30, 45, AND 60 PSIA.

Fig. 9 Flow factor as a function of pressure ratio for tee (A–N-824) fittings

upstream of the test element. Equation [1] represents the rate of weight flow through the test element for the ideal case. For the problem at hand, corrections in the form of empirical coefficients (7) are introduced. These coefficients are incorporated into Equation [1] as follows

$$W = 1.10\, AKYE \left(\frac{p_1 \Delta p}{T_1}\right)^{1/2} \quad \ldots\ldots\ldots\ldots [2]$$

where $$K = C/(1 - \beta^4)^{1/2}$$

and K is the flow coefficient, C is the discharge coefficient, Y is a compressibility factor, that is, a function of the β-ratio and the pressure ratio, ($r = p_2/p_1$), and the coefficient E corrects for thermal expansion of the element. The flow coefficient K is shown (7) to be a function of Reynolds number, diameter ratio β, pipe diameter D_1, and geometry of the fitting. However, for small diameter ratios as in the present case, and for a given fitting geometry, the effect of pipe size and β can be neglected. In addition, the discharge coefficient is shown (7) to drop about 1 per cent for $10{,}000 < \mathrm{RN} = \rho V_1 D_2/g\mu < 100{,}000$ and remain essentially constant for $\mathrm{RN} > 100{,}000$. Thus, it is assumed that K is constant if the Reynolds number is maintained above 10,000. The compressibility factor Y is also assumed to be a function of r alone since the β ratios are small. Investigation (7) of the effect of thermal expansion over the temperature range employed in these tests indicates that the effect of E can also be neglected. Assuming $E = 1$, and dividing Equation [2] by p_1 gives, after rearrangement

$$\frac{W\sqrt{T_1}}{p_1 A} = \Omega = f(r) \quad \ldots\ldots\ldots\ldots\ldots [3]$$

where Ω is called the flow factor and is seen to be

$$\Omega = 1.10\, KY\,(1 - p_2/p_1)^{1/2} \quad \ldots\ldots\ldots\ldots [4]$$

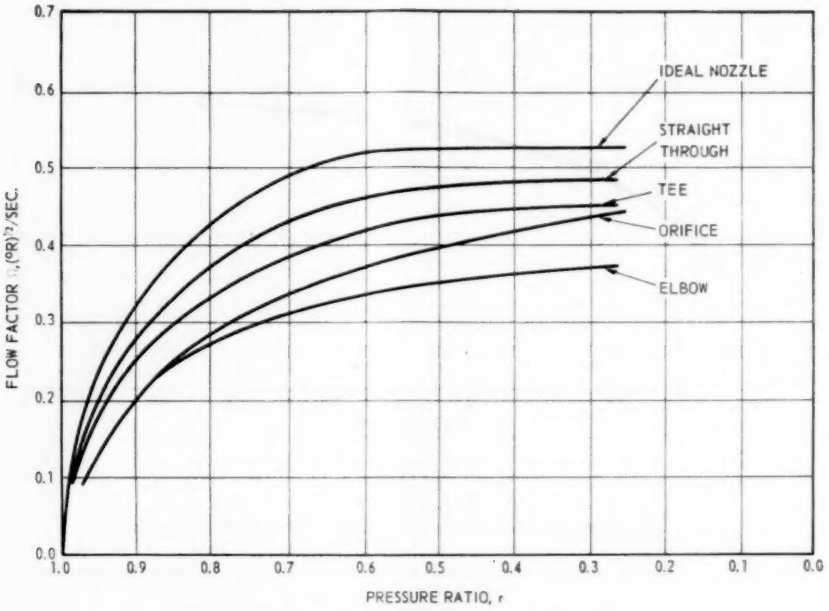

Fig. 10 Comparison of flow factors with ideal nozzle flow

Since K is assumed constant (for RN > 10,000) and Y is a function of the pressure ratio r, Ω can then be expressed as a function of r, only.

Results

The test data are shown as plots of the flow factor Ω versus the pressure ratio r for the orifices, straight-through, elbow, and tee fittings in Figs. 6, 7, 8, and 9, respectively.

In Fig. 6 the sharp-edged orifice data from Perry (5) are compared with the present data. The present data apply for temperatures ranging between room temperature and 1100 F whereas the data in reference (5) are based on room-temperature measurements. These results indicate that the rate of weight flow is inversely proportional to the square root of the absolute temperature as predicted by the theory.

Figs. 7, 8, and 9, representing the straight-through, elbow, and tee configurations, show flow-factor curves that are well defined by the experimental data.

Comparison of the flow through an ideal nozzle with the flows for the geometries investigated is presented in Fig. 10. In this latter figure it is noticed that the flow through a sharp-edged orifice is quite different from both the ideal nozzle and the various fittings tested. It is also apparent for all test specimens that the rate of weight flow increases as the pressure ratio is reduced below the critical value of 0.528 for an ideal nozzle. This is attributed to the fact that the entrance contours for the sharp-edged orifices and fittings are sharp corners and probably result in a region of separated turbulent flow near the walls. In addition the short lengths of the fittings and orifices do not permit the formation of a developed boundary layer. The resulting flow through a given geometry then consists of a central core of high-speed flow and a low-speed separated flow in an annulus near the wall. The resulting mixed flow is probably choked in the center core but as the pressure ratio is reduced below 0.528 the rate of weight flow in the separated region near the wall is increased. The net result is a slight increase in rate of weight flow as the downstream pressure is reduced. The data in Fig. 10 also indicate that the efficiency (where efficiency is defined by the rate of weight flow for a given pressure ratio) of the various geometries compared to the ideal nozzle is a strong function of the fitting geometry. As can be seen the geometry efficiency (in descending order) is first the straight-through, then the tee, sharp-edged orifice, and finally the elbow. An observation which is worthy of note was made during the test program. The tee tests were made with the single leg of the tee facing in the upstream pipe direction (as shown in Fig. 5) and then the same tests conducted with the tee holder-plate rotated 180 deg so that the single leg faced in the downstream pipe direction. Plots of flow factor as a function of pressure ratio indicated that there was no preference in the manner in which the air enters a tee fitting; i.e., entering one leg and exiting through two legs or vice versa.

In order to write empirical equations for the geometries shown in Fig. 10, Equation [4] is rewritten as

$$\Omega = 1.1\ KY\ (1 - r)^{1/2} \quad [5]$$

We now replace KY, the compressible-flow coefficient (for small β-ratios), by the symbol K_c and rewrite Equation [5] as

$$K_c = \frac{\Omega}{1.1\ (1 - r)^{1/2}} \quad [6]$$

Since the numerator and denominator of the right side of Equation [6] are functions of the pressure ratio r only, we may write

$$K_c = \frac{f(r)}{1.1\ (1 - r)^{1/2}} \quad [7]$$

The values of $f(r)$ for each geometry have been determined experimentally (Figs. 6–10). Plots of K_c versus r are shown for the straight-through, elbow, and tee fittings in Figs. 11, 12, and 13, respectively. Empirical equations for the subcritical and critical ranges of pressure ratio are presented in the Appendix for A-N fittings and similar equations for the sharp-edged orifice are taken from reference (5).

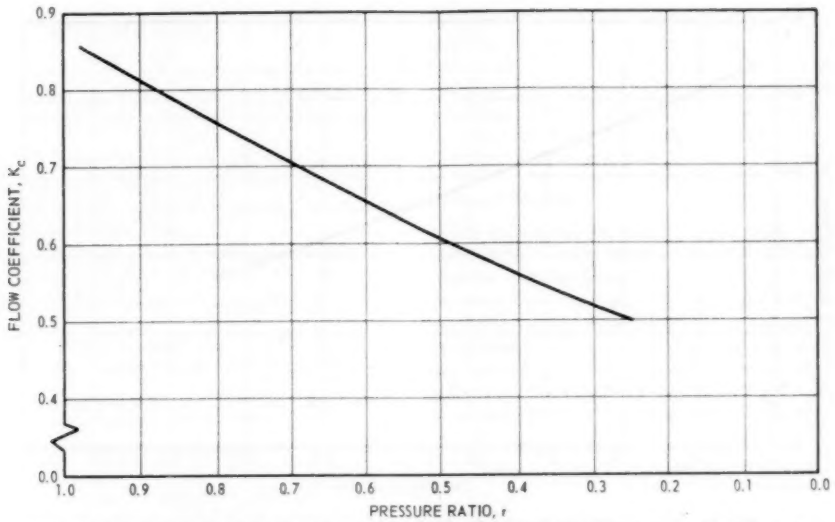

Fig. 11 Flow coefficient for straight-through (A–N-815) fittings as a function of pressure ratio

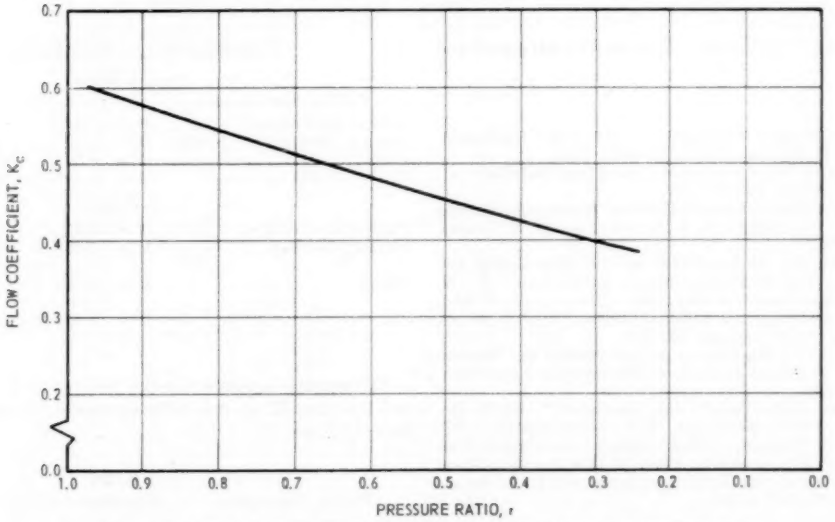

Fig. 12 Flow coefficient for elbow (A–N-821) fittings as a function of pressure ratio

Conclusions

Empirical equations for the rate of weight flow through sharp-edged orifices, straight-through, elbow, and tee fittings subject to the restrictions of negligible approach velocity, approach temperatures between 70 and 1100 F, and approach pressures ranging between 30 psia and 60 psia are derived as a function of the pressure ratio across the test specimen. Two equations are necessary to define the rate of weight flow through each test specimen; one for the region wherein the pressure ratio across the specimen exceeds the ideal nozzle critical value of 0.528 and a second for pressure ratios below this value. In contrast to the ideal nozzle flow the test specimens all exhibit an increase in rate of weight flow for pressure ratios below the critical value. The increasing rate of weight flow is attributed to the negligible approach velocity, poor entrance conditions, and short lengths of the test specimens. It appears that the resulting flow through each specimen consists of essentially a potential-type, central core, and an annulus of separated turbulent flow near the wall. Thus a reduction of the pressure ratio (below the critical value) may cause an increase in rate of weight flow in the separated region. In addition it is considered likely that this reduction in pressure ratio thins the separated region thus allowing more weight flow through the central core.

The data indicate that the rate of weight flow is influenced by the geometry of the test specimen. For a given pressure ratio, the results indicate that the efficiencies (in descending order) of the geometries tested are straight-through, tee, orifice, and elbow. On the basis of the present data it is felt that the results can be extrapolated to higher approach pressures and temperatures.

Acknowledgments

Thanks are due the Sandia Corporation which sponsored this project under consultant contract with the senior author and to

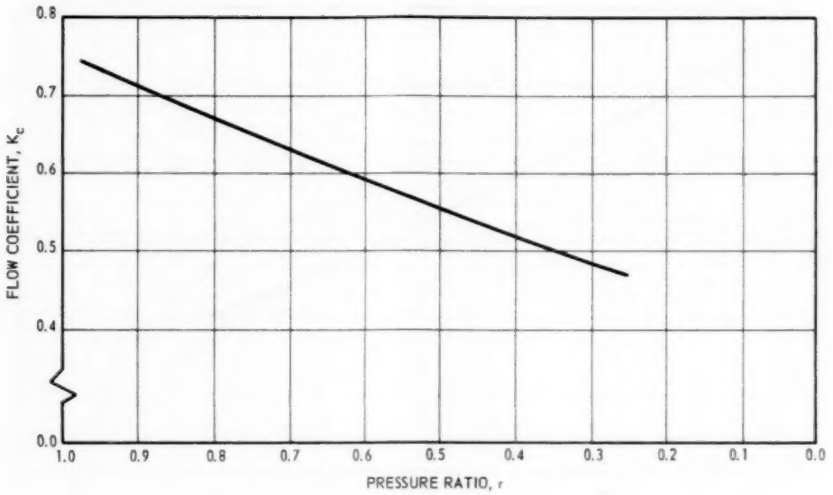

Fig. 13 Flow coefficient for tee (A–N-824) fittings as a function of pressure ratio

Mr. Harold Vaughn of the Sandia Corporation for his advice and help.

Bibliography

1 "Accuracy of Airspeed Measurements and Flight Calibration Procedure," by W. B. Huston, NACA TN 1605, 1948.

2 "Pressure Drop in Tubing in Aircraft Instrument Installations," by W. A. Wildhack, NACA TN 593, 1937.

3 "Transient Behavior of Lumped-Constant Systems for Sensing Gas Pressures," by G. J. Delio, G. V. Schwent, and R. S. Cesaro, NACA TN 1988, 1949.

4 "Experimental and Analytic Methods for Determining the Pressure and Time Lag in Pressure-Measuring Systems," by H. Vaughn, Sandia Corporation, TR 3244, 1954 (Albuquerque, N. M.).

5 "Critical Flow Through Sharp-Edged Orifices," by J. A. Perry, Jr., TRANS. ASME, vol. 71, 1949, pp. 757–763.

6 "Power Test Codes, Supplement on Instruments and Apparatus," Part V, THE AMERICAN SOCIETY OF MECHANICAL ENGINEERS, New York, N. Y., 1949.

7 "Fluid Meters, Their Theory and Application," ASME Research Publication, ASME, New York, N. Y., fourth edition, 1937.

8 "Coefficients of Discharge of Sharp-Edged Concentric Orifices in Commercial 2-In., 3-In., and 4-In. Pipes for Low Reynolds Numbers Using Flange Taps," by E. E. Ambrosius and L. K. Spink, TRANS. ASME, vol. 69, 1947, p. 805.

Appendix

Empirical Equations for Flow Coefficient, K_c

$r \gtrsim 0.528$

Fitting description	Equation
Sharp-edged orifice	$K_c = 0.425\,(1 + r)^{1/2}$
Straight-through (A–N-815)	$K_c = 0.352 + 0.516\,r$
Elbow (A–N-821)	$K_c = 0.310 + 0.298\,r$
Tee (A–N-824)	$K_c = 0.362 + 0.397\,r$

$r \lesssim 0.528$

Sharp-edged orifice	$K_c = 0.410 + 0.220\,r$
Straight-through	$K_c = 0.445 + 0.161\,r + 0.344\,r^2$
Elbow	$K_c = 0.346 + 0.130\,r + 0.187\,r^2$
Tee	$K_c = 0.414 + 0.193\,r + 0.201\,r^2$

By use of the foregoing empirical equations for $K_c\,(= K\,Y)$, equations for the flow factor Ω can be deduced by substitution in Equation [6]. The resulting equations are as follows:

Flow Equations for Flow Factor, Ω

$r \gtrsim 0.528$

Fitting description	Flow factor
Sharp-edged orifice	$\Omega = 0.465\,(1 - r^2)^{1/2}$
Straight-through (A–N-815)	$\Omega = [0.387 + 0.568\,r]\,(1 - r)^{1/2}$
Elbow (A–N-821)	$\Omega = [0.341 + 0.328\,r]\,(1 - r)^{1/2}$
Tee (A–N-824)	$\Omega = [0.398 + 0.437\,r]\,(1 - r)^{1/2}$

$r \lesssim 0.528$

Sharp-edged orifice	$\Omega = [0.451 + 0.242\,r]\,(1 - r)^{1/2}$
Straight-through	$\Omega = [0.489 + 0.177\,r + 0.378\,r^2]\,(1 - r)^{1/2}$
Elbow	$\Omega = [0.380 + 0.143\,r + 0.206\,r^2]\,(1 - r)^{1/2}$
Tee	$\Omega = [0.455 + 0.212\,r + 0.221\,r^2]\,(1 - r)^{1/2}$

Utilizing the equations for the flow factor Ω given previously and Equation [3] we may write expressions for the rate of weight flow as follows:

$r \gtrsim 0.528$

Fitting description	Equation for rate of weight flow
Sharp-edged orifice	$W = 0.465\,(1 - r^2)^{1/2}\,\frac{p_1 A}{\sqrt{T_1}}$
Straight-through (A–N-815)	$W = [0.387 + 0.568\,r]\,(1 - r)^{1/2}\,p_1 A/\sqrt{T_1}$
Elbow (A–N-821)	$W = [0.341 + 0.328\,r]\,(1 - r)^{1/2}\,p_1 A/\sqrt{T_1}$
Tee (A–N-824)	$W = [0.398 + 0.437\,r]\,(1 - r)^{1/2}\,p_1 A/\sqrt{T_1}$

$r \lesssim 0.528$

Sharp-edged orifice	$W = [0.451 + 0.242\,r]\,(1 - r)^{1/2}\,\frac{p_1 A}{\sqrt{T_1}}$
Straight-through	$W = [0.489 + 0.177\,r + 0.378\,r^2]\,(1 - r)^{1/2}\,\frac{p_1 A}{\sqrt{T_1}}$
Elbow	$W = [0.380 + 0.143\,r + 0.206\,r^2]\,(1 - r)^{1/2}\,\frac{p_1 A}{\sqrt{T_1}}$
Tee	$W = [0.455 + 0.212\,r + 0.221\,r^2]\,(1 - r)^{1/2}\,\frac{p_1 A}{\sqrt{T_1}}$

Discussion

R. Reimer.[5] The authors are to be commended for using the flow-factor technique of J. A. Perry. This is a bridge between compressible-flow theory and empirical flow-measurement methods.

The authors explain that all testing was performed on fittings having sharp entrance corners, which probably results in a region of separated flow near the walls. This is the reason for nonchoking of the fittings at high pressure ratio.

However, these fittings can be used in tubing runs behind piping that do not give separated flow into the fitting. Are the data in this report valid for such installations, and if not, how should they be applied?

Examination of Fig. 10 at a pressure ratio of 0.68, shows that the straight-through fitting passes 88 per cent of ideal flow and the orifice passes 70 per cent of ideal flow. At a pressure ratio of 0.92, the straight-through fitting passes 87 per cent of ideal flow. The orifice is behaving properly. The straight-through fitting geometry is similar to a nozzle except for the rounded inlet, so the reduction in flow is largely due to the lack of the rounded inlet. It would be very interesting to have data from A-N fittings equipped with rounded inlets.

[5] Major Test Facilities Operation, Aircraft Gas Turbine Division, General Electric Company, Cincinnati, Ohio. Mem. ASME.

Authors' Closure

The data presented herein are not valid for the condition of a nonnegligible approach velocity. Work has been completed wherein straight-through fittings have been connected to tubing (nonnegligible approach velocity) and will be submitted for publication in the near future. The present fitting data are not applicable to any conceivable piping arrangement but do represent an end-point for extrapolation when the data for nonnegligible approach velocity becomes available. At present no work is contemplated for A-N fittings with rounded inlets.

A Method for Predicting Supercompressibility Factors of Natural Gases

By R. H. ZIMMERMAN,[1] S. R. BEITLER,[2] AND R. G. DARROW,[3] COLUMBUS, OHIO

Accurate prediction of the supercompressibility factor for natural gases is of great importance to the natural-gas industry. This paper presents a working method for the accurate prediction of these factors within the pressure range of 0 to 3000 psi and in terms of gas properties generally known or conveniently determined. This method is the basis upon which the American Gas Association Supercompressibility Tables have been developed.

Nomenclature

THE following nomenclature is used in the paper:

F_{pv} = supercompressibility factor of gas mixture, based on a reference pressure of 14.7 psia
$F(t)$ = temperature-adjustment factor
$F(p)$ = pressure-adjustment factor
G = specific gravity, ratio of molecular weight of gas mixture to 28.97
H = heating value, wet basis, Btu per cu ft at 60 F and 14.7 psia
m = molecular weight
P = gage pressure of mixture, psi
P_r = reduced gage pressure of mixture, P/π
R = gas constant of mixture, ft-lb$_F$ per lb$_M$-deg R
T = temperature of mixture, deg R
T_r = reduced temperature of mixture, T/θ
v = specific volume of mixture, cu ft per lb$_M$
X = mole fraction of any component, moles per mole mixture
Z = compressibility factor of mixture
θ = pseudocritical absolute temperature, deg R
π = pseudocritical absolute pressure, psia
$a, b, c, d, e, f, k, K, q, Q$ = constants

Subscripts:

adj refers to adjusted value
c refers to carbon dioxide
f refers to flowing or actual temperature and pressure
h refers to hydrocarbon portion
i refers to any component
n refers to nitrogen

NOTE: The absence of a subscript on any variable indicates reference to a mixture of hydrocarbon gases and diluents.

[1] Professor of Mechanical Engineering, The Ohio State University. Mem. ASME.

[2] Professor of Mechanical Engineering, The Ohio State University. Fellow ASME.

[3] Senior Engineer, Columbia Gas System Service Corporation. Assoc. Mem. ASME.

Contributed by the Research Committee on Fluid Meters and presented at the Annual Meeting, New York, N. Y., December 1–6, 1957, of THE AMERICAN SOCIETY OF MECHANICAL ENGINEERS.

NOTE: Statements and opinions advanced in papers are to be understood as individual expressions of their authors and not those of the Society. Manuscript received at ASME Headquarters, July 24, 1957. Paper No. 57—A-69.

Introduction

The accurate prediction of the density of natural gas by methods other than direct experimental evaluation requires knowledge of an exact equation of state. The usual procedure in the natural-gas industry is to employ the equation of state for a perfect gas modified by the compressibility factor Z. The working equation of state is, therefore

$$pv = ZRT \quad \ldots\ldots [1]$$

All deviations for the real mixture from that of a perfect-gas mixture are absorbed in the compressibility factor Z. Thus the determination of pipeline flow rates, amount of gas in storage, and so on, are greatly dependent upon the accurate prediction of the compressibility factor from properties of natural gases which may be known generally or commonly measured. Without an accurate prediction method, it is necessary for gas-measurement engineers to rely on time-consuming and expensive experimental procedures to determine the value of the compressibility factor.

A research program was established to develop a method giving good agreement between measured and predicted values of the compressibility factor over the entire range of conditions encountered in normal gas measurements. This program led to the development of an extensive set of working data (1)[4] from the basic tables (2) covering the pressure range 0–3000 psi, temperature 0–180 F, specific gravity 0.554–0.750, carbon dioxide 0–5.0 mole per cent, and nitrogen 0–12.0 mole per cent. The working method is designed to permit rapid and convenient evaluation of the compressibility of natural-gas mixtures.

The purpose of this paper is to present the basic data, equations, and evaluation methods used in the development of the working data (1).

The compressibility data are presented in terms of the "supercompressibility factor" F_{pv} as is standard practice in the natural-gas industry. The supercompressibility factor is defined as

$$F_{pv} = (1/Z)^{1/2} \quad \ldots\ldots [2]$$

and all numerical values of the factor are defined and evaluated on the basis of F_{pv} being equal to unity at a reference pressure of 14.73 psia.

Basic Compressibility Data

Supercompressibility factors have been determined experimentally by use of the Burnett-type apparatus (7) for the pressure range 0 to 4000 psi and the temperature range −50 to 200 F. The low-temperature tests were conducted on nearly pure methane samples. A summary of all tests, excepting the low-temperature and high-pressure runs, and the character of all the gas samples have been described in detail in reference (3). Mixture heating value, specific gravity, and a fractional analysis were determined experimentally for each gas sample used in the tests.

The basic objective in the research program is to establish an accurate method for predicting supercompressibility factors which has been confirmed extensively by comparison with experi-

[4] Numbers in parentheses refer to the Bibliography at the end of the paper.

mental data. The basis of the analytical-prediction method is the "law of corresponding states" and supercompressibility data for pure methane (8). The data for pure methane were obtained through extensive correlation of data obtained from the low-temperature tests on the Burnett apparatus, the Sage and Lacey data (9), and use of the Benedict-Webb-Rubin equation of state (5, 6). The latter equation proved to be of great value to the study and appears to be exceptionally accurate over the normal range of mixture temperature. The tests on methane at low temperatures were found necessary because of the inconsistency in the low-temperature experimental data available in the literature. Table 1 presents an abridged version of the methane data obtained from this study. The data are expressed as a

Table 1 Supercompressibility factors of methane; reduced temperature and pressure data. Abridged from reference (2).

Reduced gage pressure, P_r	Reduced temperature, T_r 1.3	1.4	1.5	1.6	1.7
0	1.0000	1.0000	1.0000	1.0000	1.0000
0.30	1.0235	1.0180	1.0142	1.0112	1.0088
0.60	1.0492	1.0374	1.0288	1.0224	1.0177
0.90	1.0776	1.0574	1.0436	1.0335	1.0261
1.20	1.1086	1.0782	1.0582	1.0442	1.0339
1.50	1.1415	1.0990	1.0726	1.0543	1.0412
1.80	1.1749	1.1194	1.0861	1.0637	1.0478
2.10	1.2060	1.1382	1.0980	1.0722	1.0534
2.40	1.2308	1.1542	1.1087	1.0797	1.0587
2.70	1.2458	1.1664	1.1171	1.0860	1.0627
3.00	1.2509	1.1737	1.1228	1.0903	1.0659

function of the reduced temperature and reduced pressure of the gas mixture, defined by

$$T_r = T/\theta \quad [3]$$

and

$$P_r = P/\pi \quad [4]$$

where θ and π represent the pseudocritical temperature and pressure of the gas mixture, respectively, as defined by Equations [6] and [7].

A comparison of the experimental values of the supercompressibility factor with the data presented in Table 2 shows that the supercompressibility factor can be predicted to an accuracy of ±0.1 per cent in the majority of the cases, and to an accuracy of ±0.20 per cent for nearly all cases encountered (3).

Having defined basic compressibility factors which agree accurately with experimental data, there remains the general problem of developing an evaluation method which may be used to predict the supercompressibility factor of natural-gas mixtures in terms of gas properties which are generally known or conveniently determined.

Development of Evaluation Method

It is convenient to consider a natural-gas mixture as being composed of two main components; i.e., (*a*) hydrocarbons and (*b*) diluents. The diluents presently being considered are carbon dioxide and nitrogen. Thus

$$\Sigma X_i = 1 = X_h + X_c + X_n \quad [5]$$

where X_h, X_c, and X_n represent the mole fractions of the hydrocarbons, carbon dioxide, and nitrogen, respectively. The pseudocritical temperature of such a mixture is defined by

$$\theta = \Sigma X_i\theta_i = X_h\theta_h + X_c\theta_c + X_n\theta_n \quad [6]$$

and the pseudocritical pressure by

$$\pi = \Sigma X_i\pi_i = X_h\pi_h + X_c\pi_c + X_n\pi_n \quad [7]$$

The specific gravity of the mixture as used in the working method is defined as the ratio of the apparent molecular weight of the mixture to the molecular weight of air having standard composition. Thus

$$G = \Sigma X_iG_i = X_hG_h + X_cG_c + X_nG_n \quad [8]$$

where

$$G_i = m_i/28.97 \quad [9]$$

The heating value of a natural-gas mixture likewise may be evaluated from the fractional analysis by

$$H = \Sigma X_iH_i \quad [10]$$

For the assumption of the diluents being inert, Equation [10] reduces to

$$H = X_hH_h \quad [11]$$

The composition character of the diluent portion of the mixture has been fixed as being composed of nitrogen and carbon dioxide. The composition character of the hydrocarbon portion of the mixture is variable. If the fractional analysis of the hydrocarbon portion is known, the pseudocritical temperature and pressure as well as the heating value may be evaluated by

$$\theta_h = \Sigma(X_i\theta_i)_h, \quad \pi_h = \Sigma(X_i\pi_i)_h, \quad H_h = \Sigma(X_iH_i)_h \quad [12]$$

In most situations, however, the hydrocarbon fractional analysis is not known, and an evaluation method which is independent of Equation [12] is needed. The most desirable method is one employing independent variables which may be evaluated directly on a gross basis. Examples of such variables are mixture heating value, mixture specific gravity, carbon-dioxide content, and nitrogen content.

It is possible to circumvent the necessity of employing Equation [12] by the use of several empirical relationships for the hydrocarbon portion of the mixture. It has been demonstrated (3) that, for hydrocarbon specific gravities of less than about

Table 2 Supercompressibility factors of natural gas; base data; 0.6000 specific gravity hydrocarbon gas. Abridged from reference (1), volume VII

Flowing pressure of mixture, psig	Flowing temperature of mixture, deg F 0	20	40	60	80	100	120	140
200	1.0245	1.0213	1.0185	1.0162	1.0140	1.0123	1.0108	1.0094
400	1.0519	1.0444	1.0381	1.0328	1.0285	1.0246	1.0215	1.0189
600	1.0822	1.0691	1.0586	1.0499	1.0430	1.0370	1.0321	1.0279
800	1.1159	1.0954	1.0798	1.0676	1.0575	1.0492	1.0424	1.0366
1000	1.1520	1.1230	1.1013	1.0847	1.0717	1.0608	1.0519	1.0446
1200	1.1895	1.1505	1.1225	1.1016	1.0851	1.0718	1.0610	1.0519
1400	1.2244	1.1763	1.1422	1.1168	1.0973	1.0816	1.0690	1.0585
1600	1.2514	1.1979	1.1590	1.1301	1.1078	1.0904	1.0762	1.0642
1800	1.2665	1.2130	1.1718	1.1402	1.1161	1.0976	1.0821	1.0690
2000	1.2699	1.2207	1.1796	1.1470	1.1219	1.1027	1.0864	1.0724

0.75, the hydrocarbon pseudocritical pressure and temperature are very nearly linearly related to the hydrocarbon specific gravity. Thus to a good approximation

$$\theta_h = a + bG_h \quad [13]$$

and

$$\pi_h = c + dG_h \quad [14]$$

Furthermore, the heating values for the various hydrocarbons in natural gas exhibit an almost exact linear relationship with specific gravity of the hydrocarbons; i.e., to a very high degree of accuracy

$$H_{i-h} = e + fG_{i-h} \quad [15]$$

so that by use of Equation [12]

$$H_h = \Sigma(X_i)(e + fG_{i-h}) = e + fG_h \quad [16]$$

Equation [16] demonstrates that if the hydrocarbon-component heating values vary linearly with the component specific gravity, then the heating value of the hydrocarbon mixture varies linearly with the specific gravity of the hydrocarbon mixture. Equations [13], [14], and [16] may be used as substitutes for the three relationships listed as Equation [12] to avoid the necessity of knowledge of the hydrocarbon fractional analysis.

By use of Equations [5], [6], [7], [8], [11], [13], [14], and [16], it is possible to define the pseudocritical temperature θ and pressure π as a function of any selected set of three independent variables. The variables most easily determined for natural-gas mixtures are (*a*) mixture specific gravity, (*b*) mixture heating value, (*c*) mole-fraction carbon dioxide, and (*d*) mole-fraction nitrogen. Thus it is possible to define

$$\theta = \phi(G, X_c, X_n) = \phi(G, X_c, H) = \phi(G, H, X_n) = \phi(H, X_c, X_n) \quad [17]$$

and

$$\pi = \phi(G, X_c, X_n) = \phi(G, H, X_c) = \phi(G, H, X_n) = \phi(H, X_c, X_n) \quad [18]$$

from the specified set of eight equations. The resulting four relationships for pseudocritical temperature are as follows

$$\theta = a + bG + [\theta_c - (a + bG_c)]X_c + [\theta_n - (a + bG_n)]X_n \quad [19]$$

$$\theta = a + bG + [(\theta_c - a - bG_c) - (e + fG_c)(\theta_n - a - bG_n)/(e + fG_n)]X_c + (\theta_n - a - bG_n)(e + fG - H)/(e + fG_n) \quad [20]$$

$$\theta = a + bG + [(\theta_n - a - bG_n) - (e + fG_n)(\theta_c - a - bG_c)/(e + fG_c)]X_n + (\theta_c - a - bG_c)(e + fG - H)/(e + fG_c) \quad [21]$$

$$\theta = a + bH/f - be/f + [\theta_c - a - bG_c + (b/f)(e + fG_c)]X_c + [\theta_n - a - bG_n + (b/f)(e + fG_n)]X_n \quad [22]$$

The set of four relationships for pseudocritical pressure listed under Equation [18] may be obtained directly from Equations [19], [20], [21], and [22] by substituting c for a and d for b, as may be observed by comparing Equations [13] and [14].

The eight equations for pseudocritical temperature and pressure contain the twelve constants a, b, c, d, e, f, G_c, G_n, π_c, π_n, θ_c, and θ_n, which have been determined to have the following numerical values

$$\left.\begin{array}{llll} a = 157.50 & b = 336.60 & c = 690.0 & \\ d = -31.0 & e = 182.8 & f = 1463 & \\ G_c = 1.5192 & G_n = 0.96707 & \pi_c = 1072 \text{ psia} & \\ \pi_n = 492 \text{ psia} & \theta_c = 510 \text{ deg R} & \theta_n = 216 \text{ deg R} & \end{array}\right\} \quad [23]$$

Numerical values of the constants a, b, c, d, e, and f were determined from correlation studies based on many gas samples (3). The critical pressures of carbon dioxide and nitrogen represent actual critical values, but the critical temperatures are adjusted values so that the compressibility of nitrogen and carbon dioxide more closely agrees with that for hydrocarbon mixtures (8).

The use of the numerical values for the twelve constants allows reduction of Equations [19] through [22] and the companion set for pseudocritical pressure to the following form

$$\theta = 157.50 + 336.60G - 158.85X_c - 267.02X_n \quad [24]$$

$$\theta = 126.95 + 92.07G + 243.17X_c + 0.16711H \quad [25]$$

$$\theta = 145.43 + 239.98G + 0.066030H - 161.51X_n \quad [26]$$

$$\theta = 115.45 + 0.23004H + 394.55X_c + 100.54X_n \quad [27]$$

and

$$\pi = 690.0 - 31.0G + 429.1X_c - 168.0X_n \quad [28]$$

$$\pi = 670.8 - 184.8G + 682.0X_c + 0.10515H \quad [29]$$

$$\pi = 722.6 + 230.0G - 0.17837H - 453.0X_n \quad [30]$$

$$\pi = 693.9 - 0.021187H + 378.1X_c - 201.9X_n \quad [31]$$

Equations [24] through [31] define values of θ and π to a number of significant figures such that the supercompressibility factor is affected at most only by about 0.0001 as a result of rounding off the various coefficients.

The reduced temperature and pressure of the natural-gas mixture may be defined by use of Equations [3] and [4] and knowledge of the mixture temperature and pressure once the pseudocritical pressure and temperature have been defined by using the two appropriate equations in the group [24] through [31]. The supercompressibility factor is defined from the basic data as presented in Table 1 as a function of reduced pressure and temperature.

The specific gravity as defined for use in this analysis differs by a negligible amount from the standard definition of specific gravity when the specific gravity is less than about 0.75. A measured specific gravity first should be corrected to the specific gravity as herein used whenever the values are much above about 0.75.

Development of Working Method

For purposes of maximum convenience, the working method for predicting supercompressibility factors should be designed for minimal calculational effort for mixtures most commonly encountered and also, avoid excessive calculational effort for any other mixture.

The majority of natural-gas mixtures associated with pipeline flows have a specific gravity in the vicinity of 0.60 with negligible amounts of carbon dioxide and nitrogen. It has been considered desirable, therefore, to develop the working method around a natural-gas mixture of this type. A reference gas mixture is used which has a specific gravity of 0.600 and pure hydrocarbon composition. The pseudocritical temperature and pressure of this reference mixture are defined by Equations [13] and [14], or [24] and [28], and have numerical values of 359.46 R and 671.4 psia, respectively. On the basis of this reference mixture, the basic supercompressibility data as presented in Table 1 may be redefined as a function of the flowing pressure and temperature of the mixture. Such data are presented in Table 2. These data represent the working data and are used for the evaluation of the supercompressibility factor for any mixture through the method developed in the following.

Any natural-gas mixture having an actual mixture or flowing

temperature T_f and a pseudocritical temperature θ has a reduced temperature T/θ. The same reduced temperature may be used to define an adjusted temperature for use in Table 2 by the equation

$$T_{adj} = (T_f)(359.46/\theta) - 460 \quad [32]$$

The adjusted temperature T_{adj} defined in Table 2 is the same reduced temperature as would be used for the basic data in Table 1. Similarly, an adjusted pressure may be defined for use in Table 2 by

$$P_{adj} = (P_f)(671.4/\pi) \quad [33]$$

where P_f represents the actual or flowing gage pressure of the mixture. The difference between the corrected and mixture temperatures and the corrected and mixture gage pressures define temperature and pressure adjustments which are related by

$$T_{adj} = T_f + \Delta T_{adj} \quad [34]$$

and

$$P_{adj} = P_f + \Delta P_{adj} \quad [35]$$

Equations defining the temperature and pressure adjustments may be derived directly from the group of Equations [24] through [31] and Equations [32] and [33].

The general equations for the temperature adjustment ΔT_{adj} and the pressure adjustment ΔP_{adj} are

$$\Delta T_{adj} = T_f\,[K - F(T)]/[k + F(T)] \quad [36]$$

and

$$\Delta P_{adj} = P_f[Q - F(P)]/[q + F(P)] \quad [37]$$

where $F(T)$ and $F(P)$ are temperature and pressure-adjustment factors, respectively, and K, k, q, and Q are constants having values fixed by the selected group of independent variables. It may be shown, by use of Equations [24] through [31] that the temperature-adjustment factor and the constants k and K are defined by the following set of equations

$$F(T) = G - 0.4719X_c - 0.7933X_n, \quad \text{with } K = 0.6000,\ k = 0.4679 \quad [38]$$

$$F(T) = G + 2.641X_c + 1.815(H/1000), \quad \text{with } K = 2.525,\ k = 1.379 \quad [39]$$

$$F(T) = G + 0.2751(H/1000) - 0.6730X_n, \quad \text{with } K = 0.8919,\ k = 0.6060 \quad [40]$$

$$F(T) = (H/1000) + 1.715X_c + 0.4371X_n, \quad \text{with } K = 1.0607,\ k = 0.5019 \quad [41]$$

Also, by similar derivation, it may be shown that the pressure-adjustment factor and the constants q and Q are defined by

$$F(P) = G - 13.84X_c + 5.420X_n, \quad \text{with } Q = 0.6000,\ q = -22.60 \quad [42]$$

$$F(P) = G - 3.690X_c - 0.5690(H/1000), \quad \text{with } Q = -0.00335,\ q = -3.630 \quad [43]$$

$$F(P) = G - 0.7755(H/1000) - 1.970X_n, \quad \text{with } Q = -0.2226,\ q = 3.142 \quad [44]$$

$$F(P) = (H/1000) - 17.85X_c + 9.529X_n, \quad \text{with } Q = 1.0620,\ q = -32.75 \quad [45]$$

The choice of equation in each of the two sets would be dictated by the selected set of independent variables.

The working method for predicting the supercompressibility factor is now reduced to the following procedure: By knowledge of the numerical values of any three of the four independent variables (*a*) specific gravity, (*b*) heating value, (*c*) carbon dioxide content, and (*d*) nitrogen content, the temperature and pressure-adjustment factors, $F(T)$ and $F(P)$, may be evaluated. These factors along with the mixture flowing temperature and pressure define temperature and pressure adjustments by Equations [36] and [37], and the adjusted temperature and adjusted pressure by Equations [34] and [35]. The adjusted temperature and adjusted pressure serve to define the supercompressibility factor by use of the data shown in Table 2.

The AGA Supercompressibility Tables

The working method described in the previous section has been used as the basis for developing the AGA Tables on Supercompressibility Factors for Natural Gas (1). These tables cover the following ranges on the independent variables: Pressure, 0–3000 psi; temperature, 0–180 F; specific gravity, 0.554–0.750; carbon dioxide, 0–5.0 mole per cent; and nitrogen, 0–12.0 mole per cent. Volumes I through VI are for pure hydrocarbon mixtures. Volume VII contains the base data for the reference gas mixture of 0.600 specific gravity and temperature and pressure-adjustment factors for diluents.

Future Work

Continuing research is designed to increase the usefulness of the basic data by extending the range on all variables such as pressure, temperature, hydrocarbon specific gravity, and diluent content. It is desired to extend the specific-gravity limit to around 0.90, the pressure limit to about 5000 psi, and the diluent-content limit to about 30 mole per cent.

Acknowledgments

The research program herein reported has been sponsored by a group of companies within the natural-gas industry and the American Gas Association. The Tennessee Gas Transmission Company and the Columbia Gas System Service Corporation provided valuable assistance and extensive experimental data. The authors wish to extend appreciation to E. S. Plank of the Tennessee Gas Transmission Company, and to J. E. Overbeck and H. B. McNichols of the Columbia Gas System Service Corporation for their help in carrying out the research program.

Bibliography

1 "Supercompressibility Factors for Natural Gas," American Gas Association, New York, N. Y., vols. I through VII, 1955.

2 "Gas Measurement," American Gas Association, New York, N. Y., Committee Report no. 3, 1954.

3 "Progress Report on the Study of Supercompressibility Factors for Natural Gases," by R. H. Zimmerman and S. R. Beitler, TRANS. ASME, vol. 74, 1952, pp. 945–951.

4 "The Evaluation of Compressibility Factors for Natural Gas Mixtures," by R. G. Darrow, thesis, The Ohio State University, Columbus, Ohio, 1953.

5 "An Empirical Equation for Thermodynamic Properties of Light Hydrocarbons and Their Mixtures—I," by M. Benedict, G. B. Webb, and L. C. Rubin, *Journal of Chemical Physics*, vol. 8, 1940, p. 334.

6 "An Empirical Equation for Thermodynamic Properties of Light Hydrocarbons and Their Mixtures—Constants for Twelve Hydrocarbons," by M. Benedict, G. B. Webb, and L. C. Rubin, *Chemical Engineering Progress*, vol. 47, 1951, p. 419.

7 "Compressibility Determinations Without Volume Measurements," by E. S. Burnett, TRANS. ASME, vol. 58, 1936, pp. A-136–140.

8 "The Pseudo-Critical Method for Evaluating Deviation of Natural Gas From Boyle's Law," by R. V. Dunkle, *Gas*, vol. 20, 1944, p. 41.

9 "Thermodynamic Properties of the Lighter Paraffin Hydrocarbons and Nitrogen," by B. H. Sage and W. N. Lacey, American Petroleum Institute, New York, N. Y., 1950.

Discussion

D. L. Katz.[5] The authors are commended for their efforts to improve the accuracy and facility for determining the compressibility of natural gases. The following comments or questions are raised on the subject of the paper:

1 Many engineering problems in the natural-gas industry require compressibility data at conditions beyond the scope of this paper. Methods often employed involve the computation of reduced temperature and pressure from composition followed by finding the compressibility factor from a chart or table.[6,7] Have the authors compared their compressibility-factor data with the charts and table in common use in the industry? Assuming that the authors' results are an improvement on earlier methods, have they considered presenting a compressibility-factor chart using reduced temperature and reduced pressure, which could be used for gases having compositions outside the limits of their equations?

2 In metering gases, there are three factors which are functions of pressure, temperature, and gas gravity. It was suggested some 15 years ago that these be combined into a single factor as follows[8]

$$F_{tf}F_gF_{pv} = \left(\frac{520}{\text{GTZ}}\right)^{1/2} = F_{tgz}$$

It was shown that the variation in F_{tgz} with pressure and temperature would be no more severe than for F_{pv} and that the combination would omit two steps in meter calculations. Did the authors consider this combination of variables? Do they see any reason why it would not be possible to correlate F_{tgz} with pressure, temperature, gas gravity, and composition?

3 The last comment is a remark to the profession and gas industry and not to the authors alone. For those who have worked at pressures of 6000 psi or above, the use of the prefix "super" on the "compressibility factors" has been questionable. Presumably, the prefix is intended to connote that the gas is more compressible than an ideal gas. At higher pressures, common in natural gas reservoirs, natural gas is less compressible than an ideal gas. For those using the prefix super, it would be necessary to change the name to "subcompressibility" factors when the gas became less compressible. For this reason, elimination of the prefix super is urged, for the term compressibility factor is adequate to cover conditions at which a gas is both more compressible and less compressible.

H. B. McNichols.[9] The authors have presented a very interesting approach to a subject which has great importance to the natural-gas industry.

It should be pointed out that during the infancy of the gas industry, delivery pressures were of the magnitude of 200 or 300 psi pressure and the commodity itself was rather inexpensive. However, today the field price of natural gas has tripled and the metering pressures are around 1000 psig. The supercompressibility of natural gas was considered a straight-line function with its slope varying with temperature and specific gravity. Operating supercompressibility factors were developed to cover a pressure range up to 500 psig. As flowing pressures began to increase, the tables were extended to 1000 psig only by changing the intercept constant of the straight-line equation.

In recent years there has been a great need for a method of determining supercompressibility factors for natural gas which would more closely duplicate actual test results. The method outlined in this paper, being developed and correlated with actual test results, gives very accurate results.

Some of the larger gas companies have been making comparative studies with actual test results on natural gases having considerable amounts of carbon dioxide and nitrogen present. The results of these comparisons seem to indicate very close agreement.

It should be pointed out that owing to the number of parameters, this method of determining supercompressibility factors does not lend itself to a reasonable equation and therefore necessitates the use of the seven volumes of the "AGA Operating Tables." With the advent of electronic computers and their application to gas-measurement calculations, the use of tables rather than an equation became somewhat of a problem. However, with the advance in data-storage capacity in the newer computer equipment, the basic 0.600 specific gravity table in AGA Gas Measurement Committee Report No. 3 can easily be adapted to develop supercompressibility factors by interpolation rather than by equations.

The method outlined in this paper permits the determination of supercompressibility factors without having to make complete gas analyses which are time-consuming in themselves. Properties of the gas such as specific gravity and heating value are already known for other computations; therefore, it is necessary to obtain only the amount of carbon dioxide or nitrogen or both to develop the factors.

E. E. Stovall.[9] The authors are to be complimented on their fine presentation.

A method for more accurately predicting supercompressibility factors throughout the normal operating range of conditions in the natural-gas industry has been needed.

The method described in the paper has proved to be the answer to that need and has been widely accepted by the gas-industry engineers. Actual tests in operating practices have proved the accuracy of the method.

Authors' Closure

The authors appreciate the comments by Dr. Katz. A formal and detailed comparison of the results of this method with other methods has never been completed. The authors should complete the comparison. A study to extend the range of applicability of the present data is now in progress. It is expected that a compressibility chart will be developed which could be used for gases having compositions outside the limits of the present working method.

Relative to the use of a combined correction factor for temperature, gravity, and compressibility, the authors have given much thought to this possibility and feel that there is no significant advantage to the combined arrangement. The combination would have a basic disadvantage in that the flexibility of use would be reduced. It would be necessary to evaluate F_{pv} only as a function of the specific gravity. The present method which separates the factors allows the use of any method in defining F_{pv}, e.g., a fractional analysis, or gravity and heating value, etc. The authors agree in principle with Dr. Katz's remarks on naming of the deviation factors. However, these names have come to have certain specific meanings and it is doubtful if change would be of any benefit to natural gas industry.

The authors are grateful to Mr. McNichols and Mr. Stovall for their comments.

---

[5] Professor, Chemical Engineering, University of Michigan, Ann Arbor, Mich. Mem. ASME.

[6] "High Pressure Gas Measurement by T. A. Mathews, C. H. Roland, and D. L. Katz, *Proceedings, Natural Gas Association of America*, pp. 41–42, *Petroleum Refiner*, vol. 21, no. 6, 1942, p. 58.

[7] "Black Pressure Test for Natural Gas Wells," by J. K. Baummel and C. A. Breitung, R. R. Commission of Texas, Austin, Tex., 1950.

[8] Columbia Gas System Service Corporation, Columbus, Ohio. Mem. ASME.

[9] Superintendent of Gas, Transmission Division, Lone Star Gas Company, Dallas, Texas. Mem. ASME.

Dimensionless Correlation of Coefficients of Turbine-Type Flowmeters

By H. M. HOCHREITER,[1] HATBORO, PA.

The principles of dimensional reasoning are applied to a kinematic flowmeter of the turbine or propeller type. Experimental results are correlated over a wide range of fluid conditions and geometric variations, and coefficients compared against those predicted from a one-dimensional design equation.

Nomenclature

THE following nomenclature is used in the paper:

C = flow coefficient in practical equation, Q/nD^3
D_h = rotor hub diameter, in.
D_b = rotor blade tip diameter, in.
D = meter bore diameter, in.
E = fluid elasticity, psi
F = any force, other than fluid forces, lb
K = flow coefficient in design equation
L = rotor lead, in.
m = number of rotor blades
n = rotor angular velocity, rps
N = viscosity parameter, nD^2/ν
p = rotor axial length, in.
Q = volume flow rate, cu in. per sec
r = radius of a rotor blade section, in.
t = rotor blade thickness at blade tip, in.
V = fluid velocity at rotor, ips
V_r = relative velocity of fluid with respect to rotor blade at radius r, ips
α = ratio, D_h/D, dimensionless
θ_r = rotor blade angle at radius r, dimensionless
μ = fluid viscosity, lb per in. sec
ν = fluid kinematic viscosity, $= \mu/\rho$, sq in. per sec
ρ = fluid density, lb per cu in.

Introduction

The kinematic flowmeter described here is of the turbine or propeller type manufactured by the author's company. It is an axial flow displacement type device, Fig. 1, in which the flow passes from a flow straightening section, past a rotor with helical blades, mounted in antifriction ball bearings lubricated by the flowing fluid. The rotor turns at a speed essentially proportional to the fluid velocity. Each blade passage induces a small alternating voltage in an external magnet and coil assembly, the signal being read out on an electronic pulse counter.

Dimensional Parameters of Kinematic Flowmeters

For any device in which the fluid produces a continuous motion, and where there is no significant bearing or gearing friction, or shaft or other power input or output, the following dependency statement can be made, for incompressible flow

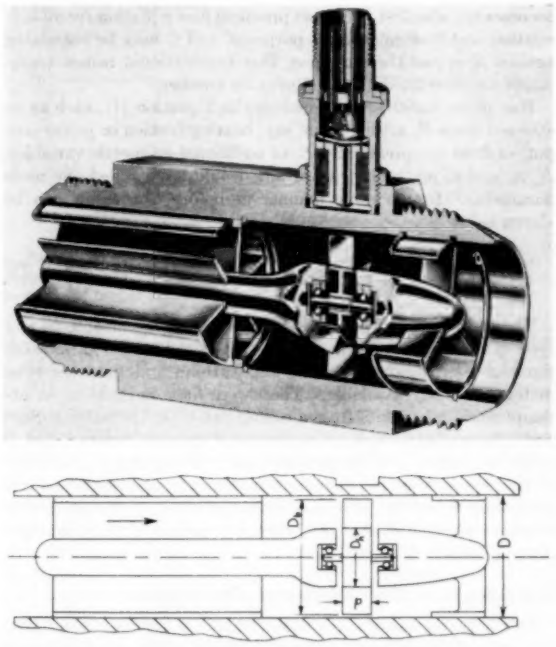

Fig. 1 A 2-in. turbine meter with sketch showing basic reference dimensions. Courtesy Fischer & Porter Company.

$$Q \text{ depends on } n, D, \rho, \mu \quad \ldots\ldots\ldots\ldots\ldots\ldots [1]$$

Since there are five variables, with three fundamental variables, there will be two dimensionless parameters, one a function of the other.[2] Choosing for example, as a matter of convenience here, n, D, and ρ as basic variables rather than mass, length, and time, the remaining variables may be expressed as functions of these, thus

$$\left.\begin{aligned} \Pi_1 &= \frac{Q}{n^a D^b \rho^c} = \frac{\mathrm{L^3T^{-1}}}{(\mathrm{T^{-1}})^a(\mathrm{L})^b(\mathrm{ML^{-3}})^c} \\ \Pi_2 &= \frac{\mu}{n^d D^e \rho^f} = \frac{\mathrm{ML^{-1}T^{-1}}}{(\mathrm{T^{-1}})^d(\mathrm{L})^e(\mathrm{ML^{-3}})^f} \end{aligned}\right\} \quad \ldots\ldots [2]$$

Since the Π's are to be dimensionless, it is seen immediately that $a = 1, c = 0, b = 3$ and $d = 1, f = 1, e = 2$, so that

$$\left.\begin{aligned} \Pi_1 &= \Pi_1\left(\frac{Q}{nD^3}\right) \\ \Pi_2 &= \Pi_2\left(\frac{\mu}{nD^2\rho}\right) = \Pi_2\left(\frac{\nu}{nD^2}\right) = \Pi_3\left(\frac{nD^2}{\nu}\right) \end{aligned}\right\} \quad \ldots\ldots [3]$$

The relationship of the variables is then

---

[1] Research Engineer, Fischer & Porter Company. Mem. ASME. Contributed by the Research Committee on Fluid Meters and presented at the Annual Meeting, New York, N. Y., December 1–6, 1957, of THE AMERICAN SOCIETY OF MECHANICAL ENGINEERS.

NOTE: Statements and opinions advanced in papers are to be understood as individual expressions of their authors and not those of the Society. Manuscript received at ASME Headquarters, July 25, 1957. Paper No. 57—A-63.

[2] "Model Experiments and the Forms of Empirical Equations," by E. Buckingham, TRANS. ASME, vol. 37, 1915, pp. 263–296.

$$\frac{Q}{nD^3} \text{ depends on } \frac{nD^2}{\nu}$$

For incompressible flow in a turbine meter free of nonfluid friction, defining Π_1 as the flow coefficient C, and Π_2 as the viscosity parameter N

$$C = \frac{Q}{nD^3}, \quad N = \frac{nD^2}{\nu} \qquad [4]$$

becomes the simplest and most practical flow equation for all correlation and flow calculation purposes, and C may be correlated against N in just the same way that conventional orifice coefficients are correlated against Reynolds number.

Had other variables been included in Equation [1], such as an external force F, arising from, say, bearing friction or power output, or fluid compressibility E, or additional geometric variables, d_1, d_2, and so on, each new variable would have added one more parameter. In the same manner as before, the result can be shown to be

$$\frac{Q}{nD^3} = f\left(\frac{nD^2}{\nu}, \quad \frac{F}{\rho n^2 D^4}, \quad \frac{E}{\rho n^2 D^2}, \quad \frac{d_1}{D}, \quad \frac{d_2}{D}, \ldots\right) \qquad [5]$$

These dimensional relationships are equally applicable to any type of continuous motion device, such as any of the various designs of positive displacement and turbine and propeller-type meters presently available. They were first derived[3] in an attempt to correlate data from a rolling-ball-type flowmeter.[4] Successfully applied here, it led to the use of the parameters C and N in the development of the present meter, as well as the realization of the necessity of freedom from influence of the nonfluid force parameter $F/\rho n^2 D^4$. It is only when the effect of this parameter is large compared to that of N that corrections for fluid density[5] are applicable.

Derivation of the One-Dimensional Flow Equation

In a metering application, where friction is kept to a minimum, the angle of attack between fluid and blade will be small and here will be neglected. Since power requirements are small, the fluid need be deflected very little in passing the blade and a flat plate, as "seen" by the fluid, represents a satisfactory geometry. The similarity of the velocity triangle and the geometric triangle for a helix in Fig. 2 shows that a helical blade will present to the fluid a flat plate geometry at a constant angle over the total blade height. In this way, opposing torques and radial flow components are minimized. Thus

$$\frac{2\pi rn}{V} = \tan \theta_r = \frac{2\pi r}{L}$$

[3] "The Kinematic Flowmeter," by V. P. Head, Fischer & Porter Company Research Report FX7-106, 1950, unpublished.

[4] "A Rolling-Ball Flowmeter for Hazardous and Corrosive Liquid," by P. I. Wood, ISA Conference, St. Louis, Mo., September, 1949, Paper No. 49-8-5.

[5] "Fluid Meters—Part 1, Their Theory and Application," ASME publication, fourth edition, 1937.

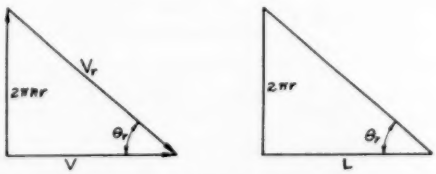

Fig. 2 Velocity and helix triangles

$$V = nL = \frac{Q}{A} = \frac{Q}{\frac{\pi}{4} D^2(1 - \alpha^2)}$$

and

$$\frac{Q}{nD^3} = \frac{\pi}{4}(1 - \alpha^2)\frac{L}{D} \qquad [6]$$

Equation [6] neglects the actual area obstructed by blades of greater than zero thickness. Based on an assumed constant blade section cut by a plane perpendicular to the flow axis, the area of blade obstruction is

$$\frac{m}{2}(D_b - D_h)t\left[1 + \left(\frac{\pi D_b}{L}\right)^2\right]^{1/2}$$

Subtracting this from the annular flow area of Equation [6] gives

$$K = \frac{Q}{nD^3} = \frac{\pi}{4}\left(\frac{L}{D}\right)\left\{1 - \alpha^2 - \frac{2m[D_b - D_h]t}{\pi D^2}\left[1 + \left(\frac{\pi D_b}{L}\right)^2\right]^{1/2}\right\} \qquad [7]$$

Obviously the complexity of this equation, compared to Equation [4], limits its usefulness to design purposes.

Since this result is based on the assumptions of fully turbulent, incompressible flow conditions and no external or nonfluid power input or output, it does not show the dependence of the coefficient on the viscosity and force parameters of Equation [5], but it does show dependence on other geometrical parameters, L/D (or blade angle), α ($= D_h/D$), and so on. It remains, then, for experiment to show under what conditions and to what extent Equation [7] is valid.

Experimental Results

All tests were made with the calibration facilities of the author's company. The test stands utilize the change in height of a mercury column to determine the change in mass of fluid in an accurately measured standpipe. The fluids used were hydrocarbons ranging in viscosity from about 0.7 ctks to 700 ctks.

Meter Coefficient as a Function of Fluid Conditions. Figs. 3 and 4 show results on a meter of 1 in. size when calibrated over a wide span of N-values, with five hydrocarbon fluids whose viscosities ranged from 0.70 ctks (gasoline) to about 700 ctks (SAE No. 50

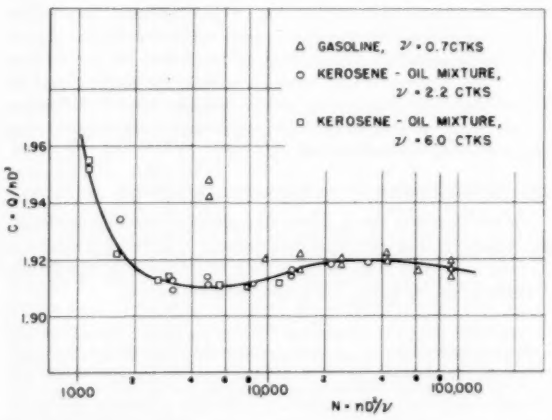

Fig. 3 Meter coefficient versus viscosity parameter in linear region for a 1-in. turbine meter

oil). Fig. 3, with an expanded scale, shows the low viscosity linear region; that is, the region of constant coefficient where flow is proportional to speed, with calibrations with fluids of three viscosities, 0.70, 2.2, and 6.0 ctks. Except at the lowest rotor speeds, all points for each fluid lie essentially on the same curve, showing the validity of Equation [4]. At the low speeds deviations occur because bearing friction, enhanced by the radial loading of the magnetic pickup, is no longer negligible compared to the fluid forces. The degree to which friction affects the coefficient depends on the lubricating qualities of the fluid. Thus gasoline, with relatively poor lubricating qualities and low viscosity, deviates 1.8 per cent at 0.05 of maximum rated speed, while the more viscous (2.2 ctks) kerosene-oil mixture deviates only 0.7 per cent at the same speed.

Fig. 4 shows the entire range, with additional calibrations at 70 and 700 ctks. The ordinate here is plotted on a log scale in order to show the approach to a straight line relationship, of slope approximately -0.190, at high viscosities. Here, even at the lowest speeds tested, about 0.025 n_{max}, there is no observable deviation from the curve due to bearing friction, since the fluid viscosity is so high that the fluid forces remain large compared to the nonfluid forces, such as nonviscous bearing friction forces.

The slope of the coefficient curve of Fig. 4, and hence the viscosity sensitivity at high viscosities is quite favorable compared to many other meter types under similar fluid conditions. At high viscosity a severe penalty is imposed by the pressure drop, illustrated in Fig. 5. For a given flow rate in a given meter size, the pressure drop may be increased by a factor of from 3 to 100 with a 100-fold increase in viscosity. This is, however, a limitation of the particular meter geometry, which was chosen for optimum performance under turbulent conditions. Typical loss at maximum flow of a jet fuel is $7^1/_2$ psi.

Geometrical Variations. In designing a full range of meter sizes, it was not feasible to maintain strict geometric similarity for all dimensional parameters. For example, since the basic design criterion was one of constant pressure drop (or flow velocity, or rotor tip speed) at maximum rated flow, it was necessary to change the number of blades in each meter size in order to maintain a constant frequency output of 600 cps at maximum flow rate. Similarly, to obtain various maximum flow rates in each size, α was also permitted to vary.

Because of the number of geometric parameters involved, it was impractical to attempt to determine the effect of each in turn, as is required by Equation [5]. However, it was found possible to obtain a satisfactory correlation with $(p/D) \times (D - D_b)/D$ as shown in Fig. 6. The effects of the geometric variables can be isolated from the force and viscosity parameters of Equation [5] by maintaining rotor speeds high enough to keep the effect of the force parameter negligible, while considering data only at specific values of N. The value of N chosen for Fig. 6 was 16,000, this point lying in the linear region for all meter sizes. Each point represents the average coefficient of a number of meters of the stated size, and the ratio C to K was used since the latter was not the same for all sizes. Because most of the meters had values of α in the neighborhood of 0.47 only this line is firmly established. Nevertheless, only the smallest meters, in the $^1/_2$-in. body sizes, fail to correlate reasonably well.

It will be noted that, although blade number varies from 2 in the smallest size to 10 in the largest, its effects are adequately accounted for in Equation [7], since the correlation of Fig. 6 does not require it. Similarly, there appears to be no effect of blade angle or rotor lead other than that accounted for in Equation [7], although the range of values investigated was quite small, the blade tip angle ranging from about 42 to 50 deg.

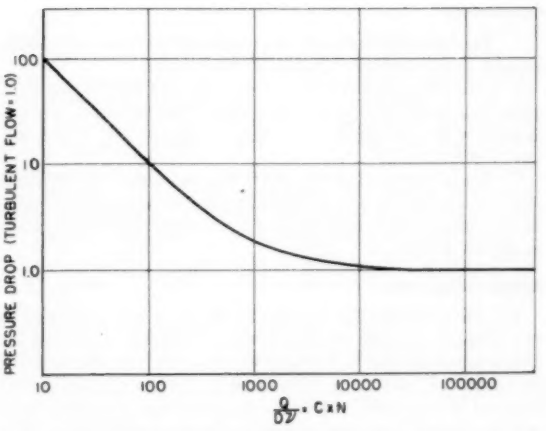

Fig. 5 Pressure drop at maximum rated flow at high viscosity referred to that in turbulent flow. Typical pressure drop at maximum flow for jet fuel is $7^1/_2$ psi.

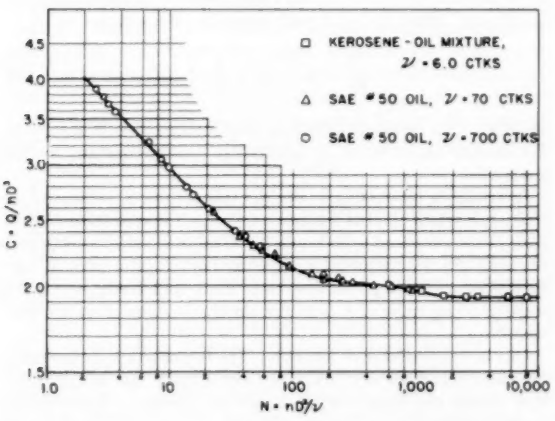

Fig. 4 Meter coefficient versus viscosity parameter over a wide viscosity range for a 1-in. turbine meter

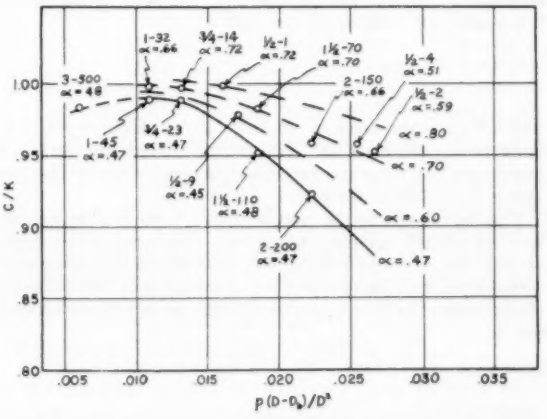

Fig. 6 Effect of geometric variations on meter coefficient. Meter designations refer to connection size in inches and maximum rated flow rate in gpm; (N = 16,000).

Conclusions

1 The foregoing methods of correlation have been successfully applied to one form of "kinematic" flowmeter.

2 Correlation methods involving the fluid density are applicable and valid only where the effects of the nonfluid forces are large compared to those of the fluid forces and are, at the same time, repeatable.

3 Use of the proposed methods can serve as a valuable tool, both to a potential user of this class of flowmeter in evaluating various design geometries, and to the manufacturer as a guide to improved design.

Acknowledgments

The author is indebted to the Fischer & Porter Company for permission to publish the results of work done in its laboratory, and especially to Mr. V. P. Head, Director of Hydraulic Research, for many valuable discussions and suggestions; also to Mr. Howard Bean of the ASME Fluid Meters Research Committee who read the manuscript and offered helpful suggestions.

Discussion

C. B. Haughton, Jr.[6] The following questions are submitted:

1 What progress is now being made in correlating turbine-type flowmeter coefficients for the compressible-flow regime?

2 Will the attempt be made to compare the meter coefficients with those predicted from a two-dimensional, and perhaps a three-dimensional flow design equation?

3 Or is it obvious at present that a one-dimensional treatment will be satisfactory for most design purposes?

H. W. Iversen.[7] The author's Fig. 4 shows a correlation of meter parameters that is useful in the application of a particular geometry of meter when the meter response speed and fluid properties are known. With similar correlations of other meter geometries a set of comparative values is available to determine the optimum meter for a particular fluid and desired meter response.

However, rapid evaluation from Fig. 4 to determine the meter indication in response speed for given conditions of flow rate and fluid properties is not direct since the response speed appears in both the meter coefficient and the viscosity parameter. A correlation to enable direct determination of the response speed may be made by noting that the viscosity parameter of the author is in reality a Reynolds number; that is

$$N = \frac{nD^2}{\nu} \propto \frac{V_R D}{\nu}$$

where V_R is proportional to nD, and V_R is the linear speed of the rotor at the diameter D. The author's Reynolds number is based upon the rotor size and upon the speed response from the action of the fluid on the rotor.

This fluid action on the rotor is related to the fluid inflow pattern immediately upstream of the rotor. The flow in the upstream conduit has a nonuniform velocity distribution with laminar or turbulent flow as the case may be. The state and distribution of the upstream flow is characterized by the conduit Reynolds number, or

$$R_c' = \frac{V_c D_c}{\nu}$$

where V_c = fluid average velocity in conduit, and D_c = conduit diameter. For convenience, the prime variable of volume flow rate is introduced from the definition of V_c

$$V_c = \frac{Q}{A_c} = \frac{4Q}{\pi D_c^2}$$

Substituting in the expression for R_c, and dropping the constants, a Reynolds number is formed in terms of the flow rate

$$R_c = \frac{Q}{D_c \nu} \quad \text{[8]}$$

(R_c' and R_c differ by the factor $\pi/4$, a constant which does not have to be carried in the numerical evaluation for correlation.)

The author's correlation of C as a function of N, Fig. 4, may be transferred directly into the correlation of C as a function of R_c since

$$R_c = \frac{Q}{D_c \nu} = \left(\frac{Q}{nD^3}\right)\left(\frac{nD^2}{\nu}\right)\left(\frac{D}{D_c}\right) = CN\,\frac{D}{D_c} \quad \text{[9]}$$

The ratio D/D_c is unity if the conduit and meter bore diameters are equal.

For a given flow rate, fluid, and meter size, R_c is known. The corresponding value of C permits direct determination of the meter response speed. This correlation may be convenient for meter selection for a particular application.

Pressure drop across the meter may be correlated by considering the Euler modulus which includes the pressure drop, flow or response velocity, and the fluid property of density.

$$\text{Euler modulus} = E = \frac{\Delta P}{\rho V^2} \propto \frac{\Delta P}{\rho n^2 D^2} \propto \frac{\Delta P D^4}{\rho Q^2} \quad \text{[10]}$$

where ΔP is the pressure drop, ρ is the fluid density, and V may be either the meter-response speed or the fluid velocity as shown by the last two forms of Equation [10].

The author's Fig. 5 is a representation of the proposed correlation of E as a function of R_c since Fig. 5 is a ratio of pressure drops at constant flow rate as a function of the Reynolds number. This can be shown as follows

$$\frac{E_2}{E_1} = \left(\frac{\Delta P D^4}{\rho Q^2}\right)_2 \Big/ \left(\frac{\Delta P D^4}{\rho Q^2}\right)_1 \quad \text{[11]}$$

In Equation [11] the subscripts 1 and 2 refer to different operating conditions. With Q and D both constant, this reduces to

$$\frac{E_2}{E_1} = \left(\frac{\Delta P}{\rho}\right)_1 \left(\frac{\rho}{\Delta P}\right)_2 \quad \text{[12]}$$

Equation [12] is the ordinate of the author's Fig. 5 except for the density ratio, which is apparently nearly constant for the fluids used.

It would be interesting to see the test results of pressure drop related in terms of E as a function of R_c. Comparative correlations of the proposed type would be of value in meter selection on the basis of pressure drop for a specified application since R_c may be evaluated for a given flow rate, fluid, and meter size. The corresponding value of E from the correlation then gives the pressure drop.

One further point is of interest. The turbine-type flowmeter is a hydraulic turbine with a shaft-power output that is essentially zero under the condition of minimum friction. The turbine model laws are

$$Q \propto nD^3 \quad \text{[13]}$$

---

[6] Experimental Engineer, Lycoming Division, Avco Manufacturing Corporation, Williamsport, Pa. Mem. ASME.

[7] Professor of Mechanical Engineering, University of California, Berkeley, Calif. Mem. ASME.

$$H \propto n^2D^2 \quad [14]$$

where H is the turbine head.

The author's definition of C is the proportionality coefficient in Equation [13], or

$$C = Q/(nD^3) \quad [15]$$

The proportionality coefficient of Equation [14] is the proposed Euler number since the head may be expressed in terms of the pressure difference divided by the fluid density, ρ

$$H \propto \frac{\Delta P}{\rho} \propto n^2D^2 \quad [16]$$

Then

$$E = \frac{\Delta P}{\rho n^2 D^2} \quad [17]$$

As stated by the author, if the external friction, such as from bearings, is large, the turbine no longer operates at zero power output and the foregoing proportionality coefficients do not depend entirely upon the flow forces as characterized by the Reynolds number, but depend also upon the external forces which may not be characterized by the Reynolds number.

M. R. Shafer.[8] The author is to be congratulated on an excellent presentation of a very timely subject. Turbine-type meters are commonly used as transducers in applications requiring flow rate as a function of an electrical signal. Examples are telemetering, digital and analog indication and recording, and process controls. Because of the continued rapid growth of the instrumentation field, a considerable increase in the use of turbine meters is expected in the future.

The writer takes this opportunity to make a few observations on the dimensionless relationships presented by the author, not from the viewpoint of meter design, but rather from that of applications in which precisions of about $^1/_2$ per cent are desired. It must be understood that, whereas only a particular design and make of meter are discussed in the paper, the comments which follow are general conclusions encompassing all makes and models of turbine meters now available. None of these comments is to be construed as applying specifically to a particular make or model.

As a first observation it is of interest to note that under properly controlled conditions very precise results can be obtained from turbine meters. With meters which are performing correctly, the standard deviation obtained from five successive calibration runs is always expected to be within 0.1 per cent and frequently this value is 0.05 per cent and less. Also, a repeatability within ± 0.1 per cent is to be expected when comparing the average results of calibration tests run at monthly intervals. Fig. 3 of the paper is a good example of the precision expected in that the points are grouped very closely to the characteristic curve except for the deviations caused by mechanical forces.

The relation $Q/nD^3 = f(nD^2/\nu)$ is useful for evaluating the general characteristics of a given meter, especially for a determination of viscosity sensitivity. However, those interested in specific applications may well ask, "Is this relation generally true for all of the different makes and sizes of turbine meters now available?"

Generally speaking, in the viscosity range 0.6 to 6.0 centistokes which we have investigated, turbine meters may deviate from the general relation expressed by Equation [4] by several per cent, especially in the lower portion of the flow ranges. Such deviations are caused by the mechanical forces which frequently are not insignificant as compared to the fluid forces. Thus we cannot expect to apply this relation to turbine meters in general and obtain the same precision as results, for example, from the coefficient of discharge versus Reynolds number relationship for orifices, nozzles, and other fixed metering devices.

Another matter of interest concerns the effect of the upstream flow conditions upon the performance of turbine meters. These meters are sensitive to rotational flow or swirl in the entering fluid stream. Thus flow straighteners consisting of vanes or tubes, as illustrated in Fig. 1, are always installed within the meters. The effectiveness of these varies considerably among the different turbine meters available. Preliminary tests at our laboratory with an induced-swirl apparatus have shown that a fairly severe swirl may influence the calibration constant within the range 1 to 20 or more per cent depending upon the flow rate and the meter design. This particular point is mentioned to illustrate that the d/D ratios of Equation [5] define the geometrical configuration of the external upstream piping as well as those of the meter itself.

Finally, it should be noted that Equations [4] and [5] are applicable only when the meter is completely filled with the fluid being metered. This very obvious requirement is sometimes overlooked in applications involving liquids of high vapor pressure. In such instances, cavitation may occur at the impeller resulting in very erratic performance. Cavitation can be detected by investigating the sensitivity of the meter to pressure level, and can be eliminated by maintaining a sufficiently high back pressure as compared to the vapor pressure of the liquid being metered.

Author's Closure

The author wishes to thank the discussers for their interest and comments. In reply to Mr. Haughton's questions, some work is now being done on gas flow applications. Results show that bearing friction will not be small enough to permit correlation of coefficients against Reynolds number alone, at least at the speeds studied to date. However, as flow rate (and hence rotor speed) is increased, compressibility becomes important and the expansion factor must then be determined unless an appropriate pressure tap location can be found which will make its effect sufficiently small.

The one-dimensional approach, combined with experimental determination of the effects of geometric variations, has proved adequate for design purposes. The ultimate in accuracy of flow coefficients must depend on precise experiment, so there is no intention, at present, to refine predicted coefficients by use of more rigorous two or three-dimensional treatment.

As Professor Iversen points out, the parameter N may not be most convenient for determination of meter response where flow rate is known. Rather, it is the parameter most convenient for determining flow rate from an observed meter response. The parameter $\frac{Q}{D\nu} = CN$ has been used in Fig. 5 to give a pressure drop variation against Reynolds number (neglecting the factor $\pi/4$) and is the same as that given in Equation [9], where the meter bore and conduit diameters are equal. Fig. 5 is meant to show the relative increase in pressure drop as viscosity is increased. However, no error is incurred if the reference turbulent flow loss of $7^1/_2$ psi (at a specific gravity referred to water of about 0.8) is converted to head loss ($\Delta p/\rho$), in which case the ordinate will be precisely Professor Iversen's Equation [12].

Mr. Shafer's question concerning the validity of the dependency of flow coefficient on Reynolds number (or N) alone is well taken. It is the author's position, however, that the low-speed regions, where such deviations with viscosity variations are not negligibly small, lie outside the useful range of the meter and should not be used in high accuracy work. These deviations are functions of the

[8] Research Engineer, National Bureau of Standards, Washington, D. C.

parameter $F/\rho n^2 D^4$ (Equation [5]), but it is felt that the non-fluid force F is not repeatable enough to permit a reliable correlation.

Upstream flow conditions do have an influence on the meter coefficient. Since a flow straightener integral with the meter necessarily represents a compromise between effectiveness on the one hand, and cost and bulk on the other, upstream piping conditions cannot be ignored where good accuracy is expected. The author has tested a 1-in. unit connected immediately downstream of a pair of 1-in. right-angle elbows, closely coupled and oriented in separate perpendicular planes. Tests were also run using a 1-in. gate valve, with varying degrees of throttling immediately upstream of the meter, and in neither case did observed coefficients deviate more than $^3/_4$ per cent from those obtained with a long run of straight pipe. As Mr. Shafer points out, the geometric ratios of Equation [5] must be interpreted as any geometry upon which the coefficient may be dependent, whether contained within the meter or externally in the piping.

Single phase liquid flow has been tacitly assumed by the author. The possibility of cavitation taking place can be minimized by designing to deflect the fluid as little as possible consistent with good performance. If local velocities within the meter do not greatly exceed the velocity in the conduit, a knowledge of the vapor pressure of the fluid is usually sufficient to set a safe minimum back pressure, since errors due to cavitation will not occur if the static pressure in the region of highest velocity exceeds the vapor pressure.

One other point of interest may be mentioned here. As the operating temperature of the meter changes, thermal expansion will cause an apparent coefficient change unless a correction is applied to the characteristic dimension D. If all components of the meter are made of materials having approximately the same thermal expansion coefficient, the geometric ratios d/D of Equation [5] remain constant when thermal equilibrium is reached. Thus the coefficient will remain precisely the same if D, in the expression for C in Equation [4], is the actual diameter at the flowing temperature. This is most easily done by multiplying the flow Q by the factor $1/[1 + 3k(T - T_0)]$ where k is the linear coefficient of thermal expansion, T the extreme temperature, and T_0 the reference temperature for which the original calibration curve was drawn.

The author is indebted to Messrs. R. E. Gorton and G. J. Lyons of the Pratt and Whitney Aircraft Company, East Hartford, Conn., for experimental verification of this correction in tests run with a hydrocarbon fuel at temperatures up to 400 F.

Liquid-Flowmeter Calibration Techniques

By M. R. SHAFER[1] and F. W. RUEGG,[2] WASHINGTON, D. C.

Calibration techniques for liquid flowmeters are discussed with emphasis on problems which are known to influence the accuracy of calibration procedures. Also, reference methods which have been used to evaluate the comparative accuracy of different calibrators are described. The results of comparative accuracy tests on four calibrators of different designs are presented and it is shown that the agreement between these is within ±0.15 per cent in the test range of 10,000 to 100,000 lb per hr. The many precautions necessary to approach this precision from the traditionally accepted "plus and minus one per cent" are given in detail.

Introduction

In the course of a continuing program of research and development at the National Bureau of Standards on aircraft fuel-metering-accessory test equipment, conducted under the sponsorship of the Bureau of Aeronautics, the performance of various liquid flowmeters has been investigated as well as equipment and techniques for their calibration. Experience has demonstrated that absolute accuracies better than ±0.3 per cent are possible in the calibration of direct-indicating flow-rate meters. It is believed that the calibration techniques used to attain such accuracies are of sufficient general interest to warrant presentation here. Thus the objectives of this paper are to present a discussion on flowmeter-calibration techniques; to present data obtained at the National Bureau of Standards and elsewhere; to demonstrate the present state of the flowmeter-calibration art; and to describe some of the limitations of existing calibration equipment and procedures.

The techniques discussed herein are applicable to totalizing meters for which calibration procedures are established and defined (1).[3] However, our primary interest and experience have been restricted to direct-reading liquid flowmeters operating under steady-flow conditions in the range 5 to 100,000 lb per hr.

A meter calibration may be considered accurate only for the conditions existing at the time the calibration data were taken. Thus those quantities which can influence the performance of the meter must be known, measured, and controlled during precise calibration work. Factors influencing the performance of the different type meters have been investigated and reported in numerous papers, among which are (2 to 7). These factors are the density, viscosity, and temperature of the liquid; upstream, and to a lesser extent, downstream flow disturbances; the vapor pressure and absolute pressure level; and the orientation and scale sensitivity of the meter. Of course, the influence of these varies widely among the different type meters.

Summarizing the possible influences on meter performance, it may be noted that the influence of density usually can be predicted through analysis. The erratic effects of viscosity are most pronounced with the smaller sized meters and can be established only through calibration tests. Temperature exerts its influence through its effects upon the configuration of the meter and upon the physical properties of the test liquid. Vapor pressure and pressure level should have no appreciable influence provided compressibility of the liquid is not significant and the pressure level is sufficient to prohibit vapor formation. Finally, meters are sensitive to external flow disturbances, and this effect generally increases with meter size and flow rate. In fact, inadequate control of flow disturbances is one of the greatest sources of error in precise work.

Although meter characteristics may seem a separate problem from that of calibration, it must be stressed that precise calibration work cannot be performed unless these are given ample consideration in specifying and controlling the conditions of calibration.

Selection and Calibration of Instrumentation

Extreme accuracy is now possible in the measurement of mass, time, and those other quantities required for the flowmeter calibration. Perhaps some thoughts regarding the selection and calibration of the separate instrumentation items may be of value before discussing representative calibration systems. The calibrator will require a timer, scales for the measurement of mass or prover tanks for volumetric determinations, thermometers, density-measuring instruments, and perhaps a viscometer. Each of these must have sufficient sensitivity and accuracy to serve its intended purpose.

Electronic-counter timers are preferred for measuring the time interval. Many different makes are now available which operate on the principle of counting the pulses from a tuning fork or quartz-crystal oscillator. These usually indicate in units of 0.001 sec and have provisions for electronic actuation. They are considered to be better suited for this application as compared to synchronous clocks and stop watches which are dependent upon the frequency of the power supply, have minimum scale divisions of 0.1 sec, and utilize mechanical methods of actuation. Standards of time and frequency are broadcast by the National Bureau of Standards over station WWV in Maryland and WWVH in Hawaii (8). These precise signals, accurate 2 parts in 100 million, are adequate and convenient references for the calibration of timers.

Volumetric calibrating systems will require prover tanks. Specifications and calibration procedures for these are given in (1). Accuracies better than 0.1 per cent of the nominal tank volume can be attained with prover tanks provided adequate and proper temperature corrections are applied.

For the gravimetric-type calibrator a scale of conventional design, equipped with weighbeam and counterpoise is recommended. The addition of quick-weighing or automatic indication devices is not considered necessary and possibly might prove detrimental to over-all accuracy as compared to the free-swinging lever system. For smaller capacities, a straight lever system or even the equal-arm balance should be used. Balances of the torsion-tape and/or flexure-plate type also will prove suitable because of their inherent stability. Features influencing their selection and use will include capacity, smallest weighbeam graduations, and sensitivity which can be adjusted by the manufacturer as required.

Before placing the scale in service, two tests extending over the

---

[1] Research Engineer, National Bureau of Standards.

[2] Physicist, National Bureau of Standards.

[3] Numbers in parentheses refer to the Bibliography at the end of the paper.

Contributed by the Research Committee on Fluid Meters and presented at the Annual Meeting, New York, N. Y., December 1–6, 1957, of The American Society of Mechanical Engineers.

Note: Statements and opinions advanced in papers are to be understood as individual expressions of their authors and not those of the Society. Manuscript received at ASME Headquarters, July 24, 1957. Paper No. 57—A-70.

load range at which it will be used should be conducted. The first should be made before, the other after installation of the weigh tank and its connections. If the two are not in agreement, connections are likely interfering with proper functioning of the scale and the conditions should be corrected. This calibration should be done with test weights that meet C tolerances (9 and 10) and not by the comparison of one scale with another. Test weights may be secured from state or city Weights and Measures Departments, or if these are not available, the services of the scale manufacturer should be secured. The National Bureau of Standards will certify test weights in Washington, D. C., or at the National Bureau of Standards Master Scale Depot located in the Clearing Industrial District of Chicago, Ill. A self-contained or built-in type scale is desired to prevent damage to which portable type scales are subject during moving and handling. Also, the scale must be protected from wind and air currents while in use, since even light air currents produce weighing errors of appreciable magnitude.

Temperatures should be indicated preferably with mercury-in-glass thermometers usually of the range 0 to 120 F graduated in single degrees and accurate to one degree or better. Standards, specifications, and methods of testing liquid-in-glass thermometers are reported in (11) for the range −110 to +750 F. This reference lists the range, subdivisions, maximum permissible scale error, and installation instructions for the numerous types of thermometers used in test work.

In those calibration applications requiring a conversion between volumetric and gravimetric units, the measurement of liquid density is of extreme importance. Instruments for determination of liquid gravity or density include the hydrometer, pycnometer, and Westphal balance. The hydrometer is the simplest of these and it yields fairly accurate results. Specifications, tolerances, and methods of certification for hydrometers are described (12). If the test liquid is a petroleum product, any necessary conversion from specific-gravity units to density and corrections for temperature differentials can be made conveniently on the basis of Petroleum Measurement Tables (13) which contain conversion and thermal-expansion factors for all liquid-petroleum products within the specific gravity range 0.46 to 1.10.

A Static Weighing Calibration System

Calibration of a liquid flowmeter involves a determination of the time interval required for a measured mass or volume of fluid to pass through the meter, at a constant indicated rate, under the specified conditions of calibration. As extreme accuracy is possible in the measurement of mass and time, the limiting factors in the procedure are the technique, the sensitivity of the meter, the constancy of the indicated flow rate, the mechanics of collection of the fluid, and the method of timer actuation.

In presenting this discussion of a representative flowmeter-calibrating system, an apparatus which was designed and constructed at the National Bureau of Standards will be described. This was developed to obtain a precision of about 0.1 per cent with two basic features in mind: (*a*) A way was sought to collect the fluid with a minimum disturbance to the steady state of flow through the meter; and (*b*) a method was desired whereby the mass of the liquid collected could be measured under a "static" condition of no flow into the collection tank. In this way the problem of accurate measurement of mass and time could be reduced to a minimum as nearly all dynamic considerations were eliminated. A schematic diagram of the apparatus is presented in Fig. 1. This particular system was used for the evaluation of flow rates in the range 5000 to 100,000 lb/hr,

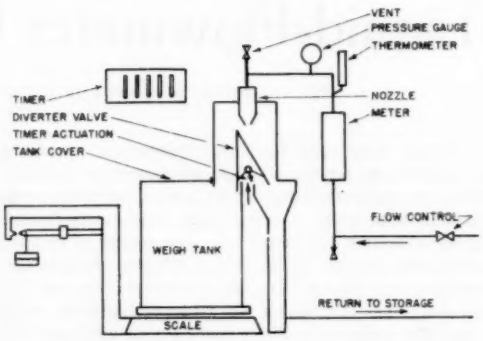

Fig. 1 NBS static weighing calibrator

which can be extended through the techniques described herein. Essential components are the flow-rate supply and control, the meter under calibration, a flow-diverter valve, an electronic timer, and a platform scale and tank.

The function of the flow-rate supply-and-control system is to deliver filtered liquid, of known physical properties, at a closely controlled temperature to the meter under test. Additional functions are to eliminate surges and pulsations within the fluid and to provide a convenient, sensitive method of control whereby all desired flow rates may be set and maintained to within 0.1 per cent of the desired value. Also, this system must contain provisions to assure positive elimination of all gas and vapor from the liquid before entering the meter with special consideration being given to the possibility of vapor formation during the throttling action of the flow-control valve.

Quantities influencing the performance of the meter under test have been discussed briefly. Of these, the upstream flow disturbances are the most difficult to detect and control when working to tolerances of a few tenths of one per cent. Such disturbances include flow distribution, pulsations, and rotational flow which originate within the pumps and fuel-supply components. They cannot be conveniently eliminated completely by placing a straight length of pipe upstream of the meter.

Some success has been obtained with a flow straightener consisting of bundles of small tubing and screens placed within a larger tube installed at or near the entrance of the meter under test. This helps in defining the calibration conditions. Also, the flow straightener in conjunction with master meters provides a more stable secondary reference for evaluating the comparative accuracy of different calibrators. As a final remark on this subject of upstream disturbances, the throttling valve should never be installed at the entrance to the meter as erratic disturbances may be introduced which will impair the precision of calibration. Rather, this valve should be located on the downstream side if possible.

The function of the diverter valve is to direct the flow as desired to storage or to the weigh tank without disturbing the rate of flow through the meter. Leak detectors should be provided to assure that none of the metered flow can bypass the weigh tank during the weigh-time interval. Also, in the static test method, the diverter valve should actuate the timer during its traverse and divert the flow quickly.

The particular diverter used in our apparatus was made of 0.035-in. cold-rolled steel in the form of an inverted V, each side being 15 in. long and 12 in. wide, with an included angle of 30 deg. The center of rotation was $2^1/_2$ in. above the base. Angular displacement was performed by a pneumatic-piston device having equal speeds in both directions with pneumatic cushions provided

at the end of the stroke. Time of positioning of the diverter was such that about 30 millisecond were required to cut through the liquid stream.

The counter-type timer should be actuated by electronic means, and in our apparatus actuation was accomplished by the diverter valve at the mid-point of its travel. This timer indicated in units of 0.001 sec and was calibrated against the standard reference time signal.

The platform scale used in this work was purchased on the open market. The scale is a self-contained, straight-lever type equipped with suspension main load-bearing assemblies and a single bar weighbeam graduated to 100 lb in $^1/_2$-lb divisions. A complement of counterpoise weights provided a total capacity of 5000 lb. Modifications performed at the National Bureau of Standards included the installation of a vernier scale on the main sliding poise to give readings to 0.05 lb. Also, concrete supports were provided for all main-lever-fulcrum bearings and for the weighbeam assembly to give a "built-in" scale. Thus the possibility of damage to which portable scales are subject during transit was eliminated.

The balance-ball elevation was adjusted to give a sensibility reciprocal of 0.1 lb at a load of 1000 lb. Sensibility reciprocal is defined as the amount of weight required to shift the weighbeam from an equilibrium position at the middle, to equilibrium at either extremity of the trig loop. Immediately prior to the flowmeter-calibration work, a scale calibration was made using 50-lb test weights known to be accurate within Class C maintenance tolerances of ±40 grains. Both ascending and descending loads were used in the range of loads to be encountered and no hysteresis was observed. Considering the sensitivity, precision of calibration, and constancy of the scale as determined by the tests, it was practicable to determine minimum net weights of 400 lb to an absolute accuracy of better than 0.05 per cent.

The weigh tank had a capacity of 64 cu ft. No connection of any kind was attached to the tank when weigh determinations were being made, and the tank was emptied by inserting the inlet hose of a transfer pump. However, a drain valve would be adequate if the tank has sufficient elevation with reference to the liquid reservoir. In installations requiring permanent, flexible tank connections, tests must be conducted to assure that these are not interfering with the proper operation of the scale.

Calibration of a meter at a selected rate of flow was performed by first determining the tare weight while the diverter valve directed the flow to "return to storage." The diverter was then operated to direct the liquid into the weigh tank and this operation automatically started the timer. After collection of an appropriate amount of liquid, the diverter was repositioned to return to storage, automatically stopping the timer. The gross weight was then measured and the net determined for the indicated time interval. It should be noted that weight determinations were not made while liquid was entering the scale tank. Weights determined by this method require a correction for air buoyancy (1) magnitude 0.1 to 0.2 per cent, to obtain the true weight.

Another important consideration in precise calibration techniques is the piping between the meter and the weigh system. This must be such as to assure that all of the flow and only that flow indicated by the meter is collected in the weigh tank during the calibration run. Aside from the obvious requirement of no leakage or bypass from these connections, complete elimination of gas and vapor must be assured so gas compression or expansion cannot occur. Always remember, one of the greatest sources of measurement inaccuracy is improper gas elimination. Thus the meter-discharge lines should be as short and small as possible with vents provided at high points for gas elimination. As a general rule, the volume of the discharge piping should not exceed 5 or at most 10 per cent of the flow collected during a calibration run.

Discharge connections of small volume also reduce the effects of thermal expansion and contraction of the liquid if an appreciable change in temperature is encountered during a run. For instance, the coefficient of cubical expansion of petroleum products is about 0.06 per cent per deg F, and 10 deg F change in temperature during the test could introduce an error of 0.06 per cent if the volume of piping is only 10 per cent of the volume of fluid collected.

Volatility of the liquid is an important consideration because of loss by evaporation. Our weigh tanks and diverter valves were provided with covers to reduce loss of vapor and the test liquid was a naphtha having a Reid vapor pressure of less than 0.1 psi. No measurable evaporation loss was detected. However, for high vapor-pressure liquids, such as gasoline, considerable refinement of the techniques described herein is required to eliminate both loss by evaporation and vapor formation in the meter-discharge lines. The ideal solution appears to be a pressurized weigh system, but this will introduce many additional complications.

Examples of Dynamic Weighing Calibrators

The static weighing method of flowmeter calibration is time-consuming and thus not well suited for those applications in which convenience of operation is important. Thus dynamic weighing is utilized frequently. This determines the time interval required to collect a preselected weight of liquid, the weighing being performed while the liquid is entering the scale tank or other weight-determining collector. Although experience has demonstrated that the accuracy of dynamic calibrators can be just as good as the static method described, additional dynamic factors must be considered.

Three different dynamic calibrators will be considered briefly. Method 1, shown schematically in Fig. 2, utilizes a free-swinging lever scale. With this arrangement, the weight of the fuel in the tank increases until it overcomes the resistance of the counterpoise weights on the end of the weighbeam which then rises and actuates the timer. At this time an additional weight is added to the pan depressing the weighbeam. When it rises again the timer is stopped. This procedure requires acceleration of the scale just prior to both the start and stop actuation of the timer.

Three important dynamic phenomena take place during this weigh cycle. They are: The change in the impact force of the falling liquid between the initial and final weigh points; the collection of an extra amount of fluid from the falling column by the rising level in the tank; and the change in inertia of the scale and weigh tank with the resultant change in time required to accelerate the weighbeam past the timer trip point.

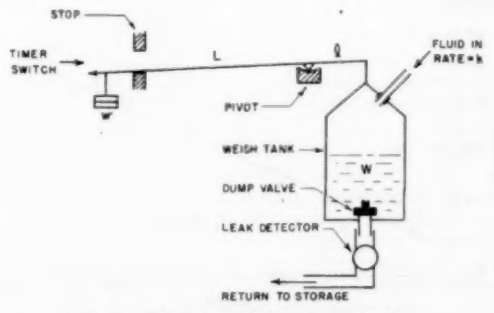

Fig. 2 Dynamic weighing calibrator 1

It can be demonstrated that the decrease in impact force is essentially equal and opposite to the additional weight collected from the falling column. Thus, even though each of these may be appreciable, they cancel each other. The effect of change in inertia between the initial and final weigh points can become appreciable and should be considered whenever the weight of liquid collected contributes significantly to the inertia of a scale system requiring a relatively large travel of its weighbeam to the point of timer actuation. This method of weighing is used frequently in other situations, and an explanation of the inertia errors involved may be of interest.

Consider a scale consisting of a single, massless lever, as illustrated in Fig. 2, having arms of length l and L. When fluid is added to a tank at a mass rate k, the collected weight W eventually will balance the counterpoise weights w. A further collection of liquid will then deflect the lever past the point of timer actuation as a result of the unbalance kt and its corresponding torque $ktgl$, where t is time measured from the instant of balance and g is the acceleration of gravity.

As a first approximation, this torque is equal to the product of the moment of inertia of the fluid and counterpoise weight and the angular acceleration $d^2\theta/dt^2$. If the scale ratio L/l is large, the moment of inertia is essentially that of the counterpoise weights, and the equation of motion of the scale may be written

$$ktgl \simeq wL^2 \frac{d^2\theta}{dt^2} \quad \ldots\ldots [1]$$

which reduces to

$$ktg \simeq WL \frac{d^2\theta}{dt^2} \quad \ldots\ldots [2]$$

as w is approximately equal to Wl/L.

Integrating twice, using constants of integration equal to zero, and rearranging, gives the time required for deflection through an angular displacement θ

$$t \simeq \left(\frac{6L\theta W}{kg}\right)^{1/3} \quad \ldots\ldots [3]$$

Thus for a constant deflection and flow rate, the time required for deflection should be approximately proportional to $W^{1/3}$. This was tested on one dynamic weighing calibrator having a scale ratio of 50:1 and constant values of $\theta = 0.007$ radian and $k = 6.4$ lb per sec. The results, plotted in Fig. 3, give a least-squares curve of

$$t = 0.031W^{0.43} \quad \ldots\ldots [4]$$

This value of 0.43 for the exponent of W is in reasonable agreement with the derived value of 1/3 considering the precision of the experimental work and the approximations used in deriving Equation [3].

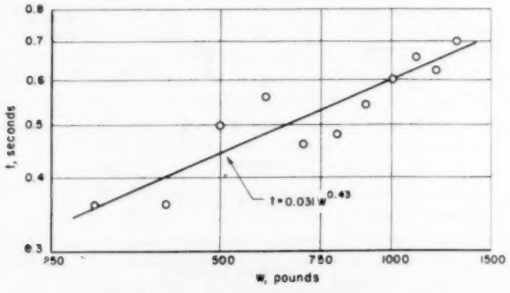

Fig. 3 Scale deflection time

The error of interest in dynamic weighing is the difference Δt between the time required for the deflection of the weighbeam at the final weight W_2 and at the tare weight W_1. Referring to Equation [3] this is derived as

$$\Delta t = t_2 - t_1 \simeq \left(\frac{6L\theta}{g}\right)^{1/3} \frac{(W_2^{1/3} - W_1^{1/3})}{k^{1/3}} \quad \ldots\ldots [5]$$

which is the inertia error in the measured time interval $T = (W_2 - W_1)/k$ required to collect the net weight of liquid. Dividing by T the percentage error is

$$\text{Per cent error} = \left(\frac{\Delta t}{T}\right) 100 \simeq 100 \left(\frac{6L\theta}{g}\right)^{1/3} k^{2/3} \left(\frac{W_2^{1/3} - W_1^{1/3}}{W_2 - W_1}\right) \quad \ldots\ldots [6]$$

The relation expressed in Equation [6] was checked by comparing dynamic calibrator 1 with the NBS static calibrator using a method to be described later. The results are plotted in Fig. 4, in which different symbols are used to designate the various flow rates. Values obtained from Equation [6], with $L = 2.2$ ft and $\theta = 0.007$ radian, are shown by the solid line. Equation [4], transposed to the co-ordinates of the figure, is shown as a dashed line.

The data of Fig. 4 are in reasonable agreement with Equations [6] and [4]. Thus it is believed that these are a measure of the inertia errors involved in this form of dynamic weighing. When the deflection of the weighbeam was reduced from 0.007 to about 0.0004 radian, the inertia effects became indistinguishable from the other small errors of the system.

At the time the tests were conducted to obtain the data of Figs. 3 and 4, we were not attempting an evaluation of the inertia error, but only demonstrating its presence. W_1 was not determined and it was necessary to estimate its value in these analyses. Thus the data should not be considered precise. However, it is believed these data are sufficient for the purpose of demonstrating that significant inertia errors may result from this method of dynamic weighing.

Dynamic calibration method 2, shown in Fig. 5, collects the liquid in a tube or cylinder of known cross-sectional area and uses the pressure existing at the bottom as a measure of the weight of liquid collected. The vertical rise in liquid between the initial or tare and the final weigh positions is usually in the range 2 to 20 ft. Thus it is necessary to measure and/or indi-

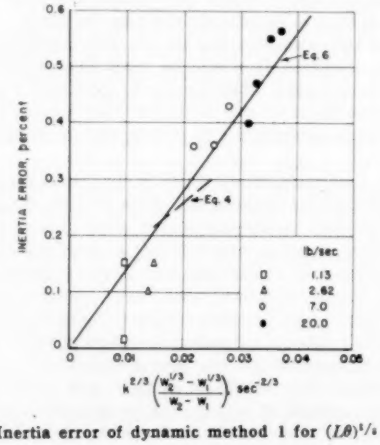

Fig. 4 Inertia error of dynamic method 1 for $(L\theta)^{1/3} = 0.249$

cate this pressure difference of 1.5 to 15 in. of mercury to a precision better than 0.1 per cent. The majority of installations use mercury manometers as the pressure-measuring device with electrodes, corresponding to different collected weights, spaced at accurately determined intervals. Contact between these and the mercury, in conjunction with electronic circuitry, provides the impulse for actuation of the timer. The contact spacing in these manometers must remain constant and any dirt or oil film which may effect the contact closure must be eliminated.

Important considerations for method 2 are: Effects of thermal expansion on the standpipe cross-sectional area and on the density of the manometer fluid; incomplete drainage of the cylinder walls before commencing the weigh-time determination, a significant factor in working with high-viscosity liquids; and changes in air pressure within either the cylinder or manometer column during the timing interval. The line between the cylinder and manometer well must never contain air or vapor. Also, the difference in elevation between its connections to the cylinder and manometer should be small so changes in the density of liquid within this line will have no influence on the height of the mercury. This is especially important when test-liquid temperatures differ from either that of the room or the mercury.

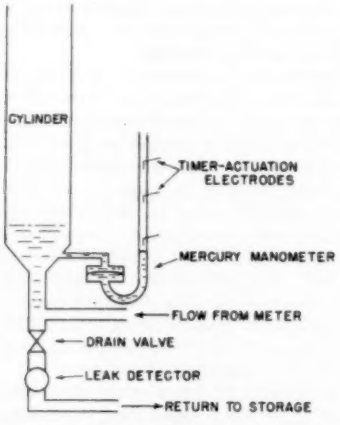

Fig. 5 Dynamic weighing calibrator 2

Dynamic considerations applicable to method 2 are first to ascertain that the pressure-measuring device has completed its acceleration and attained a constant velocity before the weigh-time interval is commenced. Also, oscillations resulting from the natural frequency of the pressure indicator must not exist. The other dynamic consideration is that of air compression in the collection vessel, especially at higher flow rates, resulting from restrictions such as flame arresters placed in the vent. It is readily seen that appreciable errors indicating higher than actual flows can result when such restrictions exist.

Dynamic calibration method 3, Fig. 6, employs bench dial scales for the measurement and indication of the weight of liquid. Nine light-beam intercepting paddles were added to the indicating dial, each corresponding to a predetermined weight. In operation, when sufficient liquid has entered the weigh tank to overcome the selected tare, the indicating mechanism of the scale commences to move around the dial. The first interruption of the light beam, occurring when the tare weight is balanced, starts the timer. An adjustable time-delay relay is provided whereby the phototrip circuit will not stop the weigh cycle until a selected time interval has been exceeded. Thereafter, when the next paddle intercepts the light beam the timer is stopped, the

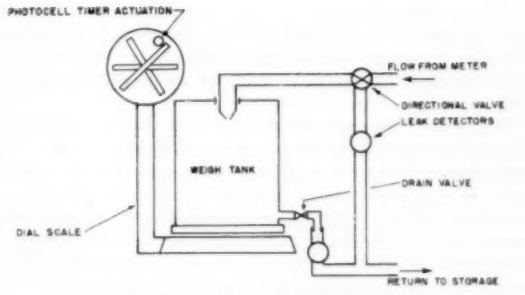

Fig. 6 Dynamic weighing calibrator 3

weight corresponding to that paddle is recorded, and the time is observed and recorded.

Dynamic considerations of method 3 are impact force and decrease in height of the falling liquid column as explained for method 1. Another consideration is the acceleration of the scale and its indicating mechanism to a constant velocity prior to the starting of the timer and maintenance of this velocity until the end of the weigh-time interval. Also, bench dial scales usually have constant sensitivity which, even when adequate at full scale, leads to larger percentage errors at the smaller weights. Thus good precision cannot be expected when the lower portion of the dial or range of the scale is used.

No attempt has been made to reveal all possible sources of dynamic errors in this discussion. These, of course, vary considerably with the different methods utilized. However, an attempt has been made to demonstrate that a static check and calibration of the instrumentation are not sufficient to prove the absolute accuracy of a dynamic-weighing method of calibration, as the response of the instrumentation used under transient conditions is a very important consideration.

Evaluation of Calibration Procedure and Equipment

The evaluation of calibration procedures and equipment includes a consideration of the ease and convenience of operation. Features which may be considered here are: The sensitivity and stability of the flow control; the temperature control; the time required to perform a weigh-time determination; and the time interval required to empty the weigh system between successive runs. All of these are of interest to the engineer in deciding whether a particular unit meets the general requirements of its intended purpose. These are not always the same for different applications, as more emphasis upon calibration time is necessary in a stand designed for production tests as compared to one used occasionally for high-accuracy tests of reference meters.

However, after these general performance characteristics are deemed satisfactory for the intended application, there still remains the all-important questions as to the precision of the measurement procedure and the absolute accuracy. The term precision as used in this paper refers to the variations or differences between repeat measurements. In the construction and operation of any calibrating unit, considerable attention will be directed towards refining the measurement procedure to reduce the variation so that it becomes insignificant. Unfortunately, this state is not always achieved and it may be necessary to evaluate the magnitude of the variations obtained.

The methods of statistics (14) define many units of variation by which the precision of a measurement procedure may be expressed. Among these are the "standard deviation," the "standard deviation of the average," the "confidence interval," and the "difference between duplicates." These are extremely useful to the engineer concerned with measurements and should

be used more extensively in flowmeter-calibration work. The ISO/TC-30 Committee of Fluid Measurements has recommended the use of twice the standard deviation as the tolerance limit in fluid-metering. An application of this tolerance is discussed by Jorissen (15).

It is beyond the scope of this paper to explain and demonstrate the application of statistics to precision of flow measured. However, the precision of the calibration procedure must be evaluated and the standard deviation provides a useful comparative unit for this purpose. A few representative statistical values will be presented to demonstrate the precision of flowmeter-calibration procedures attained in our laboratory. When data for ten successive runs are compared, using nominal timing intervals of 60 sec, the following representative values of precision result:

Standard deviation = 0.08 per cent
Standard deviation of the average = 0.03 per cent
Ninety-five per cent confidence interval = 0.06 per cent
Difference between duplicates does not exceed 0.12 per cent 80 per cent of the time

These data were obtained during calibration of sensitive float-type flowmeters. Naturally, they are dependent upon the sensitivity of the meter under calibration and meters with low-scale sensitivity will reduce this precision considerably.

Large differences between duplicate runs will be encountered occasionally. These are caused by insufficient time in bringing the meter and the liquid to operating temperature and incomplete purging of the system of gases. This happens frequently when small meters are calibrated on large-capacity stands. Other causes of large differences are insufficient tare time, with dynamic calibrators, and continuous readjustment of flow when such is necessary to provide a steady flow indication. In fact, experience generally demonstrates that minimum variability results when the flow-control valve can be left at a constant setting during the calibration time-interval.

After the calibration procedure and equipment have been adjusted to give satisfactory precision of measurement, a check of the absolute accuracy is desirable to detect the presence of constant errors. The best method for such a check is to use two or more different experimental procedures to measure the same quantity. Errors are then noted when averages disagree by an amount larger than is to be expected from the precision of the measurements. Perhaps our experience will be of help to others concerned with this problem.

In 1954 the National Bureau of Standards was requested to evaluate three dynamic weighing calibrators, one each of the designs of Figs. 2, 5, and 6, to determine whether their absolute accuracies were within the tolerance of ±0.25 per cent. Two of these stands, A and B, were in our laboratory. It was decided that the best method of detecting constant errors in these would be through the use of a different experimental procedure to measure the same flow rate. A static weighing stand, NBS, similar to that of Fig. 1, was constructed for this purpose. The third calibrator, C, is installed at another facility and some other technique was required as moving the NBS stand was not convenient. Thus it was decided to use direct-reading flowmeters as secondary references.

The following procedure was used for the determination of the accuracy of calibrators A and B at our laboratory. The calibrating stand under evaluation provided storage of liquid, pumps, filter, and flow and temperature control. In operation, the unknown flow rate was maintained constant as indicated by a sensitive float-type flowmeter operating at a constant temperature with a liquid of constant physical properties. This constant flow rate was evaluated alternately by the calibration stand under test and by the NBS static weighing method, the flow being

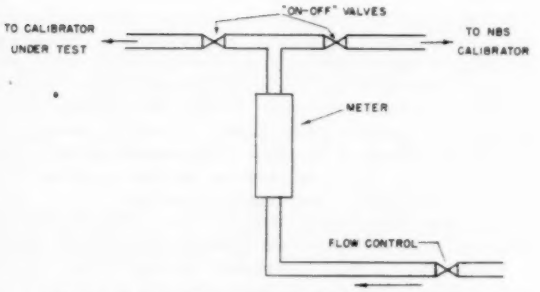

Fig. 7 Comparative accuracy-evaluation procedure

directed as desired by "on-off" valves placed downstream from the meter as shown in Fig. 7. The averages of four or five flow determinations made by each apparatus were then compared to obtain the difference between the calibrator under test and the NBS apparatus for the particular flow rate. This method has two important advantages: (*a*) The same quantity was being measured by two different procedures; and (*b*) upstream connections to the meter and downstream connections for a reasonable distance are never disturbed in directing the flow as desired to one of the two calibrating methods. Thus the conditions of calibration at the meter are identical.

For the evaluation of calibrator C, two secondary reference meters were selected. The first, range 7000 to 27,000 lb per hr, is of the float-type design having a logarithmic taper, a constant scale sensitivity of about 4 mm per per cent of indicated flow, and a stainless-steel float. All liquid passes through the metering tube. The larger meter is an experimental prototype design, range 35,000 to 100,000 lb per hr, and consists of the foregoing meter in parallel with a fixed orifice. As will be demonstrated later, this was not suitable as a secondary reference and a third meter was used. The third meter has a range 30,000 to 100,000 lb per hr, is a float-type having a 500-mm scale, and all of the flow passes through the glass metering tube. This served as an adequate secondary reference in the determination of the accuracy of calibrator C with a single exception.

Prior to the initial calibration of the three reference meters, the inlet and outlet connections were standardized. This included a 2-in. orifice upstream discharging into about 6 ft of 4-in. tubing connected to the meter inlet. The orifice was used in an attempt to obtain identical entrance flow conditions on the different calibrators. The meters were calibrated first at a few selected test points with the NBS apparatus and were then taken to calibrator C where the tests were repeated again by the same operator. Test fluids having a Reid vapor pressure of 0.1 psi and a kinematic viscosity of 1.10 centistokes were used at each location. Corrections were computed and applied for the different specific gravities of 0.783 and 0.779.

The final results of the tests are given in Fig. 8 which shows the per cent deviation of the individual calibrators from the average results for all four. Different symbols are used to designate the calibrators and each plotted point is the average of four to six separate determinations of rates of flow. Since some of these data may be considered proprietary information, we are not attempting to present the specific performance of any particular method other than the NBS static weighing apparatus represented by the open circles. Rather, the primary purpose is to show the extent of agreement obtained between four different methods of determination of flow rate. Where two identical symbols are plotted for the same flow rate, they represent the use of two different weights with corresponding timing intervals of about 30 and 60 sec. The average from which the deviations

were computed was obtained from the data within the ±0.15 per cent band with each calibrator assigned an equal weight.

As can be seen, the great majority of points are within ±0.15 per cent and the exceptions will now be discussed. Three deviations of about 1 per cent were obtained in the range 40,000 to 70,000 lb per hr with calibrator C. It must be understood that these are not an indication of the accuracy of this calibrator. Rather, they have been included to demonstrate difficulties encountered with the secondary reference meter of the orifice-bypass type. These deviations represent a change in the performance of this meter as a result of different upstream flow disturbances between the two calibrators, NBS and C. It has been concluded that a significant swirl or rotational flow difference existed between the two stands which was sufficient to affect the performance of the orifice-bypass meter by about 1 per cent.

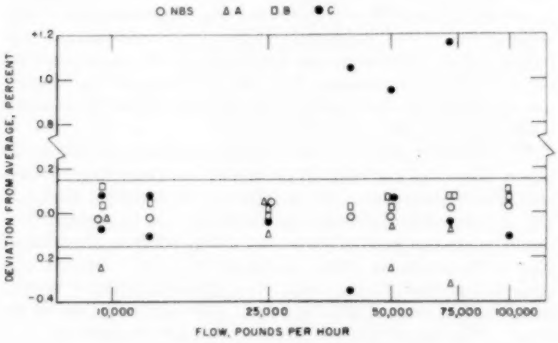

Fig. 8 Comparison of four calibrators

Still referring to Fig. 8, good results were obtained on calibrator C in the range 50,000 to 100,000 lb per hr with the third reference meter. A low reading of −0.35 per cent was obtained at 40,000 lb per hr, the lowest float position where sensitivity of this meter to upstream disturbances is a maximum. Thus it is demonstrated that two different calibrators can both be accurate and yet give different calibration results because of the influence of different upstream flow disturbances on the meter under test.

The other three low points of Fig. 8 were obtained using small test weights on a weighing mechanism of insufficient sensitivity. It is also possible that some unevaluated dynamic effects were present here.

Excluding the extreme points of Fig. 8, the resulting agreement between the four different methods of flow-rate determination may be considered quite good as it is within ±0.15 per cent. The program also enabled the detection of inertia errors of about 0.5 per cent and influences of disturbances upstream from the meter of about 1.0 per cent in one case and 0.4 per cent in another. Thus, through the procedures described herein, it has been possible to detect and correct errors in calibration equipment and procedures having magnitudes of less than 1 per cent.

Conclusions

Precise calibration of flow-rate meters requires a knowledge and control of each parameter which may influence the performance of the meter under test. Among these are the physical properties and temperature of the test liquid, at times the absolute pressure level, and the influence of upstream flow disturbances. The latter is perhaps the most difficult to specify and control when working to accuracies better than 1 per cent and is one of the primary reasons for apparent discrepancies in results between different calibrators.

Extreme accuracy is now possible and certified standards are available for the measurement of mass, time, temperature, and density which a calibrator is required to control or indicate. However, in designing a specific calibrator, an intelligent selection of the instrumentation for range and sensitivity is necessary if adequate precision and accuracy are to result. Also, provisions must be included to insure that all of the liquid and only that liquid which passes through the meter will be collected in the calibrator.

Examples of both static and dynamic weighing calibrators have been presented. For the particular calibrators and flow ranges investigated, there is not a significant difference in the absolute accuracies. However, dynamic weighing methods are subject to errors which are not exposed by a static calibration of the instrumentation. Thus it seems desirable that dynamic weighing calibrators of new designs should be evaluated for accuracy by comparisons with other calibration methods.

Acknowledgments

The suggestions and assistance of H. H. Russell of the Mass and Scale Section and H. S. Bean of the Fluid Meters Section, in advising on problems related to this work, are gratefully acknowledged. Also, we freely admit that many of the techniques and possible sources of errors described herein have been pointed out by others who have been more than liberal in advising us of their experiences. Among these are V. P. Head of Fischer and Porter Company, and A. W. Brueckner of G. L. Nankervis Company.

Bibliography

1 "ASME-API Code for Installation, Proving, and Operation of Positive Displacement Meters in Liquid Hydrocarbon Service," American Petroleum Institute Code No. 1101, Revised January, 1952, American Petroleum Institute, New York, N. Y.

2 "Discharge Coefficients of Square-Edged Orifices for Measuring the Flow of Air," by H. Bean, E. Buckingham, and P. Murphy, *National Bureau of Standards Journal of Research*, vol. 2, March, 1929, Research Paper No. 49.

3 "The Laws of Similarity for Orifice and Nozzle Flow," by J. L. Hodgson, TRANS. ASME, vol. 51, 1929, part 1, FSP-51-42, pp. 303–332.

4 "Fluid Meters, Their Theory and Application," fifth edition, 1957, in press, prepared by ASME Research Committee on Fluid Meters, ASME, New York, N. Y.

5 "Coefficients of Float-Type Variable-Area Flowmeters," by V. P. Head, TRANS. ASME, vol. 76, 1954, pp. 851–862.

6 "Correcting for Density and Viscosity of Incompressible Fluids in Float-Type Flowmeters," by M. R. Shafer, et al., *National Bureau of Standards Journal of Research*, vol. 47, no. 4, 1951, Research Paper No. 2247, pp. 227–238.

7 "Survey of Mass-Rate Flow-Measuring Principles," by Y. T. Li and S. Y. Lee, ASME Paper No. 55—SA-72, unpublished.

8 "Standard Frequencies and Time Signals WWV and WWVH," Letter Circular LC-1023, June, 1956, National Bureau of Standards Boulder Laboratories, Boulder, Colo.

9 "Precision Laboratory Standards of Mass and Laboratory Weights," National Bureau of Standards Circular 547, August, 1954, available from Superintendent of Documents, U. S. Government Printing Office, Washington, D. C.

10 "Specifications, Tolerances, and Regulations for Commercial Weighing and Measuring Devices," National Bureau of Standards Handbook H44, September, 1949, available from Superintendent of Documents, Washington, D. C.

11 "ASTM Standard on Thermometers," by T. W. Lashof and L. B. Macurdy, prepared by ASTM Committee E-1, American Society for Testing Materials, Philadelphia, Pa., December, 1953.

12 "Testing of Hydrometers," by J. C. Hughes, National Bureau of Standards Circular 555, October, 1954, available from Superintendent of Documents, Washington, D. C.

13 "ASTM-IP Petroleum Measurement Tables," ASTM Designation D1250, American edition, American Society for Testing Materials, Philadelphia, Pa.

14 "Statistical Methods for Chemists," by W. J. Youden, John Wiley & Sons, Inc., New York, N. Y., second printing, 1955.

15 "On the Evaluation of the Accuracy of the Coefficient of Discharge in the Basic Flow-Measurement Equation," by A. L. Jorissen, TRANS. ASME, vol. 75, 1953, p. 1323.

Discussion

R. L. Galley.[4] A most interesting and thorough exposition of the pitfalls awaiting the novice in calibrating flowrate-measuring devices, this paper is one of the most practical treatments of a long-neglected subject that has come to the writer's attention. The authors are to be commended on their work and on this paper. It deserves wide circulation.

As one engineer who has devoted over a quarter of a century to the measurement of flow, the writer has seen the pitiful results of many amateur calibrators who did not know of all the precautions that should be observed, as the authors point out. The following comments are offered:

1 One assumes that the work deals only with volumetric and not with the so-called "mass" or gravimetric flowmeters. Of course, the same techniques would apply with either.

2 The problem of vapor pressure in testing hydrocarbon fuels is well explained, but the user is well advised that in calibrating certain turbine-type flow sensors in the same fuels, even a satisfactory line pressure does not always preclude the possibility of local cavitation in the region of the turbine blades. This can throw results way off, and one would never suspect the reason by the vapor-pressure criterion alone.

3 The authors do not mention Reynolds numbers, and the reader is left to assume that flow conditions at the test meter are sufficiently turbulent.

4 Gravity flow through the test rig is much safer than pumped flow, as this provides a better test condition.

S. R. Grotta.[5] A flow-correlation program similar to that described in the paper was carried out by the writer's company. A different approach was made, however, in the type of meter used as a reference.

It was felt that a reference meter should feature portability and ease of installation. Since the turbine meter fills this requirement in the higher flow ranges (above 250 lb per hr) better than the variable-orifice meter, an investigation was conducted to evaluate its suitability for this application. The program involved tests of flowmeter repeatability under various conditions which probably would affect all types of volumetric flowmeters.

Most of the tests were conducted with matched pairs (same make and size) of turbine meters installed in a recirculating flow system. The output signal of each flowmeter was fed into a separate electronic pulse counter. Since the output pulse is a measure of volumetric flow, permitting the counter to totalize these pulses for a sufficient period of time a direct indication of the total volume of fluid passed through the meter was produced. When the two turbine meters were placed in series and the counting sequence started and stopped simultaneously, the total counts from the two were nearly equal, with a slight difference being due to manufacturing tolerances. The ratio of the total counts (meter A divided by meter B) was found to remain constant over a wide range of flow. The standard deviation for 15 observations was 0.02 per cent. The maximum deviation from the mean was 0.03 per cent. By interchanging the meter positions in the pipeline and repeating tests we found that the effect of the initial plumbing configuration was less than 0.05 per cent.

The effect of flow-system-plumbing configuration on meter performance was investigated using this test procedure. Valves and elbows were placed in the pipe at the locations shown in Fig. 9. An elbow immediately upstream of a 1-in. meter produced an error as great as 0.9 per cent. The addition of a straight pipe 6 diameters in length ahead of the meter reduced this error to less than 0.2 per cent. The different makes of turbine meters tested were all affected by the flow pattern set up by the elbow. The degree of effect, however, varied from make to make.

After the selection of turbine meters suitable for reference use was made, a correlation program was carried on between the NBS calibrator and the Pratt & Whitney flow-calibrating standpipes. These standpipes, as company standards, are used to perform several hundred calibrations per year. Fig. 10 shows a portion of the correlation data. These data are plotted as pulses per gallon versus frequency (cps). As can be seen, the results of the correlation were very encouraging. A distinct advantage of the turbine flowmeter for correlation studies is that the accuracy of the data

[4] Consulting Engineer, Flowmeter Specialist, Woodland Hills, Calif.

[5] Experimental Engineer, Pratt & Whitney Aircraft, East Hartford, Conn.

PLUMBING CONFIGURATION FLOW DIRECTION →	1" DIAMETER TURBINE FLOWMETERS		
	MAKE I	MAKE II	MAKE III
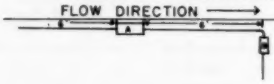	.91	.69	.84
	.21	.23	.00
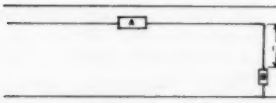	.15	.06	.00
 GATE VALVE HALF OPEN	.10	METER ERRATIC	.15
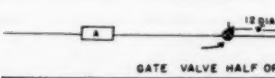 GATE VALVE HALF OPEN	.02	METER ERRATIC	.14

FIGURES ARE AVERAGE OF THREE OBSERVATIONS

Fig. 9 Per cent error in flow measurement caused by close proximity of elbow or valve to turbine flowmeter

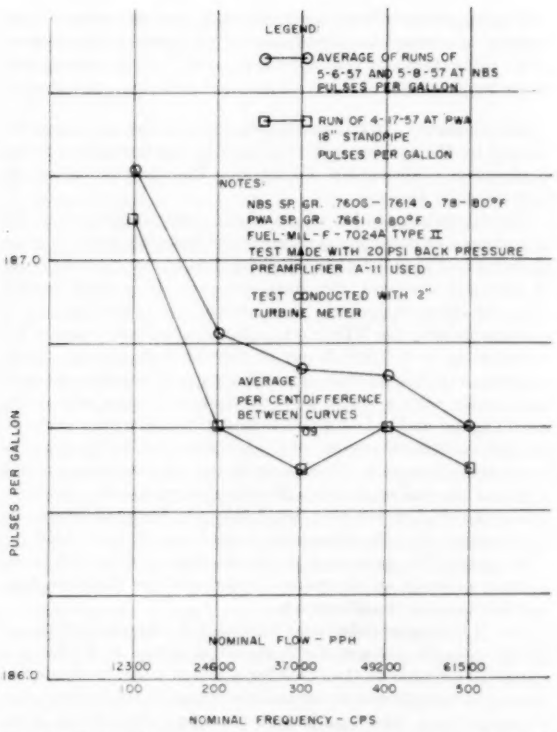

Fig. 10 National Bureau of Standards flowmeter correlation with Pratt & Whitney Aircraft

is not affected by small flowrate variations during the run. The flowrate is, in effect, averaged by the totalizing counter and timer the same as it is averaged by the weigh tank or standpipe used for calibration.

Turbine meters are not immune to all problems, however. Great care must be taken to keep the turbine rotor free of lint or other foreign material and protected from being nicked or scratched by hard objects. The observations made by the authors, emphasizing the importance of specific gravity and temperature measurements for the float-type meters, are even more important for turbine-meter applications. We also have found, as has been stated with regard to float-type meters, that air or vapor in the system causes serious error. Cavitation at the turbine-meter outlet also has been a source of trouble. This difficulty was eliminated by the application of back pressure.

It is apparent that many pitfalls have to be avoided both in calibrating turbine flowmeters and employing them for correlation studies. We feel that a document setting forth recommended procedures in the installation and use of turbine flowmeters would be very useful to those industries requiring a high degree of accuracy in flow measurements.

Finally, consideration should be given to means for conducting calibrations and correlations at elevated temperatures, up to 500 F and at pressures to 1000 psi.

V. P. Head.[6] Every fluid-mechanics laboratory should profit from the authors' treatment of inertia error. Beam travel from rest to timer operation is often $^1/_4$ or $^1/_2$ in. Note in Equation [6] that $L\theta$ is the displacement, y, of the counterweight end of the beam. Neglecting tare weight, and noting that W/k is the duration of the run T, and denoting per cent error by e, Equation [6] becomes

$$y = \frac{g}{6} T^2 \left(\frac{e}{100}\right)^3 \quad \ldots\ldots [7]$$

Using $g = 386$ in./sec^2, an average 60 sec time run requires y to be less than 0.00023 in. for 0.1 per cent, or 0.028 in. for 0.5 per cent, or $^1/_8$ in. for 1.3 per cent inertial error. Diverse beam scale dynamic rigs prevalent in university and aircraft test laboratories in past years are at best 1 per cent devices, and increasing use of the diverter, authors' Fig. 1, is to be encouraged, especially with water at low temperature where evaporation rates are negligible.

After a year of dynamic weighing experience at General Electric's A G T Division, we were using two scales and timers with pump and flowmeter between, and with 50 to 200 lb actual weights moved from receiver scale to supply scale after timers were started. Flexible hoses were hopeless. Small vertical pipes of outside diameter d extended almost to the bottom of both cylindrical liquid tanks of inside diameter D. Buoyancy of the volume of pipe plus its contained liquid was corrected by

$$W_{\text{actual}} = W_{\text{indicated}} \left(1 - \frac{d^2}{D^2}\right) \quad \ldots\ldots [8]$$

This system served only to detect gross errors in damaged meters and provide meter corrections, accurate within about 0.5 per cent, for the effects of large viscosity variations. Otherwisé, meters were probably more accurate without the supposed corrections.

The writer then undertook the development of a new primary standard for liquid-mass measurement, and a number of other aircraft laboratories contributed to its perfection. Known as the standpipe liquid weigher, and illustrated in the authors' Fig. 5, this new primary standard is not proprietary, and educational as well as industrial laboratories are encouraged to construct their own. While dynamic weighing is almost always used, static weighing by means of a single micrometer-actuated contact also could be employed, with a synchronized diverter-timer switch as in the authors' Fig. 1. When regarded as primary, with the mass per inch of mercury W/H calculated from Equation [9] (which follows), performance has consistently been ± 0.15 per cent. Attempts to determine W/H by weighing withdrawn fluid on conventional scales has led to errors as large as 0.6 per cent and proved that conventional scales are secondary devices in need of constant restandardization.

Let ρ_{hg} = mercury density at 70 F, ρ_l and ρ_a = average liquid and atmospheric densities, grams per cc. Let A_l = standpipe area, A_W = manometer well area, and A_t = manometer tube area, all in square inches at 70 F. The constant including atmospheric-buoyancy correction is

$$W/H = 0.0361276 \frac{\rho_l A_l}{\rho_l - \rho_a} \left[\rho_{hg}\left(1 + \frac{A_t}{A_W}\right) - \rho_a\left(1 + \frac{A_t}{A_l}\right) - \rho_l\left(\frac{A_t}{A_W} - \frac{A_t}{A_l}\right)\right] \quad \ldots\ldots [9]$$

Small thermal corrections, Fig. 11, are used when necessary. Variations of ρ_l and ρ_a from assumed average values have trivial effects. In the writer's opinion, this primary liquid-weight standard is as reliable as any in the world, though, of course, the many factors affecting flowmeters as well as those producing difference between flow at the meter and flow into the standard, so capably emphasized by the authors, always must be kept in mind.

[6] Director of Hydraulic Research, Fischer & Porter Co., Hatboro, Pa. Mem. ASME.

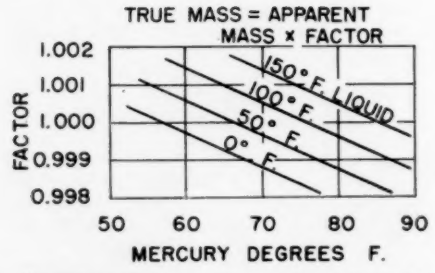

Fig. 11 Thermal-expansion corrections for standpipe liquid weigher

T. M. Morrow.[7] The authors are to be commended on the clear, concise presentation of the problems encountered in the calibration of flowmeters with dynamic weighing calibrators. They also are to be complimented on the conservative evaluation of the effect of these problems on the state-of-the-art of liquid-flow measurement.

Obviously, it is impossible to discuss in detail each source of measurement error noted in the paper. This discussion, therefore, will be limited to the presentation of an over-all picture of the effect which the results of this study can produce in the art of liquid-flow measurement.

The techniques used in the comparisons are obviously the result of careful study and planning to achieve more accurate flowmeter calibrations. Each problem is discussed with clarity noting the effects produced not only in the flow range tested, but also in the higher ranges of flow.

The careful planning and execution of the tests should be noted. Only through closely controlled and monitored test conditions could such significant results be obtained. Such tests are necessary to detect errors which many manufacturers of flowmeter-calibrating equipment consider insignificant.

To evaluate fully the extent of these errors it is necessary to have very accurate information concerning all the factors influencing the test. Only when each of these tests can be repeated a sufficient number of times to determine the existence and extent of the error, can a true evaluation be made of total error effect. By repeated tests and quantitative analysis the authors have determined that these errors are significant and their effects should be considered in precise flowmeter calibrations.

The Naval Bureau of Ordnance calibration program is confronted with accuracy requirements increasing from the nominal 1 or $\frac{1}{2}$ per cent at industrial level to a primary standard level of better than 0.1 per cent. This accuracy is not only required at the flowrates at which the National Bureau of Standards tests were conducted, but over the range of flows from 15 lb per hr to more than 2,500,000 lb per hr. This paper, therefore, represents a step toward the achievement of the required accuracy over this range. The limiting factor, until now, has been an inability to determine the rate of increase of these potential errors at higher flowrates in dynamic weighing calibration systems.

The tests and results presented in this paper are being studied carefully by the Naval Bureau of Ordnance to find a means of applying the equipment and techniques found therein to the area of high-flow, high-accuracy, liquid-flow measurement. Before further progress can be made in adapting present, or developing new, flow-measuring devices to newly developed fuels, hydraulic fluids, and liquid oxidizing agents, the characteristics peculiar to these liquids must be determined and evaluated.

These evaluations and the errors discussed in this paper should be considered for their effect on higher accuracy requirements.

[7] Measurement Standards Division, U. S. Naval Inspector of Ordnance, Pomona, Calif.

It is suggested, indeed urged, that the authors continue their program of research and evaluation of the errors of liquid-flowmeter calibrators and that it be expanded to meet existing and future requirements of increased accuracy and higher flow ranges.

E. A. Spencer.[8] It is interesting to compare the equipment developed by the authors with that used to test flowmeters at the Government's Mechanical Engineering Research Laboratory at East Kilbride, Glasgow.

This laboratory, which is one of the research stations of the Department of Scientific and Industrial Research, has a number of circuits, using water as the working fluid to cover a wide range of sizes and flowrates, the maximum capacity being 6,000,000 lb/per hr (30 cu ft per sec). A smaller version of the main rig is comparable with the NBS static calibrator and was designed for flowrates up to 180,000 lb per hr through 6-in. piping. Early experiments indicated that very high accuracies could be obtained more easily with a static weighing technique than with volumetric tanks[9] and in fact direct weighing has been adopted in all the flow-calibration systems of the laboratories. In the main rig a weighbridge capable of weighing 30 tons of water was installed while for the smaller version a 2000-lb platform machine having a sensitivity of $\frac{1}{4}$ oz has been found adequate, the minimum period for diversion into the measuring tanks being 30 sec. Like the NBS system the movement of the diverter past its mid-travel position actuates an electronic counter and the diversion time can be measured in milliseconds.

One of the major differences between the authors' system and MERL is in the siting of the flow-control valve. In the latter a spear valve similar to that used for a Pelton wheel is situated at the end of the calibration line and the round jet issuing from this is changed to a thin rectangular stream by a fishtail nozzle attached to the valve. High-speed cine films have shown that the diverter moves across this stream in about 40 millisec. Experience with this method of flow control which ensures a safe positive pressure at the meter position has been very satisfactory and is considered preferable to the upstream position selected by the authors. In view of their remarks on the dangers of upstream throttling the reason for not siting the valve between the meter and the tee-junction to the calibrators is not apparent.

Although as the authors point out a calibration is only absolutely true for the actual conditions at the time of the test, the value of such a test on a flowmeter is that it should provide data which can be applied to the subsequent use of the meter in its final installation. The introduction of flow straighteners at or near the upstream entry to the meter may produce artificial conditions which will differ substantially from those experienced in practice and give rise to significant errors. Are the authors recommending that in effect a flow straightener should become part of the meter? Even with this arrangement it is desirable that the laboratory installation should be free from rotational disturbances such as those indicated by the extreme test points in the comparison of the four calibrators. Were the authors able to measure the amount of the swirl upstream from the reference meters?

The authors are to be congratulated on the very high standards of precision achieved with the equipment in calibrating flowmeters. These figures which are dependent on the sensitivity of the meter could usefully be supplemented by results on the steadiness of the rate of flow by comparing the successive measurements of the actual flowrate determined by the NBS calibrator. At MERL it has been found that the standard deviation of such repeated determinations with the control valve at a set position is

[8] Principal Scientific Officer, Fluid Mechanics Division, Mechanical Engineering Research Laboratory, Glasgow, Scotland.

[9] "The Accurate Calibration of Flowmeters With Water," by E. A. Spencer and A. T. J. Haward, *Trans. Society of Instrument Technology*, vol. 9, 1957, p. 1.

0.1 per cent. It should, however, be noted that the supply to the calibration lines is from a constant-head tank and not direct through a pump.

Authors' Closure

The authors wish to express their appreciation for the encouraging comments of the discussers. Regarding the comments by Mr. Galley, it is correct to state that the techniques are equally applicable to either volumetric or gravimetric flowmeters. His observations on cavitation in turbine sensors are important as the high velocity at the turbine blades, with its corresponding reduction in static pressure, frequently is a cause of vapor formation especially with hydrocarbon liquids. The authors are also in agreement that the flow must be uniformly turbulent at the test meter, and that gravity flow provides a better test condition for precision work.

Mr. Grotta brings out an important characteristic to be considered in the selection of reference meters; namely, much greater precision can be obtained with reference meters of the totalizing type having a calibration constant essentially independent of flow rate. The newer electronic methods of digital readout can be employed with these and the absence of an exact flow setting will not influence the results significantly. This eliminates the human error associated with the observation and setting of flow rate and greatly increases the precision of the calibration procedure.

The treatment of inertia error by Mr. Head is correct for the assumption of zero tare weight and a massless scale and weigh tank. As they are never attained actually, his dynamic errors are the maximum to be expected. However, even if these are given due consideration, the possibility of a significant inertia influence should be considered when dynamic weighing is used.

Mr. Morrow has effectively presented the fact that the old industrial tolerances of one per cent are no longer adequate, at least in the field of national defense, and has discussed a requirement for standards approaching the accuracy level of 0.1 per cent. Although the various individual components and instruments required for this precision are available, Spencer[9] has demonstrated the considerable work involved in attempts to attain such accuracy. The problem becomes even more complicated when one realizes that new hazardous liquids at both high and low temperatures and throughout wide pressure ranges are involved.

With reference to Dr. Spencer's very constructive comments it should be mentioned that a fundamental difference in objectives exists. Dr. Spencer is attempting to establish a flow rate laboratory having the highest possible accuracy, whereas the apparatus described in this paper was constructed for the single purpose of evaluating the performance and accuracy of three dynamic type calibrators of commercial manufacture. These had been designed for installation in industrial facilities for the calibration of flowmeters used in the aircraft industry. Thus in this particular work it was necessary to use the pumps, heat exchangers, and flow control valves supplied with the calibrators as part of the evaluation procedure. This is the reason the flow control valve was located upstream from the meter. The authors are in complete agreement that throttling should be accomplished downstream from the meter whenever possible.

Regarding the subject of flow straighteners, every type of flow rate indicating meter is influenced by the upstream flow conditions. The authors still recommend that flow straighteners should be considered part of the meter in applications requiring accuracies of a fraction of one per cent. This is especially true in the aircraft field where meter installation conditions deviate considerably from the ideal. Sprenkle and Courtright[10] have recently discussed a few types of straighteners and have demonstrated their effect upon the precision of flow measurement with orifice-type metering elements.

No attempt was made to measure the swirl upstream from the reference meters, it being deemed sufficient for our purposes merely to demonstrate that its presence contributed a significant influence. The authors are in agreement that laboratory calibrators should be free from rotational disturbances and pulsations. Naturally, such is best accomplished by utilizing a gravity supply. However, this is not always feasible in industrial installations especially those using hazardous liquid-hydrocarbons as the working fluid.

[10] "Straightening Vanes for Flow Measurement," by R. E. Sprenkle and N. S. Courtright, *Mechanical Engineering*, vol. 80, February, 1958, p. 71.

Thermal Transfer in Turbulent Gas Streams—Effect of Turbulence on Macroscopic Transport From Spheres

By KAZUHIKO SATO[1] AND B. H. SAGE,[1] PASADENA, CALIF.

The rate of thermal transport from spheres in a flowing stream is of interest in many industrial operations. Limited data are available concerning the effect of turbulence level on this transfer process. Measurements of the thermal transport from spheres to an air stream at four levels of turbulence were made at four velocities varying between 4 and 32 fps. Results are presented in terms of the Nusselt number. The experimental work is a portion of a detailed study of the local thermal and material transport from spheres in turbulent air streams. The data indicate a significant increase in the thermal transport with an increase in the level of turbulence at a constant Reynolds number. For example, the Nusselt number was increased from 53 to 62 upon an increase in the level of turbulence from 0.05 to 0.12 at a Reynolds number of 7200.

Nomenclature

The following nomenclature is used in the paper:

A = area, sq ft
d = differential operator
$\mathbf{d}$ = diameter of sphere, in. or ft
E_e = electromotive force, volts
$\hat{\xi}$ = total energy flux, Btu/sec
h = thermal transfer coefficient, Btu/(sq ft)(sec)(deg F)
I_e = current, amp
k = thermal conductivity, Btu/(sq ft)(sec) (deg F/ft)
Nu = Nusselt number, $h\mathbf{d}/k$
$\hat{Q}_c$ = local convective thermal transport from sphere, Btu/(sq ft)(sec)
$\hat{Q}_c$ = total convective thermal transport from sphere, Btu/sec
Re = Reynolds number, $\mathbf{d}U/\nu$
t = temperature, deg F
u = local velocity, fps
U = gross velocity, fps
α_T = level of turbulence
θ = time, sec
θ^*_e = time required for proper averaging of electrical input, sec
ν = kinematic viscosity, sq ft/sec
T = nondimensional temperature ratio, $(t_i - t_\infty)/(t_i^* - t_\infty)$
ψ = polar angle from stagnation point, deg

Subscripts

c = convective
e = electric energy
i = solid-gas interface
0 = zero level of turbulence
t = tube
∞ = free stream

Superscript

* = average value

Introduction

Information concerning macroscopic convective thermal transport from spheres in fully developed turbulent flow is plentiful This large background of experimental information has been correlated by McAdams (1)[2] and is not considered here. In the correlations presented (1) for the convective thermal transport between spheres and air, no regard was taken of the level of turbulence and such information was not available for many of the measurements reported. However, reasonable agreement was obtained for a wide variety of sphere sizes, apparently because the flow conditions represented for the most part fully developed turbulent shear flow. Baer and co-workers (2) recently made studies of the thermal transport from a sphere in fully developed shear flow.

In contradistinction to the large amount of experimental information (1) concerning the macroscopic convective thermal transport from spheres, data relating to local transport are limited. The studies of Cary (3), Lautman and Droege (4), and Xenakis and co-workers (5) are the only recent studies that have come to the authors' attention. None of these includes any systematic investigation of the effect of the level of turbulence on thermal transport.

In the present experimental study, the steady convective thermal transport from a silver sphere 0.5-in. diam was determined for four levels of turbulence at four velocities between 4 and 32 fps. The surface temperature of the sphere was measured as a function of polar angle, taken from the stagnation point, for a number of the conditions of flow. The total energy transport from the sphere was also determined.

Methods

In principle, the methods employed in this investigation involved the use of a silver sphere 0.5-in. diam, which was provided with an internal heater and supported by two horizontal, stainless-steel tubes. The total rate of energy addition was determined by conventional calorimetric techniques involving the measurement of the current flowing in and the voltage change across the internal heater, as indicated in the following equation

$$\hat{\xi}_e^* = \frac{1}{\theta_e^*} \int_0^{\theta_e^*} E_e I_e d\theta \quad \ldots\ldots\ldots\ldots\ldots [1]$$

Guard heaters were provided along the supporting tubes in order to render negligible thermal losses from the sphere other than to

[1] California Institute of Technology.

Contributed by the Heat Transfer Division and presented at the Annual Meeting, New York, N. Y., December 1–6, 1957, of The American Society of Mechanical Engineers.

Note: Statements and opinions advanced in papers are to be understood as individual expressions of their authors and not those of the Society. Manuscript received at ASME Headquarters, February 11, 1957. Paper No. 57—A-20.

[2] Numbers in parentheses refer to the Bibliography at the end of the paper.

the air stream. In evaluating the area of the sphere exposed for thermal transfer, a correction was made for the area occupied by the supporting tubes, as indicated in the following

$$\dot{Q}_i^* = \frac{A_i}{A_i - A_t}\dot{Q}_s^* = \frac{1.0187}{\theta_s^*}\int_0^{\theta_s^*} E_s I_s d\theta = \dot{Q}_e \quad [2]$$

The electrical power supplied to the sphere, after correction for the area of the supporting tubes which was not exposed to thermal transport, was taken as the convective transport rate from a free sphere of the same diameter. The radiant transport from the silver sphere to the surroundings was considered. However, on account of the extremely low emissivity of silver the radiant-energy transport was found to be less than 0.2 per cent of the total transport and was neglected.

It should be emphasized that in this experimental investigation some effect from the supporting tubes upon the wake was present, and this may have influenced the gross thermal transport to a limited extent. For this reason, it is believed that the relative values of thermal transport as a function of the level of turbulence are more accurate than the absolute measures of the thermal transfer. The use of the guard heaters on the supporting wires decreased markedly the variation in temperature with azimuth from that experienced with this sphere in earlier studies (2) on turbulence in shear flow.

The Nusselt number for conventional convective thermal transfer is given by

$$\mathrm{Nu}_\infty = \frac{\dot{Q}_e \mathbf{d}}{A_s(t_i^* - t_\infty)k_\infty} \quad [3]$$

$$\mathrm{Nu}_i = \frac{\dot{Q}_e \mathbf{d}}{A_s(t_i^* - t_\infty)k_i} \quad [4]$$

A combination of Equation [3] with Equation [2] yields the following equation relating the Nusselt number to the experimentally measured quantities

$$\mathrm{Nu}_\infty = \frac{1.0187\mathbf{d}}{A_s\theta_s^*(t_i^* - t_\infty)k_\infty}\int_0^{\theta_s^*} E_s I_s d\theta \quad [5]$$

The time chosen for the integration θ_s^* was such as to eliminate the effect of local fluctuations in the current and electromotive force upon the recorded values. Maximum variation between the values of the integral shown in Equation [5] and the instantaneous values of the product of current and electromotive force was 0.1 per cent.

The average temperature of the sphere, which is required for the solution of Equation [5], was obtained by evaluation of the following surface integral

$$t_i^* = \frac{\oint_0^{\pi\mathbf{d}^2} t_i dA}{\pi\mathbf{d}^2} \quad [6]$$

The local temperatures of the sphere, required for the solution of Equation [6], were obtained from thermocouples imbedded in the surface of the silver sphere. Rotation of the sphere about the supporting wires permitted the local temperature to be determined as a function of polar angle, measured from the stagnation point. It is believed that sufficient information was obtained to establish the local temperature of the sphere within 0.15 deg F, and the average temperature within 0.2 deg F. In the evaluation of the Nusselt number, the molecular properties of the air under both free-stream and surface conditions were employed. The macroscopic thermal-transfer coefficient is defined as

$$h = \frac{\dot{Q}_e}{t_i^* - t_\infty} = \frac{\dot{Q}_e}{A_s(t_i^* - t_\infty)} \quad [7]$$

Equipment

The apparatus consisted of an air supply, the temperature of which was controlled within 0.05 deg F of a chosen value. The air was delivered through a duct 12 in. by 12 in. in cross section, terminating in a section which was 3 in. by 12 in. Velocities up to 32 fps were obtained with this equipment. The heated silver sphere was placed at the outlet of the converging section for studies at relatively low levels of turbulence, and a perforated plate was employed to develop a wake involving higher levels of turbulence. The level of turbulence was adjusted by locating the silver sphere at different positions downstream from the perforated plate.

Since the details of the air-supply system are already available in a study of the evaporation of drops (6, 7), it does not appear necessary to discuss this part of the equipment further. The instrumentation and methods of measurement were also the same

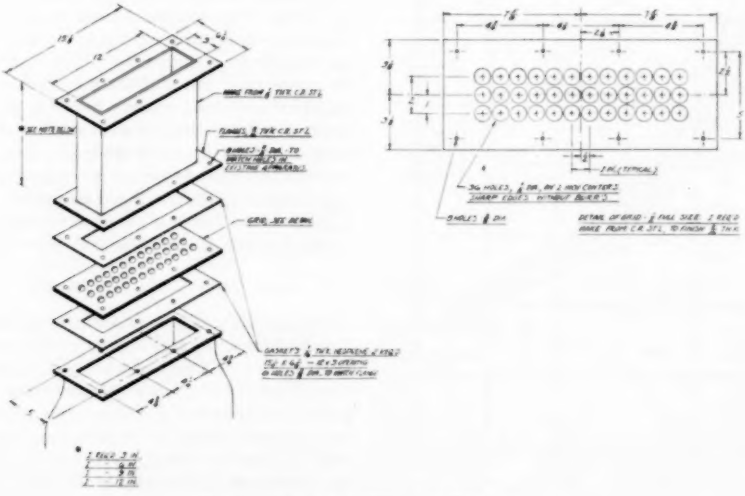

Fig. 1 Details of Grid and Extensions

as those utilized in the study of drops (6). The air stream was nearly potential in character with less than 2 per cent variation in velocity within one in. of the major axis of the jet. At the lower velocities, the local fluctuations of temperature amounted to as much as 0.09 deg F. However, at the higher velocities, these fluctuations were negligible. The average velocities were known within 0.6 per cent of the value recorded.

The equipment described (7) yielded an air stream with 0.013 fractional transverse turbulence. The fractional turbulence in the stream when no grid was present was established from measurements of the divergence in the temperature wake of a heated wire by utilizing the data of Schubauer (8).

In varying the level of turbulence, recourse was had to the measurements of Davis (9, 10), who established the character of the turbulent fluctuation in the wake of several grids prepared from perforated plates. For the present study, a grid identical to one of those used by Davis (9, 10) was prepared. The details of this grid are shown in Fig. 1. A series of rectangular extensions, of the same dimensions as the throat of the contraction section, were provided as indicated in the exploded view shown in the left-hand part of Fig. 1. These extensions permitted the stagnation point on the sphere to be located at 4, 7, and 13 in. from the surface of the grid.

By utilizing a hot-wire anemometer, the average speed in the wake was determined as a function of lateral position. Large-scale variations with position near the center of the channel were experienced at distances up to three in. from the grid (10). The "jet effect" from each of the holes in the plate was evident at these distances. The sphere was located on the axis of the jet and at distances from the grid greater than three in. Fig. 2 presents the variation in the longitudinal turbulence level with distance from the grid, based upon those measurements of Davis (10) which were made at the axis of the stream. For other particulars concerning the nature of the flow in such a wake the reader is referred to the detailed results of Davis (10). The data of Fig. 2, together with a knowledge of the distance from the trailing edge of the grid to the stagnation point of the sphere, were utilized to determine the longitudinal turbulence level. In relating the measurements in the free jet to those in the wake of the grid, it was assumed that the turbulence was isotropic.

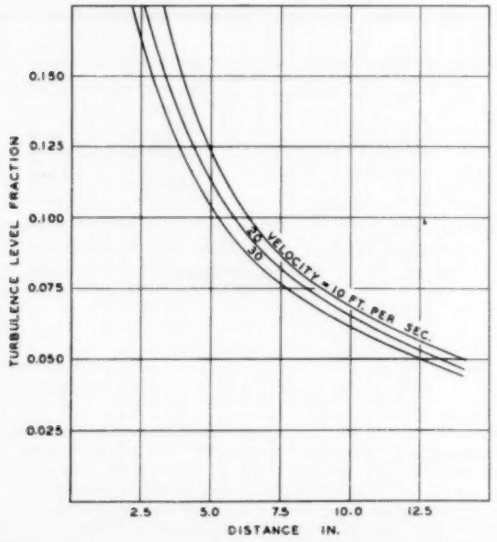

FIG. 2 LONGITUDINAL TURBULENCE IN WAKE OF GRID

Heated Sphere. The construction of the heated silver sphere is shown in some detail in Fig. 3. This sphere is the same as that utilized in an earlier investigation involving turbulent shear flow (2). It consisted of a copper core E supported upon a piano wire A. This core was provided with a spiral groove, shown at L, within which a heater was wound, and the core was covered with a silver sheath D soldered to the core. The sheath which contained a groove K for carrying thermocouple leads was connected to two 0.096-in. stainless-steel tubes B. The tubes surrounded the piano wire and carried the heater and thermocouple leads from the heated sphere to the edge of the air stream. Thermocouples were mounted at F, G, H, and J, and by rotation of the sphere about the piano wire as an axis, it was possible to obtain supplementary values of the local surface temperatures. In the course of these measurements maximum variation in surface temperature with position was found to be less than 3.0 deg F.

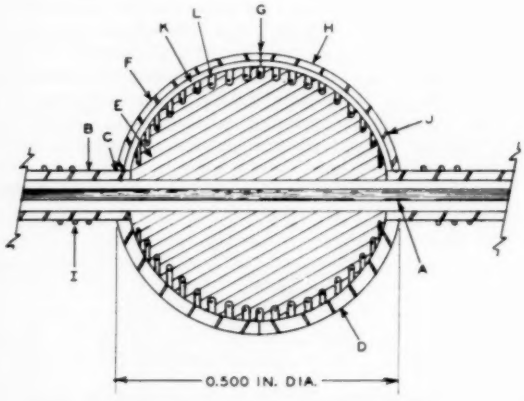

FIG. 3 ARRANGEMENT OF SILVER SPHERE

In order to avoid thermal leakage along the stainless-steel tubes and wires, guard heaters were provided, as mentioned earlier. They were located at I, ending 0.125 in. from the solder joint C. These guard heaters were so adjusted, on the basis of the indications of differential thermocouples, that the temperatures of the tubes and of the adjacent surface of the sphere were identical. Even with the careful use of the guard heaters, it is probable that some uncertainty existed in the absolute values of the thermal transfer from the sphere. Furthermore, as mentioned earlier, the wake from the stainless-steel tubes undoubtedly changed slightly the thermal transfer from the aft hemisphere from that which would be obtained without this added disturbance. The particular arrangement of the sphere and stainless-steel tubes was employed in order to permit investigations of the local temperature variation in the associated air stream. A number of the other features of the design of the sphere shown in Fig. 3 would not be required if only macroscopic transport were of interest.

MATERIALS

The humidity of the air utilized in this investigation was ascertained from wet and dry-bulb temperature measurements and was included as a part of the experimental data. Properties of air utilized in the calculations associated with this set of investigations are recorded in Table 1, the information being based in part upon an earlier critical review of properties of air (11). It is believed that uncertainty in the data submitted in Table 1 did not contribute significantly to the uncertainty in the analysis of the results.

TABLE 1 PHYSICAL PROPERTIES OF DRY AIR AT 14.696 PSI, ABSOLUTE

Property	Reference	Units	Temperature °F. 70	100	130	160	190	220	250
Viscosity x 10^7	(13,14,15,16)	(lb.)(sec.)/sq.ft.	3.82	3.98	4.14	4.30	4.45	4.60	4.76
Thermal Conductivity x 10^6	(16)	Btu/(ft.)(sec.)(°F.)	4.14	4.34	4.54	4.75	4.95	5.15	5.35
Specific Volume	(13,16,17)	cu.ft./lb.	13.348	14.105	14.862	15.616	16.372	17.127	17.883
Kinematic Viscosity x 10^4	(13,14,15,16)	sq.ft./sec.	1.641	1.806	1.980	2.161	2.345	2.535	2.727
Specific Heat	(13,16,18)	Btu/(lb.)(°F.)	0.2403	0.2406	0.2409	0.2412	0.2415	0.2419	0.2424
Thermometric Conductivity x 10^4	(16)	sq.ft./sec.	2.30	2.54	2.80	3.08	3.36	3.65	3.95

TABLE 2 EXPERIMENTAL RESULTS FOR HEATED SPHERE IN FREE JET

Test Number	Air Stream[a] Pressure lb./sq.ft.	Temperature °F.	Weight Fraction Water	Velocity ft./sec.	Heated Sphere Total Energy Flux[b] Btu/sec.	Thermal Flux Btu/(sq.ft.)(sec.)	Surface Temperature °F.
60	2064.8	100.2	0.0073	4.04	1.094×10^{-3}	0.2044	205.1
64	2065.0	100.1	0.0077	4.04	0.783	0.1463	175.9
68	2060.4	100.2	0.0098	4.07	1.533	0.2863	245.1
61	2067.8	99.8	0.0090	8.07	1.093	0.2042	176.6
66	2068.1	100.0	0.0121	8.05	0.783	0.1463	154.4
69	2069.6	100.1	0.0083	8.04	1.531	0.2859	206.9
80	2057.3	100.1	0.0057	8.05	2.085	0.3894	245.9
70	2063.8	100.0	0.0091	16.24	1.533	0.2863	178.2
71	2069.2	100.1	0.0082	16.20	2.086	0.3896	205.5
73	2044.1	100.1	0.0068	16.41	2.856	0.5334	243.8
74	2077.3	100.0	0.0095	32.08	2.086	0.3897	173.1
75	2071.3	100.1	0.0077	32.17	2.856	0.5333	199.5
79	2062.5	100.0	0.0077	32.11	4.155	0.7759	243.0

a Level of turbulence 0.013

b The total energy flux, $\dot{E}_s$, was corrected for area of the supporting tubes to obtain the thermal flux, as shown in Equation 2.

TABLE 3 EXPERIMENTAL RESULTS FOR HEATED SPHERE IN WAKE OF GRID

Test Number	Air Stream Pressure lb./sq.ft.	Temperature °F.	Weight Fraction Water	Velocity ft./sec.	Level of Turbulence[a]	Heated Sphere Distance Downstream from Grid Inches	Total Energy Flux[b] Btu/sec.	Thermal Flux Btu/(sq.ft.)(sec.)	Surface Temperature °F.
82	2074.2	99.8	0.0048	4.03	0.142	4.13	0.784×10^{-3}	0.1464	174.6
88	2065.0	100.0	0.0100	4.06	0.092	7.12	0.783	0.1463	177.7
111	2057.3	100.1	0.0064	4.07	0.054	13.04	0.783	0.1463	170.5
81	2068.0	100.0	0.0054	8.01	0.145	4.07	1.094	0.2044	171.1
87	2067.3	100.1	0.0088	8.05	0.092	7.12	1.094	0.2044	175.7
110	2055.9	100.1	0.0042	8.06	0.054	13.03	1.094	0.2044	175.4
83	2021.8	100.1	0.0057	16.13	0.129	4.13	1.533	0.2863	167.7
86	2068.6	100.0	0.0093	16.22	0.086	7.12	1.533	0.2863	173.3
109	2069.1	100.1	0.0030	16.13	0.051	13.04	1.533	0.2863	175.3
84	2067.7	100.1	0.0059	32.06	0.130	4.13	2.087	0.3898	160.2
85	2065.2	100.1	0.0093	32.19	0.080	7.12	2.087	0.3898	167.3
111	2056.3	100.1	0.0043	32.22	0.049	13.04	2.085	0.3894	170.5

a Root-mean-square longitudinal turbulence evaluated from measurements of Davis (10).

b The total energy flux, $\dot{E}_s$, was corrected for the area of supporting tubes to obtain the total thermal flux, as shown in Equation 2.

Experimental Measurements

Experimental measurements of thermal transport, made with the heated sphere in the undisturbed air jet, are recorded in Table 2. The average velocity of the stream was varied between 4 and 32 fps. Average surface temperatures of the heated sphere were determined by application of Equation [6], as described. Uncertainty in the measurement of the rate of electrical energy addition was less than one part in one thousand. However, uncertainties in the magnitude of the thermal leakage along the two stainless-steel tubes shown in Fig. 3 made it possible that uncertainties as large as two per cent might be involved in the net convective thermal transport. The measured total electrical power input and the thermal flux corrected for the area of the supporting tubes are included in Table 2.

Information similar to that in Table 2 is presented in Table 3 for the measurements which were made in the wake of the perforated plate or grid. The values of the fractional level of turbulence as determined from the data of Fig. 2 are included. No effort was made in the course of the experimental measurements to realize a fixed average value of the surface temperature. In order to permit comparison of behavior between the different sets of measurements, a normalized temperature was defined as

$$\Upsilon = \frac{t_i - t_\infty}{t_i^* - t_\infty} \qquad [8]$$

This normalized variable Υ was used to correlate the variations in surface temperature on the assumption that these variations from point to point are influenced in a linear fashion by the difference in temperature between the surface and the surrounding air stream. The temperature distribution at the surface of the silver sphere under a variety of conditions of flow is presented in Table 4 in terms of the normalized variable Υ. The values recorded in the table were smoothed with respect to polar angle for each set of flow conditions. It may be shown from Table 4 that the variation in temperature from point to point on the surface of the silver sphere is small. It does not amount to more than 1 deg F when the difference in temperature between the air stream and the sphere is about 60 deg F.

Table 4 Normalized Temperature Distribution on Surface of Sphere

Polar Angle	Velocity, ft./sec. 4	8	16	32
0	0.987[a]	0.983	0.986	0.993
30	0.989	0.985	0.988	0.994
60	0.994	0.992	0.993	0.996
90	1.000	1.001	1.002	1.000
120	1.004	1.006	1.007	1.004
150	1.006	1.007	1.008	1.007
180	1.006	1.008	1.009	1.008

[a] Values are normalized temperature described by Equation [8].

Values of the normalized temperature are shown in Fig. 4, as a function of polar angle, for several velocities of flow. The variations in surface temperature with polar angle were so small that it was not considered necessary to explore or to take into account the influence of level of turbulence on the temperature distribution. The average temperatures were determined as simple averages, and, therefore, some lack of symmetry between the upper and lower hemispheres was to be expected.

From the information submitted in Tables 2 and 3, it was possible to evaluate some of the effects of Reynolds number and level of turbulence upon the convective thermal transport from

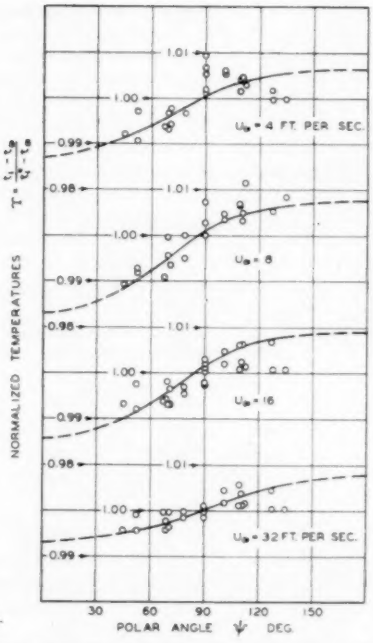

Fig. 4 Normalized Temperature Distribution on Surface of Silver Sphere

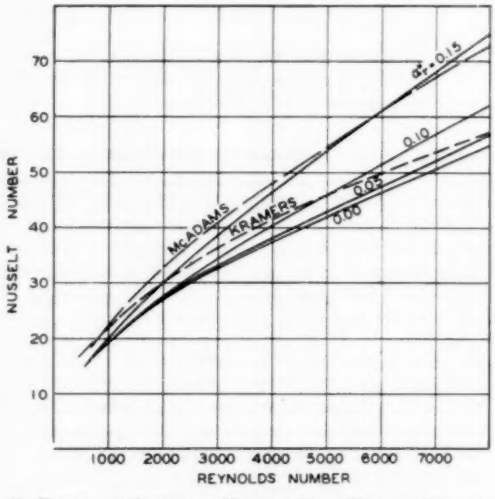

Fig. 5 Effect of Reynolds Number Upon Nusselt Number at Several Levels of Turbulence

spheres in a turbulent air stream. The Reynolds number, convective transport coefficient, and Nusselt number were established by the methods described earlier. The results are presented for the silver sphere in the free-air jet, and in the wake of the grid, in Tables 5 and 6, respectively.

Thermal Transport

Fig. 5 shows the effect of Reynolds number upon the Nusselt number based on the free-stream properties, and for comparison the data of Kramers (12) and the correlations of McAdams (1) are included. Kramers' measurements were carried out at a relatively

low but unknown level of turbulence, whereas the studies of McAdams were based for the most part upon fully developed turbulent shear flow. For some of the data employed by McAdams (1), the level of turbulence may well have increased with an increase in the Reynolds number of the flow about the spheres, although this is not necessarily true. The present information gathered in the free jet is in fair agreement with the data of Kramers and in good agreement with McAdams' values. As would be expected, the information of McAdams indicates higher Nusselt numbers for a given Reynolds number than were obtained in the free jet with a level of turbulence of 0.013. In fact, the present measurements indicate agreement with McAdams for turbulence of 0.15 which may be higher than that usually encountered in fully developed shear turbulent flow. The standard deviation of the experimental points for the silver sphere from the smooth curve shown in Fig. 5 was 0.244, assuming that all the uncertainties lay in the Nusselt number. It was not possible to show experimental points in Fig. 5 since the data were not obtained for a series at constant values of the level of turbulence.

The Nusselt number as a function of the level of turbulence is shown in Fig. 6 for several Reynolds numbers based on the properties of the free stream. The experimental points have been included with their corresponding values of Reynolds number. It is apparent that there is only a small effect of level of turbulence at Reynolds numbers below 3600. However, the influence of turbulence at the higher Reynolds numbers is significant and cannot be

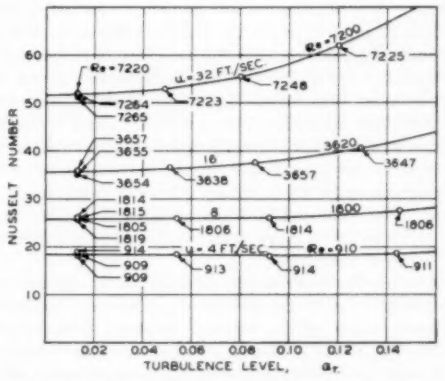

FIG. 6 EFFECT OF TURBULENCE LEVEL ON THERMAL TRANSPORT FROM SILVER SPHERE

TABLE 5 THERMAL TRANSFER FROM HEATED SPHERE IN FREE JET

Test Number	Reynolds Number[a]	Heat Transfer Coefficient Btu/(sec.)(sq.ft.)(°F.)	Nusselt Number Free Stream	Nusselt Number Surface[b]
60	909	1.948×10^{-3}	18.70	16.07
64	909	1.930	18.53	16.58
68	914	1.976	18.97	15.48
61	1819	2.659	25.53	22.80
66	1815	2.689	25.82	23.84
69	1814	2.702	25.94	22.25
80	1805	2.671	25.64	20.88
70	3654	3.681	35.35	31.32
71	3655	3.696	35.49	30.50
73	3657	3.712	35.64	29.13
74	7265	5.331	51.18	45.90
75	7264	5.365	51.51	44.62
79	7220	5.426	52.10	42.58

a Level of turbulence 0.013.

b Nusselt number calculated for thermal conductivity corresponding to conditions at surface.

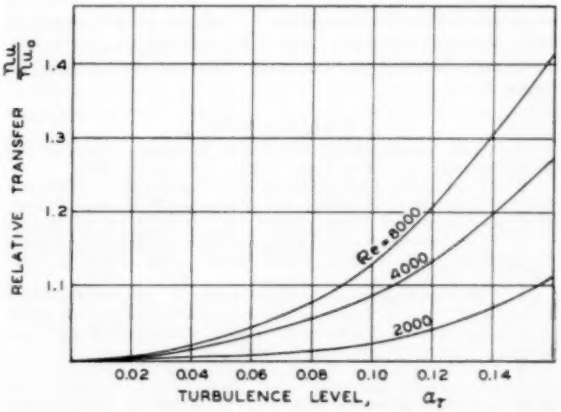

FIG. 7 EFFECT OF TURBULENCE LEVEL UPON RELATIVE NUSSELT NUMBER FOR SILVER SPHERE

TABLE 6 THERMAL TRANSFER FROM HEATED SPHERE IN WAKE OF GRID

Test Number	Reynolds Number	Turbulence Level	Heat Transfer Coefficient Btu/(sec.)(sq.ft.)(°F.)	Nusselt Number Free Stream	Nusselt Number Surface[a]
82	911	0.144	1.957×10^{-3}	18.80	16.85
88	914	0.092	1.883	18.08	16.14
111	913	0.054	2.078	19.95	17.96
81	1806	0.145	2.862	27.48	24.74
87	1814	0.092	2.703	25.95	23.20
110	1806	0.054	2.714	26.06	23.32
83	3647	0.129	4.235	40.66	36.76
86	3657	0.066	3.906	37.50	33.70
109	3638	0.051	3.807	36.55	32.71
84	7225	0.120	6.486	62.27	57.02
85	7248	0.080	5.801	55.70	50.36
111	7223	0.049	5.531	53.11	47.82

a Nusselt number calculated for thermal conductivity corresponding to conditions at surface.

overlooked. The standard deviation of the experimental points from the smooth curves as shown in Fig. 6 was 0.244.

For comparison, the relative Nusselt number is shown in Fig. 7 as a function of turbulence level, with Reynolds number as a parameter. The relative Nusselt number is defined as the ratio of the Nusselt number under the given conditions of flow to that for the same Reynolds number at a zero level of turbulence. The data illustrated in Fig. 7 indicate a rapid increase in the relative Nusselt number with increasing longitudinal turbulence at the higher Reynolds numbers. The greater influence of the level of turbulence at the higher Reynolds numbers is not unexpected because the boundary layer is thinner, and the effect of turbulence in the free stream upon the boundary transport should be more pronounced. The data of Fig. 7 are recorded in Table 7 for even values of Reynolds number based on free-stream properties for several levels of turbulence.

In reviewing the experimental information, it appears that the influence of turbulence was established with greater accuracy than the absolute value of the thermal transport from the sphere. This situation develops from uncertainty as to the thermal losses along the supporting tubes as a result of possible conduction from the silver sphere.

Acknowledgment

The assistance of Nan-Teh Hsu, a Peter E. Fluor Fellow, in connection with the experimental program is acknowledged. Betty Kendall carried out many of the calculations, and Evelyn Anderson assembled the manuscript after its review by W. N. Lacey.

BIBLIOGRAPHY

1 "Heat Transmission," by W. H. McAdams, McGraw-Hill Book Company, Inc., New York, N. Y., third edition, 1954.

2 "Temperature Distribution in the Wake of a Heated Sphere," by D. H. Baer, W. G. Schlinger, V. J. Berry, and B. H. Sage, *Journa of Applied Mechanics*, Trans. ASME, vol. 75, 1953, pp. 407–414.

3 "The Determination of Local Forced-Convection Coefficients for Spheres," by J. R. Cary, Trans. ASME, vol. 75, 1953, pp. 483–487.

4 "Thermal Conductances About a Sphere Subjected to Forced Convection," by L. G. Lautman and W. C. Droege, Report No. AIRL A 6118 50-15-3, U. S. Air Force, Air Materiel Command, Willow Run Airport, Ypsilanti, Mich., August, 1950.

5 "An Investigation of the Heat-Transfer Characteristics of Spheres in Forced Convection," by G. Xenakis, A. E. Amerman, and R. W. Michelson, Technical Report 53-117, Wright Air Development Center, Dayton, Ohio, April, 1953.

6 "Material Transfer in Turbulent Gas Streams. Influence of Shape on Evaporation of Drops of n-Heptane," by N. T. Hsu, K. Sato, and B. H. Sage, *Industrial and Engineering Chemistry*, vol. 46, 1954, pp. 870–876.

7 "Experimental Methods for Measurement of the Evaporation of Drops," by N. T. Hsu, H. H. Reamer, and B. H. Sage, Document No. 4219, American Documentation Institute, Library of Congress, Washington, D. C., 1954.

8 "A Turbulence Indicator Utilizing the Diffusion of Heat," by G. B. Schubauer, NACA Report No. 524, 1935.

9 "Measurements of Turbulence Level Behind a Set of Square-Mesh Grids and Correlation with Grid Pressure Loss," by L. Davis, Report 3-22, Jet Propulsion Laboratory, California Institute of Technology, Pasadena, Calif., 1950.

10 "Measurements of Turbulence Decay and Turbulent Spectra Behind Grids," by L. Davis, Report 3-17, Jet Propulsion Laboratory, California Institute of Technology, Pasadena, Calif., 1952.

11 "Temperature Gradients in Turbulent Gas Streams. Temperature and Velocity Distribution in Uniform Flow Between Parallel Plates," by F. Page, Jr., W. H. Corcoran, W. G. Schlinger, and B. H. Sage, *Industrial and Engineering Chemistry*, vol. 44, 1952, pp. 419–424.

12 "Heat Transfer From Spheres to Flowing Media," by H. Kramers, *Physica*, vol. 12, 1946, pp. 61–80.

13 "Thermodynamic Properties of Air Including Polytropic Functions," by J. H. Keenan and J. Kaye, John Wiley & Sons, Inc., New York, N. Y., 1945.

14 "A New Determination of the Viscosity of Air by the Rotating Cylinder Method," by G. Kellström, *Philosophical Magazine*, series 7, vol. 23, 1937, pp. 313–338.

15 "A New Modification of the Cloud Method of Determining the Elementary Electrical Charge and the Most Probable Value of That Charge," by R. A. Millikan, *Philosophical Magazine*, series 6, vol. 19, 1910, pp. 209–228.

16 "Measurements of Temperature and Velocity Distribution in Uniform Flow," by F. Page, Jr., W. H. Corcoran, W. G. Schlinger, and B. H. Sage, Document No. 3293, American Documentation Institute, Library of Congress, Washington, D. C., 1952.

17 "International Critical Tables," National Research Council, McGraw-Hill Book Company, Inc., New York, N. Y., first edition, vol. 3, 1928, p. 3.

18 "Thermodynamic Properties of Air," by R. V. Gerhart, F. C. Brunner, H. S. Mickley, B. H. Sage, and W. N. Lacey, *Mechanical Engineering*, vol. 64, 1942, pp. 270–272.

Table 7 Influence of Level of Turbulence and Reynolds Number Upon Relative Nusselt Number[a] for a Sphere

Reynolds Number	Level of Turbulence[b] 0.00	0.05	0.10	0.15
0	1.000	1.000	1.000	1.000
2000	1.000	1.007	1.022	1.092
4000	1.000	1.024	1.087	1.234
6000	1.000	1.030	1.120	1.330
8000	1.000	1.031	1.130	1.360

a Relative Nusselt number is the ratio of the Nusselt number under the conditions in question to that at the same Reynolds number for a zero level of turbulence.

b Root-mean-square longitudinal fluctuations relative to gross velocity.

Discussion

G. M. Dusinberre.[3] In the nomenclature, the authors very properly define the Nusselt and Reynolds numbers which they use, even though these ratios are widely used and well known. But the "level of turbulence," on which the whole value of the paper depends, is not defined even though this ratio is not widely used nor well known. The practicing engineer will not get much benefit from the paper without a definition and a means of prediction of this quantity.

M. V. Morkovin.[4] The authors invite the reader to refer to the detailed results of Davis (their reference 10) "for other particulars concerning the nature of the flow" (behind grids producing the turbulent flow, which was used but not measured by the authors). Since the authors' measurements are taken with the sphere at the unusually short distances behind the 1-in. mesh ($M = 1$) perforated plate, namely, 4, 7, and 13 inches and since "it was assumed (by them) that the turbulence was isotropic," it is worth while to consider a few quotations from the foregoing generally unavailable reference. Davis, p. 7, "All decay measurements were started from $x/M = 8$" (i.e., at 8 in. downstream of the grids). No data of Davis are given for smaller x, . . . for two good reasons: (*a*) The interpretation of the hot-wire data was based on the assumption of small fluctuations. (*b*) The separated boundary layer and wakes of the grid do not merge into a homogeneous field with sufficiently small mean spatial and time variations until some distance downstream, usually taken as at least 10 mesh lengths. Davis: "A typical experimental record of grid-wake profiles. . . the grid pattern is well defined at $x/M = 3$ and 5, and

[3] Department of Mechanical Engineering, The Pennsylvania State University, University Park Pa. Fellow ASME.

[4] Department of Aeronautics, The Johns Hopkins University, Baltimore, Md. Mem. ASME.

Note: The discussion was prepared in connection with studies under Contract AF 18(600)-1121 with the Air Office of Scientific Research of the Air Research and Development Command.

just perceptible at $x/M = 7$. For all grids[5] the velocity-profile variations fall to 2 to 3 per cent of the mean speed when $6 \leqslant x/M \leqslant 8$." The authors, referring to Davis' work: "Large-scale variations with position near the center of the channel were experienced at distances up to 3 in. from the grid." The scale of these wakes is, of course, 1 in., providing a local agitated (nonhomogeneous, nonisotropic) shear flow for the 0.5-diam sphere. (Recent careful investigations of Grant and Nesbit[6] suggest that the nonhomogeneity actually may be far worse than is commonly supposed and may be responsible for some of the scatter and discrepancies.)

The authors: "The data of Fig. 2 . . . were utilized to determine the longitudinal turbulence level." It would appear that these "data" go beyond the quoted reference. Unless the authors omitted to mention another source, one must conclude that the two highest utilized turbulence levels are open to question. Unfortunately, the third turbulence level 13 in. downstream from the grid is also open to question, because of the probable side-edge effects which were not present in Davis' measurements. The effect of the edge of the perforations is almost certain to spread more than 1.5 in. laterally (authors' Fig. 1) in 13 in. of downstream movement.

Thus it would seem that the main results of the paper embodied in Figs. 6 and 7 are open to some doubt.

What is more discouraging is that the paper provides little understanding for the effects of turbulence it reports. One gets little help in answering two types of basic questions: (*a*) Which aspects of the irregularities of the oncoming stream are responsible for the important changes of the heat transfer to a blunt body; e.g., the extent of nonhomogeneity, the departure from isotropy, the intensity level of turbulence, the scales of turbulence, and so on? (*b*) In which regions of the blunt body is the heat transfer mainly affected; e.g., the stagnation region, the region near the separation line (shift therein), the "base" or wake region (effects on intensity of fluctuations in the wake either directly or through earlier transition of the separated free layer, and so on)? Here the sizable cylindrical supports with their own wake characteristics are disturbing.

Clearly, to isolate the effects of the multiple parameters, which usually vary concomitantly in a given flow (such as the turbulence behind a grid) and which depend on Reynolds number (at times critically) is a difficult task. However, without serious attempts to devise telling experiments, illuminating some of these causes and effects, we shall merely cumulate approximate test data which can be confidently expected to fall in the same ballpark as that compiled by McAdams.

Authors' Closure

The authors regret the oversight pointed out by Mr. G. M. Dusinberre concerning the definition of level of turbulence. For present purposes the level of turbulence in the longitudinal and transverse directions can be defined by the following expressions:

$$\alpha_{\tau x} = \frac{\sqrt{\overline{u^2_{xf}}}}{U} \qquad \alpha_{\tau y} = \frac{\sqrt{\overline{u^2_{yf}}}}{U}$$

The quantities u_{xf} and u_{yf} are the local instantaneous fluctuating velocities in the x and y directions, respectively. Evaluation of these local instantaneous velocities is an experimental problem of some difficulty and subject to uncertainty, particularly when there exist deviations from conditions under which the time-average fluctuating velocity is a small fraction of the mean velocity.

[5] Tested by Davis.

[6] "The Inhomogeneity of Grid Turbulence," by H. L. Grant and I. T. Nesbit, *Journal of Fluid Mechanics*, vol. 2, part 3, 1957, pp. 263–272.

The interest of Prof. M. V. Morkovin in setting forth the limitations to the evaluation of turbulence level in the wake of grids is most helpful. These limitations were reviewed and discussed in some detail by Davis (10). It should be recognized that with such information as submitted in Fig. 2, no attempt was made to describe all the characteristics of the turbulent stream but only to present a single-valued parameter which, when taken in connection with the Reynolds number, forms an additional factor to describe the transport characteristics of the stream. The use of level of turbulence and Reynolds number still is inadequate to determine many of the transport characteristics of turbulent flow.

It appears desirable to offer some explanation in response to Professor Morkovin's specific comments. The punched plate used in this experimental work involved a series of 0.875-inch diameter holes spaced upon one-inch centers. Therefore there existed a significant difference between the downstream distance measured in inches and the relative downstream distance as measured in diameters. This fact was overlooked in Professor Morkovin's comments. Also in contradistinction to Professor Morkovin's interpretation, it was assumed by the authors only that the turbulence in the free jet was isotropic. Measurements by Laufer[7] indicate that under many conditions of flow, the deviations from isotropy in the center of a stream are less than ten per cent. It is probable that the longitudinal level of turbulence in the free jet was, if the lack of isotropic turbulence was taken into consideration, 0.014 rather than 0.013 as reported. This difference in the levels of turbulence was not considered to be significant because of uncertainties in the measurements of the temperature distribution in the wake of the heated wire used to establish the transverse level of turbulence.

Table 8

Downstream distance, in.	Relative downstream position	Approximate deviation from mean velocity	Ratio of longitudinal and transverse turbulence	Turbulence level[a]	
				Longitudinal	Transverse
x	$\frac{x}{M}$	$\int_{0.2}^{1} \frac{\lvert U-u\rvert}{U} d\left(\frac{y}{y_0}\right)$	$\sqrt{\frac{\overline{u^2_{xf}}}{\overline{u^2_{yf}}}}$	$\frac{\sqrt{\overline{u^2_{xf}}}}{U}$	$\frac{\sqrt{\overline{u^2_{yf}}}}{U}$
3	3.43[b]	0.17[c]	~1.38	~0.18+	~0.12[e]
4	4.58	0.10	1.26[d]	0.138[g]	0.110[g]
5	5.72	0.07	1.22	0.106[f,g]	0.087[f]
7	8.00	0.02	1.17	0.078[f]	0.070[f]
13	14.87	≤0.01	1.09	0.046[f,g]	0.042[f]

[a] Reynolds number, R_M, approximately 10,000.

[b] Hole spacing; 0.875-inch diameter, 1.0-inch centers, M = hole diameter.

[c] Estimated from hot-wire anemometer traverses by authors and from data of Davis (10).

[d] Taken from Davis (10).

[e] Estimated from temperature in wake of heated wire with data from Schubauer (8).

[f] Taken from Davis (10).

[g] Calculated from $\sqrt{\overline{u^2_{xf}}/\overline{u^2_{yf}}}$ from Davis (10) and $\sqrt{\overline{u^2_{yf}}}/U$ from wake temperature measurements.

The authors have assembled in Table 8 supplemental information concerning conditions existing in the wake of the punched plate. The footnotes to the table describe the fashion in which the numerical data were established. As stated in the text, the authors made measurements of the local time-average velocity as a function of position, and these results are given in the table. Deviations from the mean flow were significant at a downstream distance of 4 in. but appeared relatively inconse-

[7] "Investigation of Turbulent Flow in a Two-Dimensional Channel," by J. Laufer, NACA Report No. 1053, 1951.

quential at distances of 7 and 13 in. The authors also made a limited number of rough measurements of the transverse level of turbulence downstream from a punched plate by determining the temperature distribution in the wake of a heated wire. The results, based upon the data of Schubauer (8), are included in the accompanying table. The authors had refrained from including these detailed data because the application of Schubauer's data in the wake of a punched plate is open to question.

In addition, from measurements made as a function of lateral position in the jet, the authors were unable to ascertain any significant variation in the macroscopic thermal transfer or in the local temperature distribution surrounding the sphere. This situation led the authors to have greater confidence in the reproducibility of the results than is expressed by Professor Morkovin. The authors reviewed the data of Davis in detail[8] and concur with Professor Morkovin that, as the grid is approached, the deviation from homogeneity in the turbulent field increases significantly.

In any event, the measurements were made under controlled conditions, and variations in thermal transfer were obtained as recorded in Figs. 6 and 7. Whether or not the levels of turbulence reported by Davis and estimated by the authors from the measurements of Schubauer are in fact correct, it appears that the thermal transfer in the wake of a punched plate is influenced by position in the manner indicated. Measurements of the local temperature distribution in the boundary layer around the sphere indicated the turbulent field to be sufficiently homogeneous to permit time-averaged temperature gradients to have significance. Behavior similar to that illustrated in Figs. 6 and 7 has been found for material transport.[9]

[8] "Momentum Transfer in Fluids," by W. H. Corcoran, J. B. Opfell, and B. H. Sage, Academic Press, Inc., New York, 1956, p. 190.

[9] "Material Transfer in Turbulent Gas Streams. Effect of Turbulence on Macroscopic Transport From Spheres," by R. A. S. Brown, Kazuhiko Sato, and B. H. Sage, accepted by *Industrial and Engineering Chemistry* for publication in *Chemical & Engineering Data Series*.

Transient Temperature and Thermal Stresses in Skin of Hypersonic Vehicle With Variable Boundary Conditions

By SHIH-YUAN CHEN,[1] FARMINGDALE, L. I., N. Y.

The transient temperature distribution and thermal stresses resulting from aerodynamic heating in the skin of a vehicle at hypersonic speeds are found analytically for a finite slab in which one boundary has a variable coefficient of heat transfer and a variable adiabatic wall temperature while the other boundary is insulated. The purpose of this paper is to introduce the concept of using exponential functions of time to represent the coefficient of heat transfer and the adiabatic wall temperature. In general, one can choose as many exponential functions as necessary to obtain a better solution since the solution is a straightforward mathematical problem. This paper has considered the sum of two exponential functions and a constant for the coefficient of heat transfer and the sum of two exponential functions and a constant for the adiabatic wall temperature. This represents several types[2] of aerodynamic heating problems. Solutions for three special cases[3] are given to show that the general solution also can be applied to simpler problems.

Introduction and Discussion

THE structural design of hypersonic vehicles, such as aircraft and missiles, involves the problem of high thermal stressing resulting from aerodynamic heating. The computation of these thermal stresses depends directly on a knowledge of the existing temperature distribution. If the problem is restricted to one-dimensional heat flow in a solid of simple geometry, with constant material properties, there are analytical solutions for temperature distributions with particular boundary conditions readily available.

The case of constant coefficient of heat transfer and constant adiabatic wall temperature was treated in references (1)[4] and (2). The case of a finite slab in which one boundary has a linear temperature rise was presented in references (2) and (3). The case of heat flux through one surface as a quadratic function of time was analyzed in reference (4). The case of a variable coefficient of heat transfer and a constant adiabatic wall temperature was given in reference (5).

In general aerodynamic heating problems, the coefficient of heat transfer and the adiabatic wall temperature are both functions of time. It is found that both the coefficient of heat transfer and the adiabatic wall temperature for a given flight path of an aircraft, or for a given trajectory of a guided missile, generally can be approximated by sets of exponential functions of time.

The present paper has arbitrarily chosen four exponential functions and two constants, two exponential functions and a constant for the coefficient of heat transfer, and two exponential functions and a constant for the adiabatic wall temperature. The accuracy of this analytical solution depends primarily on the degree of deviation between the actual and the assumed curves for both the coefficient of heat transfer and the adiabatic wall temperature, and also on the assumption of constant material properties.

Since the temperature distribution is not symmetrical with respect to the centroid of the thickness, one has both bending stresses and normal stresses. The calculation of thermal stresses in a thin plate at a considerable distance from the ends with nonsymmetrical temperature distribution was given in reference (6). The thermal stresses obtained are contingent on the assumption that the plate is free in both the y and z-directions. This assumption is valid since buckling of the fuselage skin is objectionable for structural and aerodynamic reasons: The buckled, wavy surfaces alter the flow of air, lead to losses in aerodynamic efficiency, and may even cause aerodynamic disturbances resulting in structural failure (7).

Nomenclature

The following nomenclature is used in the paper:

A' = defined by Equation [16]
a = thickness of slab
B_1' = defined by Equation [14]
B_2' = defined by Equation [15]
B_3' = A'
b_1' = defined by Equation [9]
b_2' = defined by Equation [10]
b_3' = 0
d_1' = defined by Equation [11]
d_2' = defined by Equation [12]
e = base (2.718) of natural system of logarithms
E = Young's modulus
$f(\xi, \tau)$ = temperature-distribution function
f_i = initial temperature = const
h = coefficient of convective heat transfer
$h' = \frac{ha}{k}$
k = thermal conductivity
p = numerator of $\bar{\theta}(\xi, S)$
q' = first derivative of denominator of $\bar{\theta}(\xi, S)$ with respect to S
S = Laplace transform parameter
t = time
X = distance from insulated surface
$A, B_1, B_2, b_1, b_2, C, C_1, C_2, D_1, D_2, d_1, d_2$ = const
α = thermal diffusivity of slab

[1] Development Engineer, Republic Aviation Corporation. Assoc. Mem. ASME.

[2] See Appendix 1.

[3] See Appendix 2.

[4] Numbers in parentheses refer to the Bibliography at the end of the paper.

Contributed by the Heat Transfer Division and presented at the Annual Meeting, New York, N. Y., December 1–6, 1957, of The American Society of Mechanical Engineers.

Note: Statements and opinions advanced in papers are to be understood as individual expressions of their authors and not those of the Society. Manuscript received at ASME Headquarters, April 1, 1957. Paper No. 57—A-9.

α_j's = roots of transcendental equation
$\bar{\alpha}$ = coefficient of thermal expansion
$\beta_1 = B_1'D_1$
$\beta_2 = B_1'D_2$
$\beta_3 = B_1'C$
$\beta_4 = B_2'D_1$
$\beta_5 = B_2'D_2$
$\beta_6 = B_2'C$
$\beta_7 = A'D_1$
$\beta_8 = A'D_2$
$\beta_9 = A'C$
$\gamma_1 = b_1' + d_1'$
$\gamma_2 = b_1' + d_2'$
$\gamma_3 = b_1'$
$\gamma_4 = b_2' + d_1'$
$\gamma_5 = b_2' + d_2'$
$\gamma_6 = b_2'$
$\gamma_7 = d_1'$
$\gamma_8 = d_2'$
$\gamma_9 = 0$
$\bar{\theta}(\xi, S)$ = Laplace transform of temperature distribution $f(\xi, \tau)$
$\theta(x, t)$ = temperature distribution
θ_{aw} = adiabatic wall temperature
θ_i = initial temperature = const
λ_j = roots of transcendental Equation [50]
ν = Poisson's ratio
$\xi = X/A$
σ = thermal stress
$\tau = \dfrac{\alpha t}{a^2}$

Mathematical Analysis

Temperature Distribution. Consider the general case of transient one-dimensional heat flow in a material of constant properties with the coefficient of heat transfer and adiabatic wall temperature both dependent on time for the simple geometry shown in Fig. 1.

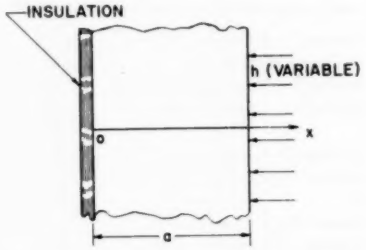

Fig. 1 Portion of Cross Section of Slab Studied

The basic differential equation is given by

$$\frac{\partial\theta(x, t)}{\partial t} = \alpha \frac{\partial^2\theta(x, t)}{\partial x^2} \quad [1]$$

The initial condition is

$$\theta(x, 0) = \theta_i \quad [2]$$

The two-boundary conditions are

$$\frac{\partial\theta(0, t)}{\partial x} = 0 \quad [3]$$

and

$$\frac{\partial\theta(a, t)}{\partial x} = -\frac{h}{k}[\theta(a, t) - \theta_{aw}(t)] \quad [4]$$

where

$$h = B_1e^{-b_1t} + B_2e^{-b_2t} + A \quad [5]$$

$$\theta_{aw} = D_1e^{-d_1t} + D_2e^{-d_2t} + C \quad [6]$$

Let

$$x = a\xi \quad [7]$$

$$t = \frac{a^2}{\alpha}\tau \quad [8]$$

$$b_1' = \frac{a^2}{\alpha} b_1 \quad [9]$$

$$b_2' = \frac{a^2}{\alpha} b_2 \quad [10]$$

$$d_1' = \frac{a^2}{\alpha} d_1 \quad [11]$$

$$d_2' = \frac{a^2}{\alpha} d_2 \quad [12]$$

$$h' = \frac{a}{k} h \quad [13]$$

$$B_1' = \frac{a}{k} B_1 \quad [14]$$

$$B_2' = \frac{a}{k} B_2 \quad [15]$$

$$A' = \frac{a}{k} A \quad [16]$$

$$\theta(x, t) = f(\xi, \tau) \quad [17]$$

and

$$\theta_i = f_i = \text{const} \quad [18]$$

Then

$$dx = ad\xi \quad [19]$$

$$dt = \frac{a^2}{\alpha} d\tau \quad [20]$$

$$\frac{\partial\theta}{\partial t} = \frac{\alpha}{a^2} \frac{\partial f}{\partial \tau} \quad [21]$$

and

$$\frac{\partial^2\theta}{\partial x^2} = \frac{1}{a^2} \frac{\partial^2 f}{\partial \xi^2} \quad [22]$$

Introducing these definitions, Equations [1] to [6] become

$$\frac{\partial f}{\partial \tau} = \frac{\partial^2 f}{\partial \xi^2} \quad [23]$$

$$f(\xi, 0) = f_i \quad [24]$$

$$\frac{\partial f(0, \tau)}{\partial \xi} = 0 \quad [25]$$

$$\frac{\partial f(1, \tau)}{\partial \xi} = -\frac{ha}{k}[f(1, \tau) - f_{aw}(\tau)] \quad [26]$$

$$h' = \frac{ha}{k} = B_1'e^{-b_1'\tau} + B_2'e^{-b_2'\tau} + A' \quad [27]$$

$$f_{aw} = D_1e^{-d_1'\tau} + D_2e^{-d_2'\tau} + C \quad [28]$$

Equation [26] can be rewritten as

$$\frac{\partial f(1,\tau)}{\partial \xi} = -f(1,\tau)\sum_{n=1}^{3} B_n' e^{-b_n'\tau} + \sum_{m=1}^{9} \beta_m e^{-\gamma_m \tau} \quad [29]$$

Let $\bar{\theta}(\xi, S)$ = Laplace transform of the temperature $f(\xi, \tau)$, where S is the Laplace transform parameter. Then Equation [23] can be rewritten as

$$S\bar{\theta}(\xi, S) - f(\xi, 0) = \bar{\theta}_{\xi\xi}(\xi, S)$$

or

$$S\bar{\theta}(\xi, S) - \theta_i = \bar{\theta}_{\xi\xi}(\xi, S) \quad [30]$$

The transformed boundary conditions are

$$\frac{\partial \bar{\theta}(0, S)}{\partial \xi} = 0 \quad [31]$$

and

$$\frac{\partial \bar{\theta}(1, S)}{\partial \xi} = -\sum_{n=1}^{3} B_n' \bar{\theta}(1, S + b_n') + \sum_{m=1}^{9} \frac{\beta_m}{S + \gamma_m} \quad [32]$$

The general solution of Equation [30] is

$$\bar{\theta}(\xi, S) = C_1 \cosh \sqrt{(S)}\xi + C_2 \sinh \sqrt{(S)}\xi + \frac{\theta_i}{S} \quad [33]$$

Differentiating Equation [33] with respect to ξ, one obtains

$$\frac{\partial \bar{\theta}(\xi, S)}{\partial \xi} = C_1 \sqrt{S} \sinh \sqrt{(S)}\xi + C_2 \sqrt{S} \cosh \sqrt{(S)}\xi \quad [34]$$

From Equation [31] one can conclude that

$$C_2 = 0 \quad [35]$$

Hence

$$\bar{\theta}(\xi, S) = C_1 \cosh \sqrt{(S)}\xi + \frac{\theta_i}{S} \quad [36]$$

From Equation [32] one obtains

$$C_1 \sqrt{S} \sinh \sqrt{S} = -\sum_{n=1}^{3} B_n' \left[C_1 \cosh (S + b_n')^{1/2} + \frac{\theta_i}{S + b_n'} \right] + \sum_{m=1}^{9} \frac{\beta_m}{S + \gamma_m} \quad [37]$$

or

$$C_1 = \frac{-\theta_i \sum_{n=1}^{3} \frac{B_n'}{S + b_n'} + \sum_{m=1}^{9} \frac{\beta_m}{S + \gamma_m}}{\sqrt{S} \sinh \sqrt{S} + \sum_{n=1}^{3} B_n' \cosh (S + b_n')^{1/2}} \quad [38]$$

Substituting Equation [38] into Equation [36], one obtains

$$\bar{\theta}(\xi, S) = \frac{\left[-\theta_i \sum_{n=1}^{3} \frac{B_n'}{S + b_n'} + \sum_{m=1}^{9} \frac{\beta_m}{S + \gamma_m} \right] \cosh \sqrt{(S)}\xi}{\sqrt{S} \sinh \sqrt{S} + \sum_{n=1}^{3} B_n' \cosh (S + b_n')^{1/2}} + \frac{\theta_i}{S} \quad [39]$$

The poles of Equation [39] are

$$S = 0$$

$$S = -b_n' \qquad n = 1, 2,$$

$$S = -\gamma_m \qquad m = 1, 2, \ldots, 8$$

$$S = \alpha_j \qquad j = 1, 2, \ldots, j, \ldots$$

where α_j's are roots of the transcendental equation

$$\sqrt{S} \sinh \sqrt{S} + \sum_{n=1}^{3} B_n' \cosh (S + b_n')^{1/2} = 0 \quad [40]$$

After performing the necessary manipulations (2, 8) and simplifications, the solution of Equation [23] becomes

$$f(\xi, \tau) = \frac{\beta_0 + \theta_i \sum_{n=1}^{2} B_n' \cosh \sqrt{b_n'}}{\sum_{n=1}^{3} B_n' \cosh \sqrt{b_n'}} + \sum_{n=1}^{2} \frac{-B_n'\theta_i [\cos \sqrt{b_n'}\xi] e^{-b_n'\tau}}{-\sqrt{b_n'} \sin \sqrt{b_n'} + \sum_{m=1}^{3} B_m' \cosh (-b_n' + b_m')^{1/2}} + \sum_{m=1}^{8} \frac{\beta_m [\cos \sqrt{\gamma_m}\xi] e^{-\gamma_m \tau}}{-\sqrt{\gamma_m} \sin \sqrt{\gamma_m} + \sum_{n=1}^{3} B_n' \cosh (-\gamma_m + b_n')^{1/2}} + \sum_{j=1}^{\infty} \frac{\left[-\theta_i \sum_{n=1}^{3} \frac{B_n'}{\alpha_j + b_n'} + \sum_{m=1}^{9} \frac{\beta_m}{\alpha_j + \gamma_m} \right] [\cosh (\alpha_j)^{1/2}\xi] e^{\alpha_j \tau}}{\frac{1 + A'}{2\sqrt{\alpha_j}} \sinh \sqrt{\alpha_j} + \frac{1}{2} \cosh \sqrt{\alpha_j} + \sum_{n=1}^{2} \frac{B_n' \sinh (\alpha_j + b_n')^{1/2}}{2(\alpha_j + b_n')^{1/2}}} \quad [41]$$

Hence, the general solution of Equation [1] with initial and boundary conditions as given by Equations [2] to [4] is

$$\theta(x, t) = \frac{\beta_0 + \theta_i \sum_{n=1}^{2} B_n' \cosh \sqrt{b_n'}}{\sum_{n=1}^{3} B_n' \cosh \sqrt{b_n'}} + \sum_{n=1}^{2} \frac{-B_n'\theta_i \left[\cos (b_n')^{1/2} \frac{x}{a} \right] e^{-b_n' \frac{a}{a^2} t}}{-\sqrt{b_n'} \sin \sqrt{b_n'} + \sum_{m=1}^{3} B_m' \cosh (-b_n' + b_m')^{1/2}} + \sum_{m=1}^{8} \frac{\beta_m \left[\cos \sqrt{\gamma_m} \frac{x}{a} \right] e^{-\gamma_m \frac{a}{a^2} t}}{-\sqrt{\gamma_m} \sin \sqrt{\gamma_m} + \sum_{n=1}^{3} B_n' \cosh (-\gamma_m + b_n')^{1/2}} + \sum_{j=1}^{\infty} \frac{2 \left[-\theta_i \sum_{n=1}^{3} \frac{B_n'}{\alpha_j + b_n'} + \sum_{m=1}^{9} \frac{\beta_m}{\alpha_j + \gamma_m} \right] \left[\cosh (\alpha_j)^{1/2} \frac{x}{a} \right] e^{\alpha_j \frac{a}{a^2} t}}{\frac{1 + A'}{\sqrt{\alpha_j}} \sinh \sqrt{\alpha_j} + \cosh \sqrt{\alpha_j} + \sum_{n=1}^{2} \frac{B_n' \sinh (\alpha_j + b_n')^{1/2}}{(\alpha_j + b_n')^{1/2}}} \quad [42]$$

Thermal Stress. Let σ_y and σ_z be the thermal stresses perpendicular to the X-axis of Fig. 1 in the y and z-directions, respectively, then

$$\sigma_y = \sigma_z = -\frac{\bar{\alpha}E\theta(x,t)}{1-\nu} + \frac{\bar{\alpha}E\theta_1(t)}{a(1-\nu)} + \frac{\bar{\alpha}E\theta_2(t)}{(1-\nu)} \quad [43]$$

where $\bar{\alpha}$ and E are constants

$$\theta_1(t) = \frac{\beta_0 + \theta_i \sum_{n=1}^{2} B_n' \cosh \sqrt{b_n'}}{\sum_{n=1}^{3} B_n' \cosh \sqrt{b_n'}}\, a + \sum_{n=1}^{2} \frac{-B_n'\theta_i a\,[\sin (b_n')^{1/2}]e^{-b_n' \frac{\alpha}{a^2}t}}{-\sqrt{b_n'} \sin \sqrt{b_n'} + \sum_{m=1}^{3} B_m' \cosh (-b_n' + b_m')^{1/2}}$$

$$+ \sum_{m=1}^{8} \frac{\beta_m a\,[\sin (\gamma_m)^{1/2}]e^{-\gamma_m \frac{\alpha}{a^2}t}}{-\gamma_m \sin \sqrt{\gamma_m} + \sqrt{\gamma_m} \sum_{n=1}^{3} B_n' \cosh (-\gamma_m + b_n')^{1/2}}$$

$$+ \sum_{j=1}^{\infty} \frac{2a\left[-\theta_i \sum_{n=1}^{3} \frac{B_n}{\alpha_j + b_n'} + \sum_{m=1}^{9} \frac{\beta_m}{\alpha_j + \gamma_m}\right][\sinh (\alpha_j)^{1/2}]e^{\alpha_j \frac{\alpha}{a^2}t}}{(1+A')\sinh \sqrt{\alpha_j} + \sqrt{\alpha_j} \cosh \sqrt{\alpha_j} + \sqrt{\alpha_j} \sum_{n=1}^{2} \frac{B_n' \sinh (\alpha_j + b_n')^{1/2}}{(\alpha_j + b_n')^{1/2}}} \quad [44]$$

$$\theta_2(t) = \sum_{n=1}^{2} \frac{-a^2 B_n'\theta_i e^{-b_n' \frac{\alpha}{a^2}t} \left\{\frac{1}{\sqrt{b_n'}}[\cos \sqrt{b_n'} - 1] + \frac{1}{2} \sin \sqrt{b_n'}\right\}}{-b_n' \sin \sqrt{b_n'} + \sqrt{b_n'} \sum_{m=1}^{3} B_m' \cosh (-b_n' + b_m')^{1/2}}$$

$$+ \sum_{m=1}^{8} \frac{a^2 \beta_m e^{-\gamma_m \frac{\alpha}{a^2}t} \left\{\frac{1}{\sqrt{\gamma_m}}[\cos \sqrt{\gamma_m} - 1] + \frac{1}{2} \sin \sqrt{\gamma_m}\right\}}{-\gamma_m \sin \sqrt{\gamma_m} + \sqrt{\gamma_m} \sum_{n=1}^{3} B_n' \cosh (-\gamma_m + b_n')^{1/2}}$$

$$+ \sum_{j=1}^{\infty} \frac{2a^2\left[-\theta_i \sum_{n=1}^{3} \frac{B_n'}{\alpha_j + b_n'} + \sum_{m=1}^{9} \frac{\beta_m}{\alpha_j + \gamma_m}\right] e^{\alpha_j \frac{\alpha}{a^2}t}\left[\frac{1 - \cosh \sqrt{\alpha_j}}{\sqrt{\alpha_j}} + \frac{\sinh \sqrt{\alpha_j}}{2}\right]}{(1+A')\sinh \sqrt{\alpha_j} + \sqrt{\alpha_j} \cosh \sqrt{\alpha_j} + \sqrt{\alpha_j} \sum_{n=1}^{2} \frac{B_n' \sinh (\alpha_j + b_n')^{1/2}}{(\alpha_j + b_n')^{1/2}}} \quad [45]$$

Acknowledgment

The author wishes to thank Mr. F. J. Mulholland, Chief Development Engineer, Republic Aviation Corporation, for permission to publish this material. This work was carried out under the supervision of Mr. H. Lu, Chief Aero-Thermo-Dynamics, Development Engineering, Republic Aviation Corporation, Farmingdale, N. Y.

Bibliography

1 "Heat Transfer," by M. Jakob, John Wiley & Sons, Inc., New York, N. Y., second printing, vol. 1, 1950, p. 270.

2 "Conduction of Heat in Solids," by H. S. Carslaw and J. C. Jaeger, Oxford University Press, London, England, first edition, second impression, 1950, pp. 85, 93, and 266.

3 "Temperature Distributions in Slabs With a Linear Temperature Rise at One Surface," by M. L. Anthony, General Discussion on Heat Transfer, The Institution of Mechanical Engineers, London, England, 1951, p. 250.

4 "Design Charts for Transient Temperature Distribution Resulting From Aerodynamic Heating at Supersonic Speeds," by J. Kaye and Victor C. M. Yeh, *Journal of the Aeronautical Sciences*, vol. 22, November, 1955, p. 755.

5 "Transient Temperature Distribution in Slabs Resulting From Aerodynamic Heating at Supersonic Speeds With Variable Coefficients of Heat Transfer and Constant Adiabatic Wall Temperature," by S. Y. Chen and D. Young, McDonnell Aircraft Corporation, St. Louis, Mo., report in preparation.

6 "Theory of Elasticity," by S. Timoshenko and J. N. Goodier, McGraw-Hill Book Company, Inc., New York, N. Y., second edition, second impression, 1951, p. 401.

7 "Thermal Buckling of Supersonic Wing Panels," by N. J. Hoff, *Journal of the Aeronautical Sciences*, vol. 23, November, 1956, p. 1019.

8 "Modern Operational Mathematics in Engineering," by R. V. Churchill, McGraw-Hill Book Company, Inc., New York, N. Y., 1944, p. 148.

Appendix 1

The sum of two exponential functions of time and a constant were chosen to represent the coefficient of heat transfer and the adiabatic wall temperature since they approximate the conditions present in actual aerodynamic heating problems to a greater degree than one exponential function of time and a constant. In general, one can choose as many exponential functions as are necessary in order to approximate actual conditions. Fig. 2 shows typical curves for various combinations of exponential functions of time.

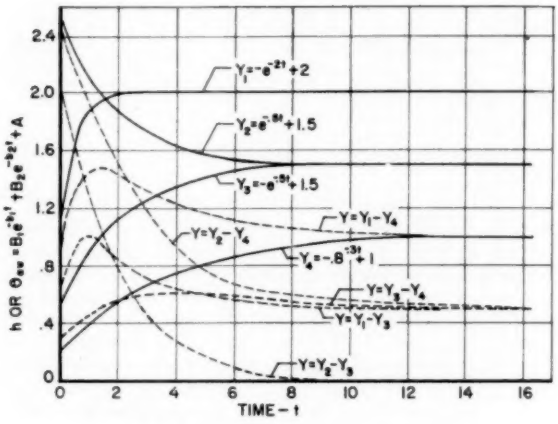

FIG. 2 h OR θ_{aw} VERSUS TIME t

Appendix 2

SOLUTIONS OF THREE SPECIAL PROBLEMS

Three special cases are chosen to show that the general solution also can be applied to simpler problems.

Case I. This is the case of constant coefficient of heat transfer and constant adiabatic wall temperature, where

$$B_1 = B_2 = b_1 = b_2 = D_1 = D_2 = d_1 = d_2 = 0$$

or

$$h = A = \text{const} \quad [46]$$

$$\theta_{aw} = C = \text{const} \quad [47]$$

Hence

$$b_1 = b_2 = d_1 = d_2 = B_1 = B_2 = \beta_1 = \beta_2 = \beta_3 = \beta_4 = \beta_5 = \beta_6 = \beta_7 = \beta_8 = \gamma_1 = \gamma_2 = \gamma_3 = \gamma_4 = \gamma_5 = \gamma_6 = \gamma_7 = \gamma_8 = 0$$

Then Equation [40] reduces to

$$\sqrt{S}\sinh\sqrt{S} + A'\cosh\sqrt{S} = 0 \quad [48]$$

Substituting Equations [16] and [46] into Equation [48] one obtains

$$\sqrt{S}\sinh\sqrt{S} + \frac{ha}{k}\cosh\sqrt{S} = 0 \quad [49]$$

It was shown (2) that Equation [49] cannot have pure imaginary roots or complex roots. Let the roots of S be

$$S = -(\lambda_j)^2 \quad [50]$$

Then Equation [49] becomes

$$-\lambda_j\sin\lambda_j + \frac{a}{k}h\cos\lambda_j = 0 \quad [51]$$

and the solution becomes

$$\theta(x,t) = \theta_{aw} - 2(\theta_i - \theta_{aw})\sum_{j=1}^{\infty} \frac{\frac{a}{k}h\left[\cos\lambda_j\frac{x}{a}\right]e^{-\lambda_j^2\frac{\alpha}{a^2}t}}{-\lambda^2\left(1+a\frac{h}{k}\right)\frac{\sin\lambda_j}{\lambda_j} - \lambda_j^2\cos\lambda_j}$$

$$= \theta_{aw} + 2(\theta_i - \theta_{aw})\sum_{j=1}^{\infty} \frac{\sin\lambda_j\left[\cos\lambda_j\frac{x}{a}\right]e^{-\lambda_j^2\frac{\alpha}{a^2}t}}{\cos\lambda_j\sin\lambda_j + \lambda_j} \quad [52]$$

This is a well-known result[5] where λ_j's are roots of Equation [49].

Case II. The case of variable coefficient of heat transfer and constant adiabatic wall temperature where

$$h = B_1e^{-b_1t} + B_2e^{-b_2t} + A \quad [53]$$

$$\theta_{aw} = C \quad [54]$$

Hence

$$D_1 = D_2 = d_1 = d_2 = d_1' = d_2' = \beta_1 = \beta_2 = \beta_3 = \beta_4 = \beta_5 = \beta_6 = \beta_7 = \beta_8 = \gamma_7 = \gamma_8 = 0$$

$$\beta_3 = B_1'C$$

$$\beta_5 = B_2'C$$

$$\beta_9 = A'C$$

$$\gamma_1 = \gamma_2 = \gamma_3 = b_1'$$

$$\gamma_4 = \gamma_5 = \gamma_6 = b_2'$$

Then Equation [40] remains unchanged or

$$\sqrt{S}\sinh\sqrt{S} + \sum_{n=1}^{3} B_n'\cosh(S + b_n')^{1/3} = 0 \quad [55]$$

and Equation [42] reduces to

$$\theta(x,t) = \frac{A'\theta_{aw} + \theta_i\sum_{n=1}^{2} B_n'\cosh\sqrt{b_n'}}{\sum_{n=1}^{3} B_n'\cosh\sqrt{b_n'}} - (\theta_i - \theta_{aw})\sum_{n=1}^{2} \frac{B_n'\left[\cos\sqrt{(b_n')}\frac{x}{a}\right]e^{-b_n'\frac{\alpha}{a^2}t}}{-\sqrt{b_n'}\sin\sqrt{b_n'} + \sum_{m=1}^{3} B_m'\cosh(-b_n' + b_m')^{1/3}}$$

$$- (\theta_i - \theta_{aw})\sum_{j=1}^{\infty} \frac{2\left[\sum_{n=1}^{3}\frac{B_n'}{\alpha_j + b_n'}\right]\left[\cosh\sqrt{(\alpha_j)}\frac{x}{a}\right]e^{\gamma_j\frac{\alpha}{a^2}t}}{\frac{1+A'}{\sqrt{\gamma_j}}\sinh\sqrt{\alpha_j} + \cosh\sqrt{\alpha_j} + \sum_{n=1}^{\infty}\frac{B_n'\sinh(\alpha_j + b_n')^{1/3}}{(\alpha_j + b_n')^{1/3}}} \quad [56]$$

where α_j's are roots of Equation [55].

Case III. The case of variable coefficient of heat transfer and variable adiabatic wall temperature approximated by one exponential function of time where

$$h = B_1e^{-b_1t} + A \quad [57]$$

$$\theta_{aw} = D_1e^{-d_1t} + C \quad [58]$$

Hence

$$B_2 = B_2' = b_1 = b_2' = D_2 = d_2 = d_2' = \beta_2 = \beta_4 = \beta_5 = \beta_6 = \beta_8 = \gamma_5 = \gamma_6 = \gamma_8 = 0$$

[5] Given in reference (1), p. 272.

$$\beta_1 = B_1'D_1 \qquad \beta_3 = B_1'C \qquad \beta_7 = A'D_1 \qquad \beta_9 = A'C \qquad \gamma_1 = b_1' + d_1' \qquad \gamma_2 = b_1' = \gamma_3 \qquad \gamma_4 = d_1 = \gamma_7$$

Then Equation [40] becomes

$$\sqrt{S}\sinh\sqrt{S} + B_1'\cosh(S + b_1')^{1/3} + A'\cosh\sqrt{S} = 0 \quad [59]$$

and the solution becomes

$$\theta(x,t) = \frac{A'C + B_1'\theta_i\cosh\sqrt{b_1'}}{B_1'\cosh\sqrt{b_1'} + A'} - \frac{(\theta_i - C)B_1'\left[\cos\sqrt{(b_1')}\,\frac{x}{a}\right]e^{-b_1'\frac{\alpha}{a^2}t}}{-\sqrt{b_1'}\sin\sqrt{b_1'} + B_1' + A'\cos\sqrt{b_1'}}$$

$$+ \frac{B_1'D_1\left[\cos(b_1' + d_1')^{1/3}\,\frac{x}{a}\right]e^{-(b_1'+d_1')\frac{\alpha}{a^2}}}{-(b_1' + d_1')^{1/3}\sin(b_1' + d_1')^{1/3} + B_1'\cos\sqrt{d_1'} + A'\cos(b_1' + d_1')^{1/3}}$$

$$+ \frac{A'D_1\left[\cos\sqrt{(d_1')}\,\frac{x}{a}\right]e^{-d_1'\frac{\alpha}{a^2}t}}{-\sqrt{d_1'}\sin\sqrt{d_1'} + B_1'\cosh(-d_1' + b_1')^{1/3} + A'\cos\sqrt{d_1'}}$$

$$+ \sum_{j=1}^{\infty} \frac{2\left[(C - \theta_i)\left(\frac{B_1'}{\alpha_j + b_1'} + \frac{A'}{\alpha_j}\right) + \frac{B_1'D_1}{\alpha_j + b_1' + d_1'} + \frac{A'D_1}{\alpha_j + d_1}\right]\left[\cosh(\alpha_j)\,\frac{x}{a}\right]e^{\alpha_j\frac{\alpha}{a^2}t}}{\frac{1 + A'}{\sqrt{\alpha_j}}\sinh\sqrt{\alpha_j} + \cosh\sqrt{\alpha_j} + \frac{B_1'}{(\alpha_j + b_1')^{1/3}}\sinh(\alpha_j + b_1')^{1/3}} \quad [60]$$

where α_j's are roots of Equation [59]. For some particular values of A', B_1', and b_1', one can find roots in reference (5).

Discussion

G. M. Dusinberre.[6] In this paper the author invites the practicing engineer to do the following:

(*a*) Confine his attention to situations where the heat flow is one-dimensional and where one boundary is adiabatic.

(*b*) Calculate h and θ_{aw} for the expected trajectory and tabulate sufficient values as functions of time.

(*c*) Assume the functional forms of Equations [5] and [6], and from the tabulated calculations determine the constants in those equations.

(*d*) Evaluate the quantities defined by Equations [7] through [16], and the β and γ defined in the nomenclature.

(*e*) Find a number of roots of the transcendental Equation [40]. Incidentally, one has no way of knowing in advance how many roots may be necessary for convergence of the series.

(*f*) Solve Equation [42] for each and every combination of x and t which may be of interest.

Whatever this may be, it is not good engineering.

The situation is well summed up in the author's reference (3). Mr. Anthony evolved several pages of equations of the same general nature as those of the present paper, though individually somewhat less appalling. In his closure Mr. Anthony said he "agreed that the analytical results reported in his paper were both distressing and a burden to the literature." He further stated that he "had been convinced that the numerical approach, with a few modifications, was the best for solving transient heat-conduction problems."[7]

In a numerical approach to the present problem we would do the following:

(*a*) If the far side of the wall were not adiabatic, we would go ahead and calculate accordingly.

(*b*) We would calculate h and θ_{aw} the same as the author.

(*c*) We would not bother to write a function relation but would use the tabulated functions of time. We would then go ahead and compute θ at selected intervals of x over the whole range of t. Each calculation is a simple arithmetical operation. A very similar problem has been worked out by the writer.[8]

When the entire temperature distribution is known, the stress distribution can, in principle, be calculated for the assumed unconstrained plate. Thus Equations [44] and [45] might also be replaceable by some simpler forms.

Incidentally, the "hypersonic" feature has nothing to do with the solution. The author's method is equally applicable to subsonic conditions.

[6] Professor of Mechanical Engineering, The Pennsylvania State University, University Park, Pa. Fellow ASME.

[7] Author's reference (3), p. 307.

Author's Closure

The author appreciates Professor Dusinberre's comments concerning the present paper. As the author has pointed out in the presentation, there are some limitations in the analytical solution. For instance, in this case, (*a*) radiation has been neglected and (*b*) the thermal properties of the material have been assumed constant. It is also required that the coefficient of heat transfer and the adiabatic wall temperature for the expected trajectory be approximated by exponential functions. The roots of the transcendental equation have to be obtained, but these limitations are encountered in most classical analytical solutions. It is not characteristic of this analysis alone. The present analysis actually gives a more general solution which includes some of those classical analyses listed in the Bibliography.

In the discussion of "Report on Strength of Welded Joints in Carbon Steel at Elevated Temperatures," TRANS. ASME, vol. 80, 1958, Professor Dusinberre said, "when a digital computer is to be used, and when an analytical solution is not obtainable anyway, there is often a great saving of time and effort in proceeding on a finite-difference basis throughout." The author fully agrees with his statement. The great advantage of the analytical solution is that the result can be applied directly to find a temperature or the thermal stress at a particular point at a particular time. The numerical solution requires the computation to be performed from the boundary and from zero time.

[8] G. M. Dusinberre, "Numerical Analysis of Heat Flow," McGraw-Hill Book Company, Inc., New York, N. Y., 1949, p. 205.

Boiling Heat Transfer to Water Containing a Volatile Additive

By G. LEPPERT,[1] C. P. COSTELLO,[2] AND B. M. HOGLUND[3]

Aspects of local boiling in forced circulation when the boiling fluid contains small percentages of alcohol are discussed. Particular emphasis is placed on the improvement in smoothness of boiling and in the decrease of average bubble size when the additive is present, as contrasted with boiling distilled water. Experimental results, including photographs, are presented for surface boiling from the outside of a cylindrical stainless-steel tube placed normal to the flow. Data are also presented for the subcooled boiling of distilled water, and comparisons are made with correlations from the literature.

Nomenclature

THE following nomenclature is used in the paper:

A = area, sq ft
C = constants; dimensions as specified by equations where they are used
c = specific heat, Btu/lb$_M$ deg F
D = diameter, ft
g = local acceleration of gravity, ft/hr^2
g_0 = constant of proportionality of Newton's second law, (lb$_M$/lb$_F$)(ft/hr^2)
G = mass flow, ρv, lb$_M$/hr-sq ft
h = film coefficient of heat transfer, Btu/hr-sq ft deg F
k = thermal conductivity, Btu/hr-ft deg F
P = pressure, lb$_F$/sq ft
q'' = surface heat flux, Btu/hr-sq ft
q''' = energy generation of unit volume, Btu/hr cu ft
R = electrical resistance, ohms
r = exponent in Rohsenow's equation
s = exponent in Rohsenow's equation
T = temperature, deg F; ΔT = temperature difference, deg F
V = volume, cu ft
x = distance, ft, measured from axis of heating surface
α = variation of electrical resistivity with temperature $\frac{1}{R_0}\frac{dR}{dT}$
β = bubble contact angle, angular degrees
γ = variation of thermal conductivity with temperature, $\frac{1}{k_0}\frac{dk}{dT}$
λ = latent heat of vaporization, Btu/lb
ρ = density, lb$_M$/cu ft
σ = surface tension, lb$_F$/ft
μ = viscosity, lb$_F$/ft hr

Subscripts

b = conditions attributable to boiling
c = conditions attributable to forced convection
cr = conditions at critical point of substance
F = force, to distinguish pounds force (lb$_F$) from pounds mass (lb$_M$)
l = liquid conditions
M = mass, to distinguish pounds mass (lb$_M$) from pounds force (lb$_F$)
o = conditions at inner surface (except as defined in connection with g_0)
p = constant pressure
sf = particular surface-fluid combination
V = vapor
w = conditions at outer wall of heating surface
x = used with ΔT, signifies temperature difference between heating surface and saturation temperature of fluid

Introduction

Utilization of the nucleate-boiling phenomenon in liquid coolants without net vapor generation is becoming more and more attractive in a number of high-performance heat-transfer applications. This mechanism, which is frequently called local boiling, permits the transfer of heat from a surface at a high rate with a relatively small temperature difference.

Typical applications for which local-boiling heat transfer may be advantageous include nuclear-reactor fuel elements, electronic-power-tube cooling coils, and rocket-engine cooling jackets. In most applications, it is desirable that vapor formation be as steady and smooth as possible, and in local boiling especially, smoothness is promoted by factors which tend to decrease the average size of bubbles leaving the heated surface.

Consequently, it was considered to be of considerable practical importance, as well as of academic interest, when it was observed that very small amounts of certain organic fluids, when added to distilled water, decreased average bubble size and produced much smoother boiling than could be obtained with water alone. Furthermore, the generally desirable characteristics of water as a coolant were not sacrificed by the small additions.

The most apparent reason for desiring smooth and steady bubble formation exists in nuclear-reactor fuel channels where the coolant also serves as a neutron moderator. In this application, the reactor power level is strongly affected by the total mass of coolant in the fuel channels. If large aggregates of vapor are continually forming and collapsing, there will be a variation in the amount of moderator in the core and a tendency for the reactor power to oscillate.

In addition to the desirability of smooth vapor formation in any boiling nuclear reactor, there is a further advantage to small bubble size in a reactor in which only local boiling is permitted. It is characteristic of forced convection local boiling that the bubbles grow on the heated surface to a maximum size, then collapse as they break away and encounter the main stream of fluid, which is at a temperature less than saturation. From the standpoint of average coolant density in a narrow channel, smaller bubble size will result in a relatively greater average volume occupied by liquid, and consequently in a greater average density.

[1] Associate Professor of Mechanical Engineering, Stanford University, Stanford, California. Assoc. Mem. ASME.
[2] Acting Instructor and Research Assistant, Stanford University, Stanford, California.
[3] Argonne National Laboratory, Lemont, Illinois. Assoc. Mem. ASME.

Contributed by the Heat Transfer Division and presented at a joint session with the Nuclear Engineering Division at the Annual Meeting, New York, N. Y., December 1–6, 1957, of THE AMERICAN SOCIETY OF MECHANICAL ENGINEERS.
NOTE: Statements and opinions advanced in papers are to be understood as individual expressions of their authors and not those of the Society. Manuscript received at ASME Headquarters, July 31, 1957. Paper No. 57—A-81.

The combination of more even boiling and smaller bubble size during forced-convection local boiling in a channel should also result in a lower static pressure drop and smaller pumping power. However, this situation has not yet been explored and will not be discussed in this paper.

The present investigation consisted of the observation of the effect of up to 2.65-per-cent-by-weight isopropyl or methyl alcohol on the nucleate-boiling characteristics of distilled water. In addition to observing and photographing the character of bubble formation, careful measurements were made to determine the variation of the heat flux with the temperature difference from the surface to the liquid. The power level was increased in increments until the burnout point was reached, at which point the nucleate boiling ended and film boiling commenced. With water, this phenomenon is generally accompanied by failure of the heater, since the surface temperature required to transmit the peak (or burnout) heat flux in film boiling is above the melting point of the common metals.

Because there is need for additional experimental information for the forced convection boiling of pure water flowing across tubes, nucleate boiling and burnout measurements are also reported without the additives which are of primary interest to this investigation. These measurements are needed here for comparison, and they are also useful as a confirming check on the correlation proposed by Rohsenow (1)[4] for nucleate boiling heat transfer.

Experimental Apparatus

The measurements reported in this paper were made on an electrically-heated Type 304 stainless-steel tube which was oriented in a $1 \times 4^1/_2$-in. rectangular channel with fluid flow normal to the tube axis. The channel was provided with pyrex glass windows front and back which permitted visual observation of the heating tube. Each tube that was used was 0.110-in. OD with 0.011-in. wall.

The tubes used in the propanol-water series of tests were cleaned before use by complete immersion in nitric acid for approximately 2 min before installation in the flow channel. The tubes used in the methanol-water series of tests were immersed in water and electrically heated to produce film boiling. The tube surface temperature was thus held at approximately 2000 F for about 2 min. After this the loose oxide scale was removed with fine emery cloth and the surface washed with a detergent. This treatment leaves a stable oxide film on the surface, which is advantageous from the standpoint of reproducibility of results in film boiling. This treatment was employed because these particular tubes were to be employed in film boiling experiments as well as in the tests reported in the present paper.

The vertical rectangular test channel formed part of a heat-transfer loop, shown schematically in Fig. 1. The piping in this loop is entirely of pyrex glass except for an Inconel section 45 in. long which adapts the circular pyrex pipe to the rectangular section housing the treated tube. The heating tube is shown in Fig. 2. Teflon gaskets are employed between all of the flanged joints, while the pump and other metallic fittings are of stainless steel.

The liquid flow rate is measured to ± 1 per cent accuracy with a gravimetrically calibrated stainless-steel orifice used with a 60-in. water manometer. Manual flow control is afforded by a throttling valve on the discharge side of the centrifugal pump.

Connections are made to the stainless-steel heater tube by silver-soldering $^1/_2$-in. diam copper pieces to each end. The copper extends $^3/_{16}$ in. into the flow stream from each side and provides the means for bringing 60-cycle ac into the tube to provide resistance heating. The rate of heat addition was measured electrically, using an ammeter and voltmeter, with voltage taps attached to the surface of the stainless-steel heat-transfer surface during the first of the tests. Later, the voltage taps were fastened to the copper rods protruding from the rectangular channel, since the voltage drop between the rods and the ends of the stainless-steel tube was shown to be negligible. The range of heat flux used in these tests was up to 1,174,000 Btu/hr-sq ft.

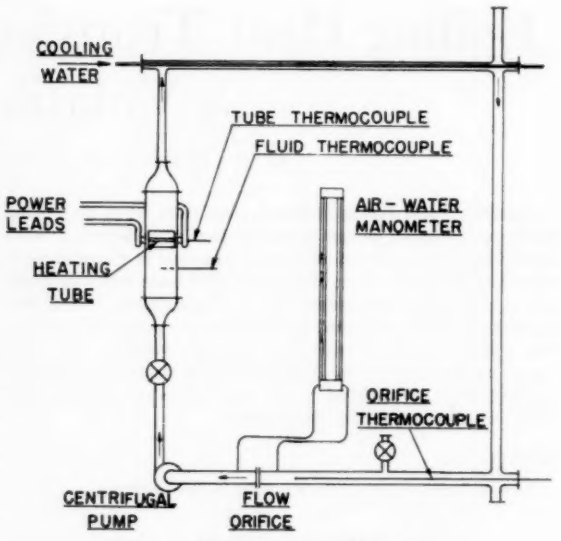

Fig. 1 Schematic diagram of test loop

Temperature measurements were made in three places: In the liquid just ahead of the flow orifice; in the liquid just ahead of the test section; and inside the heated tube, at the center of its length. Calibrated platinum to platinum-10 per cent rhodium and copper-constantan thermocouples were used to measure temperature within the tube, and copper-constantan thermocouples, housed in stainless-steel wells, were used to measure fluid temperatures. All thermocouples were calibrated to ± 0.3 F. The fluid thermocouples were immersed for at least 10 diam in the flowing liquid, and it can be demonstrated by calculation that the tube thermocouple measured inside tube-wall temperature with negligible error.

In order to know the tube outside-wall temperature precisely, it is necessary to calculate the temperature difference through the wall with considerable accuracy. It was found that the assumption of constant electrical resistance and thermal conductivity through the tube wall led to an error of as much as 16 F, so more accurate values of this temperature difference were found by solving the wall-conduction problem on an IBM 650 digital computer. The Appendix presents details of this calculation.

In all of the experimental runs, the compositions of the mixtures were checked by means of hydrometer readings carried out on samples taken from the loop from time to time. In one case a gravimetric determination was made, and it was in good agreement with the other methods.

Discussion of Results

Comparison of the two photographs in Fig. 3 shows the effect on forced-convection local boiling of 1.5-per-cent-by-weight isopropyl alcohol dissolved in distilled water. Both pictures were taken during steady-state operation at a pressure slightly above atmospheric, with a heat flux of about 590,000 Btu/hr-sq ft and liquid velocity 0.5 ft/sec.

[4] Numbers in parentheses refer to the Bibliography at the end of the paper.

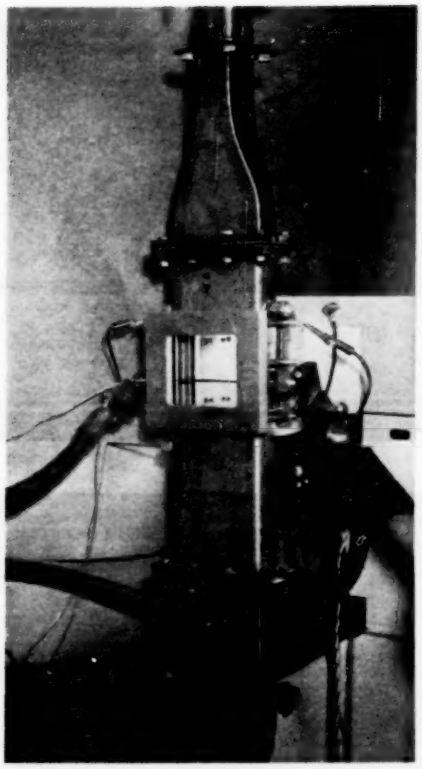

Fig. 2 Heating surface with power leads

The marked decrease in average bubble diameter which is observed in the second photograph of Fig. 3 was accompanied by a corresponding improvement in the smoothness and regularity of vapor-liquid flow adjacent to the heater. Similar effects were observed at other values of heat flux, liquid subcooling, and liquid velocity. Fig. 4 shows photographs with 1.5 per cent propanol taken at 890,000 Btu/hr-sq ft, and 4 ft/sec velocity, while Fig. 5 is with 1.5 per cent isopropanol, 663,000 Btu/hr-sq ft, and 4 ft/sec.

The degree of liquid subcooling affects bubble size to a small extent in these cases. The photographs, as noted in Figs. 3, 4, and 5, were taken while the degree of pure water subcooling was 20 F less than that of the alcohol-water mixtures, which would in itself tend to make the alcohol-water bubbles smaller. However, additional tests were made with pure water having the same subcooling as the mixtures in Figs. 3, 4, and 5, and the difference in bubble size shown by these figures was seen to persist. Moreover, photographic studies by Gunther (2) indicate that the disparity in subcooling would account for less than a seven per cent reduction in bubble radius, whereas the actual reduction observed with the mixtures was substantially greater.

Fritz (3) obtained a simple empirical relationship between the volume of a bubble during pool boiling and certain properties of the boiling fluid. Expressed in terms of the diameter of a spherical bubble it is

$$D = C\beta\left(\frac{2\sigma g_c}{g(\rho_l - \rho_v)}\right)^{1/2} \quad \ldots\ldots\ldots\ldots\ldots\ldots [1]$$

for $0 \leq \beta \leq 140$ deg

where

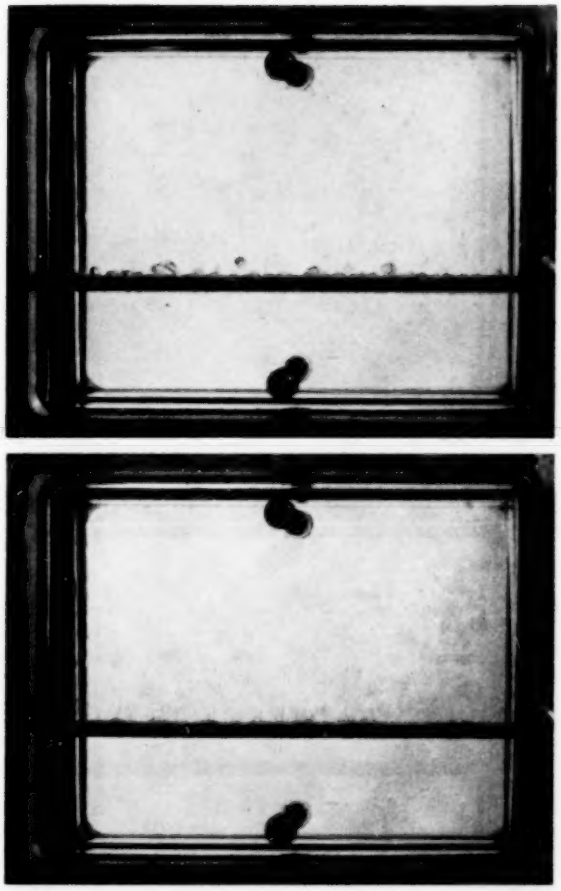

Fig. 3 ***Top:*** **Boiling with distilled water. q'' = 587,000 Btu per hr per sq ft, velocity = 0.5 fps, subcooling 25 F, surface 257.9 F, saturation temperature 218.6 F.**

Bottom: **Boiling with water containing $1^1/_2$ per cent isopropanol. q'' = 592,000 Btu per hr per sq ft, velocity = 0.5 fps, subcooling 39 F, surface 254.8 F, saturation temperature 218.6 F.**

σ = surface tension
D = bubble diameter when breaking off the heating surface
g = acceleration of gravity
g_0 = proportionality constant
C = constant
β = bubble contact angle
ρ_l = liquid density
ρ_v = vapor density

The surface tension σ decreases to 82 per cent of the surface tension for pure water when $1^1/_7$-per-cent-by-weight isopropanol is added to the water (4), while the density of the liquid decreases by only 0.5 per cent. Bonilla and Perry (5) have reported that for ethanol-water mixtures the bubble contact angle decreases by only four per cent for mixtures containing 12 per cent ethanol. No data on bubble contact angle are available for isopropanol-water mixtures.

Using linear interpolation of Bonilla and Perry's data on bubble contact angles to smaller concentrations of a different alcohol, a 9 per cent reduction in bubble radius is predicted by the Fritz equation for the 1.5 per cent isopropanol-water mixture as com-

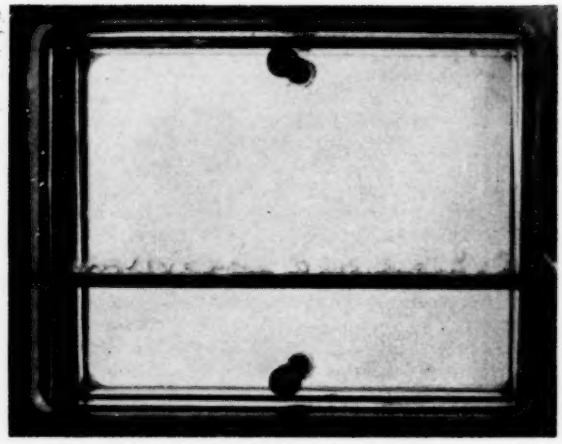

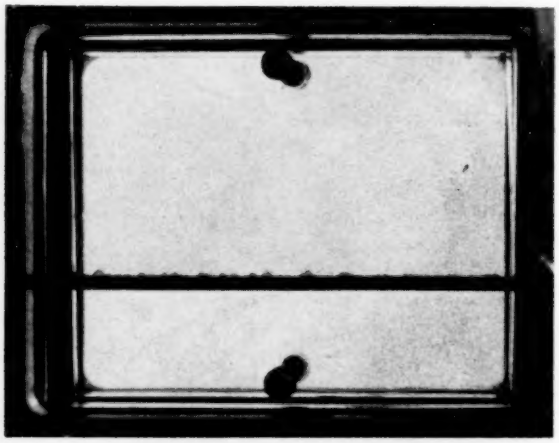

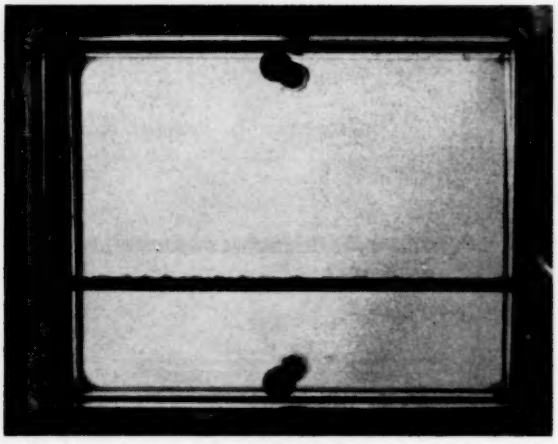

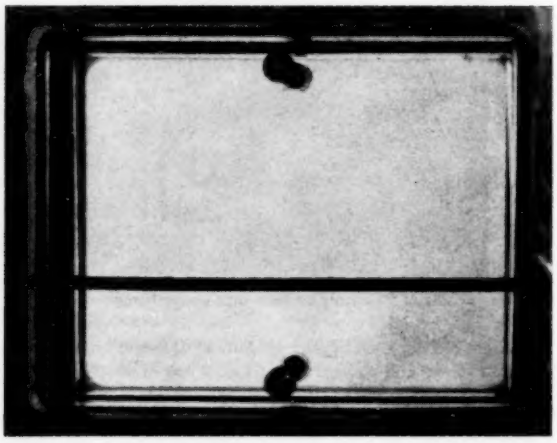

Fig. 4 *Top:* **Boiling with distilled water. q'' = 892,000 Btu per hr per sq ft, velocity = 4 fps, subcooling 20 F, surface 275.6 F, saturation temperature 218.6 F.**

Bottom: **Boiling with water containing 1½ per cent isopropanol. q'' = 881,000 Btu per hr per sq ft, velocity = 4 fps, subcooling = 41 F, surface 272.7 F, saturation temperature 218.6 F.**

Fig. 5 *Top:* **Boiling with distilled water. q'' = 663,500 Btu per hr per sq ft, velocity = 4 fps, subcooling 18 F, surface 270.6 F, saturation temperature 218.6 F.**

Bottom: **Boiling with water containing slightly over 1 per cent isopropanol. q'' = 663,500 Btu per hr per sq ft, velocity = 4 fps, subcooling = 37 F, surface 267.7 F, saturation temperature 218.6 F.**

pared to pure water. Visual observation indicates an even larger decrease in radius, even for equal degrees of subcooling. Presumably linear interpolation of the data of Bonilla and Perry is not justified, or possibly the Fritz equation does not contain all factors relevant to bubble size in local boiling.

A similar calculation, using values from Table 1, shows that predicted bubble-radius reduction is 7 per cent for 2.65 per cent by weight of methyl alcohol. As with the isopropanol, the observed reduction was greater, but qualitative agreement exists as to the effect of the additives on bubble size.

In order to determine the effect of the additive on other nucleate-boiling heat-transfer characteristics of water, a number of tests were run at liquid velocities of 0.3 and 0.5 ft/sec. Figs. 6 and 7 show curves of heat flux q'' as a function of the temperature difference, ΔT_s, from the heater's outer surface to the saturation temperature of pure water at the static pressure near the heater.

It is interesting to note the shift of these curves with different heater surface treatments. Surfaces coated with the stable oxide

Table 1 Properties of methanol-water mixtures (2.65 per cent methanol by weight) compared to those of pure water

Quantity	Value compared to that for water	Source
μ_l	1.035	(4)
c_l	0.998	(4)
k_l	0.983	(5)
σ	0.880	(4)
ρ_l	0.990	(4)
ρ_g	1.030	(5)
λ	0.919	(5)

film produced by film boiling have a higher ΔT_s for a given q'' than those of the acid cleaned tubes by some 65 per cent. This holds for runs with the alcohol-water mixtures as well as for runs with pure water. The same type of shift was noted earlier in pool-boiling tests and has been reported by other observers (6). A change of this magnitude in ΔT_s is quite small compared to the temperature of the surface, and it is, therefore, usually of second-

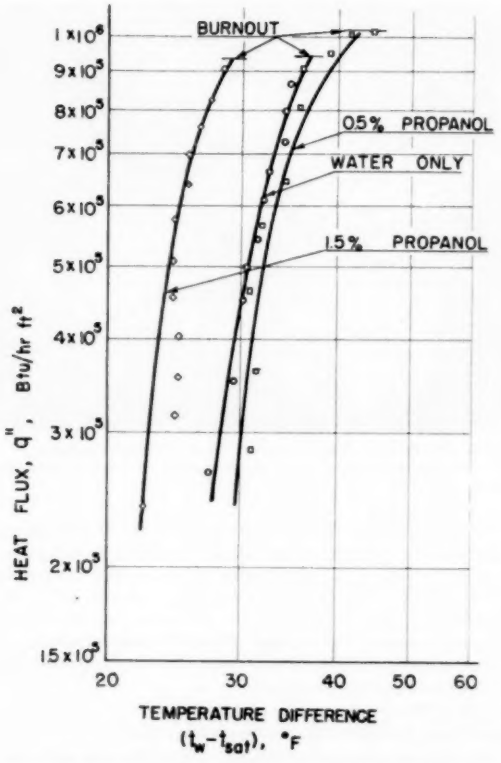

Fig. 6 Total heat flux as a function of temperature difference, wall to saturated fluid. Acid-cleaned heater. Velocity 0.5 fps.

ary interest when designing a surface to transmit a given heat flux.[4]

The curves also show that, for the smallest additions of alcohol, the q'' versus ΔT_x curve is the same as for pure water within the limits of experimental uncertainty. For greater proportions of alcohol, 1.5 per cent of isopropanol and 2.65 per cent methanol by weight, local boiling heat transfer is seen to be somewhat better than with pure water. Even at a heat flux of 800,000 Btu/hr-sq ft, however, the improvement is only 6 F, from 33 F to 27 F for the isopropanol-water mixture. For practical purposes, therefore, it may be stated that the surface temperatures were nearly independent of the small amounts of alcohol added.

A correlation which has been proposed by Rohsenow (1) for surface boiling heat transfer has proved quite successful for a number of different fluids, heating surfaces, and flow arrangements. This correlation may be written as follows

$$q'' = q_b'' + q_c'' \quad \ldots\ldots [2]$$

where

[4] Because boiling heat transfer correlations are of the form

$$q'' = C\Delta T_x^n$$

and the exponent n is large (3 or more), a moderate shift in the nucleate boiling curve affects the computed heat flux greatly for a given ΔT_x. However, most high performance nucleate boiling apparatus must be designed with heat flux, rather than ΔT_x, as the limited variable, because of the necessity for avoiding burnout. In such cases, an increase of the surface temperature of a few degrees can usually be accommodated without ill effect. Nevertheless, the greatest ΔT_x must be anticipated and provided for in the design.

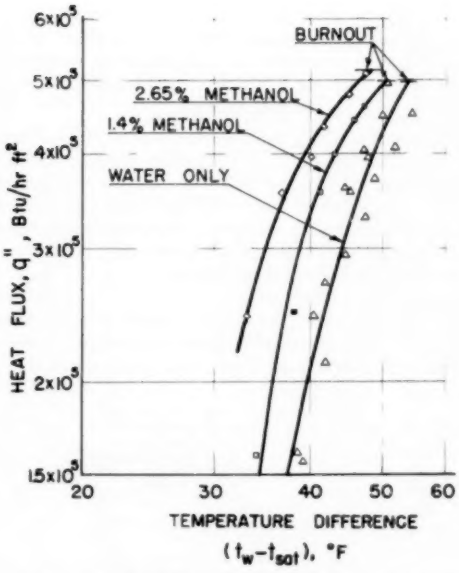

Fig. 7 Total heat flux as a function of temperature difference, wall to saturated fluid. Oxidized heater. Velocity 0.3 fps.

q'' = total heat-transfer rate per unit surface area (heat flux)
q_b'' = heat flux attributable to boiling without forced convection
q_c'' = heat flux attributable to forced convection

and the total heat flux is treated as the sum of the two quantities shown. The "convective heat flux" is that which would be calculated for the temperature difference $(T_w - T_l)$ without boiling, while the "boiling heat flux" is that which would be predicted for boiling without forced convection with the same value of the temperature difference $(T_w - T_{sat})$.

For forced convection normal to single tubes *without* boiling, the heat flux may be expressed (6)

$$q_c'' = h(T_w - T_l) \quad \ldots\ldots [3]$$

where T_w = heater surface temperature
T_l = fluid temperature

and h is defined by the relation

$$\frac{hD}{k} = 0.6\left(\frac{DG}{\mu}\right)^{0.8}\left(\frac{c_p\mu}{k}\right)^{0.31} \quad \ldots\ldots [4]$$

where

D = heater diameter
G = mass velocity
k = thermal conductivity of the liquid
c_p = specific heat of the liquid
μ = viscosity of the liquid

The pool-boiling correlation of Rohsenow (1) is presented as a relationship between dimensionless ratios

$$\frac{c_l\Delta T_x}{\lambda} = C_{sf}\left\{\frac{q_b''}{\mu_l\lambda}\left[\frac{g_0\sigma}{g(\rho_l-\rho_v)}\right]^{1/2}\right\}^r\left\{\left(\frac{c_l\mu_l}{k_l}\right)^s\right\} \quad \ldots\ldots [5]$$

where

λ = latent heat of vaporization

C_{sf}, r, and s = empirically determined constants

ΔT_x = temperature difference between the heater surface and the saturation temperature of the fluid, and the other symbols are already defined

For pure water, if it is assumed that $s = 1.7$, which Rohsenow and others have shown to be satisfactory for flow inside round tubes, the coefficient C_{sf} is found to be 0.0102 for the acid-cleaned tubes and 0.0151 for the tubes with oxide coatings. The higher value of C_{sf} for the tubes with oxide is consistent with the earlier observation that such tubes give a lower value of q'' for a given ΔT_x as compared to acid-cleaned tubes.

The exponent r, which holds for all of the curves, was found to be 0.17. Fig. 8 shows the data for pure water in local boiling with flow normal to the tube plotted in such a way that the Rohsenow coefficient of C_{sf} and the exponent r may be determined.

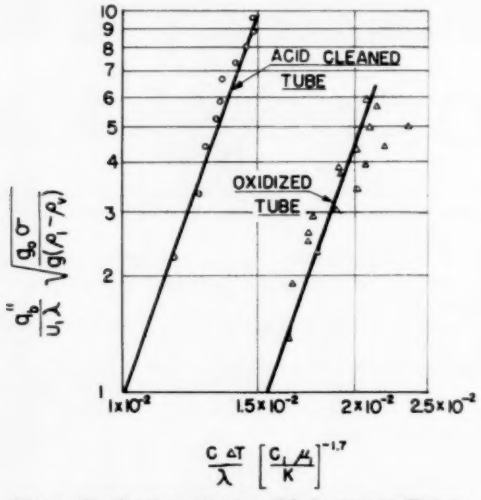

Fig. 8 Plot for determination of Rohsenow coefficients

The experimental fact that small amounts of the organic additives did not appreciably affect the values of ΔT_x for a given heat flux, although the bubble size was markedly reduced, may be investigated by expressing the Rohsenow correlation in the form

$$q_b'' = \lambda^{1-(1/r)} c_l^{(1-s)/r} \mu_l^{1-(s/r)} \left[\frac{g(\rho_l - \rho_g)}{g_0 \sigma}\right]^{1/2} k_l^{s/r} \left(\frac{\Delta T_x}{C_{sf}}\right)^{1/r} \quad \ldots [6]$$

Table 1 shows the percentage change in variables contained in the correlation, compared to pure water, when 2.65 per cent methanol by weight is added.

Taking $s = 1.7$, $r = 0.17$, regarding C_{sf} as an invariant, and substituting the percentage variations in the rewritten Rohsenow correlation, it is found that for a given ΔT_x, q_b'' should be higher by 2.5 per cent for the addition of 2.65-per-cent-by-weight methanol as compared to pure water. The reduction in bubble radius, calculated from Fritz' relation, is 7 per cent, as stated earlier.

The actual increase in q_b'' for a given ΔT_x is greater than 2.5 per cent for the addition, as may be seen from Figs. 6 and 7. However, the property values given in Table 1 are quite uncertain, and in some cases data for ethanol have been used in the absence of values for methanol. The significant points are that the direction of the shift of the q'' versus ΔT_x curves for the runs with organic additives are reasonable and consistent with the fact that bubble size is appreciably smaller, and that the calculated trends, though approximate, seem to verify the postulated mechanisms.

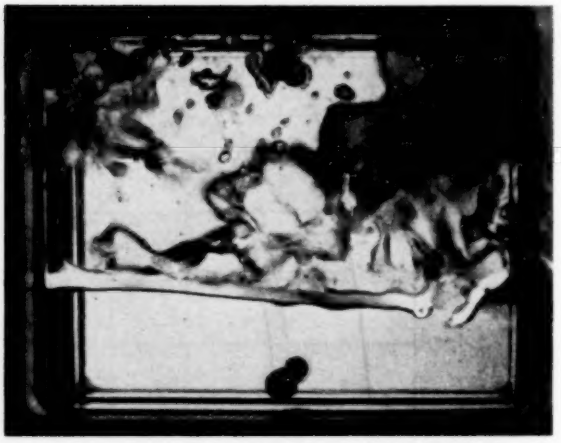

Fig. 9 Burnout in distilled water without forced circulation. Surface temperature and flux not determined. Saturation temperature 219 F.

Other tests, not to be reported in detail in the present paper, confirm the observations of various investigators that pure isopropyl alcohol, or mixtures with water where an appreciable fraction of the alcohol is present, give poorer heat transfer (greater ΔT_x for a given q'') than with pure water. This is explained by substantial changes of mixture properties other than surface tension which take place when an appreciable fraction of the organic substance is present.

Each of the experimental runs shown in Figs. 6 and 7 was continued to the onset of film boiling, to the peak heat flux. These points are indicated on the graphs, and it may be seen that the peak (or burnout) heat flux was at least as great in the runs with the organic additive as it was with pure water. At higher alcohol concentrations, the peak flux would be found to decrease.[6] Fig. 9 shows rather dramatically the appearance of the test section just after failure by burnout, at a time when the tube has failed mechanically but is still almost white-hot from the sudden temperature increase which accompanies the vapor blanketing of a heater as it goes suddenly from nucleate to film boiling.

Summary and Conclusions

The experimental investigation described here demonstrated the effect on local-boiling heat transfer of a very small amount of dissolved organic additives in distilled water. With about one per cent isopropyl alcohol or two per cent methyl alcohol by weight, the nucleate-boiling heat-transfer coefficient is either unaltered or slightly improved, while the average and maximum bubble sizes are very notably reduced. The peak heat flux is slightly elevated. The smaller average bubble size improves the dynamic characteristics of the boiling mechanism during forced convection, because the heat transfer can be effected without the ragged and uneven vapor masses characteristic of local boiling of pure water at very high heat flux [around 1 million Btu/hr-sq ft].

A possible application of this phenomenon is in the flow channel of a water-cooled and water-moderated nuclear reactor. The high heat-transfer coefficients which accompany local boiling are desirable, but the density fluctuations, lower average density, and much greater static-pressure drop are detrimental. These undesirable conditions will all be alleviated to some extent, at least, by a decrease in the average bubble size.

Because there is a lack of information in the literature on nu-

[6] See, for example, the results of Cichelli and Bonilla (7), who correlated peak flux with reduced pressure, p/p_{cr}.

cleate-boiling heat transfer from round tubes normal to the flow of subcooled pure liquid, there is included a correlation of the measurements with pure water. The dimensionless groups proposed by Rohsenow (1) were found to be adequate, and the data were sufficient to determine the necessary coefficient and exponent.

Bibliography

1 "Heat Transfer Associated With Nucleate Boiling," by W. M. Rohsenow, Proceedings of Heat Transfer and Fluid Mechanics Institute, 1953, Stanford University Press, Stanford, California, p. 123.

2 "Photographic Study of Bubble Formation in Heat Transfer to Subcooled Water," by F. C. Gunther, TRANS. ASME, vol. 73, 1951, p. 115.

3 "Berechnung des Maximalvolumens von Dampfblasen," by W. Fritz, *Physikalische Zeitschrift*, vol. 36, 1935, p. 379.

4 "International Critical Tables," published for the National Research Council by McGraw-Hill Publishing Company, New York, N. Y., 1928; vol. 3, pp. 111, 116, 309; vol. 4, pp. 467, 470; vol. 5, pp. 22, 116, 227.

5 "Heat Transmission to Boiling Binary Liquid Mixtures," by C. F. Bonilla and C. H. Perry, *Trans. AIChE*, vol. 37, 1941, p. 685.

6 "Heat Transmission," by W. H. McAdams, McGraw-Hill Publishing Company, New York, N. Y., third edition, 1954, pp. 376, 267.

7 "Heat Transfer to Liquids Boiling Under Pressure," by M. [illegible] Cichelli and C. F. Bonilla, *Trans. AIChE*, vol. 41, 1945, p. 755

8 "Metals Handbook," American Society for Metals, Cleveland, Ohio, 1939, pp. 541–543.

9 "Superior Tube Company Catalog Section 20," Superior Tube Company, Morristown, Pa., pp. 20–6, 20–7.

Acknowledgment

The major portion of the work reported herein was done with the assistance of a research grant from the Signal Oil and Gas Company of Los Angeles, Calif. In addition, a research grant from the National Science Foundation provided partial assistance, as did the use of equipment designed and built under contract with the Office of Naval Research.

APPENDIX

Calculation of Heater Surface Temperature

To establish the surface temperature of the test section from the reading of a thermocouple within the test section, it was necessary to calculate the temperature drop through the tube wall. Normally, this would be done by assuming uniform heat generation in the tube wall, in which case the calculation is quite simple. However, at high electrical inputs, where the temperature drop through the wall is substantial, properties of the tube which are functions of temperature and which affect the generation vary to such an extent that the assumption of uniform generation is invalid.

Fig. 10 shows an end view of the stainless-steel heater tube. The heat flux entering the shaded volume element dV is $-KA(dT/dx)$, the generation in volume is $q'''dV$ and the rate of heat transfer from the right side is

$$-\left(K+\frac{dK}{dx}\,dx\right)\left(A+\frac{dA}{dx}\,dx\right)\left(\frac{dT}{dx}+\frac{d^2T}{dx^2}\,dx\right)$$

where K = thermal conductivity of the tube
A = area normal to heat flow
T = temperature
x = distance measured from the tube axis

The energy balance becomes

$$-KA\frac{dT}{dx}+q'''A\,dx=-\left(K+\frac{dK}{dT}\,dx\right)\left(A+\frac{dA}{dx}\,dx\right)\left(\frac{dT}{dx}+\frac{d^2T}{dx^2}\,dx\right)$$

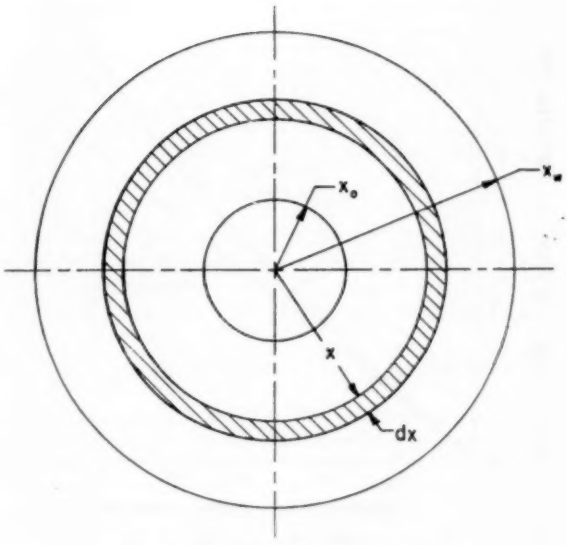

Fig. 10 Diagram of cross section of heater

Multiplying the right side out and neglecting higher order terms

$$\frac{d^2T}{dx^2}+\frac{1}{KA}\left[\frac{d(KA)}{dx}\right]\frac{dT}{dx}+\frac{q'''}{k}=0$$

But

$A = 2\pi x$ per unit length
$k = k_o[1+\gamma(T-T_o)]$

where k_o = conductivity of the inner surface of the tube
γ = variation of conductivity with temperature
T_o = temperature at the tube inner surface

and

$$q''' = \frac{E^2}{VR_o[1+\alpha(T-T_o)]}$$

where

E = voltage drop across the tube
V = metallic volume of the tube
R_o = electrical resistance at the inner surface
α = variation of resistance with respect to temperature

Substituting

$$\frac{d^2T}{dx^2}+\left\{\frac{1}{2\pi x k_o[1+\gamma(T-T_o)]}\right\}\left\{\frac{d[(2\pi x)K_o(1+\gamma\{T-T_o\})]}{dx}\right\}\left(\frac{dT}{dx}\right)+\frac{E^2}{VK_o[1+\gamma(T-T_o)]R_o[1+\alpha(T-T_o)]}=0$$

Performing the indicated differentiations

$$\frac{d^2T}{dx^2}+\frac{1}{x}\frac{dT}{dx}+\left[\frac{\gamma}{1-\gamma(T_o-T)}\right]\left(\frac{dT}{dx}\right)^2+\frac{E^2}{VR_o[1+\alpha(T-T_o)]k_o[1+\gamma(T-T_o)]}=0$$

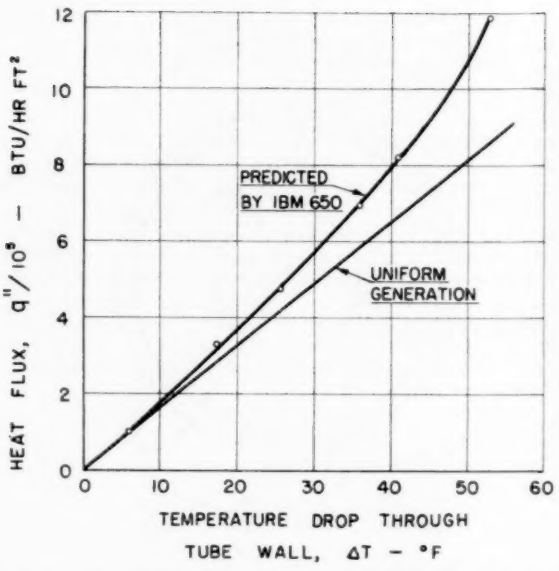

Fig. 11 Temperature drop across heater wall as a function of heat flux. Heater type 304 stainless steel, 0.110 in. OD, 0.0875 ID.

Boundary conditions: At the inner tube wall, T = the temperature given by the thermocouple inside the tube, and $dt/dx = 0$.

A model 650 IBM computer[7] was used to solve this equation by finite difference methods taking twenty equal intervals across the tube for numerical integration. The integration furnished tube-wall temperature drop for six particular values of inner-wall temperature and power input. (Power input fixes heat flux, q'' Btu/hr-sq ft). A curve of wall temperature drop versus q'', drawn through these six values was used to calculate tube surface temperatures for all tests. The curve is shown in Fig. 11.

Values of γ, α, R_o, and K_o were obtained from two sources (8 and 9) which checked each other closely and checked the values of electrical resistance observed during the tests.

Additional calculations with the computer showed that:

1 No appreciable difference in wall-temperature drop occurred due to variations of the initial-temperature value (that is, temperature at tube inner surface) within the range of initial temperature values observed at a given q'' during the tests. Hence use of the curve in Fig. 11 for all tests, in spite of variations of inner-surface temperature, is justified.

2 The probable uncertainties in K_o, R_o, α, γ, wall thickness, and initial temperature combined to give a probable uncertainty in wall drop of only ±5.1 per cent. This was found by introducing into the calculations the values corresponding to maximum uncertainties in these quantities and comparing the wall drop calculated by the computer with the original value.

3 Decreasing the size of the increment for the finite difference integration, or the required degree of convergence of answers for each increment changes the wall drop value by a negligible amount. Hence the size of the increment and degree of convergence were specified small enough to give accurate results in the calculations from which the curve in Fig. 11 was plotted.

[7] The computer is located at Electronics Research Laboratory, Stanford University. Its use was financed by the National Science Foundation, grant NSF G 3045. The authors are grateful to the National Science Foundation and to Prof. J. G. Herriott, Mathematics Department, and D. C. Baxter, Mechanical Engineering Department, Stanford University, for their assistance in this project.

Discussion

J. A. Clark.[8] The authors show that an additive more volatile than a liquid allows nucleation to occur in the liquid mixture at temperatures less than those found for the pure liquid alone. Their results given in Figs. 6 and 7 are quite reasonable. In the presence of a volatile additive it would be expected that in nucleate boiling at a given surface temperature the bubble population would be greater than for the pure liquid and hence the heat flux also would be greater. This effect is shown by the present paper. A similar effect for the case of dissolved air in water (69 cc air per liter) at 90 psia has been reported by McAdams, et al. (1).[9] At higher pressures (1000–2000 psia) dissolved gases in water appear to have no noticeable effect (2). The fact that the maximum heat flux seems to be uninfluenced by the presence of additive suggests that the vapor bubbles at this point are composed principally of the additive itself and are of sufficient volume to prevent a significant number of bubbles of water vapor to exist. It is conceivable the water could act as a stabilizing fluid delaying the actual peak flux condition. This in fact may occur but would be difficult to pick up without transient instrumentation.

For application in nuclear reactors, which the authors mention, it will be important to study these effects at much higher pressures and also to investigate the nuclear properties of the additive as regards its "poisoning," or neutron-absorption characteristics, and its susceptibility to radioactivity.

It should be pointed out that the authors' Fig. 8 is essentially their Figs. 6 and 7 for pure water as q_b'' differs very little from q''. According to the writer's computation q_o'' ranges from 22 per cent q'' to 9.4 per cent q'' for the acid-cleaned heater, and from 18 per cent q'' to 5 per cent q'' for the oxidized heater, the larger percentage corresponding to the lower flux in both instances. Since the pressure was fixed in all the tests, the co-ordinates in Fig. 8 do not indicate a correlation in the usual sense but rather another representation of the pure-water data of Figs. 6 and 7 with a change of scale in the ordinate and abscissa. The writer suggests that Rohsenow's correlation has not been tested by these data.

In their Appendix the authors derive and present the differential equation governing the temperature distribution in infinitely long circular cylinders with heat sources for the case of temperature-dependent properties of thermal conductivity and electrical resistivity. They correctly show that a general approach to this problem involves a nonlinear differential equation which they integrate using an IBM 650. This same problem has been approached by others (3, 4, 5) in a somewhat different way. Since the writer recently has had occasion to re-examine this problem, which originally was solved by Kreith and Summerfield (3), from the standpoint of a hand computation for the solution, the following is presented which may be of general interest. The outer-wall temperature T_w at radius x_w may be written in terms of the temperature T_o at x_o by a Taylor series expansion about the adiabatic point $x = x_o$ (authors' notation) for linear variation in thermal conductivity and electrical resistivity[10] as (R_m = mean resistivity)

[8] Professor of Mechanical Engineering, University of Michigan, Ann Arbor, Mich. Assoc. Mem. ASME.

[9] Numbers in parentheses refer to the Bibliography at the end of this discussion.

[10] The advantage of the Taylor series expansion is that the differential equation itself provides the second derivative, $\partial^2 T/\partial x^2$ from which all higher derivatives may be formed, and when evaluated at an adiabatic surface, the first derivative $\partial T/\partial x$ is identically zero. A nonlinear temperature variation in physical properties also may be handled.

Table 2 Results of $T_o - T_w$ calculations

q_w''	t_o	k_o	$T_o - T_w$ (geometric term), deg F	$T_o - T_w$ (thermal-property term), deg F	R_m/R_o	$T_o - T_w$ (authors' Fig. 11), deg F	Estimate of accuracy of thermal-conductivity data $\pm 5\%$ $(T_o - T_w)$, deg F
10^6	309	9.85	48.6	+0.0086	>0.99	48	±2.43
0.8×10^6	297	9.80	39.1	<0.0086	>0.99	40	±1.95
0.5×10^6	277	9.72	24.6	<0.0086	>0.99	26.4	±1.23
0.2×10^6	260	9.65	9.90	<0.0086	>0.99	10.1	±0.50

$$T_o - T_w = \frac{q''_w x_w (R_m/R_o)}{k_o[(x_w/x_o)^2 - 1]} \left\{ \left(\frac{x_w - x_o}{x_o}\right)^2 - \frac{1}{3}\left(\frac{x_w - x_o}{x_o}\right)^3 + \frac{1}{4}\left(\frac{x_w - x_o}{x_o}\right)^4 + \ldots + \frac{q_w'' x_w (R_m/R_o)}{6k_o[(x_w/x_o)^2 - 1]} \left(\frac{x_w - x_o}{x_o}\right)^4 \left[\frac{3\gamma + 4\alpha\gamma T_o + \alpha}{(1 + \gamma T_o)(1 + \alpha T_o)}\right] + \ldots \right\}$$

This result is essentially that of Kreith and Summerfield (3). Now, if one examines the first summation in the braces, two things are observed: (*a*) It contains only geometric quantities and no thermal property coefficients, and (*b*) the series, if it continues in its present form, may be written

$$\frac{1}{2}\left(\frac{x_w - x_o}{x_o}\right)^2 + \left(\frac{x_w - x_o}{x_o}\right) + \sum_{n=1}^{\infty} \frac{(-1)^n}{n} \frac{(x_w - x_o)^n}{x_o^n} = \frac{1}{2}\left(\frac{x_w - x_o}{x_o}\right)^2 + \left(\frac{x_w - x_o}{x_o}\right) - \log_e\left[1 + \frac{x_w - x_o}{x_o}\right]$$

This last form of the first summation is exactly what one would obtain assuming constant properties, i.e., $\alpha = 0$, $\gamma = 0$, and is that result which a Taylor series expansion must give for these circumstances. Hence it seems reasonable that the first series will proceed as assumed, converging to the function just written. This means the temperature drop $T_o - T_w$ can be written as the sum of two functions, the first being a geometric function (solution for constant properties) and the second a thermal-property variation function, the first term of which is written in the Taylor series just given. The equation so written enables one to assess the influence of thermal property variation on $T_o - T_w$, which does not seem to be large. To show this the writer computed several values of $T_o - T_w$ corresponding to the authors' heat-transfer data and geometry but using thermal conductivity and electrical resistivity data for 304 from Dickinson and Welch (5). The results in Table 2 were obtained.

In general, the results are equivalent. The writer is puzzled at the very large discrepancy between the authors' IBM solution and their constant-property estimation. Such a difference is not predicted by the analysis presented by the writer nor does it seem reasonable to expect it since the maximum temperature difference $T_o - T_w$ is less than 50 F. It is quite possible the root of the problem lies in the thermal-property data themselves. Perhaps the authors could report the numerical values of thermal conductivity and electrical resistivity which they used.

Bibliography

1 "Heat Transfer at High Rates to Water With Surface Boiling," by W. H. McAdams, W. E. Kennel, C. S. Minden, R. Carl, R. M. Picornell, and J. Dew, *Industrial and Engineering Chemistry*, vol. 41, 1949, p. 1945.

2 "Studies in Boiling Heat Transfer," by Buchberg, et al., UCLA, Department of Engineering, Los Angeles, Calif., March, 1951.

3 "Heat Transfer to Water at High Heat Flux Densities With and Without Surface Boiling," by F. Kreith and M. Summerfield, TRANS. ASME, vol. 71, 1949, pp. 805–815.

4(*a*) Proceedings of the Heat Transfer and Fluid Mechanics Institute, by W. M. Rohsenow and J. A. Clark, Stanford University, 1951.

(*b*) "Local Boiling Heat Transfer to Water at Low Reynolds Numbers and High Pressures," by J. A. Clark and W. M. Rohsenow, TRANS. ASME, vol. 76, 1954, pp. 553–562.

5 "Heat Transfer to Supercritical Water," by N. L. Dickinson and C. P. Welch, TRANS. ASME, vol. 80, 1958, pp. 746–754.

M. Tribus[11] **and N. Zuber.**[12] The experimental results presented by the authors are significant because they put into focus the essential features of nucleate boiling and of the "burnout phenomenon." Figs. 6 and 7 clearly illustrate the dependence of nucleate-boiling heat transfer on the condition of the surface, and the fact that the "burnout" heat flux is independent of the temperature difference ΔT_s (often called "liquid superheat"). As the authors have discussed, although a variation of 65 per cent in the temperature difference ΔT_s is small compared to the temperature of the surface, yet this variation is very important when the heat flux is computed from an equation of the form

$$q'' = c\Delta T_s^n \quad [7]$$

This result is a consequence of the fact that the exponent n is very large. Values between 3 and 24 have been reported depending on the surface conditions. The difficulty, which arises when an equation of the form of Equation [7] is used, becomes even more evident when it is realized that experimental data are not yet available which would relate quantitatively the variations of the temperature difference ΔT_s to the surface conditions.

Fortunately, for constant-heat-input systems, such as nuclear reactors, the essential information is not the temperature of the surface during nucleate boiling but rather the limiting heat flux, the so-called "burnout point." It can be seen from Figs. 6 and 7 that this flux is independent of the temperature difference ΔT_s; i.e., of the liquid superheat. The explanation for this lies in the fact that this flux is determined by the hydrodynamic stability as first proposed by Kutateladze.[13] It was shown recently[14, 15, 16] that the problem can be simplified greatly if transition boiling instead of nucleate boiling is analyzed. If such a view is adopted, then, by using a hydrodynamic-stability analysis it is possible to derive an analytic expression for the peak nucleate heat flux in pool boiling of subcooled liquids

---

[11] Associate Professor, Engineering Department, University of California, Los Angeles, Calif. Mem. ASME.

[12] Assistant Research Engineer, University of California, Los Angeles, Calif.

[13] "A Hydrodynamic Theory of Changes is Boiling Process Under Free Convections," by S. S. Kutateladze, *Izvestiya Akademiya Nauk*, S.S.S.R., Otd., Tekh. Nauk, no. 4, 1951, p. 529.

[14] "On the Stability of Boiling Heat Transfer," by N. Zuber, TRANS. ASME, vol. 80, 1958, pp. 711–720.

[15] "On the Maximum Heat Flux in Pool, Nucleate Boiling of Subcooled Liquids," by N. Zuber. (Submitted for publication in *Jet Propulsion*).

[16] "Further Remarks on the Stability of Boiling Heat Transfer," by N. Zuber and M. Tribus, Report 58-5, Dept. of Engineering, University of California, Los Angeles, Calif., 1958.

$$q'' = L\frac{\pi}{24}\rho_v\frac{\lambda}{\tau} + \frac{\pi}{24}\rho_v\frac{\lambda}{\tau}c_l(T_s - T_l) + \sqrt{(2\pi)}\frac{k_l}{(\alpha\tau)^{1/2}}(T_s - T_L) \quad [8]$$

where

$$\frac{\lambda}{\tau} = \left[\frac{\sigma g(\rho_L - \rho_v)}{\rho_v^2}\right]^{1/4}\left[\frac{\rho_L}{\rho_L + \rho_v}\right]^{1/2}$$

$$\tau = 2\pi\left[\frac{\sigma}{g(\rho_L - \rho_v)}\right]^{1/2}\left[\frac{\rho_v^2}{\sigma g(\rho_L - \rho_v)}\right]^{1/4}\left[\frac{\rho_L + \rho_v}{\rho_L}\right]^{1/2}$$

In Equation [8], L is the latent heat of vaporization, a_l the thermal diffusivity of the liquid, T_s fluid saturation temperature, and T_l the bulk-liquid temperature. The physical interpretation of the three right-hand side terms in Equation [8] is as follows: The first term is the energy required to generate the critical vapor-mass flow which causes the instability. The second is the energy required to increase the enthalpy of the liquid from bulk liquid to saturation temperature. The last term is the energy transferred from the liquid-vapor interface which is at saturation temperature to the bulk liquid which is subcooled.

Because the authors have kindly made their original data available, the writers were able to check further the validity of Equation [8]. The results are given in Table 3.

Table 3

	$T_s - T_L$, deg F	Experimental, Btu/hr sq ft	Analytical, Btu/hr sq ft
Fig. 6.....	47.6	9.10×10^5–11.74×10^5	9.89×10^5
Fig. 7.....	13.4	4.55×10^5–5.12×10^5	5.28×10^5

J. W. Westwater.[17] This interesting research shows that heat transfer to boiling mixtures is much more complicated than to pure liquids. The authors show that small quantities of a volatile material of low molecular weight can cause appreciable changes in behavior for water during subcooled, nucleate boiling. A recent paper by A. J. Lowery, Jr., and J. W. Westwater,[18] concerns the effect of nonvolatile additives of high molecular weight. For nucleate boiling of saturated methanol, the effect was not great. For transition and film boiling the effect was very large and cannot be explained in terms of changes in the surface tension or other physical properties. A few parts per million of certain agents are sufficient to produce measurable increases in the heat flux.

[17] Associate Professor of Chemical Engineering, University of Illinois, Urbana, Ill.

[18] *Industrial and Engineering Chemistry*, vol. 49, 1957, p. 1445.

Authors' Closure

The authors are indebted to Profes or Clark for his careful discussion of this paper. Some of his comments raise additional questions which we shall attempt to answer in the order of their occurrence in his presentation.

It is agreed that the effects described in the paper must be checked at higher pressures if they are to be of use in most nuclear reactors. Furthermore, any additive which is selected must be evaluated from the standpoint of stability under radiation. However, it is not necessary to investigate the "poisoning" effects of organic additives of the type described in the paper, since the absorption cross sections of these materials are generally small and, in any event, can be readily calculated from tabulated properties.

It is true that Fig. 8 does not present a test of the Rohsenow correlation. Rather, it was prepared to provide comparative values of the coefficient and exponent (C_{sf} and r) for forced flow across tubes with the materials employed in these tests. Previously published information by several authors has demonstrated the validity of the Rohsenow correlation method for flow of water inside tubes, and our presentation assumes that the method is also applicable to crossflow.

Professor Clark's method of calculating the temperature difference in the tube wall when the thermal conductivity and electrical resistivity are temperature-dependent is both interesting and helpful. To facilitate comparison, we present here the thermal conductivity and electrical resistance values which we used. These values are tabulated for the same inner wall temperatures as in Table 2:

t_s	k_o	R_m/R_o
309	9.81	>0.99
297	9.76	>0.99
277	9.67	>0.99
260	9.59	>0.99

The large discrepancy shown in Fig. 11 between the IBM solution and the constant-property estimation is incorrect. The uniform generation line on that figure was calculated for a different size of test section than was used in this experiment and should therefore be disregarded. The IBM solution is correct, however, and all the conclusions in the body of the paper are based on the results of this correct calculation.

The authors also wish to acknowledge the interesting contributions made by Professor Tribus and Mr. Zuber of the University of California at Los Angeles, as well as those made by Professor Westwater of the University of Illinois. The relation of the present work to results from research projects in other phases of boiling heat transfer will contribute to the development of a consistent theory.

Comparison of Total Emittances With Values Computed From Spectral Measurements

By J. T. BEVANS,[1] J. T. GIER,[2] and R. V. DUNKLE[2]

Spectral and total emittances have been measured for materials exposed to various oxidation conditions (total of 25 samples). The total emittance values computed from the spectral data have been found to compare favorably with the measured total values. The experimental techniques utilized for both types of determinations are described and the effect of temperature, sample preparation, and experimental errors are discussed relative to the differences obtained in the results.

Nomenclature

The following nomenclature is used in the paper:

C_1, C_2 = constants of Planck's radiation equation
E_λ = monochromatic emissive power, Btu/hr sq ft micron
E = total emissive power, Btu/hr ft²
E_{IR} = total emissive power of an ideal radiator, Btu/hr sq ft
e = emissivity or emittance; subscript λ denotes monochromatic value
n = index of refraction
r = reflectivity or reflectance; subscript λ denotes monochromatic value
T = absolute temperature, deg R
λ = wave length, microns
ρ = volume resistivity, ohm-cm; subscript denotes absolute temperature used for measurement
σ = Stefan-Boltzmann constant, 0.172×10^{-8} Btu/hr sq ft (deg R)⁴

Introduction

For several years, the authors have been engaged in developing techniques for the measurement of the spectral characteristics of materials. The purpose of this paper is to present the results of a specific program on spectral and total emittance measurements carried out for the North American Aviation Company. The twenty-five samples studied in this program consisted of typical aircraft construction materials with special surface coatings and/or thermal treatments. Samples of the untreated materials also were included for comparison. The total emittances were measured at temperatures of 200, 400, 600, and 800 deg F, while the spectral reflectances were measured at approximately 100 F. The spectral reflectances were then utilized to compute the total emittances at the four temperatures (1).[3] The discrepancies between the total emittance values obtained by direct measurement and those calculated from spectral data are discussed and the sources of the differences delineated.

The materials covered in this investigation are only moderately selective; many other materials show a much larger variation in spectral characteristics with wave length. For many engineering purposes it is essential to consider the spectral dependence of the emission and absorption of materials. This is of particular importance in the fields of control and utilization of solar energy (2, 3, 4). In the past, little attention has been paid to the importance of spectral characteristics, and even gases have been commonly treated as gray (nonselective) absorbers and emitters of radiation (6).

Experimental Procedures

Spectral Emittance[4] Measurements. The equipment used for the spectral measurements has been described previously in another journal (3). No description has been given in the engineering literature and a brief outline of the method will be presented.

The basic components of the system are (*a*) a heated ideal radiator, (*b*) a water-cooled sample, and (*c*) an infrared dispersing and detection system, Figs. 1 and 2. The sample is held by a sample holder inserted in the ideal radiator flush with the inner wall of the cavity. The radiation emitted by the ideal radiator at a particular wave length is compared with the radiation from the ideal radiator after reflection from the sample. This comparison is made by means of a Perkin-Elmer Model 83 monochromator through an optical system focussed alternately on the sample and the radiator wall, Figs. 1 and 2. Values of reflectance are obtained over the wavelength range 1 to 25 microns for 0.25-micron intervals.

[4] In scientific nomenclature the "ivity" ending refers to the characteristics of a material, whereas the "ance" ending refers to the characteristic of a body or portions of a body rather than the material composing it. Thus emissivity refers to the material in a pure, polished, and opaque form and emittance includes surface roughness, oxide films, transmission of surface films, and other deviations from the definition of emissivity. This is analogous to describing the resistivity of a metal and the resistance of a resistor made from that metal. Many engineers make no distinction between emissivity and emittance. A discussion of this terminology may be found in "Temperature, Its Measurement and Control," pp. 1164–1168, Reinhold Publishing Corporation, 1941. The same argument holds for reflectivity, reflectance, absorptivity, and absorptance.

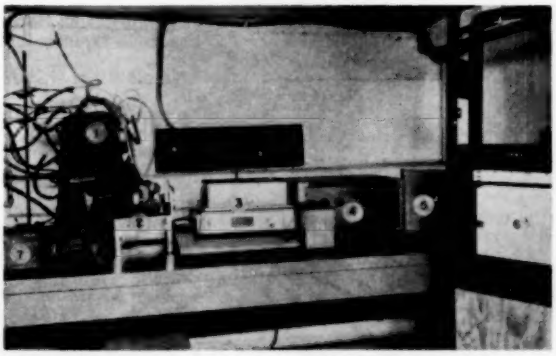

Fig. 1 View of equipment: (1) High-temperature cavity; (2) optical system; (3) Perkin-Elmer Model 83 infrared monochromator; (4) Perkin-Elmer Model 81 A-C amplifier; (5) regulated power supply; (6) indicating pen recorder; (7) potentiometer

[1] Shell Development Company, Emeryville, Calif. Assoc. Mem. ASME.

[2] Associate Professor, Department of Engineering, University of California, Berkeley, Calif.

[3] Numbers in parentheses refer to the Bibliography at the end of the paper.

Contributed by the Heat Transfer Division and presented at the Annual Meeting, New York, N. Y., December 1–6, 1957, of The American Society of Mechanical Engineers.

Note: Statements and opinions advanced in papers are to be understood as individual expressions of their authors and not those of the Society. Manuscript received at ASME Headquarters, June 10, 1957. Paper No. 57—A-29.

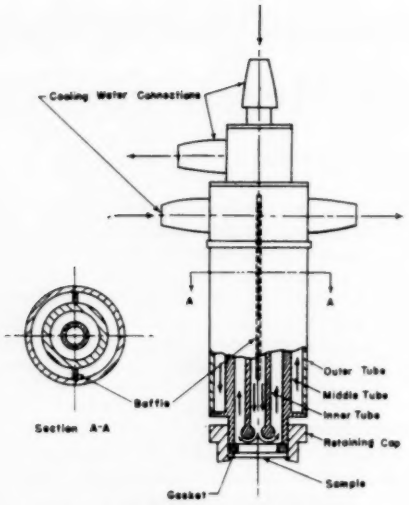

Fig. 2 Schematic-view of sample holder

The ideal radiator is heated electrically to approximately 1500 F by three separately controlled heaters and a uniform temperature established to within ±5 deg F as indicated by four chromel-alumel thermocouples peened to the cavity wall. One thermocouple is located directly opposite the sample, one in the region viewed as the reference source, and the remaining two on the sides of the cavity, midway between the top and bottom, Fig. 3. The sample must be cooled substantially below the radiation-source temperature, otherwise the sample would emit as much radiation as absorbed and it would be impossible to differentiate between emitted and reflected radiation. In addition, cooling is necessary to prevent deterioration of the test surface. In practice, the sample temperature is approximately 100 F. The construction of the sample holder and the method of cooling is shown in Fig. 4.

The values of spectral reflectance obtained are converted to

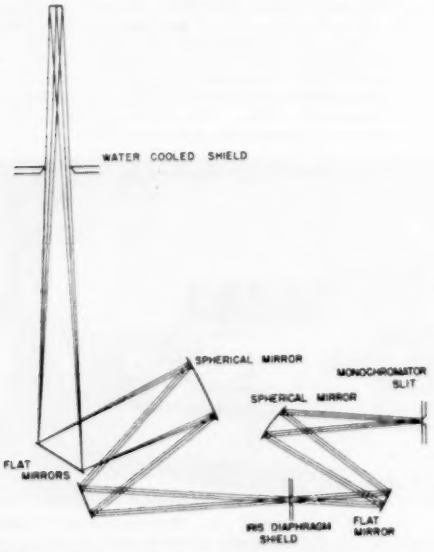

Fig. 3 Schematic view of optical system, showing relative positions of mirrors and shields

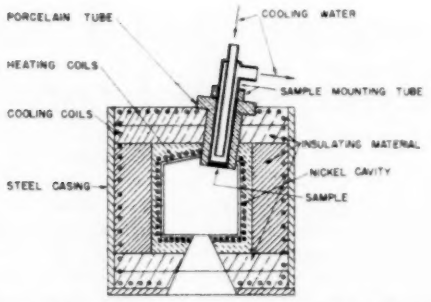

Fig. 4 Cross-section representation of heated Hohlraum

spectral emittance measurements by the relation valid for opaque materials

$$e_\lambda + r_\lambda = 1 \quad \ldots\ldots [1]$$

Total Emittance Measurements. The procedure used for measuring the total emittance of a material has been described in detail by Snyder, Gier, and Dunkle (9). The values presented are the average of a minimum of three consistent determinations at each temperature; i.e., three consecutive values obtained over an approximately 30-minute interval, which differed by ±0.01 or less.

Calculation Method. The calculations were performed using the procedure outlined by Dunkle (1), by the Computer Laboratory of the University of California. The emittances were computed at temperatures of 200, 400, 600, and 800 F. In the strictest sense, the value computed in this manner is the absorptance of the sample for an ideal radiator source at the four temperatures. This method of computation assumes that the spectral reflectance is independent of temperature.

The range of wave lengths involved in the spectral measurements is sufficiently large so that the uncertainty in the computed emittances is small for the temperature range considered. This can be shown by using the expression for the monochromatic emission of an ideal radiator, which is conveniently written as (1)

$$\frac{E_\lambda}{T^5} = \frac{C_1}{(\lambda T)^5 \left[\left(\exp \frac{C_2}{\lambda T}\right) - 1\right]} \quad \ldots\ldots [2]$$

The definition of the total emittance of a surface is

$$e = \frac{\int_0^\infty e_\lambda E_\lambda d\lambda}{\sigma T^4} \quad \ldots\ldots [3]$$

Substitution of Equation [2] in Equation [3] and changing the variable of integration to λT, transforms the latter equation into the convenient form used for computation

$$e = \int_0^\infty e_\lambda \left(\frac{E_\lambda}{\sigma T^5}\right) d(\lambda T) \quad \ldots\ldots [4]$$

The function $E_\lambda/\sigma T^5$, and the integral of this function from 0 to λT as a function of λT, are shown in Fig. 5. The value of the integral from 0 to λT represents the fraction of the power of an ideal radiator between 0 and λ for a specific temperature T. Thus less than one per cent of the total power of an ideal radiator at a temperature of 2600 R, lies in the wave length region below one micron ($\lambda T = 2600$). In a similar manner, approximately one per cent of the total power lies beyond $\lambda T = 40{,}000$. For the temperature of 200 F, and wave length limits of 1 and 25 microns, approximately 10 per cent of the power lies beyond the maximum value of $\lambda T = 16{,}500$ and negligible power lies below $\lambda T = 660$.

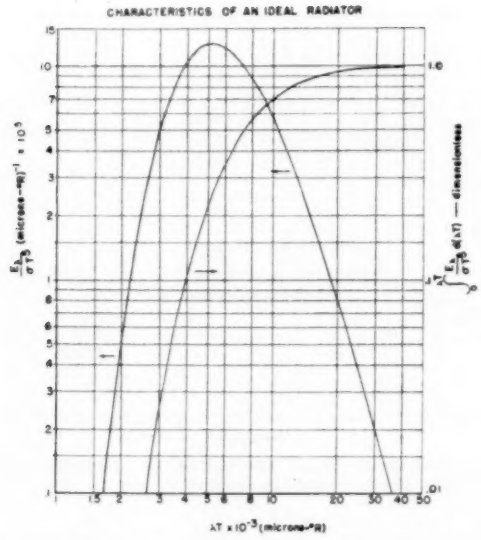

Fig. 5 Characteristics of an ideal radiator

The minimum value of λT for the 800 F temperature is 1260 at 1 micron and the power neglected in the computations is again negligible. At the long wave length end of the spectrum, 25 microns and 800 F give a value of $\lambda T = 31{,}500$ and approximately two per cent of the power is at wave lengths greater than 25 microns for this temperature. To avoid neglecting the power beyond 25 microns, the assumption was made that the reflectance of the sample from 25 to infinity was the same as the average reflectance from 24 to 25 microns. The following discussion shows the effect of this assumption upon the computations decreased as the temperature was increased.

Description of Samples

The samples were furnished by the sponsor of the work and therefore no control over the preparation of the surfaces was exercised by the authors. A description of the samples is given in Table 1 and shows the material and thermal treatment. For each test surface, two samples were furnished; namely (*a*) a disk 0.875 in. diam for spectral measurements and (*b*) a 6-in. square for total emittance measurements. Comparison of the two samples representing a single test surface indicated large variations in the visible spectrum for many surfaces. Such variations may arise from differences in the thickness of the oxide layers and/or composition of the oxides and are detectable as color differences. In addition, variations over the surface of the small disk were much

Table 1 List of radiation test specimens

Sample No.	Material	Thermal treatment
1	Titanium, Ti-75A; Mat'l Spec. AMS 4901	306 hr at 585 F
2	Titanium, Ti-75A; Mat'l Spec. AMS 4901	100 hr at 810 F
3	Titanium, Ti-75A; Mat'l Spec. AMS 4901	306 hr at 820 F
4	Titanium, Ti-75A; Mat'l Spec. AMS 4901	303 hr at 871 F
5	Titanium, Ti-75A; Mat'l Spec. AMS 4901	303 hr at 1003 F
6	Titanium, Ti-75A; Mat'l Spec. AMS 4901	None
7	Titanium alloy, C-110M; Mat'l Spec. AMS 4908	306 hr at 585 F
8	Titanium alloy, C-110M; Mat'l Spec. AMS 4908	100 hr at 810 F
9	Titanium alloy, C-110M; Mat'l Spec. AMS 4908	306 hr at 820 F
10	Titanium alloy, C-110M; Mat'l Spec. AMS 4908	303 hr at 871 F
11	Titanium alloy, C-110M; Mat'l Spec. AMS 4908	303 hr at 1003 F
12	Titanium alloy, C-110M; Mat'l Spec. AMS 4908	None
13	Titanium, Ti-75A; Mat'l Spec. AMS 4901; painted with Dow-Corning XP-310 aluminized-silicone paint	300 hr at 600 F
14	Titanium, Ti-75A; Mat'l Spec. AMS 4901; painted with Dow-Corning XP-310 aluminized-silicone paint	100 hr at 810 F
15	Titanium, Ti-75A; Mat'l Spec. AMS 4901; painted with Dow-Corning XP-310 aluminized-silicone paint	303 hr at 825 F
16	Titanium, Ti-75A; Mat'l Spec. AMS 4901; painted with Dow-Corning XP-310 aluminized-silicone paint	303 hr at 871 F
17	Titanium, Ti-75A; Mat'l Spec. AMS 4901; painted with Dow-Corning XP-310 aluminized-silicone paint	None
18	Type 321 corrosion-resistant steel; Mat'l Spec. MIL-S-6721	1000 hr at 705 F
19	Type 321 corrosion-resistant steel; Mat'l Spec. MIL-S-6721	None
20	Type 321 corrosion-resistant steel; Mat'l Spec. MIL-S-6721; silver-plated	303 hr at 682 F
21	Type 321 corrosion-resistant steel; Mat'l Spec. MIL-S-6721; silver-plated	None
22	Type 321 corrosion-resistant steel; Mat'l Spec. MIL-S-6721; painted with Rinshed-Mason black heat-resistant air-dry enamel H12144	300 hr at 497 F
23	Type 321 corrosion-resistant steel; Mat'l Spec. MIL-S-6721; painted with Rinshed-Mason black heat-resistant air-dry enamel H12144	307 hr at 690 F
24	Type 321 corrosion-resistant steel; Mat'l Spec. MIL-S-6721; painted with Rinshed-Mason black heat-resistant air-dry enamel H12144	1000 hr at 705 F
25	Type 321 corrosion-resistant steel; Mat'l Spec. MIS-S-6721; painted with Rinshed-Mason black heat-resistant air-dry enamel H12144	None

less than for the larger specimen as a result of the area differences. Consequently, some question exists as to the representative character of the disks relative to the larger squares. The discrepancies between the computed and measured values may be attributed in part to these differences. This will be discussed in a following section.

Discussion of Sources of Error

The spectral reflectances of the surfaces are presented in Table 2 and typical curves of the reflectance as a function of wavelength are shown in Figs. 6 through 12. The computed and measured values of emittance are given in Table 3 along with the differences between the two values.

The differences between the computed and measured values may be attributed to four factors:

(*a*) Dependency of the spectral emittance upon temperature.
(*b*) Errors in experimental techniques and calculations.
(*c*) Effect of heating upon the sample surfaces.
(*d*) Differences between the sample disks and the larger samples used for total measurements.

The relative importance of these factors is difficult to specify quantitatively and a qualitative discussion only can be given.

Temperature Dependency of Spectral Characteristics. The spectral emittance of the oxidized metal samples was a combina-

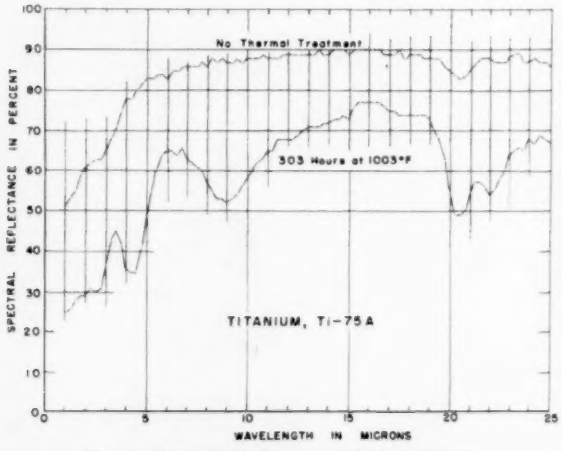

Fig. 6 Spectral reflectance: Titanium, Ti-75A

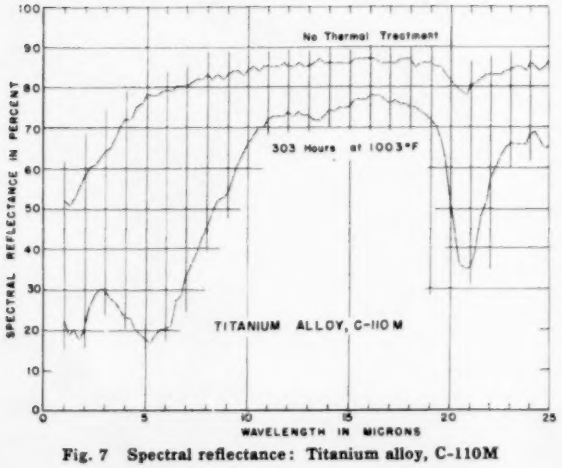

Fig. 7 Spectral reflectance: Titanium alloy, C-110M

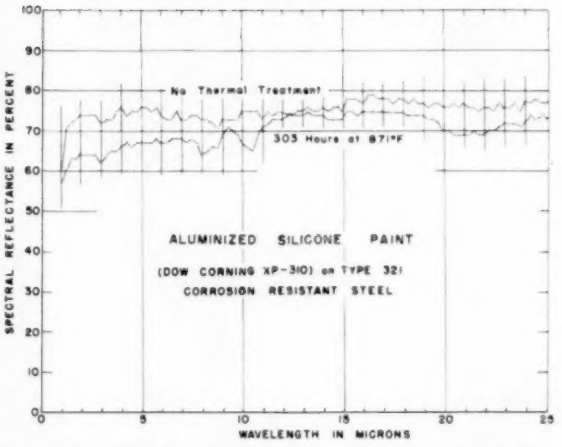

Fig. 8 Spectral reflectance: Titanium, Ti-75A; painted with Dow-Corning XP-310 aluminized-silicone paint

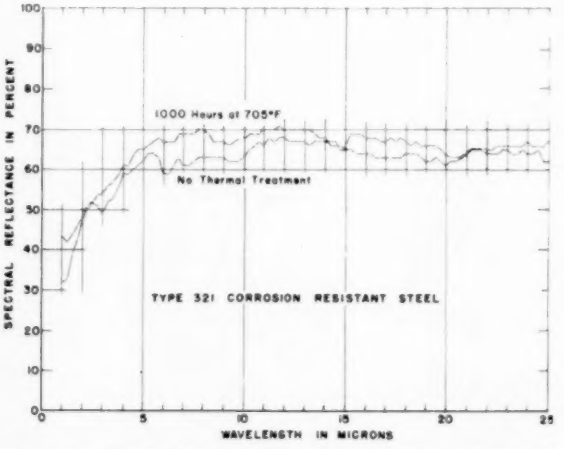

Fig. 9 Spectral reflectance: Type 321 corrosion-resistant steel

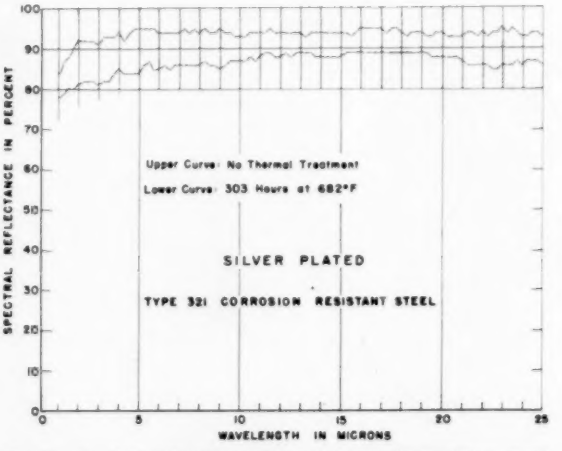

Fig. 10 Spectral reflectance: Type 321 corrosion-resistant steel, silver plated

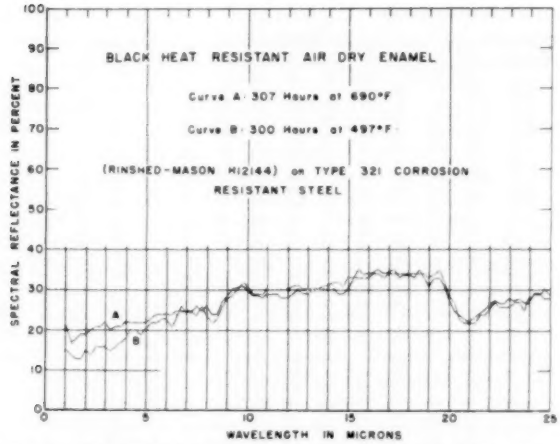

Fig. 11 Spectral reflectance: Type 321 corrosion-resistant steel; painted with Rinshed-Mason black heat-resistant air-dry enamel H12144

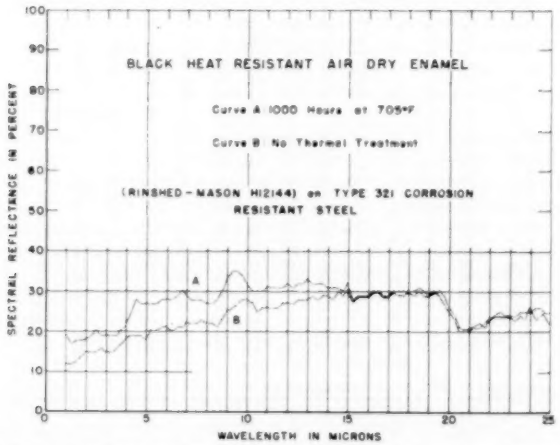

Fig. 12 Spectral reflectance: Type 321 corrosion-resistant steel; painted with Rinshed-Mason black heat-resistant air-dry enamel H12144

tion of the metal and the oxide acting together as emitters. Thus the emission was from the oxide film plus the emission from the metal transmitted by the oxide. If the emission from a pure polished metal is considered, the total emissive power can be shown to be given by (10)

$$E = \frac{36.05 C_1 \sqrt{\rho_{560}}}{C_2^{4.5}} T^4 \quad [5]$$

For an ideal radiator, the total emission is

$$E_{IR} = \frac{C_1}{15}\left(\frac{\pi}{C_2}\right)^4 T^4 = \sigma T^4 \quad [6]$$

The emissivity is given by the quotient of Equations [5] and [6]

$$\epsilon = \frac{(15)(36.05)\sqrt{\rho_{560}}}{\pi^4 \sqrt{C_2}} T \quad [7]$$

Thus the variation of the total emissivity with temperature based upon a reference temperature of 100 F, is given by

$$\epsilon_T = \epsilon_{560}\left(\frac{T}{560}\right) \quad [8]$$

Consequently, the theoretical variation of emissivity with temperature for a pure polished metal would indicate that the expected difference between a value computed from data obtained at 100 F and a value measured at 800 F would be

$$\frac{\epsilon_{1260}}{\epsilon_{560}} = \left(\frac{1260}{560}\right) \approx 2 \quad [9]$$

Inspection of the differences obtained (Table 3) will show that no change of this magnitude was found.

The emission of a pure dielectric (oxide) is not as readily analyzed since the theory of dielectrics is still somewhat inadequate. The reflection of a dielectric is given by the equations of Fresnel as derived from electromagnetic theory and may be found in most texts on optics or electromagnetic theory (e.g., 8). The relation between monochromatic reflectivity and the index of refraction for normal incidence given by this analysis is representative of the reflection of a dielectric

$$r_\lambda = \left(\frac{n-1}{n+1}\right)^2 \quad [10]$$

Using Equation [1], the expression for the reflectivity can be converted to emissivity

$$\epsilon_\lambda = \frac{4n}{(n+1)^2} \quad [11]$$

If the analysis were continued as has been done for metals, the next step would be the substitution of the expression for the indexes of refraction, as given by theory, into Equation [11]. The complexity of the equations resulting from this procedure is presented in the Appendix. Although quantitative results are not given, the analysis does indicate that the predicted increase in the monochromatic emissivity with temperature is not necessarily accompanied by an increase in the total emissivity. In addition, the theoretical effect of temperature upon the index of refraction is a function of the coefficient of thermal expansion of the dielectric. This coefficient is generally small (12) and as a consequence, the effect of temperature also should be small. Thus the use of spectral emissivity determined by the method outlined previously to calculate total emissivity at high temperatures, will not introduce theoretical errors of the magnitude indicated for metals.

When a thin layer of a dielectric covers the surface of a metal, the emittance is a function of the properties of the two materials. The variation of index of refraction and the absorption coefficient of the dielectric with wave length will then determine the importance of the base. If the surface dielectric is highly transmittant in the near infrared and visible region but highly absorbing in the infrared, the surface will have a small high-temperature emittance but a large low-temperature emittance. Surfaces which exhibit similar behavior are required frequently to minimize solar heating. An example of this is a polished metal, such as aluminum, coated with clear lacquer. Conversely, a surface with a coating over metal, highly absorbing in the visible and near infrared but transparent in the longer wave lengths, would yield a surface with a large absorptance for high-temperature sources such as the sun and a small emittance at lower temperatures. Solar-absorption surfaces have been made on this principle (11), and provide equilibrium temperatures significantly higher than other types of absorbers.

Errors of Measurement and Calculation. The errors involved in spectral reflectance measurements are partially a result of the system noise, spectral band width, and the operator.

Operator error never can be eliminated in any experimental work, and must be minimized by proper experimental methods.

Table 2 Spectral reflectance of all surfaces

WAVELENGTH	SAMPLE NO.											
Microns	1	2	3	4	5	6	7	8	9	10	11	12
1.0	50	37	37	31	25	51	43	29	20	23	22	52
1.25	47	40	35	28	26	53	45	30	19	22	19	51
1.50	50	48	42	20	28	55	47	38	22	20	20	53
1.75	54	50	47	16	29	59	50	43	26	18	18	56
2.0	56	54	51	17	29	61	52	46	35	17	20	58
2.25	58	57	55	22	31	62	53	49	39	17	26	60
2.50	58	57	56	26	30	63	54	53	42	19	29	61
2.75	60	59	57	30	31	63	56	54	47	22	30	63
3.0	62	59	59	33	38	65	56	57	48	24	30	64
3.25	65	62	61	38	43	68	60	58	50	26	28	65
3.50	69	65	63	43	45	71	62	60	55	30	27	68
3.75	73	68	66	49	42	75	64	63	58	34	25	71
4.0	76	70	69	53	36	78	67	66	62	37	23	72
4.25	75	71	70	56	35	78	69	66	64	42	23	72
4.50	78	73	71	58	35	80	71	68	65	44	20	73
4.75	80	75	73	62	41	82	72	70	68	47	19	76
5.0	82	76	75	64	49	83	74	71	69	52	18	78
5.25	82	77	76	66	55	83	75	74	70	54	17	78
5.50	83	79	77	67	60	84	77	73	71	57	19	78
5.75	84	79	77	68	64	84	78	74	73	59	20	79
6.0	83	80	78	70	66	83	78	75	72	63	20	79
6.25	83	80	78	71	65	85	78	76	74	63	21	79
6.50	84	81	79	73	64	85	79	76	74	64	27	80
6.75	85	82	79	74	66	86	80	76	75	67	29	80
7.0	85	82	79	73	63	86	80	78	78	68	33	80
7.25	85	83	80	75	62	86	80	79	76	69	36	81
7.50	86	83	81	78	61	86	81	79	78	71	39	82
7.75	87	84	81	77	60	87	82	78	77	73	43	82
8.0	86	84	81	78	57	86	82	80	77	74	45	83
8.25	87	85	82	79	55	88	83	81	77	73	49	82
8.50	87	84	82	78	53	87	83	80	78	74	52	83
8.75	87	85	81	79	53	88	84	80	78	75	53	82
9.0	86	85	82	80	52	87	84	81	78	75	54	83
9.25	87	86	83	79	53	87	84	81	79	77	58	84
9.50	87	86	83	79	54	88	83	81	79	77	61	84
9.75	87	86	84	80	56	87	83	82	80	77	64	83
10.0	88	87	84	81	58	88	83	81	80	78	66	84
10.25	87	87	85	81	60	88	85	82	80	80	68	85
10.50	87	87	84	82	62	88	85	81	81	80	70	84
10.75	88	87	85	82	63	89	85	82	81	80	70	85
11.0	89	88	85	81	65	88	86	82	82	81	72	85
11.25	89	87	86	82	65	88	86	82	82	80	73	86
11.50	90	87	86	82	68	88	86	83	82	82	73	85
11.75	89	88	85	83	68	89	86	83	82	82	73	86
12.0	89	87	86	81	68	89	87	83	81	81	74	85
12.25	89	88	86	83	68	89	86	82	82	80	73	85
12.50	88	88	85	83	69	89	86	82	82	80	74	86
12.75	88	87	85	83	70	89	86	83	82	80	73	86
13.0	88	87	86	83	71	89	86	83	82	81	73	85
13.25	88	88	86	83	71	89	86	83	82	80	72	86
13.50	89	88	86	84	71	90	87	83	82	82	72	87
13.75	89	88	86	84	72	89	87	83	83	80	73	86
14.0	89	88	86	84	72	89	87	84	83	81	74	86
14.25	89	87	86	81	73	90	86	84	83	81	74	86
14.50	88	88	86	82	73	90	86	83	83	82	75	86
14.75	89	89	86	84	74	90	88	83	83	82	75	86
15.0	89	88	86	83	73	89	85	83	83	84	75	86

WAVELENGTH	SAMPLE NO.											
Microns	13	14	15	16	17	18	19	20	21	22	23	24	25
1.0	72	69	57	57	60	32	43	78	84	15	21	19	12
1.25	73	72	60	60	71	33	42	79	87	14	17	17	12
1.50	74	74	62	63	72	39	44	80	88	13	18	18	13
1.75	76	74	63	63	73	43	48	80	90	13	19	18	14
2.0	76	74	63	64	74	47	48	81	92	18	19	18	18
2.25	77	75	64	64	74	50	51	82	92	14	20	19	15
2.50	77	75	64	64	74	52	52	82	92	16	21	20	15
2.75	76	75	63	64	74	54	51	82	92	16	21	19	16
3.0	76	74	62	62	72	54	49	81	91	16	22	19	18
3.25	76	74	64	64	73	58	52	82	93	15	20	19	15
3.50	77	75	64	65	73	57	53	82	93	16	21	19	16
3.75	77	76	65	65	75	59	56	84	93	17	21	20	17
4.0	77	77	65	66	76	61	59	85	94	18	22	21	18
4.25	77	78	65	67	74	61	59	84	92	20	22	25	19
4.50	77	77	66	66	75	64	60	84	94	20	22	28	19
4.75	77	76	67	67	75	65	61	84	95	19	22	27	19
5.0	77	77	68	67	76	65	62	84	95	20	22	27	18
5.25	78	77	67	67	76	66	64	86	95	22	23	27	20
5.50	77	77	67	67	75	67	64	87	96	22	24	27	20
5.75	77	77	67	68	76	68	63	85	95	23	24	28	21
6.0	77	77	67	67	74	67	59	85	94	23	24	28	21
6.25	77	76	66	67	73	67	59	86	94	21	24	28	20
6.50	77	76	66	68	73	67	61	85	94	24	25	29	21
6.75	77	76	67	69	75	69	63	86	94	26	25	30	21
7.0	76	76	66	68	73	69	61	86	94	25	25	29	22
7.25	76	76	66	67	73	69	61	86	95	28	25	28	22
7.50	76	75	67	68	74	69	62	88	94	24	26	28	22
7.75	75	75	66	67	74	70	63	86	95	26	25	28	23
8.0	75	73	63	64	73	70	63	86	94	24	26	27	22
8.25	75	73	64	65	73	69	63	87	95	22	24	27	22
8.50	75	74	64	66	72	67	63	86	94	23	24	28	21
8.75	75	75	66	66	71	67	63	86	94	26	27	30	23
9.0	75	76	68	69	73	67	63	85	95	28	28	33	25
9.25	76	79	69	71	73	66	62	86	94	29	30	35	26
9.50	77	79	69	70	73	67	62	87	94	30	30	35	27
9.75	77	78	67	69	73	68	62	87	93	32	31	34	28
10.0	77	77	66	67	75	68	63	87	93	31	30	32	28
10.25	77	76	65	66	75	69	65	87	93	29	29	30	27
10.50	77	76	63	65	75	69	66	88	94	29	29	30	25
10.75	77	78	67	69	75	69	67	87	94	29	29	30	26
11.0	77	78	71	71	73	70	66	88	94	30	29	31	26
11.25	77	79	72	72	75	70	68	89	94	30	29	31	26
11.50	77	79	72	73	74	70	67	89	95	30	29	31	26
11.75	77	78	73	73	75	71	68	89	94	30	28	31	27
12.0	77	79	73	73	75	70	68	88	94	30	28	32	27
12.25	77	79	73	74	74	70	67	89	94	31	29	31	27
12.50	77	79	74	74	74	70	67	88	94	31	30	32	28
12.75	78	79	72	74	75	70	67	89	94	30	29	32	28
13.0	79	79	73	74	75	70	67	89	94	30	29	33	28
13.25	78	79	73	75	76	70	68	89	93	30	30	32	29
13.50	78	79	73	74	75	69	67	89	94	30	30	32	28
13.75	78	79	74	74	75	69	67	88	94	31	30	32	29
14.0	78	79	73	74	76	68	67	88	94	31	30	31	29
14.25	78	79	74	73	75	68	67	88	94	32	30	31	28
14.50	77	79	73	73	76	68	67	88	94	32	29	31	30
14.75	78	80	73	73	76	68	68	88	94	31	29	30	29
15.0	78	80	73	73	75	68	68	88	94	33	30	32	30

WAVELENGTH	SAMPLE NO.											
Microns	1	2	3	4	5	6	7	8	9	10	11	12
15.25	90	89	87	84	76	90	86	83	83	82	77	87
15.50	90	88	87	84	77	90	87	84	83	81	77	87
15.75	89	88	87	85	77	90	87	84	83	82	77	87
16.0	89	88	88	85	77	90	86	84	83	82	78	87
16.25	89	89	88	85	77	90	87	84	84	81	78	87
16.50	90	89	87	84	77	90	87	84	84	81	78	88
16.75	90	88	87	85	76	89	86	84	83	81	77	86
17.0	89	87	87	84	75	89	86	84	83	81	76	86
17.25	90	87	87	84	75	89	87	83	83	80	77	86
17.50	89	87	87	83	74	90	85	83	82	79	76	87
17.75	89	87	86	84	74	88	86	83	83	80	76	87
18.0	88	87	86	83	74	89	85	83	82	79	75	87
18.25	88	86	86	83	74	89	85	82	82	79	75	85
18.50	88	86	86	82	74	89	85	83	82	78	74	86
18.75	88	85	86	82	74	88	85	82	81	78	73	86
19.0	87	84	85	81	73	88	85	82	81	71	72	86
19.25	87	85	84	81	70	88	84	82	80	76	70	85
19.50	86	85	84	79	69	88	84	80	77	75	67	85
19.75	85	83	83	77	63	86	82	78	75	70	62	83
20.0	83	81	80	73	55	85	80	77	67	63	53	82
20.25	80	78	78	69	49	84	76	74	67	58	43	80
20.50	80	78	77	68	49	83	76	72	68	55	36	79
20.75	80	78	78	70	50	84	76	74	72	56	35	78
21.0	82	79	79	71	54	85	77	74	73	60	35	80
21.25	83	81	80	74	57	87	79	76	74	64	40	81
21.50	84	82	82	76	57	88	81	77	76	68	48	82
21.75	84	83	82	78	58	88	81	77	77	70	51	83
22.0	85	83	83	77	54	88	81	78	78	70	57	83
22.25	85	84	82	78	55	87	82	78	78	72	60	83
22.50	85	83	83	77	58	87	82	78	78	72	63	83
22.75	85	83	84	78	60	87	83	78	78	73	65	84
23.0	85	84	85	79	64	88	81	79	77	74	66	84
23.25	86	83	84	78	65	89	84	80	78	73	66	85
23.50	86	83	82	79	66	89	83	80	76	74	66	85
23.75	85	83	83	78	65	87	84	81	77	74	66	84
24.0	86	84	84	78	66	87	82	81	76	74	68	86
24.25	85	83	83	80	67	88	82	81	77	75	69	85
24.50	86	83	83	78	69	87	82	80	76	73	67	84
24.75	87	83	82	78	68	87	81	79	78	72	65	85
25.0	84	83	80	75	67	86	81	77	76	71	65	86

WAVELENGTH	SAMPLE NO.											
Microns	13	14	15	16	17	18	19	20	21	22	23	24	25
15.25	78	80	75	75	78	65	69	89	94	33	33	29	28
15.50	78	80	75	75	78	64	69	89	93	33	35	29	29
15.75	77	80	75	74	78	64	69	89	94	33	34	29	29
16.0	78	80	75	75	77	64	68	89	95	33	34	29	29
16.25	79	80	75	75	79	64	68	89	95	34	34	30	30
16.50	78	80	75	75	79	63	69	89	95	34	35	30	30
16.75	78	80	75	75	78	63	67	89	95	33	34	29	29
17.0	78	79	75	75	78	63	67	89	95	34	34	29	29
17.25	78	80	76	75	78	63	68	89	94	34	35	30	30
17.50	77	80	76	75	77	63	67	89	95	34	33	30	29
17.75	78	80	76	75	78	63	68	89	95	34	34	30	29
18.0	78	80	76	75	78	64	67	89	94	34	34	30	30
18.25	78	80	76	74	77	64	66	89	93	34	33	30	29
18.50	78	80	76	74	78	64	67	89	94	34	35	31	30
18.75	78	80	76	74	77	63	66	89	94	34	33	30	29
19.0	78	80	75	74	77	62	66	89	94	33	31	29	29
19.25	77	80	74	73	76	62	66	89	93	34	33	30	30
19.50	78	79	74	73	77	63	66	88	93	35	33	29	30
19.75	78	78	72	72	77	62	65	88	94	32	31	27	29
20.0	77	78	71	70	76	61	64	88	94	29	28	25	26
20.25	77	78	70	70	76	62	63	88	93	27	25	23	24
20.50	77	77	69	69	77	62	63	88	93	25	23	20	21
20.75	78	78	69	69	76	63	63	88	93	22	23	20	20
21.0	77	77	68	69	77	64	64	87	93	22	22	20	20
21.25	76	78	68	69	76	65	65	86	94	22	23	21	21
21.50	77	77	68	70	76	65	65	86	94	24	24	21	22
21.75	77	77	69	69	75	65	65	86	93	24	25	22	21
22.0	76	77	69	69	76	64	65	86	94	25	26	25	23
22.25	77	78	69	70	76	64	65	86	93	27	27	24	24
22.50	77	78	71	70	75	64	66	85	94	26	27	25	24
22.75	77	79	70	71	77	65	66	86	94	28	27	24	24
23.0	77	80	70	72	76	65	66	86	95	26	26	24	24
23.25	78	79	71	72	76	64	66	86	94	27	27	24	23
23.50	78	80	72	72	77	64	66	86	95	27	28	25	24
23.75	78	79	72	71	75	65	66	87	94	28	27	25	23
24.0	78	79	73	72	77	64	67	86	93	28	27	25	26
24.25	79	79	73	74	77	64	66	87	93	29	29	26	23
24.50	79	80	74	73	78	65	66	87	94	29	29	26	24
24.75	79	79	72	74	77	62	66	87	94	30	28	25	25
25.0	78	80	73	73	77	62	67	86	93	29	28	25	22

Experimental procedures were established which required the reference energy level to be set as near full scale on the recorder as practicable. Hence the reflected energy level was also as large as practicable and the error in reading either the reference or reflected-energy level was reduced to approximately one per cent. Control of the gain is secured by varying the slit width of the monochromator which in turn determines the bandwidth viewed by the instrument. The errors in spectral values caused by large bandwidths are large in regions of rapidly varying spectral irradiation and/or regions of large variation in the spectral reflectance of the sample (6). Large changes in incident radiation will occur on the short-wave length side of the peak in the spectral emissive-power curve of the reflectometer (approximately 2.7 microns) but, fortunately, few surfaces have absorption bands in this region (see Figs. 6 through 12, or Table 2). The area of an integrated absorption band has been shown both theoretically and experimentally (6) to be independent of the spectral bandwidth under certain restrictions. The primary restriction, theoretically, is the requirement for constant incident energy over the absorption band. Experimentally, this restriction has been found to be less severe than established by theory. As a consequence of this, the errors resulting from spectral bandwidths applies primarily to spectral values and is eliminated effectively in the computed emittances (6).

The effect of emission from the sample has been shown to be less than one per cent for a sample temperature of 300 F and one tenth of this for 100 F (3). The effect of the errors in the spectral measurements are estimated to have caused an over-all error of approximately ± 0.02.

The calculations were performed with an electronic computer and were periodically checked as customary in such work. One possible source of error would be in the programming of the computations. This was partially checked by computing the total energy under the Planckian curve, Equation [4], and this value was found to be within the limit of the significant figures used for the programming. Errors in programming the spectral values are not known but the correspondence of results indicates these were a minimum.

The measurement of the total emittance of the samples and the errors involved have been fully discussed in a previous paper (9). The requirement for three consecutive values differing by less than ± 0.01 is believed to represent the magnitude of the operator error in these measurements. Analysis of the errors in calibration of the radiometer and temperature measurement have been estimated to have caused additional errors of from approximately 0.02 at the lowest temperature to 0.01 at the highest temperature.

Effect of Heating on the Surfaces. Measurement of the total emittance of a sample required the sample to be heated to a maximum of 800 F and as a consequence, each sample was subjected to oxidation in addition to that shown in Table 1. Total exposure to oxidation under all of the test conditions was approximately 10 hr. The effect of such an exposure is shown by the thermally untreated black painted sample. Reference to Fig. 17 illustrates the effect of additional oxidation above 600 F for a surface which is readily oxidized. Four black painted samples were tested, two oxidized at 700 F, one at 500 F, and one with no treatment. In each case, heating to 800 F caused an increase in the emissivity.

The emittances of the titanium, titanium alloy, stainless steel, and silver plate do not appear to have been altered by this short additional exposure to an oxidizing atmosphere, Figs. 13, 14, and 16. This is deduced from the fact that the data for different thermal treatments lie on parallel lines, differing only in the prior thermal treatment. The aluminum paint surfaces, Fig. 15, did not follow this parallel behavior pattern and a change in the effect of oxidation may occur at approximately 400 F. The change is small and experimental error may be the primary cause.

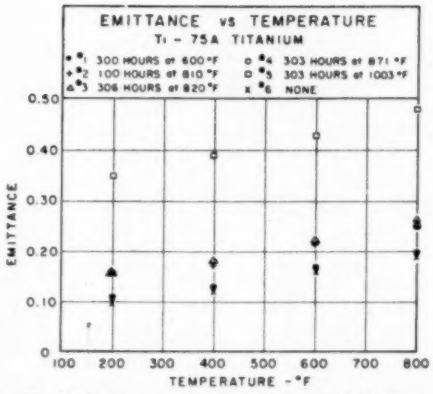

Fig. 13 Emittance versus temperature: Ti-75A titanium

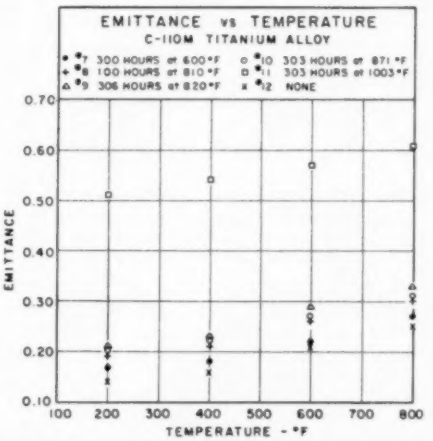

Fig. 14 Emittance versus temperature: C-110M titanium alloy

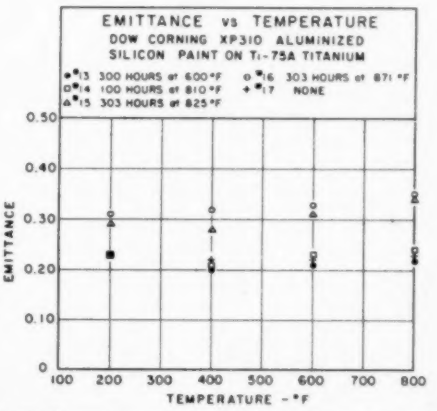

Fig. 15 Emittance versus temperature: Dow Corning XP310 aluminized silicone paint on Ti-75A titanium

Differences Between Samples Used for Spectral and Total Measurements. The two samples of each surface were compared visually as discussed previously and definite differences existed as to color and uniformity of the oxide coating. The small disks had more uniform surfaces by virtue of the small areas involved. The

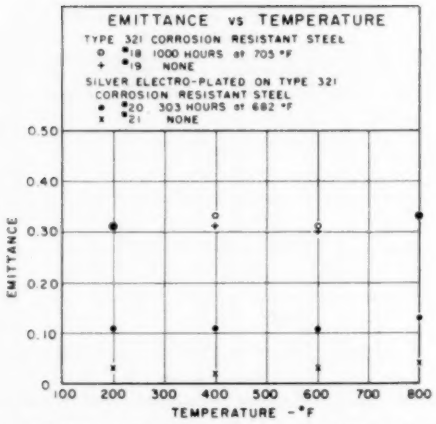

Fig. 16 Emittance versus temperature: (*a*) Type 321 corrosion-resistant steel; (*b*) silver electroplated on Type 321 corrosion-resistant steel

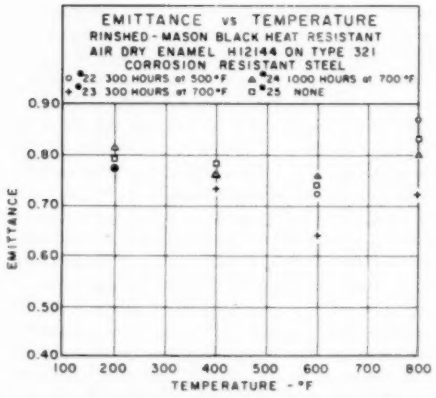

Fig. 17 Emittance versus temperature: Rinshed-Mason black heat-resistant air-dry enamel H12144 on Type 321 corrosion-resistant steel

variances observed in the visible portion of the spectrum do not necessarily indicate differences in the infrared except as representative of differences in nature and thickness of the oxides. There was no procedure available by which this could be determined.

Differences between the two samples of the same surface could have occurred from handling and preparation of the blank samples. The handling and preparation of the small sample disks would be expected to differ from those for the large square samples. Surfaces which are desired in the highly polished condition must be prepared with extreme care. Data obtained with surfaces such as aluminum or copper have indicated that such care is needed to approach the theoretical values of reflectivity (4). A surface which may appear to be clean and well polished may have a thin film which will reduce the reflectance by two per cent or more.

Discussion of Results

The foregoing discussion of the sources of error in the total and spectral emittances contains the following estimates of the total error in each measurement:

1 Spectral Emittance: ±0.02
2 Total Emittance: ±0.03

Discrepancies as large as ±0.05 may be expected therefore, between the computed and the measured values of emittance. Reference to Table 3 containing the differences between these two values will show that in the majority of surfaces, the differences are within the ±0.05 limit.

The differences for the titanium surfaces (Samples 1 through 6) were less than this value except for one, Sample 4. This surface had been oxidized for 300 hr at 850 F. For the titanium-alloy surfaces, only two were outside the established limits. Samples 10 and 11 gave results which were not within the set limits. Both had been given a maximum exposure to oxidization at elevated temperatures, Table 3. There is an apparent correspondence between extreme thermal treatments and the lack of agreement for the computed and measured emittances. The differences noted between the measured and computed emittances for Samples 4,

Table 3 Total emissivities

Sample No.	Temperature, deg F											
	200			400			600			800		
	Meas.	Calc.	Diff.	Meas.	Calc.	Diff.	Meas.	Calc.	Diff.	Meas.	Calc.	Diff.
1	0.11	0.15	−0.04	0.13	0.15	−0.02	0.17	0.18	−0.01	0.20	0.20	0.0
2	0.16	0.16	0.0	0.17	0.18	−0.01	0.21	0.21	0.0	0.25	0.23	+0.02
3	0.16	0.18	−0.02	0.18	0.19	−0.01	0.22	0.22	0.0	0.26	0.25	+0.01
4	0.16	0.22	−0.06	0.18	0.26	−0.08	0.22	0.31	−0.09	0.25	0.36	−0.11
5	0.35	0.39	−0.04	0.39	0.42	−0.03	0.43	0.45	−0.02	0.48	0.48	0.0
6	0.10	0.13	−0.03	0.12	0.15	−0.03	0.16	0.17	−0.01	0.19	0.19	0.0
7	0.17	0.18	−0.01	0.18	0.20	−0.02	0.22	0.23	−0.01	0.27	0.25	+0.02
8	0.19	0.21	−0.02	0.21	0.23	−0.02	0.26	0.25	−0.01	0.30	0.28	+0.02
9	0.21	0.22	−0.01	0.23	0.25	−0.02	0.29	0.28	+0.01	0.33	0.31	+0.02
10	0.20	0.27	−0.07	0.22	0.32	−0.10	0.27	0.38	−0.11	0.31	0.44	−0.13
11	0.51	0.44	+0.07	0.54	0.52	+0.02	0.57	0.59	−0.02	0.61	0.63	−0.02
12	0.14	0.17	−0.03	0.16	0.19	−0.03	0.21	0.21	0.0	0.25	0.23	+0.02
13	0.23	0.23	0.0	0.20	0.23	−0.03	0.21	0.23	−0.02	0.22	0.23	−0.01
14	0.23	0.22	+0.01	0.21	0.23	−0.02	0.23	0.23	0.0	0.24	0.23	+0.01
15	0.29	0.31	−0.02	0.28	0.32	−0.04	0.31	0.33	−0.02	0.34	0.33	+0.01
16	0.31	0.30	+0.01	0.32	0.31	+0.01	0.33	0.32	+0.01	0.35	0.32	+0.03
17	0.22	0.25	−0.03	0.22	0.25	−0.03	0.22	0.26	−0.04	0.23	0.26	−0.03
18	0.31	0.33	−0.02	0.33	0.34	−0.01	0.31	0.35	−0.04	0.33	0.36	−0.03
19	0.31	0.36	−0.05	0.31	0.37	−0.06	0.31	0.38	−0.07	0.33	0.39	−0.06
20	0.11	0.13	−0.02	0.11	0.14	−0.03	0.11	0.14	−0.03	0.13	0.15	−0.02
21	0.03	0.06	−0.03	0.03	0.06	−0.03	0.03	0.06	−0.03	0.04	0.06	−0.02
22	0.77	0.72	+0.05	0.76	0.74	+0.02	0.72	0.76	+0.04	0.87	0.77	+0.10
23	0.77	0.72	+0.05	0.73	0.73	0.0	0.64	0.75	−0.11	0.77	0.75	+0.02
24	0.81	0.71	+0.10	0.76	0.72	+0.04	0.76	0.73	+0.03	0.80	0.74	+0.06
25	0.79	0.75	+0.04	0.78	0.77	+0.01	0.74	0.78	−0.04	0.83	0.79	+0.04

NOTE: Difference is measured value minus calculated value.

10, and 11 may indicate a possible difference in the type and composition of the oxides formed on the titanium. A more extensive and detailed study would be necessary to determine the cause of these variations.

The surfaces of aluminum paint and electroplated silver yielded results which were satisfactory as determined by the limits of error established in the preceding discussion. The silver surfaces were subject to attack by sulfur compounds in the air and care was necessary to protect these surfaces during testing and during storage in the laboratory. The untreated stainless-steel surface (Sample 19) is an example of the difficulty involved in preparing two consistent samples of the same surface. Both the treated and untreated surfaces had approximately the same total emittance despite the fact that one of the samples had been exposed to an oxidizing atmosphere for 1000 hr at 700 F. The resistance of this material to oxidation is well known but such an exposure would be expected to cause detectable changes in the emittance. Reference to the spectral-emittance data (Table 2 or Fig. 9) will show that significant differences between the two surfaces were found for the small disk samples which would indicate similar differences in the total emittances.

The black painted surfaces furnish an example of another problem encountered in preparing samples. The effect of the thickness of a nonmetallic paint surface upon the spectral emittance is well established (4). This is the result of the transmission of such thin films and the reflection-transmission characteristics of the film and base surface in combination. In this respect, a paint surface is comparable to the oxide film on a metal surface although paints are generally less transparent. Preparing two samples of the same thickness and with the same background reflection is difficult. When this is combined with the effects of exposure to elevated temperatures for significant periods of time, the differences may be compounded. The lack of reasonable correspondence at the lowest temperature (200 F) is indicative of this problem since transmission effects should be a minimum at this temperature. Differences in the method of preparing the two sizes of samples of each surface would be apparent, however.

The total emittance variations with temperature of the various surfaces are of interest, exclusive of the comparison between the measured and computed results. The results have been presented in this form in Figs. 13 through 17. The several surfaces behave in a manner expected for the various thermal treatments; that is, as the exposure to elevated temperatures is increased, the emittance increases. The emittances remained relatively constant with temperature for the aluminum painted surfaces (Samples 13, 14, and 17) which were not exposed to the more extreme conditions. The silver-plated surfaces were most affected by the thermal treatment, Fig. 16, and conversely, the stainless steel was the least affected.

The black painted surfaces graphically demonstrate the effect of oxidation and changes in the surface coating which may occur at elevated temperatures. Large changes in the emittance occurred for a short exposure to a temperature of 800 F, Fig. 17. There is a certain anomalous behavior of the surface material which is evident by comparing the results obtained and the thermal treatments given to the various sample surfaces. For example, exposure for 300 hr at 700 F appeared to reduce the emittance more than exposure for 1000 hr at this temperature. The reasons for this behavior are unknown, but the effect of continued oxidation upon such an organic surface may initiate progressive changes which alter this decreasing trend in emittance. This black paint also displayed the negative slope with temperature frequently observed with dielectrics (see Appendix) whereas the oxidized metals tested in this program had a positive slope.

The comparison of the results computed from spectral measurements and those obtained by direct measurement have indicated that, within reasonable engineering limits and for the range of temperatures studied, either method is satisfactory. The most important advantage of the spectral method has not been discussed and that is, this procedure is the only one available for evaluating the effect of nonideal or nongray radiation sources. Consideration of such sources of radiant energy is becoming more important to the engineer as the demands of design become more restrictive. Without spectral information, there exists no means for the analysis of radiative heat absorption by a surface when exposed to a selective emission source such as the exhaust of a jet or rocket engine. The spectral characteristics of the absorbing surface are just as important in this case as they are for a solar absorber. The basic difficulty with the use of spectral reflectance data for computation of high-temperature integrated emittance or absorptance is the preparation of a sample which adequately represents the surface being considered.

Conclusions

The procedure, technique, and errors involved in using spectral reflectance data for computing total emittance at elevated temperatures, have been described and discussed. The effect of temperature upon the spectral data has been discussed and, for the temperature range considered, this effect was found to be small. This is primarily a result of the predominance of the ever-present oxide film on metals. The error in extrapolating data for a surface subject to extreme changes above a certain temperature, has been shown (Samples 22–25). A major source of error in the measurements derives from the preparation of a surface sample representative of the surface.

The technique of exposing a surface to various conditions of oxidation is one method of approaching the analysis of the transient radiation problem. This type of information is of great value in determining the changes which may be expected in the radiative heat load and to design for the worst conditions. An example in point is the behavior of the black-paint sample for oxidation at 700 F for 300 and 1000 hr. This sample also serves to illustrate the possible errors involved in the extrapolation of the emittance of a surface, particularly beyond the thermal treatment temperature.

Acknowledgments

The authors wish to express their appreciation to the various students who assisted in the performance of the experimental work, in particular Mr. D. K. Edwards, Mr. John I. Smith, and Mr. Robert R. Tipton. This work was performed within the Institute of Engineering Research, University of California, as a Service to Industry for the North American Aviation Company.

Bibliography

1 "Thermal-Radiation Tables and Applications," by R. V. Dunkle, TRANS. ASME, vol. 76, 1954, pp. 549–552.

2 "Introduction to Heat and Mass Transfer," by E. R. G. Eckert, McGraw-Hill Book Company, Inc., New York, N. Y., 1950.

3 "Measurement of Absolute Spectral Reflectivity from 1.0 to 15 Microns," by J. T. Gier, R. V. Dunkle, and J. T. Bevans, *Journal of the Optical Society of America*, vol. 44, 1954, pp. 558–562.

4 "Progress Report, Contract No. DA-11-190-ENG-3," by J. T. Gier and R. V. Dunkle, Institute of Engineering Research, University of California, Berkeley, Calif., Series No. 62, Issue No. 1, June 27, 1953.

5 "Final Progress Report, Contract No. DA-11-190-ENG-3," by J. T. Gier and R. V. Dunkle, Institute of Engineering Research, University of California, Berkeley, Calif., Series No. 62, Issue No. 5, August 31, 1955.

6 "Infrared Transmission of Synthetic Atmospheres, I. Instrumentation," by J. N. Howard, D. E. Burch, and Dudley Williams, *Journal of the Optical Society of America*, vol. 46, 1956, pp. 186–190.

7 "Heat Transmission," by H. C. Hottel, edited by W. H. McAdams, McGraw-Hill Book Company, Inc., New York, N. Y., third edition, 1954.

8 "Electromagnetism," by J. C. Slater and N. H. Frank, McGraw-Hill Book Company, Inc., New York, N. Y., 1947.
9 "Total Normal Emissivity Measurements on Aircraft Materials Between 100 and 800° F," by N. W. Snyder, J. T. Gier, and R. V. Dunkle, TRANS. ASME, vol. 77, 1955, pp. 1011–1019.
10 "Radiation in Metals," by N. W. Snyder, TRANS. ASME, vol. 76, 1954, pp. 541–548.
11 "Selective Radiation, I and II," by H. Tabor, *Bulletin of the Research Council of Israel*, Section A, First World Symposium on Solar Energy and Scientific Conference, November, 1955.
12 "Handbook of Chemistry and Physics," Chemical Rubber Publishing Company, vol. 37, 1955–1956, pp. 2059–2065.

Appendix

The classical theory of dispersion in solids is similar to the quantum theory of dispersion and differs only in the interpretation of the quantities involved. For the purposes of the following discussion, the classical theory will be adequate and yields the following expression for regions of small absorption[5]

$$n^2 - 1 = \frac{4\pi e^2}{m} N \sum_s \frac{f_s}{\omega_s^2 - \omega^2} \quad \ldots\ldots [12]$$

where n = index of refraction, e = charge of an electron, m = mass of an electron, f_s = oscillator strength, ω_s = resonant frequency, i.e., restrahlen frequency, ω = frequency of incident radiation, and N = number of oscillators per unit volume. The only temperature-dependent term is N, the number of oscillators per unit volume.

The theory of the thermal properties of solids predicts a linear variation in the volume with the absolute temperature.[6] Thus Equation [12] may be written for a specific frequency as

$$n^2 = 1 + CN_0 \frac{1}{1 + a(T - T_0)} \quad \ldots\ldots [13]$$

where C = const, N_0 = number of oscillators per unit volume at temperature T_0, and a = coefficient of thermal expansion. The value for the index of refraction is the positive root of the right-hand side of Equation [13]

$$n = \left[1 + \frac{CN_0}{1 + a(T - T_0)}\right]^{1/2} \quad \ldots\ldots [14]$$

The effect of the absolute temperature upon the index of refraction will be obtained by differentiating Equation [14] with respect to the temperature

$$\frac{dn}{dT} = -\frac{CN_0}{2}\left[\frac{1}{1 + a(T - T_0)}\right]^2 \left[1 + \frac{CN_0}{1 + a(T - T_0)}\right]^{-1/2} \quad \ldots\ldots [15]$$

The temperature-dependent expression for the monochromatic emissivity is obtained by substituting Equation [14] into Equation [11] of the text

$$\epsilon_\lambda = \frac{4\left[1 + \frac{CN_0}{1 + a(T - T_0)}\right]^{1/2}}{\left\{\left[1 + \frac{CN_0}{1 + a(T - T_0)}\right]^{1/2} + 1\right\}^2} \quad \ldots\ldots [16]$$

Substitution of Equation [16] into the dimensionless Planckian equation (Equation [4] of text) results in an expression which remains to be integrated. The temperature and the frequency terms (the constant C) in the expression occur in a manner which is difficult to handle in a closed form comparable to that for metals, Equation [5]. In addition, there is an apparent lack of correspondence between theory and experiment and the integration may not be meaningful.

The temperature dependency of the monochromatic emissivity is secured by differentiation of Equation [16]

$$\frac{d\epsilon_\lambda}{dT} = \frac{2CN_0}{[1 + a(T - T_0)]^2} \frac{\left\{\left[1 + \frac{CN_0}{1 + a(T - T_0)}\right]^{1/2} - 1\right\}}{\left\{\left[1 + \frac{CN_0}{1 + a(T - T_0)}\right]^{1/2} + 1\right\}^3} \quad \ldots\ldots [17]$$

The various factors in Equations [16] and [17] could be expanded in a binomial series and the resultant expressions simplified. However, the index of refraction in the infrared is frequently 2 or greater and to be valid, a number of terms of the series would be necessary. The resulting relations would not be a simplification.

The results obtained in Equations [16] and [17] illustrate the complexity of the problem. Furthermore, the effect of temperature is not necessarily correct. This may be shown qualitatively by observing that the monochromatic emissivity increases as the index is decreased (see Equations [3] and [11]). As a result, the theory presented indicates an increase in the spectral emissivity of a dielectric as the temperature is increased. Experimentally, the total emissivity frequently decreases as the temperature is increased for many dielectrics.[7,8] The theory is for the monochromatic value whereas the experiments are for total emissivity. Physically realizable situations can exist wherein the total emissivity will decrease, even though the spectral emissivity increases with temperature. To illustrate, consider the curves shown in Fig. 18. The emissivity at T_1 would be greater than at T_2 even though the monochromatic emissivity had increased.

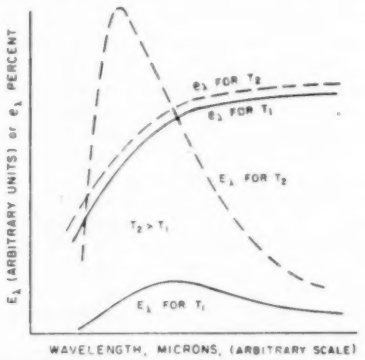

Fig. 18 Hypothetical illustration of decrease of total emittance with increased temperature although spectral emittance has increased

The conclusion may be made that the present theories for the index of refraction of dielectrics may not be adequate to explain properly the variation of total emissivity with temperature. Whether this is true, depends upon evaluation of the total emissivity by substitution of Equation [16] into Equation [4], as indicated previously. However, this is beyond the scope and intent of this presentation. Only the complexity and possible inadequacy of present theories were of interest.

5 "Light," by R. W. Ditchburn, Interscience Publishers, Inc., New York, N. Y., 1953.
6 "Introduction to Solid State Physics," by Charles Kittel, John Wiley & Sons, Inc., New York, N. Y., 1953.
7 "Measurement of Total Emissivities of Gas-Turbine Combustor Materials," by S. M. DeCorso and R. L. Coit, TRANS. ASME, vol. 77, 1955, pp. 1189–1198.
8 "Heat Transfer," by Max Jakob, John Wiley & Sons, Inc., New York, N. Y., 1949.

Discussion

G. A. Etemad.[9] The authors are to be commended for their extensive tests and excellent presentation of results. Their paper is an important contribution providing information on the emittances of the materials where few or no data existed. We at North American Aviation were interested in their data and analyzed it further in order to determine the total reflectance values of the specimens for incident energy distributions corresponding to a gray-body source at very high temperature. The analysis of the data for the samples presented in the paper and for 66 other samples, tested also by the authors, is published in a North American Aviation report.[10]

The samples investigated include materials in current use and materials being considered for future use by airframe manufacturers. The primary purpose of this investigation was to develop a material with high reflectance values for use on engine shrouds and, also, an external airframe surface material having a high emittance at the operating skin temperature but a low absorptance toward solar and nuclear fireball radiation. The spectral-reflectance data of a specimen were required to calculate the total reflectance or absorptance of the specimen when irradiated by energy from a high-temperature source.

Total reflectance, in terms of the authors' symbols, unless otherwise defined, is

$$r = \frac{\int_0^\infty r_\lambda E_\lambda d\lambda}{\int_0^\infty E_\lambda d\lambda} \quad \ldots\ldots\ldots\ldots\ldots\ldots [18]$$

E_λ, the monochromatic intensity of the incident radiation, is

$$E_\lambda = \frac{\epsilon_\lambda' c_1 \lambda^{-5}}{e^{c_2/\lambda T} - 1} \quad \ldots\ldots\ldots\ldots\ldots\ldots [19]$$

where ϵ_λ' is monochromatic emissivity of the source. Substitution of Equation [18] in Equation [19] gives

$$r = \frac{\int_0^\infty [r_\lambda \epsilon_\lambda' \lambda^{-5}/(e^{c_2/\lambda T} - 1)]d\lambda}{\int_0^\infty [\epsilon_\lambda' \lambda^{-5}/(e^{c_2/\lambda T} - 1)]d\lambda} \quad \ldots\ldots\ldots [20]$$

However, for a gray-body-source temperature range of 200 to 10,000 F, considered in this analysis, it can be shown that the limits of integration of Equation [20] can be changed from 0 and ∞ to 0.2 and 35 microns with negligible error; i.e.

[9] Research Specialist, Thermodynamics Section, North American Aviation, Inc., Los Angeles, Calif. Mem. ASME.

[10] "Spectral and Total Radiation Data of Various Aircraft Materials," by P. E. Ohlsen and G. A. Etemad, North American Aviation Report NA57-330, July, 1957.

Table 4 Description of additional radiation test specimens

Sample No.	Material	Thermal treatment
26	Black oxide coating (0.0004 in. thick) on type 321 corrosion-resistant steel	303 hr at 495 F
27	Same as above	303 hr at 682 F
28	Same as above	1000 hr at 692 F
29	Same as above	None
30	Rhodium flash (0.00002 in. thick) on nickel plate (0.0005 in. thick) on type 321 corrosion-resistant steel	200 hr at 500 F
31	Chromium plate (0.0001 in. thick) on nickel plate (0.0005 in. thick) on type 321 corrosion-resistant steel	None
32	Palladium plate (0.00005 in. thick) on silver plate (0.0005 in. thick) on nickel plate (0.0005 in. thick) on type 321 corrosion-resistant steel	None
33	Gold plate (0.0001 in. thick) on nickel plate (0.0005 in. thick on type 321 corrosion-resistant steel	None
34	Gold plate (0.0001 in. thick) on silver plate (0.0005 in. thick) on nickel plate (0.0005 in. thick) on type 321 corrosion-resistant steel	None
35	Type 17-4 PH corrosion-resistant steel	1 hr at 850 F
36	Type 17-7 PH corrosion-resistant steel	300 hr at 500 F
37	Same as above	100 hr at 1000 F
38	White paint (PV-100) on type 17-7 PH corrosion-resistant steel	None
39	Inconel X	4 hr at 1625 F Air cooled and then 10 hr at 1300 F
40	Inconel X	20 min at 1925 F Air cooled and then 10 hr at 1300 F
41	Aluminized-silicone paint (Dow Corning XP-310, 0.001 in. thick) on Inconel X	1 hr at 400 F Air cooled and then 10 hr at 1300 F

Table 5 Total reflectances in per cent

Sample No.	Temperature, deg F 200	400	600	800	1200	1600	2500	5000	10000
1	86	84	82	80	75	70	63	50	31
2	84	82	79	77	72	67	59	44	27
3	82	80	77	75	70	65	56	37	31
4	77	73	69	64	55	47	35	24	22
5	63	60	56	53	47	42	36	26	20
6	87	85	83	81	77	73	66	58	49
7	82	80	77	74	69	65	58	46	28
8	79	77	75	72	67	62	53	38	26
9	77	75	72	69	62	56	44	30	26
10	73	68	62	56	46	39	29	22	21
11	56	48	41	37	32	29	25	21	20
12	83	81	79	77	73	69	64	57	51
13	77	77	77	77	77	77	76	75	73
14	78	77	77	77	76	76	75	72	68
15	70	69	68	67	66	65	64	62	56
16	70	69	68	67	66	65	64	61	52
17	75	75	75	74	74	74	74	74	73
18	67	66	65	64	61	58	51	34	20
19	65	63	62	61	58	56	52	48	43
20	87	86	86	85	84	83	82	81	73
21	94	94	94	94	93	93	92	91	85
22	28	26	24	23	20	19	16	12	8
23	28	27	25	24	23	22	20	15	10
24	29	28	27	26	24	23	20	15	10
25	24	23	22	21	19	18	16	11	7
26	33	31	29	27	24	22	18	12	7
27	33	31	28	26	23	20	15	11	7
28	35	34	32	30	26	22	17	11	7
29	35	34	32	30	26	23	18	11	7
30	86	84	82	81	76	73	66	57	46
31	84	82	80	78	73	69	63	54	52
32	87	86	84	83	79	76	68	54	42
33	94	93	92	91	87	84	82	83	70
34	93	93	92	92	91	90	89	90	86
35	86	85	84	83	80	78	73	67	61
36	58	56	54	52	47	44	38	28	19
37	56	54	52	50	45	41	34	24	17
38	15	16	18	20	26	32	43	54	49
39	22	20	19	18	16	14	12	10	8
40	32	30	29	28	26	24	21	18	15
41	43	43	42	42	41	40	39	35	32

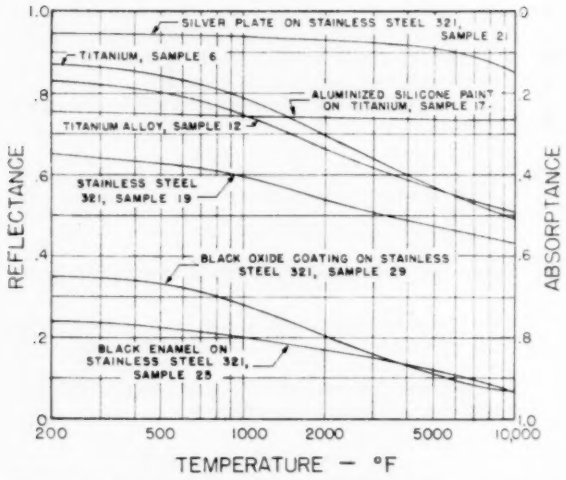

Fig. 19 Total reflectance and absorptance versus temperature

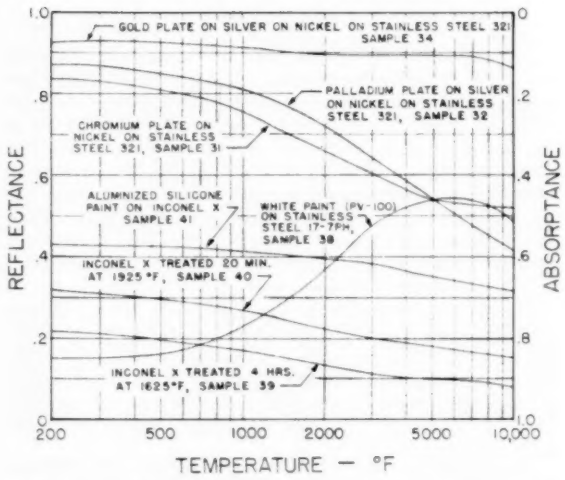

Fig. 20 Total reflectance and absorptance versus temperature

$$r = \frac{\int_{0.2}^{35} [r_\lambda \lambda^{-5}/(e^{c_2/\lambda T} - 1)]d\lambda}{\int_{0.2}^{35} [\lambda^{-5}/(e^{c_2/\lambda T} - 1)]d\lambda} \quad \ldots\ldots\ldots [21]$$

Equation [21] was programmed for IBM 704 computation by applying Simpson's rule and using wavelength increments of 0.02 micron. Since the data supplied by the authors covered a somewhat shorter wavelength range (0.4 to 25 microns) than required, it was necessary to extend the range by extrapolation. In this manner, total reflectance values for each specimen were computed for incident energy distributions corresponding to a gray-body source of nine different temperatures within the range of 200 to 10,000 F. The results, for the samples presented by the authors and some additional test specimens of interest as described in Table 4, are tabulated in Table 5, and typical curves of the reflectance and absorptance as a function of temperature are shown in Figs. 19 and 20 of this discussion.

The reflectance data of Table 5 for the temperature range of 200 to 800 F can be subtracted from unity to yield the emittance of the sample with good accuracy as pointed out by the authors. The emittances obtained in this manner agree quite well with the authors' calculated emittances.

It can be seen from the spectral data and curves of Figs. 19 and 20 that in general the reflectance of metallic surfaces decreases as the source temperature increases whereas the reflectances of paints tend to increase with temperature as the coatings build up and the surfaces assume the characteristics of the paint. A good example of this trend is white paint (see sample numbered 38). Aluminized silicone paint (see, for example, samples 17 and 41) exhibits approximately gray characteristics providing the heat-treatment is not too extreme. Sample 34 also illustrates the ability of proper plating combinations to exhibit gray characteristics.

An Investigation of Effective Thermal Conductivities of Powders in Various Gases

By R. G. DEISSLER[1] AND J. S. BOEGLI,[2] CLEVELAND, OHIO

An experimental study was made to determine the effective thermal conductivities of magnesium oxide, stainless steel, and uranium oxide powders in various gases. The gases included air, helium, argon, nitrogen, neon, and various mixtures of these gases. The variables investigated included temperature level, gas pressure, porosity, gas conductivity, and solid conductivity. A reasonably good correlation of the data was obtained by using the dimensionless groups effective thermal conductivity over gas conductivity, solid conductivity over gas conductivity, and porosity of the powder, although the effective conductivity may also be a function of the shape and arrangement of the particles. A solution for spheres in cubical array was obtained by relaxation and was in reasonable agreement with the data for porosities in the neighborhood of that for the spheres.

Nomenclature

The following nomenclature is used in the paper:

- a = fraction of space in powder occupied by gas
- Kn = Knudsen number, ratio of mean free path of gas molecules to mean particle size
- k = effective thermal conductivity of powder, Btu-ft/hr-sq ft-deg F
- k_B = Boltzmann constant, ft-lb/deg R
- k_g = thermal conductivity of gas, Btu-ft/hr-sq ft-deg F
- k_m = average effective thermal conductivity, evaluated at $(t_1 + t)/2$, Btu-ft/hr-sq ft-deg F
- k_s = thermal conductivity of solid, Btu-ft/hr-sq ft-deg F
- k_1 = thermal conductivity at r_1, Btu-ft/hr-sq ft-deg F
- L = length of tube, ft
- l_s = weighted mean sieve size required to retain particles, ft
- p = pressure, lb/sq ft abs
- p_b = breakaway pressure, pressure below which effective conductivity begins to vary appreciably with pressure, lb/sq ft abs
- Q = heat transfer, Btu/hr
- r = radius, distance from center of outer tube, ft
- r_1 = reference radius where thermal conductivity is calculated, ft
- s = molecular diameter determined from viscosity, ft
- t = temperature, deg R
- t_1 = temperature at r_1, deg R
- λ = mean free path of gas molecules, ft

Introduction

Among the materials which may be advantageous for use in nuclear reactor fuel elements are powders. In order to calculate the maximum temperatures in such fuel elements, where heat is generated by fission within the element, accurate knowledge of the thermal conductivity of the powder is required.

Although previous experimental work has been done on conductivities of powders (1),[3] the powders and temperature ranges of interest for nuclear applications were not considered. Correlations of powder conductivities were not developed to the point where predictions were certain. Accordingly, a program to obtain fundamental information on the thermal conductivities of powders of interest was initiated at the NACA Lewis laboratory.[4] The investigation used an improved measuring technique to be described later. Efforts were also made to obtain a general correlation for predicting the effective powder conductivity in terms of the solid conductivity, the gas conductivity, and the porosity of the powder.

Theory and Analysis

Maximum and Minimum Limits of Thermal Conductivity of a Two-Phase System. Before considering the thermal conductivity of a powder, it may be of value to examine the maximum and minimum limits of the thermal conductivity of any two-phase system. The maximum thermal conductivity of a two-phase system, such as a solid-gas system, is attained when the materials are arranged in alternate layers separated by planes parallel to the direction of heat flow. The minimum conductivity of such a system is attained when the materials are separated by planes running perpendicular to the direction of heat flow. These two cases are shown in Fig. 1, where the ratio of the effective conductivity of the system k to the gas conductivity k_g is plotted against the ratio of the solid conductivity k_s to the gas conductivity for various fractions a of space occupied by the gas. For $a = 0.4$ and

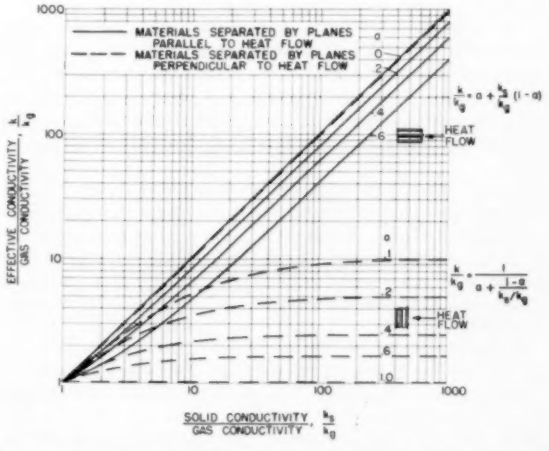

Fig. 1 Minimum and maximum effective thermal conductivities of two-phase systems; a, porosity

[1] Lewis Flight Propulsion Laboratory, National Advisory Committee for Aeronautics. Assoc. Mem. ASME.

[2] Lewis Flight Propulsion Laboratory, National Advisory Committee for Aeronautics.

Contributed by the Heat Transfer Division and presented at the Annual Meeting, New York, N. Y., December 1–6, 1957, of THE AMERICAN SOCIETY OF MECHANICAL ENGINEERS.

 Manuscript received at ASME Headquarters, August 1, 1957. Paper No. 57—A-110.

[3] Numbers in parentheses refer to the Bibliography at the end of the paper.

[4] A portion of the results were reported in references (2, 3, and 4).

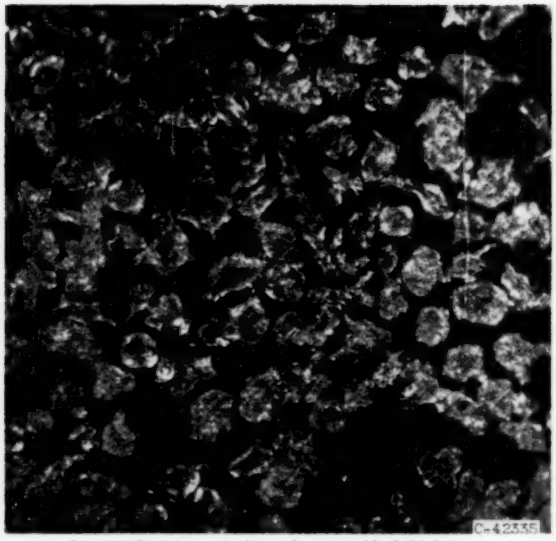

(*a*) 446 Stainless steel powder magnified 55.5 times

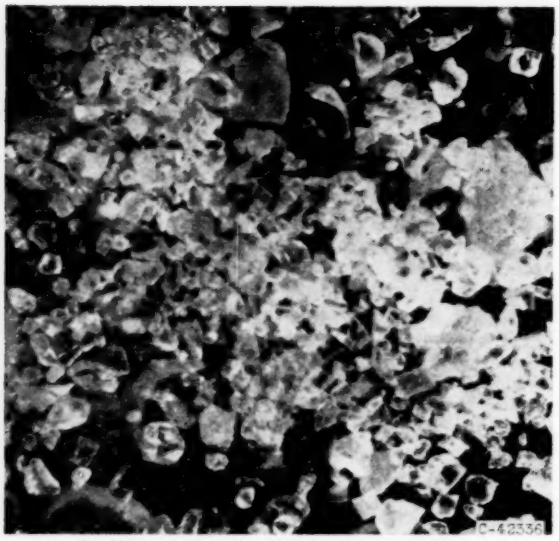

(*b*) Magnesium oxide powder magnified 55 times

Fig. 2 Enlarged photographs of powder particles

$k_s/k_g = 2$, there is a possible variation of the effective conductivity from the average of about ±7 per cent, whereas for $k_s/k_g = 1000$ there is a possible variation of ±99 per cent. This indicates that the effective conductivity of a system for a given fraction of space occupied by the gas (porosity) is greatly influenced by the arrangement of material for high values of k_s/k_g, whereas for low values of k_s/k_g the arrangement of material is of lesser importance. Inasmuch as k_s/k_g is high for most powders, the arrangement of material has an important effect on their conductivities.

Effective Thermal Conductivities of Powders. Theoretically, it should be possible to calculate the effective conductivity of a given powder from the conductivities of the solid and gas by using Laplace's heat-conduction equation in the solid and in the gas together with the boundary conditions at the interfaces. The actual calculation of results by this method, however, appears to be impracticable because of the irregular shape and arrangement of the powder particles. Fig. 2 shows photographs of typical magnesium oxide and stainless steel particles.

The most important characteristic of powders, in so far as it affects their effective thermal conductivities, is the presence of small regions or points of contact between the particles of solid in the powder. For high values of k_s/k_g most of the heat flow takes place in the vicinity of these points of contact because the gas acts as an insulator at points where the particles are separated.

Several attempts have been made to predict effective conductivities by using idealized models such as spheres or hyperbolas in regular array (2, 5). It appears, however, that any agreement with experiment obtained was probably fortuitous, inasmuch as the heat flow was assumed in those investigations to be unidirectional. However, the models might serve as a guide for correlating the data.

A somewhat more realistic model can be obtained by calculating the heat flow through a cubical array of spheres by relaxation or other appropriate means. This method avoids the assumption of unidirectional heat flow lines and will be used later in this paper. This method, of course, still does not account for the irregular arrangement and shape of the particles. It might be possible to obtain results by using the heat conduction equation in conjunction with statistical methods, but such an analysis has not yet been carried out.

Experimental Investigation

Apparatus. The apparatus used in the investigation is described in this section. In general, a different test section was used for each powder.

Fig. 3 shows a typical test section and the enclosing gas chamber and cooling jacket. The test section was 18 in. long and consisted of two concentric tubes separated by the powder under investigation. The inner ceramic tube (⅜-in. OD) was heated electrically by a carbon rod, or in some cases, where the temperatures were not excessive, by number 16 Nichrome heater wire wound on the tube. In the latter case, the Nichrome coils were coated with a high-temperature ceramic cement to give a smooth outer surface. Nichrome or platinum guard heaters 1⅛ in. long were wound on each end of the tube to compensate for end losses. The outer Monel metal tube had an inside diameter of 1¾ inches and was cooled by passing water through the cooling jacket of the gas chamber.

Temperatures were measured not only at the walls of the test section, but also at several radial locations through the powder. This method of temperature measurement was selected because of the difficulty in accurately measuring surface temperatures, especially that of the ceramic tube, and also to avoid measurements which might include contact resistance between the powder and the walls. The temperatures were obtained at ⅛-in. intervals by stretching number 28 chromel-alumel or platinum-platinum rhodium thermocouple wires through holes drilled in ceramic disks at each end of the test section. Four groups (90 deg apart) of five radially positioned thermocouple wire junctions are located in a plane across the center of the test section. Two of these groups are shown in Fig. 3. By using a large number of thermocouples at various radial positions, errors in thermal conductivity measurements due to errors in individual thermocouple readings are minimized. Mica spacers located one inch from either side of the thermocouple junctions aid in maintaining the distance between thermocouples while filling the test section with

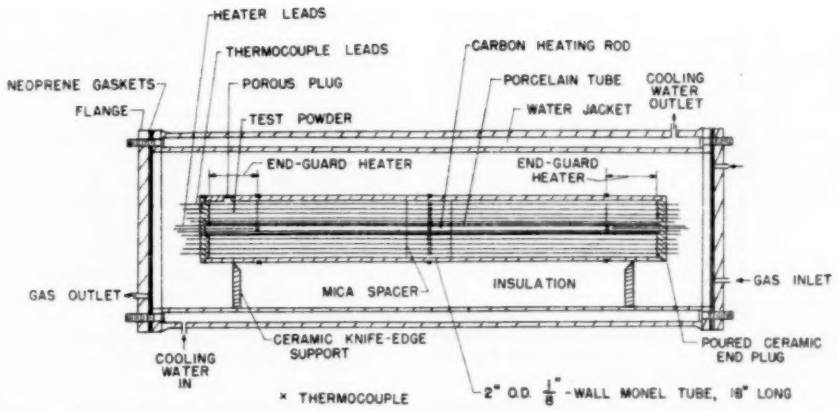

Fig. 3 Typical test section and gas chamber used for determination of thermal conductivities of powders in various gases

the powder. The thermal conductivity of mica is of the same order of magnitude as that of the powder.

Six additional thermocouples were located along the inner ceramic tube to guarantee a constant temperature along the axis of the test section and to regulate end heat losses. The outside surface temperature of the Monel tube was also measured at the center and at the ends.

A porous stainless-steel disk welded into a hole in the outer Monel tube wall allowed gas passage into and out of the powder voids.

The test section was centrally located in the gas chamber and was supported by two ceramic knife edges to minimize local heat conduction from the Monel tube. For the high temperature runs the volume between the test section and the gas chamber was filled with rock wool insulation. The gas chamber was surrounded by a water jacket to remove the heat from the test section and to aid in regulating the temperature level. It could be evacuated by the use of a vacuum pump and filled with pure, dry, bottled gas or mixtures of gases.

Electrical power from a 110-volt, 60-cycle source was supplied to the main heater and the two end heaters by individually controlled variable transformers having 2-kilovolt-amperes capacity. The power to the main heater was measured by a calibrated ammeter, voltmeter, and wattmeter. Temperature readings were obtained by a self-balancing indicating-type potentiometer.

Procedure. The test section was filled through a hole provided in one of the ceramic end disks with the powder to be investigated. The filling was done on a vibrating table.[5] The porosity or void fraction of the powder was determined by weighing the test section before and after filling, and measuring the volume of the empty test section by filling with liquid. With the density of the solid material in the powder known, the porosity could be calculated.

The positions of the thermocouple junctions distributed through the powder were determined from x-ray photographs of the filled test section.

Data were obtained for air, helium, argon, neon, nitrogen, and for various mixtures of these gases. Average powder temperatures varied from 200 to 1450 F in some cases. The pressure was varied from 0.15 to 100 psia for some runs, but most of the data were taken at pressures above the breakaway pressure, or the pressure below which the conductivity begins to vary appreciably. The calculation of the breakaway pressure will be discussed later. Replacement of one gas by another was accomplished by purging the entire system with the vacuum pumps several times and replenishing with the gas to be used. The gas pressure was held constant during each run. A small flow of water through the cooling jacket was also maintained for each run.

The power input to the main heater element was adjusted to give the desired temperature. The power input to each of the end-guard heaters was then adjusted to maintain a uniform temperature over the main heater element in order to prevent axial heat flow. After equilibrium conditions had been reached, the following quantities were measured: Power input to the main heating section, temperatures of the heating elements, temperatures through the powder, outside surface temperatures of the Monel tube, and gas pressure. For some of the runs, check points were taken after additional purging of the test section; in each case good agreement of the data with those of the initial run was obtained.

Reduction of Experimental Data. The equation for the heat flow between two concentric cylinders with uniform surface temperatures and a temperature-dependent thermal conductivity between the cylinders is

$$Q = \frac{2\pi k_m L(t_1 - t)}{\log_e\left(\frac{r}{r_1}\right)} \quad \ldots\ldots\ldots\ldots\ldots [1]$$

where t_1 and t are temperatures at the radii r_1 and r, and k_m is evaluated at $(t_1 + t)/2$. The derivation of Equation [1] is given in reference (2), where it is shown that k_m is rigorously evaluated at $(t_1 + t)/2$ if the variation of conductivity with temperature is linear. For the temperature differences occurring in the present tests, a linear variation is a sufficiently good approximation.

In calculating the thermal conductivity of the powder from the temperatures measured at various radii and the heat flow, it is desirable to plot the temperature against such a quantity that the plot is a straight line. This can be done by rewriting Equation [1] as follows

$$t = t_1 - \frac{Q}{2\pi k_1 L}\left[\frac{k_1}{(k_1 + k)/2}\log_e\left(\frac{r}{r_1}\right)\right] \quad \ldots\ldots\ldots [2]$$

where t_1 and k_1 are evaluated at the fixed reference radius r_1. Equation [2] shows that if t is plotted against $(k_1/k_m)\log_e(r/r_1)$, the plot will be a straight line with slope $-Q/(2\pi k_1 L)$. The

[5] The test sections were filled with magnesium oxide and uranium oxide powders by Knolls Atomic Power Laboratory.

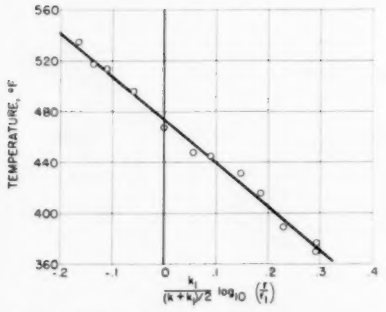

Fig. 4 Typical plot of radial temperature measurements for determination of effective thermal conductivity; k, conductivity at r; k_1, conductivity at r_1; r, radius; r_1, reference radius

thermal conductivity k_1 at temperature t_1 can be calculated from

$$k_1 = -\frac{Q}{2\pi L}\frac{1}{\text{slope}} \quad \ldots\ldots\ldots\ldots\ldots\ldots [3]$$

For plotting Equation [2], a relation between k and t must be assumed in order to calculate $k_1/[(k_1 + k)/2]$. After Equation [2] is plotted, the conductivity is calculated from Equation [3]. If the assumed values of k differ greatly from those calculated from Equation [3], the calculations are repeated using the new values.

It was found from the x-ray photographs of the test section that the center of the inner tube was usually displaced slightly from the center of the outer tube at the cross section where the radial temperature measurements were made. In order to locate the thermocouples at the positions they would occupy if the tubes were concentric, a correction derived in reference (2) was applied to the measured locations of the thermocouples.

By the use of the preceding method, a large number of thermocouple readings are used for determining each value of thermal conductivity, so that errors in conductivity caused by errors in temperature measurements are small. A typical temperature plot is shown in Fig. 4.

Results and Discussion

Effective Thermal Conductivities. Typical curves showing measured thermal conductivities of magnesium oxide, uranium oxide, and stainless steel powders in various gases are presented in Fig. 5. These data were all taken at pressures above the breakaway pressure; the breakaway pressure will be discussed in the next section. The curves indicate that the effective conductivity of the powder is a strong function of the conductivity of the gas. For the magnesium oxide powder, the effective conductivity with helium is about five times that with argon. The increase of effective conductivity with temperature is due to the increase of gas conductivity with temperature, inasmuch as the conductivity of solid magnesium oxide decreases with temperature. One would expect the gas conductivity to have more effect than that of the solid, inasmuch as most of the resistance to heat flow takes place in the gas ($k_s/k_g \sim 100 - 1000$).

Thermal conductivities of powders in various mixtures of gases are included in Fig. 5. Fig. 6 indicates an approximately linear variation of effective conductivity with gas composition.

Effect of Gas Pressure on Conductivity. The effect of gas pressure on the effective thermal conductivity of magnesium oxide powder is shown in Fig. 7. Similar curves were obtained for the

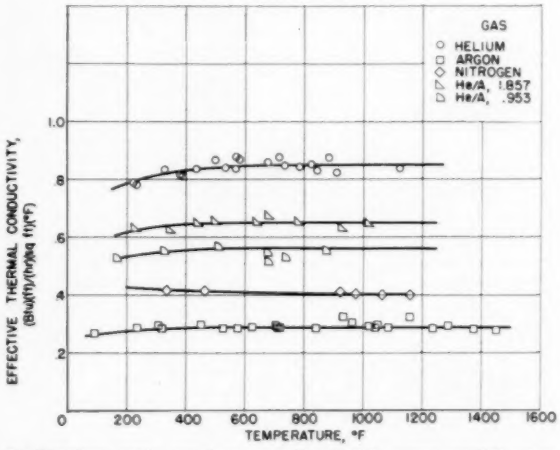

(*b*) **Uranium oxide powder; porosity, 0.405; mean particle size, 0.00027 ft**

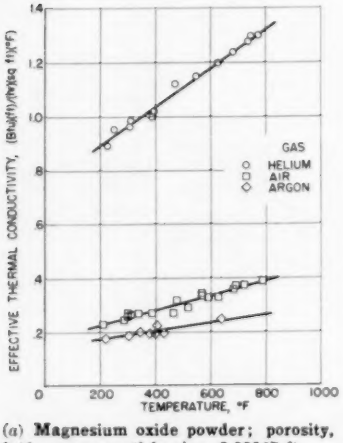

(*a*) **Magnesium oxide powder; porosity, 0.42; mean particle size, 0.00067 ft**

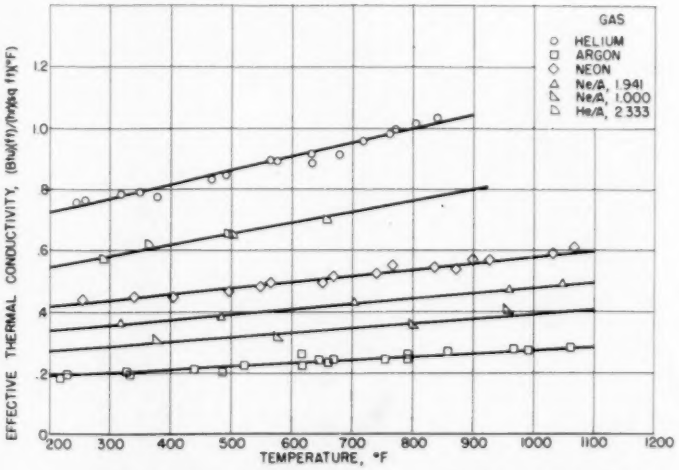

(*c*) **Stainless steel powder; porosity, 0.5; mean particle size, 0.00058 ft**

Fig. 5 Experimental effective thermal conductivities of various powders in various gases

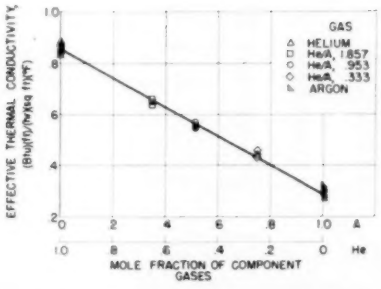

Fig. 6 Effect of gas mixture composition on effective thermal conductivity of UO_2 powder using data at temperatures above 500 F where the effective conductivities appear independent of temperature

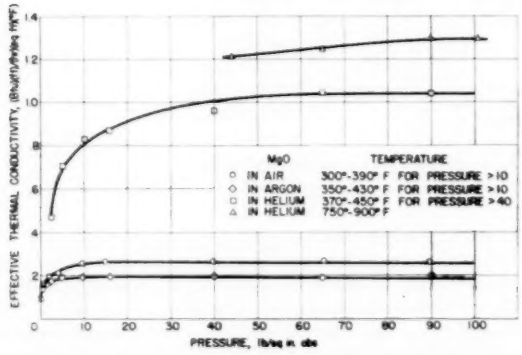

Fig. 7 Effect of gas pressure on effective thermal conductivity of MgO powder in various gases

other powders. For each curve there is a range of pressure for which the thermal conductivity is constant. Below this range the conductivity decreases rapidly as the pressure is reduced. The pressure range for constant conductivity varies with temperature and is different for different gases.

The observed effects of pressure can be explained by the kinetic theory of gases. For the range where the pressure has no effect on the conductivity, the mean free path of the gas molecules is small compared with the distances between the particles which are effective in transferring heat. For the long mean free paths which are obtained at low pressures or high temperatures the conductivity varies with pressure. The mean free path of the gas molecules also depends on the diameter of the molecules. The kinetic theory expression for the mean free path is

$$\lambda = \frac{k_B t}{\pi \sqrt{(2)} p s^2} \quad \ldots\ldots [4]$$

From dimensional analysis the ratio of mean free path to a characteristic dimension of the gas spaces (Knudsen number) must have a value, independent of the gas, the temperature, or the pressure, at which the conductivity begins to vary appreciably. It is assumed that the size of the effective gas spaces is proportional to the size of the particles, and the characteristic dimension l_s is taken as the weighted mean size of sieve required to retain the particles. The length l_s is found in reference (2) to be 0.00067 ft for the magnesium oxide powder in Fig. 7. The Knudsen number is given by

$$\mathrm{Kn} = \frac{\lambda}{l_s} = \frac{k_B t}{\pi \sqrt{(2)} p s^2 l_s} \quad \ldots\ldots [5]$$

From the data for air in MgO powder the pressure at which the conductivity begins to vary with pressure (breakaway pressure) is about 15 lb/sq in. at 340 F. The molecular diameter s for air is about 9.9×10^{-10} ft so that the breakaway Knudsen number as calculated from Equation [5] is about 0.00072. Inasmuch as this Knudsen number should be independent of the gas, the powder, the temperature, or the pressure, it can be used to predict the breakaway pressures for other gases and powders. Insertion of the value 0.00072 for Knudsen number in Equation [5] gives, for the breakaway pressure

$$p_b = 1770 \times 10^{-24} \frac{t}{s^2 l_s} \quad \ldots\ldots [6]$$

For helium, $s = 6.23 \times 10^{-10}$ ft and p_b from Equation [6] is 5850 lb/sq ft or about 41 lb/sq in. at 400 F. This value of breakaway pressure is in approximate agreement with the data for helium. For higher temperatures the data indicate that the breakaway pressure increases. This is also in agreement with Equation [6]. For argon the molecular diameter is about the same as for air, so that the breakaway pressures for the two gases should be about the same, as indicated by the data. Equation [6] is therefore in approximate agreement with the data for the three gases in MgO powder.

It was found that Equation [6] predicted the breakaway pressure satisfactorily for all the powders tested. In these powders the mean particle diameter varied from about 0.000146 to 0.00067 ft.

The value of Knudsen number corresponding to the breakaway pressure is seen to be much less than unity (0.00072 for the MgO powder in Fig. 7). This can be explained by the fact that most of the heat transfer through a powder takes place in the immediate vicinity of the points of contact of the particles so that the dimensions effective in transferring heat in the gas spaces are much less than the mean diameter of the particles.

Effect of Free Convection on Conductivity. The curves in Fig. 7 indicate that free convection is not an important factor in determining the effective thermal conductivity of a powder because at high pressures the thermal conductivity is independent of gas pressure. If there were appreciable free convection in the powder, the conductivity would continue to increase with pressure inasmuch as free convection is a function of the density of the gas. These results might not apply to particles larger than those investigated, inasmuch as free convection is a function of the dimensions of the gas spaces.

Correlation of Effective Conductivities of Powders. Fig. 1 suggests that, for a given type of arrangement of material, k/k_g should be a function of k_s/k_g and of porosity a. If all the powders tested had the same arrangement and shape of particles, the data should correlate in terms of these parameters.

Fig. 8 shows k/k_g plotted against k_s/k_g for all of the data obtained. The gas conductivities were taken from references (6 to 9), the solid conductivities from references (10, 11, and 12). The conductivities of the gas mixtures were calculated from the Enskog equation (13).

The data appear to fall into two groups, one for a, 0.36–0.405; the other for a, 0.42–0.50. The values of k/k_g are higher for the low porosities than for the high ones as would be expected. However, the variation with a is not smooth. Other factors, such as the shape and arrangement of the particles and the pressure on the particles (not gas pressure) may be affecting the conductivities.

Comparison of the data in Fig. 8 with those of other investigators as summarized in reference (1) indicates reasonable agreement in most cases for the same ranges of porosity.

It is of interest to compare the data with solutions for regular particles in regular arrangement. In reference (14) it was found that, for squares arranged in checkerboard fashion ($a = 0.5$)

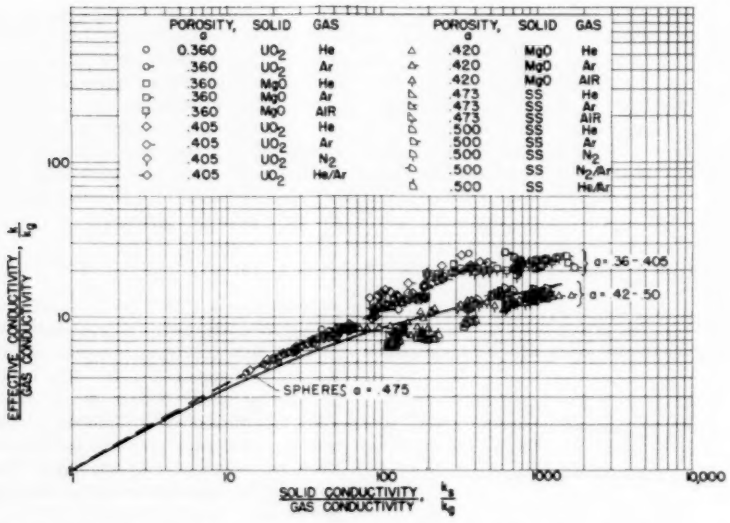

Fig. 8 Correlation of experimental effective thermal conductivities of powders in various gases and comparison with solution for spheres

$k/k_g = (k_s/k_g)^{1/3}$ for heat flow in any direction parallel to the plane of the squares. However, the value of k/k_g computed from that equation for $k_s/k_g = 1000$ is about twice that for the data.

A calculation of heat transfer through spheres in cubical array has been carried out by solving the heat conduction equations in the solid and in the gas by the relaxation method. The method of calculation is similar to that given in reference (2), wherein the materials through which heat conduction takes place are replaced by a network of rods. For spheres the thickness of the rods varies with distance from the axis of mean heat flow. Axial symmetry is assumed. This is a good assumption for large values of k_s/k_g where the heat conduction in the gas near the edges of the cube is small. It was necessary to use extremely small grids in the region near the point of contact of the spheres inasmuch as most of the heat flow takes place in that region.

The resulting curve is plotted in Fig. 8. For this case $a = 0.475$. The calculated curve is in reasonable agreement with the group of data for a, 0.42–0.50. The better agreement of the spheres than of the squares with the data is reasonable, inasmuch as the actual heat flow in the powder is three dimensional rather than two dimensional.

The correlation of the data and the agreement of the solution for spheres with the data are somewhat better than one might have expected. When an attempt was made to simulate heat transfer through powders by an electrical analog using carbon disks or spheres in an electrolyte ($k_s/k_g \sim 1000$), reproducible results could not be obtained. It was found that by pressing the particles together slightly the effective conductivity could easily be doubled. These effects are not surprising if we consider Fig. 9. Fig. 9 shows the calculated temperature distribution for heat flow through spheres in cubical array. The light solid lines are constant temperature lines. The figures indicate that, as k_s/k_g increases from 3 to 30, the constant temperature lines crowd together in the vicinity of the point of contact; that is, more of the heat flow across the gas space takes place near the point of contact. It is evident that for values of k_s/k_g on the order of 1000 nearly all the heat flow will take place through an extremely small area near the point of contact. This effect can be seen more clearly in Fig. 10, where the ratio of local heat flux to average heat flux across the plane containing the point of contact of the sphere (plane A-A in Fig. 9) is plotted against distance from the point of contact divided by sphere radius. Values of q/q_{av_g} on the order of 5000 are indicated near the point of contact for high values of k_s/k_g. The effective conductivity will therefore be very sensitive to the exact way in which the particles make contact and to slight irregularities on the surfaces near the points of contact. In view of these observations it is surprising that the effective conductivities of powders correlate as well as they do. It may be that for a very large number of particles, individual differences from particle to particle tend to cancel.

Summary of Results

The following results were obtained from the investigation of effective thermal conductivities of powders:

1 The effective conductivity of the powder is a strong function of the conductivity of the gas. For instance, the effective conductivity of magnesium oxide powder in helium was about five times that for the same powder in argon.

2 The effective conductivity of a powder becomes nearly independent of pressure at some ratio of mean free path of gas molecules to a characteristic dimension of the powder particles. For all of the powders investigated the breakaway pressure could be predicted by an equation based on the kinetic theory of gases.

3 Free convection did not affect the conductivities of the powders investigated (mean particle diameter, 0.000146 to 0.00067 ft).

4 A reasonably good correlation of the data was obtained by plotting the ratio of effective conductivity to gas conductivity against the ratio of solid conductivity to gas conductivity for various porosities. A relaxation solution for heat flow through spheres in cubical array (porosity = 0.475) was in reasonable agreement with the group of data for porosities from 0.42 to 0.50.

5 Most of the heat flow across the gas spaces between the particles takes place in extremely small areas near the points of contact. The heat flow between powder particles is therefore very sensitive to the exact way in which the particles make contact and to slight irregularities on the surfaces near the points of contact.

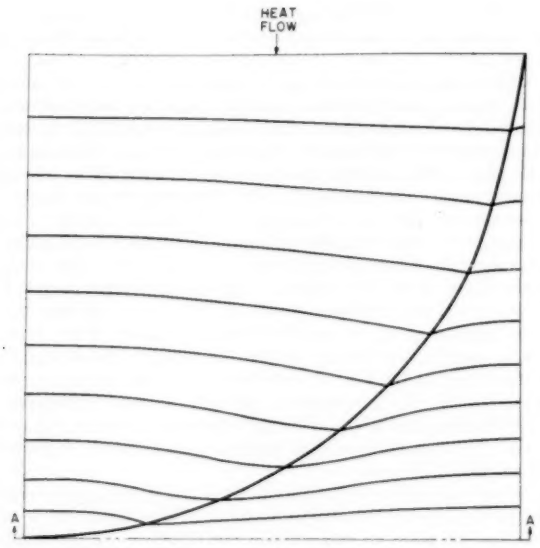

(a) k_s/k_g, 3

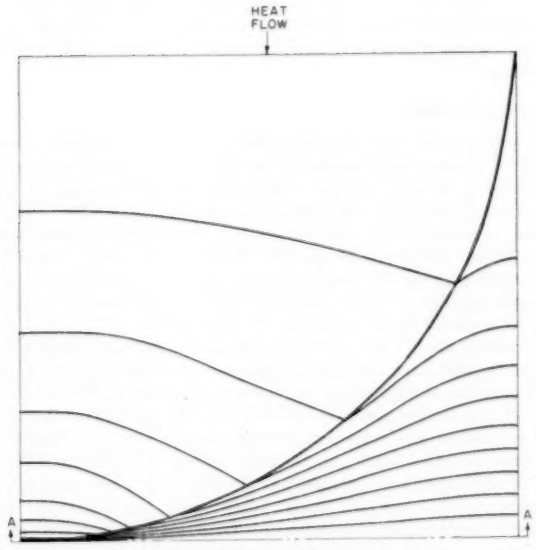

(b) k_s/k_g, 30

Fig. 9 Constant temperature lines in representative sample of spheres in cubical array as obtained by relaxation solution

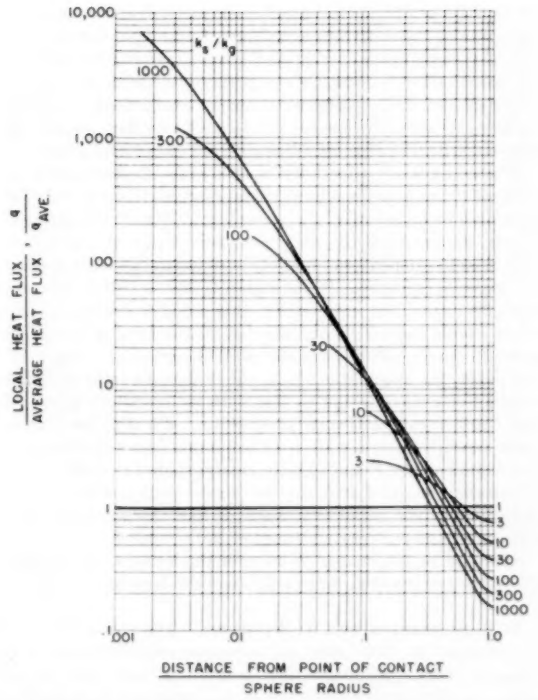

Fig. 10 Variation of ratio of local heat flux (per unit area) to average heat flux across plane A-A in Fig. 9 for various values of k_s/k_g

Bibliography

1 "Reaction Rate, Heat Transfer, and Temperature Distribution in Fixed-Bed Catalytic Converters," by R. H. Wilhelm, W. C. Johnson, R. Wynkoop, and D. W. Collier, *Chemical Engineering Progress*, vol. 44, no. 2, 1948, pp. 105–116.

2 "Investigation of Effective Thermal Conductivities of Powders," by R. G. Deissler and C. S. Eian, NACA RM E52C05, 1952.

3 "Effective Thermal Conductivities of Magnesium Oxide, Stainless Steel, and Uranium Oxide Powders in Various Gases," by C. S. Eian and R. G. Deissler, NACA RM E53G03, 1953.

4 "Measured Effective Thermal Conductivity of Uranium Oxide Powder in Various Gases and Gas Mixtures," by J. S. Boegli and R. G. Deissler, NACA RM E54L10.

5 "Heat Flow Through Granulated Material," by T. E. W. Schumann and V. Voss, *Fuel in Science and Practice*, vol. 13, no. 8, 1934, pp. 249–256.

6 "The NBS-NACA Tables of Thermal Properties of Gases. Table 2.42 Dry Air Thermal Conductivity," by R. L. Nuttall, December, 1950.

7 "The NBS-NACA Thermal Properties of Gases. Table 19.42, Argon Thermal Conductivity," by R. L. Nuttall, July, 1951.

8 "A Summary of Viscosity and Heat-Conduction Data for He, A, H_2, O_2, N_2, CO, CO_2, H_2O, and Air," by F. G. Keyes, TRANS. ASME., vol. 73, 1951, pp. 589–596.

9 "Thermal Conductivities of Gases," by F. G. Keyes, TRANS. ASME, vol. 76, 1954, pp. 809–816.

10 "The Thermal Conductivity of Ceramic Refractory Materials. Its Calculation Based on the Thermal Conductivity of the Components," by A. Eucken, *VDI Forschung*, vol. 353, 1932. (Translated by General Electric Company, July 11, 1950).

11 "The Thermal Conductivity of Metals at High Temperature," by C. L. Hogan and R. B. Sawyer, *Journal of Applied Physics*, vol. 23, no. 2, 1952, pp. 177–180.

12 "Thermal Conductivity: X, Data for Several Pure Oxide Materials Corrected to Zero Porosity," by W. D. Kingery, J. Francl, R. L. Coble, and T. Vasilos, *Journal American Ceramic Society*, vol. 37, no. 2, Part II, Thermal Conductivity, February, 1954, p. 108.

13 "Measurements of the Heat Conductivity of Nitrogen-Carbon Dioxide Mixtures," by F. G. Keyes, TRANS. ASME, vol. 73, 1951, pp. 597–601; discussion, pp. 601–603.

14 "On the Conductivities of Certain Heterogeneous Media for a Steady Flux Having a Potential," by C. H. Lees, *Philosophical Magazine*, vol. 49, 1900, pp. 221–226.

Discussion

B. E. Short.[6] The authors are to be congratulated for their paper. Possibly it is of particular interest to the writer since we were involved in a very brief and somewhat crude experimental

[6] Professor of Mechanical Engineering, The University of Texas, Austin, Texas. Mem. ASME.

study of this sort during the past summer with a fibrous insulating material. Our study was a comparison of the effective or apparent thermal conductivity of a fibrous material for high temperatures (1200 to 1500 F) used with air and with helium. Our study showed that the effective thermal conductivity of this material with helium was from 1.75 to 2.5 times that for the same material with air when at a temperature of 1000 to 1400 F.

The minimum conductivity to which the authors refer, that of parallel plates of the solid material (perpendicular to heat flow) separated by layers of the gas, according to Nusselt and quoted by Jakob, implies that the effective conductivity of the material should be less dependent on the type of gas as the temperature of the material increases. In the region of 800 to 1500 F this radiation effect should be appreciable. It is thought that the radiation effect should not be greatly affected by the type of system employed; that is, whether parallel plates or granular. Fig. 5(*a*) of the paper, for magnesium oxide, shows that the ratio of effective conductivity with helium to that with air is slightly above 4 at 200 F and slightly less than 3.5 at 800 F. Fig. 5(*b*) for uranium-oxide powder shows a ratio with helium to that with nitrogen of less than 2 at 200 F and slightly greater than 2 at 1200 F.

Nusselt's analysis with the flat plates would indicate a large reduction in the ratio with gases of like thermal-conductivity ratios over the temperature range of 200 to 1200 F.

It would be interesting to learn of the authors' evaluation of the difference between their results and the Nusselt analysis.

D. G. Stephenson[7] and W. Woodside.[7] The authors are to be commended on their clear and complete presentation of a fine piece of work. Although their concern is with heat transfer from nuclear reactor fuel elements, the results of their study are of interest in other fields of research. At the Division of Building Research of the National Research Council of Canada we have been studying heat flow and temperature distribution in soil particles. In this we also considered the idealized model of spherical particles stacked in cubical array and have determined, by experiments on a model, values of K/K_g for three values of K_s/K_g.

The model consisted of four hemispheres of marble of radius $3 \pm 1/64$ in., sandwiched between two plates of $^3/_8$-in-thick aluminum, these plates representing the isothermal planes through the centers of the spheres and the points of contact, respectively. The edges were closed in by $^1/_8$-in-thick lucite. The thermal conductivity of the marble (K_s) was determined by guarded hot-plate tests on two slabs of marble from the same source as the hemispheres. By filling the void space in the model with different materials of known conductivity (K_g), different values of the ratio K_s/K_g could be realized. The thermal conductivity K of the model was determined with an 18 × 18-in. guarded hot-plate apparatus, one of the aluminum face plates of the model fitting exactly over the 12 × 12-in. test area of the hot plate. Values for K_s/K_g of 6.4, 30, and 80 were obtained by using as fill materials dry sand, vermiculite, and silica aerogel, respectively. The corresponding values of K/K_g were found to be 3.2, 6.2, and 10.3. The maximum possible error in these values is estimated at less than 5 per cent.

Since these results differed from the authors' calculated results shown as the solid line in Fig. 8, we have tried to check by relaxation one point on their curve. For $K_s/K_g = 80$, the results in Fig. 11 were obtained. These data lead to a value for K/K_g of 8.2, whereas Fig. 8 shows a value of approximately 7.8.

It would be of interest to know why our relaxation gives a larger value of K than is obtained by the authors, and also why the relaxation solutions differ so much from the experimental results.

[7] Building Services Section, National Research Council, Ottawa Canada.

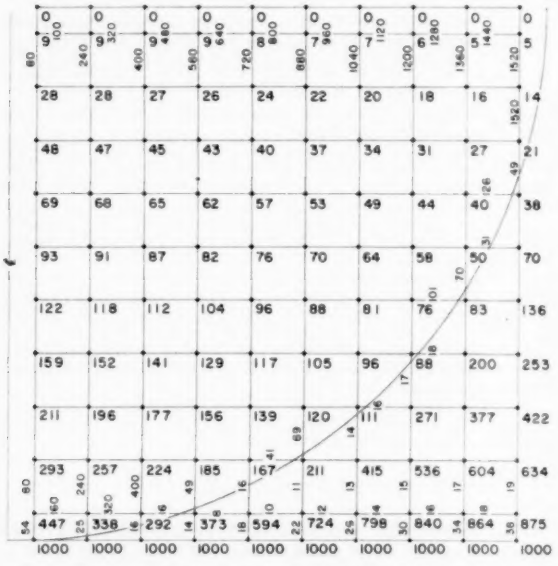

Fig. 11 Temperature distribution in a sphere which forms part of a cubical array, with $K_s/K_g = 80$. The numbers at each nodal point are the temperatures, the numbers along the grid lines are the conductances.

Authors' Closure

The authors wish to thank Messrs. Short, Stephenson, and Woodside for their interesting discussions. In connection with Professor Short's remarks concerning the comparison of the present experiments and the analysis of Nusselt, it appears that the difference in the results is due to the simplified model and radiation effect considered by Nusselt. Although Nusselt's parallel plate model indicates that we might have appreciable radiation effects in some cases, his model overestimates the relative importance of radiation. In the actual case, where the powder is made up of particles which are in contact, rather than parallel plates separated by the gas, the heat transfer by conduction will be much greater due to the contacting particles, and the heat transfer by radiation will be lower due to the fact that the form factors will be lower than for parallel plates. A rough estimate indicated that the radiation effect in the experiments probably would not amount to more than a few per cent in the worst case, so that the trends predicted by Nusselt should not apply to the present experiments. In the case of the experiments on fibrous materials mentioned by Professor Short, it is possible that Nusselt's parallel plate model might give a closer approximation than it did for the powder particles, so that in that case Nusselt's trends might apply.

In comparing Messrs. Stephenson's and Woodside's relaxation solution with that of the authors, it appears that the agreement of the two sets of calculations to within 5 per cent is probably satisfactory. In order to obtain more accurate solutions, it would be necessary to use finer grids. It should be mentioned that the grid lines used by the authors were all shifted half a grid width from those in Fig. 11. This difference will not, of course, affect the results for sufficiently fine grids.

It is difficult to say why the experimental results of Messrs. Stephenson and Woodside should differ so much from the calculated relaxation solutions. The following suggestions are offered only as possibilities. As mentioned in the paper, the high

heat flux concentration near the point of contact of the spheres at high ratios of k_s/k_g makes the effective conductivity sensitive to slight irregularities near the point of contact. Thus if the marble or the filling material happened to be inhomogeneous near the point of contact or if the surface were slightly irregular at that point, the conductivity could be affected. Slight external pressure might increase the measured conductivity by producing a finite area of contact between the spheres as in the case of the authors' electrical analog mentioned in the paper before the summary of results. The aluminum plate near the point of contact with the sphere might not be isothermal due to the high concentration of heat flux at that point. It also seems possible that heat loss from the sides of the model or through the lucite plates could have affected the measured values, although a detailed analysis would be required to determine whether or not those effects could be significant.

Effect of Vibration on Heat Transfer From a Wire to Air in Parallel Flow[1]

By R. ANANTANARAYANAN[2] and A. RAMACHANDRAN,[3] BANGALORE, INDIA

Studies on the effect of vibration of the heat-transferring surface on convective heat transfer are few and limited to natural-convection conditions. The present investigation deals with the influence of vibration on heat transfer from an electrically heated nichrome wire to parallel air streams. Air velocities ranged from 34 to 63 fps. At each air velocity, frequencies ranging from 75 to 120 cycles per second and different amplitudes were employed as vibrational variables. Both frequency and amplitude increased the heat-transfer coefficient. An increase as high as 130 per cent was obtained. The correlation of the experimental data shows that the proportional increase in heat transfer was controlled by the ratio of the mean vibrational velocity to the air-stream velocity.

Nomenclature

The following nomenclature is used in the paper:

A = surface area of test section, sq ft
C = constant
d = diameter of test wire, ft
F = vibrational frequency, 1/sec
H = amplitude of vibration, ft
h_s = heat-transfer coefficient for stationary wire, Btu/hr sq ft deg F
h_V = heat-transfer coefficient for vibrating wire, Btu/hr sq ft deg F
I = heating current, amp
k_f = thermal conductivity of air at film temperature t_f, Btu/hr ft deg F
L = length of test section, ft
m = exponent
$(N_{Nu})_s = \frac{h_s d}{k_f}$ = Nusselt number for stationary wire
$(N_{Nu})_V = \frac{h_V d}{k_f}$ = Nusselt number for vibrating wire
$(N_{Re})_f = \frac{\vartheta_f d}{\nu_f}$ = flow Reynolds number
$(N_{Re})_V = \frac{\vartheta_V d}{\nu_f}$ = vibrational Reynolds number
q_c = rate of heat transferred by convection from test section, Btu/hr
q_i = rate of heat input to test section, Btu/hr
q_r = rate of heat loss by radiation, Btu/hr
R = resistance of test section, ohms
t_a = ambient air temperature, deg F
$t_f = \frac{t_s + t_a}{2}$ = film temperature, deg F
t_s = surface temperature of test section, deg F
ϑ_f = velocity of air stream, fps
$\vartheta_V = 2FH$ = mean velocity of vibration, fps
ν_f = kinematic viscosity of air at film temperature t_f, sq ft/sec

Introduction

Convective heat-transfer rates depend on whether the flow is laminar or turbulent. Heat transfer is greater in turbulent flow than in laminar flow. Vibration of heat-transferring surfaces may set in turbulence in the case of laminar boundary layers and increase the heat transfer. With turbulent boundary layers vibrations may promote vigorous mixing and perhaps penetrate into the laminar sublayer resulting in a decrease in the resistance to heat flow.

Studies in this field can examine the scope either to utilize the increased heat-transfer rates in industrial units or to avoid over-design of heat-transfer elements subjected to induced vibrations.

Experimental investigations on heat transfer including the vibrational variables are few and provide meager information. Martinelli and Boelter (1)[4] obtained an increase of fivefold in the heat-transfer coefficients for the case of a vibrating cylinder in free convection under water. Recently experiments by Lemlich (2) on wires for free convection in air confirmed the influence of vibration and the results were correlated using a vibrational Reynolds number based on the mean vibrational velocity.

However, neither an analytical nor an experimental study appears to have been made so far with vibrating surfaces under forced-convection conditions. The only measurement of Tessin and Jakob (3) for the influence of vibration was an auxiliary part of their main problem and revealed that the heat transfer was unaffected.

In view of lack of data for the effect of vibration on forced-convection heat transfer, it is the purpose of this paper to present information for the case of a vibrating wire in a parallel air stream. In the experimental system the vibrational variables of frequency and amplitude as well as air-stream velocities were varied independently, and their effects measured for incorporating in an over-all dimensionless correlation.

Description of Apparatus

The test apparatus consisted of an electrically heated 26 S.W.G. (0.018 in. diam) nichrome wire stretched between two supports 58 in. apart and placed in a free jet of air as shown in Fig. 1. The duct-work straightened the discharge from the blower. Approximately half the length of the test wire was drawn into the duct so that the central portion of the wire taken as the test section was in the free jet. Care was taken to ensure that the wire was horizontal and along the axis of the duct. One end of the wire was fixed and the other end was connected to a tightening device.

A vibration exciter was located on the wire near the left side

[1] Based on a thesis by the junior author for the Associateship of the Indian Institute of Science.

[2] Senior Research Assistant, Mechanical Engineering Section, Indian Institute of Science.

[3] Professor of Mechanical Engineering, Indian Institute of Science. Assoc. Mem. ASME.

Contributed by the Heat Transfer Division and presented at the Annual Meeting, New York, N. Y., December 1–6, 1957, of The American Society of Mechanical Engineers.

Note: Statements and opinions advanced in papers are to be understood as individual expressions of their authors and not those of the Society. Manuscript received at ASME Headquarters, July 8, 1957. Paper No. 57—A-100.

[4] Numbers in parentheses refer to the Bibliography at the end of the paper.

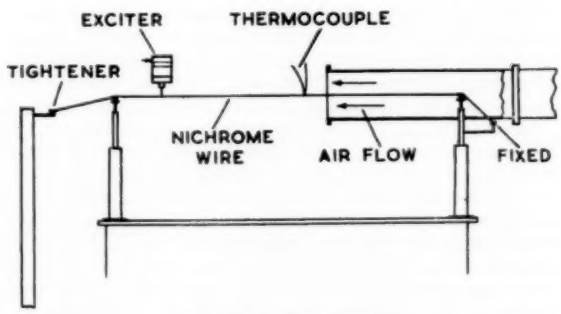

Fig. 1 Test-wire assembly

support. Power was supplied to the exciter from an audio-frequency oscillator. The segment between the fixed end and the exciter vibrated vigorously at its natural frequency when the input from the oscillator was properly tuned. Variations in the frequency could be obtained by altering the tension and by changing the position of the exciter along the wire. The vibratory amplitudes were controlled by the input voltages to the exciter.

Power-supply leads were connected to the nichrome wire near its extremities. The heating current was controlled by a variac connected to a constant-voltage supply.

The temperature at the center of the test length was measured by a 30-gage iron-constantan thermocouple connected to a Leeds and Northrup precision potentiometer. Each wire of the thermocouple was wrapped around the heating wire so as to give a split hot junction with a separation less than $^1/_4$ in. Such a technique was adopted by Lemlich (2) for experiments on heat transfer from vibrating wires by natural convection and proved to be very satisfactory.

Lemlich found welding a junction to the nichrome wire failed under sustained vibration. Because of the low-temperature coefficient of resistance of nichrome, the electrical resistance of the main wire could not be used for the measurement of temperature. Further the temperature at a point on the wire rather than the mean temperature of the entire wire had to be measured. Hence the method of forming a split hot junction by wrapping each of the thermocouple wires around the nichrome wire was adopted. A check to determine whether the potentiometer readings were influenced by the potential drop between the points where the thermocouple wires were secured to the wire was made. Heating current through the nichrome wire was adjusted to give a potentiometer reading corresponding to the boiling point of water. When the reference junction was transferred to boiling water, the potentiometer reading was found to reduce to zero. This proved that the emf in the thermocouple circuit was essentially of thermal origin and that no spurious emf was included in that circuit.

A pitot tube mounted on a traverse measured the air-stream velocities. Preliminary traverses along the wire revealed that the velocity over the wire for a distance of 1 ft downstream in the free jet was constant.

Test Procedure

Initially test data were obtained with the wire stationary. The next group of runs were made with the wire vibrating. The central portion of the wire 3 in. in length was taken as the test length for heat balance. The heat input to the test section is given by

$$q_i = 3.413\, I^2 R \quad \ldots\ldots [1]$$

The heating current was measured by a calibrated ammeter in the heating circuit and it was maintained constant at 2 amp throughout the test. The cold resistance of the test section was evaluated from direct measurements of a foot length of the test wire in tension by a Leeds and Northrup resistance bridge. Changes in the tension employed in the tests did not show any significant variation in the resistance. Alteration in the resistance resulting from heating was negligible because of the low-temperature coefficient of resistance of nichrome.

The net heat transferred by convection, q_c, from the test section was determined, taking into account the heat loss or gain due to radiation, conduction, and generation by vibration. Heat loss by radiation, q_r, was evaluated for each case and its maximum value was about 6 per cent corresponding to a maximum surface temperature of 300 F. Heat flow by conduction through the ends of the test length was found to be less than 1 per cent even when worst conditions were assumed and hence it was neglected. The absence of addition of heat due to vibration was shown by no change in the temperature of the test section, when the wire was vibrated without the heating current.

Hence the heat balance is given by

$$q_i = q_c + q_r \quad \ldots\ldots [2]$$

The convective heat-transfer coefficient is given by

$$h_s \text{ or } h_V = \frac{q_i - q_r}{A(t_s - t_a)} \quad \ldots\ldots [3]$$

The minimum value of the temperature difference $(t_s - t_a)$ was 90 deg F.

The frequency of vibration was measured on the graduated dials of the audio-frequency oscillator. Its accuracy was checked initially with a stroboscopic lamp.

The vibrational amplitudes (defined as the distance between the extreme positions of the wire axis over the course of one cycle) were measured by viewing through a telescope with a least count of 0.01 mm. Its accuracy was sufficient for the amplitudes which ranged from 3 mm to 20 mm in the experiments. The measurements were at the center of the test length. This portion of the wire was flat even at the crest of vibration because of the long distance between the supports. The amplitudes at different points on the test length were uniform.

The vibrational variables were included in a nondimensional vibrational Reynolds number given by

$$(N_{Re})_V = \frac{\vartheta_V d}{\nu_f} \quad \ldots\ldots [4]$$

This number is based on the mean vibrational velocity ϑ_V equal to twice the product of frequency and amplitude.

For the case of the vibrating wire the investigation was made for nine air velocities ranging from 34 to 63 fps. At each air velocity, different frequencies and amplitudes in the range of 75 to 120 cycles per sec (cps) and 3 mm to 20 mm, respectively, were employed as vibrational variables.

Discussion and Evaluation

Stationary Wire. Fig. 2 shows the plot of the test data for stationary wire. The relation between $(N_{Nu})_s$ and $(N_{Re})_f$ computed using the principle of least squares is given by the expression

$$(N_{Nu})_s = 0.0522\,(N_{Re})_f^{0.739} \quad \ldots\ldots [5]$$

No heat-transfer data for free flow parallel to wires were found in the literature. The only experimental data of Mueller (4) were obtained for wires of diameters 0.0007, 0.003, and 0.005 in. placed in ducts of diameters 1.81, 3.78, and 20.6 in. The diame-

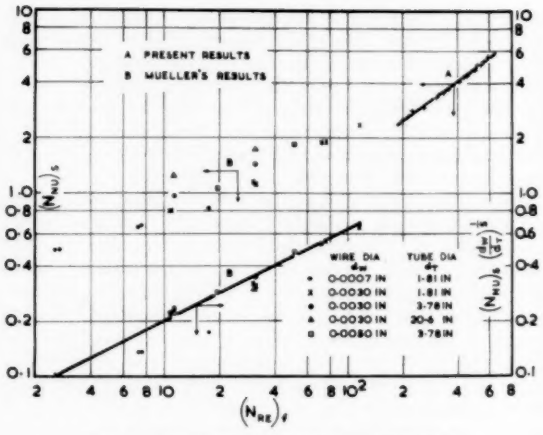

Fig. 2 Experimental data for stationary wire

ter of the ducts in which the wires were placed was found to affect the heat-transfer coefficients. The correlation of the data of Mueller along with the one for the present work is shown in Fig. 2. Mueller has used the ratio of wire diameter to tube diameter as correction factor to effect the correlation. The scatter of Mueller's data without the correction factor can be seen in Fig. 2. The Reynolds numbers in Mueller's correlation vary from 3 to 120 whereas those of the present work range from 198 to 585. The differences in the experimental setup do not permit any direct comparison of the present data. Hence extrapolation of Mueller's correlation to the range of Reynolds numbers in the present work, for purposes of comparison, is questionable. However the change in slopes of the lines in Fig. 2 from 0.5 for Mueller's to 0.729 for the correlation of this paper probably indicates transition in the character of flow as the Reynolds number changes from about 100 to 200.

With Vibration. Plots of the test data for the effect of vibration are shown in Figs. 3 to 11. Tabulated results for different air velocities revealed the increase in heat-transfer coefficients due to the vibration of the wire. Increase in heat transfer because of increase either in frequency or amplitude was indicated. Since the experimental data were obtained to effect an over-all correlation of the vibrational variables, plots of the data showing the effect of any one of the vibrational variables, such as frequency or amplitude, at some air velocity were not attempted.

Figs. 3 to 5 show the effect of vibration on Nusselt number for three air velocities. It is clear that the nondimensional vibrational Reynolds number $(N_{Re})_V$ involving frequency and amplitude may be used for the correlation of the test data. Such a number was used by investigators for free-convection studies. These figures show that the Nusselt number increased with increase in vibrational Reynolds number when the air velocity was maintained constant. But the slopes of the lines decrease with increase of air velocities. This indicates the moderating influence of higher velocities, i.e., higher flow Reynolds numbers, on the rate of increase of Nusselt number due to vibration. Fig.

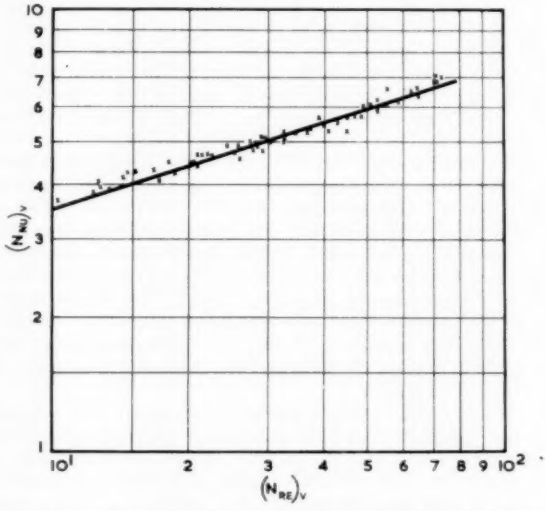

Fig. 4 Effect of vibration on Nusselt number. Air velocity 49.4 fps.

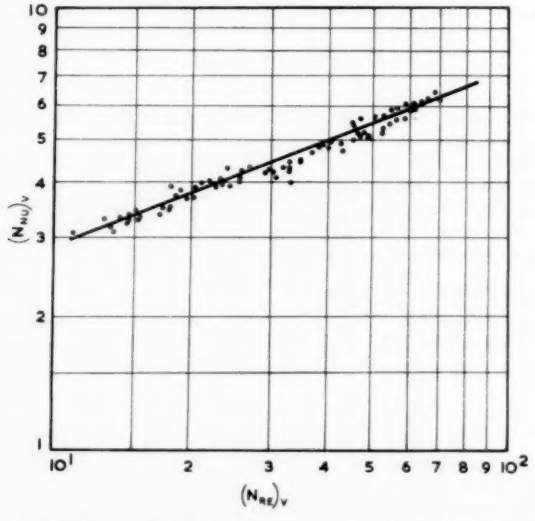

Fig. 3 Effect of vibration on Nusselt number. Air velocity 34.1 fps.

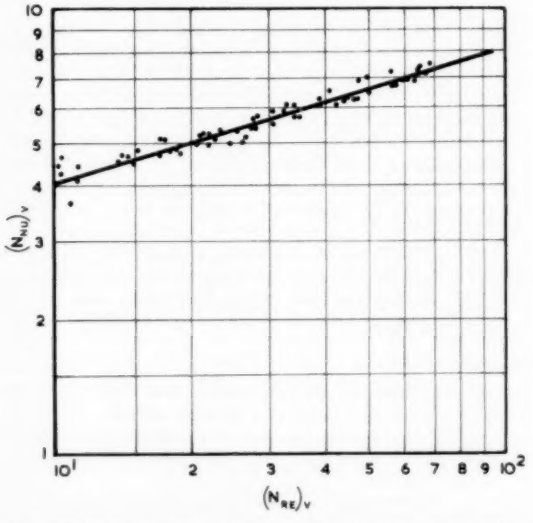

Fig. 5 Effect of vibration on Nusselt number. Air velocity 63.2 fps.

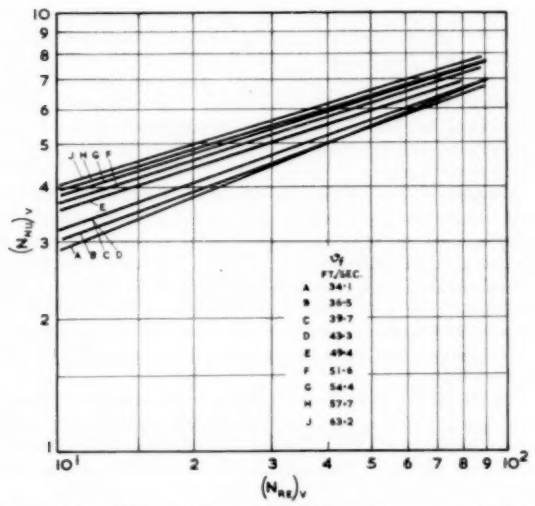

Fig. 6 Comparison of effect of vibration of Nusselt numbers for different air velocities

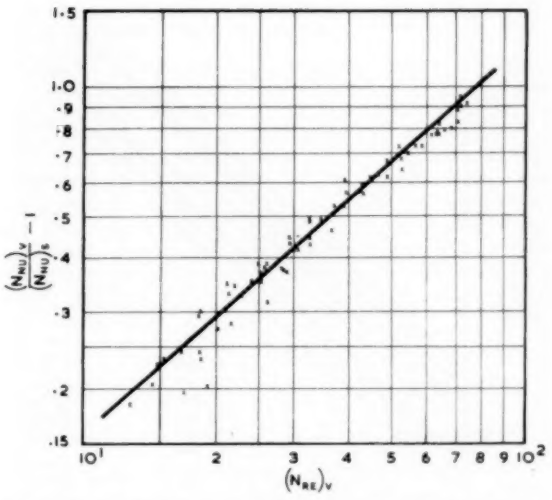

Fig. 8 Proportional increase in Nusselt number due to vibration. Air velocity 49.4 fps.

6 shows the lines for different velocities on a composite plot, the individual points being omitted in this case for clarity.

For examination of the effect of vibrational Reynolds number and air velocities on increase in heat transfer, plots of proportional increase in Nusselt number $[(N_{Nu})_V/(N_{Nu})_s] - 1$ versus vibrational Reynolds number $(N_{Re})_V$ were made with air velocity as parameter, Figs. 7 to 9. For every run the flow Reynolds number and the corresponding Nusselt number $(N_{Nu})_s$ using Equation [5] were evaluated. In Fig. 10, the lines for different velocities are brought together for purposes of comparison. It is clear that the plots are straight lines of the same slope. Hence the improvement in heat transfer due to vibration alone was a power function of the vibrational Reynolds number. A vibrational Reynolds number of 30 increased the heat transfer by 61 per cent when the air velocity was 34.1 fps. However at the same $(N_{Re})_V = 30$, the improvement fell to 31.5 per cent when the

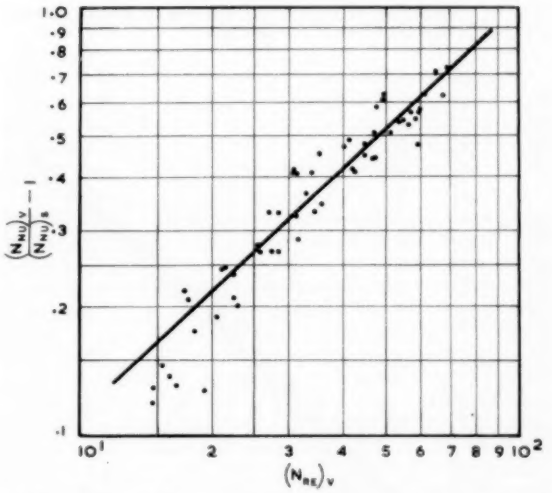

Fig. 9 Proportional increase in Nusselt number due to vibration. Air velocity 63.2 fps.

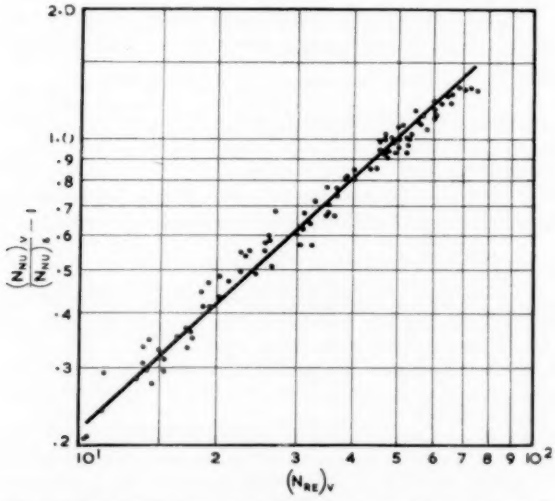

Fig. 7 Proportional increase in Nusselt number due to vibration. Air velocity 34.1 fps.

air velocity increased to 63.2 fps. The maximum increase of 135 per cent due to a vibrational Reynolds number of 72 was obtained at the lowest air velocity and hence the lowest Reynolds number. The lines for smaller air velocities are shifted upwards clearly indicating that the magnitude of improvement in heat transfer due to a vibrational velocity depended on the ratio of vibrational to flow velocities. The higher this ratio, the greater was the increase in heat transfer. Further a negligibly small increase of about 11 per cent has been obtained with a ratio of 0.035, Fig. 11.

These findings are in conformity with those of previous investigators at least in principle even though their experiments cannot be compared with the present work. Tessin and Jakob found no influence of vibration on heat transfer by forced convection. However their attention was confined to the evaluation of error introduced by any vibration that might have been picked

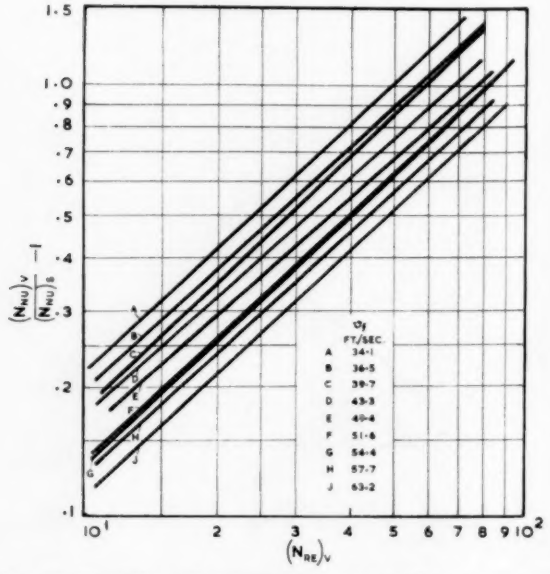

Fig. 10 Comparison of proportional increase in Nusselt numbers due to vibration for different air velocities

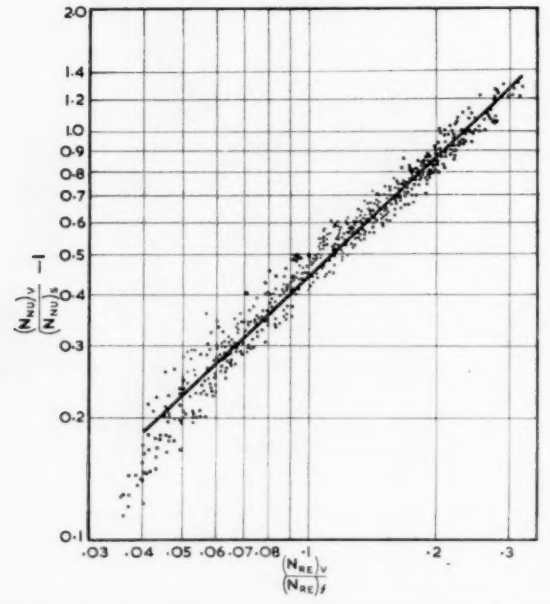

Fig. 11 Final correlations of experimental data for effect of vibration

up by the test cylinder transferring heat to parallel air streams. An analysis of their data indicated that the vibrational velocities obtained in their tests were very low compared to the air velocities and therefore did not alter the heat-transfer coefficients.

Free-convection studies with vibration also presented results similar in nature. Martinelli (1) found that for vibrational Reynolds numbers up to a critical value, the Nusselt number was independent of vibration. Further the proportional increase in heat transfer due to any vibration was greater for the smaller Grashof number. Martinelli attributed these features to the relative magnitudes of the free-convection and vibrational velocities. At low magnitudes of vibrational Reynolds number, the net resultant velocity in the viscous layer was essentially controlled by the free-convection modulus. The influence of higher vibrational Reynolds number was considerable when the free-convection velocities were lower; i.e., corresponding to lower Grashof numbers.

Kubanskii (5) also found that to obtain observable increase in heat transfer from a cylinder at right angles to an air stream with superimposed acoustic vibrations of 0.031 to 0.366 watts per sq cm, smaller air velocities had to be used. The maximum increase in heat-transfer coefficient was of the order of 50 per cent. As a preliminary conclusion, he stated that the average value of the vibrational velocity in the acoustical wave must not be less than the velocity of flow to produce acoustical currents near the walls of the solid body.

Fig. 11 shows the final correlation in a plot of $[(N_{Nu})_V/(N_{Nu})_s] - 1$ against $(N_{Re})_V/(N_{Re})_f$. The dimensionless ratio $(N_{Re})_V/(N_{Re})_f$ is the same as the ratio of the mean vibrational velocity to the air velocity. The data can be represented by the equation

$$\frac{(N_{Nu})_V}{(N_{Nu})_s} - 1 = C\left[\frac{(N_{Re})_V}{(N_{Re})_f}\right]^m \quad \ldots\ldots\ldots\ldots [6]$$

Determining the constants graphically, the following equation for the effect of vibration on forced convection heat transfer was obtained

$$\frac{(N_{Nu})_V}{(N_{Nu})_s} - 1 = 4.25\left[\frac{(N_{Re})_V}{(N_{Re})_f}\right]^{0.977} \quad \ldots\ldots\ldots\ldots [7]$$

The role of the ratio of the vibrational Reynolds number to flow Reynolds number, i.e., $(N_{Re})_V/(N_{Re})_f$ in effecting increases in heat transfer is clearly revealed by the trend of the test data in Fig. 11. The value of the ratio ranges from 0.035 to 0.34. The increase in heat transfer was about 20 per cent when $(N_{Re})_V/(N_{Re})_f$ was equal to 0.045 and reached 130 per cent with the increase of $(N_{Re})_V/(N_{Re})_f$ to 0.34. The fact that ratios of $(N_{Re})_V/(N_{Re})_f$ were obtained from different combinations of frequency, amplitude, and air velocity bears evidence to the reproducibility of the data and explains the clustering of a number of points along the mean line.

Combining Equations [5] and [7] the following expression for the heat transfer from vibrating wire to air in parallel flow is obtained

$$(N_{Nu})_V = 0.0522(N_{Re})_f^{0.729}\left[1 + 4.25\left\{\frac{(N_{Re})_V}{(N_{Re})_f}\right\}^{0.977}\right] \ldots [8]$$

Conclusions

1 The heat transfer from a wire to air in parallel flow was given by the following expression determined experimentally

$$(N_{Nu})_s = 0.0522(N_{Re})_f^{0.729}$$

2 Vibrations of heating surfaces can increase heat transfer in forced convection also, a doubling of the heat-transfer coefficient having been obtained in the present work.

3 Both frequency and amplitude increased the heat transfer from wire to air in parallel flow when the air velocity was maintained constant.

4 The proportional increase in Nusselt number due to any vibrational velocity was controlled by its ratio to air velocity.

5 A vibrational Reynolds number based on the mean vibrational velocity could be used for correlating the effect of the vibrational variables.

6 The results for the effect of vibration of wire on heat transfer could be represented by the following relationship

$$\frac{(N_{Nu})_V}{(N_{Nu})_o} - 1 = 4.25 \left[\frac{(N_{Re})_V}{(N_{Re})_f} \right]^{0.377}$$

7 The effect of vibration on heat transfer by forced convection should be studied for other ranges of the ratio $(N_{Re})_V/(N_{Re})_f$ and with different geometrical configurations.

Acknowledgment

The authors are grateful to the authorities of the Indian Institute of Science for providing the facilities for the conduct of this investigation and permission to publish the results.

Bibliography

1 "The Effect of Vibration on Heat Transfer by Free Convection From a Horizontal Cylinder," by R. C. Martinelli and L. M. K. Boelter, Proceedings of the Fifth International Congress on Applied Mechanics, 1938, pp. 578–584.

2 "Effect of Vibration on Natural Convective Heat Transfer," by R. Lemlich, *Industrial and Engineering Chemistry*, vol. 47, 1955, pp. 1175–1180.

3 "Influence of Unheated Starting Sections on the Heat Transfer From a Cylinder to Gas Streams Parallel to the Axis," by W. Tesain and M. Jakob, TRANS. ASME, vol. 75, 1953, pp. 473–481.

4 "Heat Transfer From Wires to Air in Parallel Flow," by A. C. Mueller, *Trans. AIChE*, vol. 38, 1942, pp. 613–629.

5 "The Influence of Acoustical Vibrations of Finite Amplitude Upon Boundary Layer," by P. N. Kubanskii, *Zhurnal Tekhnicheskoi Fiziki*, vol. 22, 1952, pp. 593–601.

Discussion

J. P. Hartnett.[5] The paper treats a very interesting problem but unfortunately serious questions arise regarding the instrumentation, and furthermore it is apparent that the authors have overlooked one of the important parameters in correlating their data. In regard to the instrumentation question, the authors do not show a detailed sketch of their thermocouple installation, but it appears that two thermocouples of 0.010 in. were attached to the main wire (0.018 in. diam) and, consequently, the thermocouple wires will have a major influence on the flow past the main heated wire. This would occur since the boundary layer as it builds up on the main wire encounters the thermocouple, undoubtedly giving rise to a very turbulent wake region behind the thermocouple. It would appear, therefore, that the authors are investigating a different flow situation from that indicated in the title of their paper and unfortunately the particular flow situation of the investigation is not frequently encountered in engineering situations.

With respect to the major parameter overlooked in the correlation results, this parameter is x/d where x is the distance from the apparent start of the boundary layer. This is obvious since in the limit when the radius of the cylinder becomes very large (i.e., x/d very small), the results for flow over a nonvibrating circular cylinder should reduce to the flow on a flat plate.

Finally, it would appear that the authors have overlooked considerable literature related to this problem; for example, a recent paper by Christian and Kezios[6] will yield information on the available literature.

T. W. Jackson.[7] Review of the paper indicates two technical points which should be investigated before the work is considered to be authoritative. These are as follows:

1 It is stated that a 26 B & S gage nichrome wire of 0.018 in. diam was used. According to the writer's charts a 26 B & S gage wire should have a diameter of 0.0159 in. Which is correct? Is the wire 0.018 in. and 25 gage or is it 0.0159 in. and 26 gage?

2 In measuring the temperature of the test wire a 30-gage iron-constantan thermocouple was used. A 30 B & S gage wire has a diameter of 0.010 in. In other words the thermocouple wire size is of the same order of magnitude as that of the test wire. The thermocouple leads, therefore, are large heat sinks and could easily lower the temperatures of the junctions several degrees. In Lemlich's work (reference 2 of the paper) wire sizes as follows were used:

Wire size, in.	Thermocouple wire size, in.	Error in temp reading, per cent
0.0253	0.005	2–3 of temp difference
0.0396	0.005	2–3 of temp difference
0.081	0.005	2–3 of temp difference

As can be seen from the table Lemlich's test wires were several times larger than the thermocouple wires. In contrast, for the subject paper the sizes were

Wire size, in.	Thermocouple wire size, in.	Error in temp reading, per cent
0.018 or 0.0159	0.010	?

In view of the foregoing the writer states that an experiment such as Lemlich performed of comparing the temperature inside a nichrome tube to the measured surface temperature with sizes similar to those used in the experiment is in order.

R. Lemlich.[8] With regard to the measurement of surface temperature, the writer wonders if the authors checked their thermocouple for possible local cooling or other disturbance that might be caused at the hot junction by the extension of the thermocouple wires through the film. The split thermocouple junctions employed in the work of this writer to which the authors refer (and which the writer checked by comparison with an electrically insulated thermocouple threaded through an electrically heated length of hypodermic tubing) consisted of considerably finer thermocouple wires and appreciably thicker nichrome wire than that described here. Furthermore, the writer's work was with free convection and therefore with a thicker "film blanket" than that for the forced convection employed here. Accordingly, it would appear to this writer that the authors' acceptance of the reliability of their relatively bulkier thermocouple junction, particularly with their relatively higher forced convective film coefficient, might be a bit too much to take for granted.

This writer questions the validity of the test described to determine whether or not the emf of the heating current directly influenced the potentiometer reading. However, he does go along with the conclusion, but for *a priori* reasons. The small a-c voltage drop could scarcely affect a d-c potentiometer.

The Nusselt number here appears to include the effect of any superimposed free convection as well as that for forced convection plus any vibration applied. Free convection should be appreciable at the temperature differences employed, particularly with low air velocities and weak vibration. For example, with no forced air flow and no vibration, the Nusselt number here for free

[5] Associate Professor, Mechanical Engineering, University of Minnesota, Minneapolis, Minn. Mem. ASME.

[6] "Experimental Investigation of Mass Transfer by Sublimation From Sharp-Edged Cylinders in Axisymmetric Flow With Laminar Boundary Layer," by W. J. Christian and S. P. Kezios, Heat Transfer and Fluid Mechanics Proceedings, 1957.

[7] Chief, Mechanical Sciences Division, Engineering Experiment Station, Georgia Institute of Technology, Atlanta, Ga. Mem. ASME.

[8] Department of Chemical Engineering, University of Cincinnati, Cincinnati, Ohio.

convection alone would be roughly in the neighborhood of unity. This is appreciable when compared with Fig. 2.

Results for the final correlation, Fig. 11, certainly cluster well. The slope of the line (0.977 as given in Equation [7]) is very close to unity. Do the authors attach any special significance to this?

It would be interesting to see how the authors' correlation would handle variation in wire diameter.

All in all, the authors have carried out an interesting piece of research and have prepared a simple and effective correlation of their results. Their work is a definite contribution to the rapidly expanding study of the effect of vibration on transport phenomena.

Authors' Closure

The authors wish to thank the discussers for their interest in the paper which is the first report of a comprehensive study initiated on the influence of vibration in forced convection heat transfer. It was felt that initially the vibrating surface should be of a simple configuration so that the study will throw some light on the effect of vibration on heat transfer.

As Professor Lemlich has pointed out, a simple and effective correlation of the data obtained in this investigation has been prepared. The authors are aware that the heat transfer from a cylinder to a fluid in parallel flow will not differ much from that between a plane surface and a fluid in parallel flow provided the diameter of the cylinder is large (i.e., x/d very small). The authors are familiar with the literature referred to by Professor Hartnett though not to the recent paper of Christian and Kezios which was not available to them at the time this paper was submitted. In these the heat transfer from cylinders to air streams in axial flow have been presented wherein the axial length has been used in evaluating the dimensionless groups and the parameter x/d also included. Jakob[9] has pointed out that, if the cylinder diameter is small, eddies occurring in turbulent flow may be great compared to the cylinder diameter. In this investigation d is very small (i.e., x/d large). Hence the diameter of the wire and not the axial length has been used in evaluating the dimensionless groups. Mueller (4) also has used the diameter of the wire as characteristic length in the dimensionless groups. As indicated in the paper, the airflow in this investigation is parallel to the test wire. Fig. 12 shows a photograph of the test apparatus. Fishenden and Saunders[10] have stated that the heat transfer by forced convection for flow parallel to the axis is about one half that for flow at right angles to the axis. Mueller (4) compared his results with the curve recommended by McAdams[11] for flow across wires and found that the Nusselt numbers in the range of Reynolds numbers investigated by him were only 40 per cent of those for crossflow. The Nusselt numbers obtained in this investigation for the stationary wire vary from 35 to 45 per cent of those for crossflow as the Reynolds number increased from 200 to 600, probably indicating transition in the character of flow, and is in general agreement with Mueller's finding.

In answer to Dr. Jackson's points, the diameter of the nichrome wire used in the entire investigation was 0.018 in. The split thermocouple junction technique was adopted only after several other methods had been considered and found unsuitable. An experiment such as Lemlich (2) performed, of comparing the temperature inside an electrically heated hypodermic tubing to the measured surface temperature using a split junction thermocouple, was conducted. The sizes corresponded to those used in this investigation. At different heat-flux values, the temperature indicated by the outer thermocouple was lower than that of the inner by 1 to 2.5 per cent of Δt, the difference between surface and ambient temperatures. This is of the same order of magnitude as obtained by Lemlich. Calculations indicated that loss along thermocouple leads was negligibly small. The minimum air velocity was 34.1 fps and hence the free-convection effect was small compared to the forced convection. As to how the correlation will handle variation in wire diameter, further investigations with different wire sizes are necessary. In conclusion it is felt that analytical and experimental studies on the effect of vibration on heat transfer with different configurations in gases and liquids are called for.

[9] "Heat Transfer," by M. Jacob, vol. 1, John Wiley & Sons, Inc., New York, N. Y., 1949.

[10] "An Introduction to Heat Transfer," by Fishenden and Saunders, Oxford University Press, London, England, 1950, p. 132.

[11] "Heat Transmission," by W. H. McAdams, McGraw-Hill Book Company, Inc., New York, N. Y. 1954, p. 259.

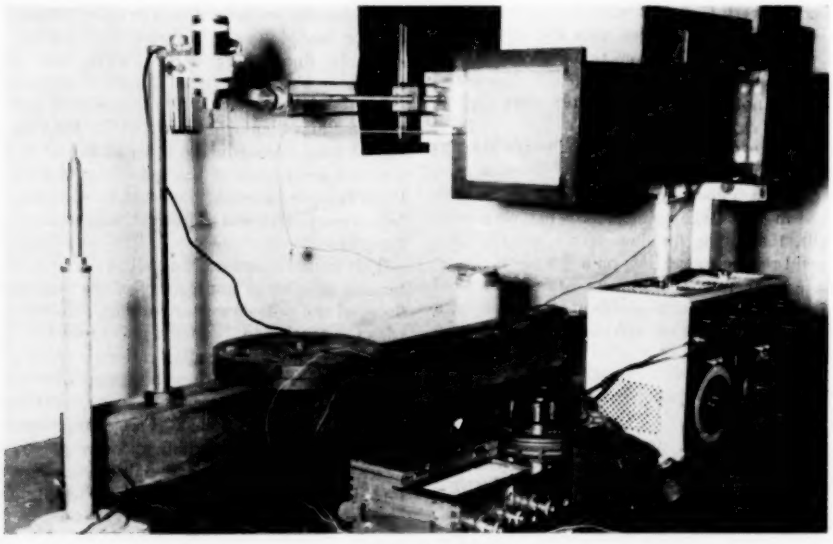

Fig. 12 Test apparatus

Local Laminar Heat Transfer in Wedge-Shaped Passages[1]

By E. R. G. ECKERT,[2] T. F. IRVINE, JR.,[3] AND J. T. YEN,[4] MINNEAPOLIS, MINN.

Heat transfer in noncircular passages recently has received increased attention in connection with various engineering applications, especially with nuclear-reactor technology. The present paper presents the results of calculations for heat transfer connected with steady laminar flow through ducts whose cross sections have the shape of circular sectors. Hydraulically and thermally developed flow is assumed. The temperature field, peripheral distribution of inner-duct surface temperature and of heat flux, as well as heat-transfer coefficients and friction factors, are presented for two boundary conditions: Peripherally constant heat flux and peripherally constant surface temperature, both with longitudinally constant heat flux. It is found that even average heat-transfer coefficients may be different by an order of magnitude for these two conditions. For this reason, it is pointed out that solutions for a class of boundary conditions can be obtained by linear superposition of the results obtained for the two conditions mentioned.

Nomenclature

THE following nomenclature is used in the paper:

a = thermal diffusivity
A = cross-sectional area
c_p = specific heat
C = circumference
C_f = friction factor
D_h = hydraulic diameter = $4A/C$
h = average heat-transfer coefficient (see Equations [10] and [4])
k = heat conductivity
n = normal to duct surface
$\overline{\mathrm{Nu}}$ = $\bar{h}D_h/k$ = Nusselt number
p = pressure
q = heat flow from inner surface of duct to fluid per unit time and area
r = radial distance from duct corner, Fig. 1
R = radial dimension of duct, Fig. 1
$\mathrm{Re} = \dfrac{\rho \bar{w} D_h}{\mu}$ = Reynolds number
T = temperature
w = velocity, Fig. 1
z = co-ordinate parallel to duct axis
α = half angle of duct, Fig. 1
θ = angular co-ordinate, Fig. 1
μ = viscosity (dynamic)
ρ = density

Subscripts

B = bulk-fluid conditions
C = center line
f = friction
h = hydraulic
w = wall

Introduction

Heat transfer connected with flow through circular ducts has been studied thoroughly, theoretically as well as experimentally. It is well known that for a fluid with constant properties the flow is independent of the heat-transfer condition and that the development of the temperature field in the fluid depends considerably on the boundary conditions which are imposed on it. The two conditions most widely investigated are either a constant wall temperature along a heated section which follows an upstream unheated section, or a constant heat flux, again with or without an unheated upstream section. More recently, methods also have been developed by which the solutions for the boundary conditions just mentioned can be used to obtain information on the temperature field in the fluid under any arbitrarily varying wall temperature (1).[5] The information obtained in such a way has shown that the development of the temperature field depends on the length of the unheated upstream section; that it is, for instance, different if the temperature field develops directly from the entrance of the tube simultaneously with the flow field or whether it starts developing only after the flow has become established. It also was found that the way in which the wall temperature varies in flow direction has a marked effect on the heat-transfer coefficients. In hydraulically and thermally established laminar flow, for instance, the local Nusselt number based on diameter and on the difference between wall and bulk temperature was calculated as $\mathrm{Nu} = 3.64$ for constant wall temperature, whereas it has the value $\mathrm{Nu} = 4.36$ for constant heat flux. The thermally established temperature field has an especially simple shape for the condition of a constant heat flux. The fluid temperature at any location increases or decreases at equal and constant rate in flow direction and the temperature profile does not change its shape in the direction of the tube axis.

A new and interesting aspect comes into consideration when heat transfer to a duct with a noncircular cross section is investigated. In such a duct, the velocity and the temperature field will not be rotationally symmetric and it has to be expected that the heat transfer from the fluid to the duct surface will depend on what boundary condition is prescribed around the periphery of the duct. It will be shown in the following section that a constant prescribed heat flow from the duct surface to the fluid generates, for instance, a surface temperature which varies around the periphery and that, on the other hand, a peripherally constant temperature can be obtained only by a heat flux which varies in a specific way around the periphery. It also will be shown that these boundary conditions not only influence the

[1] Publication from the Heat Transfer Laboratory, Mechanical Engineering Department, University of Minnesota, Minneapolis, Minn. This work was supported by the Aeronautical Research Laboratory, Wright Air Development Center, Ohio.

[2] Professor of Mechanical Engineering, University of Minnesota. Mem. ASME.

[3] Assistant Professor of Mechanical Engineering, University of Minnesota.

[4] Research Fellow, Mechanical Engineering Department, University of Minnesota.

Contributed by the Heat Transfer Division and presented at the Annual Meeting, New York, N. Y., December 1–6, 1957, of THE AMERICAN SOCIETY OF MECHANICAL ENGINEERS.

NOTE: Statements and opinions advanced in papers are to be understood as individual expressions of their authors and not those of the Society. Manuscript received at ASME Headquarters, August 1, 1957. Paper No. 57—A-133.

[5] Numbers in parentheses refer to Bibliography at end of paper.

local heat transfer but also its over-all value. In principle, asymmetric boundary conditions of course can be prescribed on a round duct as well; however, the investigations in the past appear to have considered only situations in which heat flux and wall temperature are rotationally symmetric simultaneously.

In this paper the results of a calculation will be presented which determines the temperature field and heat transfer in a fluid flowing with laminar flow through a passage whose cross section has the shape of a circular sector. Hydraulically and thermally developed flow is assumed which means that the velocity profile, as well as the temperature profile, maintain their shape in flow direction. The wall temperature is postulated to increase linearly with length. Two boundary conditions around the duct periphery are investigated, a peripherally constant wall temperature and a peripherally constant heat flux.

In actual applications, the distribution of the temperature and heat flux around the inner surface of the duct wall will depend on the characteristics of the wall as well as on the distribution of the heat transfer on the outside of the duct, or of the heat generation within the duct wall. A thick wall with good heat conductivity, for instance, will tend to equalize the inner surface temperature. It is felt that the two conditions which are considered here are limiting cases between which the situations will generally lie which are encountered in engineering applications. A circular sector has been chosen as the shape of the duct cross section because for this shape it is possible to find exact solutions for the velocity and temperature fields, and also because a variation of the opening angle of the sector leads to a family of widely varying duct cross sections. The calculations, the result of which are presented in this paper, are also paralleled by an extensive experimental program in which the transition to turbulence, the flow development, and the heat transfer for laminar and turbulent conditions is being investigated (2).

The Velocity Field

As a basis for the heat-transfer calculation, the velocity field existing in the duct must be known. In order to calculate it, a co-ordinate system is arranged in the duct as indicated in Fig. 1.

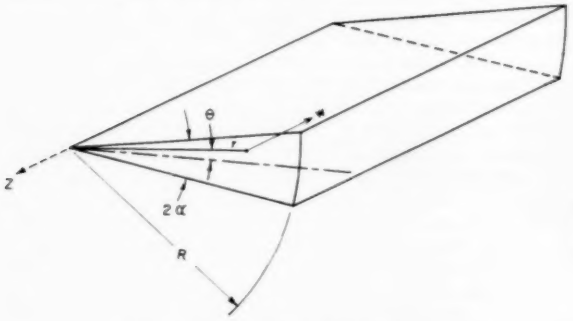

Fig. 1 Duct shape and nomenclature

The location within the duct cross section is described by the radial distance r from the corner and by the angular distance θ from the duct center line. The opening angle of the duct is 2α. Steady laminar flow of a fluid with constant properties and developed flow conditions are assumed. This means that no velocity component exists within the plane of the duct cross section and that $\partial w/\partial z = 0$. Under this condition the Navier-Stokes equation in cylindrical co-ordinates reads

$$\frac{\partial^2 w}{\partial r^2} + \frac{1}{r}\frac{\partial w}{\partial r} + \frac{1}{r^2}\frac{\partial^2 w}{\partial \theta^2} = \frac{1}{\mu}\frac{\partial p}{\partial z} \quad \ldots\ldots [1]$$

The right-hand side of the equation is a constant for developed flow conditions. The velocity field described by Equation [1] must fulfill the boundary conditions

$$w = 0 \text{ for } r = R \text{ and for } \theta = \pm\alpha \quad \ldots\ldots [2]$$

The solution of Equation [1] which satisfies boundary conditions [2] can be obtained from the analogous torsion solution as discussed in (2)

$$w = \frac{1}{4\mu}\frac{\partial p}{\partial z}\left[r^2\left(1 - \frac{\cos 2\theta}{\cos 2\alpha}\right) - \frac{16R^2(2\alpha)^2}{\pi^3}\sum_{n=1,3,5\ldots}^{\infty}(-1)^{\frac{n+1}{2}}\left(\frac{r}{R}\right)^{\frac{n\pi}{2\alpha}}\frac{\cos\frac{n\pi}{2\alpha}\theta}{n\left[n^2 - \left(\frac{4\alpha}{\pi}\right)^2\right]}\right] \quad \ldots\ldots [3]$$

The first term in the square bracket on the right-hand side of this equation describes the velocity field near the corner of the duct; the series makes it possible to adapt the velocity field to the condition $w = 0$ at $r = R$. Velocity fields described by this equation have been computed for a number of duct shapes, and for round numbers of the parameter tan α. Fig. 2(a) shows velocity profiles $w/\bar{w}$ existing along various radii in a duct with an opening angle equal to 11° 25′ 20″ which corresponds to tan $\alpha = 0.1$. It can be seen in this figure that the influence of the curved duct wall on the velocity field is felt only through a limited distance away from that wall. Fig. 2(b) presents velocity profiles encountered along the center lines for ducts with various opening angles. The opening angle is again indicated in the figure by its tangent. Table 1 gives the connection between the tangent and the opening angles themselves. As expected, the influence of the curved wall extends farther into the fluid with increasing opening angle.

Table 1 Connection between tangent and opening angles

tan α	2α
0.1	11° 25′ 20″
0.2	22° 37′ 20″
0.3	33° 24′
0.4	43° 36′ 20″
$1/\sqrt{3}$	60°

The connection between the pressure gradient in flow direction and the average velocity through any duct cross section is important for engineering calculations. It can be expressed by a friction factor C_f defined by the equation

$$\frac{\partial p}{\partial z} = C_f \frac{1}{D_h}\rho\frac{\bar{w}^2}{2} \quad \ldots\ldots [4]$$

This friction factor is conventionally based on the hydraulic diameter D_h of the duct. It can be shown from dimensional analysis that the product $C_f\mathrm{Re}$ has a constant value for each duct shape. Fig. 3 therefore presents this product plotted over the opening angle of the duct. It can be seen that the friction factor depends on the opening angle and is different from the value 64 of a round tube. This indicates that friction in laminar flow through a circular sector duct cannot be calculated from the relation for a round tube by use of the hydraulic diameter. The other curves appearing in this figure will be discussed later.

The Temperature Field

For thermally developed conditions and for a heat flux from

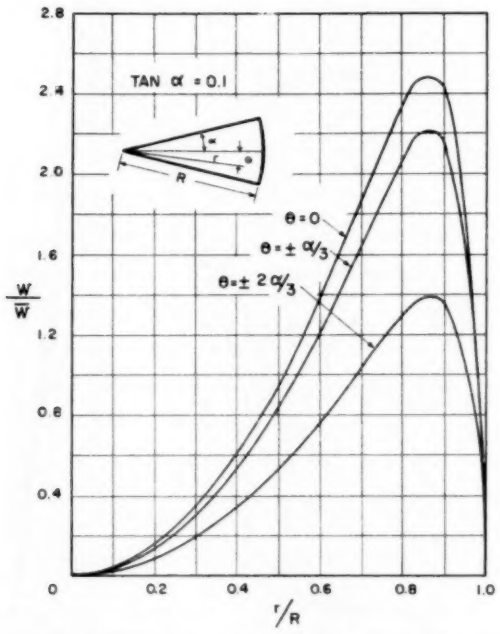

(*a*) Velocity profiles along radii *r*. Tangent of half angle of duct equals 0.1.

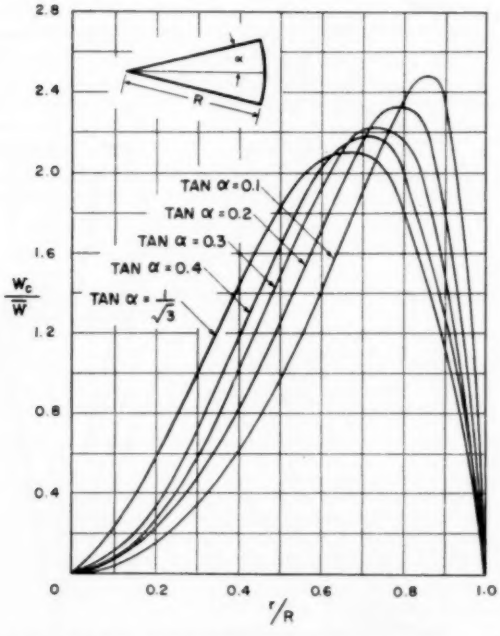

(*b*) Velocity profiles along center line of ducts with various opening angles

Fig. 2 Velocity field for developed laminar flow through a duct whose cross section is a circular sector

the inner duct surface to the fluid which is constant in axial direction, the fluid temperature at any location increases linearly in flow direction ($\partial T/\partial z$ = const). The energy equation in

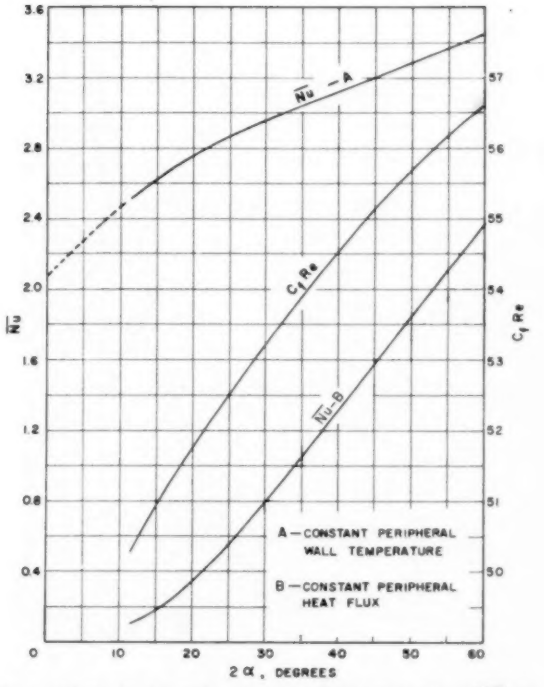

Fig. 3 Friction factor (C_f) and average Nusselt numbers ($\overline{Nu}$) for hydraulically and thermally developed laminar flow through a duct whose cross section is a circular sector

α—half angle of sector
Re—Reynolds number based on average velocity and hydraulic diameter
Nu—Nusselt number based on hydraulic diameter and difference between bulk temperature and average wall surface temperature

cylindrical co-ordinates for a constant-property fluid reads correspondingly

$$\frac{\partial^2 T}{\partial r^2} + \frac{1}{r}\frac{\partial T}{\partial r} + \frac{1}{r^2}\frac{\partial^2 T}{\partial \theta^2} = \frac{1}{a}\frac{\partial T}{\partial z}\, w \quad \ldots\ldots [5]$$

This equation can be combined with Equation [1] to give

$$\left[\frac{\partial^2}{\partial r^2} + \frac{1}{r}\frac{\partial}{\partial r} + \frac{1}{r^2}\frac{\partial^2}{\partial \theta^2}\right]\left[\frac{\partial^2 T}{\partial r^2} + \frac{1}{r}\frac{\partial T}{\partial r} + \frac{1}{r^2}\frac{\partial^2 T}{\partial \theta^2}\right] = \frac{1}{\mu a}\frac{\partial p}{\partial z}\frac{\partial T}{\partial z} \quad \ldots\ldots [6]$$

The right-hand side of this equation is again a constant.

Heat generation by internal friction has been neglected, which restricts Equations [5] and [6] to moderate velocities. However, the equation also can be applied to high-velocity flow of a fluid with a Prandtl number equal to 1 when the temperature T is interpreted as total temperature.

Constant Peripheral Surface Temperature. The boundary condition for a peripherally constant temperature on the inner duct surface is

$$T = T_w = \text{const for } r = R \text{ and for } \theta = \pm\alpha \quad \ldots\ldots [7]$$

It has been pointed out by Marco and Han (3) that the differential Equation [6] is identical with an equation occurring in solid mechanics. It, together with the boundary conditions given by Equation [7], also describes the deflection of a thin plate with a

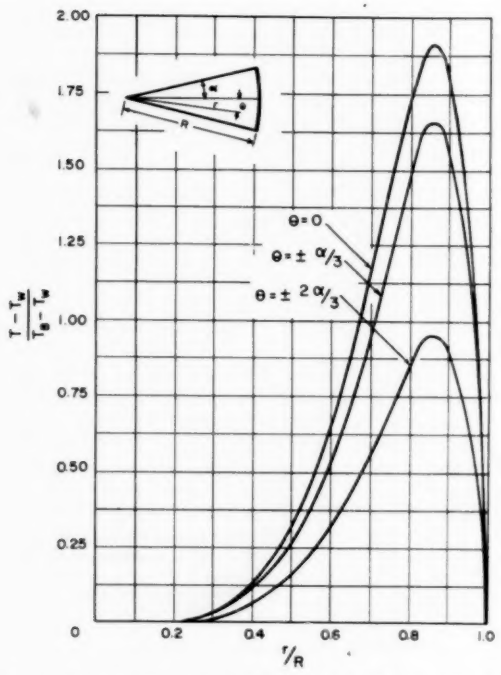

(*a*) **Temperature profiles along radii *r*. Tangent of half angle of duct equals 0.1.**

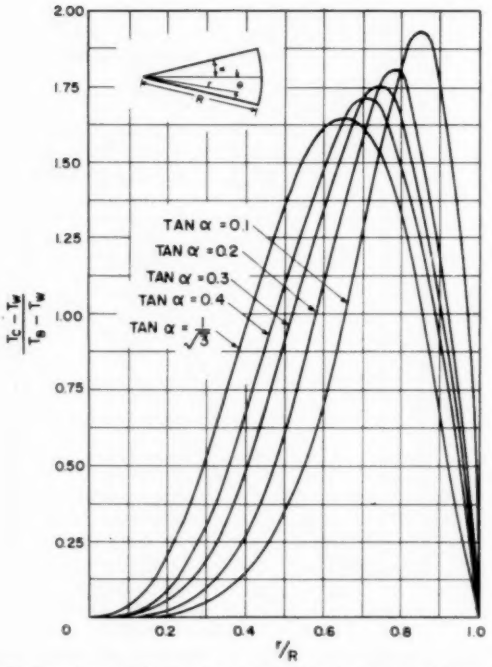

(*b*) **Temperature profiles along center line for ducts with various opening angles**

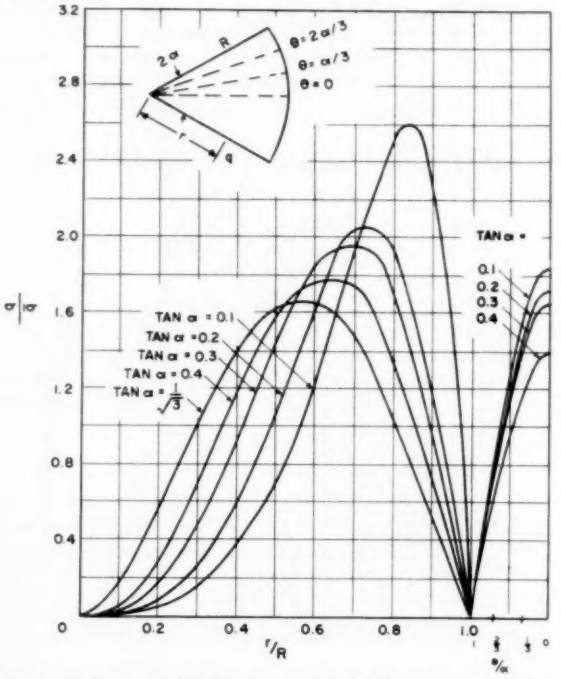

(*c*) **Local heat-flux distribution around periphery of ducts with various opening angles**

Fig. 4 Temperature field and peripheral heat flux for hydraulically and thermally developed laminar flow through a duct whose cross section is a circular sector and whose wall surface temperature is constant around the duct periphery

shape identical to the duct cross section which is simply supported around its rim and under the influence of a uniformly distributed load. A solution can be obtained by a transformation of the semicircular plate-deflection problem discussed by Timoshenko (4). The result of such a transformation which satisfies the required boundary conditions [2] and [7] is

$$T - T_w = \frac{R^4}{\mu a}\frac{\partial p}{\partial z}\frac{\partial T}{\partial z}\sum_{m=1,3,5\ldots}^{\infty}(-1)^{\frac{m+1}{2}}$$

$$\left\{\frac{4r^4}{m\pi\left[16-\left(\frac{m\pi}{2\alpha}\right)^2\right]\left[4-\left(\frac{m\pi}{2\alpha}\right)^2\right]R^4}\right.$$

$$+\left(\frac{r}{R}\right)^{\frac{m\pi}{2\alpha}}\frac{\left(\frac{m\pi}{2\alpha}+6\right)}{m\pi\left[16-\left(\frac{m\pi}{2\alpha}\right)^2\right]\left[2+\frac{m\pi}{2\alpha}\right]\left[1+\frac{m\pi}{2\alpha}\right]}$$

$$\left.-\left(\frac{r}{R}\right)^{\frac{m\pi}{2\alpha}+2}\frac{1}{m\pi\left[4-\left(\frac{m\pi}{2\alpha}\right)^2\right]\left[1+\frac{m\pi}{2\alpha}\right]}\right\}\cos\frac{m\pi}{2\alpha}\theta$$

.....[8]

Figs. 4(*a*, *b*, *c*) present temperature fields which have been calculated with this equation. The figures as shown illustrate the situation that heat flows from the fluid to the duct walls. Fig. 4(*a*) gives the temperature profiles along various radii in a duct with an opening angle characterized by tan $\alpha = 0.1$. It can be seen from Figs. 2 and 4(*a*) and also from a comparison of Equations [3] and [8] that the increase with increasing dis-

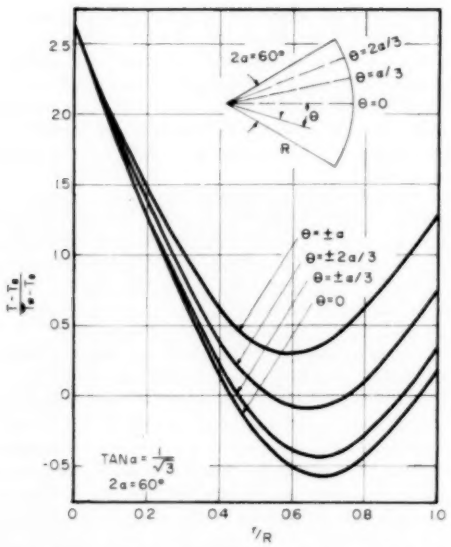

(*a*) **Temperature profiles along radii *r* for duct with 60-deg opening angle**

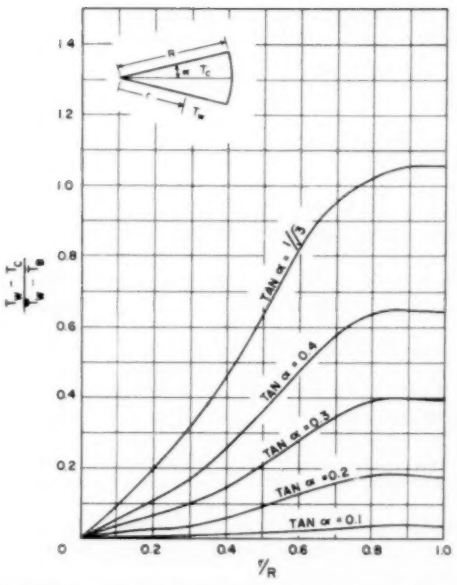

(*b*) **Difference between local wall surface temperature and centerline temperature measured at distances *r* from corner of ducts with various opening angles**

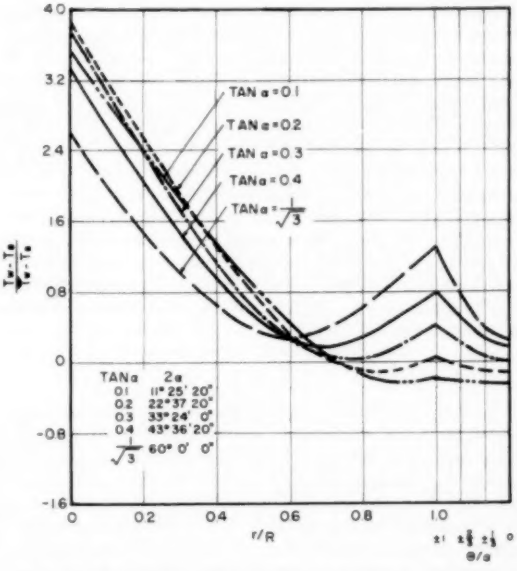

(*c*) **Wall surface temperature distribution around periphery of ducts with various opening angles**

Fig. 5 Temperature field for hydraulically and thermally developed flow through a duct whose cross section is a circular sector. A locally constant heat flux from duct surface into the fluid is prescribed.

tance from the duct corner is steeper for the temperature field than for the velocity field. Again the influence of the curved wall of the duct is felt only a moderate distance away from that wall. Fig. 4(*b*) presents the temperature profiles along the center line for ducts with various opening angles, and Fig. 4(*c*) indicates the distribution of the local heat fluxes from the fluid to the duct surface around the periphery of ducts with various opening angles. It can be observed that the heat flux drops to the value zero in the duct corners. The local heat flux q was obtained from the gradient of the fluid temperature in a direction normal to the duct surface and at the duct wall. The heat flow $\bar{q}$ averaged over the duct periphery is connected with the fluid temperature increase in the axial direction by the heat balance

$$\bar{q}C = c_p \rho \bar{w} A \frac{\partial T}{\partial z} \quad \ldots\ldots [9]$$

An average heat-transfer coefficient may be defined in the customary manner by

$$\bar{q} = \bar{h}(T_w - T_B) \quad \ldots\ldots [10]$$

where T_B is the fluid bulk temperature

$$T_B = \frac{1}{\bar{w}A} \int_A wT dA \quad \ldots\ldots [11]$$

or the temperature which would be obtained by mixing of the fluid as it passes the cross section considered. The Nusselt number $\overline{\mathrm{Nu}} = \bar{h}D_h/k$ is found to be a function of the duct shape only. Its value is inserted in Fig. 3. Again it can be seen that it is different from the value 4.36 for a round tube. This indicates that the hydraulic-diameter concept does not work for laminar heat transfer in circular sector ducts.

Peripherally Constant Heat Flux. The boundary conditions for this situation are

$$\left.\begin{aligned} -k\frac{\partial T}{\partial r} &= q = \text{const} \quad \text{for} \quad r = R \\ -\frac{k}{r}\frac{\partial T}{\partial \theta} &= \mp q = \text{const} \quad \text{for} \quad \theta = \pm\alpha \end{aligned}\right\} \quad \ldots\ldots [12]$$

The calculations necessary to obtain a solution of Equation [5] for this boundary condition are much more involved than for the constant-wall-temperature case and only the results of such a calculation will be presented here. A detailed discussion of the solution for this case together with the calculation details are

given in (6). Generally the solution of Equation [5] which satisfies boundary conditions [12] can be expressed as

$$T = \frac{1}{\mu a}\frac{\partial p}{\partial z}\frac{\partial T}{\partial z}R^4\left[C_1\left(\frac{r}{R}\right)^4 + C_2\left(\frac{r}{R}\right)\cos\theta + C_3\left(\frac{r}{R}\right)^4\cos 2\theta + C_4\left(\frac{r}{R}\right)^4\cos 4\theta + \sum_{m=1,2,3\ldots}^{\infty} A_m\left(\frac{r}{R}\right)^{\frac{m\pi}{\alpha}}\cos\frac{m\pi}{\alpha}\theta + \sum_{m=1,3,5\ldots}^{\infty} B_m\left(\frac{r}{R}\right)^{\frac{m\pi}{2\alpha}+2}\cos\frac{m\pi}{2\alpha}\theta + \sum_{m=1,3,5\ldots}^{\infty} D_m\left(\frac{r}{R}\right)^{\frac{m\pi}{2\alpha}+2}\cos\left(\frac{m\pi}{2\alpha}+2\right)\theta\right] \quad [13]$$

The constants C_1 to C_4, A_m, B_m, and D_m have to be determined in such a way that Solution [13] satisfies the boundary conditions [12]. From the results of the calculation Figs. 5(*a*, *b*, *c*) have been prepared. These figures illustrate the temperature field existing when the heat flux at the duct surface is directed from the surface into the fluid.

Fig. 5(*a*) shows the temperature profiles on various radii for the 60-deg duct. It can be observed that the temperature variation in the radial direction is considerably greater than the one in the angular direction. This is yet more pronounced for smaller duct angles as evidenced by Fig. 5(*b*). This figure gives the difference between center line and surface temperature for various positions r and for ducts with various opening angles. Since the duct with an opening angle of 60 deg comes in shape quite close to an equilateral triangle, it has to be concluded from Figs. 5(*a* and *b*) that the opening angle of a corner in a noncircular duct is the most important factor in determining how strongly the temperature varies in its neighborhood. Fig. 5(*c*) shows the distribution of the wall temperature around the periphery for ducts with various opening angles. The connection between the temperature difference $\overline{T}_w - T_B$, the axial temperature gradient $\partial T/\partial z$, and the heat flux q_w can be obtained from the following equations. The relation between heat flux and axial temperature gradient is again given by Equation [9]. With an average heat-transfer coefficient defined by the equation

$$q = \bar{h}(\overline{T}_w - T_B) \quad [14]$$

a Nusselt number $\overline{\mathrm{Nu}} = \bar{h}D_h/k$ is obtained and this parameter is inserted in Fig. 3. This figure now reveals the astonishing fact that a very great difference exists between the average Nusselt numbers for constant heat flux and for constant wall temperature. In a duct with an opening angle of 20 deg the two parameters differ almost by a factor of 10. This difference might be explainable physically by the fact that the boundary condition of constant heat flux forces more heat into regions of low velocity near the apex. From the Nusselt numbers in a circular tube obtained for axially constant wall temperature and constant heat flux, it appears that the influence of the peripheral variation of these parameters is for ducts with shapes similar to a circular sector considerably more important than the axial variation. This fact is also evident from the results of a calculation by Deissler and Taylor (5), which determined turbulent heat transfer between tube bundles and a fluid flowing in the axial direction outside the tubes. Information even on average heat-transfer coefficients for noncircular ducts with pronounced corners is practically meaningless without a clear specification of the peripheral boundary conditions.

Various possibilities for a presentation of the results of the foregoing calculations have been considered. It was felt that the method chosen here is most consistent with established practice in the field of heat transfer and that it is, for instance, not appropriate to define local heat-transfer coefficients because these parameters assume at certain locations values equal to zero or infinity when they are based on local wall temperatures.

Generalization of Results. The great difference between the Nusselt numbers of peripherally constant wall temperature and constant heat flux suggests the question how heat transfer can be calculated for arbitrarily prescribed peripheral distributions of either parameter. The solutions for a family of such distributions can be obtained in a simple way from the results presented in this paper. The fact that the energy equation [5] is linear in the temperature T makes it possible to obtain new solutions by superposition of the known ones. This means that new temperature fields for a certain duct shape can be obtained by adding the two known fields for constant wall surface temperature and for constant surface heat flux after having multiplied each one with an arbitrary scale factor. The corresponding wall surface temperature can be obtained from Fig. 5(*c*) by adding to the respective distribution curve a constant wall temperature after multiplying each value with the proper scale factor. The same procedure applied to Fig. 4(*c*) results in the proper heat-flow distribution. The average Nusselt number belonging to these temperature and heat-flow distributions is finally obtained from Fig. 3 by interpolation between the values $\overline{\mathrm{Nu}}$ for constant wall temperature and for constant heat flux in the ratio of the respective scale factors. It can be verified easily from the foregoing equations that this procedure is correct and exact.

Bibliography

1 "Forced Convection From Nonisothermal Surfaces," by M. Tribus and J. Klein, Heat Transfer Symposium, University of Michigan, Ann Arbor, Mich., 1952, p. 211.

2 "Flow in Corners of Passages With Noncircular Cross Sections," by E. R. G. Eckert and T. F. Irvine, Jr., TRANS. ASME, vol. 78, 1956, pp. 709–718.

"Laminar, Transitional, and Turbulent Flow in Triangular Passages," by E. R. G. Eckert, T. F. Irvine, Jr., and R. Eichhorn, Wright Air Development Center Technical Report 54-443, 1954.

"Analysis of Laminar Heat Transfer in Wedge-Shaped Passages," by E. R. G. Eckert, T. F. Irvine, Jr., and J. T. Yen, Wright Air Development Center Technical Report 56-98, 1956.

3 "A Note on Limiting Laminar Nusselt Numbers in Ducts With Constant Temperature Gradient by Analogy to Thin-Plate Theory," by S. M. Marco and L. S. Han, TRANS. ASME, vol. 77, 1955, p. 625.

4 "Theory of Plates and Shells," by S. Timoshenko, McGraw-Hill Book Company, Inc., New York, N. Y., 1940, pp. 272–274.

5 "Analysis of Axial Turbulent Flow and Heat Transfer Through Banks of Rods or Tubes," by R. G. Deissler and M. F. Taylor, presented at Reactor Heat Transfer Conference, New York, N. Y., November, 1956.

6 "Exact Solution of Laminar Heat Transfer in Wedge-Shaped Passages With Various Boundary Conditions," by J. T. Yen, Wright Air Development Center Technical Report 57-224, 1957.

Survey of Mathematical Methods for Nonlinear Control Systems

By JULIEN M. LOEB,[1] PARIS, FRANCE

This paper is a survey of presently known mathematical methods applicable to nonlinear control problems. After emphasizing the need for general theories which alone can facilitate equipment design, the author discusses: *a* Phase-plane and phase-space methods for graphical representation of general system behavior; *b* describing-function analysis of limit cycles; *c* piece-wise linear analysis; *d* probability calculus for the study of noise and random inputs in nonlinear systems; and *e* energy-balance and stroboscopic methods which apply to particular features of a system.

1 Introduction: Synthesis Versus Analysis

ALTHOUGH nonlinear systems cannot be analyzed by means of the standard methods that have been developed for linear systems (Laplace transform, Nyquist diagram, etc.) their analysis is far from impossible.

The analysis consists in integrating a system of nonlinear differential equations, knowing boundary conditions. Very seldom the solution appears as a combination of known functions, but this circumstance is no essential difficulty. What eventually is needed is a set of numerical values: Whether they come from tabulations of known functions or direct numerical integration is immaterial. Moreover, painstaking graphical methods belong to the past and computers have a widespread use.

But engineering principally consists of systems synthesis. If one has only analysis methods, one is condemned to a series of trial-and-error steps, without being sure he will arrive at the best design. As a guide to better understanding of the synthesis problem, there is no decisive difference between hand and machine calculations, and none of these can replace general methods in the synthesis work. These methods can be classified in two categories:

In the first category, we will put the methods such as "phase plane" that fully recognize the nonlinear nature of the problem; practically, their field of application is limited to second-order systems (although general results already are known about "phase spaces").

In the second category, we must place all the methods that try to extrapolate the knowledge already obtained in the linear domain: Such are the "describing function" method, the reduction to piecewise linear systems, the small disturbance method, etc.

With these last methods, one enters the dangerous field of so-called "approximations" (very seldom does the exposition of what is called "an approximate method" contain an evaluation of the error). However, such a shortcoming is not as important as it may seem, because the last step of the design of an equipment always is an analysis that can be performed with known and acceptable errors.

Definition of needed performance concerns the customer as well as the design engineer. In the linear field, the conditions to be fulfilled can be expressed in terms of frequency band, signal-to-noise ratio, etc. . . On the other hand, the tests to be performed are not so well known in the nonlinear case. The solution appears to be a reasonable application of probability calculus that deals with signal and disturbance statistical data.

One word more about bibliography: Hundreds of papers have been written on nonlinear control. Although only mathematical methods are considered here, relevant papers are too many. The choice of quoted literature does not imply any affirmation of priority nor any hint that other papers, not quoted, are not as good. The author knows them: That is all.

2 Phase Plane

2.1 *Differential Equations of the Second Order* (1)[2]

So-called "rational mechanics" began with the calculation of the motion of a "material point" subject to known forces. The equation of the second order was therefore thoroughly studied, and the results found for the material point rapidly were extended to the case of one solid lump of matter whose position is determined by one co-ordinate, such as the simple or compound pendulum.

Cauchy showed that a differential equation

$$f(\ddot{x}, \dot{x}, x, t) = 0 \qquad [1]$$

that relates an unknown co-ordinate x and its derivatives $\dot{x}$ and $\ddot{x}$ with respect to time t can be decomposed into two equations of the first order

$$\left.\begin{aligned} \dot{x} &= y \\ f(\dot{y}, y, x, t) &= 0 \end{aligned}\right\} \qquad [2]$$

This approach was used to derive Cauchy's classical theorem about uniqueness of the solution.

Very often, t does not appear explicitly in the equations and [2] can be written, after some manipulation, as

$$\frac{dx}{P(x, y)} = \frac{dy}{Q(x, y)} \qquad [3]$$

or

$$\frac{dy}{dx} = \frac{Q(x, y)}{P(x, y)}$$

2.2 *Phase Plane Representation*

Equation [3] immediately suggests a graphical method for the plot of the solution (Fig. 1).

The point A represents the initial state of the system: The abscissa x_A is the initial position, and the ordinate $\dot{x}_A$ is the initial velocity. From x_A and $\dot{x}_A$, one can calculate the slope $\frac{Q(x_A, \dot{x}_A)}{P(x_A, \dot{x}_A)}$ of the tangent AB to the curve AC (called a trajectory) that represents the evolution of the system. This curve can be thought

---

[1] Schlumberger Well Surveying Company.

Contributed by the Instruments and Regulators Division and presented at the Annual Meeting, New York, N. Y., December 1–6, 1957, of THE AMERICAN SOCIETY OF MECHANICAL ENGINEERS.

NOTE: Statements and opinions advanced in papers are to be understood as individual expressions of their authors and not those of the Society. Manuscript received at ASME Headquarters, August 1, 1957. Paper No. 57—A-104.

[2] Numbers in parentheses refer to the Bibliography at the end of the paper.

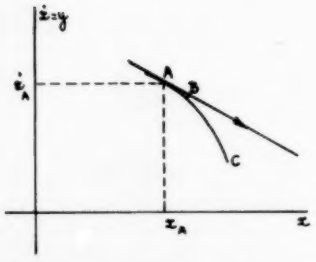

Fig. 1 Phase-plane approach—graphical integration method

of as coinciding with its tangent AB for a very small increment of time. At B, one knows the new values of co-ordinates

$$x_B \text{ and } \dot{x}_B$$

and the process can be repeated.

It has been mathematically proved that when the segments such as AB become infinitely small, the process is convergent. This means that any approximate solution consisting of small segments of straight lines tends toward the same curve, the desired solution. Equations with a forcing function also can be graphically integrated (2 and 3). As explained above, this way of doing the calculations must be classified as an *analysis* method.

2.3 *Singular Points* (Poincaré)

Fortunately enough, this method fails when $P(x, y)$ and $Q(x, y)$ are equal to zero at the same point X, Y. The slope of the tangent becomes 0/0 and is indeterminate. Such points are called "singular points." Near these points linear methods can be used, since P and Q can be expanded in increasing powers of x and y

$$\left.\begin{aligned} P &= ax + by + P_1(x, y) \\ Q &= cx + dy + Q_1(x, y) \end{aligned}\right\} \quad \ldots\ldots\ldots\ldots [4]$$

where P_1 and Q_1 do not include any constant or linear terms.

2.31 *Linear Approximation*

Around singular points, possible trajectories can be approximated by the equations

$$\left.\begin{aligned} \dot{x} &= ax + by \\ \dot{y} &= cx + dy \end{aligned}\right\} \quad \ldots\ldots\ldots\ldots\ldots [5]$$

In the vicinity of a singular point, the solution of the nonlinear equation is approximated by a linear equation of the second order. The solutions are well known, but it is interesting to use the phase plane representation. They can be classified in the following categories.

Undamped Motion

a) Periodic solutions (Equation $\ddot{x} + \omega_0^2 x = 0$). The trajectories are closed curves (ellipses for linear approximation). The singular point V never is attained: It is called a *vortex* (Fig. 2).

b) Nonperiodic solutions (Equation $\ddot{x} - \omega_0^2 x = 0$). The trajectories are open curves (hyperbolas for linear approximation). The singular point S can be attained in an infinite time, positive or negative: It is called a *saddle point* (Fig. 3). The asymptotes to the hyperbolas AA′, BB′ play a very important role in the theory. They mark the limit between regions I, II, III, IV of the plane, and therefore are called *separating curves*.

In each of these regions trajectories have the same shape, and one can be deduced from the neighboring trajectory by means of a very small adjustment. On the contrary, when the asymptote SB′ is passed, there is a jump in the shape of the curve; for instance, the final point of the trajectory abruptly jumps from A to A′.

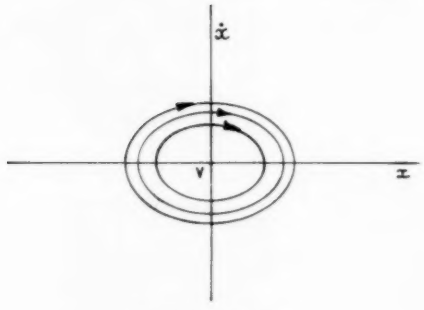

Fig. 2 Vortex point

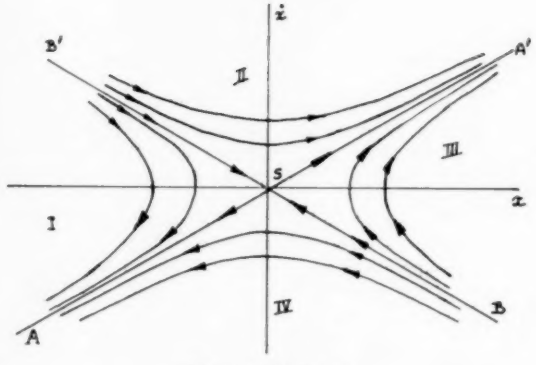

Fig. 3 Saddle point

Damped Motion (positive damping)

c) Oscillatory solutions ($\ddot{x} + 2D\dot{x} + \omega_0^2 x = 0$) with $D^2 < \omega_0^2$, i.e., damping smaller than critical value. The ellipses of Fig 2 become spirals. In the linear approximation, with suitable scales on x and $\dot{x}$ axes, the trajectories are logarithmic spirals. The singular point F is called a *focal point* (Fig. 4) and is reached after an infinite time.

d) Nonoscillatory solutions ($\ddot{x} + 2D\dot{x} + \omega_0^2 x = 0$) with $D^2 > \omega_0^2$, i.e., overcritical damping. The hyperbolas of sector IV, Fig. 3,

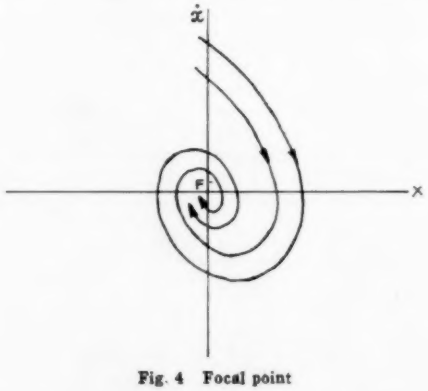

Fig. 4 Focal point

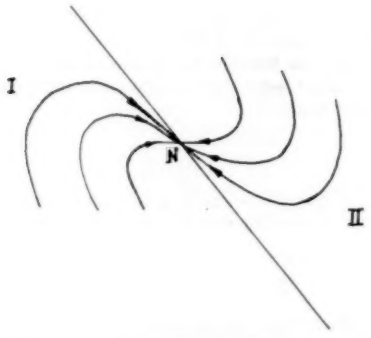

Fig. 5 Nodal point

are transformed into curves of sector I, Fig. 5. The singular point is called a *nodal point* and is reached after an infinite time.

2.32 *General Case*

Since in the neighborhood of a singular point (without damping) ellipses and hyperbolas are a good approximation, the actual curves are not substantially different and can be considered as slightly distorted ellipses or hyperbolas. This remark looks trivial; however, it shows how the phase plane approach can be not only a means of painstaking analysis, but also the powerful tool of synthesis needed by the engineers. In effect, it brings into the picture a branch of mathematics called topology.[3]

Coming back to Fig. 3, all the hyperbolas of sector I are topologically equivalent, but differ from those of sector II because it is necessary (in order to pass from one family to the other) to cross the line SB′.

[3] Topology (4) is the study of geometrical figures, regardless of their exact shape, but with an emphasis on striking features, such as their place with respect to other figures of the plane, existence of double points, closed curves, etc. . . . For instance, curves *a*, *b*, *c* of Fig. 6 are topologically equivalent (simple closed curve), but different from *d*, that shows a double point P.

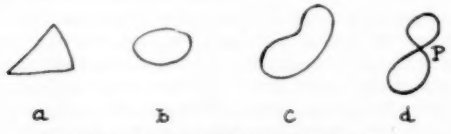

Fig. 6(*a*, *b*, *c*) Topologically equivalent curves

Fig. 6(*d*) Topologically different curve from *a*, *b*, and *c*

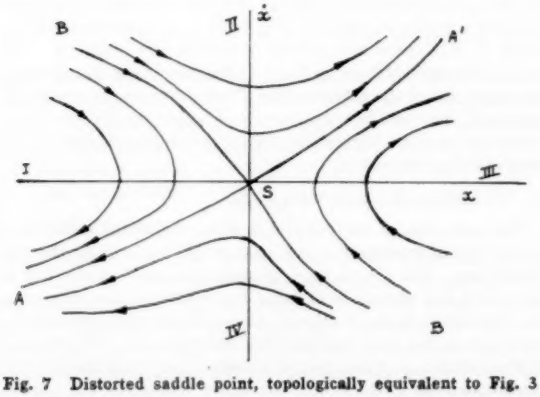

Fig. 7 Distorted saddle point, topologically equivalent to Fig. 3

Separating Curves

In Fig. 7, are represented some trajectories that are "almost" hyperbolas. The curves ASA′ and BSB′ are particular trajectories that attain S within an infinite time (positive or negative). They separate the plane into sectors I, II, III, IV where the trajectories topologically are equivalent. It is possible, when the separating curves have been drawn, to get a fairly good idea of the system behavior for any given initial conditions. In the general case, separating curves must be drawn by means of graphical methods sketched in paragraph 2.

2.4 *Limit Cycles*

Here appears a deep difference between linear and nonlinear problems. When one studies the stability of a linear device, one finds circumstances where the amplitude would increase beyond any limit if linearity could be maintained: For instance, electronic oscillators or hunting servomechanisms are systems where the origin ($x = 0$, $\dot{x} = 0$) is an unstable focal point. Linear analysis indicates that an oscillation actually will start. But it will be of no help for the calculation of amplitude or exact frequency of the oscillation.

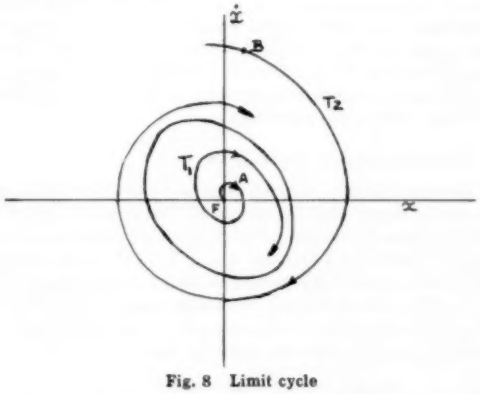

Fig. 8 Limit cycle

The phase plane approach allows one to describe sustained oscillations: The trajectory is a closed pattern that is run during one period and repeated indefinitely. Fig. 8 shows an example of self-sustained oscillation taking place after the system has been slightly disturbed from a focal point F. The curve starts at A where x_A and $\dot{x}_A$ are small. The trajectory T_1 topologically is equivalent to a logarithmic spiral diverging from F. Physically, we know that the gain of the closed loop must decrease when the amplitude increases, due to saturation. There exists a closed curve C that is a limit to expanding trajectories such as T_1. After enough time has elapsed, the asymptotic part of T_1 to C will be undistinguishable from C: The system operates on a periodic mode. If the initial point is B, the amplitude tends to decrease and the limit cycle C is attained from the outside.

H. Poincaré has done much work with limit cycles and has shown that they are alternatively stable and unstable. More recently trying a periodic solution

$$x = a_1 \cos \omega t + b_1 \sin \omega t + a_2 \cos 2\omega t + b_2 \sin 2\omega t + \dots$$

where $a_1, a_2, \dots, b_1, b_2, \dots, \omega$ are the unknowns of the problem, B. Van der Pol (5) has thoroughly examined the limit cycles of equation

$$\ddot{x} - \epsilon(1 - x^2)\dot{x} + x = 0 \dots\dots\dots\dots\dots [6]$$

2.5 *Use of Phase Plane Approach*

The general way of dealing with a nonlinear problem (of the second order) is the following:

a *Determine the singular points and the separating curves.* This can be done without solving the equation for all the initial conditions. Singular points are found by solution of simultaneous equations

$$P(x, y) = 0$$
$$Q(x, y) = 0$$

Separating curves always can be found by graphical integration.

b *Determine the limit cycles,* if any, by trial and error choice of a starting point.

These two computations give the "land marks" of the phase plane, and a fairly good idea of the behavior of any proposed system. The needed general theory now exists at least for a *qualitative* knowledge that is very helpful in the great many cases. It gives a *survey* of all possible trajectories and makes it possible, without computing the general solution, to foresee the effect of any change in the design.

3 Phase Spaces

The limitations of phase plane representation and analysis are evident: No practical control system, subject to possible hunting, is described by a second-order equation; (one can except the case, quoted in (6), of a second-order system where backlash causes self-sustained oscillations). For higher-order systems, one still can replace the unknown by a set of unknowns subjected to lower order differential equations.

3.1 *Three-Dimensional Phase Space*

It has been shown (7) how some solutions of a third-order equation can be represented by nonplanar curves whose projections on three planes are drawn. The three co-ordinates are x (representing a position or a voltage), $\dot{x}$, and $\ddot{x}$. The curves which are shown are computed for particular initial conditions, but it is also possible, although much more complicated, to define landmarks, such as vortexes, focal points, etc. . . in the 3-D space. One has first to put the equations under the form

$$\frac{dx}{P(x, y, z)} = \frac{dy}{Q(x, y, x)} = \frac{dz}{R(x, y, z)}$$

with $y = \dot{x}$ and $z = \ddot{x}$ . . . . . [7]

and study singularities defined by

$$P(x, y, z) = 0 \qquad Q(x, y, z) = 0 \qquad R(x, y, z) = 0 \text{ . . [8]}$$

3.2 *Two-Dimensional Approximation*

New mathematical methods can be applied to a very wide category of control systems. It frequently happens that a control system comprises a nonlinear part such as a relay or an elaborate computer, whose inertia can be disregarded, and a linear part such as the armature of a big electric motor, coupled to the load through resilient shafts and gears. The diagram is given by Fig. 9.

In particular, the procedures to be described can be applied to so-called "piecewise linear systems" that are discussed in Section 5. When treating these control systems, one applies the well-known

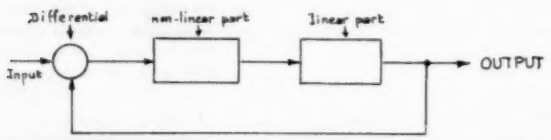

Fig. 9 Feedback system comprising a linear part and a time independent nonlinear part

algebraical process called "decomposition in simple fractions" (8) to the transfer function of the linear part.

As is known, the transfer function of a linear network (or mechanical system) can be expressed as a ratio of two polynomials in the Laplace variable s

$$\frac{N(s)}{D(s)}$$

The degree of the denominator D is higher than that of the numerator N. Such a fraction can be expanded as

$$\sum_n \frac{a_n + \tau_n S}{b_n + \xi_n T_n S + T_n^2 S^2} \text{ . . . . . [9]}$$

where n is an integer; a_n, b_n, and ξ_n are dimensionless constants; and τ_n and T_n are time constants. Among all the time constants T_n, it often happens that one or two are much larger than the others. Let us call them T_1 and T_2. Now, it is possible to choose the set of independent variables in such a way that two of them are subject to differential equations involving only T_1 and T_2.

For instance, in the case where the decomposition comprises terms like

$$\frac{a}{1 + T_1 S} + \frac{b}{1 + T_2 S}$$

there are two variables, say u and v, that obey differential equations

$$u + T_1 \dot{u} = 0$$
$$v + T_2 \dot{v} = 0$$

One often is interested in the return of the system to rest ($u = 0$, $v = 0$) after a disturbance. The time constants T_1 and T_2 assumed to be larger than the others, are a measure of the time necessary for the return to rest. So one can imagine that, after the disturbance, all the other variables die out fairly rapidly. After a short time the law of evolution of the system is approximately the same as if there were just two independent variables, i.e., if the system were of the second order. However, this procedure allows one to deal with more complicated systems than second-order ones. Multidimensional analysis can be found in (9 and 10). Following these papers and (8), one can treat the general problem by means of multidimensional geometry. The independent variables x, y, z . . . are the co-ordinates of a point in the multidimensional space. The particular study of the two variables x and y that come to zero in the longest time is equivalent to a *projection* of the multidimensional space on a particular surface described by co-ordinates x and y chosen for its practical importance. For instance, third-order systems with optimum switching have been investigated. For the representation of such systems, a particular surface (Fig. 10) is used that represents the locus of 3-D space trajectories ending at the origin O. This system is described in paper (11). If the initial point B, representing the state of the system after the disturbance, is not on the surface S, there will be a first section of trajectory Bb, run over in a very short time, the rest bO being thoroughly described by a two-variable equation.

4 "Describing Function" Methods

The basic idea of this paragraph is to provide the definition of some kind of transfer function that would be valid in the nonlinear case. For a long time, pioneers such as Van der Pol (5) have seen the advantage of using Fourier series expansion when dealing with periodic solutions. As is natural, some emphasis has been put on the fundamental Fourier component. The first step in the elaboration of generalized transfer functions is the following trivial analysis (Fig. 11). This figure represents the simplest

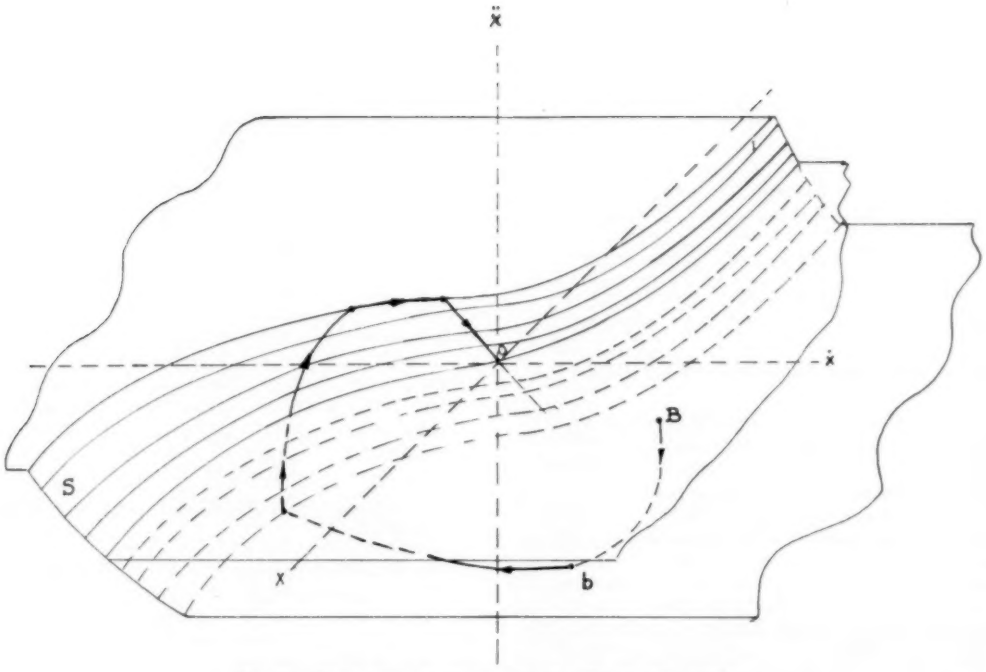

Fig. 10 Phase-space representation of optimum relay system

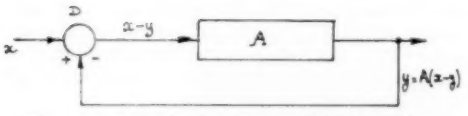

Fig. 11 General single-loop feedback system

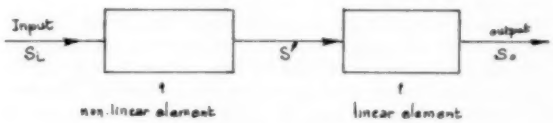

Fig. 12 Decomposition of the open loop

closed loop where A is the amplifier, generally nonlinear. If the device is to be used as a servomechanism (a position control, for instance) x represents the input, in other words, the desired value of the output y. We now will find under what conditions a closed loop can produce self-sustained periodic oscillations. When the system is hunting, the oscillations exist even if $x = 0$. This is possible only if the output y is equal to the input with a change of sign due to the action of the differential element. Then, the necessary and sufficient conditions for the existence of a periodic solution of period T defined by

$$y = f(t) = f(t + KT) \qquad (K \text{ integer}) \ldots\ldots\ldots [10]$$

is that the output y should be related to the input in such a way that *all* Fourier components would be equal (with the change of sign). In particular, the effect of the amplifier on the fundamental component must be just to change the sign of the signal. This last condition is necessary, but not sufficient, and does not give much help to the engineer.

4.1 *Filtered Systems* (12, 13)

The device represented on Fig. 9 has a very interesting property: The linear part, characterized by some inertia, can be considered as a filter for high frequencies. When the servo is hunting, the harmonics that come from the nonlinear part are approximately filtered out. It becomes useful and legitimate, in these conditions, to express the properties of the whole system by the complex ratio between output and input fundamental components. This definition relies on the possibility of performing the following experiment (Fig. 12). At the input terminals, one applies a signal

$$S_i = x \cos \omega t$$

The output S of the nonlinear element (for example, a relay) is strongly distorted, and it would not be permissible to overlook the harmonics at this point. But the output S_o is nearly sinusoidal and can be written

$$S_o = X \cos (\omega t + \phi)$$

The ratio S_o/S_i is a complex number that depends on ω and *also on* x. For instance, in a relay the ratio S/S_i tends toward zero when x increases. Doing this, we have defined a complex function

$$A(x, \omega) = \left|\frac{Y}{X}\right| + \phi$$

that is a generalization of the transfer function of linear systems. This two-variable function is a generalization of the usual "Describing Function." The describing function method can also be interpreted using the phase-space approach (Section 3). When a system actually is oscillating on a limit cycle its representative point follows a *closed* curve C in the multidimensional space. In the general case, where harmonics must be considered, the problem is too complicated for discussion. Fig. 13 is an attempt

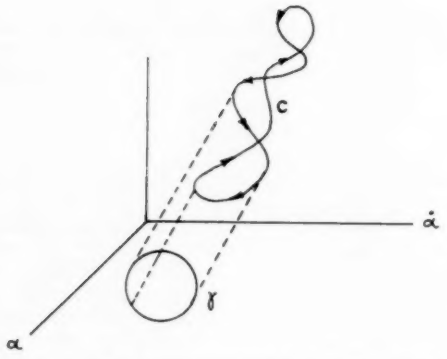

Fig. 13 Phase-space representation of limit cycle

to display (curve γ) on a two-dimensional sheet of paper, a non-planar curve C in a more-than-two-dimensional space.

Let us now assume that the system includes some part, such as the armature of an electric motor, that has a large inertia. There will be two co-ordinates, i.e., the angular position α of the shaft and its derivative $\dot{\alpha}$ by means of which the motion of the whole system can be represented very simply. In effect, if one can overlook harmonics, both are sinusoidal functions of time, and the curve in the plane α, $\dot{\alpha}$ is very close to an ellipse. This curve γ can be considered as the projection of the very complicated curve C on the plane α, $\dot{\alpha}$. In this way, the describing function method can, more generally, be considered as a suitable choice of two co-ordinates following which the projection of the complicated curve C is not very different from an ellipse.

Here now is an example of application of these ideas. Let us take an on-off servomotor controlled by a switch, that operates when the co-ordinate α changes its sign. There is only a pure inertia and the force applied has a constant modulus K. The 3-D limit cycle is shown on Fig. 14. It is composed of the arc of

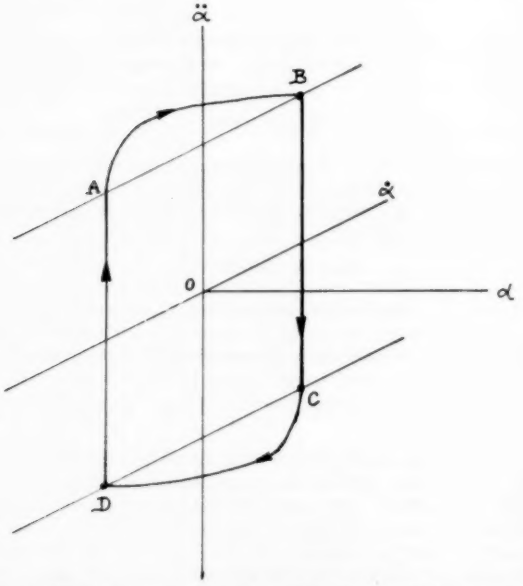

Fig. 14 Phase-space representation of the limit cycle for an on-off oscillating system

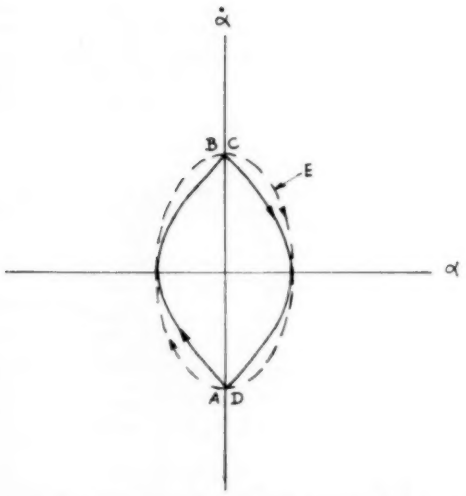

Fig. 15 Projection of 14 on the α-$\dot{\alpha}$-plane, with the describing function approximation

parabola AB in the upper plane $\ddot{\alpha} = +K$, the vertical straight line BC corresponding to the reversal of acceleration, the parabola CD in the lower plane $\ddot{\alpha} = -K$ and the straight line DA. The well-known "phase plane" trajectory of Fig. 15 really is the projection on the α, $\dot{\alpha}$ plane of the more complicated curve ABCD of Fig. 14. Now the describing function approach will consist of replacing the exact curve by the ellipse E, neglecting the harmonics associated with the angular points BC and AD.

We must keep in mind the limiting assumption that *all components other than the fundamental* are strongly reduced by the linear part, but fortunately harmonics are more reduced when the order of the differential equation is high.

Describing function methods can lead to errors when a second-order system is dealt with (it is fortunate that in this case the phase-plane approach is usable). For instance (6) an unstable limit cycle given by describing function analysis of an on-off second-order system does not really exist although the stable oscillation is correctly indicated. Moreover, a nonlinear part can also give a constant term (14) or even subharmonics. In these cases, the describing function method cannot be used, or must be very complicated (15).

In the cases where it is applicable, the describing function method is a very valuable tool since it is usable for higher order systems.

At present, it is the only approach that allows the engineer to foresee self-sustained oscillations in a higher order nonlinear servo.

4.2 *Oscillation Criteria Using Conventional and Generalized Describing Functions*

Knowledge of the generalized describing function $A(x, \omega)$ allows one to tell whether self-sustained oscillations can exist.

If so, there are one or several pairs of values (x, ω) such that

$$A(x, \omega) = -1 \quad [11]$$

A first consequence of this condition is the well-known curve intersection diagram (13), valid for the system of Fig. 9. The generalized describing function can be written

$$A(x, \omega) = f(x)g(\omega) \quad [12]$$

where $f(x)$ is the usual describing function and $g(\omega)$ is the usual frequency response (magnitude ratio and phase shift) of the linear

part. It is assumed that the nonlinear part does not depend on ω; for instance, if it is a relay, the operating lag of the armature is very small compared to the shortest period of signals that must be transmitted. In this case, one will plot, on the complex plane, two curves (Fig. 16).

The first (solid line) is the locus of the values of $f(x)$ for various values of x, say $x_0, x_1 \ldots$.

The second (dotted line) is the locus of the values of $\dfrac{-1}{g(\omega)}$ for various values of ω, say $\omega_0, \omega_1 \ldots$.

In Fig. 16(a), both curves intersect; the pair of values x_2 and ω_3 makes

$$f(x)g(\omega) = -1$$

In Fig. 16(b), the curves do not intersect, and no oscillation is possible.

It is also possible (16) to give a criterion valid for any generalized describing function $A(x, \omega)$. It suffices to plot on the complex plane the double family of curves (Fig. 17). The solid lines represent $A(\omega, x)$. Each line is labelled with a given value of x, say $x_0, x_1 \ldots$ and scanned with various values of ω. The dotted lines also give $A(\omega, x)$, each line being labelled with a given value of ω, say $\omega_0, \omega_1 \ldots$ and scanned with various values of x. These families of curves generally fill a certain region R of the plane: If R contains the Nyquist point $(-1 + j\,0)$ there are pairs of values (x, ω) for which

$$A(x, \omega) = -1$$

and the system can oscillate. If R does not contain it, no oscillation is possible.

Fig. 17 represents the following case: The nonlinear part is a relay with a threshold σ and an output voltage $\pm V_0$, the linear part is a third-order system such as an electric motor whose inductance is not neglected. One can compute the relay's transfer function $y = f(x)$, where y is the amplitude of the fundamental term of output and x the amplitude of sinusoidal input. When ξ is the instantaneous value of the input

for $-\infty < \xi < -\sigma$	$y = -K$
for $-\sigma < \xi < \sigma$	$y = 0$
for $\sigma < \xi < \infty$	$y = +K$

If the input is $\xi = X \cos \omega t$

the fundamental term Y of the output is (regardless of ω) in phase with ξ and has an amplitude

$$\frac{4V_0}{\pi}\left(1 - \frac{\sigma^2}{X^2}\right)^{1/2} \qquad \text{when } X > \sigma$$

and equal to zero when $|X| < \sigma$ [see reference (13)].

The describing function Y/X of the relay is then

$$\frac{4V_0}{\pi X}\left(1 - \frac{\sigma^2}{X^2}\right) \quad \text{or } 0$$

The motor (linear part) has the well-known transfer function

$$\frac{1}{Ts(1 + T_1 s + T_2^2 s^2)}$$

where time constants T, T_1, and T_2 are calculated from the characteristics of the motor: Inductance, inertia, voltage versus velocity in absence of load, and so on.

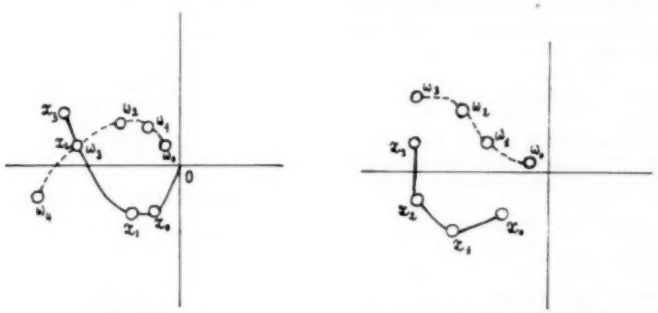

(*a*) Oscillation (*b*) No oscillation

Fig. 16 Curve intersection criterion

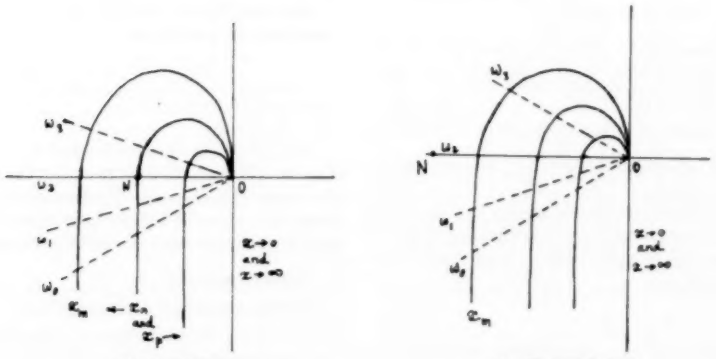

(*a*) Oscillation (*b*) No oscillation

Fig. 17 Curve-families criterion

This case presents an interesting peculiarity: When the input amplitude is smaller than the threshold, the gain is zero. It increases and reaches a maximum corresponding to curve x_m and then decreases to zero because of the effect of saturation.

In Fig. 17(a) the Nyquist point N is covered by the families of curves. Then, two modes of oscillation are possible ω_2, x_m and ω_1, x_p. In Fig. 17(b) no oscillation is possible.

This example can be considered as another, very intuitive, demonstration of Nyquist criterion for that case: The curve x_m corresponds to the gain of a linear device. In the linear language, one says that "N is enclosed by the curve x_m." This corresponds in nonlinear language to the statement "N is covered by R." Here we learn something more than the possibility of oscillations: We learn how the system actually oscillates. This knowledge is equivalent to the knowledge of limit cycles in the phase-plane approach.

4.3 *Dynamics of Limit Cycles*

At this point we have criteria about the possibility of oscillation on a mode defined by the amplitude x and the angular frequency ω. But this is not yet sufficient to allow one to predict actual hunting on this mode.

In effect, we still have to solve the problem of limit cycle stability. (Section 4.2 is purposely not entitled "Stability criteria.") Generally, a servo is called "unstable" when it is hunting, i.e., when steady oscillations take place. We would suggest that the phrase "stability of a servo" be avoided, reserving the notion of stability to characterize the hunting mode.

Let us imagine that we analyze the motion taking as initial conditions a situation (x, ω) very close to the co-ordinates (x_1, ω_1) that satisfy the relationship [11].

Two behaviors are possible: Either the mode tends toward the limit cycle: The limit cycle is then called stable; or the actual mode diverges from this limit cycle, which in this case is called unstable.

A criterion has been devised (16) for the stability of limit cycles in servos like that of Fig. 9.

Following the notation of Section 4.2, $f(x)$ is the function characterizing the nonlinear element, and $g(\omega)$ the transfer function of the linear part. It can be proved that if

$$x \frac{\frac{df}{dx}}{f} \ll 1$$

one is allowed to make the following assumption: If the initial data are such that the system operates very near the limit cycle (x_1, ω_1), x is no longer constant, but can be expressed as

$$x_1(1 + e^{-\alpha t})$$

where α is a damping factor, the sign of which must be determined. So, we add to the angular frequency ω an imaginary component $j\alpha$ and we apply Equation [11] as follows

$$f(x_1 + \xi)g(\omega_1 + \epsilon + j\alpha) = -1 \ldots\ldots\ldots [13]$$

where ξ is the difference between actual x and x_1, and ϵ is the difference between actual ω and ω_1.

The equations used to determine the unknowns ξ, ϵ, and α are two equations obtained by expanding the first member of [13] in a Taylor series with real and complex terms. They yield a proportionality between ξ and α

$$\alpha = K\xi$$

If K is positive, an increment on x gives a true damping that causes x to decrease. The limit cycle then is stable. It is unstable in the contrary case. A complete derivation of the following result would unduly load this paper but the result can be stated very simply in the following geometric way (see Fig. 18 which is related to the situation of Fig. 17). Starting from the oscillating point N, let us draw two vectors that mark the increments $\delta\omega$ of ω on the line x_n = constant and δx on the line ω = constant. If an observer standing on the half-space above the plane of the figures sees δx at the right of $\delta\omega$, the limit cycle is stable [Fig. 18(b)]. If the contrary happens [Fig. 18(a)], the limit cycle is unstable.

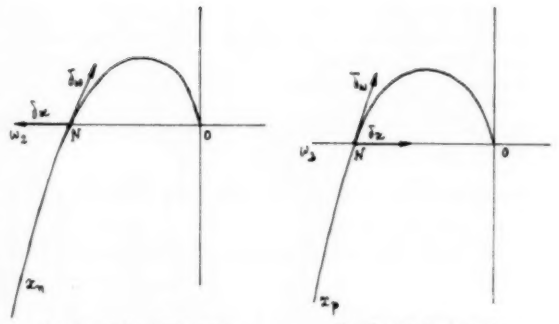

(a) Unstable limit cycle (b) Stable limit cycle

Fig. 18 Limit cycle stability criterion

For the relay system, the limit cycle determined by the saturation (x_p obtained when the gain decreases) is stable. The limit cycle related to increasing gain after the threshold is reached (x_m) on Fig. 18(a) is unstable. When Condition [12] is not fulfilled, the problem becomes very complicated because the derivatives of ω and α enter the picture.

4.4 *Subharmonics* (15)

It is possible to state in what conditions a subharmonic of frequency ω/n (n integer) can be generated:

In this case, the input of A is

$$x \cos(\omega t + \theta) + y \cos\left(\frac{\omega}{n} t + \eta\right)$$

At the output of A, we have, among other terms

$$xg(x, \omega) \cos(\omega t + \theta + \phi) + yg'(x, y, \omega) \cos\left[\frac{\omega}{n} t + \eta + \phi'(x, y, \omega)\right]$$

The functions g' and ϕ' indicate how the amplifier modifies the subharmonic; they depend on x, y, and ω in a first approximation.

The subharmonic ω/n can take place if there is an amplitude y satisfying the conditions

$$g'(x, y, \omega) = 1, \qquad \phi'(x, y, \omega) = \pi \ldots\ldots\ldots [14]$$

where x and ω are given.

4.5 *Conclusions*

The describing function method is very powerful when (a) the system is filtered, (b) limit cycles and neighboring transient modes are dealt with, (c) no rectification nor subharmonics occur. It allows one to handle higher order systems when the *problem consists of analyzing self-sustained oscillations.*

5 Series Expansion (5)

It often happens that an equation

$$f(\ddot{x}, \dot{x}, x, t) = 0$$

really depends on a small parameter ϵ in such a way that one can write

$$f(\ddot{x}, \dot{x}, x, t, \epsilon) = 0$$

For instance, the case $\epsilon = 0$ would be a linear case. Then the solution x can be expanded into a series in increasing power of

$$x = X_0(t) + \epsilon X_1(t) + \epsilon^2 X_2(t) + \dots .$$

where X_0 is the solution of the linear equation. Van der Pol has dealt with this category of problem.

6 Piecewise Linear Computation

Whenever one can apply the results of the linear differential equation theory in a calculation, one is very anxious to do so.

Cauchy's method (Section 2) is a decomposition of the trajectory in small parts where the linear equation

$$\frac{dy}{dx} = \frac{d\dot{x}}{dx} = \frac{\ddot{x}}{\dot{x}} = \text{const}$$

is valid.

The idea can be generalized in the following way. Let us deal with a second-order equation

$$\ddot{x} + f(x, \dot{x})\dot{x} + \phi(x, \dot{x})x = 0 \dots\dots\dots\dots [15]$$

6.1 *Phase-Plane Partition*

It is possible without "solving" the equation to find some regions of the phase-plane inside which f and ϕ do not vary too much. Inside these regions I, II, III . . . (Fig. 19) the equation is linear and the trajectory can be calculated, provided the starting point A_0 is given. The linear equation is valid until the representing point reaches the boundary between I and II at point A_1. Then the equation changes a bit, and the following part of the trajectory A_1, A_2 can be calculated since initial conditions are known through the co-ordinates of A_1. Such a method can replace Cauchy's method in the same way that second-degree interpolation can replace linear interpolation in algebraic equations.

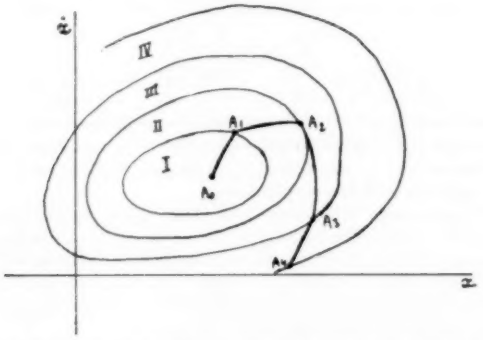

Fig. 19 Domains of approximately constant coefficients

6.2 *Relay Systems*

As often happens, people responsible for the development of some particular device have created the necessary mathematical tool for their problem. It later appears, when a general survey is carried out, that these methods find their place in a wide classification (17).

A very important class of nonlinear controls are relay systems (18). For instance, in the optimum third-order control system (11) there is a two-variable function generator that computes the desired value of acceleration. The actual value of acceleration is compared to the desired value and a relay is operated accordingly, in order to give the third derivative $\dddot{x}$ the appropriate value $+K$ or $-K$ (K is a constant). Whenever K is positive, the system obeys the equation

$$\dddot{x} = +K \dots\dots\dots\dots\dots\dots [16a]$$

When switching occurs, we have

$$\dddot{x} = -K \dots\dots\dots\dots\dots\dots [16b]$$

The 3-D phase space can be divided into two regions where respectively Equations [16a] and [16b] must be applied.

6.3 *Variable Coefficients*

Although it is not strictly correct, the term "linear" has commonly been reserved for equations with constant coefficients.

Thus equations like

$$\ddot{x} + f(t)\dot{x} + g(t)x = 0$$

whose solutions generally do not consist of known functions, sometimes are considered "not linear." It is a very useful technique to divide the total span of time into small segments. During short time intervals the coefficients f and g are almost constant, and the piecewise linear method can be applied.

7 Response of Nonlinear Elements to Random Inputs

It has become a trivial truth that control systems have only one reason for existing, their ability to perform their duty despite random disturbances and signal randomness. If there were no random features in the picture, accurately programmed systems would suffice.

So, it would be desirable to know the response of all sections of a control system to random inputs. This work has been recently done for linear elements (19). Unfortunately, the problem becomes very difficult for nonlinear elements, and the situation is far from being satisfactory in this field. We just will sketch a mathematical approach. Before we do this, we have to review some results of probability calculus we will need.

7.1 *Stationary Time Functions*

In order to define a random function of time, we must imagine the following procedure. There are a great number (in general infinite) possible functions, and only one of them actually exists. For instance, $\sin(\omega t + \alpha)$, where α is a random number, is a random function. So, the function that actually takes place can be considered as being "drawn," in the same way that a number is drawn from a hat. In general, the function will be written $f(t, \alpha)$, where α emphasizes that $f(t)$ is one member of a set of random functions. Now, there are two ways of taking average values of such functions:

First, we can find the time average

$$f_t = \lim_{T \to \infty} \frac{1}{2T} \int_{-T}^{+T} f(t, \alpha) dt$$

This operation is performed on the actual value of the function with a given α. For example let us feed a galvanometer with the noise coming out of an amplifier: Because of the inertia of the coil the displacement of the spot measures the average value of the current that actually flows. We can also imagine another experiment. Let us take a great number, say N, of amplifiers that feed as many galvanometers.

This time we suppose these galvanometers have no inertia. At the same instant t the indications $f_1, f_2, \dots, f_n$ of the galvanometers will be different, and we can perform an average

$$f = \frac{1}{N} [f_1(t) + f_2(t) + \dots + F_N(t)]$$

We note this average $f\alpha$ in order to show that it is taken at the same instant over all possible "drawings" of the function. We

will in short call the first, *the time average*, and the other the *ensemble average*. Most generally, the random functions we use have equal time and ensemble averages. Such functions are called *stationary time functions*.

7.2 *Probability Distributions*

Statistical approaches give us some information about the probabilities of these "drawings."

First, one defines as $p(x)dx$ the probability that the function lies between x and $x + dx$. Following our assumption that $f(t, \alpha)$ is a stationary function, $p(x)$ does not depend on time.

Secondly, we must analyze more sharply the probabilities of the values $f(t, \alpha)$. In the example of the inertialess galvanometers, the deflections indicate the instantaneous values of the currents. They do not depend on previous values of the currents, nor does the probability $p(x)$.

Now, let us come back to existing galvanometers that have inertia. When the current at instant t flows into the galvanometer, the position of the spot is not zero and depends on previous values of the current. We consider two instants t_0 and t_1 separated by a time span τ. The galvanometer inertia produces a causal relationship between the values of the deflection at instants t_0 and t_1. This causal relationship can be expressed as a joint probability

$$P_\tau(x, y, \tau)dy$$

which is the probability of the function lying between y and $y + dy$, when at a time $(t - \tau)$ one already knows it was equal to x.

We are allowed to write this probability $p_\tau(x, y)$ without any other time dependence since we assume the function is stationary.

7.3 *Correlations* (19)

We will now take the products of all possible values of the function evaluated at two instants separated by a constant time span. The value at time t is x and the value at time $(t + \tau)$ is y or $f(t + \tau)$. We then will compute the average values of the product xy

$$\phi(\tau) = \overline{x(t)x(t + \tau)} \quad \ldots\ldots\ldots\ldots\ldots\ldots [17]$$

We can write it in two different ways

$$\left.\begin{aligned} \text{Time average } \overline{xy_t} &= \lim_{T \to \infty} \frac{1}{2T} \int_{-T}^{+T} f(t)f(t + \tau)dt \\ \text{Ensemble average } \overline{xy_\alpha} &= \int_{-\infty}^{\infty} \int_{-\infty}^{\infty} xyp(x)p_\tau(x, y)dx, dy \end{aligned}\right\} [18]$$

These expressions are equal when the function is stationary. They only depend on τ and give the so-called *auto-correlation function* $\phi\tau$.

7.4 *Response of Linear Systems to Random Inputs*

One can predict the response of linear systems to any input when their response to sinusoidal inputs is known. The response is a function of the frequency of the input signal. For a nonrandom function, one defines the power spectral density by means of Fourier analysis. For random functions, the equivalent of this spectrum is a spectral density which can be computed from the auto-correlation function. In fact it is the Fourier transform of $\phi(\tau)$

$$\Phi(\omega) = \int_{-\infty}^{+\infty} e^{i\omega\tau}\phi(\tau)d\tau$$

A very important result related to linear networks (that unfortunately does not hold with nonlinear systems) is that the input spectral density $\phi_i(\omega)$, the output spectral density $\Phi_o(\omega)$, and the transfer function $Y(\omega)$ of the network related by

$$\Phi_o(\omega) = |Y(\omega)|^2\Phi_i(\omega)$$

7.5 *Response of a Particular Kind of Nonlinear System*

The only kind of nonlinear devices whose output can be calculated in the same way are the (20) commonly called "zero-memory" or "time-independent" class. Here the output depends only on the value of the input at the same instant. This excludes systems that have inertia. Systems that can be treated include a relay whose inertia is neglected and the detector of a radio receiver. What we want to know are statistical properties of the output. Since this output generally has to be fed into a linear component, it will be necessary to compute the spectral density of the signal transmitted by the nonlinear section.

In general the nonlinear system is described by $y = f(x)$. For example, $y = Kx^2$ represents the operation of a square law detector, while $y = \text{sgn}\ (x)$ represents the operation of a relay.

Now we have to calculate the averages of the output y knowing some statistical properties of the input x.

We cannot use the time average, because we do not know the actual shape of the function $x(t)$, and hence we cannot find the actual shape of $y(t)$. If we know however the probability distribution $p(x)$, we can easily find the mathematical expectation of any function $f(x)$. It is

$$E[f(x)] = \int_{-\infty}^{\infty} f(x)p(x)dx$$

For instance, the power, i.e., the average of x^2 is

$$\int_{-\infty}^{\infty} x^2P(x)dx$$

Now the auto-correlation also can be computed. We saw that the ensemble average of xy (where y is the value of the function at a time $t + \tau$ for a value x at the time t) is

$$\phi(\tau) = \overline{xy} = \iint_{-\infty}^{\infty} xyP(x)P_\tau(x, y)dx\,dy \ldots\ldots [19]$$

When the output is a function of the input, the average to be computed is

$$\overline{f(x)f(y)} = \phi_f(\tau) = \iint_{-\infty}^{\infty} f(x)f(y)P(x)p_\tau(x, y)dx\,dy \ldots [20]$$

It must be noticed that the knowledge of $p_\tau(x, y)$ gives much more information than the knowledge of $\phi(\tau)$. Equation [19] cannot be reversed and cannot yield $p_\tau(x, y)$ knowing $\phi(\tau)$. This discussion holds for open loop systems only.

As an example of application of these ideas, we will borrow from (21) the results concerning the operation of a square law rectifier. The input $x(t)$ is a filtered noise whose spectrum density is represented by Fig. 20(*a*).

The output shows a predominance of low frequencies coming from the detector [Fig. 20(*b*)].

This example illustrates how deeply the spectrum density of a random input can be modified by a nonlinear device.

8 Global Features

Some authors recently have suggested different approaches to the nonlinear problem. The general idea is to de-emphasize the search for a complete solution and try to get some global or general idea of the system evolution. A full explanation of these theories would go far beyond the scope of this paper, and we will just try to show how some new conceptions can work.

8.1 *Energy Balance Sheet* (22)

From this paper, let us just extract the idea of measuring what physicians call "basal metabolism." A limit cycle is characterized by the fact that the sum of kinetic and potential energy is

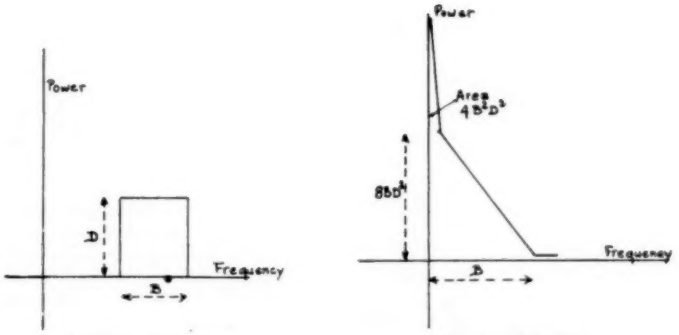

(*a*) Before detection (*b*) After detection

Fig. 20 Square-law-detected noise spectrum

the same at any instants separated by a period T. So, the average energy brought by power sources must be completely transformed into heat.

The mathematical expression of this principle in the case of a second-order system is the equation

$$\frac{d^2v}{dt^2} + \omega^2 V = -\frac{R}{L}\frac{dv}{dt} \quad \ldots\ldots\ldots\ldots [21]$$

where v is the voltage across a parallel RLC circuit whose resonant frequency is $\omega = 1/\sqrt{(LC)}$. The right-hand member of Equation [21] is a term corresponding to energy dissipation. The resistance R can, in general, be a function of v and dv/dt.

Now, let us call W the sum of potential and kinetic energy

$$W = \frac{1}{2} Li^2 + \frac{1}{2} Cv^2$$

where i is the current in the coil.

Equation [21] can be written

$$\frac{dW}{dt} = -\frac{R}{L}\left(\frac{dv}{dt}\right)^2 \quad \ldots\ldots\ldots\ldots [22]$$

During one period T, the total variation of W, say ΔW, must be equal to zero for an oscillation of fixed amplitude to occur. If there is a limit cycle, there exists a time T such that, for any t

$$\int_t^{t+T} R\left(\frac{dv}{dt}\right)^2 dt = 0 \quad \ldots\ldots\ldots\ldots [23]$$

Example of Application

In Equation [21] let us take

$$R = b_0 + b_1\frac{dy}{dt} - b_2\left(\frac{dv}{dt}\right)^2 \quad \ldots\ldots\ldots\ldots [24]$$

The author of (22) gives a first approximation by supposing that power corresponding to harmonics is negligible. Another hypothesis is that the actual period T is equal to $2\pi/\omega$. Then, let us take for the fundamental

$$v = V \sin \omega t \quad \ldots\ldots\ldots\ldots [25]$$

where V is the unknown voltage.

Now let us put into Equation [23] v taken from [25] and R taken from [24]. Equation [23] becomes

$$\int_0^T [b_0 + V_{\omega b_1} \cos \omega t - \omega_0^2 V b_2^2 \cos^2 \omega t] \cos^2 \omega t \, dt = 0 \quad \ldots [26]$$

that gives the actual amplitude of the oscillation

$$V = \frac{2}{\omega\sqrt{3}}\left(\frac{b_0}{b_2}\right)^{1/2} \quad \ldots\ldots\ldots\ldots [27]$$

(Of course, in this computation, R is not always positive and represents the action of a more complicated feedback circuit). It would be interesting to try to use this idea for higher order systems.

8.2 *Stroboscopic Methods* (23)

We will explain here a way of representation rather than a computation method.

Let us suppose we have a nonlinear system submitted to a periodic input, and that its state can be represented by two variables x and y. This is true when second-order systems are considered and can be approximately true for higher-order systems when, following the indication of Section 3, one has found two time constants much larger than the others. The evolution of the system will then be represented by the motion of a representative point in co-ordinates x and y. This representation is useful when one considers a stable system that would be at rest in the absence of an input and one wants to know whether the amplitude of oscillation will remain within reasonable limits or diverge.

The emphasis is put, not on the history of what happens inside one period, but on the general evolution. In this way, one can summarize the knowledge of one cycle by the indication of one point of the cycle. The process is identical to an optical stroboscope, where the subject is illuminated once per cycle. For instance, an exactly periodic response will be represented by a motionless point S [Fig. 21(*a*)]. An "almost periodic" response is represented by a succession of points S_1, S_2 . . very near each other [Fig. 21(*b*)]. It may happen that point S_n exactly coincides with S_1: This shows a subharmonic. In Fig. 21(*c*), there is a subharmonic of order 3, since S_4 coincides with S_1.

9 Expression of Required Servo Performance

This paragraph is directed, not only to the engineers who are responsible for the design of nonlinear control equipment, but also to the people who buy it. As long as linear servos are concerned, responses to elementary inputs, such as sinusoidal, step, or ramp inputs, allow the customer to foresee the behavior of the control system when other kinds of input are applied.

The situation is completely different with nonlinear controls. The response to actual inputs cannot be computed from the knowledge of responses to elementary inputs. Even the "describing function" can be used only in order to study the limit cycles and the behavior of a system in the neighborhood of these cycles.

Fortunately, the knowledge of the responses to elementary inputs (in the case of linear controls) is much greater than neces-

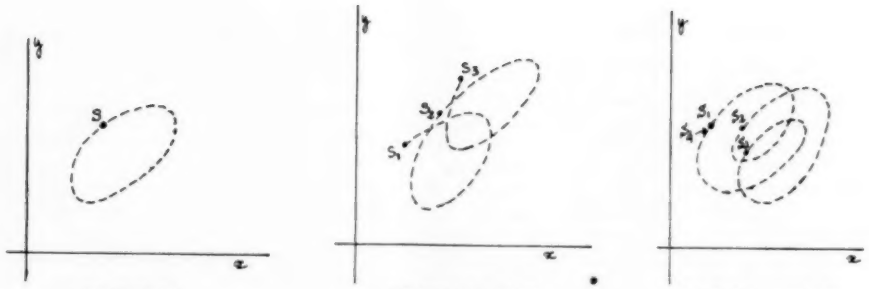

(*a*) Periodic (*b*) Almost periodic (*c*) Subharmonic (3)

Fig. 21 Stroboscopic representation

sary. Generally, a control system is intended to play a role within a given equipment that has to perform a definite job. Hence one has in advance many data concerning the actual inputs and disturbances.

In the final analysis, what is wanted is to make the error as small as possible. The computation of the error corresponding to given inputs and disturbances must be of a statistical nature. The customer should know how to express his requirements concerning the error, because they depend on the industry. For instance, in position control problems, such as radar positioning (24) the rms error must be minimized despite given target motion and given disturbances. The necessary data are the sets of probabilities indicated in Section 7. Unfortunately, as we saw, second-order averages such as auto-correlation functions theoretically do not suffice in nonlinear problems.

In other problems, on the contrary, the error must not be greater than a given value. For instance, it often happens in a chemical industry that the temperature inside a reaction tank must not exceed a given value because of the danger of explosion. In this case, it would be of no use to have a low rms error if there was one chance in 100 that the error might reach a dangerous value.

10 Conclusions

Although the accurate computation of the response of any material assembly always is possible and relatively easy through the use of modern computers, there still is a wide field of investigation for mathematicians. Engineers who are responsible for the design of equipment need much more than plain analysis methods; they need general theories as guides for their synthesis work.

For this work, fortunately, accuracy is not essential since the ultimate step always is an analysis of equipment. But a clear vision of a wide class of possible systems is necessary. So synthesis methods need representations that can be seized at a glance.

This explains the importance of the phase-plane, piecewise linear systems, and stroboscope approaches.

The describing function approach appears to be limited to the study of limit cycles and their neighborhood.

Random function theory appears as a necessary tool that has to be improved. In particular joint probabilities related to values of a random function at various intervals have to be computed.

So far as specifications for the purchase of equipments are concerned, the difficulties related to nonlinear features make impossible the advance computation of system behavior for all cases. One must give up this idea and limit the specifications to actual problems defined by the statistical knowledge of the signal and disturbances.

Bibliography

1 "Introduction to Nonlinear Mechanics," by N. Minorsky, J. W. Edwards, Ann Arbor, Mich., 1947.

2 "Etude des Oscillations Entretenues," by A. Liènard, *Revue Générale d'Electricité*, vol. 23, 1928, pp. 901–912, 946–964.

3 "Perturbations of a Nonlinear Oscillator With Low Pass Filter," by G. Cahen, Proceedings of the Symposium on Nonlinear Circuit Analysis, Polytechnic Institute of Brooklyn, Brooklyn, N. Y., April, 1953.

4 "What is Mathematics?" by R. Courant and Robbins, Oxford University Press, New York and London.

5 "On Relaxation Oscillation," by Balth Van der Pol, *Philosophical Magazine*, vol. 2, November, 1926, pp. 978–992.

6 "Backlash in a Velocity Lag Servomechanism," by N. B. Nichols, AIEE Technical Paper 53-394.

7 "Analysis of Nonlinear Coupled Circuits," by Y. M. Ku, AIEE Technical Paper 54-515.

8 "Analysis and Design Principles of Second and Higher Order Saturating Servomechanisms," by H. E. Kalman, AIEE Technical paper 55-551.

9 "Automatic Control System for Vehicles," by H. G. Doll, U. S. Patent No. 2,463,362.

10 "Predictor Control Optimalizes Control System Performance," by L. M. Silva, TRANS. ASME, vol. 77, 1955, pp. 1317–1323.

11 "Design and Analog Computer Analysis of an Optimum Third-Order Nonlinear Servomechanism," by H. G. Doll and T. M. Stout, TRANS. ASME, vol. 79, 1957, pp. 513–525.

12 "Théorie des Servomécanismes à Relais," by J. R. Dutilh, *Onde Electrique*, vol. 30, October, 1950, pp. 438–445.

13 "A Frequency Response Method for Analyzing and Synthesizing Contactor Servomechanisms," by R. J. Kochenberger, *Trans. AIEE*, vol. 69, part 1, 1950, pp. 270–284.

14 "Dyssymmetrical Servomechanisms," by J. Loeb and J. D. Lebel, *Annales des Télécommunications*, vol. 9, no. 10, 1954, pp. 282–285.

15 "The Mechanism of Subharmonic Generation in a Feedback System," by J. C. West and J. L. Douce, IME Paper 1693.

16 "Recent Advances in Nonlinear Servo Theory," by J. Loeb, TRANS. ASME, vol. 76, 1954, pp. 1281–1289.

17 "Systèmes Dynamiques Héréditaires à Déferlement," by T. Vogel, *Annales des Télécommunications*, vol. 8, no. 11, 1953, pp. 354–360.

18 "Make Servo Nonlinearity Work for You," by D. McDonald, *Automatic Control*, vol. 2, January, 1955.

19 "Extrapolation, Interpolation, and Smoothing of Stationary Time Series," by N. Wiener, Hermann et Cie, Paris, France, 1948.

20 "The Analysis of Nonlinear Control Systems With Random Inputs," by R. C. Booton, Jr., Proceedings of the Symposium on Nonlinear Circuit Analysis, Polytechnic Institute of Brooklyn, Brooklyn, N. Y., April, 1953.

21 "Threshold Signals," by J. L. Lawson and G. E. Uhlenbeck, McGraw-Hill Publishing Company, New York, N. Y., 1950.

22 "Solution Approchée de l'Equation des Phénomènes Oscillatoires," by F. Dacos, *Bulletin Scientifique de l'Association de l'Institut Montefiore*, Liège, Belgium, January, 1954.

23 "La Méthode Stroboscopique et ses Applications," by N. Minorsky, *Bulletin de la Société Française des Mécaniciens*, third trimester, 1954.

24 "Theory of Servomechanisms," by James, Nichols, and Phillips, McGraw-Hill Publishing Company, New York, N. Y., 1950.

Development of the Generalized Phase-Diagram Method

By P. M. LeFEVRE,[1] PARIS, FRANCE

The present study is concerned with the stability of linear systems with real coefficients. The author reviews the graphical method of the generalized phase diagram worked out in 1949, in collaboration with Mr. Demontvignier,[2] and presents a new rule for interpreting the phase diagram.

Introduction

For a long time, the stability of linear systems has been studied by means of the Hurwitz (1)[3] or the Routh (2) criteria both of which use coefficients of the characteristic equation with the terms ordered according to increasing or decreasing powers of the variable. The application of these criteria becomes rapidly more difficult when the equation considered is of higher order.

The harmonic method of Nyquist (3), then the method of Leonhard (4), devised in order to study electronic amplifiers, were used extensively during the last war and particularly in the United States where many research workers applied the Nyquist criterion to the study of servomechanism stability.

A few years ago, Mr. Demontvignier and the writer were led to the study of the stability of complex systems governed by a ninth-order differential equation where the Nyquist criterion could not be applied.

A new harmonic method was developed for studying the stability of linear systems. This method, just as the previous ones, is deduced from the Cauchy residue theorem and constitutes a generalization of the Nyquist criterion. It is the "graphical method of the generalized phase diagram" published in the *Revue Générale de l'Electricité* (5).

Several results, subsequently obtained in this field, were published in the "Mémorial de l'Artillerie Française" (6).

In the present paper, the graphical method mentioned is reviewed briefly. Some developments follow, including a rule for interpreting the phase diagram.

Among the results already published (6), which are not treated in this paper, the graphical method for the study of an interval of stability must be mentioned. This method, which gives the variation curve of the guaranteed damping of a given system, has led to some fruitful developments in the determination of corrective networks.

Elementary Classification of the Different Forms of Unstability

The free state of any system governed by a linear differential equation can be studied from the corresponding characteristic equation. This equation is algebraic and of any order, with real coefficients.

If this equation has a complex root

$$p = \alpha + j\omega \quad [1]$$

a term such as $e^{pt} = e^{\alpha t}(\cos \omega t + j \sin \omega t)$ appears in the general integral of the differential equation. The real part of the second term represents an oscillation of angular frequency ω, whose amplitude approaches infinity with t if $\alpha > 0$, and approaches zero when t increases indefinitely if $\alpha < 0$.

If the characteristic equation has a real root

$$p = \alpha \quad [2]$$

the integral contains the exponential $e^{\alpha t}$ which increases or decreases with t according to the sign of α. For a stable system, one should have in any case

$$\alpha \leqslant 0 \quad [3]$$

This condition can be visualized in the complex p-plane: The roots of the characteristic equation cannot lie inside the positive real half-circle. This curve is composed of the imaginary axis and is bounded on the right by a half-circle about the point at positive infinity, Fig. 1.

This curve will be called the *exclusion contour* because the roots for a stable system cannot lie within this contour.

Graphical Construction of the Generalized Phase Diagram

2.1 Number of Roots of an Algebraic Equation in Any Contour

The theorem of Cauchy relative to the integral of a holomorphic analytic function along a closed contour, and the residues theorem, lead to the following:

Theorem: Let $f(z)$ in the algebraic equation $f(z) = 0$ be a rational function of Z. If the point Z describes in the p-plane a closed contour Γ, and if this contour Γ contains N zeros and P poles of $f(z)$, the corresponding contour Γ', described the representative point of $f(z)$, circles around the origin $Q = N - P$ times, Q being counted positively if the positive directions are the same on both contours.

Remark: In most problems, one has to deal with equations involving rational functions with real coefficients. It can be seen from Fig. 1 that the contour Γ is symmetrical with respect to the real axis. Hence the contour Γ', mapping of Γ by the function $f(z)$ admits the real axis as the axis of symmetry.

In this particular case, the preceding theorem can be simplified. One can simply describe Γ^*, namely, half the contour of Fig. 1 as shown in Fig. 2, and count the number Q of half turns described by the contour Γ' (a half turn of Γ' runs from a point on the real axis to another point on the real axis because the value of z at points A and C are real) around the origin, with the sign assumption stated above. In what follows Q will be taken to be half turns.

The number Q will equal again the difference $N - P$ between the number of zeros and poles of the given equation situated inside the closed contour Γ.

2.2 Generalized Nyquist Criterion

2.21 *Proper Form of the Characteristic Equation.* Let us consider a closed-loop system, as in Fig. 3, with m components $E_1, E_2 \ldots E_m$.

---

[1] Scientific Assistant Engineer, Direction des Etudes et Fabrications d'Armement, Municipal Laboratory of Paris.

[2] Consulting Engineer, Direction des Etudes et Fabrications d'Armement, Compagnie Electro-Mécanique.

[3] Numbers in parentheses refer to the Bibliography at the end of the paper.

Contributed by the Instruments and Regulators Division and presented at the Annual Meeting, New York, N. Y., December 1-6, 1957, of The American Society of Mechanical Engineers.

Note: Statements and opinions advanced in papers are to be understood as individual expressions of their authors and not those of the Society. Manuscript received at ASME Headquarters, September 5, 1957. Paper No. 57—A-216.

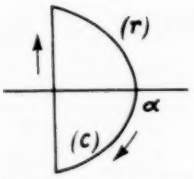

Fig. 1 p-plane contour

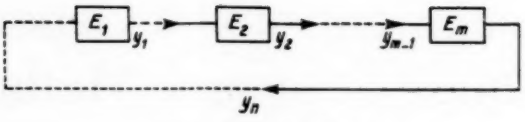

Fig. 3 Closed-loop system

Fig. 4 p-plane contour

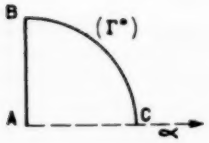

Fig. 2 Contour Γ^*

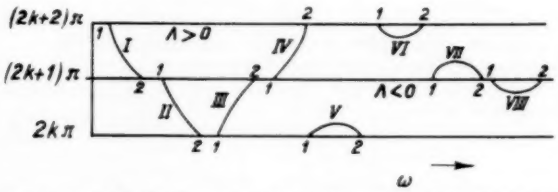

Fig. 5 Plots of the generalized phase diagram liable to change the quantity N-P

The various "boxes" shown in the loop are defined by the following differential equations:

$$\frac{y_i}{y_{i-1}} = \frac{f_{i-1}(p)}{\varphi_i(p)} = T_i(p) \quad \ldots\ldots [4]$$

where f and φ are polynomials in p.

To maintain the generality of the argument without taking into account the nature of the variables, the functions $T_i(p)$ have been referred to as "transfer functions" or "transmittances."

The characteristic equation of the system can be written as

$$T_1(p) \cdot T_2(p) \ldots T_m(p) - 1 = 0 \quad \ldots\ldots [5]$$

or

$$\frac{1}{T_1(p)} \cdot \frac{1}{T_2(p)} \cdots \frac{1}{T_m(p)} - 1 = 0 \quad \ldots\ldots [6]$$

This expression has the advantage of keeping the transfer functions of the components separated and permits a step-by-step study of the whole system.

In both cases, the characteristic equation has the general form:

$$T(p) - \Lambda = 0 \quad \ldots\ldots [7]$$

with $$T(p) = \frac{T_r(p)}{T_s(p)}$$

where $T_r(p)$ and $T_s(p)$ are polynomials of degree r and s respectively, it *being assumed that the terms of degree r and s have the same sign.*

The sign of the parameter Λ is determined by this equation. Equation [7] need not describe a system with feedback. If the system under study does not have the simple cyclic structure of Fig. 3, it is still possible to write its characteristic equation in canonical form as [7]. But, in this case, the physical meaning of $T(p) = \frac{T_r(p)}{T_s(p)}$ is not as obvious.

2.22 *General Terms.* As an application of the general theorem given in paragraph 2.1 to the characteristic Equation [7], we will now consider the curve described by the representing point $T(p) - \Lambda$ in the complex plane when the variable p follows the contour Γ. We will then determine the number of times the contour circles the origin. This is equivalent to evaluating the rotations, around the point $(+\Lambda, 0)$ of the point representing the function

$$T(p) = \frac{T_r(p)}{T_s(p)} \quad \ldots\ldots [8]$$

In the preceding theorem the poles of the transfer function $T(p)$ are taken into account. These poles are: (a) Either inside the *exclusion* contour of Fig. 1 as just stated—their number will be referred to as P, (b) or on the imaginary axis (part of this contour).

The value of P corresponds to the number of unstable solutions of the equation $T_s(p) = 0$; P can be directly obtained if the polynomial $T_s(p)$ is a product of low-order polynomials. Likewise, the number P is obtained directly by applying the method hereunder described.

As to the poles on the imaginary axis, in most cases of physical systems, one finds a pole of order μ at the origin, and a number of simple or multiple poles distributed on the positive half of the imaginary axis.

In the case of an equation with real coefficients, a conjugate pole of the same order but lying on the negative half of the imaginary axis corresponds necessarily to each of these poles.

Each pair of conjugate poles $p = \pm j\omega_0$ physically implies the presence of resonance at the angular velocity ω_0. According to the remark of paragraph 2.1 the exclusion half-contour to be used is shown in Fig. 4.

Circles of infinitely small radii are described around the origin and the poles such as $p = j\omega_0$ because Cauchy's theorem applies only to holomorphic functions. Let us study the transforms of those small contours. The presence of a pole of order μ at the origin means that $T(p)$ can be written as

$$T(p) = \frac{T_r(p)}{p^\mu Q(p)}$$

If, as shown on Fig. 4, this pole is avoided, it is seen that the point representing $T(p)$ goes along μ quadrants at infinity in the negative direction. See Appendix.

It can be seen in the same way, that a number of half-turns at infinity equal to the pole order will correspond to any pole on the positive imaginary axis (except at the origin); if there are poles like this, every pole being counted n times if n is its order, there will be $\bar{\omega}$ negative half-turns at infinity. The contour shown in Fig. 4 involves:

(a) The positive imaginary axis slightly distorted in order to avoid the poles; to these poles correspond, with the sign convention adopted, $\bar{\omega} + \frac{\mu}{2}$ half turns at infinity on the $T(p)$ plane, and therefore around the point $(+\Lambda, 0)$. On the other hand, the locus representing $T(p)$ has some branches at finite distance or going to infinity toward the circles representing the poles. Let ν be the number of turns, at finite distance, around the point $(\Lambda, 0)$

when ω goes from zero to infinity; by convention ν is positive for clockwise rotations.

(*b*) The positive quadrant at infinity, which corresponds to $(r - s)$ quarter turns at infinity on the $T(p)$ plane, if r is larger than s, and to $(r - s)$ quarter turns infinitely close to the origin if r is smaller than s [i.e., $(s - r)$ negative quarter turns] if r equals s, a point at finite distance on the real axis corresponds to the quadrant at infinity.

According to the theorem of paragraph 2.1 where $N - P$ is the number of half turns corresponding to the half contour of Fig. 4, we have

$$\text{if } r > s \qquad N - P = 2\nu + \frac{r - s}{2} + \frac{\tilde{\omega}}{2} + \frac{\mu}{2}$$

$$\text{if } r < s \qquad N - P = 2\nu + \frac{\tilde{\omega}}{2} + \frac{\mu}{2}$$

for the closed contour around the right-half p-plane encircling to the right, each pole on the imaginary axis, as in the example shown in Fig. 4.

For stability it is necessary and sufficient that N equals zero.

Thus one can obtain a very general statement of the Nyquist criterion.

Theorem I

The characteristic equation

$$T(p) - \Lambda = \frac{T_r(p)}{T_s(p)} - \Lambda = 0$$

will correspond to a stable state if, and only if, ω varies between 0 and $+\infty$, the representative point of $T(j\omega)$ circles around the point $(+\Lambda, 0)$ ν times at finite distance where ν is given by the following relation

$$\text{if } r > s \qquad \nu = -\left(\frac{\tilde{\omega}}{2} + \frac{\mu}{4} + \frac{r - s}{2} + \frac{P}{2}\right)$$

$$\text{if } r < s \qquad \nu = -\left(\frac{\tilde{\omega}}{2} + \frac{\mu}{4} + \frac{P}{2}\right) \qquad \text{[9]}$$

where P is the number of poles having a positive real part; $\tilde{\omega}$ is the total number of poles lying along the positive part of the imaginary axis, each pole being counted with its order; μ is the order of the pole at the origin.

It is advisable to recall that the Nyquist criterion assumes that there is no pole within the root-exclusion boundary, nor on its contour and, moreover, that the physical-frequency characteristic reduces to zero when $\omega = 0$ and $\omega = +\infty$. In such a case one has $r < s$, $\tilde{\omega} = \mu = P = 0$, and the Equation [9] gives $\nu = 0$.

By applying the Theorem I, we have been led into divising the polar diagram by representing the complex transfer function $T(j\omega)$ by two rectangular diagrams.

(*a*) A magnitude diagram giving $|T(j\omega)|$ in terms of ω.
(*b*) A phase diagram giving $\underline{|T(j\omega)}$ in terms of ω.

These diagrams are drawn with a logarithmic scale for magnitudes and angular velocities, and a linear scale for the phases.

There is a relationship between the phase diagram and the magnitude diagram. Bode (7) has established an equation which permits going from one diagram to the other when the frequency characteristic is limited to a finite domain.

The dependence between these two diagrams induced the author to think that it should be possible to study the stability problems from only the phase diagram and different characteristic points of the magnitude diagram.

2.3 Study of Stability From the Phase Diagram

From Theorem I, the problem can be reduced to a study of the number of circlings of the representative point of $T(p)$ around the point $(+\Lambda, 0)$. It is therefore obvious that the phase diagram assumes a particular importance, whereas the diagram of the magnitude is more limited.

2.31 *Generalized Phase Diagram.* This is a phase diagram giving the phase variation of the transfer function $T(p)$ when the variable describes, not only the positive half of the imaginary axis, but the whole half contour shown in Fig. 4, including the point of infinity.

In order to avoid a pole of order μ at the origin, as shown in Fig. 4, a half-circle infinitely small will be described from the point $(\epsilon, j0)$ to the point $(0, j\epsilon)$. The ordinate of the diagram departure point is 0 or π, according to whether $T(\epsilon)$ is positive or negative, immediately followed by the discontinuity $-\mu\frac{\pi}{2}$. The computations of those discontinuities are presented in Appendix, A.

In the same way, it can readily be seen that a pole of order μ' at the point $p = j\omega_0$, gives a discontinuity of the phase diagram which is equal to $-\mu'\pi$ for $\omega = \omega_0$. Moreover, these discontinuities are introduced when the diagram is plotted by means of the charts given in paragraph 2.44. The phase variations, occurring when p follows the contour at $+\infty$, will be plotted versus the x-axis $(\omega = \infty)$ of the diagram. These variations are equal to $-(r - s)\frac{\pi}{2}$, Appendix, B.

2.32 *Utilization of the Generalized Phase Diagram.* The procedure for using generalized phase diagrams has been established by investigating all the various circumstances under which the polar diagram can be a semicircular path about the point $(+\Lambda, 0)$ from a point of the real axis up to another point.

It has been pointed out that there *are* 8 possible plots of the phase diagram liable to cause variations of the number $N - P$. These plots are given in Fig. 5 under the Roman numbers I, II ... VIII. For each segment, only the departure and arrival points [necessarily on the lines $y = (2k + 1)\pi$ and $y = 2k\pi$] are to be taken into account, particularly the curvature is of no importance.

Table 1 gives the conditions under which the plots I, II ... VIII of the phase diagram result in an actual change of the number $N - P$. Besides, as previously stated, the subscripts 1 and 2 are the end points of the segments representing the phase diagram under consideration; they correspond, respectively, to the angular velocities ω_1 and ω_2 such that $\omega_1 < \omega_2$.

Using Fig. 5 and Table 1, it is now possible to work with any generalized phase diagram. One divides it into type I to VIII segments, and one lists for each segment the points having the amplitudes given in Table 1. The ordinate of these points is equal to $2K\pi$ for $\Lambda > 0$ and to $(2k + 1)\pi$ for $\Lambda < 0$. Then one applies the conclusion of Table 1.

Thus a summation of the variations gives the difference $N - P$ between the number of unstable solutions and the number of real positive poles for the various values of $|\Lambda|$.

2.4 A Simple Method for Constructing Phase and Amplitude Diagrams

It has been seen in paragraph 2.21 that in problems dealing with cyclic-structure systems, the symbolic transfer function, when introduced into the equation, appears as a ratio of products of rational factors of the variable p.

Use of a logarithmic scale for amplitudes and of a linear scale for phases leads to a plot of the diagrams relative to the transfer function $T(p)$ by simple addition of the elementary diagram ordinates.

Table 1 Recapitulative table of the conditions giving a change of $N - P$

$$|T(j\omega_1)| = \rho_1$$
$$|T(j\omega_2)| = \rho_2$$

CONFIGURATION	RELATIONS BETWEEN $\lvert T(j\omega)\rvert$ AND Λ	VARIATIONS OF N-P
	$\Lambda > 0$	
I	FOR ANY ρ_2 $\begin{cases}\rho_1 > \Lambda \\ \rho_1 < \Lambda\end{cases}$	$+1$ 0
II	FOR ANY ρ_1 $\begin{cases}\rho_2 > \Lambda \\ \rho_2 < \Lambda\end{cases}$	$+1$ 0
III	FOR ANY ρ_2 $\begin{cases}\rho_1 > \Lambda \\ \rho_1 < \Lambda\end{cases}$	-1 0
IV	FOR ANY ρ_1 $\begin{cases}\rho_2 > \Lambda \\ \rho_2 < \Lambda\end{cases}$	-1 0
V	$\rho_1 < \Lambda < \rho_2$ $\rho_2 < \Lambda < \rho_1$ Λ OUTSIDE THE INTERVAL ρ_1, ρ_2	$+1$ -1 0
VI	$\rho_1 < \Lambda < \rho_2$ $\rho_2 < \Lambda < \rho_1$ Λ OUTSIDE THE INTERVAL ρ_1, ρ_2	-1 $+1$ 0
VII		0
VIII		0
	$\Lambda < 0$	
I	FOR ANY ρ_1 $\begin{cases}\rho_2 > \lvert\Lambda\rvert \\ \rho_2 < \lvert\Lambda\rvert\end{cases}$	$+1$ 0
II	FOR ANY ρ_2 $\begin{cases}\rho_1 > \lvert\Lambda\rvert \\ \rho_1 < \lvert\Lambda\rvert\end{cases}$	$+1$ 0
III	FOR ANY ρ_1 $\begin{cases}\rho_2 > \lvert\Lambda\rvert \\ \rho_2 < \lvert\Lambda\rvert\end{cases}$	-1 0
IV	FOR ANY ρ_2 $\begin{cases}\rho_1 > \lvert\Lambda\rvert \\ \rho_1 < \lvert\Lambda\rvert\end{cases}$	-1 0
V		0
VI		0
VII	$\rho_1 < \lvert\Lambda\rvert < \rho_2$ $\rho_2 < \lvert\Lambda\rvert < \rho_1$ Λ OUTSIDE THE INTERVAL ρ_1, ρ_2	$+1$ -1 0
VIII	$\rho_1 < \lvert\Lambda\rvert < \rho_2$ $\rho_2 < \lvert\Lambda\rvert < \rho_1$ Λ OUTSIDE THE INTERVAL ρ_1, ρ_2	-1 $+1$ 0

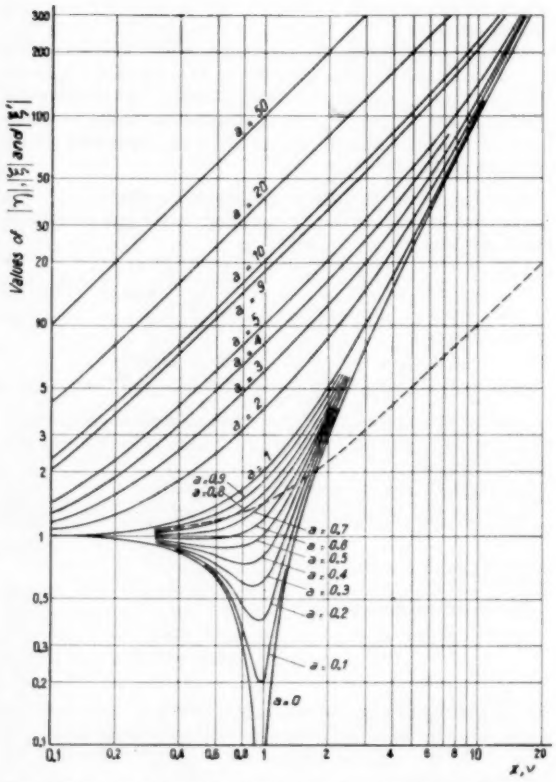

Fig. 6 Modulus of functions $\xi = 1 + jx$, $\xi = 1 - jx$, $\eta = 1 - y^2 + j2ay$, in terms of the reduced variables $x = \omega\tau$, $y = \dfrac{\omega}{\Omega}$, and the damping factor a

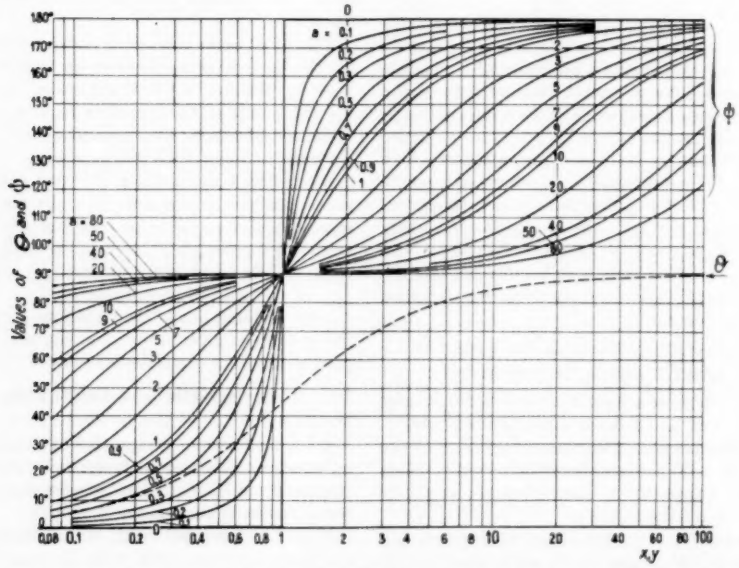

Fig. 7 Arguments $\Theta = -\Theta'$ of the functions $\xi = 1 + jx$, $\xi = 1 - jx$, and the argument ψ of the function $\eta = 1 - y^2 + j2ay$ in terms of the reduced variables $x = \omega\tau$, $y = \omega/\Omega$, and the damping factor a

Most usual rational factors are first-degree binomials of the form $a + bp$, second degree trinomials of the type $a + bp + cp^2$, or terms such as a p^n in integral powers of p.

It will be seen that elementary diagrams corresponding to these factors can be readily obtained by proper changes of variables and by use of suitable charts.

2.41 *Reduced Forms and Representative Charts of the First-Order Factors.* Let us consider a first-order factor

$$X(p) = \alpha p + \beta \quad \ldots\ldots [10]$$

By setting $p = j\omega$, we have the complex form

$$X(j\omega) = \alpha j\omega + \beta = \beta(1 \pm j\tau\omega) = \beta(1 \pm jx) \quad \ldots [11]$$

The positive sign corresponds to $\alpha\beta > 0$ and the negative sign to $\alpha\beta < 0$; τ and x are defined as follows

$$\tau = \left|\frac{\alpha}{\beta}\right| \quad \ldots\ldots [12]$$

$$x = \tau\omega \quad \ldots\ldots [13]$$

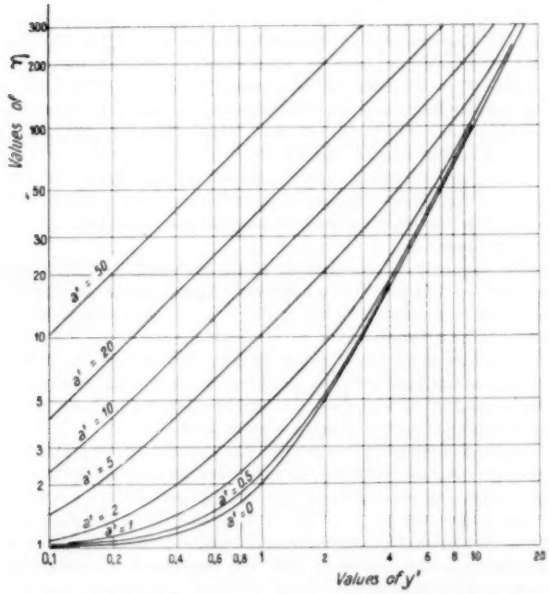

Fig. 8 Modulus of the function $\eta' = 1 + y'^2 + j2a'y'$ in terms of the reduced variable $y' = \omega/\Omega'$ and the damping factor a'

Thus the first-order factor is equal, within a constant factor β, to one of the following functions

$$\xi = 1 + jx \quad \text{if } \alpha\beta > 0 \quad \ldots\ldots [14]$$

$$\xi = 1 - jx \quad \text{if } \alpha\beta < 0 \quad \ldots\ldots [15]$$

The new variable x is proportional to the angular frequency ω and the proportionality coefficient has the dimensions of a time constant.

If Θ and Θ' are the phases relative to ξ and ξ', we have:

$$\Theta = -\Theta' = \tan^{-1} x \quad \ldots\ldots [16]$$

$$|\xi| = |\xi'| = \frac{1}{|\cos\Theta|} \quad \ldots\ldots [17]$$

The values of $|\xi| = |\xi'|$ and of $\Theta = -\Theta'$ have been plotted in dotted lines on the charts of Figs. 6 and 7. These charts use a logarithmic scale for the x-axis; for the ordinates, a logarithmic scale is used for the amplitudes and a linear scale for the phases.

2.42 *Reduced Forms and Representative Charts of Second-Order Factors.* Let us now consider a second-order factor

$$H(p) = \gamma p^2 + \delta p + \epsilon \quad \ldots\ldots [18]$$

Its complex expression can be written as

$$H(p) = \epsilon\left[-\frac{\gamma}{\epsilon}\omega^2 + 1 + j\frac{\delta}{\epsilon}\omega\right] \quad \ldots\ldots [19]$$

This implies, of course, that $\epsilon \neq 0$. Otherwise, the complex form could be reduced to a product of first-order factors.

First Case: $\gamma\epsilon > 0$; if we introduce the new variable

$$y = \frac{\omega}{\Omega} \quad \ldots\ldots [20]$$

where

$$\Omega = \sqrt{\frac{\epsilon}{\gamma}} \quad \ldots\ldots [21]$$

and

$$2a = \frac{\delta}{\sqrt{(\gamma\epsilon)}} \quad \ldots\ldots [22]$$

then we get

$$H(j\omega) = \epsilon[1 - y^2 + j2ay] \quad \ldots\ldots [23]$$

Second Case: $\gamma\epsilon < 0$: we make the new change of variable

$$y' = \frac{\omega}{\Omega'} \quad \ldots\ldots [24]$$

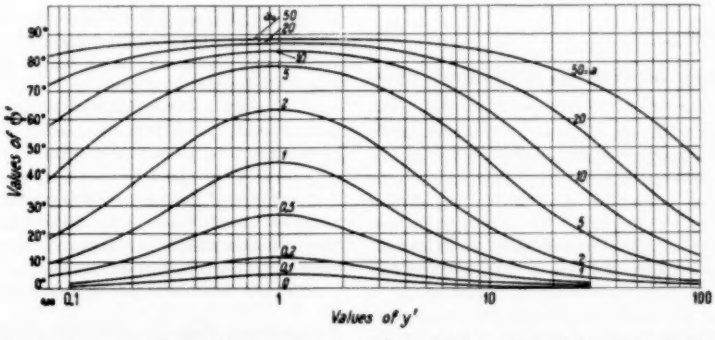

Fig. 9 Argument ψ' of the function $\eta = 1 + y'^2 + 2ja'y'$ in terms of the reduced variable $y' = \omega/\Omega'$ and of damping factor a'

where $$\Omega' = \sqrt{\frac{-\epsilon}{\gamma}} \quad [25]$$

and $$2a' = \frac{\delta}{\sqrt{(-\gamma\epsilon)}} \quad [26]$$

The factor in question can be written as

$$H(j\omega) = \epsilon[1 + y'^2 + j2a'y'] \quad [27]$$

The quantities Ω and Ω' are identified as natural angular frequencies; a and a' are nondimensional numbers called "damping factors."

The second-order factor is, in short, equal to the product by the constant ϵ of one of the following functions:

$$\eta = 1 - y^2 + j2ay \quad [28]$$

$$\eta' = 1 + y'^2 + j2a'y' \quad [29]$$

We have plotted in Figs. 6 to 9 the amplitude and phase charts relative to the functions η and η', taking into consideration only the positive or zero values of the coefficients a and a'.

The phase and amplitude diagrams of a second-order factor can be constructed by means of the following procedure:

(*a*) From Equations [21] and [22], or [25] and [26] compute the value of the coefficients Ω and a (or Ω' and a').

(*b*) On a tracing paper, draw along the x-axis and the y-axis the same scales as those of the chart.

(*c*) In the case of a phase diagram, set the point $y = 1$ of the chart on the point $\omega = \Omega$ of the tracing paper. Then make the ordinate scales coincide. In the case of an amplitude diagram, set the point $y = 1$ of the chart on the point $\omega = \Omega$ of the tracing paper. Also, superimpose the ordinate ϵ of the tracing paper upon the ordinate $\eta = 1$ of the chart.

(*d*) Finally, the diagram plot can then be constructed entirely by tracing on the chart the curve corresponding to the value of a (or a') previously computed.

2.43 *Case of Factors Composed of Integral Powers.* Let us consider a factor p^μ, where μ is a positive or negative integer. This factor is related to the complex function

$$(j\omega)^\mu = \omega^\mu e^{j\mu\frac{\pi}{2}} \quad [30]$$

If $\mu > 0$, the amplitude of this factor is reduced to zero for $\omega = 0$ and its phase is constant and equal to $\frac{\mu\pi}{2}$ as ω varies from 0 to $+\infty$. A negative value of μ means that the transfer function has a pole of order μ at the origin. The relation [30] shows a break point $\frac{\mu\pi}{2}$ at the phase-diagram origin and the phase remains constant as ω goes to infinity.

A New Method of Interpretation of the Generalized Phase Diagram

As stated in paragraph 2.32, use of phase diagrams involves, according to the preceding method, eight possible mappings of a phase diagram, and an interpretation table. It is possible to simplify this investigation procedure by replacing Fig. 5 and Table 1 by a much more convenient rule. We know already that the only amplitudes of the transfer function that are to be considered in this discussion correspond to the $x = \omega_k$ of the intersection points of the phase diagram with the lines $2k\pi$ or $(2k + 1)\pi$, according to whether the parameter Λ is positive or negative. The transfer function is said to present a *critical phase* at the angular frequency ω_k just defined.

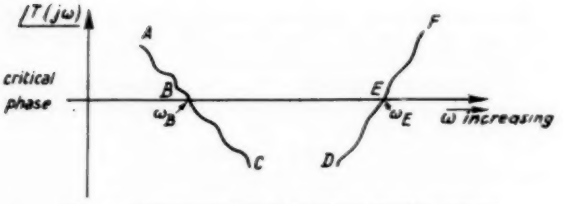

Fig. 10 Representation of the phase-diagram curves

The following analogies result from inspection of Fig. 5 and interpretation of Table 1.

(*a*) The curves I and IV show the same resulting change of the number $(N - P)$ as curve VI if $\Lambda > 0$, or as curve VII if $\Lambda < 0$.

(*b*) The curves II and III show the same resulting change of the number $(N - P)$ as curve V if $\Lambda > 0$, or curve VIII if $\Lambda < 0$.

It is therefore possible to reduce the effective curves of the diagram to four types only: I, II, III, and IV.

Table 1 also shows that the variation rules relative to curves I and II may be unified whatever the polarity of Λ may be; as a matter of fact, each of them shows a unit increase of the number $(N - P)$ when $|\Lambda|$ is less than $|T(j\omega_k)|$, where ω_k is again the angular frequency for which the transfer function presents a critical phase. On the other hand, when $|T(j\omega_k)| < |\Lambda|$, the describing curves I and II do not affect the number $(N - P)$.

These two segments are represented in Fig. 10 by the path ABC of the phase diagram that indicates their position with respect to the straight line whose ordinates correspond to the critical phase.

The segment AB corresponds to the curves II or I according to whether Λ is positive or negative. In the same way, the segment BC corresponds to the curve I for Λ positive and to the curve II for Λ negative.

When the generalized phase diagram approaches the critical phase for decreasing values or leaves it in the same way, the variation $\Delta(N - P)$ is in both cases equal to $+1$ or 0, according to whether $|T(j\omega_k)|$ is larger or smaller than $|\Lambda|$.

In the same way, it can be seen that the two curves III and IV have an identical behavior whatever the polarity of Λ may be; as a matter of fact, both of them are likely to induce a *unit decrease* of the *number* $(N - P)$. The path DEF of the phase diagram shown in Fig. 10 shows the resulting contour; DE and EF become identical to IV and III, respectively, or conversely according to the sign of Λ.

When the generalized phase diagram approaches the critical phase for increasing values, or leave it in the same way, the variation $\Delta(N - P)$ is, in both cases, equal to -1 or 0, according to whether $|T(j\omega_k)|$ is larger or smaller than $|\Lambda|$.

Every time that the phase diagram cuts a critical phase axis, we have the case of a segment similar to the curves AC or DF in Fig. 10; the variation $\Delta(N - P)$ will equal *two units or zero;* each segment under consideration involves a departure and an arrival point. Moreover, the polarity of this eventual $\Delta(N - P)$ variation will be defined by the slope of the diagram at its point of intersection with the critical-phase axis.

The points of the diagram that are likely to induce an $(N - P)$ variation of only one unit are the end points of the contour when they coincide with critical-phase ordinates; in this case there is only one departure and one arrival, both of them being remote.

It is now possible to set forth the following general rule (9).

Interpretation Rule of a Generalized Phase Diagram

The only possible variations $\Delta(N - P)$ *occur when the phase of*

Λ	$0<\lvert T_B\rvert<\lvert T_A\rvert<\lvert T_E\rvert<\lvert T_D\rvert<\lvert T_C\rvert<\lvert T_F\rvert<\infty$						
A	-2	-2	0	0	0	0	0
B	+2	0	0	0	0	0	0
C	-2	-2	-2	-2	-2	0	0
D	-2	-2	-2	-2	0	0	0
E	-2	-2	-2	0	0	0	0
F	+2	+2	+2	+2	+2	+2	0
G	+2	+2	+2	+2	+2	+2	+2
H	+1	+1	+1	+1	+1	+1	+1
N-P	-1	-3	-1	+1	+3	+5	+3

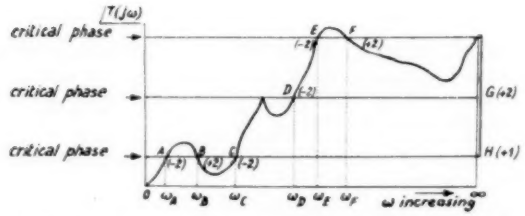

Fig. 11 Interpretation of a generalized phase diagram

the transfer function given by the generalized phase diagram takes the following critical values:

$$\underline{/T(j\omega_k)} = 2k\pi \text{ for } \Lambda > 0$$

and

$$\underline{/T(j\omega_k)} = (2k+1)\pi \text{ for } \Lambda < 0$$

The $\Delta(N-P)$ variations occur actually only if the modulus satisfies the inequality

$$|\Lambda| < |T(j\omega_k)|$$

When this condition is satisfied, this variation is equal to two units if the diagram crosses the critical phase; the variation is only one unit if the diagram departure or arrival point is on the critical phase (end-point case). The variation of polarity is opposite to the sign of the phase-diagram slope at the considered point.

This rule enables one, as in Fig. 11, to mark directly on the phase diagram all the possible $\Delta(N-P)$ variations. Only the variations for which $|\Lambda| < |T(j\omega_k)|$ will be retained. A classification in terms of increasing amplitude of $|T(j\omega_k)|$ is given by a Table, of the same type as the Table of Fig. 11 which presents a simple summing the number $(N-P)$ in terms of $|\Lambda|$.

Remarks

(*a*) The preceding investigation shows the damping influence of the generalized phase-diagram sections that admit a positive slope; as a matter of fact, any these sections are likely, under certain previously stated conditions, to decrease the number $(N-P)$. The diagram sections presenting a negative slope can only increase the instability of the system.

(*b*) Thus it can be seen that the break-points at infinity of any phase diagrams tend necessarily in every case to increase the number of unstable solutions.

When $r > s$, the phase diagram has, when ω goes to infinity, a break-point of $r - s$ quadrants with a negative slope. As $|T(\infty)|$ is equal to ∞ all the crossings of the critical phase are active and induce, each of them, an increase in the number $(N-P)$.

In return when $r < s$ the break points at infinity have actually a positive slope, but their intersections with the critical phase axis cannot have any influence, as $|T(\infty)|$ is now zero.

Bibliography

1 A. Hurwitz, "Über die Bedingungen, unter welchen eine Gleichung nur Wurzeln mit negativen rellen teilen besitze," *Mathematische Annalen*, vol. 46, 1895, pp. 273–284.

2 E. J. Routh, "Dynamics of a System of Rigid Bodies," Macmillan and Company, Ltd., London, England, 1877.

3 H. Nyquist, "Regeneration Theory," *Bell System Technical Journal*, vol. 11, 1932, pp. 126–147.

4 H. Leonhard, "Neues Verfahren zur Stabilitätsuntersuchung," *Archiv für Elektrotechnik*, vol. 38, 1944.

5 M. Demontvignier and P. LeFévre, "Une Nouvelle Méthode Harmonique d'Etude de la Stabilité des Systèmes Linéaires," *Revue Générale de l'Electricité*, vol. 58, 1949, pp. 263–279.

6 P. LeFévre, "L'Etude de la Stabilité des Systèmes Linéaires par la Méthode du Diagramme de Phase Généralisé," in "Mémorial de l'Artillerie Française," 1952, part 2.

7 H. W. Bode, "Network Analysis and Feedback Amplifier Design," D. Van Nostrand Company, Inc., New York, N. Y., 1943.

8 H. M. James, N. B. Nichols, and R. S. Phillips, "Theory of Servomechanisms," McGraw-Hill Book Company, Inc., New York, N. Y., 1947.

9 P. LeFévre, "Règle d'Interprétation du Diagramme de Phase Généralisé," *Comptes Rendus de l'Académie des Sciences*, vol. 232, 1951, pp. 381–383.

10 P. LeFévre, "Théorème sur les Systèmes Linéaires Dits Essentiellement Instables," *Comptes Rendus de l'Académie des Sciences*, vol. 232, 1951, pp. 475–477.

11 Y. Rocard, "Dynamique Générale des Vibrations," second edition, Masson, Paris, France, 1949.

APPENDIX

Study of the Phase Discontinuities of $T(p)$ Due to the Presence of Poles on the Imaginary Axis.

A. *Presence of a Pole of Order μ at the Origin.* The function $T(p)$ has the following form:

$$T(p) = \frac{1}{p^\mu} G(p) \quad \ldots\ldots [31]$$

where $G(p)$ is analytic around the origin and different from zero for $p = 0$. In order to avoid this pole, the variable p describes around the origin a quarter-circle of radius ϵ. ϵ is infinitely small and the variable p goes from the point $(+\epsilon;\ 0)$ to the point $(0,\ +\epsilon)$. This circle is defined by:

$$p_1 = \epsilon e^{j\Theta} \quad \ldots\ldots [32]$$

where Θ varies from 0 to $+\frac{\pi}{2}$ in the positive direction. This circle is transformed by the conformal mapping $T(p)$ into the following contour:

$$[T(p_1)]_{\Theta=0}^{\Theta=+\frac{\pi}{2}} = \left[\frac{e^{-j\mu\Theta}}{\epsilon^\mu} \cdot G(p_1)\right]_{\Theta=0}^{\Theta=+\frac{\pi}{2}} \quad \ldots\ldots [33]$$

Its magnitude increases indefinitely when ϵ goes to zero; the phase discontinuity is

$$\Delta\underline{/T(p_1)} = \left[-\mu\Theta + \underline{/G(p_1)}\right]_{\Theta=0}^{\Theta=+\frac{\pi}{2}} = \left[-\mu\Theta\right]_{\Theta=0}^{\Theta=+\frac{\pi}{2}} = -\mu\frac{\pi}{2} \quad \ldots\ldots [34]$$

B. *Presence of a Pole Order μ' at $p = j\omega_0$.* In that case $T(p)$ can be written as:

$$T(p) = \frac{1}{(p - j\omega_0)^{\mu'}} \cdot G(p) \quad \ldots\ldots\ldots\ldots [35]$$

where $G(p)$ is analytic around $p = j\omega_0$, and different from zero at that point.

The half-circle of radius ϵ centered at $p = j\omega_0$ corresponds to:

$$p_1 = j\omega_0 + \epsilon e^{j\varphi} \quad \ldots\ldots\ldots\ldots\ldots\ldots [36]$$

where φ varies from $-\pi/2$ to $+\pi/2$ in the positive direction. This half-circle is transformed by conformal mapping into the following contour

$$[T(p_1)]_{\varphi = -\frac{\pi}{2}}^{\varphi = +\frac{\pi}{2}} = \left[\frac{e^{-j\mu'\varphi}}{\epsilon^{\mu'}} \cdot G(p_1)\right]_{\varphi = -\frac{\pi}{2}}^{\varphi = +\frac{\pi}{2}} \quad \ldots\ldots [37]$$

Its magnitude increases indefinitely when ϵ approaches zero; the phase discontinuity is equal to

$$\Delta \underline{/T(p_1)} = \left[-\mu'\varphi + \underline{/G(p_1)}\right]_{\varphi = -\frac{\pi}{2}}^{\varphi = +\frac{\pi}{2}} = \left[-\mu'\varphi\right]_{\varphi = -\frac{\pi}{2}}^{\varphi = +\frac{\pi}{2}}$$

$$= -\mu'\pi \quad \ldots\ldots [38]$$

Discussion

R. Oldenburger.[4] The paper under discussion is one of the outstanding contributions to the modern theory of frequency response. It throws considerable light on the problem of stability with or without poles in the right-half plane. The parameter Λ corresponds to the gain of the open loop. The author's procedure therefore determines the correspondence between gain and stability. Although the theory of the paper brilliantly treats the problem of stability one is naturally led to ask whether or not this theory can be modified to shed light on the quality of the control. The control system must be designed not only to be stable but to give fast transients without too many oscillations.

The plotting of curves is a tedious matter. It appears to the writer that considerable labor can be saved by using a purely analytic approach.

[4] Professor of Mechanical Engineering, Purdue University, Lafayette, Ind. Mem. ASME.

Author's Closure

The condition [3] which excludes the roots of the characteristic equation from the positive real half-plane determines the *limit stability* only, because this condition allows roots to be situated on the negative side very near to the imaginary axis and consequently the corresponding oscillations are very slightly damped.

We can further appreciate the quality of control by introducing the notion of *guaranteed stability* which imposes a certain minimum damping on the system: The real parts α_i of the roots of the characteristic equation must not only be negative but in addition must be in absolute value superior or equal to the given minimum damping λm.

This tends to replace the initial condition [3] by the following one:

a) $\alpha_i \leqslant -\lambda m$

On the analytical plan the introduction of a guaranteed damping λ can be translated by the change of variable $p' = p - \lambda$.

The study of the guaranteed stability of the system governed by the characteristic equation:

b) $T(p) - \Lambda = 0$ thus becomes the study of the limit stability of the transformed equation:

c) $T(p - \lambda) - \Lambda = 0$

Apart from these considerations we have been able to deduce from the theory of the phase diagram a method previously published (6) which rapidly procures the guaranteed damping λ for a given control system and as the angular frequency of the oscillation the least damped.

The author wishes to express his deep gratitude to Prof. R. Oldenburger for inviting this contribution and for editing the paper.

On-Off Control With Periodic Sensing Device

By KEISUKE IZAWA,[1] LAFAYETTE, IND.

The paper describes the effectiveness of PD-type control function for the on-off control system with a periodic sensing device. When the system is subject to steady random disturbance, provided that the disturbance is varying rather slowly compared to the time constant of the controlled plant, the properly chosen PD control action can effectively decrease magnitude of fluctuation of the controlled variable.

Nomenclature

θ = temperature or controlled variable
t = time
T = time constant of the controlled plant
L = dead time of the controlled plant
Q_n = generated heat (or manipulated variable) by the heater at "on" stage
Q_f = generated heat (or manipulated variable) by the heater at "off" stage
θ_d = ambient temperature or external disturbance
d = sensing interval. Every d minutes the sensing device detects the magnitude of the actuating signal
d_n = dead time of the controller for taking "on" action after sensing is done
d_f = dead time of the controller for taking "off" action after sensing is done
λ = fluctuating time lag introduced by intermittent sensing with on-off action
$P(\lambda)$ = probability density of λ
$\tau = t/T$ = dimensionless time
$A_n = KQ_n$
$A_f = KQ_f$
K = equalization factor between plant temperature and supplied heat from heater
$x = \theta - \theta_n$
$z = \theta - \theta_d$
θ_n = reference value of the controlled variable
D_n = derivative time of the PD action for "on" stage to be taken
D_f = derivative time of the PD action for "off" stage to be taken
$B_n = D_n/T$ = dimensionless derivative time for "on" stage
$B_f = D_f/T$ = dimensionless derivative time for "off" stage
$\delta = d/T$ dimensionless sensing interval
$h_n = (L + d_n)/T$ = dimensionless dead time from controlling means to controlled plant at the "on" stage
$h_f = (L + d_f)/T$ = dimensionless dead time from controlling means to controlled plant at the "off" stage
σ_z^2 = variance of z
σ_d^2 = variance of θ_d
$\bar{z}$ = mean of z
$\bar{\theta}_d$ = mean of θ_d
$k_n = A_n - z$
$k_f = A_f - z$
$E_a(y)$ = expectation of y; the suffix a under the symbol E is a stochastic variable on which the expectation is taken
$V(y)$ = variance of y

Introduction

On-off controllers are commonly utilized throughout process industries, especially for temperature control, and there have been several papers published [1, 2].[2]

Several years ago the author noted that the magnitude of fluctuation of temperature decreased remarkably when the ordinal thermocouple was replaced by a combined thermocouple in an on-off temperature-control system with a periodic sensing device. This paper deals with this kind of on-off control problem in order to elucidate the afore-mentioned phenomenon and also to establish a reasonable design basis.

Three basic results may be emphasized concerning this problem. First, the phase-plane method can be effectively applied, if a controlled process or plant is approximated by first-order tardity (first-order lag) and dead time. Second, the time behavior of on-off control of a controlled process, whose dynamic character is approximated by first-order tardity and dead time, can be investigated by means of time co-ordinates fixed on the phase plane and not affected by the character of the on-off action [3]. Third, a periodic sensing action or sampling-plus-holding action accompanied by on-off control can be treated as if it were a dead-time element with fluctuating magnitude of dead time.

These basic results are straightforwardly applicable to those on-off control problems which have constant loads or disturbances [4], but it is still useful to consider such on-off control problems as those with steady random disturbances.

Behavior of the Control System

As one of the practical examples to which the theoretical results introduced here may be applied, the following on-off temperature-control problem is considered: A specially constructed thermocouple (so-called combined thermocouple) detects the temperature of the controlled plant plus constant times its rate of change, i.e., the couple generates proportional-plus-derivative emf signal of the controlled temperature. The difference between the output emf of the couple and the reference emf is applied to a galvanometer. A sensing bar driven by a synchronous motor pushes down an index attached to the moving coil of the galvanometer at equally spaced instants or at every d minutes.

If the sensed magnitude of galvanometer deflection is positive at a certain instant, a cam mechanism d_n min later closes the heater circuit of the plant so as to heat it up. Whereas if the sensed magnitude is negative, after an elapsed time of d_f min all or a certain part of the heater current is cut off, so that the plant temperature gradually decreases.

The dynamic characteristics of the plant are approximated with reasonable accuracy by a first-order tardity with time constant T min and dead time L min.

Fig. 1 is a sketch of a periodic sensing-and-holding and an on-off control mechanism, and Fig. 2 is a block diagram of the control system showing the outline of signal transmission in the system.

---

[1] Associate Professor of Electrical Engineering, Purdue University.

Contributed by the Instruments and Regulators Division and presented at the Annual Meeting, New York, N. Y., December 1–6, 1957, of The American Society of Mechanical Engineers.

Note: Statements and opinions advanced in papers are to be understood as individual expressions of their authors and not those of the Society. Manuscript received at ASME Headquarters, September 5, 1957. Paper No. 57—A-207.

[2] Numbers in brackets designate References at end of paper.

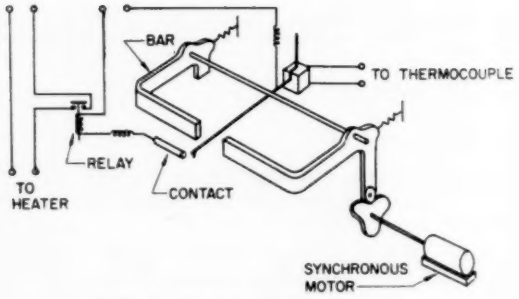

Fig. 1 Sketch of the control system

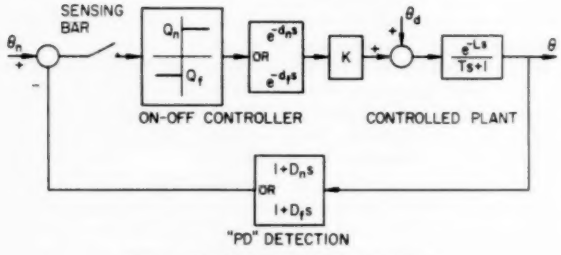

Fig. 2 Block diagram of the controller

Phase-Plane Technique for the Problem

(See references [3 and 4] or Appendix 3)

Derivation of Optimum Setting Condition

Let Q_a cal/min be the heat generated by the heater at the "on" stage and Q_f cal/min be the heat at the "off" stage, and let K deg C/cal/min be the equalization factor of the plant temperature for the heat input. The following equation expressing the "on" and "off" stages of the control system is then obtained

$$T\frac{d\theta(t+L)}{dt} + \theta(t+L) = Q(t) + \theta_d$$

Here $Q(t)$ takes on the value Q_a when

$$\theta(t - d_a - \lambda) + D_a\dot{\theta}(t - d_a - \lambda) < \theta_a \tag{1}$$

and $Q(t)$ takes on the value Q_f when

$$\theta(t - d_f - \lambda) + D_f\dot{\theta}(t - d_f - \lambda) > \theta_a \tag{2}$$

where θ_d is the ambient temperature or external disturbance, λ is a fluctuating time lag within the sensing interval d, and θ_a is the temperature setting or reference value.

Introduction of the fluctuating time lag λ is justified by the following consideration: Suppose that at an instant t the sensing bar senses the deflection of the index of the galvanometer and if then $\theta(t) + D_a\dot{\theta}(t) < \theta_a$ is fulfilled, the manipulated variable $Q(t)$ takes a value Q_a d_a min thereafter, which is a dead time of the control mechanism at "on" stage. But if immediately after the bar senses the galvanometer deflection, $\theta(t)$ changes to fulfill the inequality $\theta(t+\epsilon) + D_a\dot{\theta}(t+\epsilon) < \theta_a$, $Q(t)$ will take on the value Q_a thereafter $d_a + d - \epsilon$ minutes. Until then $Q(t)$ equals Q_f. Therefore the time delay or dead time between $\theta(t)$ and the corresponding manipulating quantity Q_a may fluctuate between d_a and $d_a + d$, and is considered as a stochastic variable distributed within this range with probability density $1/d$ (see Fig. 3). The same consideration holds for the delay between the sensing of the controlled variable and the instant the "off" stage value Q_f is taken on. Fig. 4 shows the probability density of this time delay.

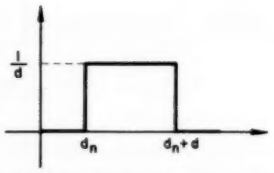

Fig. 3 Probability density of delay for "on" stage

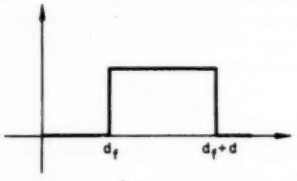

Fig. 4 Probability density of delay for "off" stage

From this discussion, λ may be considered a statistical variable with constant-probability density $1/d$ for $0 < \lambda < d$ and with zero-probability density for elsewhere. Or this is expressed by the next equation.

$$P(\lambda) = \begin{cases} 1/d \text{ for } 0 < \lambda < d \\ 0 \text{ for elsewhere} \end{cases} \tag{3}$$

By the following substitutions

$$\theta - \theta_a = x, \quad \theta_a - \theta_d = z, \quad KQ_a = A_a, \quad \text{and} \quad KQ_f = A_f \tag{4}$$

and using the dimensionless time $\tau = t/T$, Relations (1) and (2) lead to

$$\frac{dx(\tau)}{d\tau} + x(\tau) = A(\tau) - z : A(\tau) = A_a$$

$$\text{for} \quad x(\tau - h_1) + B_a\frac{dx(\tau - h_1)}{d\tau} < 0 \tag{5}$$

$$\frac{dx(\tau)}{d\tau} + x(\tau) = A(\tau) - z : A(\tau) = A_f$$

$$\text{for} \quad x(\tau - h_2) + B_f\frac{dx(\tau - h_2)}{d\tau} > 0 \tag{6}$$

where h_1 and h_2 are stochastic variables and their probabilities are

$$P(h_1) = \begin{cases} 1/\delta : h_a < h_1 < h_a + \delta \\ 0 : \text{elsewhere} \end{cases} \tag{7}$$

$$P(h_2) = \begin{cases} 1/\delta : h_f < h_2 < h_f + \delta \\ 0 : \text{elsewhere} \end{cases} \tag{8}$$

It is easily shown in phase-plane analysis that the sound control actions continue as long as the following two conditions are satisfied (see Appendix 3):

(*a*) The right-hand side of Equation (5) must be kept positive, whereas the right-hand side of the Equation (6) must be kept negative.

(*b*) B_a and B_f of Equations (5) and (6) are both less than unity. Under these conditions the system will continue to hunt with limited amplitude, although the amplitude changes due to the effect of an external disturbance and periodic sensing.

When the external temperature or disturbance θ_d is varying in a steady random fashion, with ordinal distribution characteristics

and with a certain autocorrelation function, z in Equation (4) is also a steady random variable. There exist simple relations among the mean values and variances

$$\bar{z} = \theta_a - \bar{\theta}_d \tag{9}$$

$$\sigma_z^2 = \sigma_d^2 \tag{10}$$

where $\bar{z}$ and $\bar{\theta}_d$ are the mean values of z and θ_d respectively, and σ_z^2 and σ_d^2 denote their corresponding variances. Probability for $z > \bar{z} + 3\sigma_z$ or $z < \bar{z} - 3\sigma_z$ is usually very small and might be neglected unless the distribution curve of θ_d has any intense skewness. Consequently the conditions (a) and (b) for sound control action can be expressed by the following inequalities:

$$A_a - \bar{z} - 3\sigma_z > 0, \quad A_f - \bar{z} + 3\sigma_z < 0$$

$$B_a < 1, \quad B_f < 1 \tag{11}$$

Under these conditions the plant temperature will certainly continue to cycle around its temperature setting θ_a by the behavior of the cycling, e.g., its amplitude or period of cycling will be influenced by the varying external disturbance θ_d.

Since B_a and B_f of Equations (5) and (6) are less than unity, they can be expressed in exponential form by introducing new parameters α and β:

$$B_f = 1 - e^{-\alpha h_f}, \quad B_a = 1 - e^{-\beta h_a} \tag{12}$$

Consideration of Equations (5), (6), and (12) on the phase plane leads us to the fact that the manipulating signal for the transition from the "on" to "off" stage or the "off" to "on" stage is generated a dimensionless time αh_f or βh_a before x reaches zero (Fig. 9).

Let us limit ourselves to the "on" stage and investigate the peak value x_p of x. In order to calculate the peak value, it is convenient to shift the time origin to αh_f before the instant where increasing negative x reaches to 0. The x for the "on" stage is shown as

$$x(\tau) = -k_a(0)e^{-\tau}(e^{\alpha h_f} - 1) + \int_0^\tau k_a(\xi)e^{-(\tau-\xi)}d\xi \tag{13}$$

where

$$k_a(\xi) = A_a - z(\xi). \tag{14}$$

Since $x(\tau)$ takes its peak value x_p at $\tau = h_2$ (Appendix 3)

$$x_p = -k_a(0)e^{-h_2}(e^{\alpha h_f} - 1) + \int_0^{h_2} k_a(\xi)e^{-(h_2-\xi)}d\xi \tag{15}$$

The mean value of x_p is calculated as an expectation of x_p over h_2 and k_a as follows:

(see Appendix 1)

$$\bar{x}_p = E_{h_2}E_{k_a}[x_p] = \bar{k}_a\left\{1 - e^{-h_f(1-\alpha)} \cdot \frac{1 - e^{-\delta}}{\delta}\right\} \tag{16}$$

where $k_a(\tau)$ is assumed to maintain its initial value $k_a(0)$ from $\tau = 0$ to $\tau = h_f + \delta$, since we are dealing with the case where the external disturbance changes very slowly. In other words, the autocorrelation function of $k_a(\tau)$ or $z(\tau)$ may be assumed constant within the region $0 < \tau < h + \delta$ (Fig. 5).

After calculation of $E(x_p^2)$, we have

$$V(x_p) = (\bar{k}_a^2 + \sigma_z^2)e^{-2h_f(1-\alpha)}\left\{\frac{1 - e^{-2\delta}}{2\delta} - \left(\frac{1 - e^{-\delta}}{\delta}\right)^2\right\} + \sigma_z^2\left\{1 - e^{-h_f(1-\alpha)} \cdot \frac{1 - e^{-\delta}}{\delta}\right\}^2 \tag{17}$[3]

[3] Appendix 2.

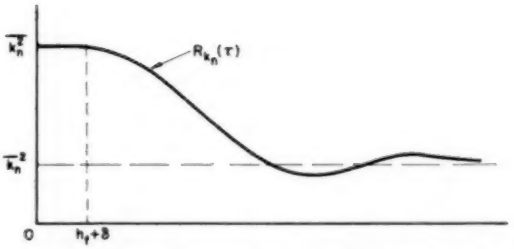

Fig. 5 Autocorrelation function of forcing term, at "on" stage

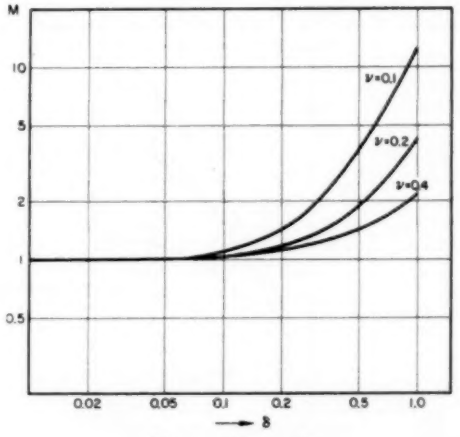

Fig. 6 M versus δ

Taking u in place of $e^{-h_f(1-\alpha)}$ and differentiating $V(x_p)$ by u, we find that the value u_0 of u which minimizes the variance of x_p or $V(x_p)$ is given by

$$u_0 = \frac{\nu^2 e^{\delta/2}}{(1 + \nu^2)\cosh(\delta/2) - [\sinh(\delta/2)]/(\delta/2)} \tag{18}$$

where

$$\nu = \sigma_z/\bar{k}_a \tag{19}$$

When we use this value of u in the Equation (6), B_f of the equation becomes

$$B_f = 1 - e^{-h_f M} \tag{20}$$

M of Equation (20) is expressed as

$$M = 1/u_0 = \frac{(1 + \nu^2)\cosh(\delta/2) - [\sinh(\delta/2)]/(\delta/2)}{\nu^2 e^{\delta/2}} \tag{21}$$

and also illustrated in Fig. 6 for a few values of ν.

We can now determine the optimum condition for the transition from "on" to "off" stage in order to minimize the fluctuation of the peak value of x. From Equations (6) and (20), the optimum transition condition is

$$x(\tau) + \{1 - e^{-h_f M}\}\frac{dx(\tau)}{d\tau} > 0 \tag{22}$$

The value of M in this condition is determined by Equation (21). Substituting u_0 from Formula (18) into (16) and (17), it is clear that the condition (22) guarantees

$$\bar{x}_p = \bar{k}_a(1 - N), \tag{23}$$

$$V(x_p) = \sigma_z^2(1 - N) \tag{24}$$

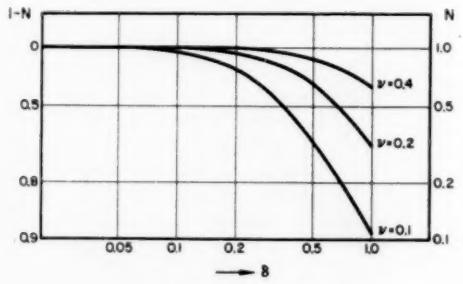

Fig. 7 N versus δ

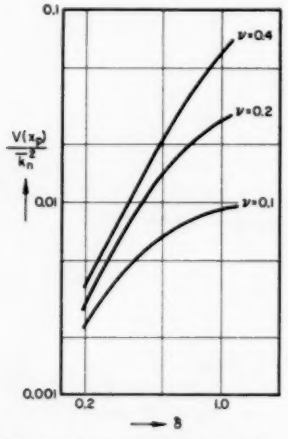

Fig. 8 Relation between variance of peak value and δ

where

$$N = \frac{\nu^2}{(1+\nu^2)(\delta/2)\cot h(\delta/2) - 1} \tag{25}$$

Fig. 7 shows the dependency of N on δ for three different values of ν. It will be worth while to note that N does not involve h_f or total dead time of controlled plant and controlling means, so that $\bar{x}_p$ and $V(x_p)$ of (23) and (24) are independent on the dead time. But if we do not set the controller as shown in (22), these values are naturally influenced by the dead time.

Fig. 8 explains the relation of $V(x_p)$ to δ for three cases of ν.

A discussion like that for x_p can be carried out for the case of the "off" stage and for the determination of the average value and variance of the minimum value of x. Simply by replacing h_f and $\bar{k}_n$ of (22), (23), and (24) by h_a and $\bar{k}_f$ respectively, we shall have the setting condition for optimum transition from the "off" to "on" stage and also the values of $\bar{x}_b$ and $V(\bar{x}_b)$ under the optimum condition.

Conclusion

Because of the practical difficulty of giving different values to B_n and B_f of (5) and (6), and because δ is usually very small ($\delta < 0.05$), it is then possible to introduce the following practical condition.

$$\theta + T\{1 - e^{-(L+d^*)/T}\}\frac{d\theta}{dt} > \theta_a \text{ for "on" to "off,"}$$

$$\theta + T\{1 - e^{-(L+d^*)/T}\}\frac{d\theta}{dt} < \theta_a \text{ for "off" to "on,"}$$

where

$$d^* = \min(d_f, d_a).^4$$

When $(L+d)/T$ is smaller than 0.1, these inequalities can be reduced with practical satisfaction to

$$\theta + (L + d^*)\frac{d\theta}{dt} > \theta_a \text{ for "on" to "off" stage,}$$

$$\theta + (L + d^*)\frac{d\theta}{dt} < \theta_a \text{ for "off" to "on" stage.}$$

This optimum setting condition is different from the one defined by Formula (22), but the difference of the control behavior between the ideal and the practical case will be small in practical sense. The PD detecting action of temperature is easily furnished by a combined thermocouple, which is also effective in attenuating annoying disturbance with high frequency when combined with a sensing-bar mechanism.

Acknowledgment

The author is grateful to Profs. Kamekichi Shiba and Yasundo Takahashi of the Univeristy of Tokyo whose guidance initiated this work. Thanks are especially due to Professor Rufus Oldenburger, the staff of Engineering Sciences of Purdue University for their interest and encouragement in this work, and to Mr. Hideo Mori, DACL of M.I.T. for providing the analog computer to check the theoretical result.

References

1 W. Oppelt, "Oscillatory Phenomena in On-Off Controls," Automatic and Manual Control, 1952, pp. 449–456.

2 D. P. Eckman, "Phase-Plane Analysis—A General Method of Solution for Two-Position Process Control," TRANS. ASME, vol. 76, 1954, pp. 109–116.

3 K. Izawa, "On-Off Temperature Control of a Single Capacity System," *Journal of the Japan Society for Applied Mechanics*, vol. 3, 1950, pp. 55–58.

4 K. Izawa, "Dynamic Behavior of a Penicillin Cultivator," *Transactions of the Japan Society of Mechanical Engineers*, vol. 18, 1952, pp. 52–55.

APPENDIX 1

Calculation of x_p

The parameter k_n of Formula (15) is assumed to vary so slowly that the difference between the value of k_n at $\tau = \tau + 0$ and the value of k_n at $\tau = \tau + h_f + \delta$ is negligibly small. This feature can be assured by means of its autocorrelation function. The constant h_2 of Equation (15) is a stochastic variable as defined by Relation (8) and is independent upon k_n. Consequently the operation of taking the expectation of x_p over h_2 and k_n can be carried separately. From Equation (15)

$$\bar{x}_p = E_{h_2}E_{k_n}\left[-k_n(0)e^{-h_2}(e^{\alpha h_f} - 1) + \int_0^{h_2} k_n(\xi)e^{-(h_2-\xi)}d\xi\right] \tag{26}$$

$$= -\bar{k}_n(e^{\alpha h_f} - 1)\frac{1}{\delta}\int_{h_f}^{h_f+\delta} e^{-h_2}dh_2 + \bar{k}_n\frac{1}{\delta}\int_{h_f}^{h_f+\delta} e^{-h_2}dh_2\int_0^{h_2} e^{\xi}d\xi \tag{27}$$

$$= \bar{k}_n\left\{1 - e^{-h_f(1-\alpha)}\frac{1-e^{-\delta}}{\delta}\right\} \tag{28}$$

---

[4] $\min(a, b) = \begin{cases} a; & \text{if } a < b \\ b; & \text{if } a > b \end{cases}$

APPENDIX 2

Calculation of $V(x_p)$

As there is a well-known relation

$$V(x_p) = E(x_p^2) - \bar{x}_p^2,$$

to determine $V(x_p)$ it is only necessary to evaluate $E(x_p^2)$. From Equation (15)

$$E(x_p^2) = E_{h_2}E_{h_1}\left[k_n^2(0)e^{-2h_2}(e^{\alpha h_f} - 1)^2 - 2k_n(0)e^{-h_2}(e^{\alpha h_f} - 1) \times \int_0^{h_2} k_n(\xi)e^{-(h_2-\xi)}d\xi + \int_0^{h_2} k_n(\xi)e^{-(h_2-\xi)}d\xi \int_0^{h_2} k_n(\eta)e^{-(h_2-\eta)}d\eta\right] \quad (29)$$

The last term of the right-hand side is rewritten by means of the autocorrelation function of k_n or $R_{k_n}(\tau)$. Then the last term will appear as

$$E_{h_2}\left[2e^{-2h_2}\int_0^{h_2} e^{\tau}d\tau \int_0^{\tau} R_{k_n}(\tau - \xi)e^{\xi}d\xi\right] \quad (30)$$

Since the argument of R_{k_n} of (30) takes place within the range $(0, h_f + \delta)$ and k_n varies very slowly, $R_{k_n}(\tau - \xi)$ in (30) can be approximated by $R_{k_n}(0)$ or $E(k_n^2)$ as

$$R_{k_n}(\tau) \fallingdotseq R_{k_n}(0) = E(k_n^2) = \bar{k}_n^2 - \sigma_k^2 \quad (31)$$

From Formulas (29), (30), and (31), expectation of x_p^2 is given as

$$E(x_p^2) = (\bar{k}_n^2 + \sigma_k^2)\left[e^{-2h_f(1-\alpha)}\frac{1 - e^{-2\delta}}{2\delta} - 2\frac{1 - e^{-\delta}}{\delta}e^{-h_f(1-\alpha)} + 1\right] \quad (32)$$

Combining Relations (28) and (32), Equation (17) is obtained.

APPENDIX 3

Phase-Plane Technique for the Problem

Assume the disturbance be constant. Then we get a phase-plane representation of $x(\tau)$ as Fig. 9 from Equations (5) and (6). A point on one of two characteristic lines, i.e., $L_1 - L_1$, goes up and when it reaches point A apart from P by nondimensional time h_2 it will immediately shift to point B. Thereafter it will go down along the other characteristic line: $L_2 - L_2$.

The point C is separated from point Q by the nondimensional time h_1. Thus we shall have a cycling of x which corresponds to the parallelogram $ABCD$ on the phase plane.

For an acceptable performance of the control condition, x should be kept close enough to 0 or x cycles around 0, so that A, B, C, and D should be located in the 1st, 2nd, 3rd, and 4th quadrant, respectively. This fact gives us the conditions (a) and (b) of this paper.

As h_1 and h_2 include constant parts, i.e., h_n and h_f, and the varying part δ which has an equal probability density $1/\delta$ within certain ranges, points A and C in the phase plane will appear everywhere on the segments (A_1, A_2) and (C_1, C_2) on the characteristic lines as shown in Fig. 10. From this figure one may conclude that there may exist many types of cycling although their amplitudes and periods are limited.

If the disturbance θ_d or z is not constant but varies, the two straight characteristic lines $L_1 - L_1$ and $L_2 - L_2$ are not exactly straight lines but curves only defined in stochastic way (see Fig. 11). If the period of the disturbance is large compared to the maximum of $L + d_n + d$ and $L + d_f + d$, the portions of the two characteristic lines on the phase plane contributing the cycling, i.e., PA and QC in Fig. 9, can be approximated by straight lines with an inclination of -1. This is the starting point of this paper.

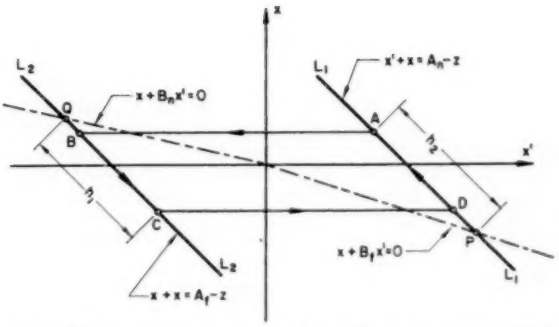

Fig. 9 Phase-plane representation of on-off control characteristics

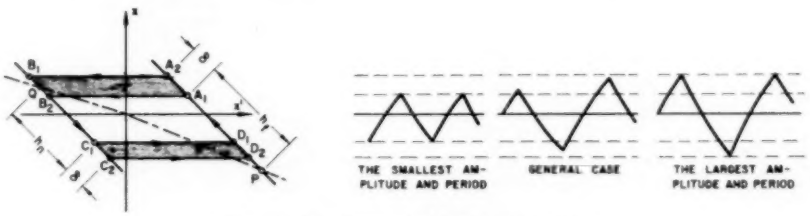

Fig. 10 On-off control with periodic sensing

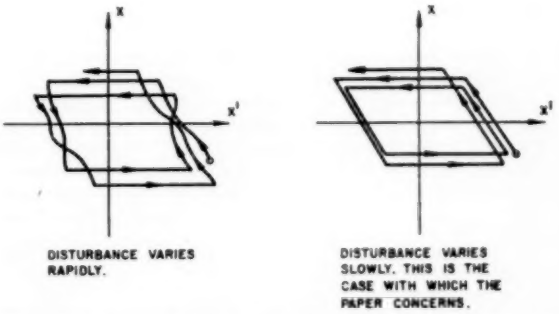

Fig. 11 Difference of phase-plane representation due to condition of disturbance

Discussion

R. Oldenburger.[6] The paper by Professor Izawa is of particular

[6] Professor of Mechanical Engineering, Purdue University, Lafayette, Indiana. Mem. ASME

interest in that the author pioneers in the treatment of the problem of optimizing on-off control systems from the statistical point of view. The restriction that the probability density of Fig. 3 be $1/d$ is made for mathematical reasons. Although this restriction simplifies the analysis it may be a severe one in practice. The theory of the paper should be much simplified if the disturbance θ_d is 0. This case should be of particular interest to the practicing engineer. Professor Izawa has chosen the minimum peak value of the error as a good measure of the quality of the control. The results may be quite different if other criteria are used. In the conventional case of on-off control the use of a proportional and derivative control function may be detrimental. Whether or not this is true for the case of the present paper is an interesting question.

Author's Closure

The author appreciates the interest shown by Prof. R. Oldenburger. One feels intuitively that the delay between sampling instant and control action will occur with equal probability within the range zero to d minutes, where d is sampling period.

The analysis of the case where θ_d is a constant gives better understanding of this approach of the problem Professor Oldenburger mentions, and it is discussed in the author's book.[6]

Whether or not a proportional plus derivative control function is detrimental due to high frequency noise may depend upon the location of the input point of the disturbance. In temperature control systems *PD* detection of temperature is achieved by a combined thermocouple.[7] This is a phase advance element with high frequency attenuation characteristics rather than a pure *PD* element. Also the controlled process has a relatively large time constant. Therefore almost all high frequency external disturbances may be considered to have no detrimental effect on control behavior.

---

[6] K. Izawa, "Introduction to Automatic Control," OHM-Sha, Tokyo, Japan, 1954, pp. 234–238.

[7] K. Izawa and T. Hosoda, "Combined Thermocouple," *Journal of the Society of Instrument Technology, Japan*, vol. 2, No. 6, 1952, pp. 266–268.

Investigation of Erosion and Corrosion of Turbine Materials in Wet Oxygenated Steam

By H. A. CATALDI,[1] C. F. CHENG,[2] AND V. S. MUSICK,[2] SCHENECTADY, N. Y.

Steam from the boiling water reactor of the Dresden Nuclear Power Station will enter the turbine at 869 psia and 525 F with 1/2 per cent moisture and with oxygen concentration higher than normal in power-plant practice. This paper discusses a series of preliminary laboratory tests evaluating the resistance of various materials for turbines and related components to erosion (impact, washing, wire-drawing) and corrosion (weight loss, pitting depths, crevice, and galvanic attack) in wet, oxygenated steam. Materials tested included carbon and low-alloy steels and cast iron, austenitic and ferritic stainless steels, Monel, cupronickels, leaded bronze, Stellite, and Ductile Ni-Resist No. 3. It is concluded that, with proper design, conventional materials may be used in the Dresden turbine except in a few critical areas.

Introduction

Object. Steam from a boiling water reactor is unusual in power-plant practice in several respects; it is radioactive, it is wet, and it contains some free hydrogen and oxygen. Because of the possibility of unexpected effects of these unfamiliar conditions on the erosion and corrosion of practical metals, it was necessary to consider carefully the selection of turbine materials for the Dresden Nuclear Power Station of The Commonwealth Edison Company. Published information indicated that the radioactivity in the turbine would not be an important materials factor. However, there was little information on the erosive action of wet high pressure steam (with or without oxygen) and only scattered data on the effect of oxygen on the corrosion of metals in high-temperature water-steam mixtures. In order to fill in some of the gaps in our experience in these fields, a two-part experimental program was undertaken: The first, a series of tests to aid in the selection of materials for the Dresden turbine; the second, a more fundamental study of the effects of temperature, pressure, oxygen, velocity, and pH on erosion and corrosion by water-steam mixtures. The purpose of this paper is to review briefly some of the potential turbine materials problems in a boiling water nuclear power plant, and to discuss some of the results of the special erosion and corrosion tests.

Dual Cycle Boiling Water Nuclear Power System. The design of the Dresden Nuclear Power Station has been described recently (1)[3]; a brief review will suffice here. Wet steam is produced in the reactor at 1015 psia (545 F), passes through a steam purifier where most of the water and "solids" are removed, and enters the first-stage nozzles of the turbine at 869 psia (525 F) with 1/2 per cent moisture, Fig. 1.

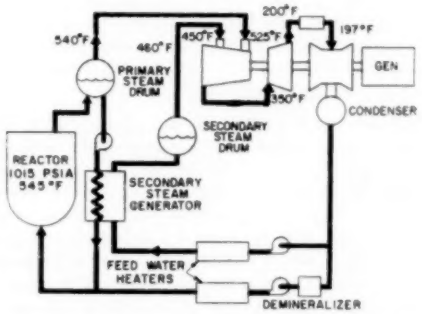

Fig. 1 Flow diagram of Dresden Nuclear Power Station

The exhaust from the turbine is condensed and pumped to air ejectors. The condensate is then split in two streams. One passes through feedwater heaters to the secondary steam generators and drum; the secondary steam then enters the ninth stage of the high pressure turbine at 415 psia (450 F). The other condensate stream passes first through demineralizers, then feedwater heaters, and finally to the reactor. The water conditions may be summarized as follows:

Reactor feedwater	
Conductivity	0.1 micromho/cm
Reactor recirculating water	
Conductivity	1 micromho/cm
Total solids	0.5 ppm max
pH	~7
Secondary steam generator (boiling side)	
Total solids	100 ppm, max
PO_4	5 ppm, max
Cl	0.1 ppm, max
NaOH	20–35 ppm, approx
Morpholene	2–4 ppm
pH	10.5 max

Corrosion by High Temperature Steam-Oxygen-Water Mixtures. When water is exposed to high intensity fluxes such as exist in a nuclear reactor, some net decomposition into hydrogen and oxygen occurs. In a boiling water reactor system, these gases pass through the turbine. It is necessary, therefore, to consider the behavior of standard turbine materials in high temperature steam-water-oxygen mixtures. In particular, the possibility of "oxygen concentration cells" raised the question of pitting and crevice attack in the turbine.

Erosion by Wet Oxygenated High-Pressure Steam. The principal questions regarding erosion in the Dresden turbine arose from the presence of moisture (and oxygen) in the high-pressure stages. In designing the erosion tests, it was convenient to visualize erosion as occurring by three processes (which might actually arise from the same mechanism),

[1] Materials and Processes Laboratory, Large Steam Turbine-Generator Department, General Electric Company.

[2] Structural Engineering Unit, Large Steam Turbine Engineering, Large Steam Turbine-Generator Department, General Electric Company.

[3] Numbers in parentheses refer to Bibliography at end of paper.

Contributed by the Power Division and presented at a joint session with the Nuclear Engineering Division at the Annual Meeting, New York, N. Y., December 1–6, 1957, of THE AMERICAN SOCIETY OF MECHANICAL ENGINEERS.

NOTE: Statements and opinions advanced in papers are to be understood as individual expressions of their authors and not those of the Society. Manuscript received at ASME Headquarters, August 20, 1957. Paper No. 57—A-134.

1 Surface or Washing Erosion. This is the eroding of a metal by high-velocity water flowing along a surface such as in a nozzle. Theoretical treatment of this problem together with early company experience with wet turbines and some published data (2) indicated that this would be minor with 12 Cr steel, even at the highest pressure prevailing in the turbine.

2 "Wiredrawing" or Channel Erosion. Wet steam leaking with high velocity past narrow restrictions can cause deep undercutting of metal. There is little information on this type of erosion.

3 Impact Erosion. This is caused by the impingement of water droplets against a surface at high velocity, and is a familiar occurrence in the last-stage buckets of condensing turbines. In a high-pressure turbine, both the high steam density and relatively low bucket velocities would tend to minimize the impact velocity and hence the damage.

Test Program. At the outset, it was expected that the most serious conditions of erosion and corrosion would be at the front end of the turbine because of the oxygen, high temperature and pressure, and pH about 7. Of particular interest was erosion due to leaks of high density, oxygenated wet steam with high velocity; and the effect of oxygen and water on pitting, galvanic, and crevice attack. The exact oxygen concentrations of particular interest could not be predicted because it was expected to depend on the precise water composition and hydrodynamic conditions in the reactor. Although the resistivity of the water in the high-temperature stages of the turbine would be high, the resistivity in restricted areas such as in crevices conceivably might be much lower. Moreover, the resistivity of pure water at 500 F is appreciably lower than that at room temperature. For these reasons it was interesting to check the effects of galvanic corrosion.

Beyond the point of secondary admission, conditions were expected to be less serious because of the lower temperature and pressure and also because of the effect of dilution by deaerated and inhibited (high pH) steam.

Tests were devised with these thoughts in mind. Conditions were chosen to approximate roughly those prevailing at various points in the high-pressure and intermediate turbines. At the high pressure (1015 psia, 545 F) only static corrosion tests were completed because of the time required to assemble a high-pressure loop. These tests were considered adequate for this preliminary evaluation.

The tests to be described are grouped under three headings, corresponding to the facilities used:

Test 1—Erosion and corrosion with wet Schenectady Plant steam: 350 psia and 430 F max; pH 6.8; with 0.05, 80, and 110 ppm oxygen, Fig. 2.

Test 2—Erosion and corrosion tests with wet steam using desuperheated steam from 14th stage of a turbine at Mystic Station of Boston Edison Company: 43 psia and 272 F, 70–110 ppm O_2, pH 8.8–9.5, Fig. 3.

Test 3—Pitting, crevice, and galvanic corrosion tests in water and steam in autoclaves, 545 F (1015 psia), 50 and 100 ppm O_2 (initially), pH 7, Fig. 4.

Materials used in these tests are described in Table 1.

Procedure and Results

Test 1. These corrosion and erosion tests were conducted in the Large Steam Turbine-Generator Department's Product Development Laboratory, using steam from the utility supply mains. This steam is produced from river water which is first treated by precipitation, then filtered and softened with zeolite. Sodium metaphosphate and sodium-hydroxide additions maintain the boiler water at pH 11.3. Steam condensate analyzed as:

pH	6.8	Specific conductivity	8.7 micromhos/cm
Fe	0.01 ppm	Total solids	4.8 ppm
Cl	0.4 ppm	Suspended matter	0.4 ppm

This steam, of a purity below that specified for the Dresden system, was admitted to a system of three loops, Fig. 2. The desired "wetness" of the steam was maintained by the automatic injection of water above the test sections so as to maintain the appropriate temperature in the calorimeter downstream from the tests. Oxygen was admitted to loops Nos. 2 and 3 from a high-pressure cylinder at a controlled rate. The concentration was checked at regular intervals by condensing the steam and measuring gas volumes.

In loops 1 and 2, which are identical except for the oxygen line, wire-drawing (channel erosion) and corrosion tests were run. In the wire-drawing tests, steam flows through three channels ($^1/_2$ in. long × $^1/_4$ in. wide × 0.005 in. high) formed by stacking 40 appropriately machined strips, Fig. 2. The pressure ratio across the specimens was 1.42. Results of the tests were appraised by the depth of erosion grooves, Figs. 5 and 6. Details of the erosion test conditions and the results are summarized in Table 2.

Each corrosion test section consisted of 26 rectangular specimens separated by 18-8 stainless-steel spacers so as to form channels for the steam, Fig. 2. Weight losses of acid-cleaned specimens were converted to corrosion rates (mils/yr). In addition, pitting tendencies were noted. Test conditions and results are shown in Table 3.

The nozzle-impingement test consisted of four miniature nozzles (two each of Types 347 and 405 stainless steel) through which steam originally at 350 psia and 6 per cent moisture was expanded to 290 psia (pressure ratio 1.61). This expanded steam was directed against a row of eight specimens (Types 347 and 403 stainless steel) about 2 in. distant, at an angle of 15 deg. Beyond these impingement specimens, the steam pressure was 245 psia, Fig. 2. These results were assessed visually only and are discussed in the next section.

Test 2. Erosion and corrosion tests were run in steam extracted from the 14th stage of a turbine in the Mystic Station of the Boston Edison Company at Everett, Mass. Boiler water treatment included disodium-phosphate and sodium-sulfate additions to the boiler; and sodium-sulfite, sodium-hydroxide, and morpholine additions to the deaerator storage tank.

Steam condensate analyzed as follows:

	pH	Specific conductivity	Total solids (boiler)
Run A	9.5	5.7 micromhos/cm	262 ppm
Run B	8.8	4.7 micromhos/cm	....

The extracted steam was desuperheated to 272 F in a water-cooled condenser and mixed with sufficient air to give the desired oxygen content.

From a common header, the steam was led to eight parallel test stations and specimens which are modifications of those used at The Detroit Edison Company (2). Steam traveled through the $^1/_4$-in-diam center hole of the plug ($1^1/_2$-in-diam × $^1/_2$-in. corrosion specimen), impinged on the erosion specimen below, and escaped radially through two $^1/_4$-in-wide × 0.025-in-high slots. The corrosion specimen was shielded from high-velocity erosive effects by a stainless-steel washer which was inserted between it and the erosion specimen, Fig. 3. With this arrangement, it was possible to distinguish the weight loss due to "corrosion" from that due to high-velocity erosion. Corrosion rates were calculated from weight losses after acid cleaning. Erosion resistance was determined both by weight loss and pit depth measurements, Fig. 7. Velocities were calculated from

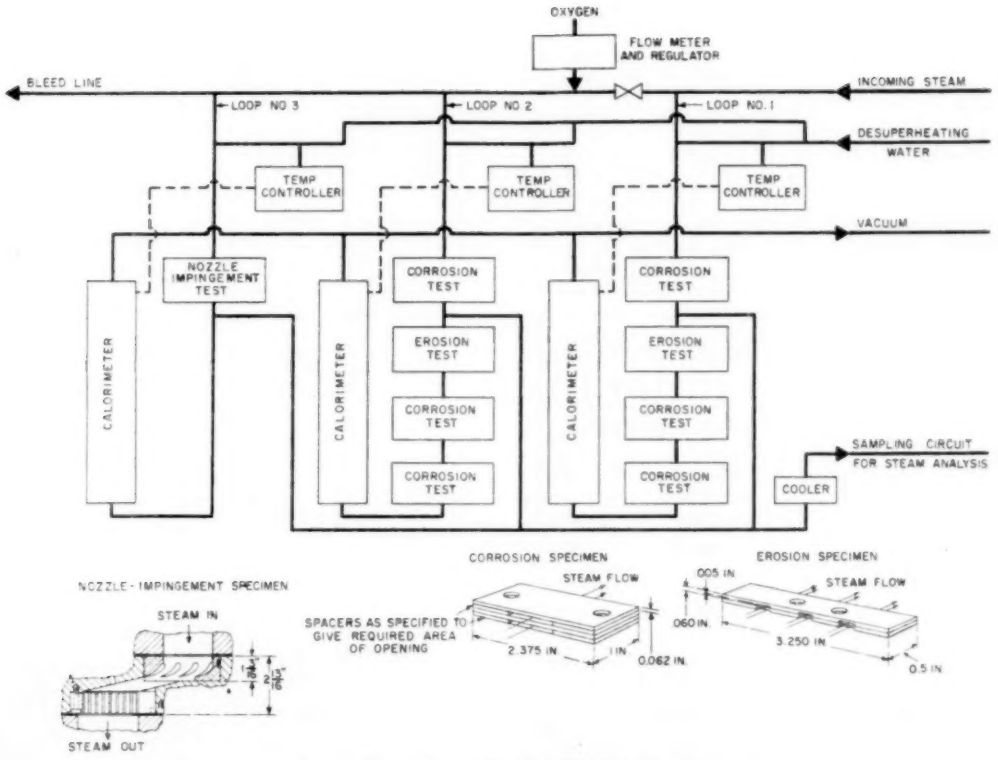

Fig. 2 Flow diagram and test specimens, Test 1

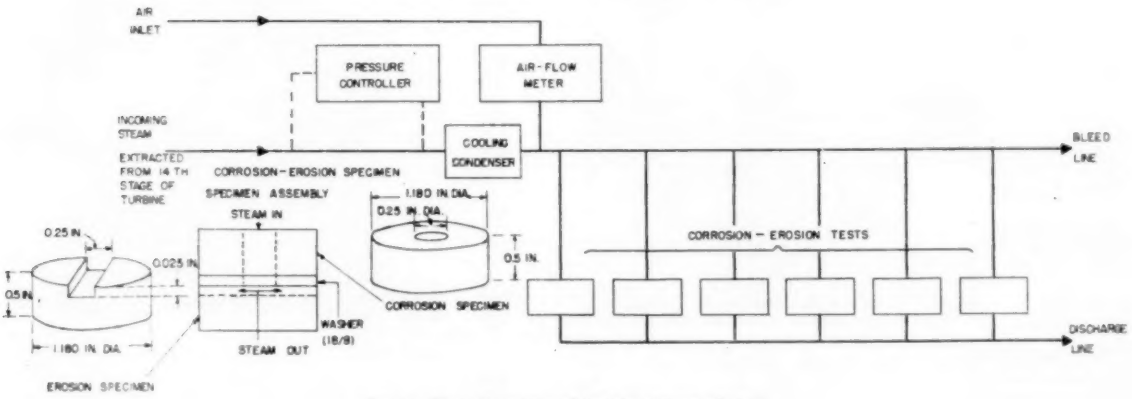

Fig. 3 Flow diagram and test specimens, Test 2

pressure-drop data. The significant details and results of these tests are included in Tables 2 and 3.

Test 3. At the maximum temperature of interest, only autoclave corrosion tests were feasible. The Type 347 stainless-steel autoclaves were of 3 liters capacity (about 3 in. diam × 20 in. long). In one series of tests, autoclaves were rocked with a period of about one-half minute so that specimens were alternately exposed to steam and water. In other tests, stationary autoclaves were provided with cooling coils in the vapor space. This allowed testing of specimens exposed to condensing steam and immersed in water.

Specimens were one-inch disks machined so that, when two were coupled (with a stainless-steel screw), a crevice 0.002 in. wide was included between them, Fig. 4. Pairs of metals were chosen to form galvanic couples which were likely to occur in a turbine. These couples were strung on axial rods and cooling coils suspended from the heads of the autoclaves.

The bombs were half filled with deionized water (less than 1 micromho/cm conductivity at room temperature). After sealing, the bombs were heated electrically to boiling at a low pressure and degassed by venting some steam. Oxygen was introduced by a high-pressure pipette sufficient to give 50 or 100 ppm based on the total weight of water (1500 grams). The temperature was then increased to 545 F (1015 psia).

Table 1 Materials tested

Type	Condition	Test no. 1	2	3	Hardness, Bhn	Chemical composition, % C	Cr	Mo	Ni	Fe	Others
Carbon steel											
ASTM A106	Seamless pipe	x	x	...	126	0.23	...	...	...	Bal.	...
ASTM A212	Boiler plate	x	...	...	179	0.31	...	...	...	Bal.	...
ASTM A201	Boiler plate	x	...	x	103	0.20	...	...	...	Bal.	...
ASTM A27 Cast	N 1925 F, T 1200 F	x	...	x	126	0.25	...	...	...	Bal.	0.50 Si
ASTM A27 Cast	N 1925 F, T 1200 F	...	x	...	146	0.25	...	...	...	Bal.	0.50 Si
Low-alloy steel											
1/2 Mo (ASTM 204)	Firebox quality	x	...	...	131	0.20	...	0.5	...	Bal.	...
1/2 Mo Cast	N 1700 F, T 1200 F	x	...	...	131	0.20	...	0.5	...	Bal.	...
1 Cr, 1/2 Mo Forged	A 1550 F, T 1100 F	...	...	x	223	0.40	1.0	0.5	...	Bal.	...
1 Cr, 1/2 Mo, 1/4 V ASTM A193–B16	HR T 1200 F	...	...	x	262	0.40	1.0	0.5	...	Bal.	0.25 V
1 Cr, 1 Mo, 1/4 V Cast ASTM A389–C24	N 1925 F, T 1200 F	x	...	...	207	0.20	1.0	1.0	...	Bal.	0.20 V
1 Cr, 1 1/4 Mo, 1/4 V Forged A293–Class 8	A 1750 F, T 1250 F	x	...	...	248	0.30	1.0	1.2	...	Bal.	0.25 V
2 Ni, 1/2 Mo, Forged ASTM A293–Class 2	A 1550 F, T 1100 F	...	...	x	248	0.30	...	0.5	2.0	Bal.	0.02 V
2 1/2 Ni, 1/2 Mo Forged ASTM A293–Class 2	A 1750 F, T 1250 F	x	...	x	229	0.30	...	0.5	2.5	Bal.	0.05 V
2 1/2 Ni, 1/2 Mo Forged ASTM A293–Class 2	& SR, 1100 F	...	x	...	262	0.30	...	0.5	2.5	Bal.	0.05 V
2 Cr Cast	Ann. 1650 F	x	...	x	229	0.15	2.0	...	...	Bal.	...
2 1/4 Cr, 1 Mo Forged ASTM A155	Ann. 1650 F FC to 500 F	x	...	x	143	0.15	2.25	1.0	...	Bal.	...
Nitrided steel											
Nitralloy[d] (ASTM A352–Class A)	HR Bar (Base)	x	...	x	60Rc	0.42	1.6	0.4	...	Bal.	1.0 Al
EME[a] nitrided	HR Bar (Base)	x	...	...	62Rc	0.15	19.0	...	12.0	Bal.	1.10 Cb + Ta
ASTM Type 410 stainless nitrided	HT Bar (Base)	x	...	...	62Rc	0.15	12.0	...	...	Bal.	...
Cast iron											
ASTM A48 cast	SR 1200 F	...	x	x	179	2.75	...	...	...	Bal.	2.0 Si
Ni-Resist #3[b]	SR 1150 F	...	...	x	97	2.75	3.0	...	30.0	Bal.	...
Ductile Ni-Resist #3[b]	SR 1150 F	x	x	...	166	2.40	2.5	...	30.0	Bal.	0.08 Mg
Stainless steel											
ASTM Type 304	CR Bar	...	...	x	241	0.08	18.0	...	8.5	Bal.	...
ASTM Type 304L	CR Sheet	x	...	...	163	0.03	18.0	...	8.0	Bal.	...
ASTM Type 304L (Sen)	Sen 1250 F	x	...	...	156	0.03	18.0	...	8.0	Bal.	...
ASTM Type 304L	HR Bar	...	x	...	143	0.03	18.0	...	8.0	Bal.	...
ASTM Type 304L (Sen)	Sen 1250 F	...	x	...	149	0.03	18.0	...	8.0	Bal.	...
ASTM Type 347	A-1800 F & OQ	x	...	x	162	0.10	18.0	...	8.0	Bal.	Cb-10X C
ASTM Type 403	HR & T 1200 F	...	x	...	235	0.12	12.5	...	...	Bal.	0.5 Si
ASTM Type 403	CR & HT to hardness	x	x	x	217	0.12	12.5	...	...	Bal.	0.5 Si
ASTM Type 405	HR Plate	x	...	x	202	0.12	12.5	...	...	Bal.	0.20 Al
ASTM Type 410	HT Bar to hardness	x	...	...	241	0.12	12.5	...	0.8	Bal.	1.0 Si
12 Cr, Mo, W, V	OQ, 1400 F, T 1200 F	...	...	x	311	0.21	13.0	1.0	...	Bal.	1.0 W, 1/4 V
12 Cr, Mo	HR Plate	x	...	x	217	0.09	13.0	1.5	...	Bal.	...
12 Cr, Cb	HR Plate	x	...	...	223	0.08	13.5	...	...	Bal.	0.35 Cb
Nonferrous alloys											
90/10 Cupro-nickel	HR Bar	...	x	...	107	...	...	...	10.0	1.15	88.6 Cu
90/10 Cupro-nickel	Ann Sheet	x	...	...	43	...	...	...	10.0	1.15	88.2 Cu
80/20 Cupro-nickel	Ann Sheet	x	...	...	40	...	...	...	20.0	0.03	80 Cu
70/30 Cupro-nickel	Ann Sheet	x	...	...	46	...	...	...	30.0	0.55	69 Cu
Monel[b]	CR Sheet	x	...	...	121	...	...	...	66.5	2.0	29 Cu
Monel[b]	HR Bar	x	x	...	143	...	...	...	66.5	2.0	29 Cu
BTH Pb bronze[e]	CC	x	x	x	50	...	...	...	12.0	0.76	65 Cu, 2.5 Sn, 5 Pb, 14 Zn
Stellite #1[c]	HR Strip	x	...	...	401	2.5	30.0	...	3.0	...	12.0 W, 52 Co
Stellite #6[c]	HR Strip	x	x	...	401	1.0	29.0	...	3.0	...	4.5 W, 60 Co
KEL-F[f]	Elastomer 3700-336 (amine cured) Co-polymer of trifluorochloroethylene and vinylidene fluoride										

[a] Trade name of Midvale Steel Co.
[b] Trade name of International Nickel Co.
[c] Trade name of Haynes Stellite Co.
[d] Trade name of Nitralloy Corp.
[e] Special General Electric Co. alloy
[f] Trade name of M. W. Kellogg Co.

A, Austenized
CR, Cold rolled
FC, Furnace cooled
HR, Hot rolled
HT, Heat-treated
CC, Centrifugally cast
N, Normalized
OQ, Oil quenched
Sen, Sensitized
SR, Stressed relieved
T, Tempered
Ann. Annealed

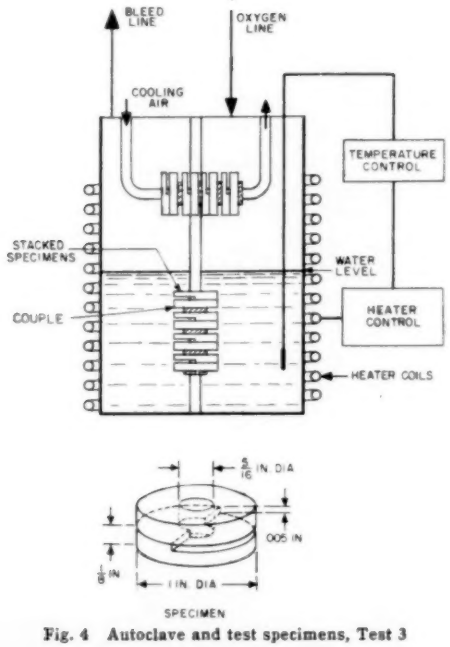

Fig. 4 Autoclave and test specimens, Test 3

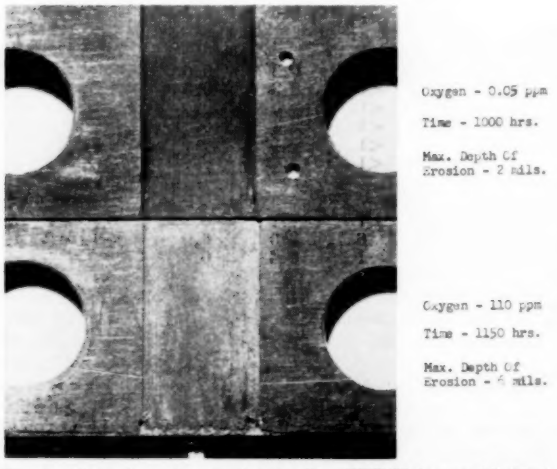

Fig. 5 Channel erosion specimens, 5X. BTH Pb bronze (50 Bhn). Erosion occurs at exit end of channel. (Bottom edge.)

Once weekly, the bombs were cooled, opened, and recharged with fresh water and oxygen as before. After 6 weeks of exposure, and again after 16 weeks, the specimens were separated, inspected, cleaned in inhibited acid, weighed, and inspected again for pitting, crevice, and galvanic corrosion. At the end of 16 weeks, the depth of the deepest pit on each specimen was determined with a microscope.

The results of this test are summarized in Table 5 where the weight losses have been converted to "average penetration" in 16 weeks (with one intermediate cleaning). The depth of the deepest pit on each specimen was measured. For each metal, the average of these maxima is shown in Table 5. In addition, the deepest pit encountered under each set of conditions also is recorded.

Some of the weight losses are shown as corrosion rates (mils/yr) in Table 3 for comparison with the corrosion under the dynamic conditions of Tests 1 and 2. "Rates" for other conditions may be inferred from Table 5.

Discussion

Erosion in Wet Steam. In Tests 1 and 2, erosion of the wire-drawing or channel type was assessed by measuring the depth of the deepest pit on each specimen. In Test 1, specimens were tested in duplicate; in Test 2, only single specimens were run.

Under the conditions of Test 1, increasing the oxygen concentration did not increase the erosion rate except in the case of BTH leaded bronze which also was the only alloy which showed a simultaneous marked increase in corrosion rate, Tables 2, 3. The maximum pitting depth in Test 1 (1000 hr) was about twice that in Test 2 (1900 hr) reflecting the greater severity of Test 1 (higher temperature, higher velocity, and lower pH). However, the relative erosion resistance of the alloys remains the same in these tests. This is seen in Table 2 which gives the ratio of the maximum depth of erosion for each alloy to the maximum depth of erosion of $2^1/_2$ Ni, $^1/_2$ Mo. In Test 2 the volume of the metal lost also was calculated from weight loss. On this basis the relative erosion resistance is the same as that obtained from pit depths.

The condition in Test 2, where the steam is obliged to make a sudden turn, simulates conditions of leakage past diaphragms and shell ledges. These ledges frequently erode in marine

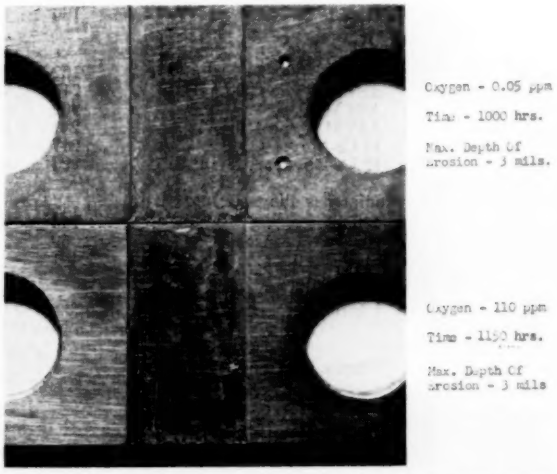

Fig. 6 Channel erosion coupon, 5X. $^1/_2$ Mo cast steel (131 Bhn). Note pitting occurs both randomly and along preferred paths.

Fig. 7 Erosion disk, 5X. $2^1/_2$ Ni, $^1/_2$ Mo steel (Bhn 262). Maximum depth of groove, 0.5 mil in 1930 hr. Note flow pattern indicated by stains. Maximum grooves in elliptical pattern below straight bore.

Table 2 Maximum depth of erosion in wet steam—mils[a]

	Test 1		Test 2
	Loop #1	Loop #2	Mystic Station
Temperature of entering steam, °F	430	430	272
Pressure of entering steam, psia	350	350	43
Moisture of entering steam, %	9	9	6
Pressure of exit steam, psia	245	245	40
Velocity of steam, ft/sec	460	460	350
pH of steam	6.8	6.8	9.2[b]
Oxygen in steam, ppm	0.05	110	90
Duration of test, hr	1000	1150	1930

Material	Hardness, Bhn	Mils[a]	Ratio[c]	Mils[a]	Ratio[c]	Mils[a]	Ratio[c]
Carbon steel							
ASTM A201	103	4	4	4	4	...	...
ASTM A27 Cast	146	3	3	3	3	...	...
Low-alloy steel							
1/2 Mo	131	3	3	3	3	...	...
1/2 Mo Cast	131	3	3	3	3	...	...
1 Cr, 1 Mo Cast	202	2	2	2	2	...	...
1 Cr, 1 Mo, 1/4 V Forged	218	2	2	2	2	...	...
2 Cr Cast	229	...	...	...	...	0.8	1.6
2 1/2 Ni, 1/2 Mo Forged	229	1	1	1	1	...	...
2 1/2 Ni, 1/2 Mo Forged	262	...	...	...	...	0.5	1.0
Nitrided steel							
Nitrided Nitralloy	62Rc	3	3	3	3	...	...
Nitrided EME	60Rc	1	1	1	1	...	...
Nitrided Type 410 stainless	60Rc	1	1	1	1	...	...
Cast iron							
ASTM A48	179	...	...	...	...	4.0	8.0
Ductile Ni-Resist #3	166	...	...	...	...	0.6	1.2
Stainless steel							
ASTM Type 347	162	<1	<1	<1	<1	0.3	0.6
ASTM Type 403	217	<1	<1	<1	<1	0.3	0.6
ASTM Type 405	202	<1	<1	<1	<1	...	...
ASTM Type 410	241	<1	<1	<1	<1	...	...
12 Cr-Mo	217	<1	<1	<1	<1	...	...
12 Cr-Cb	223	<1	<1	<1	<1	...	...
Nonferrous alloy							
Monel	143	<1	<1	<1	<1	...	...
BTH Pb bronze	50	2	2	6	6	3.0	6.0
Stellite #6	401	1	1	1	1	0.4	0.8

[a] 1 mil = 0.001 inch.

[b] Actual values: pH 9.5, 70 ppm O_2 first 780 hr.
pH 8.8, 110 ppm O_2 next 1150 hr.

[c] Ratio: $\frac{\text{Max erosion depth of alloy}}{\text{Max erosion depth of } 2\frac{1}{2} \text{ Ni, } \frac{1}{2} \text{ Mo forged steel}}$

turbines which operate with saturated steam unless they are faced with special alloys.

From Table 2 it is immediately obvious that resistance to erosion as determined by depth measurements follows roughly the order of expected corrosion behavior; that is, stainless steels are most resistant, low alloy steels intermediate, and carbon steel and cast iron least resistant. The predominance of chemical effects in erosion under the conditions of Tests 1 and 2 (calculated velocities up to 460 ft/sec, 270–430 F, pH 7–9) are further suggested by the absence of any definite influence of hardness. Stellite No. 6, the hardest material tested was not the most resistant. Carbon steel A201, however, lower in hardness than A27, was the more susceptible of the two. In the low-alloy steels, proceeding from 1/2 Mo steel to 2 1/2 Ni-1/2 Mo steel, Table 2, there is a progressive increase in hardness and a corresponding increase in erosion resistance. This apparent effect of hardness may not be real, however, since, paralleling the increasing hardness, there is also an increasing alloy content and perhaps corrosion resistance.

In other tests in wet steam at about 1000 ft/sec the erosion of 12 Cr steel was reduced by 60 per cent when its hardness was increased from 230 Bhn to 415 Bhn (3). This seems to indicate that with any particular alloy, increasing the hardness may be beneficial.

Nitrided EME and nitrided Type 410 stainless were not as resistant as the unnitrided alloys. Nitrided Nitralloy was poorer than the nitrided stainless steels, seeming to indicate an influence of the resistance of the base metal to erosion-corrosion as the hardened case eroded away. Earlier work at Mystic Station (3) showed nitrided Nitralloy to be much more resistant in alkaline steam than in acid steam.

Other published erosion results in steam show no correlation between hardness and resistance. Venton (4), with steam at 350 psi, found 18 Cr-8 Ni (169 Bhn) more resistant than hard cast iron (194 Bhn) and nitrided steels. Löbel (5), with steam at 885 ft/sec (1900 psi), obtained with Stellite No. 1 (702Hv) 40 times the weight loss obtained with 25 Cr-12 Ni (373Hv). Marshall (6), with low-pressure geothermal steam (high in CO_2

Table 3 Corrosion in wet steam

	Corrosion Rate, mils/yr											
	Test no. 1						Test no. 2		Test no. 3			
Loop or run	1	2	1	2	1	2	A	B				
Temp, °F	430	430	400	400	300	300	272	272	545	545	545	545
Pressure, psia	350	350	245	245	67	67	43	43	1015	1015	1015	1015
Moisture, %	9	9	7	7	5	5	6	6	Sat.	Sat.	Sat.	Sat.
Velocity feet per sec	30	30	30	30	45	45	90	90		Rocking	Autoclave	
pH	6.8	6.8	6.8	6.8	6.8	6.8	9.5	8.8	7	7	7	7
Oxygen, ppm	0.05	110	0.05	110	0.05	110	70	110	50	100	50	100
Duration, hr	1000	1150	1000	1150	1000	1150	780	1150	6 wk	6 wk	10 wk	10 wk
Carbon steel												
ASTM A106, A212, A201	2.0	2.2	1.0	1.4	0.2	1.0	2.6	...	1.5	1.6	2.0	1.2
ASTM A27 Cast	...	...	...	...	...	...	...	2.5	0.6	0.7	0.6	0.6
Low-alloy steel												
2 1/2 Ni, 1/2 Mo, Forged	0.9	1.3	0.4	0.6	0.3	0.4	...	1.7	0.6	0.7	0.8	0.4
2 1/4 Cr, 1 Mo, (A155)	1.1	1.4	0.5	1.1	0.2	0.4	...	0.6	0.8[a]	0.8[a]	0.5[a]	0.3[a]
Cast iron												
ASTM A48	...	...	...	...	...	...	...	1.9	2.2	3.0	2.2	1.7
Ductile Ni-Resist #3	0.2	0.4	0.2	0.2	<0.1	<0.1	...	0.7	...	0.1[b]	...	0.1[b]
Stainless steel												
ASTM Type 304L & Sen.	0.2	0.1	0.1	0.1	0.1	<0.1	0.9	...	0.2	0.2	...	..
ASTM Type 347	<0.1	0.1	Nil	Nil	Nil	Nil	Nil	...	0.2	0.2	0.1	0.1
ASTM Type 403	0.2	0.2	0.2	0.1	0.1	<0.1	...	...	0.3	0.3	0.2	0.1
Nonferrous alloys												
90/10 Cu-Ni	...	...	0.4	4.6	0.2	0.6	1.2	...	...	...	...	...
80/20 Cu-Ni	...	...	0.3	4.4	0.1	0.6	...	...	...	...	...	...
70/30 Cu-Ni	...	...	0.2	6.8	0.1	1.3	...	...	...	...	...	...
Monel	0.8	0.9	0.2	0.4	0.1	<0.1	0.7	...	...	...	...	...
BTH Pb bronze	3.2	14.5	...	...	...	...	2.4	...	4.0	3.3	...	...
Stellite #1	<0.1	0.1	<0.1	<0.1	<0.1	<0.1	...	...	...	...	...	...

[a] 2 Cr cast steel.
[b] Ni-Resist No. 3.

and H_2S) at 850–1050 ft/sec, obtained less erosion-corrosion with 18 Cr-8Ni (160 Bhn) than with 13 Cr (190 Bhn).

The relative resistance to erosion in steam obtained by Venton and by Marshall are also according to expected corrosion resistance; stainless steel, low-alloy steel, carbon steel, cast iron. No comparison is made with Löbel's work since he is concerned only with highly alloyed metals.

The wire-drawing specimens, Figs. 5, 6, showed the most severe attack at the exit edges. This is partially due to the fact that the velocity is highest at this point. There also may be effects due to peculiar turbulence and vortexes at this point.

In 1000-hr tests with wet steam flowing at about 850 ft/sec (6 per cent original moisture, 0.05 and 80 ppm O_2) there was no visible "washing erosion" of the Types 347 and 405 stainless-steel nozzles. There was one "gouge" presumably due to a hard solid particle. The impact specimens (Types 347 and 403 stainless), placed two inches from the discharge of these nozzles, suffered some roughing as expected. Some of this also might have been caused by solids. There was no difference between the Type 347 stainless steel and the hardened Type 403 stainless specimens. There was no significant effect of oxygen on either the nozzle or impingement specimens.

Turbine buckets normally are protected with erosion shields when the tip velocity and moisture exceed 1000 ft/sec and 4 per cent, respectively. The possible need for additional shielding in the Dresden turbine, where velocities may be below 1000 ft/sec but moisture above 4 per cent, is being determined with different apparatus.

General Corrosion in Wet Steam. In Tests 1 and 2 with industrial steam, all specimens became covered with thin, tenacious brown films which may have influenced the results. Similar coatings have been reported in the Borax boiling water reactor system on surfaces contacting water. Whether such films will develop also in the Dresden system, where the water purity will be higher, is not known.

All corrosion specimens in Test 1 were in duplicate; in Test 2 only single specimens were used. Weight losses in 1000 hr (after cleaning) have been converted to corrosion rates using "exposed" areas. Since some corrosion occurred on other areas of the specimens, errors from this assumption tend to make the calculated rates high. In Test 1, Table 3, Fig. 8, the corrosion rates of all the alloys tested increased with temperature (300 F–430 F), plots of the logarithm of the corrosion rate versus the reciprocal of the absolute temperature approximating straight lines. There is a marked increase in corrosion rates of high-copper cupronickel alloys (BTH leaded bronze; 70/30, 80/20, and 90/10 cupronickels) with increase in oxygen from 0.05 to 110 ppm. This effect of oxygen becomes greater with increasing temperature. Under the same conditions, Monel (a high-nickel cupronickel alloy), low-alloy steel, and Ductile Ni-Resist No. 3, show moderate increase in corrosion with added oxygen. With carbon steels, oxygen increases the corrosion rate greatly at lower temperatures, but has little effect at higher temperature. In autoclave tests (545 F, oxygen) BTH leaded bronze dezincified.

Austenitic and martensitic stainless steels showed no significant

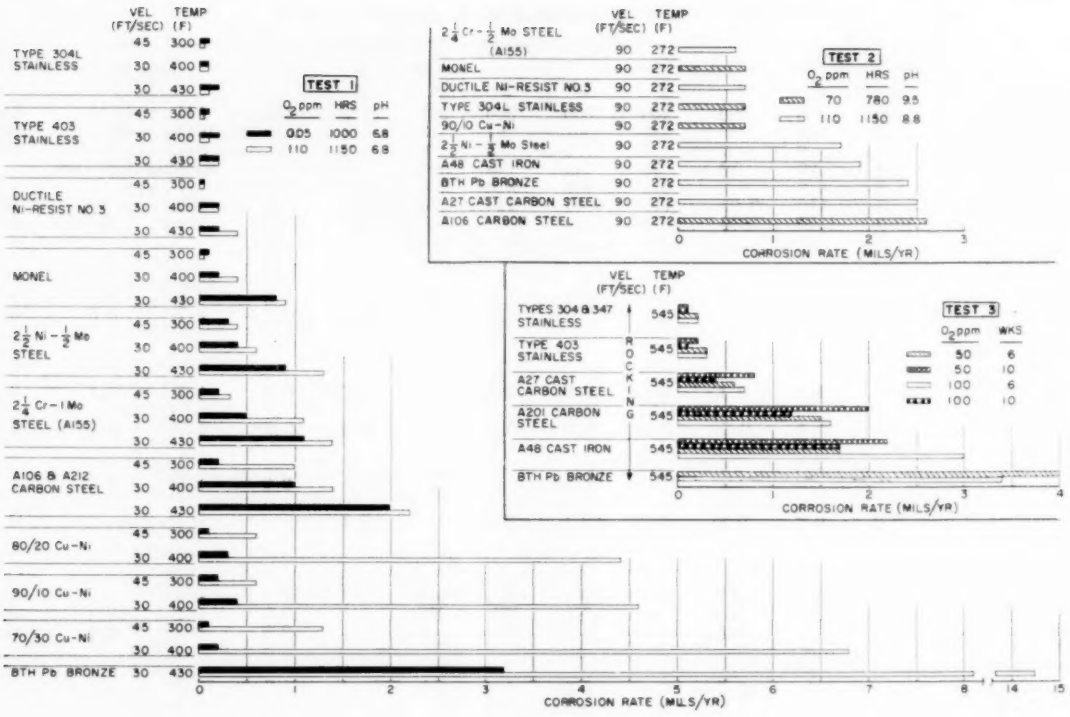

Fig. 8 Corrosion rates of materials (descaled)

effect of oxygen in Test 1 (up to 430 F). In the rocking autoclave tests (Test 3, 545 F) there was no difference in the results with oxygen initially at 50 ppm and 100 ppm in 6 weeks. After cleaning these specimens and re-exposing them for an additional 10 weeks, the corrosion was more severe with 50 ppm than with 100 ppm oxygen for all metals. In another autoclave test, results with stainless steels of Types 310, 410, 440C, and 446 reproduced the results shown for the austenitic and ferritic stainless steels in Table 3. In Fig. 8 the alloys are listed in order of decreasing resistance to corrosion in wet steam with high oxygen content.

Other autoclave corrosion rates may be obtained from the calculated average penetration values given in Table 5. Rates in water tended to be lowest; those in condensing vapor intermediate; and those under alternating (rocking) conditions highest. This may be due in part to differences in effective oxygen concentration. For instance, the specimens submerged in water developed less red oxide than the others. The rocking results also may include a velocity effect. All these effects in the autoclave tests are small, practically speaking, but they appear consistent. Couples of dissimilar metals, which included combinations of stainless steel, low-alloy steels, carbon steel, and cast iron, showed no noticeable galvanic effects.

The oxygen concentration in the liquid phase in the autoclave tests was much smaller than that in the vapor. Further, the oxygen concentration varied during the course of the weekly cycle. Thus, in one case 80 per cent of the oxygen disappeared during the first week, while only 40 per cent was consumed during the sixth week. The hydrogen accumulation also varied. For the first and sixth weeks, the ratios H_2/O_2 were 3/1 and 1/4, respectively. These reflect the decrease in corrosion rate with time. Another indication of the decrease of rate with time was the resistivity of the water which fell from its original value of over 10^6 ohm-cm to 5000 ohm-cm during the first week, but fell only as far as 300,000 ohm-cm during the sixth week.

The effects of velocity and pH cannot be distinguished in these tests. For instance, in Test 2, after 1150 hr, the corrosion rate of carbon steel at pH 9 and 90 ft/sec was about twice that in Test 1 at pH 7 and 45 ft/sec. In tests at 600 F with steel capsules filled with distilled water, Bloom (7) found that the effect of ammonia was to increase the corrosion of carbon steel by a factor of two at 1000 hr. This effect disappeared as the exposure time was increased; e.g., 150 days. There was no effect if NaOH was used. However, in earlier tests at Mystic Station (with no oxygen), the addition of morpholine to steam decreased the corrosion rates of carbon and low-alloy steels (3). Douglas (8) in autoclave tests at 600 F with no oxygen, obtained no effect on the corrosion rate of iron with additions of NaOH. It is probable, therefore, that the increased corrosion in Test 2 is due to the higher velocity.

Some comparisons with other published results are shown in Table 4. In a qualitative way, agreement is good. Results in autoclaves without oxygen indicate rates of 0.0001–0.0002 in/year for low carbon steel in 1000 hr at 500–600 F (7, 8, 9), and for stainless steel, about one tenth of these values.

There was no intergranular corrosion of Type 304L stainless at 430 F with oxygen in 1000 hr (Test 1), even when sensitized. Nor was there any cracking around heavily stamped crosses.

Pitting. In the dynamic tests with wet steam at 430 F, pH 6.8, with oxygen (Test 1, Table 3), carbon steel pitted to a maximum depth of about 0.002 in. at the periphery of crevices. In the exposed areas, the pitting was scattered and about one tenth as deep, Fig. 9. The depth of attack increased with increase in temperature between 300 and 430 F. Without

Table 4 Comparison of corrosion rates in high-temperature water at pH 7—mils per year[a]; descaled specimens

			Velocity, fps — No O_2		With O_2	
	Temp deg F	Hours	0–5	10–30	0–5	10–30
Carbon steel:						
Blaser (9)....	500 to 600	338	...	...	2	...
		500	1	2	...	...
		1000	...	1	...	...
Beeghley (11).	500	360	...	2[b]	...	...
		1440	...	0.3[b]	...	...
Present work	545	1000	...	...	1½	...
	430	1000	...	2	...	2
Stainless steel—304:						
Wroughton (10).....	500	1000	...	0.2[b]	...	...
Present work	545	1000	...	...	0.2	...
	430	1000	...	0.2	...	0.1

[a] 1 mil = 0.001 in.
[b] pH 7–11.

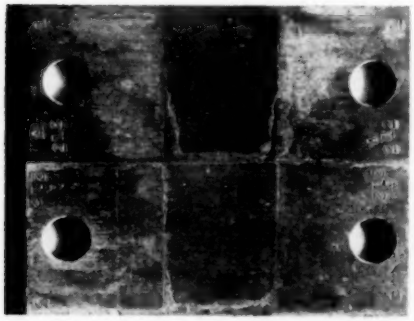

Fig. 9 Corrosion specimen, 2X. A212 carbon steel. Pitting mostly bordering crevices.

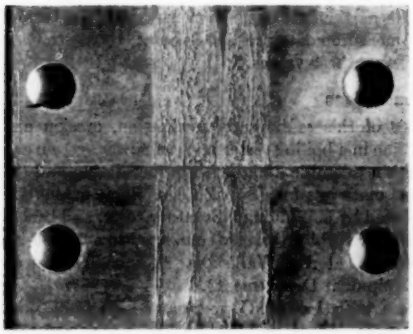

Fig. 10 Corrosion specimen, 2X. A106 carbon steel. Pitting occurred only on side facing KEL-F with high and low oxygen.

oxygen, the crevice pitting at 430 F was minor (0.0003 in., Fig. 9). Low-alloy steels showed the same behavior to a lesser extent (0.0008 in. at 430 F with oxygen, negligible pitting without oxygen). The stainless steels, cupronickels, Monel, and Ductile Ni-Resist No. 3 developed minor pits with oxygen and none without.

In Test 1, strips of KEL-F disintegrated at 430 F in less than 200 hr. With oxygen in the steam, pitting occurred on the surfaces of specimens facing the KEL-F. On carbon steel, the depth of these pits was 0.005 in., Fig. 10, and on Type 403 stainless steel, 0.002 in., Fig. 11, after 1000 hr. Without oxygen, pitting occurred on the carbon steel specimens (0.003 in.) but not on the Type 403 stainless-steel specimens, Figs. 10 and 11.

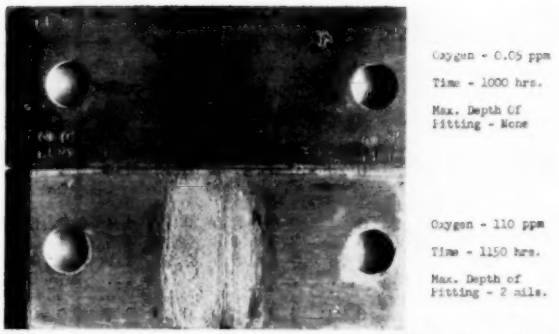

Fig. 11 Corrosion specimen, 2X. Type 403 stainless steel. Pitting occurred only on side facing KEL-F with high oxygen.

There was no pitting at crevices or exposed areas of corrosion specimens in Test 2 (Table 3) at 272 F, pH 9, with oxygen.

In the autoclave tests (545 F, with oxygen) the extent of general pitting paralleled the weight loss, indicating the major loss of metal was by pitting attack. Again, the austenitic stainless steels were most resistant; then followed ferritic stainless steel, low-alloy and carbon steel, and cast iron. Pitting on the exposed surfaces of the couples was more extensive (but not deeper) than on the contact and crevice areas. Deposits of iron oxides from solution and easier access to oxygen may explain this. Heavier deposits led to larger, but not deeper, pits. This was especially noticeable on the stainless-steel specimens since they pitted less frequently. Pitting at the 0.002-in.-wide crevices was largely confined to the mouths of the crevices.

In Table 5 is shown the average penetration calculated from the loss in weight (after descaling) obtained after exposure to steam-water-oxygen at 545 F for a total of 16 weeks. The deepest pit on each specimen was determined with a microscope. The average of these specimen maxima and the deepest pit for each alloy are also shown in Table 5. The depths of the deepest pit varied less from alloy to alloy than did the average penetration value. For cast iron and low-alloy steels the deepest pit was from 10 to 80 times deeper than the average penetration. For stainless steel, the deepest pit was from 40 to 200 times deeper than the average penetration, reflecting the greater general corrosion resistance of the stainless steels. As noted previously, the average penetration may be taken as a rough guide to the number of deep pits.

In cast iron and cast steel a few very deep pits were observed. These might have been associated with inclusions or pin-hole porosity.

In some cases, the depth of the deepest pit, rather than some average value, is of primary interest. Representative portions of the pitting data for Types 347, 403, 1 Cr-½ Mo, A48, and A201, were analyzed by the method of variance for possible differences in the maximum depth occurring:

(*a*) On different surfaces (external, contact, crevice).

(*b*) On different portions of a surface; e.g., near or removed from edges and screw heads.

(*c*) With exposure to water, condensing steam, and with alternating conditions (rocking).

(*d*) With 50 ppm and 100 ppm O_2 (initially)

(*e*) With different metals.

Table 5 Pitting of metals in autoclave tests in steam-water-oxygen; time, 16 weeks; temperature, 545 F; pressure, 1015 psia. Depth in mills (1 mil = 0.001 inch).

	Rocking (water and steam)						Water						Steam					
	50 ppm O_2			100 ppm O_2			50 ppm O_2			100 ppm O_2			50 ppm O_2			100 ppm O_2		
Carbon steel	Calc [a]	Avg [b]	Max [c]	Calc [a]	Avg [b]	Max [c]	Calc [a]	Avg [b]	Max [c]	Calc [a]	Avg [b]	Max [c]	Calc [a]	Avg [b]	Max [c]	Calc [a]	Avg [b]	Max [c]
ASTM A201	0.57	3.6	5.5	0.41	3.3	4.0	0.20	4.5	5.8	0.18	4.3	5.9	0.37	4.9	6.5	0.37	3.7	6.0
ASTM A27 Cast	0.20	10.0	17.0	0.19	4.3	6.4	0.11	[d]	7.4	0.10	7.0	7.5	0.15	[d]	8.4	0.15	5.5	6.5
Low-alloy steel																		
1 Cr, 1/2 Mo Forged	0.25	6.5	8.0	0.17	4.4	5.2	0.11	[d]	7.8	0.12	[d]	8.3	0.17	[d]	5.3	0.18	[d]	3.4
1 Cr, 1/2 Mo, 1/4 V	0.25	3.3	4.0	0.18	4.5	5.4	...	...	...	0.13	[d]	7.6	...	...	...	0.19	[d]	3.4
2 Cr Cast	0.18	5.1	8.5	0.15	4.1	5.1	0.11	5.9	8.0	0.08	4.4	4.7	0.19	3.9	4.5	0.23	7.1	10.0
2 1/4 Cr, 1 Mo, A155	...	...	...	...	...	...	0.05	2.5	2.8				0.03	2.1	2.2			
2 1/2 Ni, 1/2 Mo Forged	0.23	4.0	6.0	0.16	3.4	4.0	0.08	4.5	6.0	0.10	4.6	5.3	0.15	3.8	4.6	0.15	3.6	4.4
2 Ni, 1/2 Mo Forged	...	...	...	...	...	...	0.10	[d]	5.9	...	...	...	0.18	[d]	6.6	...	...	...
Nitralloy nitrided	0.18	...	...	...	...	...	0.13	[d]	2.5	0.25	[d]	2.5	0.12	[d]	2.8	0.18	[d]	3.2
Cast iron																		
A48	0.66	2.9	4.1	0.64	3.1	4.6	0.46	8.4	10.5	0.41	10.0	25.0	0.45	3.4	4.0	0.54	3.3	5.1
Stainless steel																		
ASTM Type 347	0.04	1.6	2.0	0.04	0.9	1.8	0.01	1.9	2.4	0.02	1.0	1.6	0.02	1.4	1.5	0.03	1.4	1.6
ASTM Type 403-HR	0.08	2.8	4.0	0.05	1.4	2.6	0.03	[d]	1.3	0.04	0.9	1.2	0.05	[d]	1.1	0.07	1.5	1.7
ASTM Type 403-CR	0.08	4.0	4.5	0.06	1.5	2.0	...	...	...	0.05	[d]	1.4	...	...	...	0.05	[d]	1.7
ASTM Type 405	0.06	2.5	4.9	0.06	1.2	2.1	...	...	...	0.03	1.5	1.9	...	...	...	0.05	1.5	2.4
12 Cr, Mo	...	...	...	...	...	...	0.00	[d]	2.2	...	...	...	0.02	[d]	1.3	...	...	...
12 Cr, Mo, W, V	0.07	2.9	4.5	0.04	4.8	8.0	...	...	...	0.02	[d]	3.3	...	...	...	0.06	[d]	2.4

[a] Average penetration calculated from weight loss after descaling.
[b] Average of specimen maxima.
[c] Deepest pit for alloy.
[d] Single specimen.

For practical purposes, the only significant differences were due to the metals themselves. The results of one analysis are shown in Fig. 12. Type 347 stainless was the most versatile metal, appearing best under most conditions. Low-alloy steel, carbon steel, and cast iron fell into one indistinguishable group. Type 403 stainless was intermediate, falling most often with Type 347 but sometimes with the low alloys. In this group, Type 403 stainless alone showed some effect due to oxygen. A greater number of specimens might have revealed other instances.

Because of the small number of specimens, it was interesting to speculate on the maximum depth that might have occurred in a large number of specimens. Extrapolation of these data was made assuming the distribution of the maxima is of the form $\Phi = \exp(-e)^{-y}$ as described by Gumbel (12). Special probability paper reduces this to fitting a straight line to the data. This line, representing points with 50 per cent assurance, may be extrapolated to any probability desired. From Table 6, for instance, for 403 stainless, the odds are even that a depth of 0.004 in. will not be exceeded in more than one specimen out of ten. With the same odds, a depth of over 0.006 in. would not be expected in more than one specimen in one hundred.

Table 6 Extrapolation of maximum pitting depths by extreme value theory $\Phi = \exp(-e)^{-y}$; 50 ppm O_2; rocking autoclave; depth in mils[a]

	No. of specimens	Max. pit observed	Pit depth with 50% assurance for probability of 0.90	Pit depth with 50% assurance for probability of 0.99
ASTM A27 cast steel	4	17	23	40
ASTM A48 cast iron	5	4	4	5 1/2
ASTM Type 403 stainless	8	4	4	6
ASTM Type 347 stainless	6	2	2 1/2	3
ASTM A201	4	5 1/2	6 1/2	10 1/2
1 Cr-1/2 Mo + 2 1/2 Ni-1/2 Mo	6	8	9	14
12 Cr alloy steels	16	5	5	7
2 Cr + 1 Cr-1/2 Mo-1/4 V	5	8	8 1/2	14

[a] 1 mil = 0.001 inch.

If the data for all alloys containing 12 per cent Cr are grouped together so as to increase the number of observations, the corresponding predictions are 0.005 and 0.007 in. A comparison of average penetration, average of the maxima measured, and the pit depth expected to be exceeded not more than 1 per cent of the time, is shown in Fig. 13, for the cases in Table 6.

There is not enough experience with pitting to indicate how significant such extrapolations are. Besides questions of the applicability of the particular distribution assumed here, errors in the pit depth measurements are not known; there were no independent checks on these values.

Summary and Conclusions

1 On the basis of this preliminary evaluation, erosion and corrosion of a turbine in a boiling water nuclear power system can be maintained within tolerable limits with proper design and the selection of special materials for critical areas. This evaluation is being supplemented by continuing laboratory tests, and by the operation of a 5000-kw turbine directly connected to a 10,000-kw boiling water reactor at the Vallecitos Atomic Laboratory (Atomic Power Equipment Department).

2 In wet steam with low (0.05 ppm) and high (100 ppm) oxygen, stainless steels, Monel, and Stellite 6 were most resistant to "wire drawing" erosion. Ductile Ni-Resist 3, low nickel steels, and low chromium steels were better than low molybdenum and carbon steels; plain cast iron was the least resistant material tested.

3 In wet steam at pH 7 and 430 F, there was no effect of oxygen on erosion in tests with high and low oxygen concentrations, except for BTH leaded bronze. With low oxygen, BTH leaded bronze resembled low chromium steel in erosion; with high oxygen, it resembled plain cast iron.

4 In wet steam at 300–430 F, and pH 7, with low and high oxygen, stainless steel, Stellite No. 1, and Ductile Ni-Resist No.

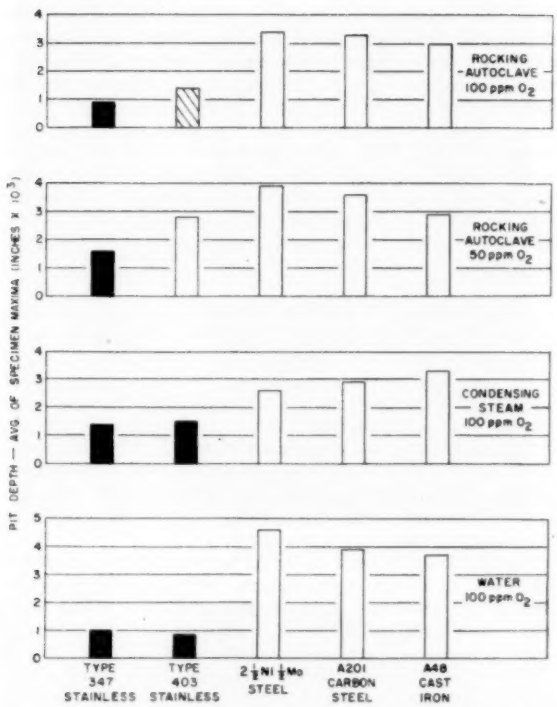

Fig. 12 Average of maximum depth of pitting; different shadings indicate averages are significantly different

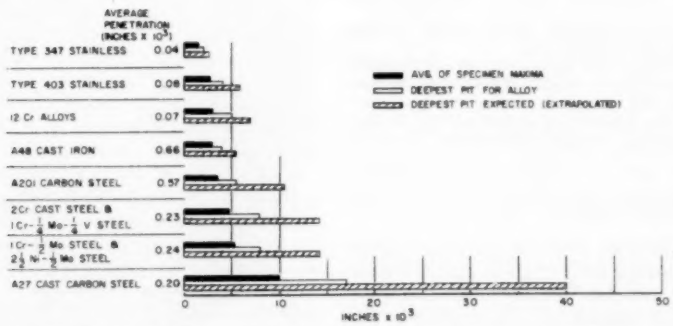

Fig. 13 Depth of pitting—comparison of calculated average penetration, average of depth maxima, deepest pit, and depth expected to be exceeded in not more than 1 per cent of test specimens (from extreme-value theory) for cases in Table 6

3 were most resistant to corrosion. Monel and low-alloy steels were superior to carbon steel. BTH leaded bronze was the least resistant material tested. At lower temperatures (300–400 F) and low oxygen, the cupro nickels were comparable to the most resistant materials; at high oxygen, they very rapidly approached the extreme corrosion rate of BTH leaded bronze.

5 At 300–430 F, pH 7, increasing the oxygen level from low to high increased the corrosion rate of all materials tested except stainless steel. In the case of carbon steel, this effect of oxygen on corrosion diminished rapidly with increasing temperature. With the cupronickels, the effect of oxygen was much more severe at 400 F than at 300 F.

6 Corrosion rates of all the materials tested, at 300–430 F, pH 7, high and low oxygen, increased with temperature, the logarithm of the corrosion rates varying approximately linearly with the reciprocal of the absolute temperature.

7 At 430 F, pH 7, with high oxygen, there was no intergranular corrosion of sensitized types 304 and 304L stainless steel specimens in 1000 hours, nor were there any cracks around heavily stamped crosses.

8 With low oxygen, at 300–430 F, pH 7, there was no pitting observed except with carbon steel, where the effect was minor. With high oxygen, all materials pitted especially at crevices. Stainless steel and Stellite No. 1 were most resistant. Monel, cupronickel, and BTH leaded bronze were better than low-alloy steel. Carbon steel pitted most severely of the alloys tested.

9 In autoclave tests in steam-water-oxygen mixtures (545 F, 1015 psia, 50 and 100 ppm O_2), run for 6 and 10 weeks, the rates of corrosion decreased with time. The maximum depth of pitting, however, did not increase significantly.

10 In the autoclave tests, the order of resistance, as measured by the maximum depth of pitting, was the same as for resistance to general corrosion. There was less difference in the maximum pitting depths among the ferrous alloys tested than there was in the corresponding weight losses. This reflects the greater number of pits in the least resistant alloys.

11 There were no significant galvanic or crevice effects in the autoclave tests. Naturally formed deposits of iron oxides were more effective in promoting pitting on all classes of steel tested than were artificial 0.002 in. crevices.

12 Cast iron and low-carbon cast steel were subject to occasional very deep pits in the autoclave tests. These may be related to inclusions and/or pin-hole porosity.

Acknowledgments

The authors wish to acknowledge the co-operation and contributions of the Atomic Power Equipment Department of the General Electric Company. It is difficult to express properly the authors' appreciation to the many persons who participated in this investigation. Tests, analyses, and other contributions were made by the Large Steam Turbine Engineering Subsections, the Product Development Laboratory, and the Materials and Processes Laboratory, all of General Electric Company. In addition, the authors and their Department express their appreciation to Mr. T. E. Nolan and his operating personnel at Mystic Station of Boston Edison Company, for their co-operation and testing facilities. It would take considerable space to acknowledge individually the authors' indebtedness to the many who contributed to this investigation, but special mention is deserved by Mr. P. H. Knowlton of Large Steam Turbine Engineering, Dr. G. V. Browning of the Materials and Processes

Laboratory, and the Turbine Advance Engineering Section.

Authors' Note: When this paper was written, the authors included information and expressed opinions they believed to be correct and reliable. However, because of the constant advance of technical knowledge, the widely differing conditions of possible, specific applications, and the possibility of misapplication, neither the authors nor their employer make any warranty with respect to, or assume any liability arising out of this paper, its contents, or its use.

Bibliography

1 "The Dresden Nuclear Power Station," by J. R. Wolcott, V. A. Elliott, G. M. Roy, E. P. Peabody, George Sege, and J. L. Schanz, ASME Paper No. 56—A-169, unpublished.

2 "Corrosion-Erosion of Boiler Feed Pumps and Regulating Valves," by J. M. Decker, H. A. Wagner, and J. C. Marsh, TRANS. ASME, vol. 72, 1950, pp. 19–24.

3 Unpublished results by T. W. Bigger, J. F. Quinlan, and C. F. Cheng.

4 "New Method of Studying Erosion Aids Selection of Valve Materials," by F. R. Venton, *Heating, Piping, and Air Conditioning*, vol. 9, 1937, pp. 34–38.

5 "Resistance of Materials Used for High Pressure Valves Against Erosion Action of Steam," by K. Löbel and F. Cerny, *Strojirenstvi*, vol. 6, no. 10, 1956, pp. 689–693, (in Czech).

6 "Corrosion by Low Pressure Geothermal Steam," by T. Marshall and A. J. Hugill, *Corrosion*, vol. 13, 1957, pp. 329–337.

7 "Hydrogen Effusion Method for the Determination of Corrosion Rates in Aqueous Systems at Elevated Temperature and Pressure," by M. C. Bloom and M. Krulfeld, *Journal of Electrochemical Society*, vol. 104, 1957, pp. 264–269; also, *Corrosion*, vol. 13, 1957, pp. 297–302.

8 "Corrosion of Iron in High Temperature Water," by D. L. Douglas and F. C. Zyzes, *Corrosion*, vol. 13, 1957, pp. 361–374.

9 "Special Corrosion Study of Carbon and Low Alloy Steels," by R. V. Blaser and J. J. Owens, ASTM Symposium on High Purity Water Corrosion, 1956, pp. 37–53.

10 "Structural Materials for Use in Pressurized Water Power Reactor," by D. M. Wroughton and D. J. DePaul, AIME "Nuclear Metallurgy"—Symposium on Behavior of Materials in Reactor Environment, 1956.

11 "Preliminary Report on Status and Evaluation of Carbon Steel," by H. F. Beeghley, WAPD-CP-622, 1954.

12 "Statistical Theory of Extreme Values and Some Practical Applications," by E. V. Gumbel, U. S. Bureau of Standards, Applied Mathematics Series 33, 1954.

"Probability Tables for the Analysis of Extreme-Value Data," U. S. Department of Commerce, Applied Mathematics Series 22, 1953.

Discussion

D. L. Douglas.[4] The authors are to be congratulated on a fine contribution to the accumulating body of knowledge concerning the behavior of structural materials in high-temperature water systems. Despite the great amount of work done under the auspices of the Atomic Energy Commission in support of the design and construction of water-cooled and moderated reactors our theoretical understanding and empirical knowledge of these systems are sufficiently limited that predictions of behavior in untried combinations of the many variables are not reliable enough for design purposes.

The authors' findings indicate that erosion and corrosion will not be serious problems in a turbine if proper materials are used. A gratifyingly wide range of conditions covered in the tests puts this conclusion on a firm basis.

Regarding the autoclave tests, one of the purposes of which was to look for galvanic and crevice corrosion, the question of the effect of the considerable hydrogen content of the water on the results may be raised. DePaul[5] states, "Tests made in high-oxygen bearing water (1–10 cc/kg) caused all material combinations with clearances up to and including 0.002 in. to seize within a few weeks of testing." While the authors here do not specifically state which couples were tested it is fair to assume that the 132 couples in the work reported by DePaul covered some if not all of the same ones. DePaul in fact suggests that oxygen contents as low as 1 cc per kg (approximately 1 ppm) will lead to serious crevice corrosion. It is proposed that the hydrogen present in the water accounts for the limited amount of crevice corrosion found by the authors. Previous work has shown that hydrogen is effective in preventing crevice corrosion.[6] Would the authors comment on this?

C. R. Breden.[7] The authors of this paper are to be congratulated on a very timely, significant, and interesting paper. At the time the experimental work, reported here, was started, there was a very large gap in our knowledge as to what materials could be used in a boiling water reactor and its associated steam plant. At that time the materials suitable for a pressurized water reactor, and its steam plant, had been quite well defined. The steam plant being isolated from the primary circuit could be conventional. The primary circuit being pressurized could use excess hydrogen to minimize the water dissociation, and corrosion could be minimized by maintenance of high pH.

The picture, with regard to the boiling water reactor, was not at all clear. In absence of experimental evidence, some people assumed that the degree of water dissociation in a boiling water reactor would not be appreciably different from that in a pressurized water reactor. Others were of the opinion that it could be much greater. When a determination was finally made of the amount of water dissociation occurring in BORAX, the boiling reactor experiment in Idaho, it was found to be significantly higher than that in a pressurized water reactor. Due to this dissociation into hydrogen and oxygen, the steam issuing from the reactor contained an appreciable amount of oxygen. The important question then was, what happens to conventional turbine materials when the steam contains oxygen? An additional factor of uncertainty was the effect on materials of using saturated steam instead of superheated steam. When we started inquiries on these two points, we were informed that no one could remember what happened to the early turbines operated in this manner.

Being already committed to a turbine of conventional materials for EBWR, the simplest expedient appeared to be to coat the inside of the turbine (except for the rotor) with Kanigen nickel.

After the plant was put into operation, it was found that the amount of oxygen present in the steam was about 30 ppm. Since no corrosion coupons were placed in the steam lines of EBWR until very recently, it is difficult to determine exactly what is happening to the materials. From such observations as have been made through various openings, there appears to be no cause for alarm. When the test coupons are removed for examination we should be able to tell more about it.

As a result of the extensive experimental work described in this paper, and the supplemental test work being carried out with the boiling water reactor at Vallecitos, the authors should be able to specify the materials for the Dresden power plant with considerable more confidence than was available when EBWR was built.

The authors set out to study the corrosion behavior of possible materials under all of the conditions that they could anticipate would occur in the Dresden boiling reactor steam plant. The results reported here cover about every possible condition except the effect of irradiation. This factor, according to the authors, is to be examined at Vallecitos.

[4] Research Laboratory, General Electric Company, Schenectady, N. Y..

[5] "Corrosion and Wear Handbook for Water Cooled Reactors," by D. J. DePaul, ed., USGPO, Washington, D. C., 1957, p. 156.

[6] Ibid., p. 157.

[7] Reactor Engineering Division, Argonne National Laboratory, Lemont, Illinois.

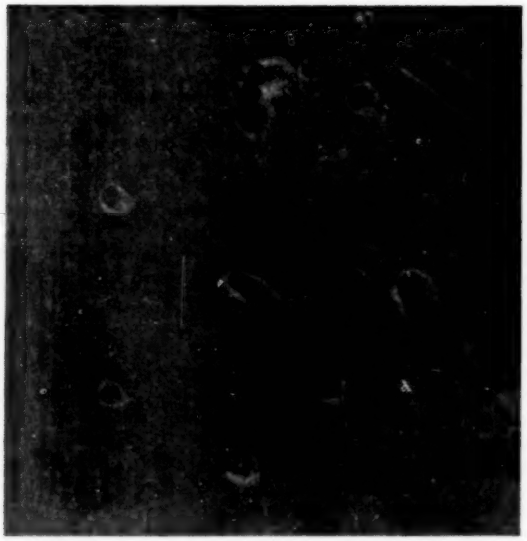

Fig. 14 2 per cent boron, stainless steel, A 4494 G

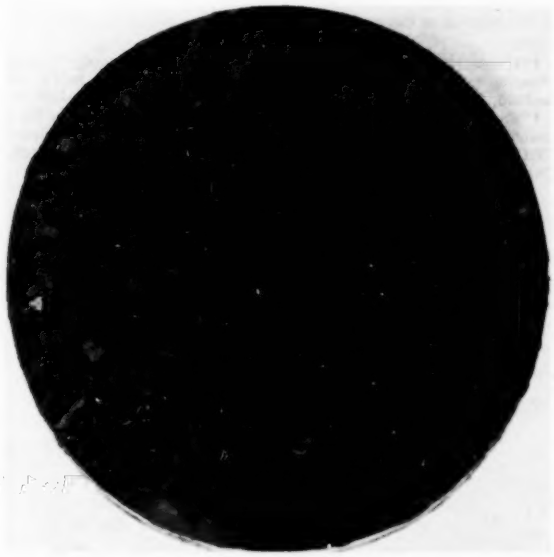

Fig. 15 4 per cent boron, stainless steel, A 4561

Of particular interest was their approach to the problem of evaluating the pitting characteristics of the various materials, and the degree of correlation they obtained. Their experience with 403 SS in water and steam, however, is similar to ours with 410 SS in water. Sometimes it behaved like 347 and showed very good corrosion resistance. At other times it behaved like carbon or low alloy steels, showing excessive attack.

Some of our biggest corrosion problems would be minimized if we only knew enough about pitting corrosion to be able to predict it consistently.

As an extreme example of the apparently inconsistent behavior that is occasionally met with in testing materials subject to pitting attack, see Figs. 14 and 15, pictures of two samples we examined a short time ago. Fig. 14 shows a sample of 304 stainless steel to which 2 per cent boron had been added. Fig. 15 shows a sample containing 4 per cent boron. These samples had been tested in an autoclave in 550 F degassed water for 5 consecutive periods totalling 2073 hours without any evidence of pitting. After the sixth period had been in progress for 299 hours, the electrical heater failed and the temperature dropped to that of the room. Due to not being able to get repairs, the samples remained in the autoclave for 1920 hours at room temperature before the autoclave was opened and the samples examined. They then had the appearance seen in the figures, rust spots with pits beneath. Without cleaning the samples they were returned to the autoclave and tested further at 550 F. At the next examination the rust spots had disappeared, but of course, the pits remained, and showed no further attack with additional testing. This would appear to indicate that corrosion can be worse at low temperature than at high temperatures. We have had, occasionally, other indications of this apparently reverse temperature effect, particularly with the Martensitic stainless steels.

Test 3 in Fig. 8 of the paper seems to indicate that an oxygen concentration of 50 ppm was more corrosive than that of 100 ppm. Several years ago some dynamic tests of ours indicated a rather low oxygen concentration as being more corrosive than a higher one. It begins to look as if this question of oxygen concentration should be examined in more detail; as well as the effect of temperature.

In conclusion this discusser would like to ask the authors a question that has nothing to do with the experimental work. The author's diagram (Fig. 1) of the Dresden Nuclear Power Station shows only one clean-up system, the demineralizer in the feed line going to the reactor. Is there a blowdown or other clean-up system in the recirculating part of the primary system?

Authors' Closure

The authors wish to thank Drs. D. L. Douglas and C. R. Breden for their contributions to this paper. Because of differences in types of specimens and conditions of exposure, a direct comparison between our crevice corrosion results and those referred to by Dr. Douglas is not possible. In the AEC work, crevice effects were determined visually and by the torque required to turn a journal-sleeve combination after exposure to oxygen-bearing water. Our assessment of the crevice corrosion effects was made visually and in terms of specific applications in a steam turbine. Presumably, had we run journal-sleeve type crevice corrosion specimens, we would have observed some seizure also. As in the AEC work, all our specimens became pitted and covered with corrosion product to varying degrees. A few of our couples actually became bonded at the contacting surfaces. In the case of the corrosion-resistant stainless steels, it seemed clear this bonding was due to precipitation of oxides from solution as fine black crystals on the contacting surfaces. The source of these deposits was largely the much more rapidly corroding low alloy steels. In no case did we find any bonding across the 0.002-in. wide crevices in tests lasting ten weeks. In our autoclave tests we found deposition and pitting was more extensive on the external surfaces of our coupled specimens than on the recessed surfaces. It is possible that in autoclave tests with stainless-steel specimens only, the process of solution and precipitation would be so reduced as to make crevice corrosion very noticeable relative to other effects.

We do not know what effect the hydrogen corrosion product might have had on our autoclave experiments since the hydrogen was not under control. In the AEC work with water containing 500 cc/kg of hydrogen and 0.5 to 1 cc/kg of oxygen it is not definitely stated whether the oxygen was maintained at this level or whether it might have been consumed by reaction with hydro-

gen or metal. In our autoclave tests, the oxygen was never completely consumed before it was renewed.

Twenty-four materials, most of which are described in Table 1, were tested in 39 combinations in our autoclave crevice and galvanic corrosion work:

SS 304	versus	1 Cr, 1/2 Mo pipe
SS 310	versus	2 1/2 Ni, 1/2 Mo forged
SS 310	versus	ASTM A201 boiler plate
SS 310	versus	1 Cr, 1/2 Mo forged
SS 347	versus	ASTM A48 cast iron
SS 347	versus	1 Cr, 1 Mo cast
SS 347	versus	ASTM A201
SS 347	versus	Nitrided Nitralloy
SS 347	versus	ASTM A155
SS 347	versus	12 Cr, 1 Mo, 1 W, 1/4 V
SS 347	versus	Ni Resist #3
SS 347	versus	SS 410
SS 403	versus	SS 403
SS 403	versus	2 1/2 Ni, 1/2 Mo forged
SS 403	versus	SS 405
SS 403	versus	ASTM A193-B16
SS 405	versus	ASTM A48
SS 405	versus	2 Cr cast
SS 405	versus	ASTM A27
SS 410	versus	ASTM A201
SS 410	versus	ASTM A48
SS 440C	versus	SS 440C
SS 440C	versus	1 Cr, 1 Mo
SS 440C	versus	ASTM A27
SS 446	versus	SS 446
15 Cr, 2 Mo	versus	ASTM A201
2 1/2 Ni, 1/2 Mo forged	versus	1 Cr, 1/2 Mo forged
2 1/2 Ni, 1/2 Mo	versus	ASTM A155
2 1/2 Ni, 1/2 Mo	versus	2 Ni, 1/2 Mo
ASTM A155	versus	2 Cr cast
ASTM A155	versus	ASTM A48
2 Cr cast	versus	2 Cr cast
2 Cr cast	versus	ASTM A27
2 Cr cast	versus	ASTM A48
2 Cr cast	versus	BTH bronze
ASTM A201	versus	ASTM A48
ASTM A201	versus	BTH bronze
ASTM A48	versus	ASTM A27
ASTM A48	versus	BTH bronze

The Large Steam Turbine-Generator Department is conducting tests with experimental turbine parts, as well as with corrosion coupons, in a 5000-kw turbine operating with a boiling water reactor at Vallecitos. In Schenectady we are studying the effects of variables such as velocity, moisture content, and density on erosion and corrosion by steam. Independently, the Atomic Power Equipment Department is conducting various investigations in a number of laboratory loops. It will be interesting to compare these results with the information from the EBWR turbine at the Argonne National Laboratory.

The stimulation of pitting in high-temperature water by preexposure to low-temperature oxygenated water may occur both with stainless steels as illustrated by Dr. Breden, and with carbon steel as reported by Dr. Bloom.[8] We do not have sufficient data to prove that a nominal 50 ppm oxygen was more severe than a nominal 100 ppm in our autoclave tests. The corrosion rate of carbon steel in flowing water at 90 F and pH 7, with 3 to 5 ppm O_2, was found to be 0.002 inch per year,[9] approximately the rate obtained in our tests at higher temperatures. It would be interesting to know whether the corrosion rate of steel in water does pass through a maximum at relatively low-oxygen concentrations and temperatures.

There is another clean-up demineralizer in the primary system of the reactor as shown in reference (1).

---

[8] "Observations Regarding the Nature of Films Formed—Pitting Phenomena," by M. C. Bloom, M. J. Boehm, M. Krulfeld, and R. E. Seebold, NRL Quart. Nuc. Sci. and Tech., January 1, 1957, pp. 29–31.

[9] "Some Loop Experiments in the NRX Reactor to Study the Corrosion of Mild Steel by Flowing Water at 90 F," by G. M. Allison, CRDC 645, November, 1956, Atomic Energy of Canada Limited, Chalk River, Ontario, Canada.

On the Economics of the Basic Turning Operation

By R. C. BREWER,[1] SALFORD, ENGLAND

The general economic problem of turning is fairly well appreciated from a qualitative viewpoint; viz., that the reduction in machining cost as the cutting speed is increased will be eventually more than offset by increased tool changing and grinding costs. The problem involves, however, a great number of variables and it must be conceded as axiomatic that the number of variables which can be conveniently handled mathematically is such that a great deal of generality is lost. There is a further risk of loss of generality in attempting to represent the mathematical results in a form suitable for application, preferably graphical. This paper attempts to achieve the initial goal of including at least the fundamental variables in the analysis and representing the results in a reasonably useful form.

Nomenclature

The following nomenclature is used in the paper:

a, b = indexes for feed and depth of cut in tool-life equation
C_c = cutting cost per piece
C_i = idle cost per piece
C_p = total cost per piece
C_{pf} = premature failure cost per piece
C_{tc} = tool changing cost per piece
C_{td} = tool depreciation cost per piece
C_{tg} = tool regrinding cost per piece
D = diameter of workpiece
d = depth of cut
f = feed rate
L = length of workpiece to be machined
N = number of tools
n = index of T in tool life equation
q = index of W in premature failure equation
R_1 = general labor and overhead costs per minute
R_2 = constant regrinding costs
R_3 = cost of grinding 1 in. off clearance face of tool
r = number of times a tool can be reground
T = tool life
T_0 = specific tool life for an amount of wear W_0
t_c = tool-changing time
t_f = final cost of tool
t_i = idle time per piece
t_0 = initial cost of tool
u = fraction of tools which prematurely fail between each regrind
V = cutting speed
W = amount of flank wear
$\alpha = a/n$
$\beta = b/n$
γ = clearance angle of tool
Δ = limiting amount which can be ground off before a tool is useless for its present purpose
ξ = ratio of tool-changing and regrinding costs to labor cost plus overheads per unit time $= \dfrac{C_{tc} + C_{tg}}{R_1}$
ρ = number of pieces machined by any one tool between regrinds
$\sigma = \dfrac{C_{td} + C_{pf}}{C_{td}}$

[1] Formerly, Senior Lecturer in Mechanical Engineering, The Royal Technical College, at present, Lecturer in Production Engineering, Imperial College of Science and Technology, University of London, London, England.

Contributed by the Research Committee on Metal Processing and presented at the Annual Meeting, New York, N. Y., December 1–6, 1957, of The American Society of Mechanical Engineers.

Note: Statements and opinions advanced in papers are to be understood as individual expressions of their authors and not those of the Society. Manuscript received at ASME Headquarters, January 15, 1957. Paper No. 57—A-58.

Introduction

The problem of economic machining has been acknowledged for many years and there has been some appreciation (albeit imperfectly) of the solution from a qualitative angle which may be summarized as follows: Faster speeds and higher feed rates are required to reduce machining times and hence reduce costs but the implementation of either leads to shorter tool life, which increases costs. It is supposed that there is some optimum set of conditions which will lead to a minimum cost. If this be true, there remains the further point as to whether the machine tool has sufficient power to meet the requirements of these optimum conditions.

Put qualitatively, this seems to be a simple problem; a quantitative solution, however, is beset with many difficulties, the principal of which are:

1 The mathematical manipulations involved.

2 The difficulty of obtaining sufficient reliable data (this, despite the amount of published information on metal cutting).

3 The formulation of any conclusion which could be regarded as general.

The problem of economic cutting conditions has been previously investigated with varying degrees of generality and often from rather different aspects. The earliest references to economic cutting speeds appear to have been made in the early 1930's by Leyensetter (1),[2] Paasche (2), and Wallichs and Schöpke (3). These form a "technical" rather than "economic" study of machining conditions as does the more recent paper of Škrgatić (4). This latter paper gives many comprehensive data on the relationship of economic cutting speed to other machining variables and even material properties, but this economic cutting speed is arbitrarily defined in terms of a specified tool life.

The first analyses of a more general nature seem to have been given by Witthoff (5, 6, 7), who considered the effect of cutting speed and, to a less satisfactory extent, that of feed. He deduced an expression for cost in the form

$$\text{Cost} = k_1 + \frac{k_2}{fV} + \frac{k_3}{cfV^{\left(1-\frac{1}{n}\right)}} \quad \ldots\ldots\ldots\ldots [1]$$

It was not made sufficiently clear that c includes a term of the form f^a since the symbol c is derivable as follows: The generalized tool-life expression is of the form $VT^nf^ad^b$ = const, which for a given depth and feed, reduces to

[2] Numbers in parentheses refer to the Bibliography at the end of the paper.

$$VT^n = \text{const}/(f^a d^b) = c$$

Differentiating Equation [1] with respect to V and setting the result equal to zero gives as the cutting speed for minimum cost

$$V_0 = \frac{c}{\left[\xi\left(\frac{1}{n} - 1\right)\right]^n} \quad [2]$$

where ξ is some constant.

Substitution of this value into the tool-life expression $VT^n = c$ yielded the possibly unexpected result that the tool life for minimum cost was

$$T_m = \left(\frac{1}{n} - 1\right)\xi \quad [3]$$

i.e., the value c had disappeared and the answer to the economic problem appeared to be independent of the feed. Indeed Witthoff indicates this in his first paper (5) and suggests that the general procedure should be to determine the tool life for minimum cost from Equation [3] and then to use tool life/cutting speed curves to find V_0. This is evidently where the paradox is explained, for the question immediately arises—the tool life/cutting speed curve for which feed?

Witthoff argues, with some conviction, that the feed to be selected should be the greatest consistent with the power available, but since power is a function of feed and cutting speed and, as yet, the cutting speed (for minimum cost) cannot be found until the feed is known, the problem has evidently reached the vicious-circle stage. This point was not made explicitly in Witthoff's paper and it is perhaps significant that all three of his numerical examples start with a feed as one of the given quantities.

This difficulty has arisen because feed was not considered satisfactorily in the first place and a problem in two independent variables was made to look as though only one variable was effective; this cannot be so. As will be seen later in the paper, there is another aspect of the problem that this treatment has not clarified.

Independently, Atalay (8) and Gilbert (9, 10) gave analyses of the problem considering only cutting speed as variable. Accordingly they arrived at the same forms of equations as Witthoff but they gave an interpretation of the constant; viz., the ratio of the cost of changing and regrinding a tool to the cost of labor, and overheads per unit time. As the analysis did not consider feed rate, there was no need to consider methods for its selection but the disappearance of the "constant" in the tool-life equation was again noted and Gilbert (10) states: "This means then that the tool life is independent of the loading time, the idle time, the size of part being machined, the tool shape, size of cut, cutting fluid, etc. . . . . ." This is true and the implication of it will be discussed later; nevertheless the reference to size of cut may have created the impression that feed does not enter into the problem.

Lickley and Chisholm (11) considered the effect of speed and feed on cost but formulated no general expression. Their prime objective seems to have been to compare laboratory tool-life tests with shop conditions. They did not consider wear as a variable nor allow for the premature failure of a certain number of tools which occurs, especially when using carbide as a cutting medium. Some of the discrepancy between their predicted and actual results may well be attributable to omission of this latter consideration.

The General Cost Expression

For the purposes of the present analysis, the total cost/piece C_p will be broken down into the following parts:

1 Idle cost/piece, C_i
2 Cutting cost/piece, C_c
3 Tool changing cost/piece, C_{tc}
4 Tool regrinding cost/piece, C_{tg}
5 Tool depreciation cost/piece, C_{td}
6 Premature failure cost/piece, C_{pf}

With this definition, it follows that

$$C_p = C_i + C_c + C_{tc} + C_{tg} + C_{td} + C_{pf} \quad [4]$$

Each of these terms will now be considered in turn.

Idle Cost/Piece. If t_i be the idle time/piece, then the idle cost/piece will be

$$C_i = R_1 t_i \quad [5]$$

where R_1 represents the general labor and overhead costs per minute. This will include operators' wages, maintenance, power, depreciation (excluding tool depreciation), and so on.

Cutting Cost/Piece. This will be directly related to the time actually taken to machine each piece; i.e.

$$C_c = (\text{cost/minute})(\text{cutting time per piece})$$
$$= R_1 \frac{L\pi D}{fV} \quad [6]$$

where L, D, f, and V are in consistent length units (inches in this paper).

Tool Changing Cost/Piece. It is usually accepted that the tool-life relationship is given by

$$VT_0^n f^a d^b = \text{const} = \lambda \quad [7]$$

where T_0 is the specific tool life for a given amount of wear W_0. This may be transformed to give

$$T_0 = \frac{\lambda^{1/n}}{V^{1/n} f^{a/n} d^{b/n}} = \left(\frac{\lambda}{V}\right)^{1/n} \frac{1}{f^\alpha d^\beta} \quad [8]$$

where $\alpha = a/n$ and $\beta = b/n$.

The costs of regrinding are affected by the amount of wear that has taken place and hence, if this is to be allowed for, some functional relationship must be established (or assumed) between the general tool life T and the general amount of wear W. The evidence available suggests that different relationships may hold for different work materials and cutting conditions Shaw (12) gives four curves (fig. 22 of the paper cited) indicating a direct proportionality between wear and time of cutting and this is largely supported by the results of Pekelharing and Schurmann (13). Results which appear to conflict with this have been quoted by Bickel (14) and, in a more recent paper, Shaw and Dirke (15) have given many wear curves (for different work and tool materials) which suggest that the linear law is a special case of a more general relationship. In this paper, the linear law will be considered but evidently the same treatment will apply to other more general laws.

Thus for any wear W other than the standard wear W_0 we may write

$$\frac{\text{Time for wear } W}{\text{Time for wear } W_0} = \frac{T}{T_0} = \frac{W}{W_0} \quad [9]$$

or

$$T_0 = \frac{W_0 T}{W} \quad [10]$$

Substituting into Equation [8] we have a general expression relating the machining parameters to the amount of wear, viz.

$$\frac{W_0 T}{W} = \left(\frac{\lambda}{V}\right)^{1/n} \frac{1}{f^\alpha d^\beta}$$

or

$$T = \left(\frac{\lambda/W_0^n}{V}\right)^{1/n} \frac{W}{f^\alpha d^\beta} \quad \ldots\ldots\ldots\ldots\ldots [11]$$

If we now assume that the tool changing time t_c is independent of the amount of wear (which seems reasonable) we may write down the tool-changing cost/piece as

$$C_{ct} = (\text{cost/tool change})(\text{number of tool changes/piece})$$

$$= R_1 t_c \frac{L\pi D}{fV} \left(\frac{V}{\lambda/W_0^n}\right)^{1/n} \frac{f^\alpha d^\beta}{W} \quad \ldots\ldots\ldots\ldots\ldots [12]$$

Tool Regrinding Cost/Piece. There are certain costs associated with regrinding which are quite independent of the amount of wear allowed; e.g., the general handling associated with removing the tool, inspection, lapping where necessary, and so on. Let these costs be denoted by R_2 dollars/regrind.

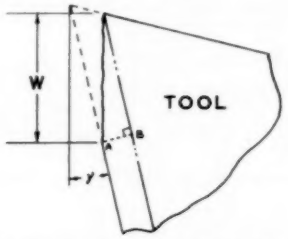

Fig. 1 Schematic representation of a tool with flank wear of amount W

Fig. 1 shows the profile of a tool with clearance-face wear of amount W inches. Theoretically, the amount to be ground off in order to produce a satisfactory clearance face is $AB = W \sin \gamma$ but in practice an amount $(W \sin \gamma + A)$ must be ground off as the worn face is not a well-defined line. Then if R_3 be the cost of grinding per inch (measured in the direction of AB), the total cost per regrind is

$$R_2 + R_3 (W \sin \gamma + A) = (R_2 + R_3 A) + R_3 W \sin \gamma \ldots [12a]$$

Hence regrinding cost per piece = (cost/regrind)(regrinds/piece)

$$= \{(R_2 + R_3 A) + R_3 W \sin \gamma\} \left\{\frac{L\pi D}{fV} \left(\frac{V}{\lambda/W_0^n}\right)^{1/n} \frac{f^\alpha d^\beta}{W}\right\}$$

$\ldots\ldots\ldots [13]$

Tool Depreciation Cost per Piece. Let the initial cost of the tool be t_0 and, in general, we may assume that the tool has a final value t_f when it is of no further use for the particular operation considered; in particular t_f may often be zero. If the tool is reground r times before it is of no use for the particular job, then the loss in value of the tool $(t_0 - t_f)$ is spread over $(1 + r)$ usages. The value of r is determined from the amount ground off each time $(W \sin \gamma + A)$ and the limit imposed when further regrinding becomes impossible (Δ); i.e.

$$r = \frac{\Delta}{W \sin \gamma + A}$$

$$\therefore C_{td} = \left\{\frac{(t_0 - t_f)}{1 + \frac{\Delta}{W \sin \gamma + A}}\right\} \left\{\frac{L\pi D}{fV} \left(\frac{V}{\lambda/W_0^n}\right)^{1/n} \frac{f^\alpha d^\beta}{W}\right\} \ldots [14]$$

Premature Failure Cost per Piece. Witthoff concludes his first paper (5) by remarking that, as the analysis is mathematical, the results need no practical verification. The results, however, are no more reliable than the data will permit and the weakest link for the brittle tool materials is that there is no guarantee that each tool will last the time predicted by tool-life tests. This has been noted by Lickley and Chisholm (11).

Although this phenomenon is not completely explicable it seems reasonable to assume that if a tool is allowed to wear more before being reground, its chances of reaching the expected tool life will be reduced. Quantitative evidence of this is scanty but some small details have been given by Burmester (16). The numerical part of his deductions therefrom is not clear but the author has plotted his premature-failure figures bilogarithmically and obtained the fact that the percentage of premature failures is proportional to the 2.78 power of the amount of wear permitted.

There are thus two alternatives:

(*a*) To accept the sum of the costs 1–5 as the total cost, realizing that for brittle materials especially, it is unlikely to give a true picture except at small values of wear.

(*b*) To attempt to incorporate the notion of premature failures into the general theory, accepting that it must be based on certain assumptions which are either only partially justified or whose justification may not be verifiable directly.

The first alternative leads to the expression for cost per piece as

$$C_p = R_1 t_l + R_1 \frac{L\pi D}{fV} + \frac{L\pi D}{fV} \left(\frac{V}{\lambda/W_0^n}\right)^{1/n} \frac{f^\alpha d^\beta}{W}$$

$$\times \left\{R_1 t_c + R_2 + R_3 A + R_3 W \sin \gamma + \frac{t_0 - t_f}{1 + \frac{\Delta}{W \sin \gamma + A}}\right\}$$

The second alternative will now be discussed. It is evident from the foregoing discussion that, due to premature failure, the cost will increase as the wear permitted increases (provided that this is taken over a considerable number of pieces.) This concept may be incorporated into the cost equation if we assume that this cost may be divided by the number of pieces so as to give an average cost per piece; this average will be greater than that for tools exhibiting no premature tool failure. A further assumption which must be made, and about which there is no experimental evidence at all, is that premature failure is independent of the number of times a tool has been reground; this appears reasonable.

Initially there are N tools and if $(100u)$ per cent of the tools fail between each regrind, then at the first regrind there are only $N(1 - u)$ tools which have not failed; the uN tools which have failed are regarded as now useless for the present operation.[3] At the second regrind there will be only $N(1 - u)^2$ tools and, in general, at the rth regrind there will be $N(1 - u)^r$ tools. After the r th regrind, the tools remaining cannot be reground and therefore the number of pieces machined by the tools which do not fail

$$= N[(1 - u) + (1 - u)^2 + (1 - u)^3 + \ldots\ldots\ldots + (1 - u)^{r+1}]\,\rho$$

$$= N\rho(1 - u)\left[\frac{1 - (1 - u)^r}{1 - (1 - u)}\right] \ldots\ldots\ldots\ldots\ldots [15]$$

where ρ = number of pieces machined by any one tool between regrinds.

Estimating the number of pieces produced by the tools which fail prematurely is more difficult since the number will vary from

[3] If this should not apply to all uN tools, under similar assumptions to the foregoing, we could make allowance for this by reducing the value of u.

tool to tool. This difficulty was overcome by Burmester (16) in an indirect manner, from which it was concluded that, on the average, each tool produced, before failure, 80 per cent of the components produced, between regrinds, by a tool which did not fail; i.e. 0.8ρ.

With these data we may proceed as follows: In the period before the first regrind Nu tools fail, producing $0.8\rho Nu$ pieces before failure. Between the first and second regrinds, there are initially $N(1-u)$ tools, of which $(100u)$ per cent fail prematurely; i.e., $uN(1-u)$; these produce $0.8\rho Nu(1-u)$ pieces before failure. Proceeding in this manner, we may again sum a geometric series to give the total number of pieces machined by the tools which fail

$$= 0.8Nu\rho[1 + (1-u) + (1-u)^2 + \ldots\ldots\ldots\ldots + (1-u)^r]$$

$$= 0.8Nu\rho\left[\frac{1-(1-u)^r}{1-(1-u)}\right] \ldots\ldots\ldots\ldots\ldots\ldots\ldots [16]$$

Hence adding Equations [15] and [16], the total number of pieces machined by N tools

$$= N\rho\left[\frac{1-(1-u)^r}{1-(1-u)}\right][(1-u) + 0.8u]$$

$$= N\rho\,\frac{1-(1-u)^r}{1-(1-u)}(1-0.2u) \ldots\ldots [17]$$

and the number of pieces machined per tool

$$= \rho(1-0.2u)\left[\frac{1-(1-u)^r}{u}\right] \ldots\ldots\ldots [18]$$

This may be regarded as increasing the tool-depreciation cost in the ratio

$$\sigma = \frac{\text{total number of pieces machined with no premature failures}}{\text{total number of pieces actually machined}}$$

$$= \frac{\rho(r+1)}{\rho(1-0.2u)\left[\dfrac{1-(1-u)^r}{u}\right]}$$

$$= \frac{u(r+1)}{(1-0.2u)[1-(1-u)^r]} \ldots\ldots [19]$$

Hence

$$C_{td} + C_{pf} = C_{td}\sigma \ldots\ldots\ldots\ldots [20]$$

Adding the various costs we have for the total cost/piece

$$C_p = R_1 t_l + R_1\frac{L\pi D}{fV} + \frac{L\pi D}{fV}\left(\frac{V}{\lambda/W_0^n}\right)^{1/n} f^\alpha d^\beta \frac{f}{W}$$

$$\times\left\{R_1 t_c + R_2 + R_3 A + R_3 W\sin\gamma + \frac{t_0 - t_f}{\left(1 + \dfrac{\Delta}{W\sin\gamma + A}\right)}\right.$$

$$\left.\times\frac{u(r+1)}{(1-0.2u)[1-(1-u)^r]}\right\} \ldots\ldots [21]$$

Discussion

It is seen from Equation [21] that the cost per piece is a function of four variables, viz., W, d, f, and V; u is a function of W which will be expressed more explicitly later. The effect of these variables on C_p will now be discussed.

Effect of W. From the bilogarithmic plot mentioned previously it was found that the incidence of premature failures was related to the amount of wear permitted before regrinding, by the relationship $u = mW^q$. Substituting for u in Equation [21] yields a functional relationship between C_p and W which is too complex to permit a general mathematical treatment. However, for use in the present analysis, a specific set-up is considered, details of which are given in the Appendix; many of these data are difficult to assess with information available at present but the order of magnitude should be correct.

For given values of feed, depth of cut, and cutting speed, the variation of C_p is governed by the third term in Equation [21]; as W is increased, the quantity in braces increases, slowly at first and then more rapidly while the other variable part, $1/W$, evidently decreases. The result is a curve, shown in Fig. 2, exhibiting a minimum cost at approximately 0.03 in. wear. Evidently alteration of feed, depth, and speed would affect the magnitudes throughout the range of wear but the general shape of the curve would not be affected since it is controlled by the two quantities stated previously, both of which are independent of f and V.

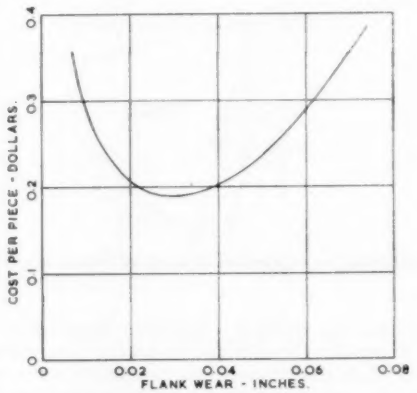

Fig. 2 Variation of cost/piece with amount of flank wear permitted before regrinding

Effect of f and V. The foregoing paragraphs have indicated that there is an optimum amount of wear to be permitted before regrinding. Assuming that this value has been chosen, Equation [21] may be simplified to give

$$C_p = R_1 t_l + R_1\frac{L\pi D}{fV} + \frac{L\pi D}{fV}\left(\frac{V}{\lambda/W_0^n}\right)^{1/n} f^\alpha d^\beta B \ldots [22]$$

where B is a constant equal to the term in braces in Equation [21] divided by W.

Differentiating Equation [22] with respect to f and V in turn and equating to zero, we may establish the conditions (if any) for minimum cost.

$$\frac{\partial C_p}{\partial V} = -R_1 L\pi D/fV^2 + \frac{L\pi D f^{\alpha-1} d^\beta B W_0}{\lambda^{1/n}} V^{\left(\frac{1}{n}-2\right)}\left(\frac{1}{n}-1\right) = 0$$

i.e.

$$V^{1/n} f^\alpha = \frac{R_1\lambda^{1/n} n}{d^\beta B W_0(1-n)} \ldots\ldots [23]$$

$$\frac{\partial C_p}{\partial f} = -R_1 L\pi D/f^2 V + \frac{L\pi D}{V}\left(\frac{V}{\lambda/W_0^n}\right)^{1/n} f^{\alpha-1} d^\beta B(\alpha - 1) = 0$$

i.e.

$$V^{1/n}f^{\alpha} = \frac{R_1\lambda^{1/n}}{d^{\beta}BW_0(\alpha - 1)} \quad \ldots\ldots\ldots\ldots [24]$$

It should be emphasized that both of these equations are independent of the physical dimensions of the workpiece. Since Equations [23] and [24] cannot be simultaneously true, it is evident that there is no absolute minimum value of C_p considered as a function of f and V. It is known, however, that for a given value of f, there is a value of V which will give minimum C_p and for a given value of V, there is a value of f which will give minimum C_p. Further, from Equation [23] it is seen that as f is increased the value of V for minimum cost decreases as would be expected; indeed if both sides of Equation [23] are multiplied by d^{β} we see that $V^{1/n}f^{\alpha}d^{\beta}$ is a constant; i.e., the tool life for minimum cost is constant (compare with Equation [11]). Gilbert's comments on this have been noted already.

Using the data given in the Appendix and $d = 0.05$ in., Equation [22] takes the numerical form

$$C_p = 0.05 + \frac{2.83}{fV} + \frac{f^{1.8}}{522}\left(\frac{V}{163.8}\right)^7 \quad \ldots\ldots\ldots [25]$$

(C_p in dollars per piece). Fig. 3 shows curves of C_p against V for various values of feed from which it is seen that, as f increases, not only does the value of V for minimum cost decrease but also the cost itself decreases, although not spectacularly.

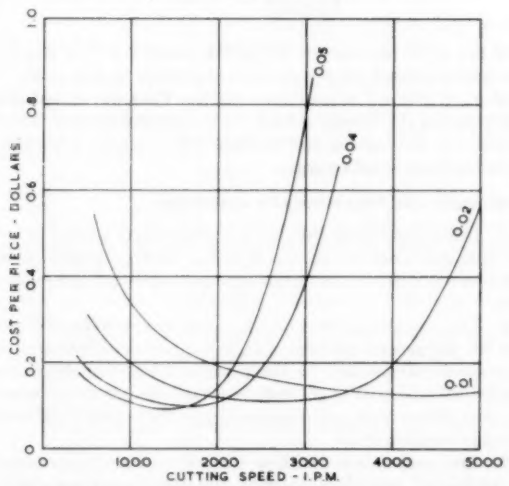

Fig. 3 Variation of cost/piece with speed. Numbers against curves refer to feed rates in inches/revolution.

Fig. 3 is useful for interpreting Equation [25], but is not the best representation of the effect of varying feed and cutting speed since it gives no facile impression of how much change in C_p is effected by any given change in f or V. In Fig. 4 is shown the locus of the points of minimum cost; thus for any given feed the cutting speed for minimum cost can be read off easily. As has been pointed out, there is no absolute minimum of C_p as a function of f and V but in the range covered by Fig. 4 the lowest cost is at $f = 0.05$ ipr and $V = 1400$ ipm. If we call this C_p', then all combinations of f and V which will give costs, some given percentage above C_p', must satisfy an equation of the form

$$0.05 + \frac{2.83}{fV} + \frac{f^{1.8}}{522}\left(\frac{v}{163.8}\right)^7 = \mu C_p', \quad (\mu > 1) \ldots [26]$$

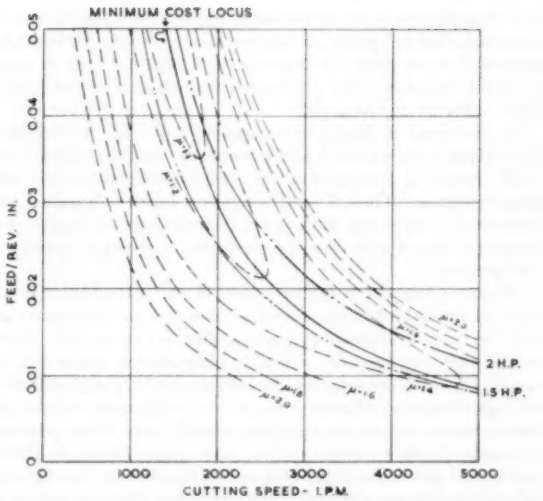

Fig. 4 Relationship between cost/piece, feed, and cutting speed. Broken lines are loci of equal cost (expressed as multiples of C_p'). Chain lines are loci of constant power.

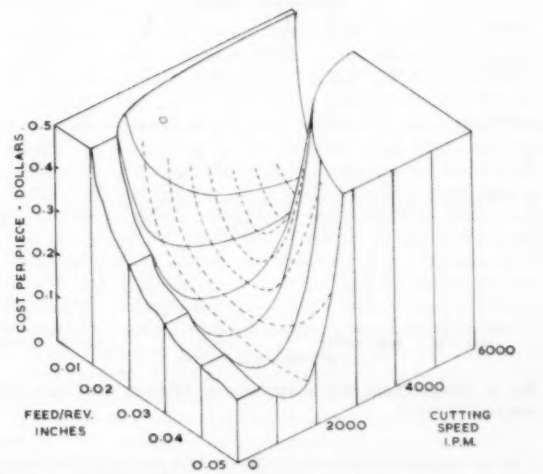

Fig. 5 Three-dimensional plot of relationship between cost/piece, feed, and cutting speed. Full lines are curves at constant feed rate and broken lines are curves at constant speed.

In Fig. 4 are shown constant-cost loci for $\mu = 1.1$, 1.2, 1.4, 1.6, 1.8, and 2.0 (i.e., 10, 20, 40, 60, 80, and 100 per cent above C_p'). These do give some indication of how critical, or otherwise, is the selection of speeds and feeds and incidentally show how the "valley" of the minimum cost rises toward the lower feeds. This valley is seen in the three-dimensional representation of Fig. 5 but the rise in the valley is too gradual to be apparent in a pseudo-perspective view. Fig. 4 is essentially a plan view of Fig. 5.

A point of great practical importance is whether the machine has sufficient power to enable minimum cost conditions to be realized. To assist in answering this, curves of constant horsepower have been added. [Horsepower at the tool tip has been used to avoid introducing the (variable) efficiency of the machine.]

The diagram is now in a fairly complete form inasmuch as one can select a feed and cutting speed to achieve either the best re-

sult or the nearest to it. However, in application it has the serious drawback that it applies to only one depth of cut. It would be preferable to sacrifice the trajectories of constant cost in order to be able to indicate the various loci of minimum cost corresponding to different depths of cut.

At this point it should be recognized that Figs. 3 through 5 have given some insight into the complex cost relationships but would involve a great deal of very tedious calculation work and graph plotting. Thus, if some alteration which will reduce the amount of preparation work is not forthcoming, the analysis remains of interest only from the viewpoint of giving an insight of the problem.

However, any curve can be replotted as a straight line if the axes are subdivided in the correct manner and in the present case it is fortunate that the most important loci are power laws, which means that commercially available bilogarithmic paper can be used. Fig. 6 shows much of the information of Fig. 4 replotted on logarithmic co-ordinates. The locus of minimum cost and the loci of constant horsepower are now straight lines; the trajectories of constant cost, however, are still curved since Equation [26] is not a pure power law, but as the curves recede from their turning points they become effectively straight and of slope -1 (see $\mu = 1.4$ and 1.6 trajectories in Fig. 6) due to the predominant effect of one term.

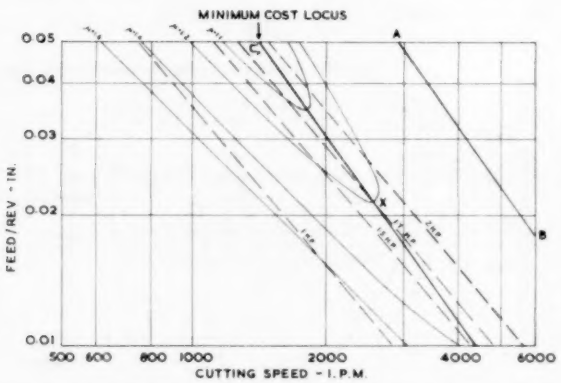

Fig. 6 Bilogarithmic plot of relationship between cost/piece, feed, and cutting speed

In the comments made on Witthoff's first paper, another aspect of the problem was mentioned but deferred until later. It is now convenient to refer to this, making reference to Fig. 6. Consider a lathe having 1.7 hp at the tool tip; up to the point X the power line lies to the right of the minimum cost line and hence a speed can be selected to give minimum cost at that feed. Above X there is insufficient power to achieve minimum cost for a given feed so that the question arises "is there any point in increasing the feed beyond this critical value?" Fig. 6 shows clearly that the answer is "yes," this hinging upon one point; viz., that the horsepower line has a steeper slope than the constant-cost trajectories. Hence as one proceeds along a constant power line towards higher feed rates the cost is steadily decreasing although, from point X upward, the minimum cost for a given feed can never be achieved; indeed if one tried to achieve minimum cost conditions under such circumstances a self-inconsistent result would be obtained. It is felt that Witthoff's treatment did not clarify this point.

Had the machine in question had 2 hp at the tool tip then, up to the limiting feed shown, minimum cost conditions could have been achieved at any feed while for 1.5 hp at the tool tip, the limiting conditions throughout would have been power. The problem is thus more complex than has been indicated in the previous literature and there are two zones (a) where minimum cost conditions can be realized, and (b) where power is the limiting factor.

Effect of d. The effect of depth of cut may be considered as follows. Two questions need answering: (a) Whether to take the depth in one cut or more; (b) for more than one cut whether to take the cuts in equal amounts or not? Considering the first question we have, using Equation [22], the cost/piece using only one cut

$$C_{p1} = R_1 t_1 + R_1 \frac{L\pi D}{fV} + \frac{L\pi D}{fV}\left(\frac{V}{\lambda/W_0^n}\right)^{1/n} f^\alpha d^\beta B \ldots [27]$$

Remembering, that with two cuts, the time taken per piece is doubled, the cost per piece for two cuts is

$$C_{p2} = R_1 t_1 + 2R_1 \frac{L\pi D}{fV} + \frac{2L\pi D}{fV}\left(\frac{V}{\lambda/W_0^n}\right)^{1/n} f^\alpha \left(\frac{d}{2}\right)^\beta B \ldots [28]$$

The boundary dividing the zones where these two desiderata represent the minimum cost is given by equating the right-hand sides of Equations [27] and [28]; i.e.

$$R_1 = \left(\frac{V}{\lambda/W_0^n}\right)^{1/n} f^\alpha d^\beta (1 - 2^{1-\beta}) B \ldots\ldots\ldots [29]$$

For the data of the Appendix this reduces to

$$\left(\frac{V}{163.8}\right)^8 f^{3.6} = 545 \ldots\ldots\ldots\ldots\ldots [30]$$

This line is the one marked AB in Fig. 6 and it will be seen that the region covered by the previous discussion is well inside the zone where one cut is more economical. Thus the second question posed in the foregoing need not be considered here; the use, in practice, of roughing and finishing cuts is largely a matter of securing dimensional accuracy.

Conclusions and Suggestions for Application

1 It has been shown that there is an optimum amount of wear for minimum cost but the analysis has drawn attention to the need for much more information on many aspects of this relationship.

2 The question of the number of cuts has been discussed and this left the general problem of C_p as a function of feed and cutting speed. Dependent on the power available, minimum cost conditions might, or might not, be attainable but it was true to say that, if they were not attainable, then the heaviest feed would give the lowest cost.

3 The analysis is not without its cross currents; for example, an additional overriding criterion of surface roughness may be present, the fact that continuously variable feeds and speeds (easily attainable in a mathematical analysis) do not obtain in general practice, and so forth. It is, as already stated, axiomatic that the more variables one wishes to include, the less hope there is of any easy scheme of application but the following suggestions are offered in the light of the analysis given:

(a) Bilogarithmic graph paper may be used for a general feed-speed chart, similar to Fig. 6, or if the chart is for a given machine a tracing may be made showing only the feeds available on that machine.

(b) Using available or acquired tool-life data, lines of minimum cost for various relevant depths of cut may be added.

(c) Using data on hp/cu in/min and the (power law) correction factors for depth of cut and feed, suitable horsepower lines may be added (a chart for a specific machine would have only one hp line per depth of cut.)

(*d*) If desired, the horizontal axis, being logarithmically divided, may be used as one line of a nomogram, the other two lines for spindle speed and workpiece diameter being added below as horizontal lines suitably divided (again for a specific machine, only the spindle speeds available would be graduated).

It is realized that when all this has been done, the chart is still only valid for one material but it is felt that much of the information available would often be more useful in the form of such a chart than as tool-life data where economic considerations are not evident, although it is recognized that not all machining is governed by economic considerations. It is hoped, however, that the analysis has clarified some aspects of the problem. As the point does not seem to have been mentioned specifically before, it is as well to add that the conditions for minimum cost need not coincide with those which enable the operator to make his greatest wage and thus some attention would need to be given to bonus and incentive schemes.

Finally, the treatment could be modified a little to consider the maximum production rate instead of minimum cost, the optimum speed for maximum production rate being rather higher than that for minimum cost.

Bibliography

1 "Die wirtschaftliche Schnittgeschwindigkeit," by W. Leyensetter, *AWF Mitteilungen*, vol. 15, no. 4, 1933.

2 "Kennzeichen und Bestimmung der wirtschaftlichen Schnittgeschwindigkeit," by J. Paasche, *AWF Mitteilungen*, vol. 15, no. 6, 1933.

3 "Beitrag zur Frage der wirtschaftlichen Schnittgeschwindigkeit," by A. Wallichs and H. Schöpke, *AWF Mitteilungen*, vol. 15, no. 7, 1933.

4 "Iz Teorije Rezanja i Obradivanja Metalnog Materijala," by M. Škrgatić, *Tehnički Progled*, vol. 5, no. 3, 1953, p. 107.

5 "Die rechnerische Ermittlung der günstigsten Arbeitsbedingungen bei der spanabhebenden Formung," by J. Witthoff, *Werkstatt und Betrieb*, vol. 80, 1947, p. 77.

6 "Ermittlung und betriebswirtschaftliche Bedeutung der Werkzeugkosten," by J. Witthoff, *Werkstattstechnik und Maschinenbau*, vol. 39, 1949, pp. 148 and 179.

7 "Die Ermittlung der günstigsten Arbeitsbedingungen bei der spanabhebenden Formgebung," by J. Witthoff, *Werkstatt und Betrieb*, vol. 85, 1952, p. 521.

8 "A Study of Cutting Speed for Maximum Production Rate," by A. Atalay, thesis for MS degree, University of Michigan, Ann Arbor, Mich., 1948.

9 "The Economics of Metal Cutting," by W. W. Gilbert, ASME Manual on Cutting of Metals, second edition, 1952, p. 313.

10 "The Economics of Machining," by W. W. Gilbert, in "Machining—Theory and Practice," American Society for Metals—31st National Metal Congress.

11 "The Economics of Machining Operations," by J. M. Lickley and A. J. Chisholm, *Machinery* (London), vol. 75, 1949, p. 673.

12 "Usinabilité des Métaux et Usure des Outils," reproduced (from notes taken during a lecture by M. C. Shaw at Liège) in Revue Universelle des Mines, April, 1953, p. 159.

13 "Wear of Carbide Tools," by A. J. Pekelharing and R. A. Schurmann, *The Tool Engineer*, October, 1953, p. 51.

14 "Der heutige Stand der Zerspanungsforschung," by E. Bickel, *Schweizer Archiv für angewandte Wissenschaft und Technik*, vol. 19, 1953, p. 105.

15 "On the Wear of Cutting Tools," by M. C. Shaw and S. O. Dirke, *Microtecnic* (English edition), vol. 10, 1956, p. 187.

16 "Das Standzeitkriterium in kostenmässiger Betrachtung," by H. J. Burmester, *Werkstatt und Betrieb*, vol. 84, 1951, p. 512.

APPENDIX

Numerical Data for Setup Considered in Body of Paper. A turning operation on a nickel-chrome steel 3 in. diam, 6 in. long; tool material, cemented carbide. Tool life relationship

$$T = \left(\frac{163.8}{V}\right)^8 \frac{W}{d^{3.06} f^{0.6}} \qquad (V \text{ in in. per min})$$

Cost ratios: $R_1 = 0.05$ dollars/min, $R_2 = 0.2$ dollars/regrind, $R_3 = 16$ dollars/in.

Idle time:

Loading, min	0.63
Approach, etc., min	0.05
Engage feed, min	0.02
Remainder reduced to a time/piece, min	0.30
Total, min =	1.00

Tool costs: $t_0 = 5$ dollars; $t_f = 0$

Tool grinding data: $A = 0.008$ in. $\Delta = 0.2$ in.

Premature failure data: $u = 1600\ W^{2.78}$

Discussion

B. N. Colding.[4] The author is to be commended for an interesting contribution to an extremely important subject.

Although the particular economic machining problem with which the author deals was first considered (as far as is known to the writer) as early as 1929 by Forsberg (1),[5] no one has solved this problem satisfactorily. The reason lies probably in the fact that tool life is generally studied at only a few different feeds chosen within a rather narrow feed range. The generalized tool-life equation obtained is therefore too uncertain to enable one to state a certain optimum of cutting data with certainty. Unfortunately this is often done.

Witthoff's cost Equation [1] in this paper yields the commonly recognized economic tool life Equation [3]. Forsberg's economic tool-life equation established in 1929 was indeed Equation [3], but it was derived considering the maximum production rate. The author's main conclusion, "The heaviest feed would give the lowest cost" agrees well with that of Svahn (2), who states that in rough milling "choose as heavy feed per tooth as possible in regard to tensile strength of the tooth and a relatively low cutting speed suitable to it." However, it will be shown that the economic optimum of cutting variables may be a combination of feed and cutting speed available on standard machine tools. For other types of material the heaviest feed and depth of cut should be chosen. The final result depends on the validity of the approximation made in the use of a generalized equation of this type $VT^n f^a d^b = \text{const}$. There are at least three limiting factors involved when using the foregoing equation: (*a*) The Taylor exponent n varies in practical cases with feed f and depth of cut d. (*b*) When tool life T is plotted on logarithmic co-ordinates for a constant speed, V versus f or d, the resulting function is better approximated by a curve than by a straight line. (*c*) Log T versus log V or log T versus log f (or d) can only be regarded as a good straight-line approximation within certain limiting feeds or speeds. The two first mentioned causes of uncertainty will be included in the first of the two examples to be given while the third cause is considered in the second example.

The author's cost expression Equation [22] is rewritten in the following form:

$$C_p = R_1 \left[t_l + t_c \left(1 + \frac{B}{T} \right) \right] \qquad [22a]$$

where

$$t_c = \frac{L\pi D}{fV}$$

[4] Research Supervisor, Department of Physical Research, Cincinnati Milling Machine Company, Cincinnati, Ohio.

[5] Numbers in parentheses refer to the Bibliography at the end of this discussion.

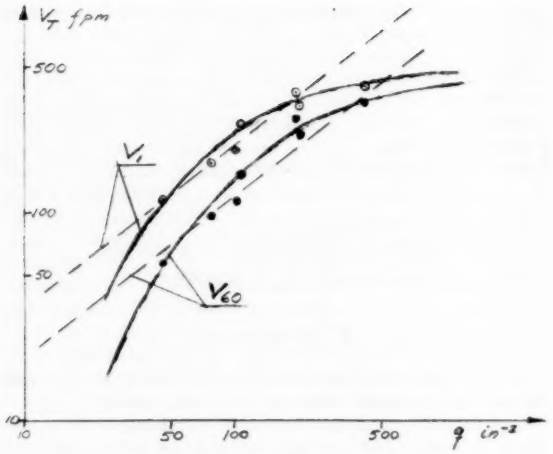

Fig. 7(*a*)

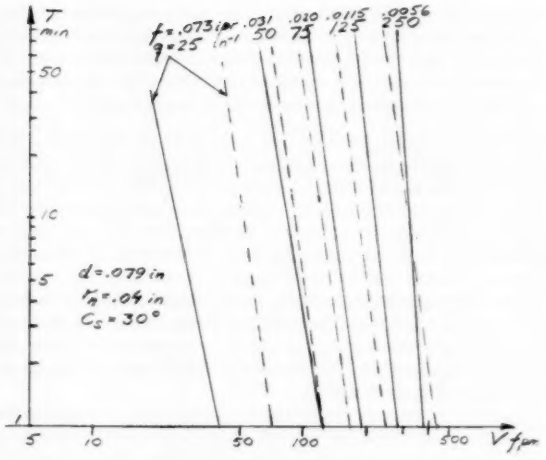

Fig. 7(*b*)

However, defining the material to be taken off more generally, one can also write

$$L\pi Dd = \Delta \quad [31]$$

where

Δ = volume to be removed per part
d = depth of cut

Hence

$$t_c = \frac{\Delta}{fdV} \quad [32]$$

$$C_p = R_1\left[t_1 + \frac{\Delta}{fdV}\left(1 + \frac{B}{T}\right)\right] \quad [22b]$$

From Equation [31] it is seen that $(L\pi D)$ is also a function of the depth of cut d, a fact which should be kept in mind when differentiating Equation [22*a*] with respect to d.

An expression similar to that given by Equation [22*b*] but which is valid for maximum production is readily shown to be

$$t_{avg} = t_1 + \frac{\Delta}{fdV}\left(1 + \frac{t_{tc}}{T}\right) \quad [33]$$

where t_{avg} is the average time to produce a part and t_{tc} is the tool changing time.

From the similarity of Equations [22*b*] and [33] it appears that the following function should be considered in an economic analysis

$$F = Vfd\,\frac{T}{T + B} \quad [34]$$

where $B = t_{tc}$ in the case of maximum production.

The function F may be called the "productivity function," a maximum of which will yield a minimum cost or a minimum time to produce one part.

An easy and illustrative way of investigating extreme values of F without having to refer to an approximate equation of the form $VT^nf^cd^b$ = const will be illustrated in the first example, for which tool-life data from Svahn (2) are given in Fig. 7(*a*) where V_1 and V_{60} are plotted against the chip equivalent, q, on bilogarithmic paper. The chip equivalent q introduced by Woxén (3) in 1931 is defined in Fig. 8 where it is seen that q is a function

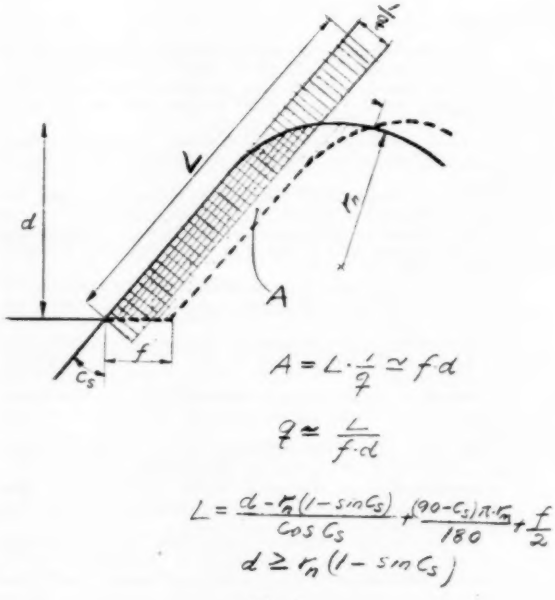

Fig. 8

of depth of cut, feed, nose radius, and side cutting-edge angle. In the present example the only variable is feed. In orthogonal cutting q is simply the inverse value of the feed. The advantage of using the q-value in an economic analysis is evident as it includes feed, depth of cut, nose radius, and side cutting-edge angle in one, single variable.

The difference between a straight-line approximation (dashed lines) and the curve approximation (solid lines) is seen in Fig. 7(*a*) and also in Fig. 7(*b*) where tool life is plotted against cutting speed for different values of chip equivalent ($\sim$ inverse value of feed). The dashed lines have a constant Taylor exponent n in analogy with the relation $VT^nf^cd^b$ = const. From these figures and from Equation [3] the particular economic tool life for each q-value is readily obtained. The corresponding values of V are found by means of Fig. 7(*b*). Introducing the simultaneous values

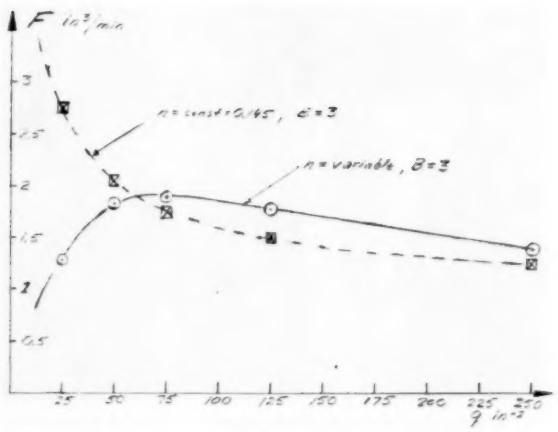

Fig. 9

into Equation [34] yields the two curves given in Fig. 9, where the productivity function, F, is plotted versus q for the case $B = t_{in} = 3$ min. The dashed curve, corresponding to the case where n was constant, does not appear to have any maximum for practical values of q (or f). This would indicate the use of the heaviest feed possible, but the "true" F-q curve which is based on the solid curves in Fig. 7 yields a maximum for a value of $q = 70$ in.$^{-1}$ corresponding to a feed of $f = 0.020$ in. per revolution (ipr).

This example shows the extreme importance of having an accurate tool-life equation which takes into account the variation n with feed and depth of cut (= chip equivalent). The problem illustrated also suggests the practical procedure in establishing tool-life relations for economic considerations; namely to run tests for at least three feeds which have to be of considerably different magnitude; e.g., $f = 0.040$ in., 0.020 in., and 0.005 ipr for $d = 0.10$ in. Notice that in general a different economic tool life is obtained for each q.

Typical tool-life data covering a large range of machining data may be illustrated by Schicharen's (4) ceramic tool-life studies in Fig. 10. In Fig. 10(a) tool-life is plotted against speed while against feed in Fig. 10(b) and against depth of cut in Fig. 10(c). Two straight lines of different slope are drawn in each of Figs. 10(b and c) in order to illustrate the fallacy in basing economic solutions on approximate relations within narrow ranges of feed and depth of cut. The solid curve in Fig. 10(a) is an ellipse which fits the data rather well. The right-hand portion of the ellipse up to the maximum tool life is of importance in an economic study. An analysis of these data also reveals that there exists an optimum combination of feed, depth of cut, and cutting speed for this tool material and work material.

As these results are in disagreement with the author's statement, it would be of great interest to the writer to be able to check the author's tool-life data (if they are available) using the method applied in the foregoing. However, the writer (5) has shown that there exists a relationship between V, q, and T which is a better approximation than $VT^nf^ad^b$ = const. Using this relationship and the productivity function F he shows that either the feed should be as heavy as possible or a particular combination of cutting variables would determine machining economics.

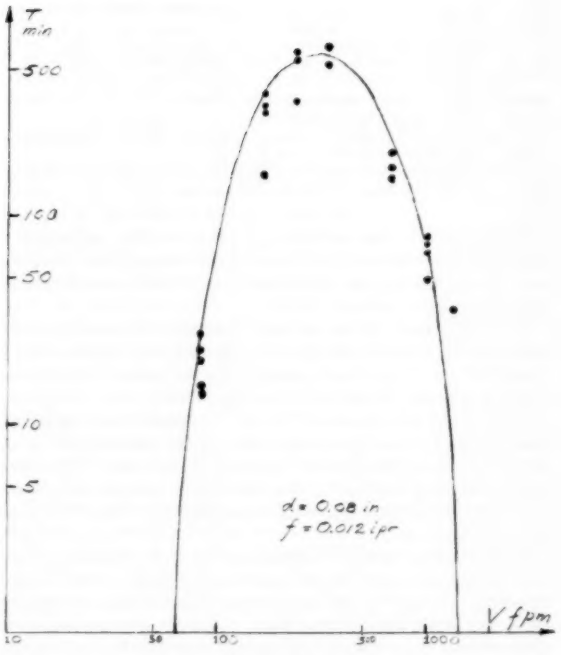

Fig. 10(a)

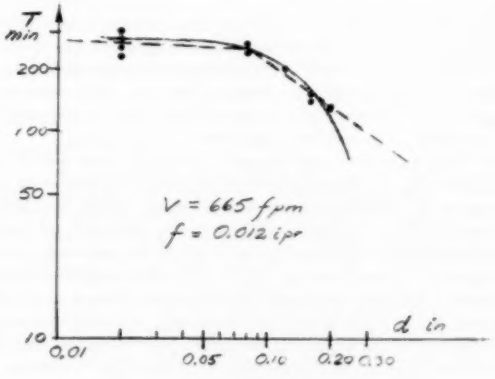

Fig. 10(b)

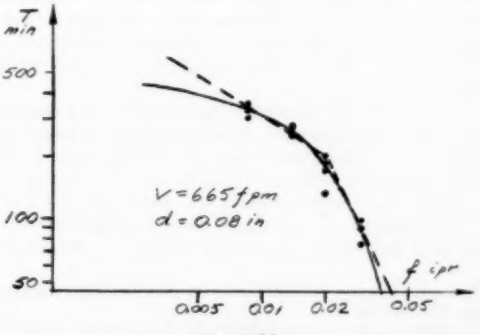

Fig. 10(c)

Bibliography

1 "Investigations as to Cutting Speeds for Swedish Materials," by E. A. Forsberg, *Ingeniörs Vetenskaps Akademien*, Handlingar No. 95, Stockholm, Sweden, 1929, 108 pp. (in English).

2 "Machining Properties and Wear of Milling Cutters," by O.

Svahn, Kungl. Tekniska Hogskolans, Avhandling No. 55, Stockholm, Sweden, 1948, 104 pp. (in English).

3 "A Theory and an Equation for the Life of Lathe Tools," by R. Woxén, Kungl. Tekniska Hogskolans, Stockholm, Sweden, 1932.

"Tool-Life and Balance of Heat in Lathe Work," by R. Woxén, *Ingeniörs Vetenskaps Akademien*, Handlingar No. 42, Stockholm, Sweden, 1937, 39 pp. (in English).

4 "The Use of Ceramic Tools in Machining," by V. I. Schicharen, *Stanki i Instrument* (Moscow), No. 2, 1956.

5 "A Three Dimensional Tool-Life Equation. Machining Economics," by B. Colding. To be published.

V. Šolaja.[6] In the writer's opinion this paper represents a valuable contribution to the subject. However, the following comments, although they do not contradict the main conclusions drawn, may be of interest:

1 Usually tool life is expressed as the time to destruction of the tool, and it is directly related only to the planning of tool change. From the point of view of productivity (including over-all economical aspects), volume of chips produced in unit of time in roughing, and area generated in unit of time in finishing operations, related in an appropriate way to the rate of tool wear, appear to be of a far greater practical importance. Therefore without altering the basic treatment, certain changes may be introduced into the proposed expressions and these may be of considerable interest.

2 In dealing with tool regrinding, the author takes into account tool-flank wear W. Most research papers on wear of the clearance face of the tools, including also some national standards, relate to a mean value of wear land. Consequently, the quantitative recommendations are not usually based on the maximum value of W which determines the reconditioning of the tool. The phenomenon of the concentrated tool wear in the form of grooves localized at the boundaries of the areas of contact between rake face and chip and between clearance face and workpiece was noticed and described earlier; e.g., references (1–6)[7] and it has been shown recently (7) that under some circumstances the mean value of wear land may account for only 25 per cent of the length of the grooves. The accompanying microphotograph, Fig. 11, resulting from this work may illustrate this point.

3 The depth of crater formed on the rake face is of a much smaller order of magnitude than the width of the wear land. However, in reconditioning tools it is usually necessary to remove all wear marks, and consequently grinding of both faces, or more grinding of only one face, e.g., rake face in the case of form tools, is required. Thus Equation [12*a*] of the paper has to be modified slightly. Roughly speaking, only less than 15 per cent of the volume of a tool tip is worn off in cutting, whereas more than 70 per cent is lost in regrinding, the remainder being the rest of the tip which has to be discarded. Therefore the technical and economical importance of the optimum initial tool shape, and of the best method of reconditioning may be appreciated. According to work by Weber (8), crater wear can be expressed in terms of cutting ratio and workpiece material. It appears that some relationship between the wear on both faces may be found, which would facilitate the analytical handling in the author's treatment.

4 The inclusion of premature tool failure is of a considerable value. However, it appears that more practical information is needed to prove the quantitative relationships derived from the work by Burmester (reference 16 in the paper). In this connection, it may be of interest to refer to a recent paper by Reznikov (9). In this paper the conclusions are not definite also but, being based on a considerable amount of practical results obtained in mass production of ball bearings, they may contribute toward clarifying this important aspect.

5 The author correctly asserts that, in fine turning, surface finish is the main criterion of machining. From recent work (10) it may be seen that the pattern of tool wear shown in Fig. 11 of this discussion, i.e., the length of grooves and the width of wear land, is directly related to surface finish. It is interesting to mention here that the surface finish in finish turning may be expressed as $h_{CLA} = k(r/f^2)^n$, where h_{CLA} = center-line-average roughness, r = tool-nose radius, f = tool-feed, while k and n are functions of various cutting factors (cutting speed, workpiece material, condition of the machine, cutting with or without coolant, and so on), as well as of the length of cutting or time of cutting. As an example, Fig. 12 shows the h_{CLA}-values obtained in a series of experiments, plotted against r/f^2 for five values of L and W_{max}. For the experimental conditions employed n varies from $n = -0.83$ for $L \simeq 0$ ft, to $n = -0.23$ for $L = 8500$ ft, and k decreases from $k = 10{,}700$ for $L \simeq 0$ ft, to $k = 600$ for $L = 700$ ft, after which it increases slightly. It has been concluded that

Fig. 11 Clearance face of a carbide-tipped tool showing concentrated wear when 0.35 per cent C steel is finish turned and after the length of cutting $L = 8500$ ft; $r = 0.019$ in., $\alpha = 0$ deg, $\gamma = 8$ deg, $f = 0.0065$ ipr, $v = 900$ fpm. Direction of cutting from left to right. Photographed on a Vickers microscope, $\times 180$.

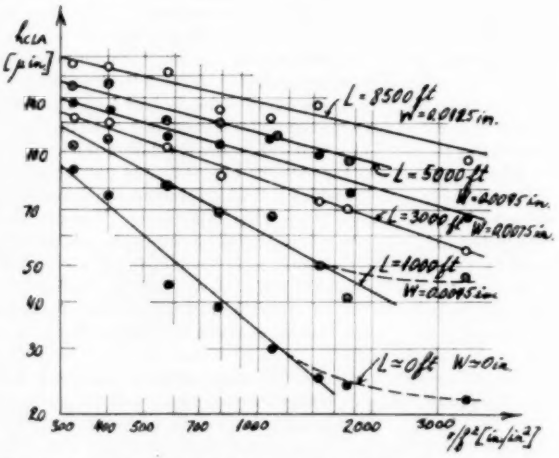

Fig. 12 h_{CLA}-values obtained in series of experiments with varying feed as dependent on the variable r/f^2 for five different lengths of cutting L and maximum values of wear-land W (10). Worn tool for $r/f^2 \simeq 400$ is shown in Fig. 11.

[6] Lecturer, Faculty of Mechanical Engineering, University of Belgrade, Yugoslavia.

[7] Numbers in parentheses refer to the Bibliography at the end of this discussion.

the surface finish generated is a function of the length of cutting, time of cutting, and tool wear, and, consequently, it appears that, in the author's analysis of the economics of the turning operation, fine finish turning also may be approached in the same manner as rough turning.

Bibliography

1 "An Account of Some Experiments on the Action of Cutting Tools," by E. G. Coker and K. C. Chakko, discussion by R. E. B. Crompton, *Proc. of The Institution of Mechanical Engineers*, vol. 1, 1922, p. 567.

2 "Wear of Carbide Tools," by A. I. Pekelharing and R. A. Schurmann, *Tool Engineering*, vol. 3, no. 4, 1953, p. 51.

3 "Some Remarks Regarding Wear on the Flanks of Carbide Cutting Tools," by L. H. Hovenkamp and E. van Emden, *Microtecnic*, vol. 7, 1953, p. 116.

4 "An Explanation of Tool Wear," by P. Albrecht, *Microtecnic*, vol. 10, 1956, p. 145.

5 "Measuring Chip-Deformation and Wear-Land on Clearance Face in Fine Turning With Carbide Tools," by W. Leyensetter, *Zeitschrift des Vereines Deutscher Ingenieure*, vol. 10, 1956, p. 187 (in German).

6 "On the Wear of Cutting Tools," by M. C. Shaw and S. O. Dirke, *Microtecnic*, vol. 10, 1956, p. 187.

7 "Concentrated Wear of Turning Tools," by V. Šolaja, *Research (London)*, vol. 11, 1958, p. 11.

8 "A Contribution to the Analysis of Tool-life," by G. Weber, *Industrie-Anzeiger*, vol. 77, 1955, p. 237 (in German).

9 "Evaluation of the Working Characteristics of Carbide-tools According to the Wear-Rate of the Cutting Edge," by A. N. Reznikov, *Vestnik mashinostr.*, vol. 36, 1956, No. 7, p. 39 (in Russian).

10 "Wear of Carbide Tools and Surface Finish Generated in Finish Turning of Steel," by V. Šolaja, 1957, sent for consideration to The Institution of Mechanical Engineers, London, England.

Author's Closure

The author thanks the discussers for their kind remarks about the paper.

Mr. Colding gives three factors which, he thinks, limit the use of the generalized tool life equation $VT^n f^a d^b$ = constant. The first of these is that n is not constant but a function of feed and depth of cut. The data available are probably not sufficient to enable this statement to be made with a high confidence level but, if it be true, then only a revision of the analysis from Equation [7] onward can really rectify the deficiencies; Mr. Colding's Equation [22*b*] has expressed the tool life simply as T and not in the parametric form of Equation [7]. However, although this produces a neat equation, T must still be related to V either simply, for constant values of f and d, or in a more complex parametric form, of which the author's Equation [7] is one example; a symbolic form of the data presented in Mr. Colding's graphs could be another form.

An objective glance at Fig. 7(*a*) will show that, for both the V_1 and the V_{60} curves, there is only one point which suggests that the full lines are a better correlation than the dashed lines. It is felt that much more evidence than Fig. 7(*a*) is needed before a decision can be made either way. Also, there is no information on how q varied. This is of importance because, if the feed or depth of cut were varied, Equation [7] would not lead one to expect a single straight line in any event.

The other two factors which Mr. Colding mentions reduce, in effect, to one consideration. It is generally conceded that a straight line log-log law relating either V, f, or d to T is not true over the complete range of variables; Mr. Colding suggests that a straight line is never the best approximation and reproduces a graph of Zhikharev's (Fig. 10) in which he (Mr. Colding) has added an ellipse as the best approximation. This illustration appears to be the same as one used by the author on a previous occasion (1).[6] The curve drawn by the author is better to the extent that it does not involve any question of interpreting the infinite slope of the ellipse at about 1500 fpm. In the article quoted (1) the author draws a straight line for the right-hand half of Mr. Colding's ellipse and would stress the presence of a fair degree of scatter in Zhikharev's results.

The left-hand side of the ellipse is, in the case of ceramics, due to crumbling of the cutting edge and has been discussed by the author elsewhere (2). In this closure, the author restricts himself to pointing out that, whether the left-hand side is an ellipse or not, it has definitely a positive slope and will only serve to make costs at lower speeds even higher than predicted by the analysis given in the paper.

The suggestions offered by Mr. Colding and Mr. Šolaja are valuable contributions to the theory of machining economics and it is hoped that, in time, a more refined theory will be advanced and that interest, of an intensity exhibited in fundamental machining work, will be applied to the economic aspects of machining.

Bibliography

1 "An Appraisal of Ceramic Cutting Tools," by R. C. Brewer, *The Engineers' Digest*, vol. XVIII, no. 9, 1957, pp. 381–418.

2 "Turning With Ceramic and Sintered Oxide Tools," by R. C. Brewer, Paper No. 24 read at the Conference on the Technology of Engineering Manufacture, The Institution of Mechanical Engineers, London, England, March, 1958.

[6] Numbers in parentheses refer to the Bibliography at the end of the author's closure.

Oil-Whip Resonance

By E. H. HULL,[1] SCHENECTADY, N. Y.

A series of oil-whip resonances has been demonstrated by applying a rotating force to a shaft running in a hydrodynamically lubricated bearing. These resonances appear at the ratios of shaft speed to exciting-force frequency of approximately 2 which is normal oil whip, 3, 4, 6, 8 . . . . and −2, −4, −6 . . . . The locus of the shaft center at these resonances traces a trochoid containing a number of loops related to the ratio of shaft speed and force frequency. Inside loops are formed at positive frequency ratios, outside loops at negative ratios. A qualitative explanation of the formation of these resonance figures is offered.

Introduction

Oil whip occurs commonly in lightly loaded[2] fluid-film bearings. Hydrodynamic forces in the oil film cause a circular motion of the shaft center at $^1/_2$ shaft running speed (or slightly less than $^1/_2$ shaft speed under most practical conditions) and in the direction of shaft rotation. A more vigorous form of this phenomenon is observed when oil-whip frequency coincides with a shaft critical speed. This disturbance starts when the shaft is turning at approximately twice its critical speed and builds up in amplitude at higher speeds. The oil-whip condition allows large displacements of the journal in its bearing clearance which build up larger amplitudes in the shaft span at its resonant frequency. This doubly resonant phenomenon may be called critical-speed oil whip.

Oil whip was described quite completely by Newkirk and Taylor (1)[3] in 1925. These authors recorded the several forms in which this phenomenon appears as well as a nearly complete list of palliatives. Since that time, the resonant nature of oil whip has been realized; i.e., the capacity of a bearing to carry load is small when the load rotates at $^1/_2$ journal speed and in the direction of journal rotation. As in other forms of resonance, a small force causes a disproportionately large displacement.

This paper will describe a series of oil-whip resonances occurring at a number of ratios of shaft speed to exciting-force frequency. These ratios may be either positive or negative. The frequency-ratio sign is assumed positive when both shaft and force vector rotate in the same direction and negative when rotating in opposite directions.

Oil Whip

There are several conventions for visualizing oil whip as a resonant phenomenon. A shaft, running in a hydrodynamically lubricated sleeve bearing, carrying a load which may rotate with respect to the shaft will show a load-carrying capacity about as depicted in Fig. 1 (2).

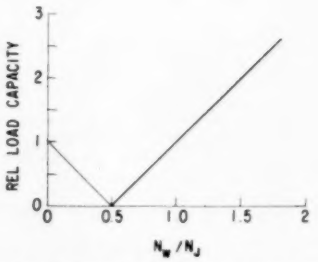

Fig. 1 Relative load-carrying capacity of a hydrodynamic bearing versus frequency ratio, load speed N_W over shaft speed N_J

Burwell (3) has suggested that we visualize the situation at the critical condition, $N_W/N_J = 0.5$, as follows: An observer stations himself at the bearing center O in Fig. 2. Additionally, the observer rotates at the load speed or $^1/_2$ shaft speed which allows him to look along the line OO' to the point of minimum oil-film thickness. Under these conditions he will see the shaft and bearing passing by at the speed $N/2$ and in opposite directions. Furthermore, our observer will see that there is no oil circulation past the point of minimum clearance. The oil pumped in by the shaft on one side of h_{min} will be removed by the bearing and conversely on the other side of h_{min}.

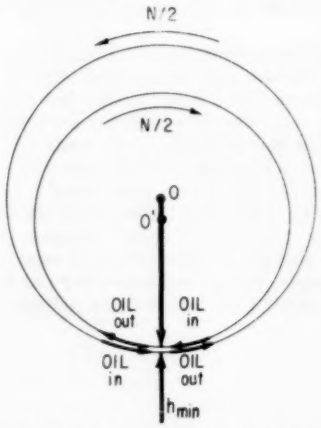

Fig. 2 Observer's view of a bearing in which load is rotating at $^1/_2$ journal speed. O is the bearing center, O' the shaft center, N equals journal speed, and h_{min} minimum oil-film thickness.

A journal-and-bearing combination which does not circulate oil past the point of minimum clearance will support very little load and none hydrodynamically. In this respect a speed ratio of $N_W/N_J = 0.5$ may be looked upon as a resonant condition in the bearing. A small load rotating at $^1/_2$ shaft speed will cause a greater displacement of the journal than the same load rotating at any other speed ratio with respect to the shaft. Furthermore, small changes in speed ratio cause relatively large changes in shaft displacement. Each of these effects is typical of a lightly damped resonant system. Thus normal oil whip may be considered as a form of resonance.

---

[1] Mechanical Engineer, Research Laboratory, General Electric Company, The Knolls. Mem. ASME.

[2] The bearing loading below which oil whip may occur varies with many factors. In the shaft and bearing combination used in the work reported here, oil whip has not been noted above 50 psi.

[3] Numbers in parentheses refer to the Bibliography at the end of the paper.

Contributed by the Lubrication Division and presented at the Annual Meeting, New York, N. Y., December 1–6, 1957, of The American Society of Mechanical Engineers.

Note: Statements and opinions advanced in papers are to be understood as individual expressions of their authors and not those of the Society. Manuscript received at ASME Headquarters, August 30, 1957. Paper No. 57—A-169.

Apparatus

For some time we have been studying the behavior of a shaft in a hydrodynamically lubricated bearing under the action of sinusoidal and nontransient forces. In the work reported here we have applied to the shaft a rotating radial force controllable in value, frequency, and direction of rotation as shown schematically in Fig. 3.

The apparatus itself has been complicated by additional requirements as indicated in Fig. 4, although the parts essential to the work reported here may be recognized. A test shaft 1 is driven by motor 2 through a step-up gear 3. This shaft is supported at its driven end by a pair of preloaded ball bearings 4 and at the near end by a test bearing, somewhat hidden at 5. The babbitted test bearing is 2 × 2 in., containing a central circumferential oil groove receiving oil at a few psi pressure. A radial clearance of 1.8 mils is allowed between the shaft and bearing.

The mechanism for applying a rotating load to the shaft appears in the foreground of Fig. 4. A load-driving motor 6 turns a two-output-shaft bevel-gear box 7. The vertical output shaft from this box drives a cam which oscillates the right-hand end of spring 8 by means of a suitable cam-follower mechanism. At its left end spring 8 bears against vertical lever 9 pivoted to the machine frame at its lower end and attached, near its upper end, to two bearing boxes 10 and 11 running on the test shaft at either side of the test bearing. A similar mechanism is operated by the horizontal output shaft of the bevel-gear box also terminating at the bearing boxes 10 and 11. By these means a sinusoidal displacement at the right end of spring 8 is translated into sinusoidal force on lever 9 and thence to a sinusoidal horizontal force on the test shaft via the bearings in 10 and 11. The companion mechanism produces a vertical sinusoidal force on 10 and 11. Since the vertical and horizontal cams are set 90 deg apart on their shafts, the horizontal force leads or lags (depending on the direction of cam rotation) the vertical force. The resultant of these two sinusoidal forces is a single force which may be represented by a fixed magnitude vector rotating about the shaft, Fig. 3. The speed and direction of rotation of this force vector may be varied by means of the driving motor 6. Bias springs 12 and 13 serve to center the rotating force.

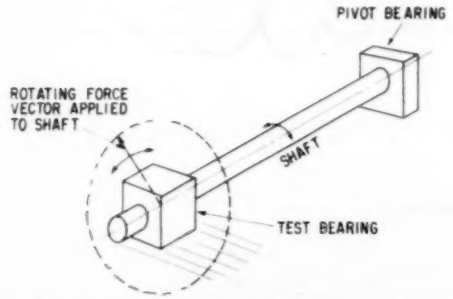

Fig. 3 Rotating force is applied to shaft at test-bearing center

The position of the test shaft with respect to the test bearing is measured continuously by means of two pairs of capacitance shoes supported from the test bearing. Two capacitance bridge circuits (one for the vertical pair of shoes and the other for the horizontal) lead through suitable electronics to a galvanometer oscillograph for recording, or a cathode-ray oscilloscope for observing, the locus of the test-shaft center with respect to the bearing.

Within the bearing boxes 10 and 11 are strain gages which measure the horizontal and vertical components of force applied to the shaft. Outputs of these gages are operated upon electronically for recording by the oscillograph.

Test-shaft speed and rotating-force-vector speed are detected magnetically for recording by the oscillograph or measuring to four figures on a digital counter.

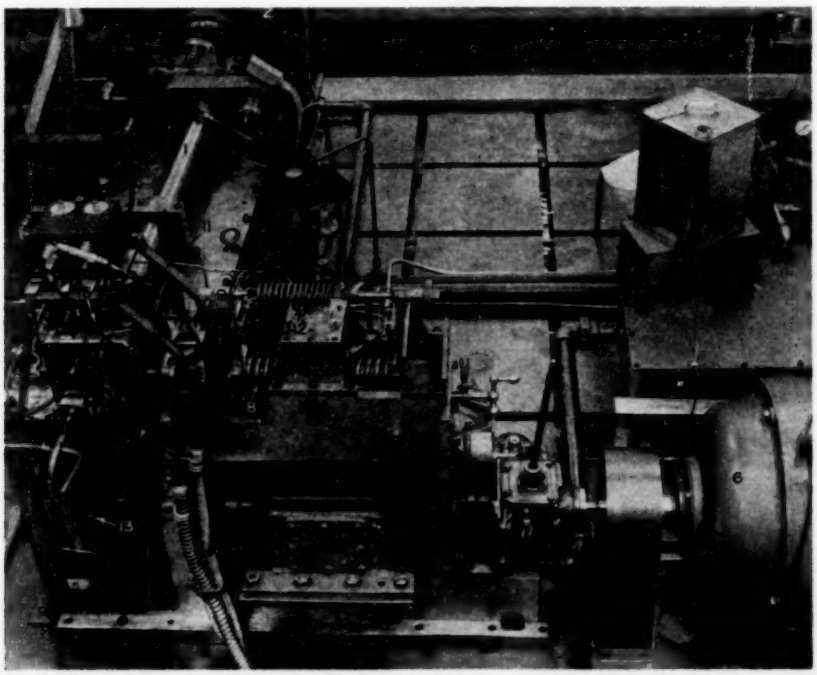

Fig. 4 General view of oil-whip apparatus

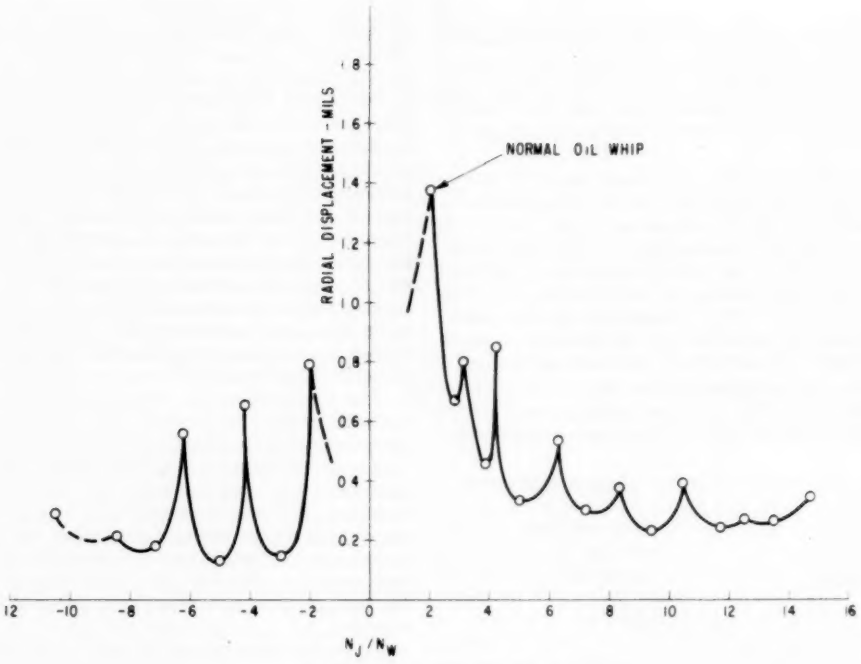

Fig. 5 Oil-whip resonance series

Experiments and Discussion

Using the apparatus just described, we find that when the shaft speed N_J is set at some constant value while the rotating speed of the force vector N_W is varied over a wide range, a series of oil-whip resonances appears as shown in Fig. 5. These resonances occur when the shaft and rotating force are turning in opposite directions as well as in the same direction.

At the ratio N_J/N_W of about $+2$ the locus of the shaft center in the bearing describes a nearly circular path as shown in Fig. 6. This is normal oil whip. As the ratio of shaft speed to rotating-force speed rises the number of loops in the shaft-locus figure at resonance increases as indicated at the upper right in Fig. 6. At positive ratios of N_J/N_W the figures traced out by the shaft center are epitrochoids. When this ratio becomes negative, hypotrochoids are formed as in lower left of Fig. 6.

The frequency ratio N_J/N_W and the number of loops formed are related linearly as shown in Fig. 6. A straight line passing through each resonant point is defined by the following relation

$$L = \frac{N_J/N_W}{2.16} - 1 \quad \ldots\ldots\ldots\ldots\ldots\ldots [1]$$

where L = number of loops in the shaft-locus figure. Inside loops are considered positive and outside negative.

When using this expression one must employ the appropriate sign for the speed ratio as well as for the loop number.

If one examines these figures carefully the resemblance to oil-whip resonance becomes more apparent. Take for instance the 4-loop epitrochoid formed at the speed ratio of approximately 10. We see that the shaft-center locus turns through 4 complete loops or 4 revolutions plus four 90-deg arcs or 1 revolution making a total of 5 revolutions while the shaft is rotating through 10 revolutions. This is the 2 to 1 frequency ratio obtained in oil whip. If we consider the 4-loop hypotrochoid formed at a frequency ratio of about -6 we will find that the shaft center locus

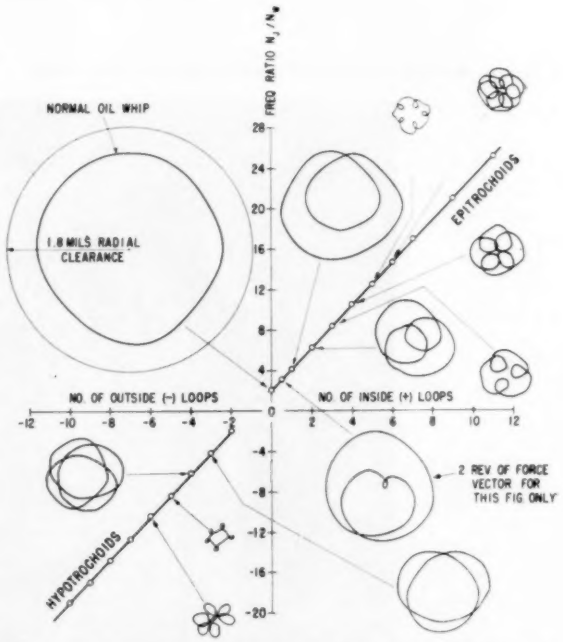

Fig. 6 Figures drawn by shaft center for various frequency ratios. Each figure is completed in one revolution of the force vector except for ratio +3.1 which requires two force-vector revolutions as explained in text.

completes 3 revolutions while the shaft is turning 6 times. The fact that the 4-loop shaft-locus figure is formed by only 3 turns

of the shaft center may be demonstrated by tracing the figure with a pencil. Starting at any point on the figure we find that our pencil passes through only 6 points of horizontal tangency or 3 complete revolutions before returning to the starting point. Again while the shaft is rotating through about 6 revolutions the shaft locus turns through 3 revolutions indicating oil whip.

In these figures, the locus of the shaft center moves in the same rotational sense as the shaft, independent of the direction of the force rotation.

One of the more interesting shaft-center-locus traces occurs at a frequency ratio of about +3. Applying Expression [1] to this ratio we find that there should appear a figure containing one half of a loop. This appears rather difficult but nature solved the problem by drawing the design shown in Fig. 6 in 2 revolutions of the force and 6 of the shaft, thus satisfying the required number of loops for this frequency ratio; i.e., $^1/_2$. All other figures shown were generated in one revolution of the force. As indicated in Fig. 5, the peak at the frequency ratio 3 is less marked than that at 2 or 4, suggesting a minor resonance in the series. Although we did not find similar resonances at 5, 7, 9 and so on, it is probable that they exist and can be identified with sufficiently accurate speed control, considerable patience, and sensitive instrumentation.

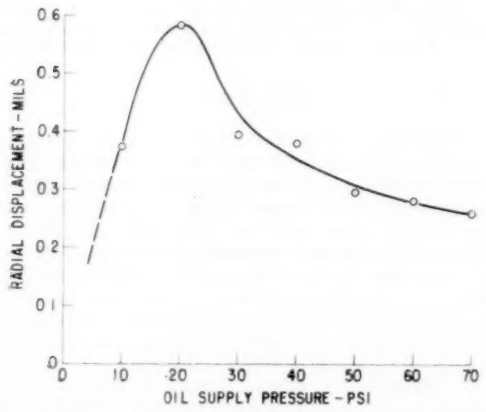

Fig. 7 Dependence of figure amplitude on bearing-oil-supply pressure for $N_J/N_W = +12.5$, giving a 5-loop epitrochoid

The effect of test-bearing oil-supply pressure on this form of oil whip was investigated. As indicated in Fig. 7, taken at a frequency ratio of +12.5, producing a 5-loop epitrochoid, the diameter of the figure maximizes at 20 psi bearing oil-supply pressure. The sharp downward slope of this curve at 10 psi suggests zero displacement at zero oil pressure, although we did not run the bearing without oil. Oil whip depends on a plentiful oil supply to the oil wedge which drives the journal around in its bearing. As the bearing oil supply is reduced, so will the driving force of the wedge until at zero oil supply there can be no oil whip. The dependence of this type of shaft perturbation on oil pressure indicates an oil-whip phenomenon.

A qualitative demonstration of the forces acting on the journal during the formation of a 2-loop epitrochoid indicates the mechanics of formation in these figures. Fig. 8 shows this epitrochoid redrawn with vectors representing forces acting on the journal center at four different positions of that center. Three forces operate on the journal:

1 Applied rotating force which is continuously measured and recorded during these experiments. This vector makes one complete revolution during the formation of Fig. 8. Its scalar value is 40 lb.

2 Oil-film restoring force. A journal running under load in a bearing assumes an attitude in that bearing such that the high-pressure oil wedge formed between the journal and bearing will support the applied load. This oil-film restoring force acts in a direction 85 to 90 deg from the line connecting the bearing center with the instantaneous journal center at the relatively high shaft speeds and small displacements pertaining in these experiments.

3 As the journal center moves in the bearing along the paths indicated, its motion is resisted by oil viscosity and by a small amount of damping from the associated apparatus which moves with the journal. The resultant force from these sources is represented by a vector opposing the direction of motion of the shaft center. Its scalar value is unknown but is assumed to be proportional to journal-center velocity. Since all forces between the shaft and the rotating force generating and transmitting mechanism are measured by the strain gages in the bearing boxes 10 and 11 (Fig. 4), the small amount of damping associated with the test apparatus is included in the applied rotating force (1, above). Thus the resistance vector shown in Fig. 8 includes the damping effect within the bearing only.

The resultant of these forces accelerates that part of the shaft mass and associated apparatus which can be considered as concentrated at the bearing center. After consideration of the weight concentrated at the journal center, its displacement and frequency of displacement, one may estimate the mass reaction force at about 5 lbs. This indicates that the resultant of the three applied vectors should be small.

Referring to point (1) of Fig. 8, the rotating force is shown at its measured value and direction. The oil restoring force is drawn in a direction and at a value which have been measured for this journal-bearing combination under nontransient conditions. An approximation of the viscous force is shown opposing the

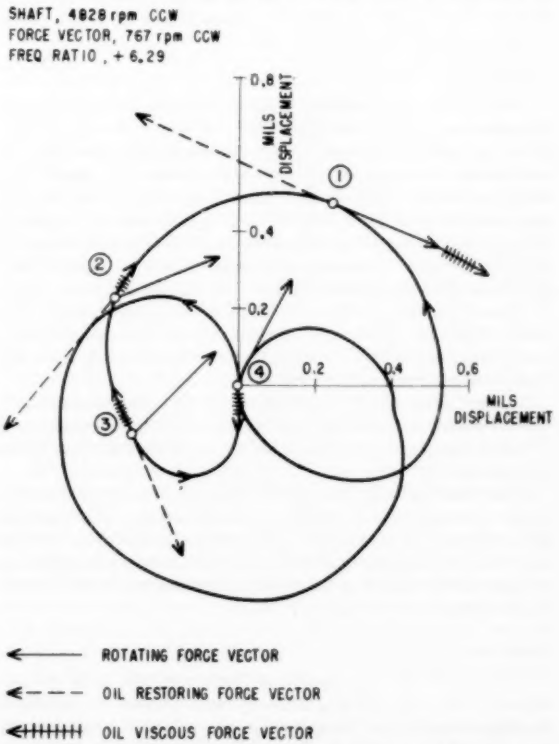

Fig. 8 Graphic representation of forces operating on journal center

motion of the journal center and proportional to the instantaneous velocity of that center. Vectors at points (2) and (3) were drawn in the same manner. At point (4) the oil restoring force vector is zero since the journal is momentarily centered in the bearing. One may see that at each of these points the resultant of these forces will urge the journal along the path which we have found it to follow under these conditions.

Returning to Expression [1] it will be noted that the experimentally obtained constant 2.16 is not an integral number. For our apparatus it is necessary to run the shaft about 8 per cent faster than the theoretical ratio 2 in order to obtain maximum displacements in the several figures. Since the energy necessary to maintain oil whip comes from the high-pressure oil wedge generated by shaft rotation and which ideally may rotate at $^1/_2$ shaft speed, we suggest that, in a system containing damping, there should be some slip between half shaft speed and oil-whip frequency. This effect may be likened to induction-motor slip; that is, energy output is proportional to slip.

Several investigators (4, 5) have observed figures somewhat similar to the epi and hypotrochoids shown in Fig. 6. Pinkus (4) used no definite excitation other than residual shaft unbalance and the usual disturbances from gear sets, oil pumps, and so on. He included these figures as a matter of interest. In some cases Pinkus reports rotation of the figures on the oscilloscope screen. This agrees with our experience when the frequency ratio N_J/N_W is not on resonance. At maximum displacement (resonance) the figures do not rotate in our apparatus. This condition may be obtained by careful frequency-ratio adjustment.

Shawki (5) used unidirectional shaft excitation only. In this case it is rather difficult to determine the sign of the frequency ratio N_J/N_W. In fig. 10 Shawki (5) shows a 2-loop epitrochoid at a frequency ratio N_W/N_J of 1/0.167 or, using the notation of this paper, $N_J/N_W = 6$. If we may assume that this is a positive ratio this agrees with the data shown in Fig. 6 of this paper for a 2-loop epitrochoid at 6.27 ratio.

Applications

There are several practical situations in which one might expect to encounter oil-whip resonances. For instance, if a shaft is run above its critical speed in lightly loaded oil-film bearings, the well-known critical-speed oil whip appears when the shaft is rotating at twice critical speed. As explained previously, the oil-whip frequency at $^1/_2$ shaft speed and the shaft natural frequency coincide producing a vigorous resonance. In the same manner, one would expect a reinforcing resonance between shaft critical speed and the epitrochoidal forms of oil whip at frequency ratios of about 3, 4, 6, 8, and so on. These resonances should be less severe than that at a frequency ratio of 2 since the oil-whip harmonic resonances show relatively less displacement than the fundamental as indicated in Fig. 5.

A planet gear carried on sliding friction bearings in an epicyclic-gear assembly may be excited by ring-gear inaccuracies at a negative frequency ratio producing a hypotrochoidal locus of the gear center.

It may be possible for one of the forms of oil-whip resonance to build up a self-induced vibration in combination with an adaptable exciting force which exhibits no inherent periodicity. In this case the particular form of oil-whip resonance chosen would determine the frequency of the exciting force and hence of the combined resonant vibration.

Summary

A series of oil-whip resonance harmonics has been demonstrated with a journal and hydrodynamic-bearing combination. In these experiments the journal supported by the test bearing was excited by a rotating force. Resonances occur at several ratios of the shaft speed to the exciting-force frequency both when the sense of rotation is the same and opposite.

In each of these resonances the number of turns of the journal-center locus is equal to one half the number of shaft revolutions as required for normal oil whip. The peak displacement at resonance is dependent on the test-bearing oil-supply pressure.

Acknowledgments

F. P. Bundy inaugurated the design of the apparatus used in the work reported in this paper. O. Brusdal produced the detail design. All experimental work and data reduction were done by K. A. Darrow.

Bibliography

1 "Shaft Whipping Due to Oil Action in Journal Bearings" by B. L. Newkirk and H. D. Taylor, *General Electric Review*, vol. 28, 1925, pp. 559–568.

2 "Analysis and Lubrication of Bearings," by Shaw and Macks, first edition, McGraw-Hill Book Company, Inc., New York, N. Y., 1949, p. 203.

3 "The Calculated Performance of Dynamically Loaded Sleeve Bearings," by J. T. Burwell, *Journal of Applied Mechanics*, TRANS. ASME, vol. 69, 1947, p. A-231.

4 "Experimental Investigation of Resonant Whip," by O. Pinkus, TRANS. ASME, vol. 78, 1956, pp. 975–983.

5 "Journal-Bearing Performance for Combinations of Steady, Fundamental, and Low-Amplitude Harmonic Components of Load," by G S. A. Shawki, TRANS. ASME, vol. 78, 1956, pp. 449–455.

Discussion

E. M. Simons.[4] The author is to be commended for this very fine experimental study. The inability of an oil film to support a periodic or rotating load applied at a frequency of one half the journal speed has been discussed widely in the literature, and oil-whip resonance above twice the critical speed of the shaft is a well-known phenomenon. However, little attention has been paid to resonance effects at other multiples of the journal speed. Furthermore, although a number of investigators, including the writer, have observed trochoidal journal-center orbits under cyclic loads, attempts to characterize such orbits analytically in terms of operating parameters have been successful only for the simplest cases. The author's qualitative characterization is indeed a significant contribution.

The results of an investigation conducted by the writer some years ago[5,6] are in general agreement with the author's findings as reported in this paper. For example, both studies show that the maximum eccentricity ratio occurs when N_J/N_W is slightly greater than the theoretically predicted ratio of 2. Furthermore, in neither case was the theoretical eccentricity ratio of unity observed. For comparison purposes, some typical values are tabulated below:

	Hull	Simons	Theoretical
Frequency ratio N_J/N_W at which maximum eccentricity occurs	2.16	2.02	2.00
Value of maximum eccentricity ratio	0.73	0.82	1.00

The writer has found that the theoretical values can be approached by extreme refinements in the testing machine through the elimination of slight misalignments and any other factors which tend to produce unintentional whirl-inhibiting effects. The fact

[4] Consultant, Engineering Mechanics Division, Battelle Memorial Institute, Columbus, Ohio. Mem. ASME.

[5] E. M. Simons, "The Hydrodynamic Lubrication of Cyclically Loaded Bearings," TRANS. ASME, vol. 72, 1950, p. 805.

[6] R. W. Dayton, E. M. Simons, and F. A. Fend, "Discrepancies Between Theoretical and Observed Behavior of Cyclically Loaded Bearings," NACA Technical Note 2545, November, 1951.

that the author's values deviate from the theoretical more than those of the writer would suggest that the author's test equipment had a greater amount of inherent damping as a result of such factors as inertia of the lubricant, inertia of moving masses, elastic deformations, and the like.

If this is true, one would guess that the writer's experiments should have uncovered the harmonic resonances at N_J/N_W values greater than 2. The fact is that no indication of such a series of oil-whip resonances was found. Fig. 9 shows the author's Fig. 5 and the writer's Fig. 6,[5] replotted to the same scale. With the exception of the resonance peaks, the agreement is rather remarkable (and may be fortuitous) considering the great difference in test equipment, speed, load, and probably lubricant viscosity. Several possible explanations for the discrepancy regarding harmonic resonances come to mind. Perhaps the writer missed the

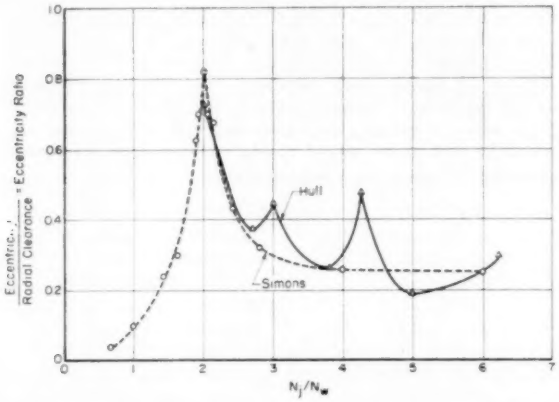

Fig. 9 Eccentricities under constant load, rotating at constant speed. Comparison of results.

resonance peaks because his load-rotation frequency was varied stepwise and the steps were too far apart. Actually, it would be possible to draw a curve which passes through all of the circled points in Fig. 9 and still would have peaks and valleys which are roughly parallel to those in the author's curve. An alternative explanation is that the resonances may be peculiar to the author's test equipment, being induced by natural-frequency phenomena associated with the loading springs or other components. Although the author makes no mention of this possibility, the writer cannot help but feel that it has been considered and ruled out and that, consequently, the first explanation is the more tenable one.

To add to the author's examples of trochoidal journal-center loci actually observed by other investigators, the writer would like to present Fig. 10(*a*). This is a single-loop epitrochoid which appeared, in accordance with the author's findings, when N_J/N_W was 4. The same series of tests produced the predicted 2-loop epitrochoid when N_J/N_W was 6. However, in both cases the load was a unidirectional one varying in magnitude sinusoidally, rather than a constant rotating load. Since Mr. Shawki[7] also obtained epi rather than hypotrochoids with unidirectional loading, one wonders whether this type of loading always corresponds to positive values of N_J/N_W and what the governing factors are.

Figs. 10(*b* and *c*) show the orbits obtained under a constant rotating load with $N_J/N_W = 4$ and 6, respectively. In these cases, the paths were nearly circular, and no loop was evident. However, the speed of the journal center was not uniform, but showed pauses where the analysis indicates loops should have been. These orbits were obtained with flood lubrication of the test bearing. It

[7] Author's reference (5).

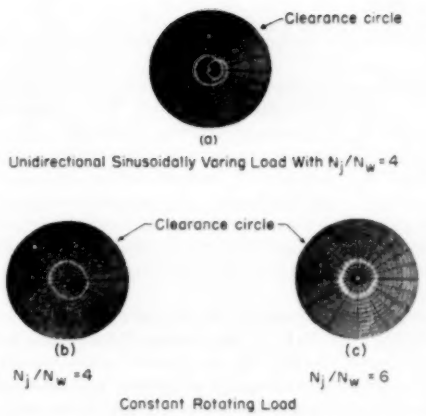

Fig. 10 Journal-center paths under two types of cyclic loading

was found that loops could be made to appear simply by increasing the oil-feed pressure. This agrees in part with the author's observation that lubricant feed pressure has an influence on oil whip. Actually, in the cases cited, increasing the feed pressure made the loops appear, but, unlike the author's example in Fig. 7, had no noticeable effect on the maximum eccentricity.

Incidentally, the author does not make it clear what is meant by "radial displacement" in the cases where the eccentricity varies continuously throughout each cycle. The writer assumes that this refers to the maximum eccentricity in the orbit.

H. Poritsky.[8] This paper forms an interesting addition to the subject of oil whip and adds further information on this puzzling phenomenon.

While there are almost as many definitions of oil whip as there are workers in this field, engineers working with high-speed machinery like turbines and generators are generally concerned with oil whip which occurs when the rotation frequency is greater than double the critical frequency and takes place in such a way that the center of the shaft whips at a frequency close to the critical frequency, even though the speed of rotation varies over a wide range. The conditions of the experiments in this paper are quite different and are characteristic of a light shaft, rather than a shaft provided with a heavy rotor and capable of critical speed vibrations. Likewise, the author's definition certainly differs from the one of concern to high speed machine rotor engineers.

If it is assumed that the inertia of the oil film is negligible, then the instantaneous oil flow, pressure distribution, and resultant force exerted on the shaft can only depend upon the position of the shaft center in its circle of clearance and upon the instantaneous velocity of this center. Roughly speaking, the oil film is not able to distinguish at any instant of time whether it is part of a rotor whipping at a particular frequency and revolving at some other frequency, or whether it is part of a light shaft which is being acted on by an artificially provided unbalance force. It appears to this writer that from the point of view of explaining oil-whip phenomena the most important task is to calculate or derive from experiments the resultant force of the oil film and its direction as functions of position of the shaft center, and velocity and direction of this center. If a way could be found to analyze the data obtained in this paper so as to furnish this reaction force, a solid foundation for a general study of oil-whip phenomena will have been laid.

[8] Consulting Engineer, General Electric Company, Schenectady, N. Y. Mem. ASME.

Author's Closure

The author is indebted to Dr. Simons for his careful consideration of the paper.

It seems reasonable that, since Dr. Simons' equipment appears to have less inherent damping than the author's apparatus, the resonances at N_J/N_W values greater than 2 should have appeared providing frequency ratios were adjustable within sufficiently close limits. Fig. 5 is plotted with the aid of only two experimental points per resonance peak. If more points had been taken and plotted, perhaps the narrowness of the resonant ranges would have indicated that, even with less damping, the resonant range would not have been entered with the frequency ratios available to Dr. Simons.

As inferred by Dr. Simons, the author did consider seriously the possibility that the resonances reported were a characteristic of the apparatus. Some work was done to assure ourselves and local critics that this was indeed an oil-whip phenomenon. The forms shown in Fig. 6 may be obtained at any of the shaft speeds we have tried in the range 1550 to 5250 rpm. Below this range there is difficulty in obtaining constant cam speeds for the higher N_J/N_W ratios. Minor resonances in the apparatus are excited at greater than 5250 rpm shaft speed.

Great care in adjusting the frequency ratio N_J/N_W and reasonable co-operation of the apparatus in maintaining speed while data are recorded will produce traces such as shown in Fig. 6 for N_J/N_W equals -4 and -6. In these examples the loops and circumscribing circle are nearly the same size. In other cases such as at -8 and -10 the data apparently were not obtained exactly at the resonance peak. This effect may be observed in Fig. 5 also.

Radial displacement as used in this paper is the average radius of an elliptically shaped figure circumscribing the shaft center displacement trace.

Dr. Poritsky has called our attention to the nonuniformity in the technology of oil film disturbance phenomena. More work leading to publication will improve the general understanding and inevitably tend toward standardization in terminology.

As pointed out by Dr. Poritsky and in the Introduction of this paper, oil-whip phenomena, as generally encountered, occurs when a rotor is turning at two or more times its critical speed. Data reported in this paper were obtained with a "stiff" shaft. The advantages in working with one phenomenon at a time are obvious. A flexible shaft carrying a rotor has been prepared for this apparatus. We anticipate a certain amount of complexity if the forms of oil-whip resonance described in this paper are combined with rotor critical speeds and the normal oil whip occurring at twice rotor critical and above.

Theory of Oil Whip for Vertical Rotors Supported by Plain Journal Bearings

By FINN ØRBECK,[1] OSLO, NORWAY

This paper endeavors to show that by considering the pressure forces, the viscous drag forces, and the centrifugal forces acting on the journal in a plain journal bearing in oil whip, it is possible to obtain a rational explanation of this phenomenon. The conditions of force equilibrium of the journal lead to two equations, the first of which determines the ratio of frequency of whirl to frequency of rotation in terms of the eccentricity ratio. The second equation relates the eccentricity ratio to the frequency of rotation. These equations therefore suffice to describe oil whip in frequency and amplitude. Numerical studies of the problem indicate some agreement with published experimental studies.

Nomenclature

THE following nomenclature is used in the paper:

M = mass of the rotor, lb sec^2/in.
r = radius of journal, in.
C_r = radial clearance, in.
D = diameter of journal, in.
C_D = diametral clearance, in.
L = length of bearing, in.
μ = viscosity, lb sec/in.^{2}
f = viscous drag per unit area of journal, lb/in.^{2}
p = oil pressure, lb/in.^{2}
x = co-ordinate (around the journal), in.
y = co-ordinate (along the journal), in.
z = co-ordinate (across the oil film), in.
β = angle around the journal measured from point of maximum oil film thickness
u_x = oil velocity in x-direction, in./sec
u_y = oil velocity in y-direction, in./sec
e = eccentricity, in.
ϵ = eccentricity ratio
h = oil film thickness, in.
v = linear velocity of journal center, in./sec
ω_1 = frequency of whirl of the journal, 1/sec
ω = frequency of rotation of the journal, 1/sec
N' = angular velocity of journal, rps
T_1 = force component due to oil pressure, lb
T_2 = force component due to oil pressure, lb
F_1 = force component due to viscous drag, lb
F_2 = force component due to viscous drag, lb
C.F. = centrifugal force, lb
P = resultant force on the journal due to the oil film pressure, lb
α = attitude angle, deg
p' = average pressure on journal = P/LD, lb/in.^{2}
Ω = $(\omega - 2\omega_1)$, 1/sec
$1/C_a$ = load number, dimensionless
γ = index, dimensionless
I_1, I_2, etc., I_8 denote integrals (Appendix 2)

Terminology

The terminology referring to the instability of journal bearings used in this paper is, in its main features, taken from Newkirk [1],[2] see Fig. 6.

(*a*) *Shaft Resonance.* The first peak of the whirling amplitudes as shown by Fig. 6 is due to shaft resonance, and it is therefore primarily determined by the mass and the stiffness of the rotor shaft.

(*b*) *Oil Resonance.* The second peak of the same curve is due to the quasi-elastic properties of the oil film, which establish resonance conditions with the rotor mass.

The shaft resonance and the oil resonance are really two of the resonance values for a vibrational system which consists of the rotor mass, the rotor stiffness, and the elastic properties of the connected journal bearings. The vibrations are the result of an external exciting force (rotor out of balance) and the frequency of the vibrations will be the same as this exciting force.

(*c*) *Oil Whip.* This is a result of the centrifugal force acting on the rotor due to its whirling motion. Since the oil-film resistance to this force is a minimum for whirling motions at frequencies just below one half of that of the rotor rotation, oil whip will occur at this frequency.

The amplitude of oil whip increases with increasing speeds and oil whip is *not* a resonance phenomenon.

(*d*) *Whirl.* This is a collective term to cover any of the above three whirling phenomena.

Introduction

The object of this paper is to study oil whip. It endeavors to show that a consideration of the force equilibrium of the journal in a journal bearing which is subjected to oil whip leads to two equations which describe this phenomenon in frequency and amplitude.

The forces considered are: (*a*) The force on the journal due to the pressure in the oil film; (*b*) the force due to viscous drag by the oil film on the journal; and (*c*) the centrifugal force acting on the journal due to its whirling motion.

In order to avoid the effect of gravity, the analysis has been restricted to rotors with vertical axes and, further, the assumption that the journal moves in a circular path with constant velocity is essential.

Since the shell as well as the journal of a plain bearing are circular, the oil-film forces on the journal will be of constant magnitude and rotate with a constant angular velocity if the journal moves according to the afore-mentioned assumption. The same holds for the centrifugal force.

Force equilibrium for the journal is therefore possible if it moves in a circular path with constant velocity and, consequently, this motion is possible [2]. However, since this is not the only motion possible, our analysis will not furnish a general treatment of oil whip.

[1] Research Department, Det Norske Veritas.

Contributed by the Lubrication Division and presented at the Annual Meeting, New York, N. Y., December 1–6, 1957, of THE AMERICAN SOCIETY OF MECHANICAL ENGINEERS.

NOTE: Statements and opinions advanced in papers are to be understood as individual expressions of their authors and not those of the Society. Manuscript received at ASME Headquarters, March 14, 1957. Paper No. 57—A-171.

[2] Numbers in brackets designate References at end of paper.

Forces Exerted by the Oil Film on the Journal

Generally, the oil film will exert a pressure which acts perpendicularly to the surface of the journal, as well as a viscous drag which acts tangentially to the surface of the journal resisting its motion. When considering the static load-carrying capacity of a bearing, the effect of viscous drag is so small that it can be neglected and, consequently, only the pressure needs to be considered.

For a study of oil whip, however, when the shaft center describes a circular motion approximately equal to half that of the shaft about its own center, it will be necessary to consider also the effects of viscous drag, as the pressure effects are small. Fortunately the two effects can be treated separately and let us start by considering the effects of the pressure.

Pressure Effects. Referring to a co-ordinate system as shown by Fig. 1, the differential equation for the pressure in the oil film will be as follows

$$\partial/\partial\beta(h^3\partial p/\partial\beta) + r^2\partial/\partial y(h^3\partial p/\partial y) = 6(\omega - 2\omega_1)r^2\mu\epsilon C_r \sin\beta \quad (1)$$

when the journal, as well as rotating about its own center, moves in a circular path with constant velocity. (For derivation see Appendix 1.)

The oil-film thickness h is given by the following expression

$$h = C_r(1 + \epsilon \cos\beta)$$

Introducing $\Omega = (\omega - 2\omega_1)$ in the above equation gives

$$\partial/\partial\beta(h^3\partial p/\partial\beta) + r^2\partial/\partial y(h^3\partial p/\partial y) = 6\Omega r^2\mu\epsilon C_r \sin\beta \quad (2)$$

which corresponds to the case when the journal center is stationary and the journal rotates with an angular velocity Ω about its own center.

Any solution of Equation (2) will therefore also apply to Equation (1).

Unfortunately, in spite of the fact that extensive studies of the constant-load characteristics of plain journal bearings have been made, the author is unaware of any complete solution of Equation (2). There are, however, two important approximate solutions to the plain-journal-bearing problem, the first after Sommerfeld [3]. The second is after Michell [4] and Dubois and Ocvirk [5]. Further, numerical solutions based on the relaxation method [5], as well as a wide selection of experimental studies, are available. But, before we proceed to discuss these studies, it will be convenient to introduce a dimensionless parameter $1/C_n$, which will be called the load number

$$1/C_n = \frac{2\pi p'}{\mu\Omega}\left(\frac{C_D}{D}\right)^2\left(\frac{D}{L}\right)^\gamma, \quad (3)$$

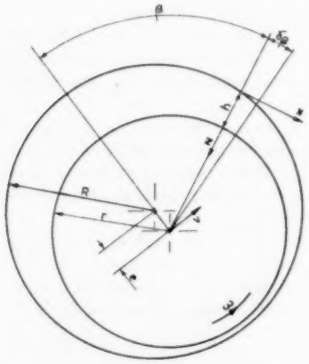

Fig. 1 Co-ordinate system

The index γ is left to be determined.

Sommerfeld's approach [6] to the journal-bearing problem is based on the assumption that $\partial p/\partial y$ in Equation (2) can be neglected. This leads to a load number

$$1/C_n = \frac{2\pi p'}{\mu\Omega}\left(\frac{C_D}{D}\right)^2, \text{ i.e., } \gamma = 0 \quad (4)$$

Michell suggested that $\partial p/\partial\beta$ in Equation (2) could be put equal to zero, and this was made use of by Dubois and Ocvirk in their solution. This leads to the load number

$$1/C_n = \frac{2\pi p'}{\mu\Omega}\left(\frac{C_D}{D}\right)^2\left(\frac{D}{L}\right)^2, \text{ i.e., } \gamma = 2$$

Since the first of these solutions applies to infinitely long bearings and the second to infinitely short bearings, it is to be expected that in actual fact γ takes a value between 0 and 2.

Kreisle [7] obtains an experimental value of $\gamma = 1.73$ for very short bearings, thus indicating the load number for an intermediate case.

The load number is an important parameter since the general procedure is to present solutions of the journal-bearing problem as functions relating the eccentricity ratio and the attitude angle to the load number, i.e.

$$\epsilon = f(1/C_n) \quad \text{or} \quad 1/C_n = F(\epsilon) \quad (5)$$

$$\alpha = g(\epsilon) \quad (6)$$

For the theoretical treatment of oil whip which we will now proceed to develop, it is sufficient to know that functional relationships exist between the eccentricity ratio, the attitude angle, and the load number, as shown by Equations (5) and (6).

The actual forms of these functions will not be required before we want to solve a numerical example.

At this stage it should be emphasized that the purpose of our theory of oil whip is to furnish a link between the constant-load characteristics of a bearing and the oil-whip characteristics. In order to simplify experimental verification, the best procedure would therefore seem to be: (*a*) Select an experimentally obtained constant-load characteristic for the bearing; (*b*) apply the theory to obtain the oil-whip characteristics; and (*c*) measure the oil-whip characteristics experimentally.

Further progress of this analysis will therefore be as follows:

A typical curve which relates the eccentricity ratio to the load number for a journal bearing is shown by Fig. 3. Fig. 4 shows the variation of attitude angle with eccentricity ratio for the same bearing [8].

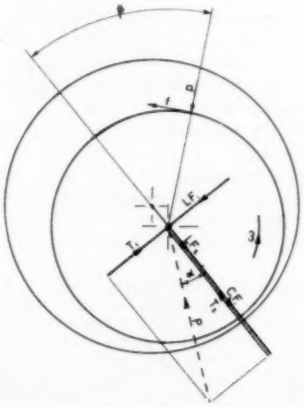

Fig. 2 Force diagram

Let us assume that the two curves just mentioned are obtained by experimental measurements on a bearing in which the journal, subjected to a constant load, rotates with the angular velocity Ω. These curves then represent the resultant effect of viscous-drag forces as well as pressure forces on the journal.

However, since during test the frequency of rotation of the applied force is kept well away from half the frequency of rotation of the shaft, the effect of the oil-film pressure will be very large compared to that of the viscous drag.

Consequently, the curves of Figs. 3 and 4 may be taken to represent the effect of the oil-film pressure alone, i.e., the solution of Equation (2).

Let us now replace Ω by $(\omega - 2\omega_1)$ in the expression for the load number, Equation (3), and further make use of $\gamma = 1.73$ as indicated by Kreisle [9].

This leads to the following equation

$$1/C_n = \frac{2\pi p'}{\mu(\omega - 2\omega_1)} \left(\frac{C_D}{D}\right)^2 \left(\frac{D}{L}\right)^{1.73} \tag{7}$$

It will accordingly be necessary to extend the curves of Figs. 3 and 4 to cover negative values for the load number as shown by the dotted lines.

The complete curves of Figs. 3 and 4 will now represent the solution of Equation (1).

Let us now for a moment consider the cross section of a journal bearing as shown by Fig. 2. If P denotes the total force on the journal due to the pressure in the oil film and α is its attitude angle, the components of this force perpendicular to and in line with the eccentricity will be given by Equations (8) and (9).

$$T_1 = P \sin \alpha \tag{8}$$

$$T_2 = P \cos \alpha \tag{9}$$

Since $P = p'LD$, it is possible to express P in terms of the load number by making use of Equation (7).

$$P = \mu(\omega - 2\omega_1)LD \left(\frac{D}{C_D}\right)^2 \left(\frac{L}{D}\right)^{1.73} \left(\frac{1}{C_n}\right) \Big/ 2\pi \tag{10}$$

Thus Equations (8) and (9) can be rewritten as follows

$$T_1 = \mu(\omega - 2\omega_1)LD \left(\frac{D}{C_D}\right)^2 \left(\frac{L}{D}\right)^{1.73} \left(\frac{1}{C_n}\right) \sin \alpha/2\pi \tag{11}$$

$$T_2 = \mu(\omega - 2\omega_1)LD \left(\frac{D}{C_D}\right)^2 \left(\frac{L}{D}\right)^{1.73} \left(\frac{1}{C_n}\right) \cos \alpha/2\pi \tag{12}$$

Viscous-Drag Effects. The force per unit area of the journal due to viscous drag will be given by the following equation

$$f = \mu(\partial u_x/\partial z)_h \tag{13}$$

The velocity gradient $\partial u_x/\partial z$ is obtained from Appendix 1, Equation (34) and, consequently, Equation (13) can be rewritten as

$$f = \frac{h}{2} \partial p/\partial x - \frac{\mu\omega r}{h} \tag{14}$$

Putting $x = r\beta$ and $h = C_r(1 + \epsilon \cos \beta)$ in Equation (14) leads to the following expression

$$f = \frac{1}{2}\left(\frac{C_r}{r}\right)(1 + \epsilon \cos \beta)\partial p/\partial\beta - \mu\omega \left(\frac{r}{C_r}\right) \frac{1}{1 + \epsilon \cos \beta} \tag{15}$$

We shall see later that the term containing $\partial p/\partial\beta$ in this equation can be neglected.

To be able to show that this is the case, it is convenient and sufficiently accurate to derive an expression for $\partial p/\partial\beta$ according to Sommerfeld's theory—i.e., neglecting side leakage. On this basis, it can readily be shown that

$$\partial p/\partial\beta = 6(\omega - 2\omega_1)\mu\epsilon \left(\frac{r}{C_r}\right)^2 \frac{\cos \beta_0 - \cos \beta}{(1 + \epsilon \cos \beta)^3} \tag{16}$$

Hence

$$f = -\mu\omega \left(\frac{r}{C_r}\right) \frac{1}{1 + \epsilon \cos \beta} + 3\mu\epsilon(\omega - 2\omega_1) \left(\frac{r}{C_r}\right) \frac{\cos \beta_0 - \cos \beta}{(1 + \epsilon \cos \beta)^3} \tag{17}$$

where $\cos \beta_0$ is given in Appendix 2.

The effect of viscous drag on the journal may be represented by two force components, F_1, perpendicular to the line of eccentricity, and F_2, in line with the eccentricity (see Fig. 2). These two components can be expressed in terms of f by the following equations

$$F_1 = r \int_{-\pi}^{\pi} f \cos \beta d\beta \tag{18}$$

$$F_2 = -r \int_{-\pi}^{\pi} f \sin \beta d\beta \tag{19}$$

Making use of Equation (17), these two equations can be rewritten as follows

$$F_1 = -r\mu\omega \left(\frac{r}{C_r}\right) \int_{-\pi}^{\pi} \frac{\cos \beta d\beta}{1 + \epsilon \cos \beta} + 3r\mu\epsilon(\omega - 2\omega_1) \left(\frac{r}{C_r}\right) \left\{\cos \beta_0 \int_{-\pi}^{\pi} \frac{\cos \beta d\beta}{(1 + \epsilon \cos \beta)^3} - \int_{-\pi}^{\pi} \frac{\cos^2 \beta d\beta}{(1 + \epsilon \cos \beta)^3}\right\} \tag{20}$$

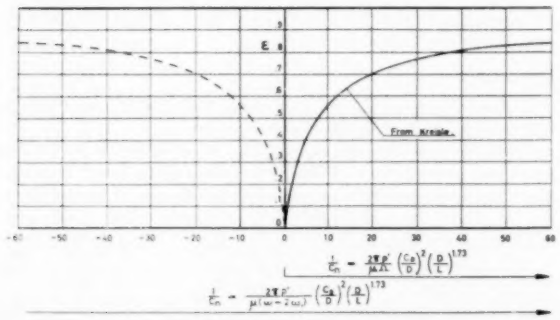

Fig. 3 Eccentricity ratio versus load number

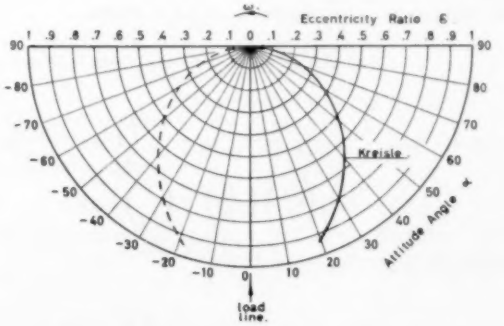

Fig. 4 Attitude angle versus eccentricity ratio

$$F_2 = r\mu\omega\left(\frac{r}{C_r}\right)\int_{-\pi}^{\pi}\frac{\sin\beta d\beta}{(1+\epsilon\cos\beta)} - 3r\mu\epsilon(\omega-2\omega_1)\left(\frac{r}{C_r}\right)\left\{\cos\beta_0\int_{-\pi}^{\pi}\frac{\sin\beta d\beta}{(1+\epsilon\cos\beta)^2} - \int_{-\pi}^{\pi}\frac{\cos\beta\sin\beta d\beta}{(1+\epsilon\cos\beta)^2}\right\} \quad (21)$$

Let us denote the integrals which occur in Equations (20) and (21) by I_1, I_2, I_3, I_4, I_5, and I_6, respectively. The evaluated forms of these integrals are given in Appendix 2, which shows that

$$I_4 = I_5 = I_6 = 0$$

Hence

$$F_2 = 0 \quad (22)$$

The expression for the force F_1 may be rewritten in the following way

$$F_1 = 2\pi r\mu\left(\frac{r}{C_r}\right)\left\{-\frac{\omega}{\epsilon}\left(1-\frac{1}{(1-\epsilon^2)^{1/2}}\right) + 3\epsilon(\omega-2\omega_1)\left[\frac{3\epsilon^2}{(2+\epsilon^2)(1-\epsilon^2)^{5/2}} - \frac{1}{\epsilon^2}\left(1-\frac{1-2\epsilon^2}{(1-\epsilon^2)^{5/2}}\right)\right]\right\} \quad (23)$$

Centrifugal Force

It will be remembered from the Introduction that the center of the journal is assumed to describe a circular path about the center of the shell with constant tangential velocity. The only acceleration which acts on the journal is, consequently, an acceleration of constant magnitude directed toward the center of the shell and the only resulting inertia force is the centrifugal force.

Let M denote the mass of the journal and the following expression will give the centrifugal force which acts radially outward.

$$\text{C.F.} = M\omega_1^2 C_r\epsilon \quad (24)$$

Force Balance

Let us now assume that the journal is perfectly balanced and, further, that there are no lateral forces acting on it in addition to those treated in the previous two sections. The conditions of force equilibrium for the journal will then lead to the following two equations

$$LF_1 = T_1 \quad (25)$$

$$LF_2 + \text{C.F.} = T_2 \quad (26)$$

The force components T_1, T_2, F_1, and F_2, and C.F. are given by Equations (11), (12), (23), (22), and (24) respectively. Equations (25) and (26) can therefore be rewritten as follows

$$-\frac{2\pi\omega}{\epsilon}\left\{1-\frac{1}{(1-\epsilon^2)^{1/2}}\right\} + 6\pi(\omega-2\omega_1)\epsilon\left\{\frac{3\epsilon^2}{(2+\epsilon^2)(1-\epsilon^2)^{5/2}} - \frac{1}{\epsilon^2}\left(1-\frac{1-2\epsilon^2}{(1-\epsilon^2)^{5/2}}\right)\right\} = (\omega-2\omega_1)\left(\frac{D}{C_D}\right)\left(\frac{L}{D}\right)^{1.73}\left(\frac{1}{C_n}\right)\sin\alpha/\pi \quad (27)$$

$$M\omega_1^2 C_r\epsilon = \mu(\omega-2\omega_1)LD\left(\frac{D}{C_D}\right)^2\left(\frac{L}{D}\right)^{1.73}\left(\frac{1}{C_n}\right)\cos\alpha/2\pi \quad (28)$$

In Equation (27) there are two terms containing the factor $\omega - 2\omega_1$. It will be noticed that the second of these terms contains the factor (D/C_D) as well whereas the first does not. For this reason the second term will be very large compared to the first and, consequently, the first term can be neglected.

Physically this means that we neglect the effect of the oil-film pressure on the viscous drag, and our procedure in deriving the effect of the viscous drag is thereby justified.

Equation (27) then becomes

$$\frac{2\pi^2\omega}{\epsilon}\left(\frac{1}{(1-\epsilon^2)^{1/2}}-1\right) = (\omega-2\omega_1)\left(\frac{D}{C_D}\right)\left(\frac{L}{D}\right)^{1.73}\left(\frac{1}{C_n}\right)\sin\alpha \quad (29)$$

Rearranging Equation (29) now gives the following expression for the ratio of the whirling frequency to the frequency of rotation

$$\frac{\omega_1}{\omega} = \frac{1}{2}\left\{1-\frac{\frac{2\pi^2}{\epsilon}\left(\frac{1}{(1-\epsilon^2)^{1/2}}-1\right)}{\left(\frac{D}{C_D}\right)\left(\frac{L}{D}\right)^{1.73}\left(\frac{1}{C_n}\right)\sin\alpha}\right\} \quad (30)$$

Further, Equations (28) and (29) give an expression relating the frequency of rotation to the eccentricity ratio

$$\omega = \frac{2\pi\mu L\left(\frac{1}{(1-\epsilon^2)^{1/2}}-1\right)\left(\frac{D}{C_D}\right)^2\cot\alpha}{M\left(\frac{\omega_1}{\omega}\right)^2\epsilon^2} \quad (31)$$

Equations (30) and (31) describe completely the motion of the journal in oil whip.

Numerical Example

The following dimensions will now be assumed for the purpose of carrying out a numerical example

$$M = 3 \text{ tons}; \quad L = 6 \text{ in.}; \quad D/C_D = 1000; \quad L/D = \frac{1}{2};$$

$$\mu = 5 \times 10^{-6} \text{ lb sec/in.}^2$$

It will also be assumed that the bearing response to a constant load is given by the experimental curves obtained by Kreisle, as shown in Figs. 3 and 4.

Making use of Equation (30), values of the frequency ratio have been calculated for a range of different eccentricity ratios.

Further, values of the frequency of rotation corresponding to the various eccentricity ratios are obtained from Equation (31).

The results of the calculations are given in Table 1 and the variation of eccentricity ratio with frequency of rotation has also been presented graphically in Fig. 5.

Discussion

A short discussion of the results given by Table 1 and Fig. 5 will be required before this paper is concluded.

Let us first consider the ratio of the whirling frequency to the frequency of rotation. A range of values from 0.497 to 0.499 has been obtained for this ratio by the theory. In comparison, Shawki [10] gives experimental values of 0.491, 0.497, and 0.499 which indicates good agreement. Other experimental works, however, give values down to 0.41 which is below the values calculated in our numerical example. It should be noticed from Equation (30), however, that the various bearing dimensions affect the ratio of whirling frequency to frequency

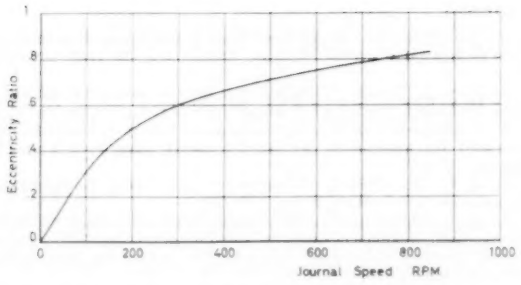

Fig. 5 Eccentricity ratio versus journal speed

Table 1 Frequency ratio and frequency of rotation versus eccentricity ratio

ϵ	$1/C_n$	α, deg	$\frac{\omega_1}{\omega}$	ω, rpm
0.05	0.26	85.5	0.497	17
0.1	0.63	81	0.497	33
0.15	1.05	77	0.498	48
0.2	1.65	74	0.498	60
0.3	2.86	67	0.498	95
0.4	4.75	59	0.498	142
0.5	7.7	52	0.498	202
0.6	12.2	44	0.498	301
0.7	19.5	37	0.498	452
0.8	37	30	0.499	749

of rotation. Bearings with large clearances will have low values for this ratio and, for example, with $D/C_D = 100$, frequency ratios down to 0.467 would be predicted.

The curve of Fig. 5 shows the eccentricity ratio plotted against the frequency of rotation. It will be seen from this curve that the theory predicts oil-whip at all speeds for vertical rotors supported by plain journal bearings. This is in accordance with general experience. It is true that as exceptions rotors of this type have run without oil-whip. This, however, can easily be explained by out of alignment of the bearings.

Finally, the calculated curve of Fig. 5 has been superimposed on an experimental curve obtained by Newkirk [1], as seen in Fig. 6. This latter figure is presented primarily as a convenient reference for our classification of the various whirling phenomena as given in the terminology, but it will also furnish a comparison for the calculated results.

It is seen that agreement is possible for high speeds. At the beginning of oil whip, however, the calculated curve deviates considerably from the experimental curve. The main reason for this is that Newkirk's results apply to a horizontal rotor for which the effect of gravity is important.

The effect of gravity for horizontal rotors is to shift the neutral position of the journal off the center of the bearing. As a result, a stiffer part of the bearing characteristics will determine the stability of the journal which, therefore, remains stable until a higher instability threshold is reached [13].

When first unstable, however, the journal will gain approximately the same amplitude as though it were vertical.

APPENDIX 1

Differential Equation for the Pressure in the Oil Film

If u_x and u_y denote the velocity of the oil in the x and y-directions respectively, p the oil pressure, and μ the viscosity, the following two equations express sufficiently the conditions of viscous flow in a journal bearing:

$$u\partial^2 u_x/\partial z^2 = \partial p/\partial x \tag{32}$$

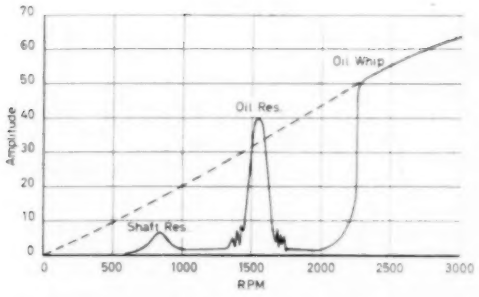

Fig. 6 Amplitude versus shaft speed (*broken line* indicates suggested oil whip amplitudes for vertical rotor, *solid line* is the experimental curve from Newkirk [1])

$$u\partial^2 u_y/\partial z^2 = \partial p/\partial y \tag{33}$$

These two equations can be integrated twice with respect to z. Further, the following boundary conditions will be introduced:

When $z = 0$, $u_x = u_y = 0$, and
when $z = h$, $u_x = -\omega r$ and $u_y = 0$.

Thus two expressions are derived for the velocity components

$$u_x = \frac{1}{2\mu}\,\partial p/\partial x(z^2 - hz) - \frac{\omega r}{h}\,z \tag{34}$$

$$u_y = \frac{1}{2\mu}\,\partial p/\partial y(z^2 - hz) \tag{35}$$

Let us now consider an element of length δy and breadth δz of the oil film in a journal bearing. The difference between the flow out of and the flow into this element will be given by

$$\partial/\partial_x\left(\int_0^h u_x dz\right)\delta x\delta y + \partial/\partial_y\left(\int_0^h u_y dz\right)\delta x\delta y$$

For the compression of the same element per unit time we have

$$v \sin \beta \delta y \delta x$$

Based on the assumption of incompressible fluid flow, the following equation may therefore be put down

$$\partial/\partial x\left(\int_0^h u_x dz\right)\delta x\delta y + \partial/\partial y\left(\int_0^h u_y dz\right)\delta x\delta y = v \sin \beta \delta y \delta x \tag{36}$$

Making use of Equations (34) and (35) in Equation (36) gives

$$\partial/\partial x(h^3\partial p/\partial x) + \partial/\partial y(h^3\partial p/\partial y) = -6\mu r\omega\,\frac{\partial h}{\partial x} - 12\mu v \sin \beta \tag{37}$$

Let us now make use of the following relations

$$v = C_r \epsilon \omega_1$$

$$x = r\beta$$

And further introduce

$$h = C_r(1 + \epsilon \cos \beta)$$

in the left-hand side of Equation (37). Thus the following differential equation will be obtained for the pressure in the oil film of the bearing

$$\partial/\partial\beta(h^3\partial p/\partial\beta) + r^2\partial/\partial y(h^3\partial p/\partial y) = 6(\omega - 2\omega_1)r^2\mu\epsilon C_r \sin \beta \tag{38}$$

APPENDIX 2

Integrals

$$\cos \beta_0 = -\frac{3\epsilon}{2 + \epsilon^2} \tag{39}$$

$$I_1 = \int_{-\pi}^{\pi} \frac{\cos \beta d\beta}{(1 + \epsilon \cos \beta)} = \frac{2\pi}{\epsilon} \left(1 - \frac{1}{(1 - \epsilon^2)^{1/2}}\right) \tag{40}$$

$$I_2 = \int_{-\pi}^{\pi} \frac{\cos \beta d\beta}{(1 + \epsilon \cos \beta)^2} = -\frac{2\pi\epsilon}{(1 - \epsilon^2)^{3/2}} \tag{41}$$

$$I_3 = \int_{-\pi}^{\pi} \frac{\cos^2 \beta d\beta}{(1 + \epsilon \cos \beta)^2} = \frac{2\pi}{\epsilon^2} \left(1 - \frac{1 - 2\epsilon^2}{(1 - \epsilon^2)^{3/2}}\right) \tag{42}$$

$$I_4 = \int_{-\pi}^{\pi} \frac{\sin \beta d\beta}{(1 + \epsilon \cos \beta)} = 0 \tag{43}$$

$$I_5 = \int_{-\pi}^{\pi} \frac{\sin \beta d\beta}{(1 + \epsilon \cos \beta)^2} = 0 \tag{44}$$

$$I_6 = \int_{-\pi}^{\pi} \frac{\cos \beta \sin \beta d\beta}{(1 + \epsilon \cos \beta)^2} = 0 \tag{45}$$

References

1 B. L. Newkirk, "Varieties of Shaft Disturbances Due to Fluid Films in Journal Bearings," TRANS. ASME, vol. 78, 1956, pp. 985–988.

2 G. S. A. Shawki, "Whirling of a Journal Bearing Experiment Under No Load Conditions," *Engineering*, vol. 179, 1955, pp. 243–246.

3 A. Sommerfeld, "The Hydrodynamic Theory of Lubrication," *Zeitschrift für angewandte Mathematik und Physik*, vols. 1 and 2, 1904, pp. 97–155.

4 A. G. M. Michell, "Progress of Fluid-Film Lubrication," TRANS. ASME, vol. 51, 1929, pp. 153–163.

5 G. B. Dubois and F. W. Ocvirk, "Analytical Derivation and Experimental Evaluation of Short Bearing Approximations of Full Journal Bearings," National Advisory Committee for Aeronautics Technical Report 1157, 1953.

6 Sommerfeld used a parameter equal to the inverse of the load number, which is called Sommerfeld's number.

7 L. F. Kreisle, "Very Short Journal-Bearing Hydrodynamic Performance Under Conditions Approaching Marginal Lubrication," TRANS. ASME, vol. 78, 1956, pp. 955–963.

8 The curves of Figs. 3 and 4 are reproduced from Kreisle for a ratio $L/D = 0.502$.

9 Taken from Kreisle, op. cit., p. 7, for $L/D = 0.502$.

10 Shawki, op. cit., p. 4.

11 G. F. Boeker and B. Sternlicht, "Investigation of Translatory Fluid Whirl in Vertical Machines," TRANS. ASME, vol. 78, 1956, pp. 13–19.

12 Poritsky's theoretical treatment of instability in journal bearings should apply to the instability threshold of the horizontal rotor. See H. Poritsky, "Contribution to the Theory of Oil Whip," TRANS. ASME, vol. 75, 1953, pp. 1153–1161.

13 Newkirk, op. cit., p. 3.

Static and Dynamic Characteristics of Compensated Gas Bearings[1]

By HERBERT H. RICHARDSON,[2] CAMBRIDGE, MASS.

A static and dynamic analysis of a general configuration of a compensated gas bearing is presented for the case in which the effects of shaft rotation on performance are negligible. The equations developed can be used quantitatively and are particularly useful in assessing the effects on static and dynamic performance of changes in design parameters such as fluid properties, compensation schemes, and geometry. To illustrate the use of the equations developed, a comparison is made between two common types of hydrostatic gas bearings—the pool bearing and the inherently compensated bearing—and a design example for a specific bearing requirement is worked.

Nomenclature

The following nomenclature is used in the paper:

A = flow area of compensating orifice, sq in.
A^* = area of hypothetical choked orifice permitting flow W_c, sq in.
A_e = effective area $(\beta b/2)(L_p)$, sq in.
a_1, a_2 = dimensionless pressure-flow sensitivities,

$$(P_{ms}/W_s)(\partial W/\partial P_m)$$

b = circumferential distance between adjacent inlet orifices, in.
b_1, b_2 = dimensionless displacement-flow sensitivities,

$$(h/W_s)(\partial W/\partial h)$$

b_p = circumferential width of pool, in.
C_d = orifice discharge coefficient
c_p = specific heat at constant pressure, ft-lb$_F$/lb$_M$ deg R
D_B = diameter of bearing, in.
$D\ \}$ / $d/dt\ \}$ = time derivatives, sec^{-1}
d = diameter of inlet orifice, in.
F = resultant pressure force in full journal bearing, lb
F_B = amplitude of sinusoidally varying force, lb
F_m = resultant pressure force in simplified model of bearing, lb
F_0 = dimensionless parameter
g = local acceleration of gravity, 386 in/sec^2
h = radial clearance, in.
h_p = pool depth, in.
i = subscript indicating initial steady or quiescent value
j = $\sqrt{-1}$
k = ratio of specific heats (1.4 for air)
k_d = dynamic spring stiffness of full journal bearing, lb/in.
k_s = static spring stiffness of full journal bearing, lb/in.
L = bearing length, in.
L_p = pool axial length, in.
n = polytropic exponent
P = pressure, psia
$\mathcal{P}$ = power, hp
P_e = ambient or exhaust pressure, psia
P_m = pressure just downstream of inlet orifice, psia
P_s = bearing-supply pressure, psia
R = gas constant, ft-lb$_F$/lb$_M$ deg R
R_{ex} = external flow restriction
R_O = orifice flow restriction
R_1, R_2 = bearing-clearance restriction
T_s = bearing-supply temperature, deg R
$\mathcal{V}_c$ = volume of fluid film in simplified model, $\mathcal{V}_c = bLh$, cu in.
$\mathcal{V}_p$ = volume of fluid in pool, $\mathcal{V}_p = b_p L_p h_p$, cu in.
W = mass flow rate, lb$_M$/sec
Y = amplitude of sinusoidally varying shaft deflection, in
y = shaft deflection, in.
β = constant relating ΔF_m to ΔF, $\beta = \Delta F/\Delta F_m$
Δ = small change
μ = viscosity, lb$_F$-sec/sq ft
ρ_m = pool density, lb$_M$/cu in.
τ_1 = lead time constant, sec
τ_2 = lag time constant, sec
ω = frequency, radian/sec

Introduction

The present trend toward higher speeds and higher temperatures has created a major design problem in the support of shafts and other moving elements in airborne equipment. Conventional bearings such as oil-hydrodynamic and rolling-contact or antifriction types currently are being operated near their ultimate limits of speed and temperature.

The gas-lubricated bearing offers one attractive solution to this problem of supporting high-temperature and high-speed shafts. However, in the technical literature, little information currently is available that would enable a design engineer to compute reliably the load capacity, power loss, or dynamic characteristics of such a device. Even qualitative effects of various design parameters on the dynamic characteristics of a given bearing configuration in many instances cannot be deduced. Thus a need exists for information that would permit a designer to evaluate the feasibility of a gas bearing for a given application, and to compute its operating characteristics within an acceptable degree of accuracy.

Functionally, an almost direct analogy exists between a fluid bearing and a conventional hydraulic or pneumatic fluid-control system. A fluid bearing is essentially a position control system that tries to hold a bearing journal centered in a bearing sleeve. This position device is subjected to disturbances in the form of loads that must be carried by the bearing elements, and a satisfactory bearing must have load stiffness sufficient to keep deflection less than a prescribed fraction of the bearing clearance when the system is subjected to the maximum expected load force.

[1] The work reported in this paper was supported by the United States Air Force under Contract AF 33(616)-3173 with the Division of Sponsored Research, Massachusetts Institute of Technology, and monitored by the Flight Control Laboratory at the Wright Air Development Center.

[2] Research Engineer, Dynamic Analysis and Control Laboratory, Massachusetts Institute of Technology.

Contributed by the Lubrication Division and presented at the Annual Meeting, New York, N. Y., December 1–6, 1957, of The American Society of Mechanical Engineers.

Note: Statements and opinions advanced in papers are to be understood as individual expressions of their authors and not those of the Society. Manuscript received at ASME Headquarters, June 4, 1957. Paper No. 57—A-138.

Limited investigations, which dealt analytically and experimentally with the static and dynamic behavior of one type of externally pressurized gas bearing, were carried on at the Dynamic Analysis and Control Laboratory from 1953 to 1955. This work resulted in several publications (1, 2, 3)[3] that present limited design information for the special bearing configuration that was studied.

In view of the increasing need for high-speed and high-temperature shaft supports, a renewed effort to analyze and study the gas bearing was initiated. The results obtained thus far deal with externally pressurized gas bearings in which any effects of shaft rotation on static or dynamic characteristics can be neglected. Because of the complexities of compressible fluid flow in passages of varying geometry, refined analyses of gas bearings usually are precluded. However, by removing distributed effects through the use of lumped parameters, the gas-bearing problem can be simplified to the point where analysis can be used to yield quantitative design information. An incremental analysis of the static and dynamic characteristics of a generalized pressurized-bearing configuration has been made employing lumped-parameter assumptions. The results obtained in this way can be used quantitatively to compute the effects of various design parameters on bearing performance.

Compensated Hydrostatic Gas Bearings

Principle of Operation. In the hydrostatic bearing, a fluid film that separates the shaft and journal is maintained by a source of pressurized fluid external to the bearing. The pressures in this fluid are regulated, or compensated, in such a way that they resist shaft deflection. This regulation is accomplished by the action of flow restrictions in and external to the bearing. Fig. 1, a schematic diagram of the common pool-type bearing, illustrates the principle of pressurized-bearing operation. Fluid at pressure P_s enters into pools or pressure cavities in the clearance through external capillary or orifice restrictions R_{ex} and exhausts to atmosphere through the bearing-clearance restrictions R_1 and R_2. When the shaft is centered in the bearing, the pressures P_{m1} and P_{m2} in the upper and lower pools, respectively, are equal, and no net force is exerted on the shaft. But when the shaft is deflected to increase the clearance h_1, the restrictions R_1 and R_2 decrease and increase, respectively, thus causing P_{m1} to decrease and P_{m2} to increase. This action may be visualized with the aid of the schematic bridge shown in Fig. 1. A net force, proportional to the shaded area in the pressure-distribution diagram, acts to oppose the shaft deflection. Consequently, the bearing has a load capacity that is a function of the rate-of-change of pressure with clearance and of the pressure distribution.

Fig. 2 shows a second common bearing configuration. This type of bearing is simpler in construction than the pool bearing, because no external flow restrictions are employed and the fluid is introduced directly into the clearance through straight-drilled holes. The function of the upstream restriction R_{ex} of Fig. 1 is accomplished by the restriction of the annular orifice R_O formed by the clearance height h and the periphery πd of the inlet hole. When the shaft is deflected to increase h_1 in Fig. 2, R_{O1} and R_1 both decrease; but since R_{O1} varies inversely with h_1, while R_1 varies inversely with h_1^3, the intermediate pressure P_{m1}, just downstream of R_{O1}, decreases. Similarly P_{m2} increases, and a net force that resists the deflection acts on the shaft. Because no external compensating flow restrictions are present, this bearing is termed the *inherently compensated* (IC) hydrostatic bearing. This configuration was chosen for the limited studies reported in references (1, 2, and 3). Since R_{O1} and R_{O2} change in the same direction as R_1 and R_2 in the bearing of Fig. 2, a given shaft deflection produces less pressure change than occurs in a comparable pool bearing. Comparison of the pressure distribution in Figs. 1 and 2 shows that a given pressure change produces less shaft force in the IC bearing than the pool bearing. Therefore, qualitatively, the static load capacity of the inherently compensated bearing is inferior to that of the pool bearing. However, as will be shown later, the inherently compensated bearing has superior dynamic characteristics.

Analysis. The problem of journal-bearing analysis can be simplified by replacing the full journal by an equivalent single-pad bearing. By replacing actual pressure distributions with linear pressure distributions, or straight-line segments, and by assuming that each fluid-inlet region behaves essentially independently of the other inlet regions and that shaft deflections are small relative to the total clearance, a correspondence can be established between a full journal bearing and the model shown in Fig. 3. The change in force on the full bearing, ΔF, is related to the change in force in the model, ΔF_m, by the equation

$$\Delta F = \beta \Delta F_m \quad \ldots\ldots\ldots\ldots\ldots\ldots\ldots\ldots [1]$$

where the constant β normally is equal to one half the number of inlet regions in the bearing. In Fig. 3, b is the circumferential distance between adjacent inlet regions and L is the axial length of the journal bearing. If the actual pressure distributions in the

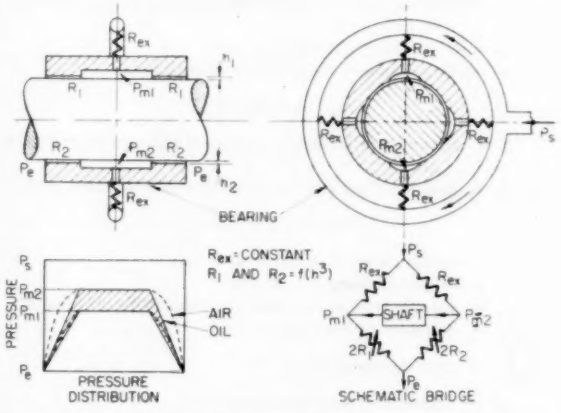

Fig. 1 Pool-type hydrostatic bearing (adapted from fig. 2 of reference 3)

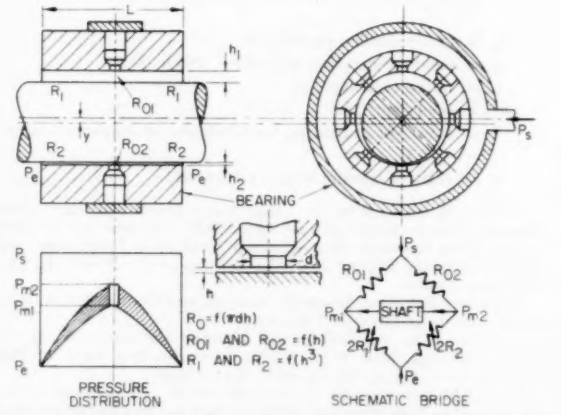

Fig. 2 Hydrostatic bearing with inherent orifice compensation (adapted from fig. 4 of reference 3)

[3] Numbers in parentheses refer to the Bibliography at the end of the paper.

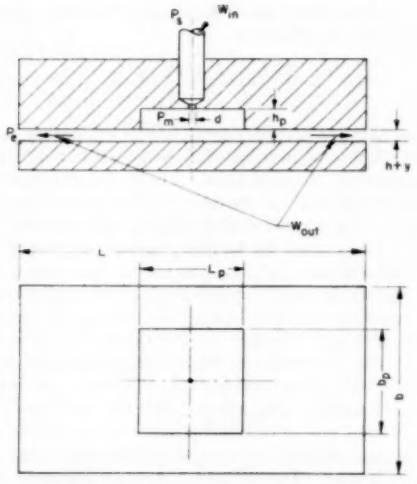

Fig. 3 Simplified model of a pressurized journal bearing

pad are replaced by a constant circumferential pressure and a linearly decreasing axial pressure, the change in pad force ΔF_m as a function of change in pad pressure ΔP_m is found to be

$$\Delta F_m = \frac{b(L + L_p)}{2} \Delta P_m \quad [2]$$

and the corresponding shaft force is

$$\Delta F = \beta \frac{b(L + L_p)}{2} \Delta P_m \equiv A_e \Delta P_m \quad [3]$$

where A_e is an effective area over which ΔP_m can be assumed to act.

The flow into and out of the pad is controlled by the combined valving action of the inlet restriction and the clearance-space restriction. With the assumption that the bearing operates with small percentage changes from the centered position, the incremental-flow equations for the equivalent pad can be written in the form

$$\frac{\Delta W_{in}}{W_i} = \left(\frac{h}{W_i}\frac{\partial W_{in}}{\partial h}\right)\frac{y}{h} - \left(\frac{P_{mi}}{W_i}\frac{\partial W_{in}}{\partial P_m}\right)\frac{\Delta P_m}{P_{mi}} \quad [4]$$

$$\frac{\Delta W_{out}}{W_i} = \left(\frac{h}{W_i}\frac{\partial W_{out}}{\partial h}\right)\frac{y}{h} + \left(\frac{P_{mi}}{W_i}\frac{\partial W_{out}}{\partial P_m}\right)\frac{\Delta P_m}{P_{mi}} \quad [5]$$

where h is the radial clearance, y is shaft deflection, and P_{mi} and W_i are the pool pressure and the mass flow through the pad, respectively, when $y = 0$. For simplicity, Equations [4] and [5] are written in the form

$$\frac{\Delta W_{in}}{W_i} = b_1 \frac{y}{h} - a_1 \frac{\Delta P_m}{P_{mi}} \quad [6]$$

$$\frac{\Delta W_{out}}{W_i} = b_2 \frac{y}{h} + a_2 \frac{\Delta P_m}{P_{mi}} \quad [7]$$

The quantities a_1, a_2, b_1, and b_2 are effective "valve" parameters for the bearing. The net flow into the pad is

$$\frac{\Delta W_{in} - \Delta W_{out}}{W_i} = (b_1 - b_2)\frac{y}{h} - (a_1 + a_2)\frac{\Delta P_m}{P_{mi}} \quad [8]$$

The conservation of mass requires that the net mass flow rate into the pad equal the rate of change of mass inside the pad. In Fig. 3

$$W_{in} - W_{out} = \frac{d}{dt}(\text{mass})_{pad}$$

$$= \frac{d}{dt}\left[\rho_m L_p b_1 h_p + \rho_m b L_p (h + y) + \frac{\rho_m}{2} b(L - L_p)(h + y)\right]$$

$$= \frac{d}{dt}\left\{\rho_m \left[\mathcal{V}_p + \frac{b(L + L_p)}{2}(h + y)\right]\right\} \quad [9]$$

where ρ_m is the pool density and $\mathcal{V}_p$ is the pool volume. Linearizing Equation [9] for small changes from the steady-state conditions $y = 0$, $\rho_m = \rho_{mi}$, and $d\rho_m/dt = 0$ yields

$$\Delta W_{in} - \Delta W_{out} = \rho_{mi}\frac{b(L + L_p)}{2}\dot{y} + \left[\mathcal{V}_p + \frac{b(L + L_p)h}{2}\right]\frac{d\rho_m}{dt} \quad [10]$$

In order to continue the analysis, a relationship between the density and pressure in the pad is required. It is assumed that the pressure and density are related by the polytropic equation

$$\frac{P_m}{\rho_m^k} = \text{constant} \quad [11]$$

Since the changes occurring in fluid properties inside the pad are small and are likely to be rapid in comparison with thermal lags, the polytropic exponent is taken equal to k, the ratio of specific heats. Then

$$\frac{\Delta P_m}{P_{mi}} = k\frac{\Delta \rho_m}{\rho_{mi}} \quad [12]$$

Combining Equations [3], [8], [10], and [12] gives

$$\left\{\left[\frac{1}{W_i}\mathcal{V}_p + \frac{b(L + L_p)h}{2}\right]\frac{\rho_{mi}}{k}D + (a_1 + a_2)\right\}\frac{\Delta F}{A_e P_{mi}} = -\frac{y}{h}\left[\frac{\rho_{mi} b(L + L_p)h}{2W_i}D + (b_2 - b_1)\right] \quad [13]$$

where D denotes differentiation with respect to time. Equation [13] can be rewritten in the form

$$k_d = k_s\left(\frac{\tau_1 D + 1}{\tau_2 D + 1}\right) \quad [14]$$

where k_d is the dynamic spring stiffness

$$k_d = -\frac{\Delta F}{y} \quad [15]$$

k_s is the static spring stiffness

$$k_s = \frac{A_e P_s}{h}\left(\frac{P_{mi}}{P_s}\right)\frac{(b_2 - b_1)}{(a_1 + a_2)} \quad [16]$$

τ_1 is the lead time constant

$$\tau_1 = \frac{\rho_{mi} b(L + L_p)h}{2(b_2 - b_1)W_i} \quad [17]$$

and τ_2 is the lag time constant

$$\tau_2 = \frac{\left[\mathcal{V}_p + \frac{b(L + L_p)h}{2}\right]\rho_{mi}}{k(a_1 + a_2)W_i} \quad [18]$$

Therefore, the dynamic-force–displacement relationship for a pressurized bearing is equivalent to a static spring stiffness with a lead and lag.

When the bearing is deflected very slowly, equilibrium flows and pressure distributions are achieved in the clearance spaces, and the restoring force depends on the static stiffness k_s. When the bearing is deflected very rapidly, no appreciable flow can enter or leave the clearance spaces, and a restoring force occurs because of compression or extension of the essentially trapped fluid film. The latter force depends on the compressibility of the film and is determined from the quantity $k_s(\tau_1/\tau_2)$.

Stability. If a steady sinusoidal displacement of amplitude Y and frequency ω is impressed on a bearing, then, in complex notation, the amplitude of the resulting force F_B is given by

$$F_B = k_s\left(\frac{j\omega\tau_1 + 1}{j\omega\tau_2 + 1}\right) Y \quad \ldots\ldots\ldots\ldots [19]$$

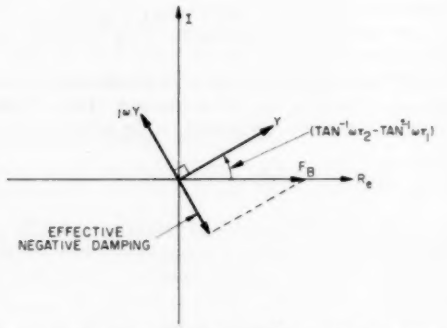

Fig. 4 Vector diagram for compensated gas bearing

This result is plotted in the vector diagram of Fig. 4. If $\tau_2 > \tau_1$, as shown, the force F_B lags the displacement Y. Then, since one component of the force is 180 deg out of phase with the velocity vector $j\omega Y$, an effective negative damping exists for any value of the frequency ω. Consequently, in the absence of sufficient dissipation or positive damping from an external source (load damping), the bearing is dynamically unstable when $\tau_2 > \tau_1$. Similarly, if $\tau_1 > \tau_2$, the bearing is positively damped and stable. Therefore, as indicated by Equation [14] and the condition that $\tau_1 > \tau_2$, the dynamic spring constant in a stable bearing must be larger at high frequencies than at low frequencies. The spring constant at high frequencies, $k_s(\tau_1/\tau_2)$, results from the compression of the fluid film without any flow occurring into or out of the film. Hence an upper limit exists for the stiffness of any fluid bearing, regardless of the method of compensation. This limiting value is the spring stiffness of the trapped fluid film. The magnitude of τ_1/τ_2 gives an indication of the amount of inherent positive damping in the bearing. From Equations [17] and [18] the condition for stability is

$$\frac{\tau_1}{\tau_2} = \frac{k(a_1 + a_2)}{(b_2 - b_1)}\left[\frac{1}{\dfrac{2\mathcal{V}_p}{b(L + L_p)h} + 1}\right] > 1 \quad \ldots\ldots [20]$$

When load damping is present in the bearing system, the external load characteristics (mass, external springs, damping, and so forth) influence the stability; however, since Equation [19] represents the dynamic-force characteristics of the fluid film, the effects of load characteristics on stability can be assessed in a straightforward manner. In any event, Equation [20] is a conservative criterion for stability when normal load characteristics are present.

Effect of Parameters on Stiffness and Stability. Combining Equations [3] and [16] gives

$$\frac{k_s h}{P_s} = \frac{\beta b(L + L_p)}{2}\left(\frac{P_{mi}}{P_s}\right)\frac{(b_2 - b_1)}{(a_1 + a_2)} \quad \ldots\ldots [21]$$

Equations [20] and [21] provide a basis for evaluating a proposed bearing configuration in terms of its geometry and of its pressure-displacement-flow characteristics. These characteristics vary as a function of the nature of the inlet orifices or other compensating restrictors and as a function of the type of flow that occurs in the clearance spaces (that is, laminar, turbulent, choked, and so forth). The stiffness k_s of a bearing may be increased by increasing the flow-displacement sensitivity $(b_2 - b_1)$ or by decreasing the flow-pressure sensitivity $(a_1 + a_2)$. However, according to Equation [20], any changes of this nature that also decrease τ_1/τ_2 are reflected directly in reduced damping in the bearing.

Since the value of the quantity $k(a_1 + a_2)/(b_2 - b_1)$ is normally near unity, Equation [20] indicates that the volume of any pressure pools must not be of a higher order of magnitude than the clearance-space volume and that the smaller the pool, the more stable the bearing. The stiffness k_s may be increased by an increase in inlet pressure P_{mi}, or, when h_p/h, L_p/L, and b_p/b are constant, by a decrease in clearance, without compromising stability. However, increase in pressure increases the quiescent flow W_s required to sustain the fluid film and hence increases the power that must be supplied externally to the bearing.

Comparison of the Pool Bearing With the Inherently Compensated Bearing. In a pool bearing such as shown in Fig. 1, the inlet-orifice area is independent of shaft deflection y; hence from Equation [4], $b_1 = 0$. For the IC bearing, the inlet-orifice area πdh is proportional to the deflection y and therefore $b_1 = 1$. When laminar flow occurs in the clearance space ($W_{out} \sim h^3$), $b_2 = 3$. When two bearings having inlet orifices rather than capillaries, for example, are compared, the pressure-flow sensitivities a_1 and a_2 are the same functions of the inlet-pressure ratio P_{mi}/P_s for both bearings. In the IC bearing no pools exist and $\mathcal{V}_p = 0$.

If two bearings having equal numbers of inlet regions, equal sizes, and equal values of inlet-pressure ratio are considered, Equation [21] gives

$$\frac{(k_s)_{\text{pool}}}{(k_s)_{\text{IC}}} = \frac{3}{2}\left(1 + \frac{L_p}{L}\right) \quad \ldots\ldots [22]$$

For practical bearing designs L_p/L can vary from approximately one half to zero. Then the ratio of $(k_s)_{\text{pool}}$ to $(k_s)_{\text{IC}}$ varies from 1.5 to approximately 2.25. Consequently, much of the advantage in load capacity of a pool bearing derives from the fact that b_1 is zero (fixed upstream orifice). If a bearing could be constructed with an inlet orifice that *decreased* its area as clearance in the inlet region *increased*, then b_1 would be negative, giving further increase in load stiffness. However, a feasible way of constructing such a bearing has not been found.

From Equation [20]

$$\frac{\left(\dfrac{\tau_1}{\tau_2}\right)_{\text{pool}}}{\left(\dfrac{\tau_1}{\tau_2}\right)_{\text{IC}}} = \frac{2}{3\left[\dfrac{2\mathcal{V}_p}{b(L + L_p)h} + 1\right]} \quad \ldots\ldots [23]$$

and

$$\left(\frac{\tau_1}{\tau_2}\right)_{\text{IC}} = \frac{k(a_1 + a_2)}{2} \quad \ldots\ldots [24]$$

For a given bearing configuration, the parameters a_1, a_2, and P_{mi}/P_s can be found as follows: By setting the equation for flow

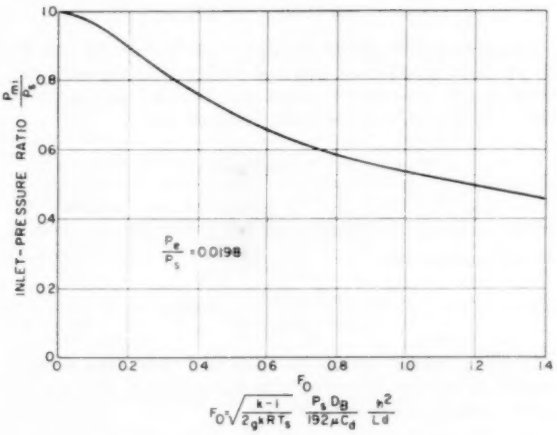

Fig. 5 Inlet-pressure ratio versus design parameter F_0 (adapted from fig. 10 of reference 2)

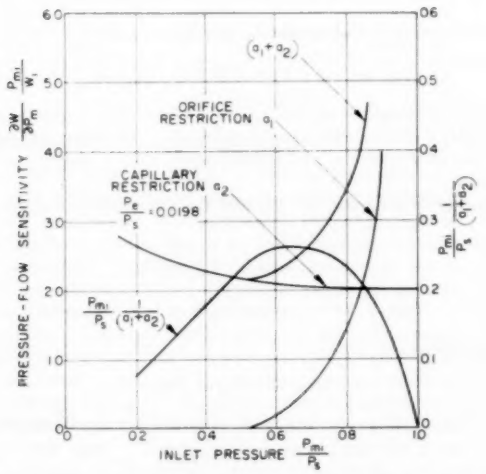

Fig. 6 Plots of orifice and capillary pressure-flow characteristics (adapted from fig. 9 of reference 2)

into the simplified pad equal to the equation for flow out, P_{mi}/P_s is determined as a function of a design parameter, for example, F_0. The parameter F_0 is not a generalized function but depends on the type of compensation employed and on the nature of the flow in the clearance spaces. Physically, it determines the ratio of the clearance restriction to the compensating inlet restriction. The inlet-pressure ratio P_{mi}/P_s is plotted in Fig. 5 as a function of F_0 for the IC bearing with adiabatic orifice flow into and isothermal compressible laminar flow out of the bearing. The results of Fig. 5 are also directly applicable to an orifice-compensated pool bearing with $\mathcal{U}_p$ small if F_0 is multiplied by $4h/d$, and if d is interpreted as the inlet-orifice diameter. From Equations [4] and [5] and the controlling flow equations, a_1 and a_2 can be determined as functions of P_{mi}/P_s. These functions, reproduced from reference (2), are presented in Fig. 6. The curve for the capillary restriction a_2 was computed for $P_e/P_s = 0.0198$. Curves of combined pressure-flow sensitivity $(a_1 + a_2)$ and $(P_{mi}/P_s)[1/(a_1 + a_2)]$ have been added. Reference to Figs. 5 and 6 shows that $(a_1 + a_2)$ is always greater than 2. Therefore $(\tau_1/\tau_2)_{IC}$ is always greater than 1.4. Hence the IC bearing is inherently stable for any combination of system parameters. Further discussion of the dynamic properties of the IC bearing in the presence of various load characteristics can be found in reference (2). A bearing operating near maximum stiffness per unit supply pressure has $(a_1 + a_2) \approx 3$, $\tau_1/\tau_2 \approx 2$, and the bearing is well damped. With substitution of the latter value into Equations [23] and $[20]_b$ the pool-bearing stability condition is

$$\left(\frac{\tau_1}{\tau_2}\right)_{pool} \approx \frac{4}{3}\left[\frac{1}{\dfrac{2\mathcal{U}_p}{b\left(1+\dfrac{L_p}{L}\right)hL}+1}\right] > 1 \quad \ldots\ldots [25]$$

For stability under these conditions

$$\frac{\mathcal{U}_p}{\mathcal{U}_e} < \frac{1}{6}\left(1+\frac{L_p}{L}\right) \quad \ldots\ldots [26]$$

where $\mathcal{U}_e$ = clearance volume = bLh. Therefore, in order to operate a pool bearing in its most efficient region, $(a_1 + a_2) \approx 3$, and yet maintain stability, the pool volume must be less than 25 per cent to 30 per cent of the clearance volume. Of course, a bearing with a larger pool may be stabilized at the expense of stiffness by changing $(a_1 + a_2)$. Even when $\mathcal{U}_p \approx 0$, the pool bearing is less stable than the inherently compensated bearing, as shown by Equation [23].

As the shaft of a pool bearing is given large displacements relative to the clearance, the effective clearance volume $\mathcal{U}_e$ decreases in regions of reduced clearance, and increases in regions of increased clearance. From Equation [20], the ratio of τ_1/τ_2 then becomes very small on the side of the bearing where clearance is becoming very small, thus introducing a relatively large destabilizing effect. However, on the side where clearance is increasing, τ_1/τ_2 can change by only a few per cent because the initial $\mathcal{U}_p/\mathcal{U}_e$ must be small for stability at small shaft deflections. For this reason, pool bearings that are stable when unloaded have a tendency to become unstable as they are loaded. Since the pressure-flow sensitivity $(a_1 + a_2)$ also can increase in the region of reduced clearance, the statement does not hold that all pool bearings become unstable when heavily loaded. Whether or not a given pool bearing tends to become unstable as it is loaded can be determined by reference to Figs. 5 and 6. In any case, since $(a_1 + a_2)$ goes to infinity as P_{mi}/P_s goes to unity and local clearance goes to zero, a pool bearing that becomes unstable when loaded regains stability eventually as the bearing is deflected further. In the IC bearing, no such difficulties occur because $\mathcal{U}_p$ is zero.

The advantages of dynamic stability and manufacturing simplicity usually make the inherently compensated bearing preferable to the pool bearing, particularly for critical high-speed applications. When load capacity is at a premium, stiffness can be increased 50 per cent, with corresponding decrease in τ_1/τ_2, by introducing a pool of small volume compared with the clearance volume.

Sample Design. To illustrate the use of the equations developed for the compensated hydrostatic gas bearing, a bearing is designed to meet the following requirements:

1 Maximum load 25 lb.
2 Maximum available supply pressure P_s = 100 psig.
3 Minimum bearing diameter consistent with economy of fluid supply.

To conserve supply fluid, the bearing clearance should be as small as possible. A value of h of 0.0008 in. is taken here as a practical minimum. If the bearing is to be used for high-temperature operation, this value probably would have to be increased to

minimize effects of thermal distortion, and the resulting increase in gas flow would have to be accepted.

Since the stiffness for small loads, k_s, normally drops off somewhat as the bearing is subjected to large loads, the maximum load that can be applied to the bearing probably will be less than $k_s h$. For design purposes, the maximum allowable load is taken equal to $0.5k_s h$. Then

$$0.5k_s h = 25 \text{ lb}$$

$$k_s = \frac{25 \text{ lb}}{(0.5)(0.0008 \text{ in.})} = 6.25 \times 10^4 \text{ lb/in.} \quad [27]$$

To minimize bearing size by maximizing stiffness, a pool of very small volume is assumed. Then $\mathcal{V}_p/\mathcal{V}_c \approx 0$, but $b_1 = 0$. For laminar flow in the clearance, $b_2 = 3$.

Eight inlet regions are chosen for this design; then $\beta = 4$ and $b = \pi D_B/8$. From Equation [3]

$$A_s = \frac{\beta b L}{2} = \frac{4 \times \pi D_B \times L}{(2)(8)} = \frac{\pi}{4} D_B L \quad [28]$$

Then Equation (16) becomes

$$\frac{k_s h}{A_s P_s} = \frac{50 \text{ lb}}{\left(\frac{\pi}{4} D_B L \text{ sq in.}\right)\left(115 \text{ lb/sq in.}\right)} = \frac{2}{1.15\pi D_B L}$$

$$\leqq \frac{P_{mi}}{P_s} \frac{3}{(a_1 + a_2)} \quad [29]$$

or

$$\frac{P_{mi}}{P_s} \frac{1}{(a_1 + a_2)} > \frac{2}{3.45\ \pi D_B L} \quad [29a]$$

The quantity $(P_{mi}/P_s)[1/(a_1 + a_2)]$, plotted in Fig. 6, has a maximum value near $P_{mi}/P_s = 0.8$. Then $a_1 + a_2 \approx 3.5$, and

$$D_B L > \left(\frac{2}{3.45\pi}\right)\left(\frac{3.5}{0.8}\right) = 0.808 \text{ sq in.} \quad [30]$$

if

$$L_{max} = D_B, \quad D_B^2 = 0.808, \quad D_B = 0.90 \text{ in.}$$

Therefore, for convenience

$$D_B = \frac{15}{16} \text{ in.} = 0.937 \text{ in.}$$

$$L = \frac{15}{16} \text{ in.} = 0.937 \text{ in.}$$

From Fig. 5, for $P_{mi}/P_s = 0.8$, $F_0 \approx 0.35$. For a pool bearing with a small pool, the relationship for F_0 must be multiplied by $4h/d$

$$0.35 = \left(\frac{k-1}{2gkRT_s}\right)^{1/2} \frac{P_s D_B}{192\mu C_d} \frac{4h^3}{Ld^2} \quad [31]$$

For air at 530 deg R

$$k = 1.4$$
$$R = 53.35 \text{ ft-lb}_F/\text{lb}_M \text{ deg R}$$
$$\mu = 3.72 \times 10^{-7} \text{ lb}_F\text{-sec/sq ft}$$

and $$C_d = 0.9$$

Then, the inlet-orifice area is found to be, from Equation [31]

$$d^2 = \frac{(4)(115 \text{ lb/sq in.})(8 \times 10^{-4})^3 \text{ cu in. } (12 \text{ in/ft})}{(0.35)(2.52 \times 10^3 \text{ ft/sec})(192)(3.72 \times 10^{-7} \text{ lb}_F\text{-sec/sq ft})(0.9)}$$

$$= 5.0 \times 10^{-5} \text{ sq in.}$$

$$d = 7.08 \times 10^{-3} \approx 0.007 \text{ in.}$$

This value of d is actually too small to be drilled. The value of d can be increased to a practical minimum of approximately 0.013 in. by increasing clearance and therefore quiescent mass flow. To keep F_0 constant, from Equation [31]

$$\frac{h^3}{d^2} = \text{constant}$$

and $$h = 0.0012 \text{ in., when } d = 0.013 \text{ in.}$$

From Equation [20]

$$\frac{\tau_1}{\tau_2} = \frac{(1.4)(3.5)}{3} = 1.63 \quad [32]$$

Therefore, stability is assured. The pool dimensions were assumed to be small compared with the volume of the clearance space; that is, in Equation [20]

$$\frac{2\mathcal{V}_p}{b(L + L_p)h} < 0.10 \quad [33]$$

Then $$2b_p L_p h_p < 0.10bh(L + L_p)$$

A minimum practical size for L_p and b_p is $^1/_{16}$ in.

$$h_p < 0.31\ h \quad [34]$$

This pool depth is too shallow to be effective as a pool because h_p is only a fraction of the radial clearance. Therefore the design is changed so that the pool is eliminated; that is, the IC bearing is used.

For the IC bearing, $b_1 = 1$, and Equation [29a] becomes

$$\frac{P_{mi}}{P_s} \frac{1}{(a_1 + a_2)} > \frac{1}{1.15\ \pi D_B L} \quad [35]$$

$$D_B L > 1.17 \text{ sq in., and } D_B = L > 1.08 \text{ in.}$$

Again, for convenience

$$D_B = L = 1\ ^3/_{16} = 1.062 \text{ in.}$$

In Fig. 5, the expression for F_0 is correct for the IC bearing

$$0.35 = \left(\frac{k-1}{2gkRT_s}\right)^{1/2} \frac{P_s D_B}{192\mu C_d} \frac{h^3}{Ld} \quad [36]$$

$$d = \frac{(115 \text{ lb/sq in.})(64 \times 10^{-4} \text{ sq in.})(12 \text{ in/ft})}{(2.52 \times 10^3 \text{ ft/sec})(0.35)(192)(3.72 \times 10^{-7} \text{ lb}_F\text{-sec/sq ft})(0.9)}$$

$$\approx 0.0156 \text{ in.}$$

Then, from Equation [20]

$$\frac{\tau_1}{\tau_2} = \frac{(1.4)\ (3.5)}{2} = 2.45 \quad [37]$$

In order to complete the design, a knowledge of the mass flow W_i is required. For adiabatic orifice flow (4)

$$\frac{W_i}{A^*} \frac{\sqrt{T_s}}{C_d P_s} = 0.532 \sqrt{\text{deg R/sec}} \quad [38]$$

$$W_i = A \left(\frac{W_i}{A^*}\right)\left(\frac{A^*}{A}\right) = (\pi d h\ C_d) \frac{0.532 P_s}{(\sqrt{T_s})} \frac{A^*}{A} \quad [39]$$

where A^* is the area of a choked orifice that would permit the flow W_i. For $P_{mi}/P_s = 0.8$, $A/A^* = 1.21$, as shown on p. 614 of reference (4). Thus

$$W_i = (\pi)(1.56 \times 10^{-3}\text{ in.})(8 \times 10^{-4}\text{ in.})\frac{(0.9)(0.532)\,(\sqrt{\text{deg R}}/\text{sec})(115\text{ lb/sq in.})}{(23\sqrt{\text{deg R}})(1.21)}$$

$$= 7.76 \times 10^{-6}\text{ lb}_M/\text{sec}$$

For eight inlet regions, $8W_i = 6.2 \times 10^{-4}$ lb$_M$/sec.

The quiescent power requirement depends on the state of the fluid emerging from the bearing. A conservative estimate is obtained by assuming that the fluid expands isentropically to the ambient pressure P_a. Then

$$\mathcal{P} = 8W_i c_p T_s \left[1 - \left(\frac{P_a}{P_s}\right)^{\frac{k-1}{k}}\right] \quad [40]$$

≈ 0.05 hp where $\mathcal{P}$ is the power required.

The design results are summarized as follows:

load capacity = 25 lb
stiffness = 6.3×10^4 lb/in.
length = diameter = $1^1/_{16}$ in.
number of inlet holes = 8
no pressure pools
inlet hole diameter $d = 0.016$ in.
supply pressure $P_s = 100$ psig
quiescent flow $8W_i = 6.2 \times 10^{-4}$ lb/sec
quiescent power ≈ 0.05 hp

Summary, Conclusions, and Recommendations

The relationships developed in this memorandum can be used to obtain qualitative and quantitative design information regarding the performance of compensated hydrostatic gas bearings. The results presented should be particularly useful in pointing out the effects of changes in design parameters, for example, fluid properties (such as pressure, temperature, and viscosity), compensation schemes, and geometry.

In order to illustrate the use of the equations developed, a comparison is made between two common types of hydrostatic bearing—the pool bearing and the inherently compensated bearing—and a design example for a specific bearing requirement is worked.

Previous experimental work (2, 3) has indicated that the type of analysis used in this report is valid. However, many more static and dynamic test data with various bearing configurations are required before the design equations presented here can be employed with a high degree of confidence. Characteristics of bearings at large shaft deflections would be of particular interest.

When a hydrostatic bearing is operated at high shaft speeds, fluid flow is induced between adjacent inlet regions by the relative motion between journal and sleeve. Also, with values of speed and clearance currently contemplated in hydrostatic bearings, hydrodynamic effects in the fluid film can become of the same order of magnitude as hydrostatic effects. Therefore investigations should be made to evaluate the effects of shaft rotation on gas-bearing performance.

Bibliography

1 "A Study of Pressurized Air Bearing Design; Steady Loading—No Rotation," by S. K. Grinnell, M.I.T., Department of Mechanical Engineering, MS thesis, Cambridge, Mass., 1954.

2 "A Dynamic Analysis of Externally Pressurized Air Bearings," by H. H. Richardson, M.I.T., Department of Mechanical Engineering, MS thesis, Cambridge, Mass., 1955.

3 "Design Study of a Hydrostatic Gas Bearing With Inherent Orifice Compensation," by S. J. Grinnell and H. H. Richardson, TRANS. ASME, vol. 79, 1957, pp. 11–12.

4 "Compressible Fluid Flow," by A. H. Shapiro, The Ronald Press Company, New York, N. Y., vol. 1, pp. 85, 99–100.

Discussion

L. Licht.[4] The author has made a valuable contribution in the field of externally pressurized gas bearings.

His remarks on the dependence of bearing stiffness on the frequency of the disturbance should certainly be borne in mind by those who habitually refer to the bearing-spring "constant" in the literal sense of the word.

It is, indeed, gratifying to note that the author's stability criteria agree with the analysis, and confirm the conclusions arrived at by this writer for the case of a circular-pad bearing.

One must emphasize, however, that results based on such analyses cannot be expected to be in better agreement with experiment than the assumptions on which they are based are with reality.

Generally, even in the absence of shaft rotation, circumferential flow cannot be neglected. Concepts of linear pressure distributions and mean annulus widths should be applied with caution and re-examined in the light of bearing geometry, eccentricity, and whenever large shaft deflections y or high rotative speeds render such simplifying assumptions invalid.

The paper should be of interest to all concerned with new lubrication concepts. It also represents a useful guide in estimating the magnitude of parameters which influence the performance of hydrostatic gas bearings of this type.

Author's Closure

The author wishes to thank Mr. Licht for his valuable discussion of this paper.

Many assumptions have been employed in connection with this work in order to reduce the analysis to a simple form. The experience of this author with inherently orifice-compensated bearings has indicated that the type of approach detailed here can be used to predict bearing performance to a reasonable degree of accuracy up to eccentricity ratios of about 0.5 when the shaft is not rotating. Under rotating conditions below the whip range, the predicted static and dynamic performance usually is conservative.

The greatest difficulty in applying the results presented often comes in establishing the quiescent conditions for a given proposed bearing; that is, the quantity P_{ms}/P_s in Fig. 5. Determination of this parameter requires matching of inlet flows to exhaust flows, which in turn involves considerations of pressure gradient. This gradient is of course determined by the assumed pressure distribution and may be in considerable error. Once the operating point has been determined, however, other performance characteristics can be evaluated with a high degree of confidence.

The author feels that the greatest value of this paper will be in giving to the reader an understanding of the phenomena that occur in compensated gas bearings and to show the effects on static and dynamic performance of changes in various bearing design parameters.

In closing, the author would like to express his sincere appreciation to Dr. John Hrones,[5] director, and the staff of the Dynamic Analysis and Control Laboratory; notably Drs. J. L. Shearer[6] and T. C. Searle,[7] and Mr. J. L. Coakley,[8] for the inspiration, the atmosphere, and the support, which made this work possible.

---

[4] Research Engineer, The Franklin Institute, Philadelphia, Pa. Assoc. Mem. ASME.

[5] Vice-President for Academic Affairs, Case Institute of Technology, Cleveland, Ohio. Mem. ASME.

[6] Associate Professor of Mechanical Engineering, M.I.T., Cambridge, Mass. Mem. ASME.

[7] Vice-President, Hydel, Inc., Cambridge, Mass.

[8] Senior Engineering Super visor, Hydel, Inc., Cambridge, Mass.

Solution of the Tapered-Land Sector Thrust Bearing[1]

By O. PINKUS,[2] W. LYNN, MASS.

Reynolds' equation in polar co-ordinates was solved on a digital computer for the actual sectorial geometry of finite thrust bearings. The oil-film shape is that of a uniform taper in the circumferential direction. Minimum film thickness, side and end leakage, power loss, and centroids are given in general dimensionless form as functions of a dimensionless group $(\mu N/P)(L/b)^2$. A wide range of bearing parameters is covered and solutions are given for very heavy unit loadings. A short discussion is included on how to perform thrust bearing calculations using the results and expressions derived in the paper.

Nomenclature

The following nomenclature is used in the paper:

a = minimum film thickness, in.
b = amount of taper, in.
c_p = specific heat, Btu/lb deg F
h = film thickness, in.
j = power-loss coefficient, dimensionless
k = number of pads, dimensionless
p = pressure, psi
q_s = side-flow coefficient, dimensionless
q_e = end-flow coefficient, dimensionless
r = radius, in.
t = temperature deg F
r_0 = inner radius of sector, in.
$\bar{r}_0$, = $r - r_0/L$, radial co-ordinate of centroid, dimensionless
θ = angular co-ordinate, radians
θ_0 = angular span of sector, radians
$\bar{\theta}_0$ = θ/θ_0, angular co-ordinate of centroid, dimensionless
μ = viscosity, lb-min/sq in.
μ_2 = outlet viscosity, lb-min/sq in.
F = frictional force, lb
F_v = vertical load number, dimensionless
F_H = horizontal load number, dimensionless
H = power loss, lb-in/min
L = radial length of bearing, in.
N = speed of runner, rpm
P = unit loading, psi
Q = oil flow, cu in/min
R = outer radius of sector, in.
T = thrust factor $(\mu N/P)(L/b)^2$, dimensionless
U = linear speed, in/min
W = bearing load, lb
ρ = specific weight, lb/cu in.
λ = friction coefficient, dimensionless

Introduction

The foremost handicap in lubrication studies is the difficulty of obtaining analytical solutions of Reynolds' equation. While in the case of journal bearings, due to the trigonometric expression of the oil film, this task is almost insurmountable, there were some successful attempts in solving analytically Reynolds' equation for thrust bearings. The most important contribution was made by Michell (1)[3] who, for the first time, obtained a purely analytical expression for the pressure distribution in a plain slider with a constant slope. But the main task of obtaining the integrated load capacity, the side leakage, and so on, remained unsolved. It was Muskat, Morgan, and Meres (2) who, using a similar approach, obtained workable solutions for rectangular sliders running at light loads. Archibald (3) in turn obtained solutions for the stepped bearing, solving essentially Laplace's equation with one nonzero boundary condition. Charnes, Saibel, and Ying (4) did get a solution for a sector-type element but this work assumes an exponential oil-film shape which is only an approximation to actual tapers.

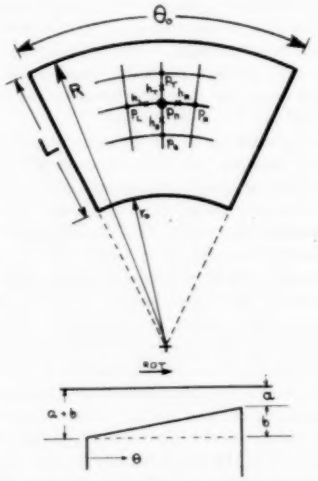

Fig. 1 Geometry of sector thrust bearing

This paper offers solutions for tapered-land thrust bearings of finite width. The results obtained on a 650 digital computer[4] are based on the solution of Reynolds' equation in polar co-ordinates, thus considering the sectorial geometry of actual bearings as shown in Fig. 1. The solutions, covering a wide range of parameters and operating conditions, are plotted as functions of a dimensionless group $(\mu N/P)(L/b)^2$ which can be considered as equivalent to the Sommerfeld number in journal bearings. The

[1] When this paper was written, the author included information and expressed opinions he believed to be correct and reliable. However, because of the constant advance of technical knowledge, the widely differing conditions of possible specific applications, and the possibility of misapplication, neither the author nor his employer makes any warranty with respect to, or assumes any liability arising out of this paper, its contents, or its use.

[2] General Electric Company. Assoc. Mem. ASME.

Contributed by the Lubrication Division and presented at the Annual Meeting, New York, N. Y., December 1–6, 1957, of The American Society of Mechanical Engineers.

Note: Statements and opinions advanced in papers are to be understood as individual expressions of their authors and not those of the Society. Manuscript received at ASME Headquarters, August 22, 1957. Paper No. 57—A-152.

[3] Numbers in parentheses refer to the Bibliography at the end of the paper.

[4] IBM 650 computer.

solutions were obtained for a 7×7 mesh; i.e., for about 50 points per bearing pad.

Solution of Reynolds' Equation

Reynolds' equation in polar co-ordinates is given by

$$\frac{\partial}{\partial r}\left(\frac{rh^3}{\mu}\frac{\partial p}{\partial r}\right) + \frac{1}{r}\frac{\partial}{\partial \theta}\left(\frac{h^3}{\mu}\frac{\partial p}{\partial \theta}\right) = 6U\frac{\partial h}{\partial \theta} \quad \ldots\ldots [1]$$

In order to transform Equation [1] into dimensionless form the following substitutions are used

$$\bar{r} = \frac{r}{R}, \quad \bar{\mu} = \mu/\mu_{\text{avg}} = 1$$

$$\bar{h} = h/b$$

$$\bar{p} = \frac{p}{\mu N}\left(\frac{b}{L}\right)^2$$

$$U = 2\pi rN = 2\pi R\bar{r}N$$

With these transformations Reynolds' equation becomes

$$\frac{\partial}{\partial \bar{r}}\left(\bar{r}\bar{h}^3\frac{\partial \bar{p}}{\partial \bar{r}}\right) + \frac{1}{\bar{r}}\frac{\partial}{\partial \theta}\left(\bar{h}^3\frac{\partial \bar{p}}{\partial \theta}\right) = 12\pi\bar{r}\left(\frac{R}{L}\right)^2\frac{\partial \bar{h}}{\partial \theta} \quad [2]$$

Referring to Fig. 1 and replacing the differentials by finite increments, we obtain for anyone of the n discrete points in the mesh

$$\bar{p}_n = \frac{12\pi\bar{r}_n\left(\frac{R}{L}\right)^2\left(\frac{\bar{h}_L - \bar{h}_R}{\Delta\theta}\right) + \frac{\bar{h}_T^3\bar{r}_T}{\Delta\bar{r}^2}\bar{p}_T + \frac{\bar{h}_B^3\bar{r}_B}{\Delta\bar{r}^2}\bar{p}_B + \frac{\bar{h}_R^3}{\bar{r}_n\Delta\theta_n}\bar{p}_R + \frac{\bar{h}_L^3}{\bar{r}_n\Delta\theta_n}\bar{p}_L}{\frac{\bar{h}_T^3\bar{r}_T}{\Delta\bar{r}^2} + \frac{\bar{h}_B^3\bar{r}_B}{\Delta\bar{r}^2} + \frac{1}{\bar{r}_n\Delta\theta^2}(\bar{h}_R^3 + \bar{h}_L^3)} \quad \ldots\ldots [3]$$

For the n points there will result n equations in n unknowns, which will have to be solved simultaneously. After getting the pressure distribution the total load capacity is obtained from

$$W = \sum_1^n p_n\bar{r}_n\Delta\theta\Delta r = R^2\mu N(L/b)^2\Delta\bar{r}\Delta\theta\sum_1^n \bar{p}_n\bar{r}_n$$

The area of a pad is given by

$$A = \theta_0/2\pi[\pi(R^2 - r^2)] = \frac{\theta_0 R^2}{2}\left[1 - \left(1 - \frac{L}{R}\right)^2\right]$$

$$W = PA = P\frac{\theta_0 R^2}{2}\left[1 - \left(1 - \frac{L}{R}\right)^2\right]$$

Equating the two expressions for W we obtain

$$P = \frac{R^2\mu N(L/b)^2\Delta\bar{r}\Delta\theta\Sigma\bar{p}_n\bar{r}_n}{\frac{\theta_0 R^2}{2}[1 - (1 - L/R)^2]}$$

$$= \frac{2\mu N(L/b)^2 F_v}{\theta_0[1 - (1 - L/R)^2]}$$

Defining the dimensionless thrust factor as

$$T \equiv \frac{\mu N}{P}(L/b)^2$$

$$T = \frac{\mu N}{P}(L/b)^2 = \frac{\theta_0}{2}[1 - (1 - L/R)^2]\frac{1}{F_v} \quad \ldots\ldots [4]$$

A sector-pad thrust bearing yields a dimensionless parameter $T = (\mu N/P)(L/b)^2$. This is analogous to the Sommerfeld number, $(\mu N/P)(D/C)^2$. This dimensionless parameter also could have been defined in terms of the minimum film thickness a, but this would be a definite disadvantage. The value of a is usually unknown beforehand and so the finding of the correct value of a would involve a trial-and-error solution. Using b as a reference dimension eliminates this complication. From Equation [2], it is seen that a unique solution is provided by three parameters: The L/R ratio, the span θ_0, and film shape. An equal number of parameters, L/D ratio, arc length, and attitude, is involved in the solution of journal bearings. The simplification in the case of thrust bearings consists in the fact that no attitude angle is involved which eliminates the laborious process of satisfying the conditions $\Sigma F_H = 0$.

The solutions obtained in this paper are for thrust bearings having a circumferential taper only The shape of the oil film is given by the equation

$$h = a + b(1 - \theta/\theta_0) \quad \ldots\ldots [5]$$

as shown in Fig. 1, with θ positive in the direction of rotation In dimensionless form h becomes

$$\bar{h} = h/b = a/b + (1 - \theta/\theta_0) = \left(\frac{a+b}{b}\right) - \left(\frac{\theta}{\theta_0}\right)$$

Thus the ratio a/b is, along with L/R and θ_0, the third necessary parameter for a unique solution of the differential equation.

Results of Analysis

The results obtained in this paper cover a wide range of values of the three determinant parameters. All these are tabulated in Table 1. The L/R ratios which must be less than unity and more than zero are represented by 2/3, 1/2, and 1/3. The values of the angle θ_0 had to be related to the number of pads employed in thrust bearings. In practical cases this number will rarely be less than 4 or more than 10. Solutions were obtained for θ_0 equal to 80, 55, 40, and 30 deg which, allowing space for the oil grooves correspond roughly to thrust bearings having correspondingly 4, 6, 8, or 10 pads. The values of a/b reflect the operating conditions and this parameter is represented by 1, 1/2, 1/4, and 1/8 which give ratios of inlet to outlet-film thickness up to 9. The solutions thus cover cases of high loading which cannot be obtained from the previous solutions of Muskat, Morgan, and Meres (2).

The three basic quantities involved in bearing calculations are minimum film thickness, lubricant flow, and power loss. An additional item of interest in case of thrust bearings is the center of pressure which is of importance for pivoted-shoe bearings. All these quantities are plotted in the following graphs and discussed.

Film Thickness. Fig. 2 shows the relation between the minimum film thickness and the thrust factor $(\mu N/P)(L/b)^2$ which in functional form is given by

$$a/b = f\left(\frac{L}{R}, \theta_0, T\right) \quad \ldots\ldots [6]$$

Figs. 3 and 4 are replotted from Fig. 2 to facilitate interpolation with respect to L/R and θ_0. Fig. 5 shows two typical pressure plateaus and Fig. 6 gives one-dimensional pressure profiles at the radial and circumferential mid-section of the bearing pad.

The plots suggest the following observations:

(*a*) Effect of parameter θ_0. There is, as shown in Fig. 4, an optimum θ_0 for a given L/R ratio. This is shown in Table 2. Thus,

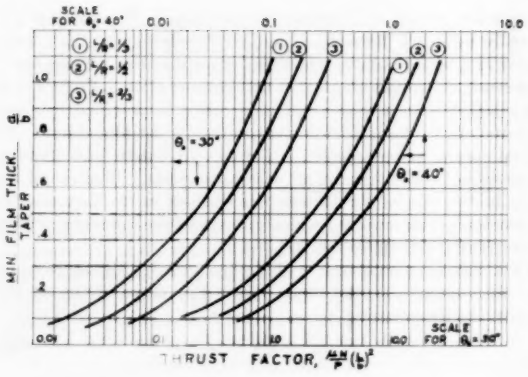

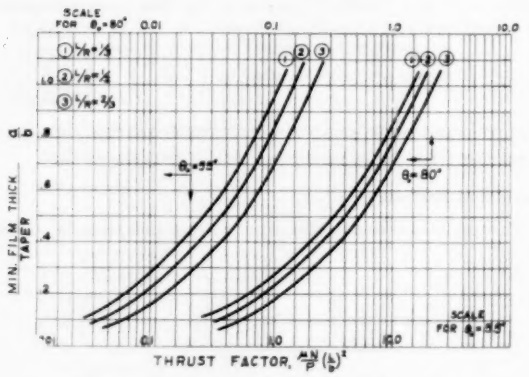

Fig. 2 Plot of thrust factor T as function of a/b

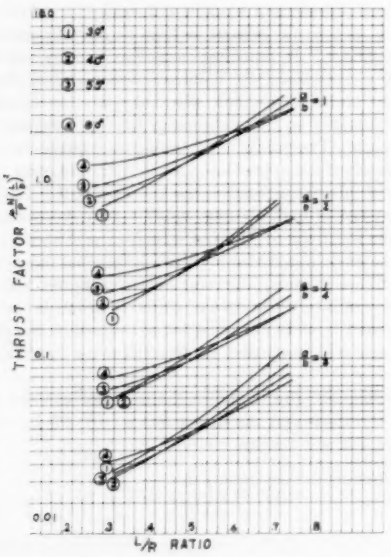

Fig. 3 Plot of thrust factor T as function of L/R ratio

by using the optimum number of pads, the highest load capacity or thickest oil film is assured. In general the higher the load and the higher the L/R ratio, the fewer pads are desired. High values of θ_0 bring the peak pressures closer to the trailing edge.

Table 1 Performance data for thrust bearings

a/b	θ_0	T	q_s	q_s	$\bar{x}$ θ_0	$\bar{x}$ r_0	λ	j
				L/R = 1/3				
1	80	1.423	0.81	0.062	0.64	0.37	0.17	2.44
	55	1.108	0.755	0.096	0.625	0.45	0.23	1.685
	40	0.947	0.68	0.13	0.61	0.49	0.36	1.26
	30	0.870	0.59	0.165	0.605	0.51	0.40	0.95
1/2	80	0.321	0.82	0.053	0.71	0.37	0.73	3.94
	55	0.257	0.76	0.082	0.69	0.47	0.94	2.70
	40	0.225	0.68	0.11	0.67	0.50	1.09	2.00
	30	0.211	0.60	0.14	0.66	0.51	1.18	1.57
1/4	80	0.0855	0.83	0.038	0.78	0.41	2.54	5.96
	55	0.0714	0.77	0.057	0.76	0.48	3.13	4.25
	40	0.0652	0.70	0.076	0.74	0.505	3.54	3.23
	30	0.0635	0.61	0.094	0.73	0.52	3.71	2.54
1/8	80	0.0278	0.83	0.020	0.83	0.465	7.15	8.51
	55	0.0247	0.78	0.029	0.815	0.50	8.38	6.23
	40	0.0238	0.71	0.037	0.795	0.51	8.98	4.86
	30	0.0242	0.625	0.045	0.78	0.565	9.07	3.91
				L/R = 1/2				
1	80	1.72	0.65	0.099	0.62	0.48	0.20	2.90
	55	1.494	0.55	0.14	0.61	0.51	0.23	1.96
	40	1.435	0.46	0.17	0.60	0.53	0.24	1.47
	30	1.489	0.37	0.20	0.59	0.55	0.24	1.13
1/2	80	0.402	0.655	0.083	0.685	0.46	0.81	4.72
	55	0.3585	0.56	0.11	0.67	0.52	0.93	3.33
	40	0.352	0.46	0.14	0.655	0.53	0.97	2.49
	30	0.370	0.37	0.16	0.65	0.55	0.93	1.92
1/4	80	0.1138	0.66	0.058	0.755	0.48	2.69	7.32
	55	0.1062	0.57	0.078	0.735	0.52	2.97	5.29
	40	0.108	0.47	0.095	0.72	0.54	2.98	4.065
	30	0.1163	0.38	0.11	0.71	0.56	2.80	3.18
1/8	80	0.0402	0.67	0.029	0.81	0.50	7.02	10.81
	55	0.0399	0.585	0.038	0.78	0.53	7.35	8.06
	40	0.0423	0.485	0.045	0.77	0.55	7.12	6.30
	30	0.0470	0.39	0.050	0.765	0.57	6.50	5.01
				L/R = 2/3				
1	80	2.240	0.48	0.12	0.61	0.50	0.18	3.06
	55	2.185	0.38	0.15	0.60	0.55	0.19	2.12
	40	2.320	0.30	0.18	0.59	0.58	0.18	1.57
	30	2.590	0.24	0.20	0.59	0.61	0.16	1.20
1/2	80	0.538	0.48	0.10	0.67	0.51	0.74	5.07
	55	0.537	0.38	0.13	0.66	0.56	0.75	3.59
	40	0.578	0.30	0.15	0.65	0.59	0.71	2.70
	30	0.653	0.24	0.16	0.645	0.61	0.63	2.07
1/4	80	0.1598	0.49	0.070	0.735	0.53	2.34	8.00
	55	0.1655	0.39	0.086	0.72	0.57	2.31	5.79
	40	0.1820	0.30	0.098	0.71	0.60	2.13	4.43
	30	0.2085	0.25	0.11	0.705	0.62	1.89	3.46
1/8	80	0.0599	0.50	0.034	0.79	0.55	5.79	12.07
	55	0.0649	0.40	0.040	0.78	0.58	5.52	8.98
	40	0.0737	0.31	0.045	0.765	0.61	4.95	6.94
	30	0.0861	0.24	0.049	0.76	0.63	4.31	5.47

Table 2 Optimum θ_0 values

L/R	a/b	θ_0	No. of pads
1/3	1	<30	More than 10
	1/2	<30	More than 10
	1/4	35	9
	1/8	40	8
1/2	1	40	8
	1/2	45	7
	1/4	50	6
	1/8	60	5
2/3	1	50	6
	1/2	60	5
	1/4	80	4
	1/8	>80	Fewer than 4

(*b*) Effect of parameter L/R. Higher L/R ratios will raise the unit load capacity. This trend is stronger at low values of θ_0.

(*c*) Effect of a/b. As in a journal bearing the load capacity goes up very rapidly with lower values of a. There is a 40-fold increase in load capacity when going from $a/b = 1$ to $a/b = 1/8$.

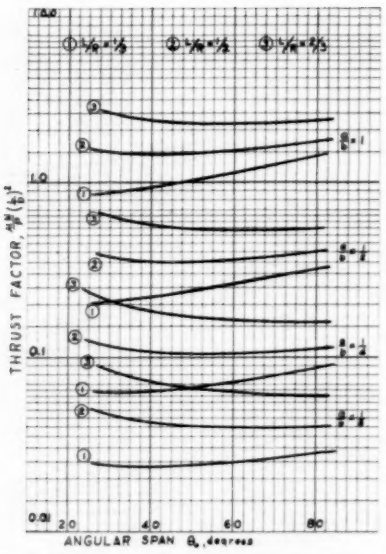

Fig. 4 Plot of thrust factor T as function of span θ_0

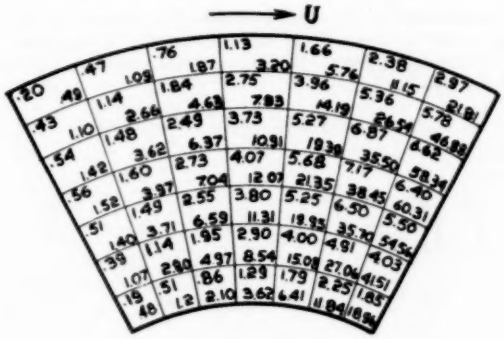

Fig. 5 Sample pressure distribution in a sectorial pad in terms of F_v

(*d*) The peaks of the radial-pressure profiles occur somewhat at the outside of the radial center line. The peaks of the circumferential-pressure profiles occur close to the trailing edge.

Lubricant Flow. The flow of lubricant out of any bearing, in the absence of feed pressure, is made up of two components; that due to shear and that due to the pressure gradients. The side leakage is due only to the hydrodynamic forces; the end leakage is made up of both the shear and pressure flows. The expressions for the two flows are as follows

$$Q_s = \int \frac{h^3}{12\mu} \left.\frac{\partial p}{\partial z}\right|_e dx \qquad [7]$$

$$Q_e = \int \left\{ \frac{Uh}{2} - \frac{h^3}{12\mu} \left.\frac{\partial p}{\partial x}\right|_e \right\} dz \qquad [8]$$

Expressing arbitrarily the hydrodynamic components of the two flows in terms of outward linear velocity, radial length, and taper as

$$Q = q\,\frac{U}{2}\,Lb = q\pi RNLb$$

we then have

$$Q_s = \int \frac{i^3}{12\mu} \left.\frac{\partial p}{\partial z}\right|_e dx = q_s \pi RNLb$$

$$Q_s = \int \frac{Uh}{2}\,dz = \int \frac{h^3}{12\mu} \left.\frac{\partial p}{\partial x}\right|_0 dz = q_s \pi RNLb$$

Using the substitutions employed in Equation [1] and remembering that $x = r\theta$, $z = r$, we have

$$q_s = \frac{1}{12\pi}\left(\frac{L}{R}\right)\int_0^{\theta_0} \bar{h}^3 \bar{r} \left.\frac{\partial p}{\partial \bar{r}}\right|_{R,\,r_0} d\theta$$

$$q_s = \frac{1}{12\pi}\left(\frac{L}{R}\right)\int_{r_0}^{R} \frac{\bar{h}^3}{\bar{r}} \left.\frac{\partial p}{\partial \bar{r}}\right|_{0,\,\theta_0} d\bar{r}$$

In view of the numerical nature of the solution of Equation [1] the foregoing equations too were summed on the computer. The shear component of Equation [8], however, can be integrated directly

$$\int_{r_0}^{R} \frac{Uh}{2}\,dr = \int_{r_0}^{R} \frac{2\pi rN}{2}\,a\,dr = \frac{\pi Na}{2}(R^2 - r_0^2) = \frac{\pi NLa}{2}(R + r_0)$$

Thus the side leakage of a sector thrust bearing is given by

$$Q_s = q_s \pi RNLb \qquad [9]$$

and the end leakage

$$Q_e = \frac{\pi NLa}{2}(R + r_0) + q_e \pi RNLb = \pi RNLb\left\{\left[1 - \frac{1}{2}\left(\frac{L}{R}\right)\right]\frac{a}{b} + q_e\right\} \qquad [10]$$

where q_s and q_e are found in Figs. 7 and 8.

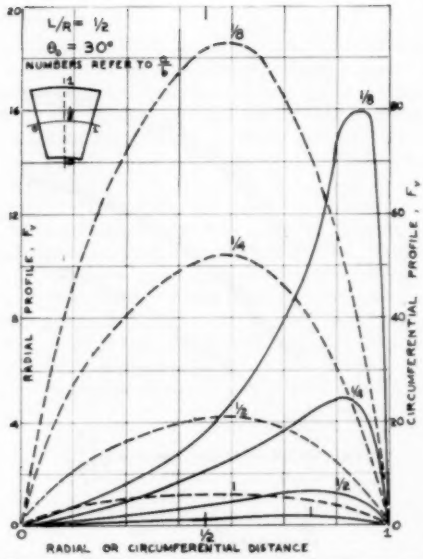

Fig. 6 Sample of radial and circumferential pressure profiles in terms of F_v

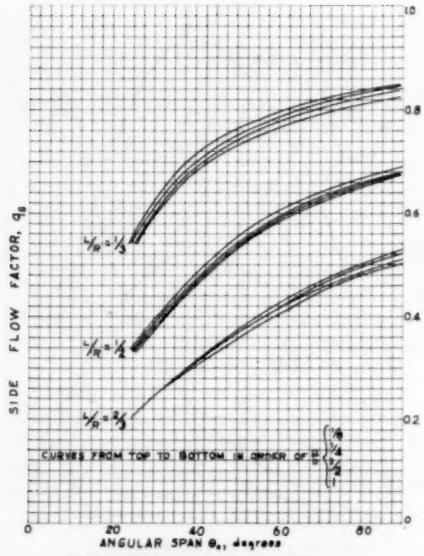

Fig. 7 Plot of side-flow coefficient

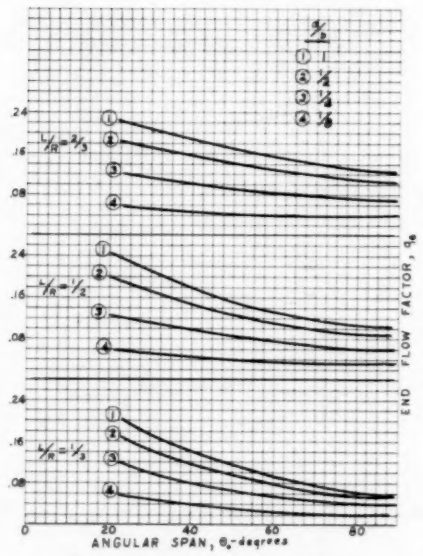

Fig. 8 Plot of end-flow coefficient

The striking phenomenon here is that the side flow is practically independent of the minimum film thickness. This is due to the fact that, as the gradients rise sharply with a decrease in a, the total film thickness h decreases and, since the flow is proportional to the cube of the clearance, the two effects cancel each other. The end flow naturally decreases with a drop in the maximum film thickness. With the end flow playing only a minor part, it develops that once the geometry of the bearing is fixed the oil flow through the bearing changes only with speed but is independent of such things as viscosity and load.

Power Loss. The linear velocity at any point across the oil film is given by

$$u = U\left(\frac{h-y}{h}\right) - y\left(\frac{h-y}{2\mu}\right)\frac{\partial p}{\partial x}$$

Differentiating this with respect to y

$$\frac{du}{dy} = \frac{U}{h} \pm \frac{h}{2\mu}\frac{\partial p}{\partial x} \quad \ldots\ldots\ldots\ldots\ldots [11]$$

where the + sign refers to the surface at the runner and the − sign to the surface at the bearing. The frictional force is then

$$dF = \mu\frac{du}{dy}\,dA$$

and the power loss at the runner surface

$$dH = U\,dF = \mu 2\pi rN\left(\frac{2\pi rN}{h} + \frac{h}{2\mu}\frac{\partial p}{r\partial\theta}\right) r\,dr\,d\theta$$

or

$$H = 2\pi\mu N\int_{r_0}^{R}\int_{0}^{\theta_0}\left(\frac{2\pi r^2 N}{h} + \frac{hr}{2\mu}\frac{\partial p}{\partial\theta}\right)d\theta\,dr$$

$$= 4\pi^2\mu N^2\int_{r_0}^{R}\int_{0}^{\theta_0}\frac{r^3}{a + b(1-\theta/\theta_0)}\,d\theta\,dr + \pi N\Sigma\Sigma hr\frac{\partial p}{\partial\theta}\Delta r\Delta\theta \quad \ldots\ldots [12]$$

The second term on the right-hand side of Equation [12] is again transformed by means of the substitutions used in Equation [1] into dimensionless form. With these transformations, Equation [12] becomes

$$H = 4\pi^2\mu N^2 I + \lambda\frac{\pi\mu(RNL)^2}{b}$$

where

$$I = \int_{r_0}^{R}\int_{0}^{\theta_0}\frac{r^3}{a + b(1-\theta/\theta_0)}\,d\theta\,dr = \frac{(R^4 - r_0^4)}{4b}\,\theta_0\ln\left(1 + \frac{b}{a}\right)$$

and

$$\lambda = \Sigma\Sigma h\bar{r}\frac{\partial p}{\partial\theta}\Delta\bar{r}\Delta\theta$$

Thus the expression for power loss is given by

$$H = \frac{\pi^2 N^2\mu}{b}(R^4 - r_0^4)\theta_0\ln\left(1 + \frac{b}{a}\right) + \lambda\frac{\pi\mu(RNL)^2}{b}$$

$$= \frac{\pi\mu N^2}{b}\left\{\pi\theta_0(R^4 - r_0^4)\ln\left(1 + \frac{b}{a}\right) + \lambda R^2L^2\right\}$$

Taking all dimensional parameters outside the parentheses, the equation becomes

$$H = \frac{\pi\mu N^2R^4}{b}\left\{\pi\left[1 - \left(1 - \frac{L}{R}\right)^4\right]\theta_0\ln\left(1 + \frac{b}{a}\right) + \lambda\left(\frac{L}{R}\right)^2\right\} \quad \ldots\ldots [13]$$

with λ given in Table 1.

Equation [13] also can be expressed in terms of a constant dependent on the bearing parameters and the operating variables

$$H = j\frac{\pi\mu N^2R^4}{b} \quad \ldots\ldots\ldots\ldots\ldots [14]$$

where

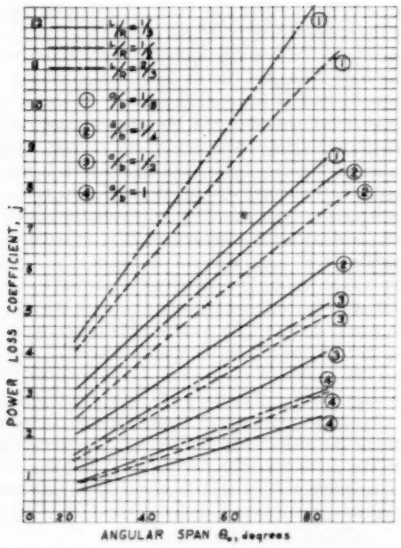

Fig. 9 Plot of power-loss coefficient

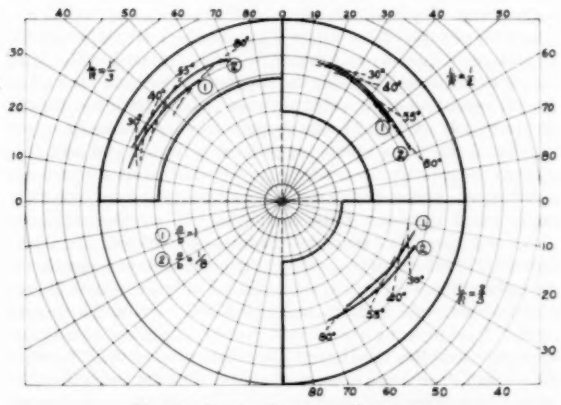

Fig. 10 Locus of centers of pressure

$$j = \left\{\pi[1 - (1 - L/R)^4]\theta_0 \ln\left(1 + \frac{b}{a}\right) + \lambda\left(\frac{L}{R}\right)^2\right\}$$

is given in Table 1 and Fig. 9.

Centers of Pressure. The values of the centers of pressure, i.e., the co-ordinates through which the resultants act, are listed in Table 1. In general the value of the radial co-ordinate $\bar{r}_0$ lies between 0.5 and 0.6; the angular co-ordinate $\bar{\theta}_0$ is between 0.6 and 0.8. These trends could be anticipated from the shape of the pressure plateaus sketched in Figs. 5 and 6. The loci of the centroids are plotted in Fig. 10 and the shifting tendency of the centroids for a clockwise rotation can be summarized as follows:

(*a*) The centroid shifts counterclockwise and downwards with a rise in θ_0 and a/b.

(*b*) The centroid shifts counterclockwise and upwards with a rise in L/R ratio.

These shifts, of course, are to be understood as relative to the sector whose radial and circumferential lengths are taken as unity.

Performance Calculation

The dimensionless group $T = (\mu N/P)(L/b)^2$ along with the L/R ratio and θ_0 provide all the necessary information for calculating bearing performance. The function (a/b) which is a criterion of load capacity will provide the maximum allowable loading if a minimum is set on the value of a. Power loss can be obtained directly from Equation [14]. The amount of lubricant flow depends on the geometry of the bearing. If the space between the sectors is wide and open then the total flow will include the end leakage. If, as is more common in practical bearings, the oil grooves are narrow and with small inlet orifices for the oncoming lubricant then the lubricant pumped out the trailing edge will be carried over into the next pad and, after being recirculated, will be discharged eventually as side leakage. The temperature rise, assuming that most of the heat is dissipated in the fluid film, is determined by the power loss and amount of flow of the lubricant. Collecting all the equations required to perform bearing calculations, we have

$$a = bf\left\{L/R,\ \theta_0,\ \frac{\mu_2 N}{P}\left(\frac{L}{b}\right)^2\right\} \quad \ldots\ldots [6]$$

$$Q = \begin{cases} Q_s = kq_s\pi RNLb & \ldots\ldots [9] \\ Q_s + Q_e = k\pi RNLb\left\{q_s + q_e + \frac{1}{2}\left[1 - \frac{1}{2}\left(\frac{L}{R}\right)\right]\left(\frac{a}{b}\right)\right\} & \ldots [10] \end{cases}$$

$$H = j\frac{k\pi\mu_2 N^2 R^4}{b} \quad \ldots\ldots [14]$$

$$\Delta t = \frac{H}{Jc_p\rho Q} \quad \ldots\ldots [15]$$

where k is the number of pads of the bearing.

All relations derived in the foregoing contain viscosity and the question arises what value should be assigned to it. Since no accurate $\mu = f(t)$ can be derived and since surely no expression embracing all possible lubricants exists that would enable the derivation of general dimensionless solutions, the best method was found to be that of using a representative or average viscosity. From tests and experience it has been found that the viscosity of the outlet temperature approximates closely such an average value. This constitutes the reason for using μ_2 in the performance equations.

This approach necessitates a few trials before the final, correct solution is obtained. A value of μ_2, corresponding to an estimated Δt, is assumed and the calculations are performed using this assumed μ_2. The Δt calculated from Equation [15] should correspond with the assumed value. If it does not, a different value of Δt is assumed and the process repeated. When the trial points, the assumed μ_2 versus calculated t_2, are plotted on the viscosity chart of the lubricant used and a line drawn through the points, this line will intersect the viscosity curve at the correct μ_2. Using then this last, correct value of μ_2, all correct bearing characteristics can be obtained.

Comparison With Other Results

The results of this analysis are here compared with those obtained by previous workers. Reference (4) expresses the load capacity in terms of a coefficient C_p given as follows

$$W = C_p\frac{\mu\omega R^4}{a^2}$$

where ω is the angular velocity. From the identity

$$P = \frac{\mu N}{T}\left(\frac{L}{b}\right)^2 = C_p \frac{\mu\omega R^4}{L^2 a^2}$$

we obtain after some rearrangement

$$C_p = 0.0625\,\frac{(a/b)^2}{T}\left(\frac{h_1/h_2 + 1}{2}\right)^2$$

where h_1 and h_2 are respectively the inlet and outlet film thickness. The comparative values of C_p are as follows:

	Value of C_p			
h_1/h_2	Muskat, et al. (2)	Brand (5)	C. S. & Y. (4)	Present work
2.00	0.081	0.081	0.0819	0.0826
2.50	0.113	0.116	0.1137	0.106
2.85	0.135	0.145	0.135	0.1253

It is indeed surprising that these various results obtained as they were by radically different analytical methods and also for somewhat different configurations and film shapes should be that close to each other.

A comparison was also made for the value of the friction coefficient C_F

$$F = C_F \frac{\mu\omega R^4}{a}$$

which in our case will yield

$$C_F = 0.305\,(a/b)\left\{2.35 \ln\left(1 + \frac{a}{b}\right) + 0.32\lambda\right\}\left(\frac{h_1/h_2 + 1}{2}\right)$$

The comparative values are as follows:

	Value of C_F			
h_1/h_2	Muskat, et al. (2)	Brand (5)	C. S. & Y. (4)	Present work
2.00	0.66	0.80	0.81	0.78
2.50	0.74	0.87	0.875	0.825
3.04	0.84	0.94	0.95	0.88

Acknowledgment

Acknowledgment is due to Mr. F. J. Maginnis of the General Electric Company for programming and supervising the computer solutions. The author also wishes to thank T. W. Steele of the General Electric Company for his help in checking the obtained results.

Bibliography

1 "Die Schmierung ebener Flächen," by A. G. M. Michell, *Zeitschrift für Mathematik und Physik*, vol. 52, 1905, pp. 123–138.

2 "Studies in Lubrication—VII, Lubrication of Plane Sliders of Finite Width," by M. Muskat, F. Morgan, and M. W. Meres, *Journal of Applied Physics*, vol. 11, 1940, pp. 208–219.

3 "A Simple Hydrodynamic Thrust Bearing," by F. R. Archibald, TRANS. ASME, vol. 72, 1950, pp. 393–400.

4 "On the Solution of the Reynolds' Equation for Slider-Bearing Lubrication—V, The Sector Thrust Bearing," by A. Charnes, E. Saibel, and A. S. C. Ying, TRANS. ASME, vol. 75, 1953, p. 1125.

5 "The Hydrodynamic Lubrication of Sector-Shaped Pads," by R. S. Brand, TRANS. ASME, vol. 73, 1951, pp. 1061–1063.

Discussion

D. F. Hays.[b] The increased use of digital computers in the analysis of two-dimensional lubrication problems is evident from a survey of current literature. This particular computer solution for the sector thrust bearing has been presented clearly and the content of the paper is comprehensive, covering a wide range of bearing operations. Since the problem was treated very thoroughly, the only comment to be made regards the warped-surface one-dimensional film configuration. Would it not be of greater interest to consider the two-dimensional film extent, wherein the taper is also a function of the radius? This would allow the design of pivoted-shoe bearings, which is not possible from this paper. It would also be helpful in the case of thrust bearings designed to equalize oil flows across the pads. Since a computer is used, this two-dimensional film distribution should not be too difficult.

In regard to the computer solution, the author's comment on the probable error introduced by a 7 × 7 mesh would be appreciated. It would appear that considerable error could result in attempting to evaluate the pressure gradients with such a coarse grid. Since the gradients are used in the flow expressions, these flows may vary considerably from the true differential-equation solutions. We have experienced some difficulty in using a grid size $^1/_4$ that of the author's in the case of one-dimensional problems where the gradients changed rapidly. The size of the grid chosen is also influenced by the computer space available and it was perhaps this factor which dictated the 7 × 7 mesh.

[b] Research Staff, General Motors Technical Center, Detroit, Mich.

Author's Closure

With regard to the first point raised by Mr. Hays, it should be realized that if a comprehensive set of solutions were to be obtained for two-directional tapers, the radial taper would constitute a new basic parameter and thus if four dimensionless values were picked for it (as was done for the circumferential taper) the number of required solutions would have been nearly 200 instead of the 50 given here. While the film shape treated here would imply a warped surface for a pivoted shoe bearing, it is a practical geometric configuration for a fixed plate of which most thrust bearings consist. In this connection the values given at the end of the paper are of interest. These values, as well as other available data, seem to indicate that once the inlet and outlet oil film thicknesses are fixed, the actual shape of the oil film is of no great importance. Thus the exponential film of reference (4) is almost identical with the uniform taper of Brand and of the present work. In comparing the present results with some incomplete data on a two-directional taper, the author found the differences to be small when using average values for the inlet and outlet film on the two-directional bearing. While the attainment of exact solutions for two-directional tapers remains a desirable goal, it is comforting to know that the one-directional taper solutions can be used as a fair approximation.

The grid size in numerical analyses makes little difference on the shape of the pressure profiles but may be of importance in the integrated values of load capacity. However, this too can be obtained with a high degree of accuracy without increasing the density of the network. Either additional pressure points can be fitted in on a linear basis and the results integrated, or trapezoidal integration can be used instead of the customary step function. This latter method was used in the present work. Thus trapezoidal integration used on a 7 × 7 grid yielded results very close to a 14 × 14 grid using step integration. The saving in computer time in this case was almost 75 per cent. The problem of obtaining accurate values for pressure gradients at the boundary remains critical even with a dense grid. In the paper the boundary points were located at a distance of half the ordinary grid interval from the boundary lines, i.e., at a distance of $^1/_2\Delta r$ and $^1/_2\Delta\theta$, to obtain a closer spacing of points. But the main problem still remains and that is the lack of a mathematical expression for the pressure field which alone could provide an accurate first derivative.

"DeCew Falls, Abitibi" Turbine Tests

By A. E. AEBERLI[1] and R. A. WALKER,[2] TORONTO, CANADA

This paper describes the results of Gibson tests for efficiency and performance of the DeCew Falls, Abitibi Francis turbine. This turbine was installed initially at the Abitibi Canyon station to operate under 237-ft head and was later removed and reinstalled at a new site in the DeCew Falls station to operate under 280-ft head. A comparison is developed to show the results "expected" at DeCew Falls from the original Abitibi tests versus the actual field test results obtained at DeCew Falls.

Introduction

THE function of laboratory tests on hydraulic turbine models in relation to predicted and guaranteed prototype field performance is of continuing interest, particularly when some form of penalty or bonus incentive clause for efficiency performance is written into the customer's specifications to develop a competitive atmosphere among prospective bidders. The question of test tolerances to be allowed in the absolute measurements of both hydraulic and electrical quantities becomes very important; namely, water-turbine discharge and generator output.

This paper reports an outline of the results of performance and efficiency tests carried out on the 66,000-hp Francis-type turbine originally installed at Abitibi Canyon G.S. under 237-ft head to operate at 150 rpm for 25-cycle service and later removed to DeCew Falls G.S. to operate at higher capacity under 280-ft head and 171.4 rpm synchronous speed with the generator rebuilt for 60-cycle service. Gibson tests for turbine discharge were carried out at both sites.

It was unusually fortunate that variable-speed tests from about 23 to 26 cycles synchronous speed were carried out in the original setting, but on another unit at Abitibi Canyon G.S., to provide some data to reasonably forecast the expected performance and efficiency of the Abitibi prototype turbine runner when moved to DeCew Falls G.S. and to compare these results with the model test data.

The Abitibi tests were carried out in 1936. In 1943, the unit, complete with generator, was moved to DeCew Falls and the turbine was provided with a new scroll case, embedded parts, and penstock. In 1955, the generator was rebuilt for 60-cycle service and the DeCew Falls tests were carried out in 1956.

Turbine-Discharge Measurements. At Abitibi four units were tested at 25-cycle synchronous speed over the full range of gate opening using the Gibson "time-pressure" method for turbine-discharge measurement and the individual units showed good agreement. The Gibson method also was used to test the Abitibi unit in the DeCew Falls setting at 60-cycle synchronous speed. The variable-speed tests at Abitibi unfortunately were not carried out on the particular unit brought to DeCew, but this is not considered too important since the variable-speed tests are intended mainly to show the relative rather than the absolute change in performance as speed and head are varied. The absolute values already had been established during the Gibson tests. Turbine-discharge measurements during the Abitibi variable-speed tests were made by index test correlated to the original Gibson test on that unit; the load consisted of an isolated nonsynchronous electric boiler supplied through an independent transmission circuit.

It is agreed generally that the Gibson measurements and power readings were carried out by competent engineers at both Abitibi and DeCew, respectively. All hydraulic and electrical quantities were corrected to the net pressure head effective at the turbine scroll-case inlet.

Turbine Setting. The general arrangement of the turbine installation particularly with regard to setting of the center line of the distributor in relation to tailwater level is shown in Fig. 1 for Abitibi and in Fig. 2 for DeCew. A cross section of the turbine is shown in Fig. 3.

Tests. The performance data given in Tables 1, 2, and 3 were taken directly from the curves in Figs. 4, 5, 6, 7, and 8. It is to be expected that the reader will disagree with the author as to what constitutes a proper analysis. However, the tables, summaries, and comments are shown in detail to enable the reader to follow the authors' conclusions.

Abitibi Test Results

Each of the turbines in this station is rated nominally at 66,000 hp, 150 rpm under 237-ft net head, with "best" efficiency expected at about 53,000–54,000 hp, all based on step-up to drawing dimensions from the model performance data, Table 2.

The actual field test performance of the units at Abitibi varies somewhat from the expected values owing to individual variations, in actual prototype runner dimensions "as cast," from the core-box drawing dimensions. A review of the original runner check sheet (as cast) showed the discharge diameter of the particular unit now at DeCew to be 139½ in.; or ½ in. below drawing of 140 in.; and similarly, the actual opening between blades at the discharge side averaged 7.2 per cent below drawing. Consequently the runner "as cast" had a discharge area 8.0 per cent below drawing dimensions.

1 *Gibson Tests (25-Cycle Synchronous Speed) on Abitibi No. 3 Unit.* This unit is the one that was installed later at DeCew Falls. For performance and efficiency test results see Figs. 4 and 5.

Best gate was found to occur at about 60 per cent of full servomotor stroke to develop 51,000 hp with 2020 cusecs (efficiency = 93½ per cent plus).

Maximum power was found to be 62,600 hp at approximately 87½ per cent gate, using about 2740 cusecs (efficiency 85 per cent). The unit at Abitibi may be said to be "overgated" since power output fell off appreciably at turbine-gate openings above 90 per cent of full servomotor stroke.

2 *Index Tests at Variable Speeds (23 to 26-Cycle) on Abitibi No. 2 Unit.* The performance of unit No. 2 at Abitibi had performance characteristics very similar to unit No. 3 and for this reason the results of variable-speed index tests were considered to be applicable to unit No. 3.

The results of the variable-speed tests on No. 2 unit are shown in Fig. 6. The data were reduced to equivalent values at 1-ft head for the prototype wheel. $N_1 = 9.75$ corresponds to 150 rpm operation at Abitibi under 237-ft net head. At the DeCew site, under a net head of 280 ft and a synchronous speed of 171.4 rpm, the value of $N_1 = 10.25$.

[1] Mechanical Engineer, Generation Department, Ontario Hydro.

[2] Assistant Hydraulic Engineer, Generation Department, Ontario Hydro. Mem. ASME.

Contributed by the Hydraulic Prime Movers Committee and presented at the Annual Meeting, New York, N. Y., December 1–6, 1957, of THE AMERICAN SOCIETY OF MECHANICAL ENGINEERS.

NOTE: Statements and opinions advanced in papers are to be understood as individual expressions of their authors and not those of the Society. Manuscript received at ASME Headquarters, July 25, 1957. Paper No. 57—A-57.

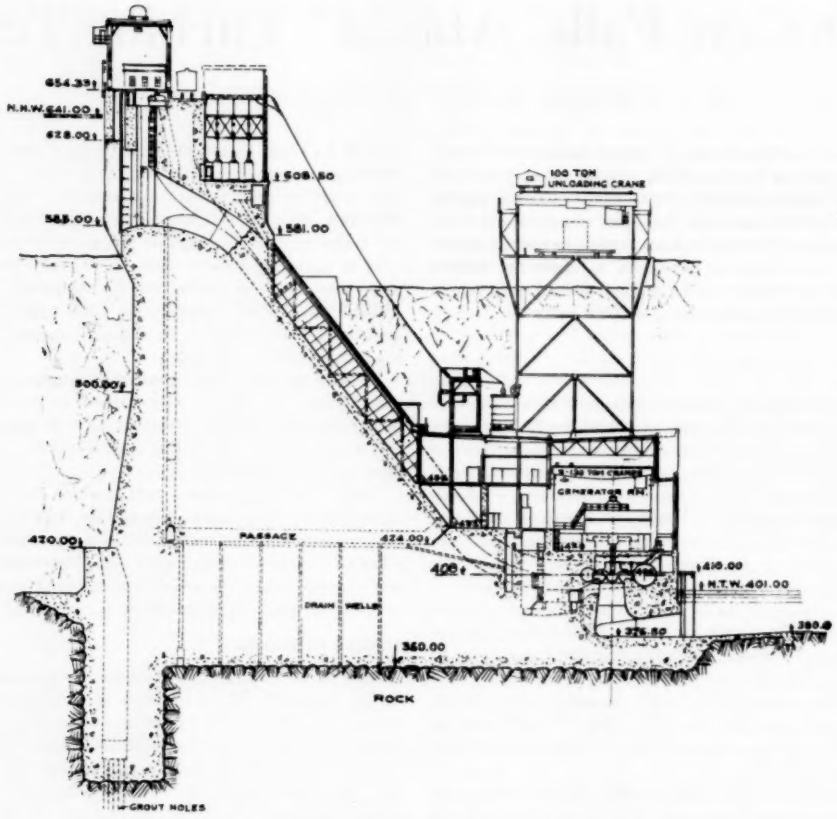

Fig. 1 Powerhouse—cross section—Abitibi Canyon

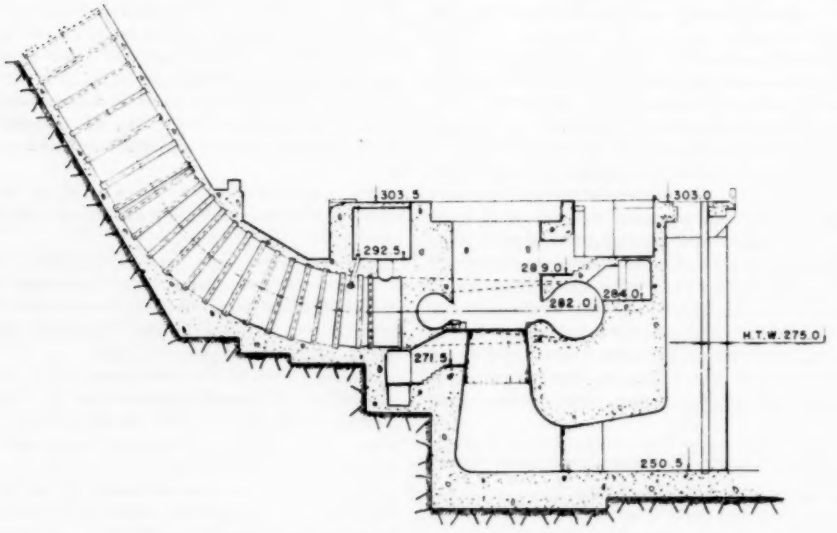

Fig. 2 Section through Unit No. 1—DeCew Falls

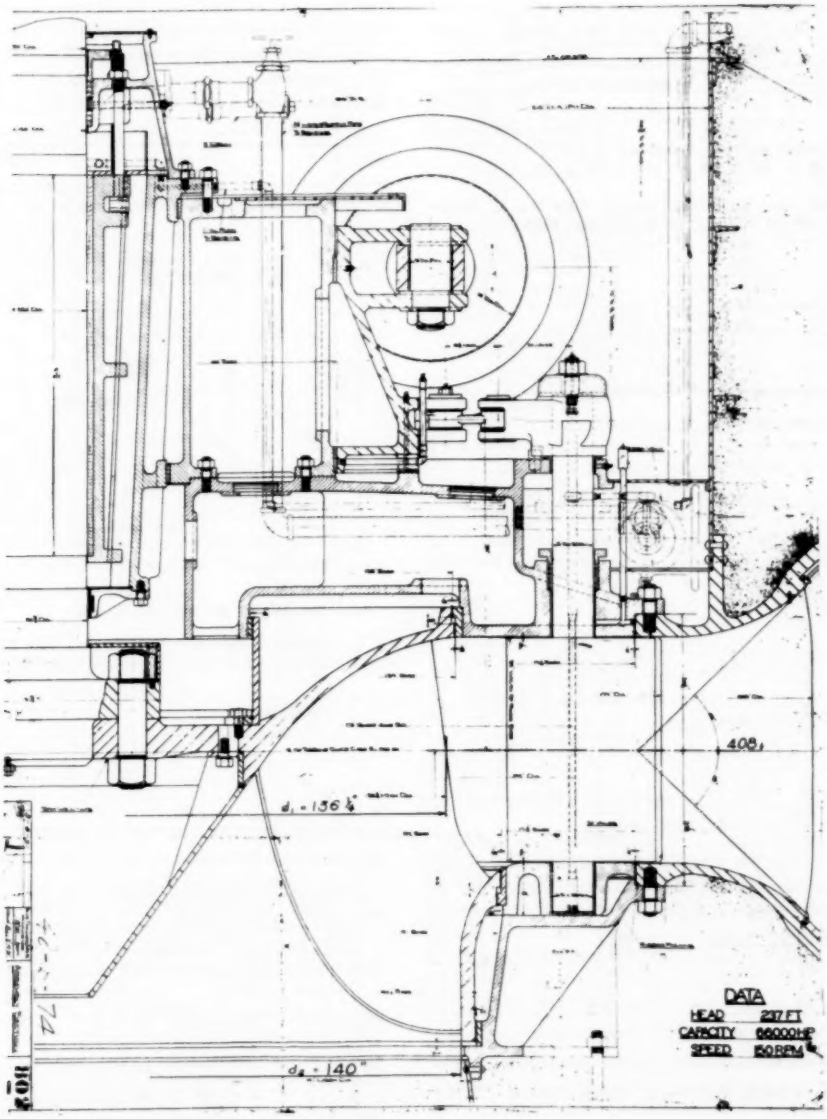

Fig. 3 Turbine arrangement

3 *Estimated Performance of DeCew No. 1 Unit (Formerly Abitibi No. 3 Unit) Under 280-Ft Net Head and Operating at 171.4 Rpm 60-Cycle Synchronous Speed.* It is of course obvious that a speed of 164 rpm would have been desirable at DeCew to duplicate the Abitibi speed coefficient. The decision to adopt 171.4 rpm at DeCew was mainly to accommodate the generator manufacturer in rebuilding the unit for 60-cycle service.

Reference to Fig. 6 indicates the basis for determining the expected performance of this unit as cast for the DeCew setting derived as outlined in Table 1. For the DeCew setting we would have expected best gate conditions to be 64,000 hp using 2160 cusecs and efficiency of 93.4 per cent (i.e., practically no loss in efficiency).

However, the foregoing conclusion neglects runner maintenance over the past 21 years. A recent inspection showed that stainless-steel protection had been added to both runner band and blades; to reduce the discharge diameter to 139 in. (1 in. below drawing of 140 in.) and the opening between blades 9.2 per cent below drawing. The discharge area is now a total of 11 per cent below drawing. Thus the present-day performance of the runner now installed in DeCew No. 1 unit is expected to be about 3 per cent less in power and discharge because of these further reductions (throat diameter, $^1/_2$ in., and discharge opening between blades, 2 per cent).

Making allowance for this change, the final expected performance is submitted in Table 1 and summarized as follows:

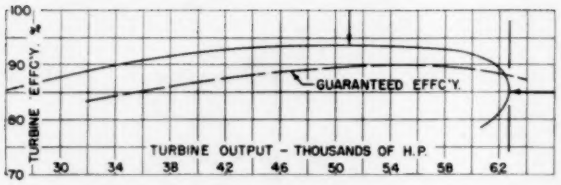

Fig. 4 Turbine efficiency on turbine output, Unit No. 3, Abitibi Canyon. Net head 237 ft; Gibson test of January, 1936.

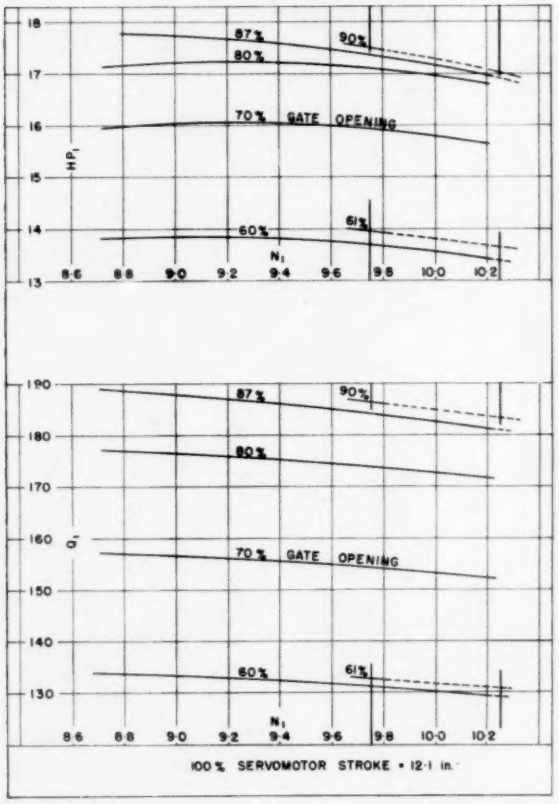

Fig. 6 Variable speed tests, Unit No. 2, Abitibi Canyon. Test of February, 1936.

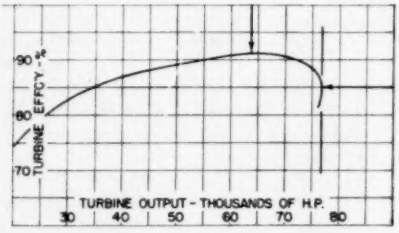

Fig. 7 Turbine efficiency on turbine output, Unit No. 1, DeCew Falls. Net head 280 ft; Gibson test of May, 1956.

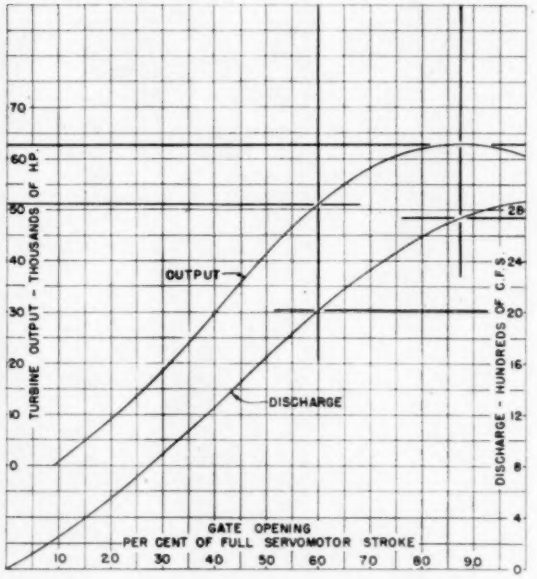

Fig. 5 Turbine output and discharge on gate opening, Unit No. 3, Abitibi Canyon. Net head 237 ft; Gibson test of January, 1936.

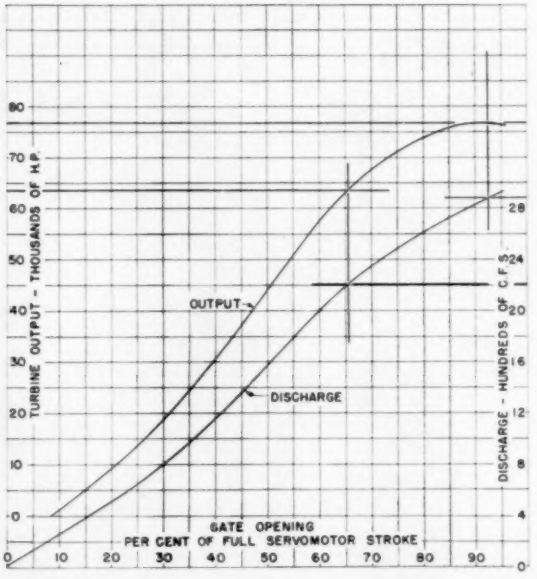

Fig. 8 Turbine output and discharge on gate opening, Unit No. 1, DeCew Falls. Net head 280 ft; Gibson test of May, 1956.

Table 1 As-cast expected performance on Unit No. 1, DeCew Falls (Unit No. 3, Abitibi Canyon) from data of prototype Unit No. 2, Abitibi Canyon; e.g., variable speed tests (Fig. 6)

	At Abitibi Site		At DeCew Site	
	Abitibi No. 2	Abitibi No. 3	Abitibi No. 2	Abitibi No. 3 - DeCew No. 1*
Net Head - feet	237	237	280	280
Synchronous Speed - rpm	150	150	171.4	171.4
Original Servomotor Stroke inches - 100% gate	12.1	12.1	12.1	12.1
Best Gate (Variable Speed Data) 61%		-	61%	-
H_1	9.75	-	10.25	-
HP_1	13.96	-	13.65	-
Q_1	133	-	131.1	-
Best Gate (Gibson Tests)	61%	60%	61%	60%
Power - Hp	51,000	51,000	64,000 Est.	64,000 Est.
Discharge - Cusecs	2,050	2,020	2,195 Est.	2,160 Est.
Efficiency	93%	93-1/2% plus	92% Est.	93.4% Est.
Max. Power Gate (Variable Speed Data)	90%	-	90%	-
H_1	9.75	-	10.25	-
HP_1	17.5	-	17.01	-
Q_1	186.2	-	183.2	-
Max. Power Gate (Gibson Tests) 90%		87-1/2%	90%	87-1/2%
Power - Hp	64,000	62,600	79,900 Est.	78,200 Est.
Discharge - Cusecs	2,870	2,740	3,070 Est.	2,930 Est.
Efficiency	83%	85%	82% Est.	84% Est.

Summary for DeCew No. 1 Unit*

	Hp	Q	E
Best Gate Expected (adjusted - 3% for stainless repairs)	62,100	2,095	93.4%
Max. Power Gate Expected (adjusted - 3% for stainless repairs)	75,900	2,845	84%

	DeCew
Net head, ft	280
Speed, rpm	171.4
Best gate:	
HP, expected	62100[a]
Cusecs, expected	2095[a]
Efficiency, expected per cent	93.4
Maximum power gate:	
HP, expected	75900[a]
Cusecs, expected	2845[a]
Efficiency, expected per cent	84

[a] Corrected for stainless repairs.

4 *Gibson Tests at DeCew Falls Site—60-Cycle Synchronous Speed.* The results of performance and efficiency tests conducted at DeCew in 1956, are shown in Figs. 7 and 8.

As already noted, Table 1 outlines the arithmetic basis to step up the Abitibi performance data to determine the results expected in the DeCew setting. The comparison between these expected results and the Gibson test results is shown as follows:

	1956 test	Expected
Best gate:		
HP	63700	62100
Cusecs	2200	2095
Efficiency, per cent	91.2	93.4
Maximum power gate:		
HP	76700	75900
Cusecs	2880	2845
Efficiency, per cent	85	84

It will be noted that some discrepancies are present between the expected and the test results. It may be mentioned, however, that the test results for DeCew No. 1 unit did in fact allow a very close estimate and agreement with test data on another unit at DeCew. The latter turbine as cast had water passages equally as much oversize from drawing dimensions as the Abitibi, DeCew unit was below drawing.

Model Tests. Data based on a step-up of the manufacturer's model tests are submitted in Table 2 and summarized as follows:

Table 2 Data from manufacturer's model tests. Unit No. 3, Abitibi Canyon, later relocated at DeCew Falls, Unit No. 1

	Model	At Abitibi No. 3	At DeCew No. 1
Net Head - feet	-	237	280
Synchronous Speed - rpm	-	150	171.4
Servomotor Stroke inches	0.798"	11"	11"
Full Stroke - 100% gate	-	12"	12"
Best Gate	0.532"	60%	60%
n_{10} (d_2 = 140.0")	-	136.0	143.0
hP_{10}	-	0.0755	0.0742
e	-	91.2%	91%
Power - Hp (Expected from Dwg.)		54,000	68,200
Power (adjusted for actual blade openings - as cast)	(-8%)	49,700 Est.	-
Power (adjusted for stainless repairs)	(-11%)	-	60,700 Est.
Maximum Power Gate	0.798"	90%	90%
n_{10} (d_2 = 140.0")		136.0	143.0
hP_{10}		0.0922	0.0912
e		84.4%	83.8%
Power - Hp (Expected from Dwg.)		*66,000	83,700
Power (adjusted for actual blade openings - as cast)	(-8%)	60,600 Est.	-
Power (adjusted for stainless repairs)	(-11%)	-	74,500 Est.

Summary	At Abitibi No. 3		At DeCew No. 1	
Best Gate	HP	e	HP	e
Expected	49,700	91.2%	60,700	91%
Maximum Power				
Expected	60,600	84.4%	74,500	83.8%

*Rated (Full Load) Output was 66,000 horsepower

	Abitibi	DeCew
Net head, ft	237	280
Speed, rpm	150	171.4
Best gate, HP, expected	49700[a]	60700[b]
Test	51000	63700
Maximum power, HP, expected	60600[a]	74500[b]
Test	62600	76700

[a] As cast.
[b] Correction for stainless repairs.

Table 3 is a comparison of all data for the unit under discussion; both at the Abitibi site and later at the DeCew site. For the Abitibi location, we have shown the turbine output and efficiency to be expected from the manufacturer's model data versus the field test data for best gate and maximum power gate. For the DeCew location the same information is given, together with the results to be expected at DeCew from the actual performance of the unit at Abitibi.

Conclusions

The high best-gate values of the field efficiency tests (93 per cent or better) obtained in 1936 on the Abitibi turbines were accepted with satisfaction by both the customer and manufacturer. The fact that the turbines did not quite meet the rated capacity of 66,000 hp under 237-ft head was of minor consequence and was easily explained by the condition of the actual runner castings in comparison to the core-box drawings.

The most interesting information in Table 3 is in the comparison of the actual efficiency performance of the turbine in the DeCew setting relative to the results expected from a step-up of the prototype test data obtained on the same wheel in the Abitibi setting (outlined in Table 1).

At DeCew, the Abitibi unit was expected to produce at best gate about 62,100 hp using 2095 cusecs at 93.4 per cent efficiency; whereas the field test data for DeCew indicated that best efficiency of 91.2 per cent was attained over a broad range in power

Table 3 Comparison of performance from tests and by calculation

	At Abitibi No. 3 Unit		At DeCew No. 1 Unit (Formerly Abitibi No. 3 Unit)	
Net Head - feet	237		280	
Synchronous Speed - rpm	150		171.4	
Best Gate	**Hp**	**Efficiency**	**Hp**	**Efficiency**
Field Test	51,000	93-1/2%	63,700	91.2%
Expected from Abitibi Prototype Test - Table I	-	-	62,100	93.4%
Manufacturer's Model Test - Table II	49,700	91.2%	60,700	91%
Maximum Power				
Field Test	62,600	85%	76,700	85%
Expected from Abitibi Prototype Test - Table I	-	-	75,900	84%
Manufacturer's Model Test - Table II	60,600	84.4%	74,500	83.8%

output averaging about 63,700 hp. The expected maximum power was 75,900 hp at 84 per cent efficiency and 76,700 hp was actually obtained at 85 per cent efficiency.

At DeCew the efficiency is about 2.2 per cent less than expected at best gate; and 1 per cent higher than expected at maximum power output (full gate). These variations are greater than anticipated because the expected values were derived from the prototype runner operating in the Abitibi setting. The results indicate a need for caution in eulogizing or alternatively deprecating the performance data of any individual model or prototype turbine unless a reasonable tolerance band of 1 or possibly 2 per cent is allowed in the accuracy of the test findings.

Consequently, the validity of penalty or bonus incentive clauses for efficiency performance to a decimal point should always be reviewed and evaluated by responsible engineers, since the absolute values of variations in efficiency are magnified by any errors in power and discharge measurements.

Discussion

M. Braikevitch.[3] The authors are to be congratulated on dealing with very efficient turbines, which is not surprising seeing the care with which their principals order and inspect the machinery.

The paper is a valuable contribution to the deduction of turbine performance from model tests. It would be interesting to know the diameter of the model runner, and whether a completely homologous model including inlet bend, spiral, and draft tube was constructed or whether just the runner and gate apparatus were homologous.

From the figures in Table 2 it would appear that the model runner was about 10 in. in diam. This seems small by present-day standards, because with a small model the increase in efficiency works out rather large and as such is somewhat uncertain. Thus taking the modern Moody formula with the 5th root, the best model efficiency works out at 85.1 per cent, while with the older formula using the 4th root the corresponding figure is 83.0 per cent; this gives a majoration of 6.1 and 8.8 per cent, respectively, to get to the expected figure of 91.2 per cent given in Table 2.

It would be interesting to see the contour curves of the model runner; i.e., the plots of equal efficiency contours on a diagram having unit speed n_1 horizontally and unit quantity q_1 vertically. Such a diagram readily indicates the change in performance with an alteration in the speed and head, and gives a good idea of the behavior of the wheel under varying conditions.

When model tests are relied on, it is essential to check the model accurately against the drawing, and it is equally essential to check the full-size runner against the model. This especially applies to vane shape at the exit where the vane angle must be correct in addition to the actual openings between the vanes being to drawing. It will be noted that the full-size wheel differs appreciably from the model in having a somewhat smaller outlet area. A further point is that the full-size wheel must be well finished to have smooth vanes.

Apparently after 20 years of service the runner has lost about 2 per cent in peak efficiency. This is not surprising as evidently a fair amount of stainless-steel welding had to be done. This may have thickened the vanes slightly at the outlet and so changed the shape. In any case maintenance appears to have been excellent.

When a penalty and bonus incentive clause is written into a contract it would be reasonable to allow a tolerance of plus-minus 1 per cent (2 per cent if test conditions are difficult) to cover for the possible inaccuracies of measurement which are many, however carefully the tests are conducted.

Papers such as this are very valuable when we are relying more and more on model test data instead of costly field tests.

J. B. Holt.[4] This is an interesting paper from at least three points of view: (*a*) It is seldom that tests are made on the same turbine located in different powerhouses operating under different heads, and are available for study. (*b*) The test results and turbine measurements indicate that the maximum power output attained at the second installation could have been predicted within 0.3 per cent. (*c*) The test results indicate that the inaccuracies of measurement may be as much as 2 per cent.

The writer does not agree with the authors in their calculation method of adjusting the expected power output because of the difference in runner dimensions. To determine a cross-section flow-area comparison between the two runners the difference of area at discharge and the difference of area between buckets should not be added since the opening areas are upstream from the discharge area.

The expected power output could have been predicted to within 0.3 per cent by using the ratio of the discharge areas between buckets. This should not be used in direct proportion to power output, but should be adjusted by a factor determined from the original plant Gibson tests and runner measurements, or the original plant Gibson test, the model test, and runner measurements. The Gibson test at the original plant showed 62,600 horsepower or a reduction of 5.15 per cent below the 66,000 hp indicated by the model. The runner-bucket openings were 7.2

[3] Technical Manager, Water Turbine Department, The English Electric Company, Ltd., Rugby, England.

[4] Supervisory Engineer, Hydraulic Department, Allis-Chalmers Manufacturing Company, Milwaukee, Wis.

per cent small. Then by direct proportion 9.2 per cent small openings should result in a 6.58 per cent reduction in power below the 66,000 hp. Adjusting this for the change in head and speed between the two plants, the calculated expected maximum horsepower output for the Abitibi unit No. 3 in the Decew Falls Plant becomes

$$66{,}000 \times (1.00 - 0.0658) \times \left(\frac{280}{237}\right)^{5/2} \times \frac{17}{17.5} = 76{,}912 \text{ hp}$$

Compared with 76,700 hp measured on the Gibson test at DeCew Falls this is 0.27 per cent.

G. D. Johnson.[5] It is easy to subscribe to the authors' opening statement, "the function of laboratory tests on hydraulic turbine models in relation to predicted and guaranteed prototype field performance is of continuing interest." It is also especially interesting to study their paper on these unusual field tests . . . . on the same prototype unit in two different generating stations . . . . together with corresponding model test data.

The authors' conclusion that a reasonable tolerance of 1 or 2 per cent should be allowed in the accuracy of the test findings when evaluating any performance test data is endorsed enthusiastically by the writer. Because of the real difficulties and expense involved in reducing over-all field-test inaccuracies to less than this, there is no reason to doubt the authors' statement that the Abitibi and DeCew tests were carried out by competent engineers.

The authors' comparisons between model and prototype indicate field-test outputs 3 per cent greater than the corresponding laboratory data corrected for runner-discharge areas. This discrepancy is slightly greater than similar comparisons made by the writer's company, the agreement always being within ±2 per cent when the complete laboratory model is essentially homologous to the prototype. Apparently, the maximum model efficiency of approximately 91 per cent compares directly with the DeCew field-test efficiency (no step-up), whereas the Abitibi test indicates a peak efficiency increase of over 2 per cent above the model.

These results of well-conducted field tests certainly support the authors' final conclusion that the validity of efficiency penalty or bonus clauses dealing in hundredths or tenths of 1 per cent should always be reviewed and evaluated by responsible engineers who take all of the inaccuracies of measurement into account.

W. J. Rheingans.[6] The authors have made an interesting comparison of field tests on the same unit installed in two different powerhouses. Such a comparison should give some indication of the accuracy that can be expected from actual field tests. However, in making such a comparison we must consider certain factors which may have influenced the performance of the unit at DeCew Falls as compared to its original performance at Abitibi.

One factor is the difference in unit speed between the two installations. The author states that there is practically no loss in efficiency between the two speeds, based upon index tests that were made at variable speeds on Abitibi unit No. 2. Fig. 6 shows unit horsepower and discharge. Since the scale is rather small it is difficult to determine the efficiency from this figure with a great degree of accuracy. However, going back to the original test report, where the values were plotted on a large scale, we find that there is a difference of 0.8 per cent in efficiency at 0.60 per cent gate between the two unit speeds.

Thus the efficiency of the Abitibi unit No. 3 at the DeCew Falls unit speed would be 93.5 − 0.8 = 92.7 per cent.

The DeCew Falls generator consists of the old 25-cycle Abitibi generator rebuilt for 60-cycle service. The authors make no mention of whether a field test was made on this rebuilt generator to determine its losses. Estimation or calculation of generator losses could be in error by as much as 0.5 per cent.

Maintenance of the runner over a period of 21 years reduced the discharge area 3 per cent below the original area. The author makes allowance for this in comparing the output but not in comparing the efficiency. In making repairs such that they reduced the discharge areas, the shape of the runner blades must have been changed. The addition of stainless steel must have increased the thickness of the trailing edge of the runner blades. Experience has shown that this has a measurable influence on efficiency, the thicker the blade, the less efficiency.

Another factor that was neglected is the wear on the runner, wicket gates, and guide case during 21 years of operation. Although the authors make no mention of it, we assume that the running clearances at DeCew Falls were the same as the original clearances at Abitibi. However, during 21 years of operation there certainly was sufficient wear on the runner and wicket gates to influence the efficiency.

A. Puyo[7] concluded that even after reconditioning, the influence of wear on efficiency in Francis turbines is 1 to 2.5 per cent during first years of service, with relatively clean water. This was based on tests on units operating under 330 to 660 ft head. This is an indication of what can be expected under somewhat lower heads, during a period of 21 years of operation.

Taking into account all of these factors, the 91.2 per cent efficiency actually obtained at DeCew Falls seems to be an excellent check.

However, the authors' conclusion that a tolerance band of 1 or possibly 2 per cent be allowed in accuracy of test findings has considerable merit.

P. A. Soicher.[8] The Hydro-Electric Power Commission of Ontario and the authors are to be commended for the expense and effort involved in carrying out and reporting the tests described in this paper. Field tests on hydraulic turbines are useful to the purchaser and plant operators in evaluating the performance of the machines they have purchased with respect to expected and guaranteed characteristics, and in establishing the power production regime of a station or of a particular unit in a station. From the turbine manufacturer's point of view the results of field tests are a source of invaluable information in correlating and evaluating model test results carried out in the laboratory. Without field testing information the turbine manufacturer would lack a very essential check on the accuracy and adequacy of his model test results and testing methods.

In view of the fact that the unit tested was in service for 20 years, was removed and reinstalled, fitted with a new scroll case and embedded parts, and that no allowance is made for the effect on performance of the repair welding, other than the reduction in throat diameter and discharge area, it is believed that the difference between the estimated and actual performance of the DeCew unit is not really excessive.

The realistic attitude that the authors take toward the degree of accuracy that reasonably can be attained in a field test is most commendable. To place a high premium on an unusually high guarantee when evaluating tenders may often be rewarding a manufacturer for his willingness to gamble on a high test or on

[5] Chief Hydraulic Engineer, S. Morgan Smith Company, York, Pa. Mem. ASME.

[6] Manager, Hydraulic Department, Allis-Chalmers Manufacturing Company, Milwaukee, Wis. Mem. ASME.

[7] "Francis or Impulse, the Influence of Wear and Operating Conditions," by A. Puyo, ASME Paper 49—A-111. (Unpublished.)

[8] Sales Manager, Hydraulic Division, Dominion Engineering Company, Ltd., Lachine, Quebec, Canada.

the fact that the unit cannot be tested in accordance with an approved test code. It should be realized, however, that a manufacturer is entitled to credit for a high guarantee if his guarantee is consistent with the average results of a number of field tests performed according to the code on hydraulically similar units.

Authors' Closure

The authors wish to express their sincere thanks to the various hydraulic engineers who have taken part in discussions to this paper.

In conclusion, we note particularly Mr. Rheingans' comments and can offer the assurance that, after the generator was rebuilt for 60-cycle service, field tests were made to determine electrical performance.

Subsequent to the preparation of this paper, it now has been decided to install a new runner of higher output in the DeCew No. 1 unit and to return the runner referred to in this paper back to Abitibi. The runner will be reinstalled as Abitibi unit No. 3 with the original embedded parts together with new guide vanes, headcover, etc., rebuilt to the original drawings. Thus we will in 1959 have an opportunity to retest the turbine for the third time and the results should again be rather interesting.

Symposium on Laboratory Testing of Hydraulic Turbine Models in Relation to Field Performance[1]

This report includes, in full, the five prepared statements by representatives of the major American manufacturers and, in condensed form, the written and oral discussions presented at the 1956 Annual Meeting. These discussions have been condensed by Mr. G. Dugan Johnson, the 1956 Chairman of the Hydraulic Prime Movers Subcommittee, to reduce the over-all length of this publication and have not been edited by the respective authors. Therefore they may not reflect the intended and fully considered opinion of the parties quoted and where this is the case these authors are particularly requested to submit written discussions, correcting or appending this record. The Summary has also been prepared by Mr. Johnson and reflects his personal and tentative summation of the points on which the panel members and discussers appear to him to agree. It is offered as a basis for discussion at the 1957 Annual Meeting, particularly by each panel member and discusser quoted in this report.

Prepared Statement by Mr. Rheingans

DURING the latter part of the nineteenth century and the first part of this century, American waterwheel manufacturers used the facilities of the Water Power Company of Holyoke to test the performance of model runners. In those days, it was taken more or less for granted that the runner was the principal factor and little thought was given to draft tube design, casing design, or settings, as affecting runner performance. Thus the majority of the Holyoke model tests were conducted with long straight draft tubes, in a large open flume setting with high sigma values; ideal conditions for producing optimum runner performance. Gradually it was recognized that draft tube design, casing design, and setting had considerable influence upon the performance of a given runner. Beginning about 1916, hydraulic turbine manufacturers started construction of their own laboratories and started to test their model runners, first with the draft tubes and later also with the casings they were using in the field. This changed the entire concept of model testing, until today it is recognized that in order to predict the field performance of a prototype with accuracy, the model test must be made with homologous intake, casing, wicket gates, guide case, and draft tube, in addition to the runner.

In comparing the performance of a model test with the field test of a prototype, quite a number of factors have to be taken into consideration. First, the model must be homologous in all respects to the prototype, including intake, spiral casing, stay ring, wicket gates, guide case, runner, and draft tube.

The model must be tested with the cavitation sigmas corresponding to the field sigmas. Furthermore, the measurement of the quantities that determine the performance must be made with close absolute accuracy. This is sometimes difficult to obtain. It is not too difficult to measure the torque, speed, and head with a fair degree of accuracy. However, accurate measurement of water quantities is not a simple matter. It might appear that accurate measurement of flow under laboratory conditions should be relatively easy. This is not the case. Up until about five years ago, the writer's company used weirs for measuring the water quantities in hydraulic turbine model testing. It was found that these gave inconsistent results and the measurements would depend upon temperature and other factors which were difficult to evaluate. Although attempts were made to calibrate the weirs, it was always felt that the absolute accuracy of the test results was in considerable doubt.

The next step was to use calibrated venturi meters. However, even here it was found that unless the venturi meters are actually calibrated in place under the exact model test conditions there can be considerable errors in the absolute measurements. It is surprising how often such "in place" calibrations will give venturi coefficients close to 1.00 or even above.

Thus it is the opinion of the writer that careful consideration must be given to all the measurements involved in model testing to get an absolute accuracy within 1 per cent.

The next step in comparing the performance of a model with the field prototype is to obtain an accurate field test. Based upon the difficulties encountered in obtaining accurate laboratory tests, especially the measurement of the quantity of water, accurate field tests become a herculean job. It is unfortunate that not many engineers in the hydroelectric field appreciate the problems and difficulties to be overcome in obtaining accurate field performance data. This is particularly true of the water

---

[1] A report on the session held at the Annual Meeting on Tuesday afternoon, November 27, 1956, in the Hotel Statler, New York, N. Y., by G. Dugan Johnson, 1956 Chairman, Hydraulic Prime Movers Subcommittee.

The members of the panel were as follows:

H. J. PETERSEN, *Chairman*, Vice-President and Power Consultant, United Engineers and Constructors, Inc., Philadelphia, Pa. Mem. ASME.

G. F. CROWE, *Vice-Chairman*, Assistant Mechanical Engineer, New England Power Service Company, Boston, Mass. Mem. ASME.

WILLIAM J. RHEINGANS, Manager, Hydraulic Department, Allis-Chalmers Manufacturing Company, Milwaukee, Wis. Mem. ASME.

WILLIAM R. MACNAMEE, Chief Engineer, Hydraulic Turbines and Marine Products Department, Baldwin-Lima-Hamilton Corporation, Eddystone, Pa. Mem. ASME.

ROBERT S. SPROULE, Manager, Hydraulic Division, Dominion Engineering Company, Ltd., Montreal, Quebec. Mem. ASME.

BRUCE L. VANDERBOEGH, Hydraulic Engineer, Newport News Shipbuilding and Dry Dock Company, Newport News, Va. Mem. ASME.

G. DUGAN JOHNSON, Chief Hydraulic Engineer, S. Morgan Smith Company, York, Pa. Mem. ASME.

Contributed by the Hydraulic Prime Movers Subcommittee of the Hydraulic Division and presented at the Annual Meeting, New York, N. Y., December 1–6, 1957, of THE AMERICAN SOCIETY OF MECHANICAL ENGINEERS.

NOTE: Statements and opinions advanced in papers are to be understood as individual expressions of their authors and not those of the Society. Manuscript received at ASME Headquarters, July 26, 1957. Paper No. 57—A-124.

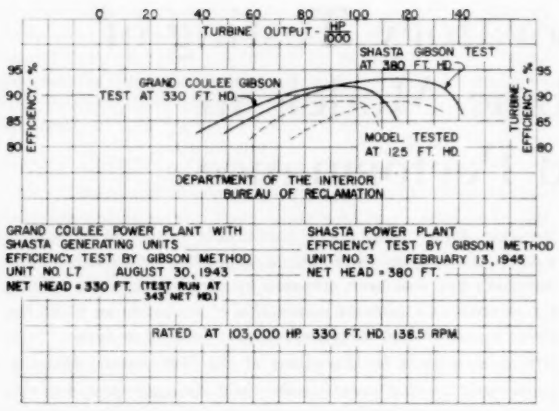

Fig. 1 Comparison of model tests with field tests of duplicate units installed in two different installations (Grand Coulee and Shasta)

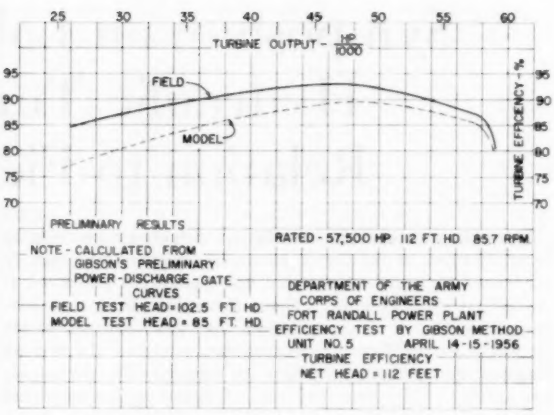

Fig. 2 Comparison of model test with field test (Fort Randall)

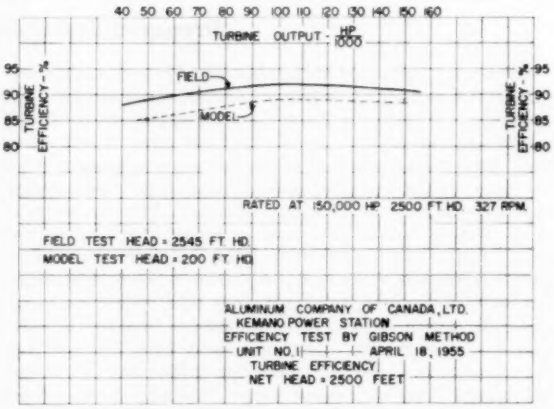

Fig. 3 Comparison of model test with field test for impulse turbine (Kemano)

measurement although power output and head measurements also pose serious difficulties. When it is realized that in laboratory testing, instruments are calibrated and recalibrated, tests are checked and rechecked, and close control is kept over all the work in order to assure an absolute accuracy in the order of 1 per cent, it then becomes highly doubtful whether field tests, which are usually a one-shot test, with large quantities of water to be measured, can consistently approach such absolute accuracy. Certainly, there is no evidence nor assurance that this can be done in all field tests. As a matter of fact, there is considerable evidence available to throw doubt on many field tests, whether the results showed unusually low or unusually high efficiencies, or even just "get by" efficiencies. For example, the very fact that a large number of field tests are conducted without properly calibrated electrical instruments for measuring the generator output or without accurate determination of generator losses is an indication of the lack of knowledge of the problems involved in obtaining accurate field data.

All of this resolves itself into the axiom that, in order to make a fair comparison of model test performance with prototype field test performance, the test of both the model and the prototype must be made with extreme care and, furthermore, the water measurement of the prototype must be made under ideal conditions for the method used.

Another factor involved in comparison of model tests with prototype field tests is the accuracy of step up of the model to the prototype. With the present system of making castings of runners, it was felt that certain commercial tolerances were permissible and would not affect the results. Recent test work has indicated that such tolerances or variations can probably be somewhat greater than is normally accepted, without changing the performance. In a recent installation of hydraulic turbines it was found desirable to increase the capacity of the units by increasing the discharge openings. An increase in capacity was obtained as expected, but no information was available as to its effect on efficiency. There were also indications that there might be some variations in the discharge edge blade thickness between the model and the prototype. Therefore, careful measurements were made of the entire shape of the field runner, including in addition to the discharge openings, inlet angles, discharge angles, shape and thickness of the blades, etc.

Comparing these measurements with the original model runner showed certain variations. It was then decided to make a new model runner, based upon the field measurements, and test it in comparison with the original model runner.

Table 1 shows some of the comparative measurements. As was expected, the model of the actual field runner showed more capacity than the original model because of the difference in discharge openings. However, the efficiencies checked within $^1/_{10}$ of one per cent which is within the laboratory recheck tolerances, thus indicating that there can be considerable variations in the prototype runner, without affecting performance.

On the other hand, there have been a number of excellent demonstrations that variations in performance of a test model due to certain changes in design were duplicated nearly exactly in the field when similar changes were made on the prototype.

All of this leads to the conclusion that careful and accurate model tests can be used to determine field performance, probably with a greater degree of accuracy than the actual field test. In this connection the question arises as to what step up, particularly in efficiency, should be used between the model test and the prototype performance. Everyone is familiar with the Moody formula for step up which has been in use for many years. However, it is felt that the efficiencies predicted by this formula are seldom achieved. Furthermore, the use of the formula assumes that all test laboratories give accurate absolute values. It is very doubtful whether this is true. Thus the next step is for each laboratory to establish its own step-up formula. Figs. 1, 2, and 3 show field test results on some of the prototypes as compared to model tests conducted in the laboratories of the

writer's company. The Moody efficiency step ups as compared to the actual step ups for the Francis runner installations are as follows, using the formula $E = 1 - (1 - e)\,(d/D)^{1/5}$ for the Moody step up:

Fig. no.	Power plant	Step up computed by Moody formula, per cent	Actual step up, per cent	Actual step up as per cent of Moody formula
1	Shasta Dam	4.1	3.3	80.5
2	Fort Randall	4.3	3.5	81.5

This indicates that the step up to be expected from this particular laboratory is about 80 per cent of what the Moody formula indicates. However, it may take a number of additional field tests conducted under ideal conditions, with corresponding model tests of the actual field installations to obtain a more accurate relationship between model tests and field performance.

Fig. 3 shows the comparison between model and field tests on impulse wheels. Although the Moody formula was not developed to apply to impulse wheels it is interesting to note that the step up is approximately of the same order as for the Francis units.

Fig. 1 also shows two interesting field tests on identical units in different installations. The unit was first installed at Grand Coulee and field tested. It was then taken from Grand Coulee, installed at Shasta Dam. Although this actual unit was not tested at Shasta Dam, a duplicate unit was tested there. Although tested at two different heads, the level of efficiency was $1^1/_4$ per cent different in the two tests. This probably gives a good indication of the variation in field tests even under practically ideal conditions, when the identical units are tested in two different installations. Tests on similar units in the same power plant have sometimes been used as a criterion for the accuracy of the test. However, such tests were usually made with similar penstocks, electrical instruments, head measurement setups, and similar generators.

The question regarding field tests is not so much the ability to repeat tests or to obtain comparative results on identical units in the same plant, as it is the question of the degree of absolute accuracy that is obtained under the conditions existing at that particular installation.

In order to put the laboratory testing of models in the hydraulic turbine industry on a firmer footing and to obtain greater confidence in such tests and possible future recognition of model tests as a universal means of determining fulfillment of contract obligations, it is suggested that the hydraulic turbine builders arrange to test at least one model each of the same Francis and Kaplan runner in all of their laboratories to determine what might be called the basic efficiency and power level of each laboratory.

These considerations lead to the following conclusions:

1 Model tests do not necessarily give true absolute values. Water measurements can produce errors of 1 to 3 per cent in absolute accuracy.

2 Field tests can never be as accurate as model tests and therefore are always subject to question. Even under ideal conditions extreme care must be taken to obtain correct absolute values.

3 There are certain tolerances permissible in the physical step up of the prototype from the model, which do not affect the results.

4 Since each test laboratory probably has its own level of absolute test accuracy the Moody formula cannot be applied correctly to the model tests from all laboratories. Thus each test laboratory must establish its own step-up formula.

5 The laboratories of the various turbine manufacturers should be "calibrated" by testing the same model in all the laboratories.

6 Since field testing even under ideal conditions is usually subject to question, careful model testing may eventually replace the need for field testing.

Prepared Statement by Mr. MacNamee

The preparation and testing, in a laboratory, of a model of a hydraulic turbine installation prior to construction is now very generally practiced and accepted. Such testing is useful to the manufacturer in the development and proving of new designs, and, to the customer, an indication, in advance of manufacture, that the turbine will deliver the expected performance. As is well known, many Kaplan and propeller turbine installations cannot be tested for efficiency in the field, and model tests are frequently relied on as the basis for the acceptance of the design.

As model and field test experience accumulates, it is interesting to review the efficiencies obtained and to check against established formulas relating the two. In the U. S. A., the commonly used formula for this purpose is that of Moody, most generally used in its revised form, which states that turbine losses vary inversely as the $^1/_5$-power of the diameter ratio. It is generally agreed that the increases in efficiencies so predicted from model tests are considerably higher than usually realized, particularly for the larger turbines.

We have reviewed the turbines manufactured by this company during the past twenty years, with a view toward checking the field tests against this formula or some other relation.

Only three plants of the propeller or Kaplan type have been field tested. The following comments, therefore, apply only to Francis turbine installations. During this period, field efficiency tests have been made on a total of seventeen turbines in twelve different plants. Completely homologous models of six of the plants were tested. Models of the remaining plants differed in minor details which would be expected to cause efficiency variations at the peak of the curve of less than $^1/_2$ per cent. These also were reviewed.

Unfortunately, the comparison of the field and model tests shows a scattering which makes it impossible to find any formula that fits the experimental results in a satisfactory way.

As mentioned, the Moody formula definitely indicates a greater step up in efficiency than justified by results. A step up two-thirds of that indicated by the Moody formula would be much closer to the average. It may be that the step-up ratio would be different for another model laboratory.

Obviously, the scattering shown by these tests can be due to:

1 Variations in model tests.
2 Variations in field tests.
3 Deviations from true similarity in model and field unit.

The first of these possible causes can be eliminated, if we compare tests of duplicate units. One plant in which three units were tested showed the same peak efficiencies. A second plant, with three units, showed a variation of 0.5 per cent. A third plant, with two units, showed a variation of 0.6 per cent. No tests are available of exactly duplicate units installed in different plants. However, units for two different installations, differing only in runner bucket design, were built and installed at the same time. Model tests were made with a completely homologous setting,

and with both model runners. In the laboratory, one design showed ½ per cent better efficiency than the other, while in the field the second showed higher efficiency by 1 per cent.

In the discussion of field tests, hydraulic engineers tend to concentrate on the methods and procedures of water discharge measurement. This is a difficult measurement and well deserves the attention of specialists in the field. In some cases the measurement of electrical power output of the generator has been handled rather casually. Methods of connection, calibration of meters, and correction for transformer errors all require careful consideration, if the resulting measurements are to be correct within ½ per cent. The calibration of wattmeters before and after one of the field tests just mentioned showed a discrepancy of ½ per cent.

In general, the horsepower at which the peak efficiency occurred agreed well with the model test. The maximum power was generally 5 or 6 per cent greater in field than the model test predicted, but one plant showed about 15 per cent maximum power increase. No good reason for this large increase has been found.

The field and model tests just reviewed lead to the conclusions that:

1 The Moody formula is unrealistic, at least for this laboratory.

2 Discrepancies between model and prototype performance are considerable and cannot justify any but the simplest formula relating them.

3 Continued efforts to improve test techniques are needed to minimize the "scatter" of model-field relationships now existing.

Prepared Statement by Mr. Sproule

The subject of this symposium can be divided into two parts:

A The use of laboratory testing by the manufacturer as an aid to design and for establishing predicted and guaranteed prototype performance before the prototype has been built.

B The use of laboratory testing to establish to the satisfaction of the customer that the prototype will meet or has met a guaranteed efficiency curve.

A Laboratory Testing for Design and Predicting

This type of testing may be done as part of a test program not related to a specific project, or it may be done before tendering to establish guarantees and sizes, or it may be done in the initial design stages of a contract. This type of testing involves measuring the power and efficiency over a range of speeds, observing the effect of cavitation on the power and efficiency as the pressure at the runner discharge is lowered, and noting the visible and audible effects of increasing cavitation. It usually involves testing a series of variations of a given model and often a series of different models. The emphasis in this testing is on the measurement of relative values rather than on the absolute value of the efficiency. It is, however, general practice to measure the absolute value of efficiency accurately in order to be able to compare the results with tests done at different times and, to some extent, in different laboratories.

This type of testing is important for success in the manufacture of hydraulic turbines as constantly improving designs permit more economical speeds and setting with relation to the tailwater level. The writer's company considers this testing so important that two laboratories are in constant operation on development testing.

This type of testing is often done with standard laboratory equipment where the principal changes made are in the shape of the runner. It is frequently done in a flume without a spiral case.

B Acceptance Tests

Acceptance testing of hydraulic turbine models is done in lieu of field efficiency tests where it is considered that an accurate field test is not practical. For acceptance testing the model is usually completely homologous to the prototype, from the turbine case inlet to the exit from the draft tube. Here absolute accuracy is important, so extensive and carefully made calibration tests of the laboratory measuring devices are a necessary part of the tests.

The principal factors involved in evaluating laboratory tests when used as acceptance tests are the following:

1 Accuracy of the laboratory.

2 Exactness of similarity between model and prototype.

3 Relative heads between model and prototype.

4 Relative cavitation parameter values.

5 Relative Froude numbers.

6 Model size.

7 Ratio of model size to prototype.

8 Step-up formula for converting from model to prototype performance.

The attitude of the writer's company to the use of model tests for turbine acceptance may be summed up as follows:

The use of homologous model tests is approved under agreed test conditions when conditions preclude the possibility of making field tests with reasonable accuracy.

The laboratory measuring equipment should be carefully calibrated before and after the test.

The test should be conducted at or near the minimum sigma value specified for the prototype.

The test head may be less than the operating head for the prototype but should be high enough to permit good test accuracy. It is unnecessary and often undesirable to reduce the head so that the Froude number of the model and the prototype will be the same.

If the model test is required to check a guaranteed performance of the prototype, then the efficiency step-up formula should be specified in the contract.

Stepped-up model tests are not equivalent to field tests of the prototype and should not be so represented.

Field tests of the prototype are preferred as a basis of checking performance guarantees for the following reasons:

1 It is desired to use the research facilities for research work rather than for acceptance testing, which is usually of a repetitive character.

2 The requirement of making model and prototype closely homologous may involve undesirable restrictions on design changes and manufacturing procedures.

3 There may be serious discrepancies between a model test and measured field performance of the prototype. In other words, the step-up formulas in use are not accurate over the full range of power, although reasonably accurate for predicting the maximum efficiency.

4 It is impossible to make model and prototype exactly homologous. The degree of approximation is difficult to specify and may be the subject of disputes which cannot be resolved satisfactorily to both parties.

Prepared Statement by Mr. VanderBoegh

Modern hydraulic turbine design is based upon development of theories confirmed in the laboratory by model testing. The results of such testing are used to predict the performance of the prototype units. The verification of the predictions is borne out by testing the units in the field. The accuracy of the predictions depends upon experience and upon how closely the laws of similitude were followed in reproducing prototype conditions in the model and model test.

In order to predict what the performance of the prototype will be, precise similarity between it and the model must obtain. The types of similarity to be considered may be termed geometric, kinematic, and dynamic:

By geometric similarity is meant the similarity in form and shape. That is, the ratios of all physical dimensions must be equal and the dimensions to exact scale.

By kinematic similarity is meant the similarity of motion, so that the ratio of velocities is equal.

By dynamic similarity is meant the similarity of masses and forces. The different types of similarity are related to and dependent on each other.

Certain difficulties in obtaining true similarity are found. The inability to provide precise duplication of physical dimensions is often present. The accuracy of model castings, especially in the innermost part of the runner water passages, cannot always be maintained. Surface finishes must be smooth and fair, and it is readily seen then, that a question of economics is also involved to keep hand finishing from being the major cost of the test. And yet, if the surfaces are not uniform and to scale finish, an indeterminate roughness factor is involved.

The departure from true kinematic similarity is introduced by the failure to maintain geometric similarity. If surfaces are uneven and rough, certainly the pattern of the flow may vary and disturbances foreign to the design may form, and the ratios of the velocities of the flow particles will no longer be related.

In dynamic similarity, the effect of elasticity and surface tension may be neglected, as the cold fresh water medium is usually the same in model and prototype. However, the effects of viscosity and gravity are not so easily overlooked. This involves choosing the size and operating speed of the model with respect to the practical and minimum values of the Froude and Reynolds numbers. Obviously all of the dynamic problems cannot be solved by the mechanics of similitude. Thus, while the foregoing variances from the ideal may be minimized by accurate construction and operation, each small discrepancy may contribute to the whole, and the sum may be of some significance, and vary the results from the absolute.

Some of the pitfalls of model design have been discussed, with the recognition of possible errors to be anticipated in deriving the test data.

Let us now consider the actual testing and the relation of the data secured to the absolute, for upon the accuracy of the testing will depend the limits to which we can project the data for estimating prototype performance.

The final derivation will depend upon measurements of head, power, speed, and discharge. Of these, perhaps the discharge measurement is the most critical, as the others are more a matter of calibration and mechanics. The classical measurement of discharge is through use of the weighing tank. The practical

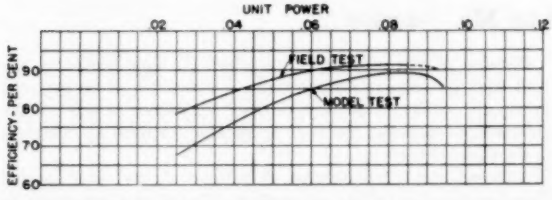

Fig. 4 Comparison between field and homologous model tests (N_s = 22.6)

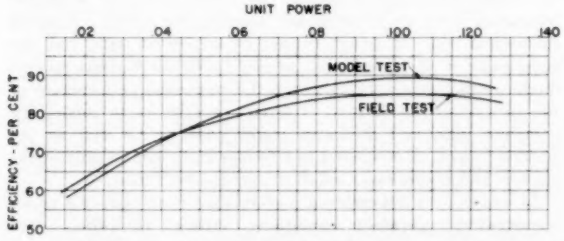

Fig. 5 Comparison between field and homologous model tests (N_s = 33.1)

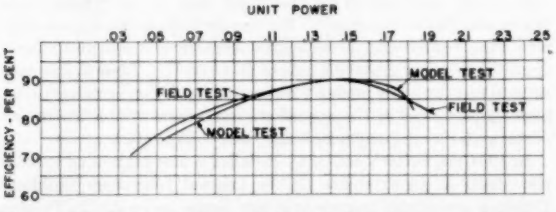

Fig. 6 Comparison between field and homologous model tests (N_s = 56.0)

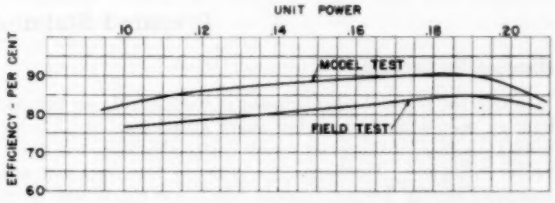

Fig. 7 Comparison between field and homologous model tests (N_s = 67.6)

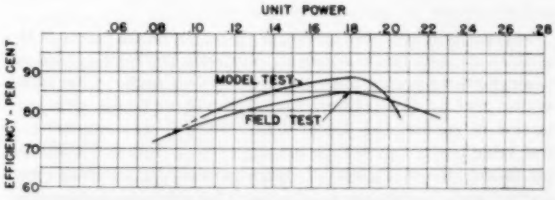

Fig. 8 Comparison between field and homologous model tests (N_s = 70.6)

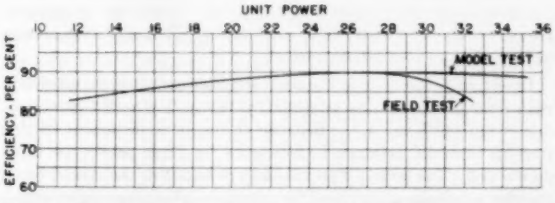

Fig. 9 Comparison between field and homologous model tests (N_s = 136.8)

method is the use of a weir or a venturi meter. Both of the latter require frequent calibration, especially so when it is considered how small an amount of fungus or extraneous matter in the water is required to produce surprisingly erroneous results.

Losses due to bearing friction must be carefully calculated for each model. These may vary due to assembly procedures and different operating speeds for different models and should not be disregarded. Another loss which is obviously disproportionate is that found through the runner seals. Due to required operating clearances, the model sealing area may be as much as five times larger than the corresponding prototype area reduced by the scale ratio. Depending on the model test head, the leakage loss then is much higher in proportion. This is actually a loss of energy and will vary over the range of gate openings.

It is vital also that the model be tested at or near field sigma and preferably at the field temperatures. There is also to be considered the problem of air entrapment in a closed model circuit and its importance or unimportance in the final data.

Two of the recognized methods for measuring flow of a prototype turbine are the Gibson time-pressure method and the Allen salt-velocity method. The accuracy of the Gibson method has been stated to be within ±0.6 per cent of the absolute. The accuracy of the Allen method is probably similar. The accuracy of testing a model in a well-designed laboratory may also be within these limits. If it is considered that the extremes of the accuracy tolerances are used in both cases, that is, the field test is 0.6 per cent high combined with the model test being 0.6 per cent low, a discrepancy of well over 1 per cent is already noted, even before all the other variances mentioned are introduced.

In relating model efficiencies to the prototype the well-known Moody formula is often used. This formula is based on the assumption that the total losses in a turbine will vary in the same ratio as the friction losses and that these total losses are inversely proportional to the linear dimensions raised to some exponential power. In other words, it is based on a size ratio and makes no allowance for the ratio of velocity or viscosity. Furthermore, it is the same for turbines of all specific speeds, and it is believed the step up afforded by the formula is not realistic.

An attempt has been made here to point out some of the factors which must be considered if the differences between model results stepped up to the prototype are to be explained. If we are to assume comparable testing techniques for both field and model tests, and the verity of the Moody formula, certain differences do exist, as inspection of the following figures will show. In each case shown here, the model was completely homologous in all water passages to the prototype. (See Figs. 4 to 9 inclusive.)

Both field and model efficiencies were reduced by the Moody formula using an exponent of 0.2. Relationship was based in each case on an equivalent model top draft tube diameter of 12 inches. It is noted that the peak efficiencies of both model and field occur at about the same output, but the curves diverge at high and low outputs. The field data for the highest specific speed runner were taken from an index test, so naturally the efficiencies coincide at maximum. The agreement in shape is very good, however, and the divergence at high output is due to the presence of cavitation. The cavitation occurred because the tail water elevation at the time of test was much lower than it was when the unit went into commercial operation.

Prepared Statement by Mr. Johnson

Historical Background

In 1880 the Water Power Company of Holyoke, Massachusetts, built an open-flume turbine test stand with a head of 17 ft for testing commercial size water wheels (up to approximately 48-in. runner diameter). Discharge was measured by a 14-ft weir and computed by the Francis formula which was considered to be reasonably accurate up to a maximum flow of 225 cfs. This facility furnished American manufacturers with the opportunity to test and compare the relative efficiencies of their various runner and wheel-case designs at reasonable cost.

Beginning in 1915 the hydraulic turbine manufacturers of this country started construction of their own low-head open-flume laboratories to permit more frequent testing, under closer observation of their own engineers, at lower cost, and with better protection of confidential design data. Since it was impossible to test large modern prototype runners even at Holyoke, a reasonable model size was required, large enough for accurate reproduction and testing but small enough for economical laboratory construction and operation. Instead of the larger and larger test runners being sent to Holyoke because of the higher efficiencies indicated as the size increased, an effort was made to "standardize" on runners with 16-in. discharge diameters. However, there is very little evidence of efficiency correlations between the various laboratories.

Eventually the Moody formula for increase in peak efficiency with size of runner was adopted by the entire hydro power industry (in the U. S. A.). Because of the basic structure of this step-up formula, estimated efficiencies for large prototype units do not reflect as large differences as are found in the model tests, thereby minimizing the need for accurate laboratory calibrations and comparisons.

Because of the admitted (and obvious) inaccuracies in the field tests on large prototype units, a guarantee of 90 per cent maximum efficiency on any turbine, regardless of size or the stepped-up efficiency, has been acceptable for most installations in the United States.

Although the fundamentals of turbine theory, such as the Eulerian theorem (1754), are well-established and important in turbine design, in actual practice no important installation is consummated without confirming the calculations by complete laboratory tests on a reasonably homologous model. A sound theoretical basis of design cannot be dispensed with, but the complexity of flow conditions in any hydraulic turbine renders model testing necessary to assure the successful performance of the prototype installation. Current practice is to model the complete inlet and discharge water passages as well as the turbine proper, as compared to a former Holyoke test on just the runner, wicket gate case, and short vertical draft tube.

In addition to determining performance characteristics under conservative operating conditions, critical cavitation data are also determined in all modern hydraulic turbine laboratories. The first turbine cavitation laboratory in the United States went into operation in 1930 at the Holtwood plant of the Pennsylvania Water and Power Company. Sixteen-inch diameter Kaplan runners were tested with homologous semi-spiral cases and elbow-draft tubes under gravity heads of 50 to 60 ft. Thus it was possible to test the same models for comparison of performance under high sigma values in the open-flume test stand at the laboratory of the writer's company which had been built in 1921.

In 1954 the writer's company installed a new high-head turbine test stand in an extension to the original laboratory building. Utilizing centrifugal pumps to create heads up to 325 ft, Francis turbine models with 12-in. discharge diameters can be tested

conveniently at very low values of sigma and 12-in. Kaplan and propeller models can be tested under prototype head conditions, all with homologous spiral or semi-spiral cases and elbow draft tubes.

Many turbine development programs include model tests without spiral or semi-spiral cases although they are required on all contract tests. However, since they are concerned with accelerating flow, losses are almost negligible in any reasonably well-designed case and corrections to the so-called open-flume tests are insignificant.

But the same considerations do not apply to draft tubes, except possibly for very low specific speed Francis wheels. Because the flow is decelerating, losses tend to be considerable (increasing with the specific speed of the unit) and to be critically affected by the various runner discharge velocity and whirl patterns. Consequently, Kaplan and propeller models as well as medium to high specific speed Francis designs must be tested with draft tubes essentially homologous to the prototype installations in order to closely approximate expected field performance characteristics.

Contract Model Tests

Many large prototype units, especially Kaplan and propeller turbines, are installed under conditions that render it practically impossible to conduct a reasonably accurate field acceptance test in accordance with any approved test code. The effective head and the horsepower output usually present no special problems, but accurate measurement of the large quantities of water involved is not economically feasible.

Consequently, current practice in such cases is to specify accurately conducted laboratory tests on homologous models including inlet and discharge water passages, and the contract guarantees are based on model performance. The various turbine manufacturers propose guarantees on the basis of previous tests of similar models, but they must be confirmed on a completely homologous model before the prototype structure and turbine-generator equipment are actually processed. The major items to be settled are the draft tube and spiral case details and dimensions, the elevation of the distributor center line, the design of the turbine proper including the speed and size required to achieve the specified outputs and efficiencies under the various heads and flow rates without exceeding the critical cavitation limits, as well as the maximum runaway speed and hydraulic thrust for which the generator must be designed.

After the turbines have been installed and placed in satisfactory operation, "index" tests are conducted in accordance with the ASME Test Code (1953) to determine the shapes of the efficiency-horsepower curves and to confirm the guaranteed output capacities and cavitation limits under various head and tailwater conditions. In order to draw the prototype efficiency-horsepower curves, the maximum model test efficiency is stepped up to prototype size by the Moody formula (U. S. A.) or by the Ackeret formula (Europe).

It is desirable that more units be installed under favorable conditions so that they can be accurately field tested at reasonable expense for comparison with laboratory tests on completely homologous models and thereby assist in the establishment of a reliable efficiency step-up formula.

Cavitation Testing

Since the advent of very large hydroelectric units in the 1920's, the various hydraulic turbine manufacturers have experienced little difficulty in designing and building units capable of attaining 92 to 94 per cent peak efficiencies. The major field of exploration in the laboratories, therefore, has been the development of runners with improved cavitation resistance and better operating characteristics.

In the new high-head test stand, medium and high specific speed Francis wheels and all Kaplan and propeller models may be tested under heads equal to those on the respective prototypes. Under these conditions, the Thoma cavitation index, sigma, is obtained with the same draft head between the runner discharge elevation and tailwater as will exist in the field, thereby not only reproducing sigma but actually utilizing the same absolute pressure (average) under the runner as will occur in the prototype. When running cavitation tests in low-head test stands, in order to obtain low sigma values, it is necessary to utilize large suction heads which frequently cause air to come out of solution and "cloud" the validity of the results as well as "fouling" the manometer lines. By testing under a higher head, the required suction head is smaller for a given sigma value with less suction on the gages and less likelihood of air coming out of solution.

Laboratory tests *duplicating* field conditions and permitting investigation of the effects due to their variations are much more likely to lead to trouble-free operation of the prototype units than are tests under much lower heads. The higher test heads are not only more suitable for cavitation research, but the larger horsepower outputs also facilitate a higher degree of accuracy, thereby permitting extremely satisfactory tests to be conducted for both performance and cavitation characteristics on the same model.

For a cavitation test, five men are located at the following stations: Dynamometer control console, venturi manometer, headwater manometer, tailwater manometer, and computer's desk. During the design stages, the use of measuring equipment that would allow the stand to be operated by one or two men was considered, but it was felt that greater accuracy and more consistent results could be obtained initially by taking a number of simultaneous readings on all instruments during each run—in the same way that prototype field tests are usually conducted. However, the use of accurate remote indicating or recording instruments is still being considered for future application.

A high degree of accuracy is especially desirable for development work, because any specific design modification may produce only a small change in performance that cannot be discovered if it is smaller than the errors of measurement, which must therefore be kept as small as practicable. The repeatable accuracy of any test point in the new stand appears to be within plus or minus one quarter of one per cent. The absolute accuracy is considered to be within one per cent, since each component has been carefully calibrated against recognized standards.

Conclusion

By *duplicating* prototype conditions while maintaining laboratory control and accuracy, homologous model tests can obviate the need for expensive, time-consuming field tests. This is particularly true in cases where Paragraphs 2 and 3 of the ASME Test Code, dealing with inaccuracies of measurement and failure to conform to "ideal" testing conditions, are obviously significant. Also worthy of mention is the fact that a field test is usually limited to the small head range existing at the time, whereas the homologous laboratory model may be conveniently and accurately tested throughout the entire prototype operating head range.

Written Discussions[2]

E. B. Strowger.[3] The Moody formula for efficiency step up from geometrically homologous model to prototype assumes that all turbine losses are in the nature of friction losses. On the other hand, if it is assumed that the frictional losses can be treated as dynamic losses, the Froude number rather than the Reynolds number becomes the basis of comparison and there is no efficiency step up. It is reasonable to expect the true answer to be somewhere between these extreme views and the discusser is inclined to agree with Mr. MacNamee, who suggests a step up of two thirds of that computed by the Moody formula using an exponent of one fifth (instead of the original one quarter), especially since available test data seem to indicate that Moody step ups are too large.

It is desirable to have several models, each tested in more than one laboratory, and these results published together with the corresponding prototype field test data. The discusser takes issue with Mr. Johnson, who suggests the use of index tests to determine the shape of the efficiency versus horsepower curve with the position of the curve determined by making the maximum efficiency coincide with the maximum model efficiency stepped up to prototype size, but admits that this procedure may be desirable for installations with short or complex intakes even though it is not recognized by the ASME Test Code as fulfilling the requirements of an acceptance test. However, he agrees with Mr. Johnson on the importance of a completely homologous model, including turbine case and draft tube, when a step up to prototype size is to be made.

I. A. Winter.[4] In the experience of the discusser, laboratory tests are subject to the same possibilities of error as are found in the field; possibly more so, since the larger sizes and capacities of the prototype units may permit a higher degree of accuracy. Also, he prefers the highly accurate standard meters for measuring generator output to specially developed laboratory dynamometers.

The discusser feels that field measuring sections for the determination of water flow rates are superior to those in the laboratories, which tend to be too short for accuracy and do not have adequate means for calibration, both dictated by the need for economy. Also, laboratory testing is generally under the direction of a junior engineer in training, whereas field tests are handled by responsible engineers of long standing experience. Since all of the physical measurements used in the conduct of a field test can be determined within plus or minus 0.2 per cent, the law of averages leads to the conclusion that the probable error in field measurements is zero. Inaccuracies in field testing have been accepted because of the practice of following abridged procedures, which "points up the need for better planning of the test installation and procedures."

The discusser prefers the use of a power step-up formula, which corrects for Reynolds number and other important variables but does not predict prototype efficiency like the Moody and Ackeret formulas, which he considers unreliable because of the inconsistent relationships between the various laboratories, model construction, and field tests.

Grant H. Voaden.[5] This discussion pertains to the relation

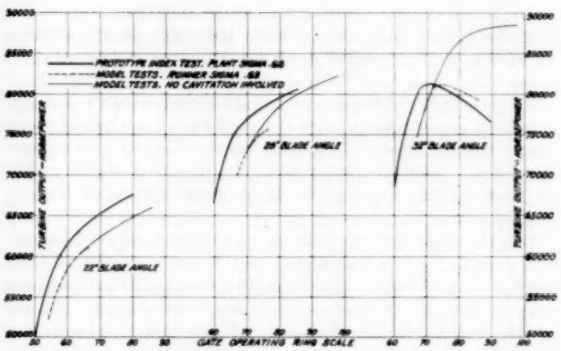

Fig. 10 Comparison of model and prototype tests (Bonneville)

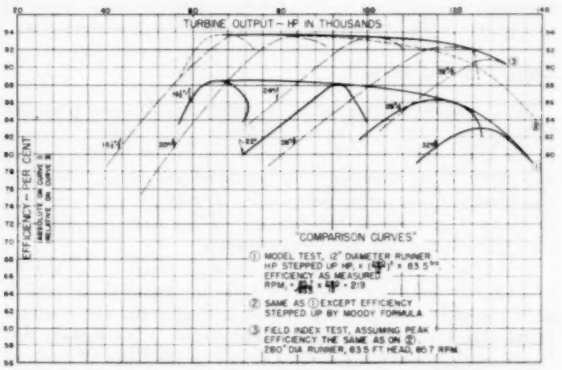

Fig. 11 Comparison of model and prototype tests (McNary)

between the power delivered by hydraulic turbines in the field and that of completely homologous laboratory models. It is generally recognized that there is some step up in efficiency from model to prototype. The basis of the Moody formula is that in the prototype the proportion of the total head lost in the turbine is less than in the model and it is because of the method that must be used to measure the head that we have an efficiency step up. Consequently, there must be a power step up which should be approximately the three-halves power of the efficiency step up.

However, comparison of 37 field tests on Francis turbines with laboratory tests on reasonably homologous models failed to indicate any power step up (beyond the three-halves power of the head ratio and the direct ratio of the runner discharge areas), even though the measured efficiency step up was approximately as calculated. Sixty tests of Kaplan turbines, on the other hand, have consistently shown an additional power step up closely approximating the three-halves power of the Moody efficiency step up (using the one-fifth exponent). Fig. 10, comparing Bonneville prototype and homologous model outputs under noncavitating conditions, indicates an average "extra" power step up of 7.3 per cent, very close to the 8.5 per cent indicated by the three-halves power of the efficiency step up. Fig. 11 illustrates how this additional power step up tends to flatten out the prototype efficiency versus horsepower curves at outputs beyond the maximum efficiency point.

S. Logan Kerr.[6] There are differences between laboratory testing, where small quantities of water are measured, where installations can be checked and rechecked, and where expe-

[2] Condensed by 1956 Chairman, Hydraulic Prime Movers Subcommittee.

[3] Chief Hydraulic Engineer, Niagara Mohawk Power Corp., Buffalo, N. Y. Mem. ASME.

[4] Chief, Hydraulic Machinery Branch, United States Bureau of Reclamation, Denver, Colo. Mem. ASME.

[5] Assistant Chief Hydraulic Engineer, S. Morgan Smith Co. Mem. ASME.

[6] Consulting Engineer, Flourtown, Pa. Fellow ASME.

rienced personnel are available for carrying out the tests and also for acquiring familiarity with the test apparatus and the methods of measurement and field testing, where these optimum conditions are not always found and tests have to be made under service conditions in the full scale plant at the convenience of the operating department. Nevertheless, it is the field performance of the hydraulic turbine unit that the owner of the plant has purchased and not the laboratory results.

These difficulties in making field tests should not be a deterrent, but should rather be a challenge to the hydraulic turbine manufacturers to confirm in as accurate a manner as possible their engineering expectations of the finished product. With these improved methods (Allen and Gibson) of measuring large quantities of water, a degree of accuracy rarely attained with other methods was made available for checking guaranteed performance.

Holyoke tests of the runner (usually 30 or 36-in. diam) and wheel case on a conical draft tube were never truly homologous to the prototype. When the turbine manufacturers built their own laboratories (about 1920), they standardized on 16-in. diameter model runners for reasons of economy. These showed somewhat lower efficiencies than those obtained at Holyoke and gave rise to the need for a step-up formula. The writer participated with the late Professor Moody in the development of the original theoretical formula with an exponent of one quarter, which was used to correlate the early tests in one manufacturer's laboratory with previous Holyoke tests, and then had to be changed to an exponent of one fifth because the stepped-up efficiencies far exceeded the field results.

A shift in the absolute efficiency of the laboratory's results would cause the stepped-up efficiency to change very substantially. Negative increases in efficiency from model to prototype occurred in some cases, particularly for impulse turbines, thereby casting doubt on model testing. The power step up and the shape of the efficiency curves have also failed to be confirmed in field tests. Although the philosophy that the "field test was in error" seemed to be a convenient explanation, in many cases the prototype intake and draft tube were not homologous to the model. In one instance, even the runners were not homologous. The outflow area was stepped up exactly but excessive curvature of the prototype vanes caused additional contraction of the outflow jets, reduced the discharge, and distorted the performance. On other installations, the location of the penstock valve, wye pipes, and elbows ahead of the turbine had a marked effect on the field performance.

In the light of these actual experiences, the stepping up of model turbine performance obtained in the laboratory to the conditions of the full scale installation is always subject to doubt unless every detail of the main unit is reproduced precisely in the model, or vice versa. The ability to check laboratory and research work in full scale installations by means of field tests has a great value in stimulating the development of the art, since actual performance is subject to measurement and not speculation. Although a number of field tests have produced unsatisfactory results, usually investigation disclosed that the ASME Test Code had not been followed or that the plant design had not made proper provision for a field test.

The purchaser buys the finished product and in fairness to him, the actual performance in the field, both as to efficiency and output, should be the true basis of compliance with contractual guarantees.

Oral Discussions[7]

At this point, Mr. Petersen opened the meeting to questions and extemporaneous discussions from the floor, which would then be answered or clarified by the panel members.

Dr. Robert T. Knapp[8] divided the subject into three main points: (1) Are laboratory tests accurate? Are the actual measurements made better than in field tests? (2) If so, what is the relationship between these accurate laboratory measurements and actual field performance? (3) Is laboratory performance really essentially the same as field performance? Apart from accuracy, is the fluid behavior in the laboratory the same as it is in the field?

Dr. Knapp then said "categorically that the laboratory tests can be made as accurate as you want them." There is no question of being able to minimize inaccuracies; it is merely a question of how far you want to go and if you are willing to pay the money for it. Consequently, laboratory measurements can be more accurate than you can hope for in the field. Back in 1934, the Cal Tech hydraulic machinery laboratory had a probable absolute over-all accuracy within ±0.1 per cent, the various individual measurements being within 0.05 per cent; today, that error could be divided by ten.

Regarding a step-up formula for the relationship between the accurate laboratory measurements and the observed field performance, Dr. Knapp thinks that we must analyze the various phenomena involved and treat each one in a suitable manner. "The ship people, for example, have been confronted with this (problem) for a long time and they have broken down their step up into pieces"... "There is no reason why we should search for a universal omnibus factor that we lump everything into and think it is going to be the same for every machine." For example, leakage losses are entirely different from friction losses and should be handled differently.

It is the opinion of Dr. Knapp that for the normal performance characteristics of capacity, head, horsepower, and efficiency, under noncavitating conditions, the behavior of the flow in the model and in the field can be said to be the same, provided that true geometric similarity exists. In some cases, "we could use accurately made models to predict prototype performance better than we can measure it in the field." Each factor, or detail, must be carefully modeled and considered separately. With cavitation occurring, it is not possible to satisfy all prototype conditions in a single model at the same time. However, with careful analysis, it should be possible to test for separate effects under different conditions.

Dr. Knapp admits that we do not know too much at the present time about using model tests to predict actual cavitation damage (or pitting). It may be possible to study pressure variations and vibration, where the rigidity of the construction can have resonance with the hydraulic phenomenon, if proper model analyses are made. But he feels that you can predict the major characteristics of a unit in the field with a good model test, provided that it is an accurate model of the actual machine. Prototypes involving detail changes from the basic model design tested should be modeled again for an accurate performance check. As an example, Dr. Knapp cited the case of two different pump impeller castings from the same patterns with as much as 2 per cent difference in performance (efficiency?) due to the finish.

Mr. Rheingans agreed with Dr. Knapp that it is possible to get a very accurate model test in spite of what Mr. Winter had written. He also pointed out that there are many cases where you run into trouble in a "one-shot" field test.

Mr. Johnson thought that the relationship between accuracy and expense as pointed out by Dr. Knapp, should be emphasized, and agreed that a reasonably accurate field test can also be per-

[7] Condensed by 1956 Chairman, Hydraulic Prime Movers Subcommittee.

[8] Director of Hydrodynamics Laboratory, California Institute of Technology, Pasadena, Calif. Mem. ASME.

formed, provided that conditions are suitable and expense is not of primary importance.

Mr. Sproule thought that accuracy within 0.1 per cent, as mentioned by Dr. Knapp, was pretty good to expect from a closed-circuit cavitation laboratory.

Mr. MacNamee commented "that the application of cavitation model tests to the field unit is a very large question and certainly not one that we would like to get into right now," but pointed out that the peak efficiency is usually well away from the cavitation limit so that the efficiency step up is not likely to be affected by cavitation, which might have to be considered near full gate.

Mr. Johnson read the following paragraph from Section 10 of the "1917 Machinery Builders' Testing Code": "The power of the model when operating at the hydraulic equivalent of the speed of the large unit in the tests of the latter, at the same proportional gate opening, is to be multiplied by the ratio of the area of the discharge orifices of the large turbine runner to that of the model and by the three-halves power of the ratio of the head existing in the tests of the large unit to the head in the model tests. When the power so computed agrees exactly with that obtained from the installed unit, the efficiency of the large unit shall be considered to be identical with that of the model; and when the power of the large unit exceeds that thus computed from the model, the efficiency of the large unit shall be considered to be in excess of that of the model." He considered this a very good piece of basic thinking that was done many years ago and that tended to agree with the Kaplan turbine data presented by Mr. Voaden, but was not in accordance with observed Francis turbine test results.

Richard E. Krueger[9] tried to explain some of the comments made by Mr. Winter regarding the accuracy of laboratory testing not being as good as that in the field. He had personally measured and rechecked a head of 1000 ft within 1 in., or 0.01 per cent, making allowance for the change in barometric pressure, and so forth, which (he said) is not done in the laboratory. He then mentioned that the USBR department under Mr. Parmakian was applying strain gages to turbine shafts for measuring horsepower with very consistent results (within ±0.5 per cent).

Mr. Krueger referred to the need for careful planning of field tests mentioned by Mr. Kerr, and pointed out that the USBR prepares a test brochure several months in advance to have the field personnel alerted and the preliminary work done before the test experts arrive on the job. He did not care to discuss the difference between Gibson and Allen tests but, based on the consistency of the results, the Bureau has a lot of confidence in both. Mr. Krueger also noted that all piezometer connections are arranged for when the plant is designed, and the piping is put in prior to the test so that the test engineer merely connects up his equipment and dresses up the piezometer orifices. In this connection, he has never found a difference of more than about 1 per cent of the velocity head among the various piezometers on a traverse, although the (ASME) Code allows as much as 10 per cent (or 20 per cent).

Mr. Rheingans questioned Mr. Krueger as to whether the accuracy within 1 in. of his 1000 ft head measurement was repetitive or absolute. Mr. Krueger admitted that it was repetitive, using the same instruments, but felt that the absolute accuracy was also very close by comparison with the (static) difference in water surface elevations determined by accurate field surveys, including corrections for barometric pressure and temperature from the top to the bottom of the 1000-ft water column.

Mr. Rheingans agreed that the USBR " is very careful in their tests" but "that isn't true universally." In many cases, commercial instead of calibrated transformers are used for measuring power output, and the water measuring people take such data along with their own discharge measurements and calculate the official efficiencies of the unit. This situation will have to be corrected; the person who signs the official report should be responsible for the accuracy of all measurements, including electrical output, head, and discharge. He also cautioned that the condition of the unit in the field must be carefully considered, since differences of several per cent in output could be attributed to growths or bitumastic (paints) on stay rings and wicket gates.

Mr. Johnson pointed out that he is not recommending only accurate laboratory tests and no field tests, but either accurate laboratory tests or accurate field tests under satisfactory conditions. He felt that there was a lot of agreement among Mr. Kerr, Dr. Knapp, Mr. Rheingans, and quite a few others, and read the following paragraph from his letter of January 24, 1955 to Mr. Kerr: "It should be noted that field conditions seem to be getting more and more difficult for conducting accurate and reliable tests. It should also be noted that good upstream flow conditions, which favor convenient and accurate tests, are also conducive to good turbine performance. Possibly our plant designs are actually lowering turbine (and over-all) efficiencies by appreciable amounts (up to several per cent) merely to effect economies in plant construction that may amount to less than one per cent of over-all project costs. If such be the case, instead of attempting to conduct field tests under difficult conditions in order to justify these economies by obtaining seemingly satisfactory results, we should be testing complete models in laboratories to determine the extent to which such economies are warranted."

I. M. White[10] had made a summary of the best reaction turbine tests in their records, as compared with essentially homologous laboratory tests. They had calculated the value of the exponent in the Moody formula required to make the model and the prototype curves coincide at the peak point, and found a range from 0.07 to 0.23. He had also made a survey of what various qualified people thought of field test accuracies, by either of the two accepted methods (Allen and Gibson), and found a range from ±0.25 to ±2.0 per cent. If you take anything approaching 1 to 2 per cent into account, it makes a tremendous difference in the Moody exponent. Mr. White felt that it would be nice to improve the accuracies of both field and laboratory tests, but that it would also be possible to co-ordinate all of the tests conducted to date and arrive at a more realistic Moody exponent, say, 0.15.

He also pointed out that a field test inaccuracy of 1 per cent could mean as much as $100,000 to the turbine manufacturer; if the test is low by 1 per cent, he may be gambling $100,000 . . . . or a new runner.

Mr. Petersen agreed with Mr. White that it would be highly desirable to arrive at a Moody exponent acceptable to all concerned, and wondered whether Mr. Jaski of Allis-Chalmers might have something to say in regard to pump-turbine efficiency step ups, especially for the pump cycle.

Robert E. Turner[11] suggested that careful correlation of unit outputs with stream flow gagings would indicate variations of 0.5, 1, or even 2 per cent due to changes like coating the runners, adjusting the water-lubricated guide bearings, et cetera. Field test runs last only 3 to 5 minutes, but they operate the Conowingo units at fixed gate openings for hours and "get a pretty good index of the relative efficiencies" from their operating records. As far as absolute efficiency is concerned, he has his choice since the two methods (Allen and Gibson) ran into some difficulty there and they never did agree on a final report.

[9] Mechanical Engineer, Hydraulic Machinery Branch, United States Bureau of Reclamation. Mem. ASME.

[10] Manager of Engineering, Pelton Division, Baldwin-Lima-Hamilton Corp., San Francisco, Calif. Mem. ASME.

[11] Hydrographer for the Susquehanna Electric Co., Conowingo, Md. Mem. ASME.

Frank E. Jaski[12] questioned the apparent increase in power reported by Mr. Voaden as possibly being due to larger prototype discharge openings, even at the same blade angle (on Kaplan runners). He also mentioned the possibility of duplicate units showing different test results because of different inflow or outflow conditions at various locations in a given powerhouse. Anything but a direct inflow to the turbines and a direct outflow into the tailrace is "not conducive to good hydraulic flow." In reply to Mr. Petersen regarding the Moody step up for pumps, Mr. Jaski pointed out that the decelerating flow through pumps is the reverse of the accelerating flow through turbines "and the Moody formula does not have the same application."

Clyde W. Hubbard[13] mentioned the lack of consistency between index tests on the same unit at the Rock Island Plant, as the other five units went into service one at a time, and considered that this was evidence of what Mr. Jaski had noted about the importance of flow conditions approaching and leaving the turbine proper.

Mr. Rheingans mentioned some difficulty experienced by Mr. Aeberli of the Hydro-Electric Power Commission of Ontario (Canada) in connection with index tests using Winter-Kennedy piezometers. It appeared that model tests had indicated some variations in results due to wicket gate and runner blade positions and that index testing methods might be due for considerable revision.

Mr. Voaden replied to Mr. Jaski by saying that the runner discharge openings had been checked within ±1 per cent and that even ±2 per cent would not account for the "apparent" power step ups of 7 per cent or more.

Prof. L. J. Hooper[14] quoted Professor Gerber of Zurich and Mr. Bovet of Charmilles as saying that the Moody formula gives a step up that is too high, whereas the Ackeret formula gives too low a step-up value. He also quoted the laboratory at Kristinehamm (Sweden) as reporting that when they tested models at full prototype head (and therefore full prototype velocity) there was a very small efficiency step up, if any. Professor Hooper also mentioned the difficulty involved in making the model and prototype accurately homologous.

Mr. Rheingans referred to his prepared statement in which (Table 1) he had shown the average measurements for four fairly large runners. These prototype runners checked each other quite closely but were considerably different from the test model; therefore, a new model runner was made from the stepped-down measurements and the new test efficiency checked the old one within 0.1 per cent.

Prof. C. P. Kittredge[15] cited the difficulties experienced a few years back in obtaining extremely accurate (within 0.01 per cent) venturi meter calibrations. For this class of work, not only the meters but the manometers and even the manometer fluids must be accurately calibrated in place.

Paul D. Hess[16] agreed with Professor Kittredge on the need for accurate calibration of any venturi meter right in its own test circuit because of the effect of uneven velocity distribution on the indicated discharge coefficient. Certain combinations of upstream flow conditions can even result in coefficients slightly greater than unity, a theoretically impossible value with so-called normal flow patterns. Mr. Hess also referred to pressure

Table 1

	Average dimensions of four prototype runners stepped down to model size	Original model dimensions
Max. blade thickness, in.		
At crown	0.246	0.281
At band	0.186	0.218
Camber of horizontal section below *c/l* distributor, in.		
Point 1	0.068	0.073
Point 2	0.100	0.115
Point 3	0.088	0.099
Point 4	0.056	0.052
Thickness of blades at *c/l* distributor, in.		
Point 1	0.121	0.162
Point 2	0.170	0.242
Point 3	0.153	0.209
Point 4	0.096	0.073
Discharge openings after alterations, in.		
Point 1	0.720	0.677
Point 2	0.714	0.668
Point 3	0.585	0.528
Point 4	0.517	0.462
Point 5	0.528	0.485
Point 6	0.526	0.479
Discharge angles (back of blades)	18°-20′	17°-0′
Inlet angles (back of blades)	33°-37′	30°-54′

reading accuracies within 0.01 per cent as unrealistic; it may be possible to duplicate gage readings that closely but with water flowing in the pipe the actual pressure is affected by the upstream piping configuration and the piezometers are affected by the condition of the inside pipe surface. Since careful laboratory calibrations had revealed errors of the order of 1 per cent in venturi coefficients, he guessed that some field pressure tap readings might be in error by as much as 5 per cent.

Mr. Krueger again emphasized the importance of cleaning the pipe wall near the piezometers and carefully checking the condition of the piezometers themselves. He cited the case of a recent test where it was not convenient to check the piezometers on the inside of the pipe and the traverse of the individual piezometers showed variations up to 30 per cent of the velocity head. Since the conditions responsible for this excessive variation could not be corrected, it was necessary to cut those piezometers out of the test.

Mr. Kerr also emphasized that the word "piezometer" does not mean accuracy per se, but that the design and conditions of installation must be in accordance with approved practices. He referred to the classic work of Professors Allen and Hooper at the Alden Hydraulic Laboratory of the Worcester Polytechnic Institute. Mr. Kerr pointed out that negligence in the checking of penstock piezometers does not prove that all field tests are inaccurate, since the same negligence would produce corresponding errors in laboratory work.

Mr. Kerr then referred to the difficulties experienced in the field tests at Conowingo mentioned by Mr. Turner. He admitted that substantial discrepancies (approximately 4 per cent) had appeared between the Allen and Gibson water measurements on one of the units tested. On another identical unit, the same personnel with the same instruments checked water quantities very closely (within about 1 per cent). Actually, conditions at Conowingo were not favorable for the application of either method of water measurement. According to Mr. Kerr, a leak in the piezometer piping to the Gibson apparatus was responsible for the

[12] Pump-Turbine Engineer, Hydraulic Department, Allis-Chalmers Manufacturing Co. Mem. ASME.

[13] Hydraulic Engineer, Stone & Webster Engineering Corp., Boston, Mass. Mem. ASME.

[14] Director of Alden Hydraulic Laboratory, Worcester Polytechnic Institute, Worcester, Mass. Mem. ASME.

[15] Mechanical Engineering Department, Princeton University, Princeton, N. J. Mem. ASME.

[16] Chief Engineer, Hydraulic Department, Allis-Chalmers Manufacturing Co. Mem. ASME.

discrepancy on the one unit, and he feels very definitely that it is unfair to discredit all field tests because of the unfortunate experience in this particular case.

L. H. Kessler[17] said that in his experience with pumps each 1 per cent in efficiency could be worth as much as $22,500 .... as compared to $100,000 for turbines (Mr. White). He hoped that ASME would soon be able to take a definite stand as to whether there is or isn't a step up in efficiency from model to prototype, or to recommend that the model efficiency be regarded as the guaranteed efficiency (for the prototype).

Wm. C. Osborne[18] felt that the Moody formula just happened to be published and well known, but that it did not apply correctly to pumps.

Mr. Petersen thanked the panel members and the discussers from the floor for their efforts in bringing the various points to the attention of all interested parties, and adjourned the meeting with the thought that these recorded presentations would form the basis for a written summary on the present state of the art.

Personal Commentary[19]

Although that was not the basic idea behind this symposium, the discussions tended to be divided in favor of field tests for determining prototype performance or in favor of laboratory tests on homologous models as being more accurate.

Mr. S. Logan Kerr, Chairman of ASME Power Test Code Committee No. 18 on Hydraulic Prime Movers, and also Chairman of the International Electrotechnical Commission Technical Committee No. 4 on Hydraulic Turbines, emphasized that it is the field performance of the hydraulic turbine unit that the owner of the plant has purchased and not the laboratory results.

Actually, no one disagreed with this statement—the real question was whether the more accurate representation of prototype performance could be attained by one-shot field tests of the prototype unit or by carefully conducted (and easily repeated) laboratory tests of a completely homologous model. Even Mr. Kerr pointed out the greater difficulties attendant upon an accurate field test as compared to an accurate laboratory test. In so doing, he answered the questions raised by Mr. Winter, the only one to suggest that field tests are more accurate than laboratory tests. In all fairness to Mr. Winter, it must be admitted that laboratory tests are subject to significant errors in the same way as field tests, but such errors are much more easily controlled and limited in the laboratory by rechecking tests and recalibrating instruments.

Several representatives of the turbine manufacturers agreed that careful consideration must be given to all of the measurements and calibrations involved in a laboratory model test in order to obtain an absolute over-all accuracy within 1 per cent, even though repetitive accuracies within ±0.1 per cent to ±0.25 per cent are usually attained. By contrast, even the 1949 ASME Test Code for Hydraulic Prime Movers (Paragraph 24) accepts individual point (or repetitive) accuracies within ±1.5 per cent—and does not specify just what absolute accuracy is expected in a field test conducted with conditions and procedures in strict accordance with the provisions of the Code. A popular estimate of the over-all accuracy attainable in a well-conducted field test is ±2 per cent—and extreme care under ideal test conditions is required even to approximate this value.

There was a great deal of discussion about the proper method of stepping up the laboratory performance of a homologous model to predict prototype efficiency and output characteristics. In addition to the universally accepted procedure of stepping up the power output by the ratio of the prototype-to-model runner discharge areas and by the three-halves power of the prototype-to-model effective test head ratio, the use of the popular Moody efficiency step up was analyzed. Basic considerations, pointed out by Mr. Voaden and the 1917 Machinery Builders' Testing Code, indicate that a step up in efficiency would correspond to a reduction in head loss which should be accompanied by an increase in power output (to the three-halves power of the efficiency step-up ratio). This does not appear to agree with observed output measurements for Francis-type turbines, which do not show this extra power due to measured efficiency increase, and therefore it is rational to doubt that there is actually any step up in efficiency from model to prototype for Francis turbines. As a matter of fact, a number of field tests have failed to show any efficiency step up, and practically all of the step ups reported to date could be eliminated on the basis of the combined inaccuracies of the laboratory test (±1 per cent) and the field test (±2 per cent).

In this connection, it is extremely significant that, even when the peak efficiency points of the exemplary model and prototype tests seemed to agree approximately with the Moody step up formula, there was no consistent relationship between the shapes of the model and prototype efficiency-horsepower curves. It appears that the suggestions made by Dr. Knapp—that we must analyze the various phenomena involved and treat each one separately in a suitable manner: break down the step-up into pieces as in the marine industry; stop trying to use a universal omnibus factor that will be the same for every machine regardless of type—should receive serious consideration.

Another point that was mentioned several times was the desirability of calibrating the various laboratories by having each one test the same model. Although such results would be extremely interesting, they would not have any permanent value because of inevitable changes in equipment, instruments, or calibrations. What we really need is agreement upon the degree of over-all absolute accuracy desired and a set of corresponding specifications covering the methods and accuracies required in the various individual measurements and calibrations. As Dr. Knapp pointed out, any conceivable degree of accuracy can be achieved in the laboratory—if we are willing to spend enough money.

Similarly in field testing, we should agree upon the over-all absolute accuracy desired and write a test code that specifies in detail how accurately the individual measurements and calibrations must be made to achieve it. In order to guarantee field test inaccuracies of less than 2 per cent, it will be necessary for the plant designers to make proper provisions for reasonable test conditions—in accordance with code requirements. Although the present ASME Test Code for Hydraulic Prime Movers is one of the best in the world today, it leaves too many details that materially affect test accuracy either to the judgment of the experienced men conducting the test or to agreement between representatives of the parties to the contract.

For the benefit of those who honestly believe that field tests are generally conducted with an over-all accuracy within ±1 per cent, serious consideration of the following items is recommended:

1 Practically all of the experts admit that field discharge measurements within ±1 per cent are extremely difficult under ideal conditions—and therefore impossible under normal conditions.

2 Several of the experts mentioned the fact that most field output measurements were hardly within ±0.5 per cent under optimum conditions—and casual optimism could easily double this inaccuracy.

3 Even the simple pressure head measurement can be made

[17] Chief Engineer, Hydraulic Division, Fairbanks, Morse & Co., Kansas City, Mo. Mem. ASME.

[18] Manager of Engineering, Worthington Corporation, Harrison, N. J.

[19] By G. Dugan Johnson.

under the ASME Code with individual piezometers varying by as much as 20 per cent of the velocity head at the turbine inlet. Since the usual inlet velocity head is approximately 4 to 5 per cent of the total head on the turbine, the Code accepts variations up to 1 per cent of the head as reasonable—which certainly corresponds to an inaccuracy of at least ±0.5 per cent—and this does not allow for the inevitable errors of observations and inaccuracies in the instruments and their calibrations.

It should be obvious just from these points that those field tests with over-all inaccuracies of less than ±2 per cent are the exception rather than the rule, since most field tests are conducted under difficulties or short cuts of some kind.

Although there was very little discussion concerning the effects of cavitation upon the relationship between model and prototype performance, all of the experts agreed that the models should be tested at values of the Thoma sigma coefficient corresponding to field conditions.

Another very significant point that all of the experts agreed upon was that reasonably homologous model tests were required to assure the successful performance of the prototype installations. All of the manufacturers conduct laboratory model tests to enable them to predict the field performance of the prototypes with sufficient accuracy to make firm output and efficiency guarantees, and to convince the customers in advance of manufacture that the prototype turbines will deliver the expected performance. After the model tests have convinced both the manufacturer and the purchaser that the prototype turbines "can't miss," conducting a difficult, expensive, and/or potentially inaccurate field test on the prototype unit to confirm that the guaranteed predictions have been fulfilled hardly seems necessary. In view of the obvious difficulties and inaccuracies inherent to prototype field tests, it does not seem fair or practical to penalize a reputable manufacturer $100,000 for an indicated deficiency of only 1 per cent in turbine efficiency—as mentioned by Mr. White.

Consideration of all of the previous comments and discussions makes it appear obvious that, when compliance with the prototype efficiency guarantees is to be based upon model tests, the efficiency step-up formula should be specified in the contract—or the guarantees should be in terms of model efficiencies, which amounts to the same thing.

All of the experts agreed that the laboratory model must be completely homologous to the prototype unit, when the field efficiencies are to be based upon the model tests. Not just the runner and wicket gates, but the entire water passage from the spiral case inlet to the draft tube exit should be modeled for an acceptance test. However, the degrees of dimensional accuracy required in the various portions of the model and prototype have not been settled. Some reasonable tolerances are obviously permissible, as pointed out by Mr. Rheingans, but industry-wide agreement on a set of specifications is highly desirable. This could be reached by rational analysis and common sense, but some comparative model tests (and/or field index tests) might expedite its general acceptance.

Messrs. Rheingans and Johnson seem to prefer accurate laboratory tests on homologous models to the dubious results expected even from the better field tests and indicate that such model tests may eventually eliminate the need for field tests. On the other hand, Mr. Sproule prefers field tests for checking performance guarantees, except when field conditions preclude the possibility of conducting prototype tests with reasonable accuracy.

In closing, the author wishes to emphasize that his criticism of the present ASME Test Code is not intended as a personal reflection on the ability and/or integrity of any practicing test engineers. Since the Code does not include detailed specifications for the accurate performance of individual measurements and calibrations, the special care usually required in at least one of the major quantities would involve delays and expenses that the owner of the plant did not anticipate and is not willing to assume. Consequently, most field tests involve potential inaccuracies much greater than is generally realized, even when carefully conducted under the supervision of competent, experienced engineers.

Summary[19]

The present state of the art may be outlined as follows:

1 All of the major manufacturers now have their own laboratories, well-equipped for model performance and cavitation tests.

2 Two types of model testing are performed in these laboratories, development of improved designs and contract acceptance tests.

3 For accurate prediction of prototype performance, a completely homologous model (including inlet casing and draft tube discharge) must be carefully built and tested.

4 The required degree of dimensional accuracy between model and prototype has not been settled, but obviously some reasonable tolerances are permissible.

5 There is no universally accepted model-to-prototype efficiency step-up formula probably because of the difficulties encountered in both laboratory and field tests as well as in both model and prototype construction.

6 It is easier to obtain any specified degree of test accuracy in the laboratory than in the field.

7 The smaller the allowable inaccuracies are, the more expensive the tests will be—in laboratory or field.

8 The various laboratories should be calibrated against each other—and against universally acceptable standards.

9 Acceptance tests on homologous models are desirable whenever field conditions are not suitable for accurate prototype tests. Only the maximum prototype efficiency is based on the model test, the shape of the prototype efficiency-horsepower curve is determined by field index tests—as are the actual cavitation limits.

10 It is desirable that more units be installed under favorable conditions for accurate field testing at reasonable expense so that comparisons with accurate laboratory tests on homologous models can assist in the development of a reliable efficiency step-up formula.

11 Since upstream flow conditions affect test accuracy as well as turbine performance, provisions for accurate field tests must be made in the design of each plant. The conduct of the tests should be carefully planned, in advance, and the unit should be in first-class condition at the time of the test.

Acknowledgments

The author gratefully acknowledges the assistance of the other panel members, Messrs. Rheingans, MacNamee, Sproule, and VanderBoegh, the Chairman, Mr. Petersen, and the Vice-Chairman, Mr. Crowe, in arranging the program for this extremely interesting session. The contributions, both written and oral, of all the other experts who took part in the discussions, have also contributed greatly to the value of this report as an up-to-date picture of the relationship between laboratory and field testing of hydraulic turbines.

1957 Annual Meeting Discussion

L. J. Hooper.[20] There are several points concerning the test of a hydraulic turbine model and the prediction of the field per-

[20] Professor of Hydraulic Engineering; Acting Director of Alden Hydraulic Laboratory, Mechanical Engineering Department, Worcester Polytechnic Institute, Holden, Mass. Mem. ASME.

formance which can be emphasized more strongly. Mr. S. Logan Kerr points out that a distinction should be made between model and prototype test performance. It is true that very good accuracy can be obtained in the laboratory while testing a hydraulic turbine model but fundamentally the customer is not using the model but rather the full-scale turbine in the field.

Of course guarantees of performance, particularly with respect to efficiency, can be made on a model test alone with no reference to field performance. This arrangement is legally definite but is hardly satisfactory so far as a guarantee of field performance is concerned.

The next possibility is that the field of performance may be compared with the model performance by means of an index test with the power carefully measured as by a normal field-efficiency test under test-code conditions. To be significant this index test must be supported by very careful measurements of the runner dimensions and angles. The area at outflow by itself does not seem sufficient to determine similarity of discharge conditions between model and prototype. The angles of convergence of the water passages at the outlet are also important. This all leads to guaranteeing geometric similitude between the model and the prototype runner. This also leads to the question of tolerances for inaccuracies in these measurements. Everyone realizes that all measurements do not have to be made with similar accuracy, but there is little information available at the present time to tell hydraulic engineers in general which dimensions are critical and which can be measured less exactly. In this connection the measurement of a Kaplan blade of which all the surfaces are readily accessible should be a fairly simple and accurate matter. The same cannot be said for the measurement of a Francis runner where some of the surfaces are very difficult to reach.

The final arrangement which is possible is the prediction of field efficiency by similitude and a suitable step-up formula. In the discussion by the panel this arrangement has been assumed tacitly but not spelled out. It presumes a step-up formula such as the Moody formula and only this formula has been mentioned in the discussion. However, there are several step-up formulas and, significantly they do not give the same increase in efficiency for a given relation between the model and its prototype. There is reason to believe also that test stands operating with different diameters of models and heads will have differing step-up experience. There is reason further to believe that the step-up relation for Kaplan, Francis, and impulse wheels may all differ. Finally, there is no general information available in engineering literature as to the operating experience with these step-up factors as determined by the various manufacturers' laboratories and their prototype installations. Under such circumstances the acceptance of a step-up formula would seem to be a supreme act of faith on the part of the customer.

In conclusion it would seem as though the prediction of prototype efficiencies from accurate model test data is still subject to uncertainties which are comparable to those of direct determination of field-test efficiency.

S. L. Kerr.[21] In this symposium on laboratory testing in relation to field testing, there is an opportunity to bring to light a great deal of information concerning the relationship between these two methods of establishing the performance of hydraulic turbines. It should be borne in mind, however, that there are distinct differences between field and laboratory testing where small quantities of water are measured, where installations can be checked and rechecked, and where experienced personnel are available for carrying out the tests, and also for acquiring familiarity with the test apparatus and the methods of measurement.

[21] Consulting Engineer, Flourtown, Pa. Fellow ASME.

In field testing these optimum conditions are not always found and yet it is the field performance of the hydraulic turbine unit that the owner of the plant has purchased and not the laboratory results. Instead of well-heated rooms, convenient quarters for office work, and the ability to check and recheck results, field tests have to be made under service conditions in the full-scale plant at the convenience of the operating department, with full representation by both parties to the contract together with strict adherence to the test code and the contract provisions.

These difficulties in making field tests should not be a deterrent, but should rather be a challenge to the hydraulic-turbine manufacturers to confirm in as accurate a manner as possible their engineering expectations of the finished product.

Field testing of hydraulic turbines was a very difficult operation in the days before the Allen and the Gibson methods became available. With these improved methods of measuring large quantities of water, a degree of accuracy rarely obtained with other methods was made available for checking guaranteed performance. It is interesting to note that a philosophy had developed concerning field testing. If the efficiency was high and a bonus and penalty clause was in effect, the test was wrong. If the efficiency was low, irrespective of whether a penalty clause was in the contract, the turbine was always to blame.

Some classic examples in the years from 1900 to 1920 showed efficiencies in excess of 100 per cent and even the manufacturers were unwilling to believe these results.

The Holyoke Water Power Company testing flume was one of the original "model test laboratories" and many contracts stated that the guarantees were based on "Holyoke tests." An examination of the Holyoke test flume would indicate that no turbine with an elbow draft tube or with an inclosed casing was used. A Holyoke setting stepped up to the full-scale installation was never truly homologous to the prototype.

About this time (1920) the Holyoke laboratory was superseded to a large extent by the construction of laboratories by the individual turbine manufacturers. For reasons of economy, the size of the model runner in most cases was set at 16 in. diam whereas 30 or 36 in. was customary at Holyoke. The efficiencies on the smaller diameter model runners were somewhat lower than those obtained at Holyoke. This gave rise to the need for a "step-up" formula.

In checking my notes as one of the participants in the development of the Moody formula, I find a curve sheet dated July 16, 1924, from which the original formula was derived. It consisted of five different runner designs, four of which were tested at Holyoke with diameters between 32 and 36 in., and one in the manufacturer's laboratory with a diameter of 16 in. The exponent of the ratio of diameters was fixed at 0.25 and a master sheet for the "Moody formula" was prepared for general use by the manufacturer.

This chart was mercifully cut off at 95 per cent efficiency and later the exponent was reduced to 0.20 as the step up from 16-in. models using the exponent 0.25 far exceeded the field results.

It should be emphasized that only five or six field tests with runners ranging from about 50 to 160 in. in throat diameters were related to laboratory tests.

A shift in the absolute efficiency of the laboratory's results would cause the step-up efficiency to change quite substantially. In some cases the efficiency from the model tests showed a negative increase from the model to the full-scale unit. This was particularly true in the field of impulse turbines and unfortunately cast doubt on model testing in this field. An arbitrary ceiling of 85 per cent on field performance of impulse turbines received general acceptance.

While efficiency step up alone has been emphasized, the power step up and the shape of the efficiency curves also have failed to

be confirmed in field tests. Here again the philosophy that the "field test was in error" seemed to be a convenient explanation. In many cases, however, the intake, the scroll case, and draft tube of the full-scale unit departed substantially from the model tests and introduced other factors which seriously affected the performance of the main unit.

In a number of these cases corrective measures were undertaken by the manufacturer and when the discrepancies were traced to their source, many interesting deviations came to light. In one instance, the outflow area of the runner was stepped up exactly from the model, but the curvature of the vanes introduced an added contraction of the outflow jet, reduced the discharge, and distorted the performance.

On other installations, the location of the penstock valve, wye pipes, and elbows, or changes in direction of the water passages ahead of the turbine had a marked effect on the field performance.

With impulse wheels this was particularly true. Many models were tested where the flow was below the turbulent point, whereas the full-sized unit operated under conditions of extreme turbulence. The buckets of the impulse wheels may have been superbly designed, but the flow conditions leading up to the nozzle produced a turbulent or funnel-shaped jet and much of the water never reached the buckets.

In the light of these actual experiences, the stepping-up of model turbine performance obtained in the laboratory to the conditions of the full-scale installation is always subject to doubt unless every detail of the main unit is reproduced precisely in the model or, conversely, every detail of the model is reproduced in the design, construction, installation, and operation of the main unit.

The ability to check laboratory and research work in full-scale installations by means of field tests has a great value in stimulating the development of the art, since actual performance is subject to measurement and not speculation.

In July, 1956, at a meeting of Technical Committee 4, Hydraulic Turbines, International Electrotechnical Commission in Munich, much discussion was given to the feasibility of making field tests, and numerous examples were cited whereby field tests had produced unsatisfactory results. In most of the cases that were analyzed, it was found that either the tests were not made in accordance with provisions of a code such as the ASME Power Test Code for Hydraulic Prime Movers, or the designer of the plant had not made proper provision for a field test.

At that time, a section was adopted for the International Code that called for the designer of a hydroelectric plant to make provision in the design in advance of construction for the carrying out of field tests within the provisions of the new Code.

It should be emphasized again that the purchaser buys the finished product and, in fairness to him, the actual performance in the field, both as to efficiency and output, should be the true basis of compliance with contractual guarantees.

W. R. MacNamee.[22] A review of the discussions of a year ago shows universal agreement on one point only; namely, that field-test efficiencies cannot be predicted accurately by model tests. This appears to be so regardless of the model laboratory involved or the step-up formula employed.

A manufacturer's model laboratory is in daily use and subject to repeated recheck and recalibration, at least with respect to relative efficiencies. In the writer's company, two test stands, independently calibrated, are available for testing a given model. Several models of widely different specific speeds have been tested over the complete operating range. In each case the efficiency curves have differed by less than $1/2$ per cent throughout.

Under the circumstances, when field tests do not correlate with model tests, it is difficult for the manufacturer to believe that the model tests are at fault.

It is natural that the user, unfamiliar with the laboratory, is concerned primarily with the field test. This concern is fundamentally correct, the only question being whether the field test truly represents the field performance.

The writer does not advocate the abandonment of field tests; to do so would be to give up any hope of producing real proof that the prototype performance can be tied to model tests. Moreover, it is the writer's opinion that many, though by no means all, field tests have suffered from indifferent preparation, untrained observers and rigid time schedules. Sometimes, the personnel directly concerned do not appreciate the difficulties involved in obtaining accurate measurements nor recognize the importance of the tests. Such deficiencies can be eliminated readily at little expense when the problem is recognized. Attention to the requirements of testing during the design of the power plant also can be helpful, although here an economical solution may not be easy.

It has been pointed out that the large size of many turbines results in an evaluation of efficiency that may run into many thousands of dollars for each 1 per cent. Surely field tests beyond the bare minimum should be considered when so much is at stake. At times, minor design modifications can be investigated at slight cost. In any event, additional knowledge of the scope and limitation of testing procedures will be helpful to all.

Whatever the cause, the present unsatisfactory correlation between field and model tests offers a serious problem to both the manufacturer and user when performance "guarantees" are considered. Basically, the establishment of such guarantees calls for engineering judgment, based on model tests and past experience with similar machines. The design engineer has learned, however, that the field-test efficiency of what appears to be a sound design may vary over a range that is quite broad. In view of the penalties that may be assessed for failure to meet guarantees, the margin between "expected" and "guaranteed" performance is a compromise between the engineer's innate conservatism and the commercial pressures to be competitive. While the prospective purchaser may be able to evaluate bids in considerable detail, based on guaranteed performance, it is obvious that the conclusions cannot be more exact than the data on which they are based. At the present time, much more is to be learned.

W. J. Rheingans.[23] A considerable portion of the symposium deals with the accuracy of field tests. It is apparent that all the commentators agree that field tests of hydraulic turbines can be made with satisfactory accuracy, provided the tests are made in strict accordance with the ASME Test Code for Hydraulic Prime Movers. The difficulties with field tests have largely been due to two factors:

1 Using short cuts in making the test.

2 Trying to use methods of water measurement under conditions outside the limitations set by the Test Code or using these methods where good judgment indicates that the methods may not give accurate results.

The usual short cuts which affect the test accuracy are as follows:

1 Use of the station instrument transformers for measuring generator output. The commercial calibration of these transformers is used, disregarding the extra burden put on them by the test instruments. The Code calls for the test transformers to be

[22] Chief Engineer, Hydraulic Turbines and Marine Products Division, Baldwin-Lima-Hamilton Corporation, Philadelphia, Pa. Mem. ASME.

[23] Manager, Hydraulic Department, Allis-Chalmers Manufacturing Company, Milwaukee, Wis. Mem. ASME.

calibrated with the actual burden (including leads) to be used during the test.

2 Failure to calibrate the electrical output-measuring instruments both before and after the test.

3 Use of generator losses calculated by the generator manufacturer in lieu of an actual generator-loss test in the field. Probably the hydraulic-turbine manufacturer should calculate the turbine losses and the generator performance should be determined based on such calculations. However, we doubt that the generator manufacturer would agree to this.

4 Failure to measure the tail-water elevations in accordance with the provisions of the code.

5 Failure to make an accurate measurement of the Gibson or Allen test section, using instead the design dimensions or measuring the circumference of the penstock, to determine the inside area.

6 Failure to inspect the water passages before and after the test.

7 Failure to compute and agree upon test results before the testing personnel shall have left the field, and before the test equipment is removed. One of the major criticisms of field tests has been that the test results as agreed upon in the field are changed by as much as 1 to 2 per cent in the final report 4 or 5 months after the test is completed.

8 Failure to obtain the agreement of the manufacturer before the results are embodied in the final report.

The use of methods of water measurement under conditions outside the limitations set by the test code applies to all methods but particularly to current meters, Allen salt velocity, and the Gibson method. It is quite true that under certain conditions these methods sometimes will give fairly accurate results even if used outside the limitations set forth by the test code. However, they also can give quite erroneous results, which immediately tend to give the method a bad reputation.

It would certainly increase the all-around confidence in these methods if their proponents recognized the possibility of obtaining inaccurate results and would refuse to conduct a test unless all test conditions were ideal.

There is a definite reason for each of the conditions set forth in the ASME Test Code. The code was written by engineers with many years of background and experience in field testing. They tried to foresee every eventuality in such a way that if the test were conducted in strict accordance with the code it had every chance of being successful.

However, the shortcuts mentioned previously, and the attempt to use water-measurement methods under conditions not ideally suited to that method, are practices that have brought field testing into ill repute among many engineers.

It appears that the subject of model tests has been covered fully by the various commentators. It is evident that model tests can be made with greater accuracy than field tests since the accuracy is dependent only upon the amount of money and time one wishes to expend on such tests. Furthermore, model tests can produce a greater wealth of over-all information on the performance of the unit than the ordinary field test. Thus model-acceptance tests eventually could take the place of field-acceptance tests.

However, before this can be accepted universally, the accuracy and consistency of model tests must be demonstrated either by making all the model-acceptance tests at an independent, proven laboratory, or by a calibration of the various acceptable laboratories; such calibration to consist of a careful check by independent parties of all the test constants, and also the establishment of a laboratory performance level, in comparison with other laboratories by testing certain identical models in all of the laboratories.

R. S. Sproule.[24] The writer's prepared statement mentions, "It is unnecessary and often undesirable to reduce the head so that the Froude number of the model and the prototype will be the same." This is not only unnecessary and undesirable, it is impractical in the case of cavitation tests of models of very large turbines.

If the head under which the model is tested is less than $^1/_{10}$ the field head, and it may be even less than this for Froude similitude of very large turbines, the pressure level in the apparatus has to be so low, to obtain the critical sigma, that stable operation and accurate measurements become extremely difficult, if not impossible. If cavitation does not occur, that is, if the test is not done near the critical sigma, there is no question of operating at the Froude number equivalent to the field, because Froude's criterion of similitude is significant only when there is a free water surface present. It is usual to test at a high enough head to make dynamometer readings accurate and to permit obtaining sigma values low enough to make cavitation troubles apparent. The lower the critical sigma, the higher the test head must be for stable operation.

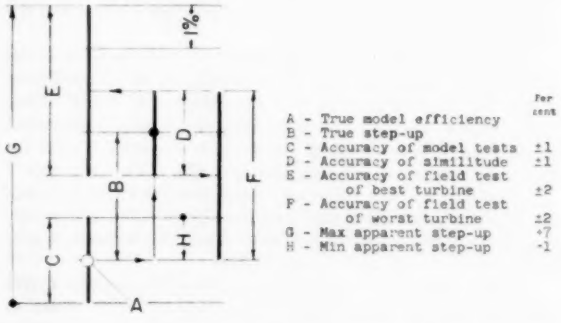

Note: Accuracies assumed for this demonstration are not suggested limits, but may be similar to those existing in some cases which have been used as evidence of the validity or otherwise of the Moody and other step-up formulas.

Fig. 12

The writer does not believe that the data correlating field tests and model tests are extensive or accurate enough to draw conclusions about what step up has been experienced. Suppose that the true step up from a given model to its prototype is 3 per cent. Suppose again that the model test may be wrong by 1 per cent, the field tests may be wrong by 2 per cent and the inaccuracy of reproducing the model may cause 1 per cent discrepancy. This combination could show the field efficiency from 1 per cent lower than the model test to 7 per cent above, as shown by Fig. 12 of the comment.

It is not suggested that these are the limits of obtainable accuracy. The diagram exaggerates. Few field tests 1 per cent below the model efficiency have been reported, but at least one ASME paper quotes a field test where the turbine, at certain loads, was 9 per cent above the model.

In view of the foregoing remarks, it seems superfluous to point out that a number given in the paper of 3.3 per cent step up at Shasta Dam, contradicts Fig. 1 of the paper which shows over 4 per cent, or very close to the Moody step up.

B. L. VanderBoegh.[25] The amount of interest displayed by

[24] Manager, Hydraulic Division, Dominion Engineering Company, Limited, Montreal, Quebec. Mem. ASME.

[25] Hydraulic Engineer, Newport News Shipbuilding and Drydock Company, Newport News, Va. Mem. ASME.

contributors to this symposium indicates that there was a definite need for a reappraisal of the relationship of model-test results to field-test results. Two definite issues have appeared—one, whether the model and field tests were each sufficiently accurate, and also, whether there may be hydraulic phenomena influencing the prototype performance which are unrecognized or indeterminate thus far in model studies. It appears from the discussions that whenever difficulty arises in relating model tests to field results, the laboratory adherents doubt the accuracy of the field tests, and vice versa, and each disputes the step-up formula. This question has remained somewhat dormant prior to this symposium.

If laboratory accuracy is a direct function of the budget, it is not unlikely that, to some degree, the same would hold for field tests.

Whenever a prototype exceeds its output and efficiency guarantees, the manufacturer does not evidence too much curiosity as to why the unit did particularly well. It is only when the guarantees are not met, or at least are marginal, that interest is awakened and some investigational program is instituted.

Data would indicate that frequently there are differences between actual field-test results and stepped-up model results. The majority of comparisons between field results and homologous model results reveals that best efficiency occurs at about the same relative output. The curves themselves frequently are not parallel. Therefore, it would seem that we should investigate thoroughly the means by which model data pertain to the prototype.

Dr. Knapp has suggested that the many and various factors involved in hydraulic flow be considered individually and separately weighted. This conceivably could require a series of graduated tests with carefully selected variables, co-ordinated with a program of intensive study and deliberation by qualified investigators. It is certainly worthy of a great deal of reflection. A beginning towards the problem might well be the establishing of a test code for model testing, whereby certain standards, tolerances, and/or allowable inaccuracies would determine comparison levels between laboratories. Until such criteria are established the testing of the same model in different laboratories is subject to question.

The development of a single new step-up factor, or a series of factors to be applied to model data is a definite need. The present factor allows the estimate of efficiencies which cannot be verified by recognized field-testing techniques, but its use is tolerated because nothing better has been derived.

Author's Closure[26]

When this report was presented at the 1957 Annual Meeting, the other panel members were requested to comment specifically on the author's eleven-point summary of the present state of the art. The results of this "poll" were as follows.

1 Unanimous agreement, except for Mr. Sproule who questioned whether all manufacturers' laboratories are well-equipped for cavitation testing over the full range of turbine specific speeds. However, he agreed that this is desirable and stated that his company was rebuilding its laboratory to increase its practical testing range.

2 Unanimous agreement.

3 Unanimous agreement, except for Mr. Sproule who felt that reasonable changes could be made in turbine runner design, and the effects accurately predicted from comparison of "open flume" tests (without inlet casings).

4 Unanimous agreement.

5 Unanimous agreement.

6 Unanimous agreement, except for Mr. Sproule who qualified his agreement specifically to point out that the laboratory test applies only to the model tested and is not necessarily a more accurate indication of what would be obtained in the field with a full-scale turbine.

7 Unanimous agreement.

8 Apparently, this item suffered from a poor choice of words, since it seems obvious that there must be some basis upon which potential customers can compare the model efficiencies attained in the laboratories of the various manufacturers. The general consensus of opinion seemed to be that this is desirable, but that calibration of the various laboratories against each other would be impractical, although calibration of all measuring devices against universally acceptable standards would be feasible for all laboratories.

9 Unanimous agreement, except for Mr. Sproule who felt that neither field tests nor acceptance tests on completely homologous models are justified unless the purchaser of the equipment (or his representative) feels that he can obtain some return for the additional expense of making the test. He pointed out that the test can produce no revenue unless it results in changes being made to the turbine equipment.

10 Unanimous agreement, except for Mr. Rheingans who did not feel that field tests are sufficiently important to justify design features that are favorable to test accuracy but add to the cost of the power plant.

11 Unanimous agreement, except for Mr. Rheingans who felt that field tests are not important enough to justify that provisions for accurate tests be incorporated in the design of each plant—at considerable extra expense.

Before attempting another summary of the present state of the art that is more or less universally acceptable, the author would like to synthesize the more recent comments with the original symposium. In a sincere effort to give "the opposition" to the manufacturers' representatives another opportunity to get "on record," the author contacted all of the original contributors to the Symposium plus a truly representative list of the other experts in this field—requesting the presentation of additional data and/or opinions. The only responses to this appeal were from Professor Hooper and Mr. Kerr.

Professor Hooper's statement that the arrangement of guaranteeing the performance of the model "is legally definite but is hardly satisfactory so far as a guarantee of field performance is concerned" is contradicted conclusively by the large number of huge Kaplan turbine contracts that have been processed on this basis to the complete satisfaction of the purchasers and the manufacturers. The author anticipated Professor Hooper's discussion of dimensional accuracy between model and prototype in his personal commentary and pointed out that "some reasonable tolerances are obviously permissible, as pointed out by Mr. Rheingans, but industry-wide agreement on a set of specifications is highly desirable."

Professor Hooper's statement that only the Moody efficiency step-up formula had been mentioned is an obvious oversight, since the author's prepared statement in 1956 mentioned the use of the Moody formula in the United States and the Ackeret formula in Europe. In this connection, the author's personal commentary (1957) pointed out that "practically all of the step ups reported to date could be eliminated on the basis of the combined inaccuracies of the laboratory test (± 1 per cent) and the field test (± 2 per cent)." This point is brought out vividly by Mr. Sproule's 1957 discussion and Fig. 13—even if his ± 1 per cent for the "accuracy of similitude" is disregarded completely

Professor Hooper's suggestion that "the acceptance of a step-up formula would seem to be a supreme act of faith on the

[26] Written by G. Dugan Johnson.

part of the customer" has been obviated by the author's 1957 personal commentary which states that "when compliance with the prototype efficiency guarantees is to be based upon model tests, the efficiency step-up formula should be specified in the contract—or the guarantees should be in terms of model efficiencies, which amounts to the same thing." No "supreme act of faith" is involved, since the purchaser's representative witnesses the acceptance tests on the model and must be convinced of the accuracy of the tests as well as of the laboratory instrument calibrations. Professor Hooper's "parting shot" also has been anticipated in the author's 1957 commentary which states that "it must be admitted that laboratory tests are subject to significant errors in the same way as field tests, but such errors are much more easily controlled and limited in the laboratory by rechecking tests and recalibrating instruments."

Mr. Kerr's discussion adds very little to his 1956 comments, which had been condensed slightly for inclusion in the original report. Consequently, most of the items mentioned by him have been discussed in the author's 1957 personal commentary. It is interesting to note that the philosophy concerning field test efficiencies has changed—bonus and penalty clauses are seldom used nowadays, but if the field test efficiency falls below the guarantee it is the test that is "suspect" rather than the turbine.

Mr. Kerr's version of the origin of the Moody efficiency step-up formula should do more to discredit that formula than all of the contradictory evidence collected to date. As mentioned in the author's prepared statement (1956), the Holyoke weir "was considered to be reasonably accurate up to a maximum flow of 225 cfs" which led to "larger and larger test runners being sent to Holyoke because of the higher efficiencies indicated as the size increased." Although the Moody formula was based to some extent upon rational theory, it would appear that it was originated as a scientific "explanation" for the obvious inconsistencies to be expected from uncalibrated weirs. As pointed out by the author in 1956, "because of the basic structure of this step-up formula, estimated efficiencies for large prototype units do not reflect as large differences as are found in the model tests, thereby minimizing the need for accurate laboratory calibrations and comparisons."

Mr. Kerr stated that the forthcoming International Test Code (IEC/TC4) would call for "the designer of a hydroelectric plant to make provision in the design in advance of construction for the carrying out of field tests within the provisions of the new Code." Messrs. Rheingans and Sproule have pointed out the uneconomic aspects of field tests which add to the cost of a plant without producing any compensating revenue.

The results of the "poll," together with the several 1957 discussions, indicate that the following commentary on the summary of the present state of the art would not be too repetitious.

1 No further comment.

2 No comment.

3 Although the author is inclined to agree with Mr. Sproule that inlet casing losses usually are not significant, it must be realized that, for a completely homologous model (per contract), the customer would not be satisfied with an "open flume" test—nor with an "indicative" test on a runner not completely homologous to the prototype.

4 No comment.

5 No comment.

6 Mr. Sproule's qualification is correct, but was not necessary.

7 No comment—except that the author hopes that its true significance is universally appreciated.

8 The calibration of all laboratory measuring equipment against universally acceptable standards is not only feasible, but the International Electrotechnical Commission, Technical Committee 4 on Hydraulic Turbines, is currently engaged in drafting a Test Code for Hydraulic Turbine Models.

The United States National Committee IEC/TC4/US, is being assisted in this task by the Hydraulic Turbine Section of the National Electric Manufacturers' Association. In this connection, the author's 1957 personal commentary included: "What we really need is agreement upon the degree of over-all absolute accuracy desired and a set of corresponding specifications covering the methods and accuracies required in the various individual measurements and calibrations."

9 Mr. Sproule's point that neither model nor field test expenses are justified unless the purchaser obtains some return for the additional expense is well taken. Actually, field tests rarely result in significant changes being made to the turbine—except for the optimum adjustment of the blade-gate cam on a Kaplan turbine as the result of an index test. However, field index tests (even on Francis type turbines) enable the purchaser to arrange for the most efficient scheduling of operations—based on the prevailing load demand, head, and quantity of water available.

10 No further comment.

11 Mr. Rheingans' point that field tests are not important enough to justify considerable extra expense for the incorporation in plant design of special provisions that favor test accuracy is also well taken. Laboratory tests of the complete structure, as well as of the turbine itself, would indicate whether or not upstream conditions favoring test accuracy are justified by resulting improvements in turbine efficiency and performance. Mr. VanderBoegh pointed out that field testing of any unit immediately after it goes into commercial operation is the best way to assure that it is in first-class condition at the time of the test.

In his closing discussion (1957), Mr. MacNamee pointed out that many field tests have suffered from indifferent preparation, untrained observers, and rigid time schedules, and that the indicated field-test efficiency of an established design may vary considerably.

Mr. Rheingans stated that field tests can be made with "satisfactory" accuracy if they are conducted in strict accordance with the ASME Test Code, but admitted that the Code allows the use of the various methods of water measurement under conditions where good judgment indicates that they might not give accurate results. He listed eight common short cuts, not in accordance with the Code, some of which are encountered in almost every formal acceptance test. The author agrees that "one of the major criticisms of field tests has been that the test results as agreed upon in the field are changed by as much as 1 to 2 per cent in the final report 4 or 5 months after the test is completed." The use of calculated generator losses in many so-called "absolute" turbine tests is inconsistent; the same confidence should also apply to modern hydraulic turbine guarantees, thereby obviating the need for anything more expensive than a field index test.

Mr. Sproule emphasized the impracticality of making laboratory cavitation test under conditions of Froude similitude between model and prototype. The model test heads indicated by this criterion are too low for general test accuracy—especially under critical sigma conditions.

Mr. VanderBoegh mentioned another point that should be emphasized. Most manufacturers (and purchasers) are not too inquisitive when the indicated field test efficiencies are higher than expected, but get "up in arms" when the indicated efficiencies are marginal or fail to meet the guarantees. It should be noted that inaccuracies can lead to either high or low efficiencies, and a completely honest approach to the problem does not permit accepting the high efficiencies and repudiating only the low ones.

In closing, the author would like to repeat a point that was made to the Power Division of the American Society of Civil Engineers at their 1958 Chicago Convention as a commentary on a committee report on "The Value of Efficiency, Index, and Acceptability Tests for Hydro-Electric Units" by Mr. M. G. Salzman. In a field index test, preferably using the Winter-Kennedy system of spiral case piezometers, the shape of the output versus efficiency curve can be determined and only the peak efficiency point need be taken from the manufacturer's data. Since the manufacturer's "expected" curves are based on applicable (i.e., reasonably homologous) model tests, it is inconceivable that an indicated peak efficiency of 92 per cent could be in error by more than ± 2 per cent (minimum field test inaccuracy) in any case. This is based on the assumptions that the usual peak efficiency guarantee of 90 per cent has been met or exceeded by the laboratory model and that an indicated peak efficiency of more than 94 per cent on the field test would be "taken with a grain of salt." Consequently, it is obvious that if the manufacturer can show the purchaser an efficiency of approximately 90 per cent on a reasonably homologous model test, the extra cost of a so-called "absolute" test over an index test is entirely without justification.

The following statement of the present state of the art is based upon all of the previous discussions; the author is not listing merely his personal convictions but is summarizing those points upon which all of the panel members agreed. Once again, the author wishes to thank all of those who have contributed to the success of this symposium.

1 All of the major manufacturers now have their own laboratories for model performance and cavitation tests.

2 Two types of testing are performed in these laboratories, (*a*) development of improved designs and (*b*) contract acceptance tests.

3 A completely homologous model (including inlet casing and draft tube discharge) should be carefully built and tested to satisfy any contract based upon laboratory acceptance tests.

4 The required degree of dimensional accuracy between model and prototype has not been settled, but obviously some reasonable tolerances are permissible.

5 There is no universally accepted model-to-prototype efficiency step-up formula, probably because of the difficulties encountered in both laboratory and field tests, as well as in both model and prototype construction.

6 It is easier to obtain any specified degree of test accuracy in the laboratory than in the field.

7 The smaller the allowable inaccuracies are, the more expensive the tests will be—in laboratory or field.

8 All of the measuring devices used in the various laboratories should be calibrated against acceptable standards. The specifications covering the methods and accuracies required in the various individual measurements and calibrations should be incorporated in a universally accepted test code for hydraulic turbine models.

9 When the purchaser insists upon a formal acceptance test and field conditions are not suitable for accurate prototype tests, a homologous laboratory model should be tested. The efficiency step-up formula should be specified in the contract—or the guarantees should be in terms of model efficiencies, which amounts to the same thing.

10 If the purchasers continue to insist upon field acceptance tests, they should provide favorable conditions for accurate field testing. Accurate field tests could then be compared with accurate laboratory tests on homologous models to assist in the development of a reliable efficiency step-up formula.

11 Since upstream flow conditions affect test accuracy as well as turbine performance, when the purchaser insists upon a field acceptance test he should provide for an accurate field test in the design of the plant. The conduct of the tests should be carefully planned, in advance, and the unit should be in first-class condition at the time of the test.

The Effect of Wakes on the Transient Pressure and Velocity Distributions in Turbomachines[1]

By R. X. MEYER,[2] LOS ANGELES, CALIF.

In general, the blades of a multistage turbomachine move through a row of wakes shed from the blades of the preceding stage. This interaction between blade rows results in a transient fluctuation of the pressure distributions, which in turn can be expected to have an important effect on the drag, the maximum lift coefficient and, in the case of hydraulic machines, on the cavitation characteristics of the affected blades. In the paper, the time-dependent pressure gradient and the velocity are determined for the case of two-dimensional incompressible flow through lightly loaded cascades.

Nomenclature

The following nomenclature is used in the paper:

a = amplitude of v_g
b = half-width of wake
c = chord
C = free-stream velocity, relative to stationary blades
c_d = profile drag coefficient
f, g, h = functions related to wake velocity-profile
J_0, J_1 = Bessel functions of the first kind
K_0, K_1 = modified Bessel functions of the second kind
p_x = pressure gradient
s = step function
t = time
t' = dimensionless time
u, v = x, y-components of velocity perturbation
u_g, v_g = x, y-components of velocity perturbation due to undisturbed wake
U = circumferential velocity of rotor blades
V = free-stream velocity, relative to rotor blades
w = velocity defect of undisturbed wake
W = integrated velocity defect of undisturbed wake
x, y = co-ordinates
x' = dimensionless co-ordinate
β = angle between airfoil and wake
λ = parameter, Equation [8]
ρ = density
ψ = stream function
ω = dimensionless frequency; also vorticity
S = stator blades (subscript)
(0) = part of perturbation which is independent of wake width (superscript)
(1) = part of perturbation which is independent of chord (superscript)

Introduction

Each blade of a turbomachine has trailing behind it a viscous wake, i.e., a region of fluid of diminished velocity originating from the boundary layer of the blade. In a multistage turbomachine, the rotor blades move through a row of wakes shed from the preceding stationary blades, and vice versa. The result of this interaction between neighboring blade rows is a nonsteady flow accompanied by a fluctuation of the pressure distribution on the affected blades.

The present considerations are confined to axial-flow machines, more specifically to two-dimensional incompressible flow through lightly loaded cascades. On the assumption that only the wakes shed from the directly adjacent upstream cascade have a material effect on the downstream blades, the analysis is restricted to this case.

Although perfect fluid theory does not offer an adequate means of description of wakes, it nevertheless can be used to obtain approximately the effect of interaction between a viscous wake and an airfoil situated in its path. The wake appears in this type of analysis as a region of fluid containing vorticity, the transport of which is governed by the vortex laws of perfect-fluid theory.

The fluctuating parts of lift and aerodynamic moment have been investigated by Sears and Kemp in a number of papers (1–3).[3] The lift and moment can be obtained more directly, i.e., without integration of the pressure distribution, from a consideration of the change of momentum. The present investigation makes use of results obtained by Küssner (4, 5) and Schwarz (6) for the pressure distribution of a single airfoil in nonuniform motion.

Reduction to Potential-Flow Problem

To give more definiteness to the formulation, it will be assumed that the upstream blades, from which the wakes are shed, are stationary, and that the blades located downstream are rotating.

The case of a compressor stage is illustrated in Fig. 1(a). The velocity distribution in the wake, as it would be in the absence of the rotor blade, is shown in Fig. 1(b), which is self-explanatory. Fig. 1(b) is drawn to scale, for an assumed profile drag coefficient of the stator blades of 0.01, utilizing the semi-empirical relations for turbulent wakes found by Silverstein, Katzoff, and Bullivant (7). In the present investigation, it will be assumed that the velocity defect is small compared with the free-stream velocity, and that the corresponding small terms of higher order therefore may be neglected.

It also is assumed that the flow about the rotor blade may be considered to be the one of a perfect fluid, a flow which is nonsteady and rotational. The fact that the velocity distribution

[1] Based on a dissertation submitted to The Johns Hopkins University in June, 1955, in conformity with the requirements for the degree of Doctor of Engineering. The investigation was supported by the Office of Naval Research, under Contract Nonr 248 (45).

[2] The Ramo-Wooldridge Corporation.

Contributed by the Fluid Mechanics Committee of the Hydraulics Division and presented at the Annual Meeting, New York, N. Y., December 1–6, 1957, of The American Society of Mechanical Engineers.

Note: Statements and opinions advanced in papers are to be understood as individual expressions of their authors and not those of the Society. Manuscript received at ASME Headquarters, August 2, 1957. Paper No. 57—A-83.

[3] Numbers in parentheses refer to the Bibliography at the end of the paper.

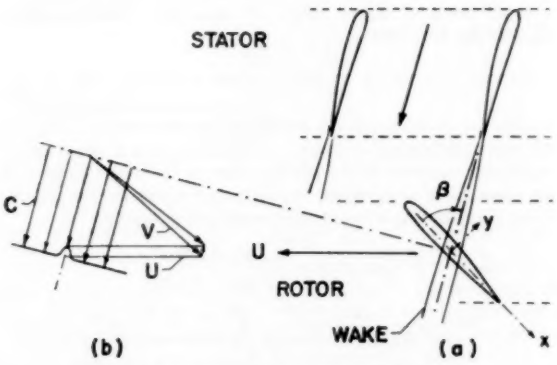

Fig. 1 Compressor blades and velocity diagram

in the wake flattens and that its width increases because of viscosity as it progresses downstream cannot be taken into account in a theory which assumes that the fluid is inviscid. It is necessary therefore to assume that—at least in the vicinity of the location of the rotor blade—the velocity profile of the wake would be the same for all cross sections if the rotor blade were absent. It is natural to select for this constant profile the one which would occur at the mid-chord location.

For lightly loaded thin blades, the effects of camber, angle of attack with respect to the flow outside of the wakes, thickness, as well as the effects produced by the neighboring blades, may be computed without reference to the wakes, by known methods, and the results added to the ones obtained for a flat plate at zero angle of attack in the presence of wakes. Fig. 2 illustrates this latter case.

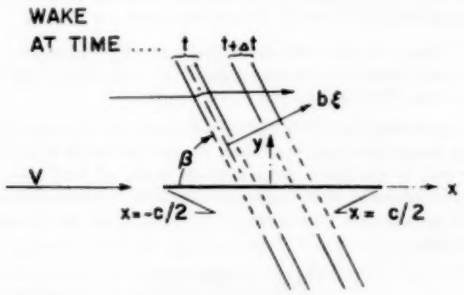

Fig. 2 Flat-plate-airfoil approximation

The region of the wake is swept downstream at a velocity (relative to the airfoil) equal to the free-stream velocity V. Also indicated in the figure is a streamline, typical for all those streamlines which are at a large distance from the airfoil.

Owing to the previously introduced assumptions, the problem reduces to one of potential flow. In order to show this, the velocity at any point and at any instant of time is decomposed into:

(a) The (constant) free-stream velocity V parallel to the x-axis.

(b) The perturbation due to the wake alone; i.e., in the absence of the blade. Its velocity components are designated by $u_g(x, y, t)$, $v_g(x, y, t)$ and its vorticity by $\omega_g(x, y, t)$.

(c) The additional perturbation introduced by the presence of the blade (flat plate) with velocity components $u_a(x, y, t)$, $v_a(x, y, t)$ and vorticity $\omega_a(x, y, t)$.

The total velocity perturbation is designated by (u, v)

$$u = u_g + u_a; \quad v = v_g + v_a \qquad [1]$$

and the total vorticity by

$$\omega = \omega_g + \omega_a \qquad [1a]$$

Helmholtz' equation in the present case reduces to $D\omega/Dt = 0$, or, neglecting small terms of higher order

$$\left(\frac{\partial}{\partial t} + V\frac{\partial}{\partial x}\right)\omega = 0 \qquad [2]$$

The same reasoning applied to the flow perturbed by the wake alone, in the absence of the blade, leads to an identical equation with ω_g instead of ω. Subtraction from Equation [2] yields

$$\left(\frac{\partial}{\partial t} + V\frac{\partial}{\partial x}\right)\omega_a = 0 \qquad [2a]$$

The effect of the blade is imperceptible at infinity, except—due to the trailing vorticity—on the positive x-axis. The seemingly trivial solution of Equation [2a], which requires that ω_a vanish identically, except on the positive x-axis, is the physically pertinent one, since it is capable of satisfying all the imposed boundary conditions.[4] This signifies that (u_a, v_a) represents a potential flow to which the results of the theory of oscillating airfoils can be applied.

Expressions for u_g and v_g

In order to describe the instantaneous location of a wake relative to the blade, it is convenient to define a wake axis for which, for instance, the line connecting the points of maximum velocity defect may be chosen. It is also convenient to introduce a characteristic half-width b of the wake. If $b\xi$ denotes the perpendicular distance from the wake axis, Fig. 2, one has the transformation

$$\xi = \frac{(x - Vt)\sin\beta + y\cos\beta}{b} \qquad [3]$$

where it is assumed, without loss of generality, that the axis of the particular wake considered passes through the origin of the (x, y) co-ordinate system at the time $t = 0$.

The angle β between the airfoil and the wake is taken as positive in the case illustrated in Figs. 1 and 2. For simplicity, the following equations are restricted to $0 < \beta < \pi$. No loss of generality ensues, since the case in which $0 > \beta > -\pi$, can be reduced to the previous one by a mirror reflection.

The velocity defect w can be expressed by putting

$$w = \text{const}\ g(\xi)$$

where the function $g(\xi)$ describes the wake profile. Also, it shall be normalized to unity, i.e.

$$\int g(\xi)\, d\xi = 1$$

where the integral is extended over a single wake.

Introducing the integrated velocity defect[5] W

$$W = b\int w(\xi)\, d\xi$$

there is

$$u_g = -\frac{W}{b}\cos\beta\, g(\xi)$$
$$v_g = +\frac{W}{b}\sin\beta\, g(\xi) \qquad [4]$$

[4] Cf. James (8).

Representing $g(\xi)$ as a complex Fourier transform

$$g(\xi) = \int_{-\infty}^{+\infty} f(\eta)\, e^{-i\xi\eta} d\eta \quad \ldots\ldots [5]$$

and introducing the dimensionless quantities

$$t' = \frac{2V}{c} t, \qquad x' = \frac{2}{c} x \quad \ldots\ldots [6]$$

where c is the chord of the blade, one obtains

$$v_y = \frac{2W}{c} \int_{-\infty}^{+\infty} f(\lambda\omega) e^{-i(x'-t')\omega} d\omega \quad \ldots\ldots [7]$$

for points located on the airfoil, i.e., for $y = 0$, if Equation [3] is taken into account.[5] λ is a dimensionless parameter characterizing the relative magnitudes of wake width and chord

$$\lambda = \frac{2b}{c \sin \beta} \quad \ldots\ldots [8]$$

Sinusoidal Wake

The form in which v_y appears in Equation [7] suggests first examining the case where, on the airfoil

$$v_y = a\, e^{-i(x'-t')\omega} \quad \ldots\ldots [9]$$

(a = const) which corresponds to a sinusoidal profile of the velocity defect in the wake.

This problem is equivalent to the case, considered by Küssner (5), of a thin elastic airfoil executing a sinusoidal "snaking" motion (9). The following expression is obtained for the pressure gradient p_x

$$p_x = \pm \frac{2\rho a V}{c} e^{i\omega t'} S(\omega) \frac{1}{\sin\theta(1 + \cos\theta)} \quad \ldots\ldots [10]$$

where ρ is the density, and where

$$\cos\theta = x'; \qquad 0 \leq \theta \leq \pi \quad \ldots\ldots [11]$$

The function

$$S(\omega) = \frac{1}{i\omega[K_0(i\omega) + K_1(i\omega)]} \quad \ldots\ldots [12]$$

which occurs frequently in Sears' work, and where K_0 and K_1 are modified Bessel functions of the second kind, is tabulated by Kemp (10). The upper sign in Equation [10] as well as in the subsequent equations pertains to the side of the airfoil which corresponds to $y > 0$, the lower sign to $y < 0$.

The result expressed by Equation [10] is very curious, inasmuch as it states that the pressure distribution on the flat plate remains similar at all times and for all frequencies. In fact, this distribution is the same as for steady flow about a flat plate at constant angle of attack, except for a scale factor depending on time and frequency. Because the equations are linear, the same must be true not only for a sinusoidal wake, but for a wake of arbitrary, but permanent, shape which can be represented by a Fourier series or Fourier integral. However, no such similarity exists in the case of the velocity distribution on the airfoil, as will be found presently.

Euler's equation of motion, if applied to the flow along the airfoil, yields

$$\frac{\partial u}{\partial t} + V \frac{\partial u}{\partial x} = -\frac{1}{\rho} p_x \quad \ldots\ldots [13]$$

[5] Term ω represents a dimensionless frequency. There should be no occasion to confuse it with the previously considered vorticity, designated by the same symbol.

if small terms of higher order are neglected. Since u varies sinusoidally with time

$$\frac{\partial u}{\partial t} = i \frac{2V}{c} \omega u$$

Equation [13] is therefore a differential equation for u with x as the only independent variable. Integrating, and making use of the Kutta condition at the trailing edge for the determination of the constant of integration, the following expression for the velocity perturbation is found, after some calculation (9)

$$u = -a e^{i\omega(t'-x')} \left\{ \operatorname{ctn}\beta \pm \pi \frac{J_0(\omega) - iJ_1(\omega)}{K_0(i\omega) + K_1(i\omega)} \mp \frac{1}{i\omega\,[K_0(i\omega) + K_1(i\omega)]} \int_0^\theta \frac{e^{i\omega\cos\theta}}{1 + \cos\theta} d\theta \right\} \quad \ldots\ldots [14]$$

$$0 \leq \theta < \pi$$

Single Wake of Small Width

The results obtained for the sinusoidal wake serve to obtain corresponding results for the more general wake expressed by Equations [4]. Of particular interest in the application to turbomachines is the limiting case, in which the characteristic width of the wake is small compared with the chord of the airfoil. The parameter λ characterizes this ratio. No quantitative definition has been attached as yet to the half-width b, which occurs in the expression for λ. For the usually encountered, nearly symmetric wake, the most pertinent definition is to set

$$2b = W/w_{max}$$

where w_{max} is the maximum velocity defect in the wake. Term λ has been computed, based on the data of (7), and is listed in Table 1 for some values of the profile drag coefficient (of the stator blades) and some values of β. The table applies to the case—which may be regarded as more or less typical for most axial flow machines—where:

(a) Chords of stator and rotor blades are of equal length.

(b) And where the average length[6] of the wake to its intersection with the blade is one chord length.

The following analysis is based on the assumption that $|\lambda| \ll 1$. As one recognizes from the table, the case in which a high drag coefficient is combined with a small angle of incidence, may hardly be expected to be rendered adequately by a solution based on this assumption. This case is excluded from the present investigation.

Table 1 Parameter λ

Drag coeff	$\beta = 30°$ 150°	60° 120°	90°
0.01	0.14	0.078	0.068
0.03	0.24	0.14	0.12
0.05	0.30	0.18	0.15

Pressure Gradient. Comparison of the expression for v_y in the case of the sinusoidal wake with the corresponding expression for an arbitrary wake indicates that the amplitude a is to be replaced by

$$2Wf(\lambda\omega)\, d\omega/c$$

Substituting this term in the equation for the pressure gradient and integrating, one obtains

$$p_x = \pm \frac{4\rho V W}{c^2} \frac{1}{\sin\theta(1 + \cos\theta)} \int_{-\infty}^{+\infty} f(\lambda\omega) S(\omega) e^{i\omega t'} d\omega \quad \ldots [15]$$

[6] The wake length is measured from the 85 per cent chord point on the stator blade, since this point may be regarded approximately as the (virtual) vertex of the parabolic wake contour (7).

In the case of a narrow wake of arbitrary shape, it is convenient to write

$$g(\xi) = \delta(\xi)$$

where the right-hand side is Dirac's δ-function. Since $f = 2\pi)^{-1}$ in this case, one obtains

$$p_z = \pm\frac{2\rho VW}{c^2}\,\frac{1}{\sin\theta(1+\cos\theta)}\,T(t') \quad \ldots\ldots [16]$$

where

$$T(t') = \frac{1}{\pi}\int_{-\infty}^{+\infty} S(\omega)e^{i\omega t'}\,d\omega; \qquad t' \neq -1 \quad \ldots\ldots [17]$$

$t' = -1$ signifies the time at which the wake intercepts the leading edge of the airfoil. The fact that the leading edge is associated with a singularity is to be expected, since the same is true in the case of the steady flow about a thin airfoil.

The function T, which is real for real arguments (9), is tabulated in Table 2. It is the derivative of a function which occurs, e.g., in Küssner's work (5, 11). T is discontinuous at -1 and zero for all arguments smaller than -1.

The velocity in the case of the narrow wake of arbitrary shape is obtained by extending the Fourier integral over the right-hand side of Equation [14]. Each of the three terms in the bracket of this equation will give a contribution to the velocity. The first term represents the velocity component which had been designated by u_q.

Velocity u_p. Considering now the last term of this bracket, its contribution to the velocity is, if designated by u_p

$$u_p = \pm\frac{W}{c}\,\frac{1}{\pi}\int_{\omega=-\infty}^{+\infty} e^{i\omega(t'-x')}\,S(\omega)\,d\omega\int_{\vartheta=0}^{\vartheta}\frac{e^{i\omega\cos\vartheta}}{1+\cos\vartheta}\,d\vartheta; \qquad 0 \leq \theta < \pi \quad \ldots\ldots [18]$$

The order of the integrations may be reversed, yielding

$$u_p = \pm\frac{W}{c}\,\frac{1}{\pi}\int_{\vartheta=0}^{\vartheta}\frac{d\vartheta}{1+\cos\vartheta}\int_{\omega=-\infty}^{+\infty} S(\omega)e^{i\omega(t'-\cos\theta+\cos\vartheta)}\,d\omega = \pm\frac{W}{c}\int_0^{\vartheta} T(t'-\cos\theta+\cos\vartheta)\,\frac{d\vartheta}{1+\cos\vartheta}$$

where T is the same function which occurred previously in the expression for the pressure gradient. However, the argument of T is different. Introducing the quantity

$$\tau = t' - x' \quad \ldots\ldots [19]$$

which represents the (dimensionless) time counted from the instant at which the wake passes the point defined by x', one has

$$u_p = \pm\frac{W}{c}\,P(x', t') \quad \ldots\ldots [20]$$

if

$$P(x', t') = \int_0^{\vartheta} T(\tau+\cos\vartheta)\,\frac{d\vartheta}{1+\cos\vartheta}; \qquad -1 < x' \leq 1 \quad \ldots\ldots [20a]$$

The integrand is continuous for $t' > -1$. Numerical methods to obtain P from the previously tabulated function T are therefore easily applied. $P(x', t')$ is a universal function in the sense that it is independent of the shape of the wake, and is tabulated in Table 3.

Table 2 Function

$$T(t') = \frac{1}{i\pi}\int_{-\infty}^{+\infty}\frac{e^{i\omega t'}\,d\omega}{\omega[K_0(i\omega)+K_1(i\omega)]}$$

t'	T
−1.0	∞
−0.8	0.9582
−0.6	0.6458
−0.4	0.5036
−0.2	0.4167
0	0.3567
0.2	0.3118
0.4	0.2769
0.6	0.2487
0.8	0.2252
1.0	0.2053
1.5	0.1668
2.0	0.1390
2.5	0.1180
3.0	0.1014
3.5	0.0882
4.0	0.0773
4.5	0.0684
5.0	0.0608
7.5	0.0366
10	0.0239
20	0.0069
30	0.0029

Table 3 Function $P(x', t')$

t' \ x' =	−1.0	−0.6	−0.2	0.2	0.6	1.0
−1.0	∞	1.043	0.626	0.456	0.342	0
−0.6	∞	0.761	0.462	0.335	0.241	0
−0.2	∞	0.564	0.346	0.249	0.172	0
0.2	∞	0.452	0.278	0.198	0.135	0
0.6	∞	0.375	0.232	0.164	0.110	0
1.0		0.318	0.196	0.139	0.092	0
1.4			0.169	0.119	0.079	0
1.8				0.103	0.068	0
2.2					0.059	0

Velocity u_q. Next, the Fourier integral extended over the second term in the bracket of Equation [14] is considered. The function which occurs in this term

$$\frac{J_0(\omega)-iJ_1(\omega)}{K_0(i\omega)+K_1(i\omega)} = i\omega S(\omega)\,[J_0(\omega)-iJ_1(\omega)] \quad \ldots\ldots [21]$$

is continuous everywhere in the finite part of the ω-plane. In order to decide on the convergence of the Fourier integral, it is therefore sufficient to consider the asymptotic expansion for large $|\omega|$ of the Function [21]. This expansion is computed in the Appendix, Equation [40]. As one recognizes from this equation, the value of the function tends on the real axis to $+i/\pi$ as $\omega = \infty$, and to $-i/\pi$ as $\omega = -\infty$. It is therefore clear that the Fourier integral with $f(\eta) = 1/2\pi$ cannot converge, or, in other words, that the contribution to the velocity due to the term [21] must depend upon the shape of the wake. Also, the form obtained for the asymptotic expansion of this term suggests splitting it into two parts, to be investigated separately

$$\frac{J_0(\omega)-iJ_1(\omega)}{K_0(i\omega)+K_1(i\omega)} = \frac{i}{\pi}\,[s(\omega)-R(\omega)] \quad \ldots\ldots [22]$$

where $s(\omega)$ is the step function

$$s(\omega) = \left\{\begin{array}{lll} +1 & \text{if} & Re(\omega) > 0 \\ 0 & \text{if} & Re(\omega) = 0 \\ -1 & \text{if} & Re(\omega) < 0 \end{array}\right\} \quad \ldots\ldots [23]$$

The remainder $R(\omega)$ has the expansion, from Equation [40]

$$R(\omega) \sim ie^{2i\omega}\left[\frac{1}{4}\frac{1}{i\omega} + \frac{1}{16}\frac{1}{(i\omega)^2} + \frac{11}{128}\frac{1}{(i\omega)^3} + \frac{59}{512}\frac{1}{(i\omega)^4} + \cdots\right] \quad [24]$$

valid in the whole (cut) plane[7] $-(3/2)\pi \leq \arg\omega \leq +(1/2)\pi$.

If the Fourier integral is extended over $R(\omega)$, the following contribution, designated by u_q, to the velocity tangential to the airfoil results

$$u_q = \mp\frac{W}{c}Q(\tau) \quad [25]$$

where

$$Q(\tau) = \frac{1}{i\pi}\int_{-\infty}^{+\infty} R(\omega)e^{i\omega\tau}\,d\omega \quad [25a]$$

since the integral converges.

In the interval $-2 < \tau < 0$, $Q(\tau)$ is computed from a contour integral involving the expansion Equation [24]. Different expansions are needed in other intervals (9), and serve to construct Table 4.

Table 4 Function

$$Q(\tau) = \int_{-\infty}^{+\infty}\left[\frac{s(\omega)}{i\pi} + \frac{J_0(\omega) - iJ_1(\omega)}{K_0(i\omega) + K_1(i\omega)}\right]e^{i\omega\tau}d\omega$$

τ	Q
−2.0	0.182
−1.6	0.169
−1.2	0.158
−0.8	0.148
−0.4	0.139
0	0.131
0.4	0.124
0.8	0.118
1.2	0.112
1.6	0.107
2.0	0.102
3.0	0.0911
4.0	0.0819
5.0	0.0747
10	0.0505
20	0.0296

Velocity u_h. Having determined the effect of the term $R(\omega)$ in Equation [22] on the velocity, it is now necessary to consider the effect due to the step function $s(\omega)$. It follows from the previous discussion, that the Fourier transform $f(\eta)$ no longer can be set equal to $(2\pi)^{-1}$ as corresponds to the representation of the wake by the δ-function, but that the complete expression, namely, the inverse of the Fourier transform Equation [5], is needed. If this contribution to the velocity is designated by u_h, there is

$$u_h = \mp 2i\frac{W}{c}\int_{-\infty}^{+\infty} f(\lambda\omega)e^{i\omega(t'-x')}s(\omega)\,d\omega \quad [26]$$

A simple physical interpretation of u_h can be given. In order to show this, $s(\omega)$ is represented by (VP = principal value)

$$s(\omega) = \mathrm{VP}\,\frac{i}{\pi}\int_{-\infty}^{+\infty}\frac{e^{-i\omega x'}}{z'}\,dz'$$

a form of Dirichlet's discontinuous factor. Consequently

$$u_h = \pm\frac{2}{\pi}\frac{W}{c}\int_{-\infty}^{+\infty} d\omega\,\mathrm{VP}\int_{-\infty}^{+\infty} f(\lambda\omega)e^{-i\omega(x'+z'-t')}\frac{dz'}{z'}$$

The sequence of the two integrals can be reversed, and one finds with the new variable of integration $\zeta = z'/\lambda$

$$u_h = \pm\frac{2}{\pi}\frac{W}{c\lambda}\,\mathrm{VP}\int_{-\infty}^{+\infty}\frac{d\zeta}{\zeta}\int_{-\infty}^{+\infty} f(\lambda\omega)e^{-i\lambda\omega(\zeta+\xi)}\,d(\lambda\omega)$$

$$= \pm\frac{2}{\pi}\frac{W}{c\lambda}\,\mathrm{VP}\int_{-\infty}^{+\infty}\frac{g(\zeta+\xi)}{\zeta}\,d\zeta$$

since $y = 0$ on the airfoil. Finally, if $\zeta - \xi$ is substituted for ζ, and if λ is replaced by the expression defining it (Equation [8])

$$u_h = \mp\frac{W}{b}\sin\beta\,h(\xi) \quad [27]$$

where

$$h(\xi) = \frac{1}{\pi}\,\mathrm{VP}\int_{-\infty}^{+\infty}\frac{g(\zeta)}{\xi-\zeta}\,d\zeta \quad [27a]$$

A comparison of this result with the theory of steady linearized flow over an airfoil, indicates that u_h represents the effect produced by the wake, if the plate were of infinite extent.

Comparing the order of magnitude of u_x and u_h with the one found for u_y and u_q, it is found that the former is larger by a factor of c/b, which is large in the case of a narrow wake. On the other hand, u_x and u_h are large only in the immediate neighborhood of the point of intersection with the wake. Since, roughly speaking, the effect on the boundary layer on the airfoil in the case of a large, but localized disturbance, can be of the same order of magnitude as in the case of a weaker, but diffuse disturbance, both types of terms are retained in the present considerations.

In contrast to the previously encountered functions, $h(\xi)$ is not strictly a universal function, but depends upon the velocity profile of the wake. Measurements in the turbulent wake behind aircraft wing models indicate that the dynamic-pressure-loss distribution through a cross section of the wake is very nearly the same, except for a scale factor, for all cross sections and all models tested (7). Accordingly, the velocity defect also has an approximately universal distribution, which, in the notation of the present paper, can be described by the empirical formula

$$g(\xi) = \left\{\begin{array}{ll}\frac{1}{2}\cos^2\left(\frac{\pi\xi}{4}\right) & \text{if } |\xi| \leq 2 \\ 0 & \text{if } |\xi| \geq 2\end{array}\right\} \quad [28]$$

from (7). For this choice of the function $g(\xi)$, the velocity defect at the distance b from the center of the wake is, since in this case $|\xi| = 1$

$$w = \frac{1}{2}w_{\max}$$

The actual dimensions of the wake essentially depend on the profile drag of the airfoil producing the wake, and on the distance of the cross section from the airfoil. The lift appears to be of little influence on the dimensions of the wake; in particular, it does not affect the symmetry of the wake profile significantly. From the semiempirical relation for the width of the wake (7) one finds

$$b = 0.24\,c_S\,[c_{dS}(x_S' - 0.70)]^{1/2} \quad [28a]$$

where c_S is the chord length of the blade shedding the wake (stator blade), c_{dS} its profile drag coefficient, and x_S' the dimensionless co-ordinate analogous to x', but with respect to the stator blade. Furthermore, from conservation of momentum

$$W = \frac{1}{2}c_S c_{dS} C \quad [29]$$

[7] Although $R(\omega)$ is discontinuous on the imaginary axis, its asymptotic expansion is nevertheless continuous, a phenomenon which may be regarded as the inverse of Stokes' phenomenon.

The empirical relations Equations [28] and [28a], together with the last equation, determine the shape and size of the wake completely.

The integral in Equation [27a] can be expressed in terms of the sine-integral and cosine-integral functions. h is an odd function of ξ since g is even, and is tabulated for positive arguments in Table 5.

Table 5 Function $h(\xi)$

ξ	h
0	0
0.4	0.175
0.8	0.296
1.2	0.330
1.6	0.280
2.0	0.194
2.4	0.149
2.8	0.123
3.2	0.105
3.6	0.0923
4.0	0.0824
5.0	0.0651
6.0	0.0538
8.0	0.0401
12	0.0271
16	0.0200
20	0.0159

Perturbation Velocity u. Collecting all results found for the various contributions to the velocity perturbation u, since

$$u = u_p + u_q + u_g + u_h \quad [30]$$

one has

$$u = \pm\frac{W}{c}\,[P(x', t') - Q(t' - x')] - \frac{W}{b}\,[\cos\beta\, g(\xi) \pm \sin\beta\, h(\xi)] \quad [31]$$

It will be found convenient to write

$$u = u^{(0)} + u^{(1)} \quad [32]$$

where

$$u^{(0)} = \pm\frac{W}{c}\,[P(x', t') - Q(t' - x')] \quad [32a]$$

$$u^{(1)} = -\frac{W}{b}\,[\cos\beta\, g(\xi) \pm \sin\beta\, h(\xi)] \quad [32b]$$

$u^{(0)}$ depends on the abscissa expressed in terms of the chord c; $u^{(1)}$ depends on the abscissa expressed in terms of the wake half-width b. Similarly

$$p_x = p_x^{(0)} + p_x^{(1)} \quad [33]$$

where, from Equation [16]

$$p_x^{(0)} = \pm\frac{2\rho VW}{c^2}\,\frac{1}{(1 + x')(1 - x'^2)^{1/2}}\,T(t') \quad [33a]$$

$$p_x^{(1)} = 0 \quad [33b]$$

The present results were obtained from an application of thin-airfoil theory; i.e., a method of small perturbations. However, as shown in the next section, this method is inadequate to render correctly the velocity and pressure distributions in the immediate neighborhood of the intersection of wake and airfoil and must be substituted there by the solution of a differential equation which is no longer linear. As a consequence, it will be found that, whereas the expressions found for $u^{(0)}$ and $p_x^{(0)}$ can be retained without change, the expressions found for $u^{(1)}$ and $p_x^{(1)}$ must be modified.

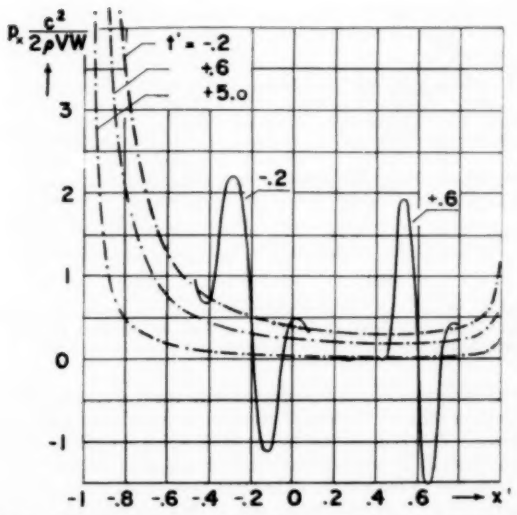

Fig. 3 Pressure gradient. Dash-dot lines, thin-airfoil theory, for $y > 0$; solid lines, corrected solution for $\beta = \pi/2$, $\lambda = 0.15$, and $cW/(2b)^2V = 1.08$.

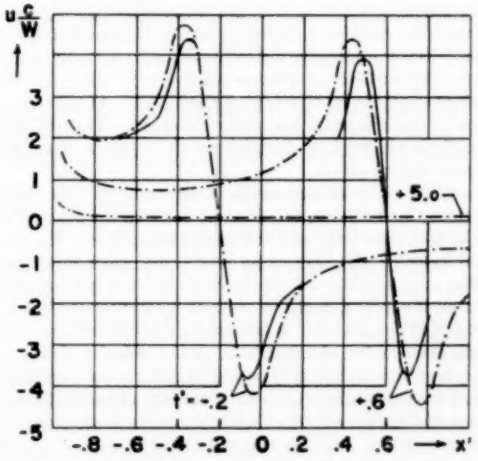

Fig. 4 Velocity perturbation. Dash-dot lines, thin-airfoil theory, for $y > 0$, $\beta = \pi/2$, $\lambda = 0.15$; solid lines, corrected solution for $cW/(2b)^2V = 1.08$.

The pressure gradient p_x obtained from thin-airfoil theory is plotted in dimensionless form in Fig. 3, and is represented by the dash-dot curves. Each of these curves represents the pressure gradient at a fixed time t', and applies to the side of the airfoil on which $y > 0$. For $y < 0$, the pressure gradient is of opposite sign. Similarly, the curves in Fig. 4 represent the velocity perturbation, in the case where $\beta = \pi/2$ and $\lambda = 0.15$.

Conditions in the Vicinity of the Wake

Two distinct limiting processes were involved in the previous section: (*a*) It was assumed that the deviation of the velocity from the free-stream velocity was small compared with the latter. (*b*) It was assumed that the width of the wake was small compared with the chord of the airfoil. It is necessary to investigate the physical significance of this particular sequence in which the two limits have been taken.

The first limit implied Equation [2], which means that the vor-

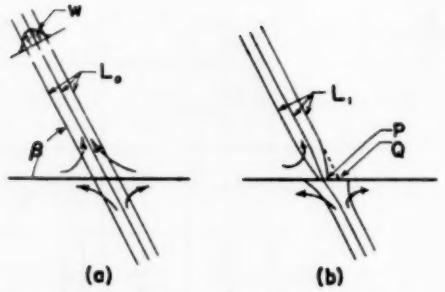

Fig. 5 Sketch of vorticity distribution. L_0 = lines of constant vorticity in thin-airfoil theory; L_1 = lines of constant vorticity in exact theory.

ticity is assumed to be transported with the free-stream velocity V, rather than by the actual velocity, as is the case in the exact theory. This is illustrated in Fig. 5(a), which is similar to Fig. 2, but where it is assumed for convenience, that a velocity $-V$ is imparted to the airfoil. The wake then appears as a *jet* which sucks off air from the upper side of the airfoil and impinges on the lower side. The parallel lines inclined at an angle β, connect points for which the vorticity is constant spatially, as well as in time.

In contrast to this, Fig. 5(b) illustrates schematically the exact theory. The velocity induced by the jet in the vicinity of the airfoil causes a progressive distortion of the lines connecting points of constant vorticity, a process which starts when the wake is intercepted by the leading edge of the airfoil. At least the initial stages of this distortion are easily discerned. The width of the wake (jet) will tend to diminish on the upper surface, and increase on the lower one.

Next, the order of magnitude is estimated of this distortion, for which, for instance, the distance between the points P and Q of Fig. 5(b) may be considered as representative. The time interval between the instant at which the wake intercepts the leading edge and the instant at which it intercepts an arbitrary point on the airfoil, is of the order of magnitude $0(c/V)$. Since in Fig. 5(b) the vorticity is transported with a velocity which is of the same order of magnitude as the velocity defect of the wake, the distortion at the considered point must be of the order $0(cw/V)$. Comparing this with the width of the wake, one has the result that the relative magnitude of the distortion is of the order

$$0\left(\frac{w}{V}\,\frac{c}{b}\right)$$

For turbomachines, the first factor in the foregoing expression is much smaller, and the second one much larger than unity. If it is assumed in accordance with current design practice of axial-flow machines that the stator chord, rotor chord, and average wake length (to its intersection with the downstream blade row) are all of the same order of magnitude, it follows from Equation [28a] that

$$\frac{c}{b} = 0\,(c_{dS}{}^{-1/2}) \qquad [34]$$

which is a large number. Furthermore, since it is permissible to assume that the free-stream velocity C relative to the stator is of the same order of magnitude as the free-stream velocity V relative to the rotor, it follows from Equation [29] that

$$\frac{w}{V}\,\frac{b}{c} = 0(c_{dS}) \qquad [34a]$$

Consequently

$$\frac{w}{V}\,\frac{c}{b} = 0(1) \qquad [35]$$

Since, therefore, the distortion is of the same order of magnitude as the width of the wake, it follows that the thin-airfoil theory, which neglects it entirely, is not applicable in the immediate vicinity of the wake; i.e., at points, the distance of which from the center of the wake is of the order of b. At all other points of the airfoil the thin-airfoil theory constitutes a valid approximation in the case of a sufficiently small c_{dS}.

Since the exact theory differs from thin-airfoil theory only in the vicinity of the wake, it suffices to restrict the present considerations to this region. The problem is therefore equivalent to the one in which a flat plate of infinite extent is suddenly (at $t = 0$) inserted into a two-dimensional jet.[8]

The stream function $\psi^{(1)}(x, y, t)$ satisfies the relation

$$\frac{\partial}{\partial t}(\Delta\psi^{(1)}) + \frac{\partial\psi^{(1)}}{\partial y}\frac{\partial}{\partial x}(\Delta\psi^{(1)}) - \frac{\partial\psi^{(1)}}{\partial x}\frac{\partial}{\partial y}(\Delta\psi^{(1)}) = 0 \qquad [36]$$

where Δ is the Laplacian. Although this equation is nonlinear, it resembles the equation of conduction of heat. Somewhat similarly as in the case of the latter equation, an approximate numerical solution can be obtained as follows: Replacing the derivative with respect to t by finite differences

$$\Delta\psi_{n+1}{}^{(1)} - f_{n+1} = 0 \qquad [37]$$

where

$$f_{n+1} = \Delta\psi_n{}^{(1)} - \delta t\left[\frac{\partial\psi_n{}^{(1)}}{\partial y}\frac{\partial}{\partial x}(\Delta\psi_n{}^{(1)}) - \frac{\partial\psi_n{}^{(1)}}{\partial x}\frac{\partial}{\partial y}(\Delta\psi_n{}^{(1)})\right] \qquad [37a]$$

where δt is a (small) time interval and where the subscripts indicate the value assumed by t, in terms of multiples of δt, as, for instance, in $\psi_n{}^{(1)} \equiv \psi_{(x,y,t=n.\ \delta t)}{}^{(1)}$. If $\psi_n{}^{(1)}$ is known, f_{n+1} is found from Equation [37a]. Equation [37], which is a Poisson's equation, is then solved to find $\psi_{n+1}{}^{(1)}$. Starting from the known initial condition for $\psi^{(1)}$, the complete solution can be found by a repetition of the foregoing process.

By means of the relaxation method, the dimensionless pressure gradient and velocity have been computed for $\beta = \pi/2$ and for the side of the airfoil corresponding to $y > 0$ (Figs. 6 and 7). Replacing the expressions for $p_s{}^{(1)}$ and $u^{(1)}$ given by the thin-airfoil theory by those obtained from the exact theory, and adding to them $p_s{}^{(0)}$ and $u^{(0)}$, the solid lines in Figs. 3 and 4 are obtained, representing the exact solutions for pressure gradient and velocity. Whereas the required correction of the thin-airfoil theory is relatively minor in the case of the velocity distribution, a strong local pressure disturbance appears at the intersection with the wake, a disturbance which is entirely absent in the results yielded by the thin-airfoil theory.

Acknowledgment

This investigation was carried out under the sponsorship of the Office of Naval Research, Mechanics Branch. The author wishes to express his appreciation to Prof. Hsuan Yeh, now at the University of Pennsylvania, and to Prof. Francis H. Clauser of the Johns Hopkins University, for their guidance and encouragement.

[8] The time $t = 0$ is the instant at which the leading edge intercepts the wake. For convenience, the origin of t was defined differently in the previous sections. Similarly, the origin of the abscissa x in this section will be placed into the center of the wake, rather than into the center of the airfoil.

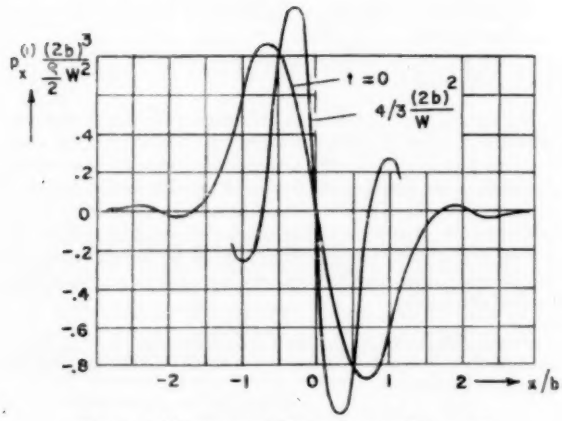

Fig. 6 $p_x^{(1)}$ from exact theory, for $y > 0$, $\beta = \pi/2$

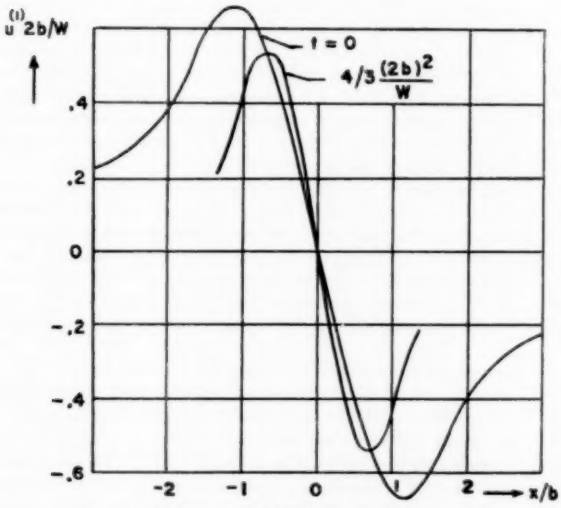

Fig. 7 $u^{(1)}$ from exact theory, for $y > 0$, $\beta = \pi/2$

Bibliography

1 "Aerodynamic Interference Between Moving Blade Rows," by N. H. Kemp and W. R. Sears, *Journal of the Aeronautical Sciences*, vol. 20, no. 9, 1953, pp. 585–597.

2 "The Unsteady Forces Due to Viscous Wakes in Turbomachines," by N. H. Kemp and W. R. Sears, *Journal of the Aeronautical Sciences*, vol. 22, no. 7, 1955, pp. 478–483.

3 "Some Aerodynamic Problems of Compressors and Turbines," by W. R. Sears, University of Maryland Institute for Fluid Dynamics Lecture Series No. 30, 1953.

4 "Zusammenfassender Bericht über den instationären Auftrieb von Flügeln," by H. G. Küssner, *Luftfahrtforschung*, vol. 13, no. 12, 1936, pp. 410–424.

5 "Das zweidimensionale Problem der beliebig bewegten Tragfläche unter Berücksichtigung von Partialbewegungen der Flüssigkeit," by H. G. Küssner, *Luftfahrtforschung*, vol. 17, no. 11/12, 1940, pp. 355–361.

6 "Berechnung der Druckverteilung einer harmonisch sich verformenden Tragfläche in ebener Strömung," by L. Schwarz, *Luftfahrtforschung*, vol. 17, no. 11/12, 1940, pp. 379–386.

7 "Downwash and Wake Behind Plain and Flapped Airfoils," by A. Silverstein, S. Katzoff, and W. K. Bullivant, NACA Technical Report 651, 1938.

8 "Two-Dimensional Airfoils in Shear Flow, Part I," by D. G. James, *Quarterly Journal of Mechanics and Applied Mathematics*, vol. 4, 1950, p. 407.

9 "Interference Due to Viscous Wakes Between Stationary and Rotating Blades in Turbomachines," by R. X. Meyer, Doctor of Engineering thesis, The Johns Hopkins University, 1955.

10 "On the Lift and Circulation of Airfoils in Some Unsteady-Flow Problems," by N. H. Kemp, *Journal of the Aeronautical Sciences*, vol. 19, no. 10, 1952, pp. 713–714.

11 "Berechnung der Funktionen $U_1(s)$ und $U_2(s)$ für grössere Werte von s," by L. Schwarz, *Luftfahrtforschung*, vol. 17, no. 11/12, 1940, pp. 362–369.

12 "Theory of Bessel Functions," by G. N. Watson, Cambridge University Press, Cambridge, England, second edition, 1944.

Appendix

The expansions (12), suited for large values of $|\omega|$

$$J_0(\omega) \sim \left(\frac{2}{\pi\omega}\right)^{1/2} \left[\cos\left(\omega - \frac{\pi}{4}\right) \sum_{n=0}^{\infty} \frac{(-1)^n (0, 2n)}{(2\omega)^{2n}} - \sin\left(\omega - \frac{\pi}{4}\right) \sum_{n=0}^{\infty} \frac{(-1)^n (0, 2n+1)}{(2\omega)^{2n+1}}\right] \quad [38]$$

and similarly for $J_1(\omega)$, are valid for $-\pi < \arg \omega < +\pi$. As usual in the theory of Bessel functions, the symbol (ν, m) is introduced, where

$$(\nu, m) = \frac{(4\nu^2 - 1^2)(4\nu^2 - 3^2) \ldots [4\nu^2 - (2m-1)^2]}{2^{2m}\, m!}$$

$$(\nu, 0) = 1$$

Since the range of $\arg \omega$ is less than 2π, it is necessary, in order to cover the whole plane, to introduce a second expansion, valid for $-2\pi < \arg \omega < 0$, derived from the former by noting that

$$J_0(-\omega) = +J_0(\omega)$$

$$J_1(-\omega) = -J_1(\omega)$$

Also, one has the expansions for the K-functions (12)

$$K_0(i\omega) \sim \left(\frac{\pi}{2\omega}\right)^{1/2} e^{-i\left(\omega + \frac{\pi}{4}\right)} \sum_{n=0}^{\infty} \frac{(0, n)}{(2i\omega)^n} \quad [39]$$

and similarly for K_1 valid in the whole plane $-(3/2)\pi \leq \arg \omega \leq (1/2)\pi$ (actually, the validity extends even further) and where, as before, the principal branch of the square root is meant. Collecting terms of equal powers of ω, and then dividing out the fraction on the left-hand side of Equation [21], one finds

$$\frac{J_0(\omega) - iJ_1(\omega)}{K_0(i\omega) + K_1(i\omega)} \sim \frac{i}{\pi} \left\{ \pm 1 - ie^{2i\omega} \left[\frac{1}{4} \frac{1}{i\omega} + \frac{1}{16} \frac{1}{(i\omega)^2} + \frac{11}{128} \frac{1}{(i\omega)^3} + \frac{59}{512} \frac{1}{(i\omega)^4} + \ldots \right] \right\}$$

for $-\pi < \arg \omega < +\pi$ (upper sign)

$$-2\pi < \arg \omega < 0 \text{ (lower sign)} \quad [40]$$

for the first few terms of the expansion.[9]

[9] The two regions of validity overlap in $-\pi < \arg \omega < 0$. But the contradiction which results from the fact that then the first term in the expansion is both $+1$ and -1 is only apparent. The term $e^{2i\omega}$ for large ω increases exponentially in this region; the error committed by breaking off the series at any given term, if multiplied with $e^{2i\omega}$, is of the same order as ± 1. The discontinuity of the asymptotic expansion is an example of the Stokes' phenomenon.

Discussion

W. G. Cornell.[10] The author is to be congratulated on an excellent and interesting paper, having considerable practical utility to the turbomachine designer in improving his notions of the mechanism of mutual interference between adjacent rows of blades. It should be pointed out that the author's use of the Kutta condition, viz., assumption of smooth, separation-free flow off the blade trailing edges, may yield misleading results, especially in the blade-surface pressure distribution near the trailing edge. The Kutta condition is never quite satisfied in actual, steady flow over an airfoil, a small separation normally occurring on the suction side near the trailing edge. In the present unsteady case, it is probable that conditions near the trailing edge vary even further from the Kutta condition and that in a time-dependent fashion.

[10] Jet Engine Department, General Electric Company, Cincinnati, Ohio. Mem. ASME.

Author's Closure

Mr. Cornell is quite correct in pointing out that the Kutta condition is only approximately satisfied by a real fluid. The same problem is encountered in the application of unsteady-flow theory of airfoils to the stability and control of aircraft, and a number of corrections to the Kutta condition have been proposed.[11] It is quite possible, that some of the simpler approaches, such as the semiempirical Rott-George method, could be incorporated into the present paper, perhaps without introducing undue mathematical difficulties.

[11] "Some Recent Developments in Airfoil Theory," by W. R. Sears *Journal of the Aeronautical Sciences*, vol. 23, no. 5, 1956, pp. 490-499

Possible Similarity Solutions of the Laminar, Incompressible, Boundary-Layer Equations[1]

By A. G. HANSEN,[2] CLEVELAND, OHIO

A review of research on the problem of obtaining similarity solutions of the three-dimensional, laminar, incompressible, boundary-layer equations is presented along with a general method of analysis for treating the problem. Restrictions on main flow velocity components and co-ordinate systems which lead to similarity solutions are tabulated. Finally, a discussion is given of the practical application of similarity solutions and the problems which remain to be solved.

Introduction

THE analysis of boundary-layer flows over various aerodynamic configurations continues to be a problem of major importance. Efficient design procedures for both internal turbomachine components and external surface components must allow for boundary-layer development. In the past it has often been possible to make gross allowances for the boundary layer by using empirical relations in combination with results predicted from two-dimensional boundary-layer theory. However, in many current design problems, this method has serious shortcomings. One of the major shortcomings is that this approach does not readily account for three-dimensional boundary-layer characteristics such as secondary flow phenomena. Often it is precisely the three-dimensional characteristics that are of major importance. As a consequence, a great deal of experimental and theoretical research on three-dimensional boundary-layer flows has been carried on in recent years.

In spite of past efforts, a need still exists for theoretical analyses which will lead to quantitative as well as qualitative predictions of boundary-layer behavior. Theoretical research, however, has been restricted because of the complex nature of the equations describing the flow. For example, in a number of problems of practical concern, the boundary layer is turbulent. Examination of the nonlinear partial differential equations which describe turbulent flow discloses that the equations are all but intractable. Some success, however, has been achieved in the analysis of the three-dimensional laminar equations. The practical importance of this research is threefold: (*a*) Experimental evidence indicates that laminar boundary-layer flows can usefully provide qualitative information concerning turbulent boundary-layer behavior. (*b*) As in the two-dimensional case, laminar-flow solutions may provide a basis for approximating more general flows. (*c*) Certain boundary-layer problems such as external-surface boundary-layer flows for high-altitude flight might well be encompassed by a laminar-flow analysis.

One important phase of the theoretical attack on boundary-layer problems has been the search for exact solutions of the laminar, incompressible, boundary-layer equations for special types of main stream flows. References (1 to 7)[3] might be cited as typical of such investigations. The principal approach for finding exact solutions of the equations has been the use of the similarity technique. In instances where the technique is applicable, the partial differential equations of the boundary layer reduce to a system of ordinary differential equations. The corresponding solutions for the boundary-layer velocity components are such that the velocity profiles differ, at most, by scale factors along the co-ordinate directions.

To date, similarity solutions have been found for only very special types of main stream flows and for special types of co-ordinate system. A question has always existed, therefore, as to the applicability of the similarity technique to general problems and what limitations are inherent in its use. This question was successfully answered for the case of two-dimensional, laminar flows in references (8–12). These investigations showed that, in general, similarity solutions can only be found for main stream flows in which the velocity varies as a power of the distance along a surface or as an exponential. Recently, several investigations (13–16) have attempted to determine the conditions under which similarity solutions exist for laminar, incompressible, three-dimensional boundary-layer flows. In investigations of this kind, the type of co-ordinate system employed plays an important role as a result of similarity of velocity profiles in the co-ordinate directions. Consequently, reference (13) considers the special case of a stationary rectangular co-ordinate system and determines what possible main stream flows referred to such a system lead to similarity solutions. Reference (14) determines permissible main stream flows referred to polar co-ordinates. In references (15) and (16) an arbitrary orthogonal co-ordinate system is assumed but certain additional assumptions are then made regarding either the main stream flow or the surface over which the flow takes place. Requirements for similarity equations then lead to restrictions on both the co-ordinate systems and main stream flows.

As a completely general analysis of possible similarity solutions does not exist at present, it will be one of the purposes of this paper to outline a technique used for attacking this problem. In addition a review of the progress made to date (13–16) will be made and a comparison of results presented. Finally, an evaluation of the practical applications of similarity solutions will be attempted along with a discussion of certain problems remaining to be solved.

Conditions for Similarity Solutions

Consider a surface in space in which an arbitrary orthogonal co-ordinate system (x_1, x_2) has been imbedded. Let y^* be a co-ordinate normal to the surface, Fig. 1. The boundary-layer equations referred to such a system are the following (16)

---

[1] Based in part on results obtained in a PhD thesis submitted to Case Institute of Technology.

[2] Aeronautical Research Scientist, Lewis Flight Propulsion Laboratory, National Advisory Committee for Aeronautics.

Contributed by the Fluid Mechanics Committee of the Hydraulics Division and presented at the Annual Meeting, New York, N. Y., December 1–6, 1957, of THE AMERICAN SOCIETY OF MECHANICAL ENGINEERS.

NOTE: Statements and opinions advanced in papers are to be understood as individual expressions of their authors and not those of the Society. Manuscript received at ASME Headquarters, August 2, 1957. Paper No. 57—A-79.

[3] Numbers in parentheses refer to the Bibliography at the end of the paper.

$$\left.\begin{aligned}\frac{u_1}{h_1}\frac{\partial u_1}{\partial x_1}+\frac{u_2}{h_2}\frac{\partial u_1}{\partial x_2}+\frac{v}{\sqrt{\nu}}\frac{\partial u_1}{\partial y}+u_1u_2k_1-u_2^2k_2-\frac{\partial^2 u_1}{\partial y^2}\\ =\frac{U_1}{h_1}\frac{\partial U_1}{\partial x_1}+\frac{U_2}{h_2}\frac{\partial U_1}{\partial x_2}+U_1U_2k_1-U_2^2k_2\end{aligned}\right\}\ldots[1a]$$

$$\left.\begin{aligned}\frac{u_1}{h_1}\frac{\partial u_2}{\partial x_1}+\frac{u_2}{h_2}\frac{\partial u_2}{\partial x_2}+\frac{v}{\sqrt{\nu}}\frac{\partial u_2}{\partial y}+u_1u_2k_2-u_1^2k_1-\frac{\partial^2 u_2}{\partial y^2}\\ =\frac{U_1}{h_1}\frac{\partial U_2}{\partial x_1}+\frac{U_2}{h_2}\frac{\partial U_2}{\partial x_2}+U_1U_2k_2-U_1^2k_1\end{aligned}\right\}\ldots[1b]$$

$$u_1k_2+u_2k_1+\frac{1}{h_1}\frac{\partial u_1}{\partial x_1}+\frac{1}{h_2}\frac{\partial u_2}{\partial x_2}+\frac{1}{\sqrt{\nu}}\frac{\partial v}{\partial y}=0\ldots.[1c]$$

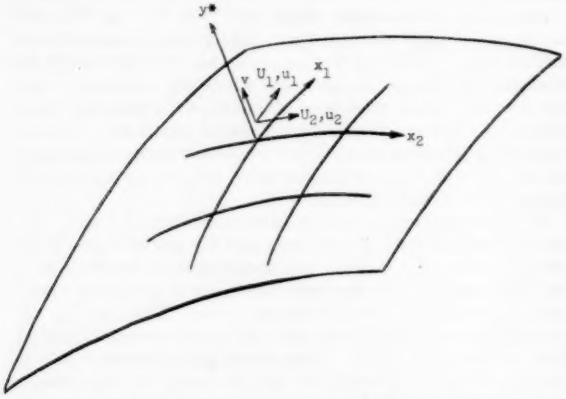

Fig. 1 Co-ordinate system and orientation of velocity components for flow over a surface

where

$y = y^*/\sqrt{\nu}$

ν = coefficient of kinematic viscosity

u_1, u_2, v = boundary-layer velocity components in the x_1, x_2, and y^*-directions, respectively

U_1, U_2 = main flow velocity components in vicinity of surface

k_1, k_2 = geodesic curvatures of co-ordinate lines x_1 = const and x_2 = const, respectively

$$\left(k_1=\frac{1}{h_1h_2}\frac{\partial h_1}{\partial x_2};\ k_2=\frac{1}{h_1h_2}\frac{\partial h_2}{\partial x_1}\right)$$

h_1, h_2 = metric tensor components related to differential of arc length by $ds^2 = h_1^2dx_1^2 + h_2^2dx_2^2$

The boundary conditions are the following

At

$$y=0,\quad u_1(0)=u_2(0)=v(0)=0\ldots\ldots[2]$$
$$\lim_{y\to\infty}u_1=U_1\qquad\lim_{y\to\infty}u_2=U_2$$

Without loss of generality, we can assume that $U_1 \not\equiv 0$.

Two possible situations now exist. Either $U_2 \not\equiv 0$ or $U_2 \equiv 0$ in which case the streamlines of the flow coincide with the co-ordinate lines x_2 = const. It is first assumed that $U_2 \not\equiv 0$. Following the classical approach for obtaining similarity solutions it is assumed the u_1 and u_2 are expressible as

$$\frac{u_1}{U_1}=F'(\eta)\ldots\ldots[3]$$

$$\frac{u_2}{U_2}=G'(\eta)\ldots\ldots[4]$$

where $F(\eta)$ and $G(\eta)$ are as yet undetermined functions of the "similarity variable" η defined as

$$\eta=yg(x_1,x_2)\ldots\ldots[5]$$

where $g(x_1, x_2)$ is an arbitrary function of x_1 and x_2. (See reference 13 for a detailed explanation on specification of the form of η.)

For the case of one main stream velocity component, U_2, identically zero, it is assumed that

$$\frac{u_1}{U_1}=F'(\eta)\ldots\ldots[6a]$$

$$\frac{u_2}{U_2^*}=G'(\eta)\ldots\ldots[6b]$$

where $U_2^* = U_2^*(x_1, x_2)$ is a function which will be determined from the analysis.

Transformed Equations for U_1 and U_2 Not Identically Zero. From Equation [1c] and the definitions for u_1 and u_2, it is possible to obtain an expression for the boundary-layer velocity component v. Substituting Equations [3] and [4] into Equation [1c] and using Equation [5] we obtain

$$U_1F'k_2+\frac{U_1F''}{h_1}y\frac{\partial g}{\partial x_1}+\frac{F'}{h_1}\frac{\partial U_1}{\partial x_1}+U_2G'k_1+\frac{U_2G''}{h_2}y\frac{\partial g}{\partial x_2}+\frac{G'}{h_2}\frac{\partial U_2}{\partial x_2}+\frac{1}{\sqrt{\nu}}\frac{\partial v}{\partial y}=0\ldots[7]$$

Solving Equation [7] and integrating partially with respect to y, we have

$$v=-\frac{\sqrt{\nu}}{g}\left[F\left(U_1k_2+\frac{1}{h_1}\frac{\partial U_1}{\partial x_1}-\frac{U_1}{h_1}\frac{\partial \ln g}{\partial x_1}\right)+G\left(U_2k_1+\frac{1}{h_2}\frac{\partial U_2}{\partial x_2}-\frac{U_2}{h_2}\frac{\partial \ln g}{\partial x_2}\right)+\frac{U_1}{h_1}\frac{\partial \ln g}{\partial x_1}\eta F'+\frac{U_2}{h_2}\frac{\partial \ln g}{\partial x_2}\eta G'\right]+f(x_1,x_2)\ldots[8]$$

At this point, it would be well to discuss restrictions on the functions $F(\eta)$ and $G(\eta)$ resulting from the boundary conditions on u_1, u_2, and v. From Equations [3], [4], and [5] we have:

1 The boundary conditions $u_1(0) = u_2(0) = 0$ for $y = 0$ imply

$$F'(0)=G'(0)=0$$

2 The conditions $\lim_{y\to\infty}u_1=U_1$ and $\lim_{y\to\infty}u_2=U_2$ imply

$$\lim_{\eta\to\infty}F'(\eta)=1 \text{ and } \lim_{\eta\to\infty}G'(\eta)=1$$

3 The condition $v(0) = 0$ implies

$$\frac{g}{\sqrt{\nu}}f(x_1,x_2)=F(0)\left(U_1k_2+\frac{1}{h_1}\frac{\partial U_1}{\partial x_1}-\frac{U_1}{h_1}\frac{\partial \ln g}{\partial x_1}\right)+G(0)\left(U_2k_1+\frac{1}{h_2}\frac{\partial U_2}{\partial x_2}-\frac{U_2}{h_2}\frac{\partial \ln g}{\partial x_2}\right)$$

Now, it can be shown by a slight extension of an argument presented in reference (13) that there is no loss of generality if it is assumed that $F(0) = 0$ and $G(0) = 0$ which in turn implies $f(x_1, x_2) = 0$. This result will be used in the following development.

Substitution of Equations [3], [4], and [5] into Equations [1a] and [1b], respectively, yields

$$\frac{1}{h_1}\frac{\partial U_1}{\partial x_1}F'^2 - \left(\frac{1}{h_1}\frac{\partial U_1}{\partial x_1} - \frac{U_1}{2h_1}\frac{\partial \ln g^2}{\partial x_1} + U_1k_2\right)FF'' - g^2F''' + \left(\frac{U_2}{h_2}\frac{\partial \ln U_1}{\partial x_2} + U_2k_1\right)G'F' - \left(\frac{1}{h_2}\frac{\partial U_2}{\partial x_2} - \frac{U_2}{2h_2}\frac{\partial \ln g^2}{\partial x_2} + U_2k_1\right)GF'' - \frac{U_2^2}{U_1}k_2G'^2 - \left(\frac{1}{h_1}\frac{\partial U_1}{\partial x_1} + \frac{U_2}{h_2}\frac{\partial \ln U_1}{\partial x_2} + U_2k_1 - \frac{U_2^2}{U_1}k_2\right) = 0 \quad \ldots [9]$$

$$\frac{1}{h_2}\frac{\partial U_2}{\partial x_2}G'^2 - \left(\frac{1}{h_2}\frac{\partial U_2}{\partial x_2} + U_2k_1 - \frac{U_2}{2h_2}\frac{\partial \ln g^2}{\partial x_2}\right)GG'' - g^2G''' + \left(\frac{U_1}{h_2}\frac{\partial \ln U_2}{\partial x_1} + U_1k_2\right)G'F' - \left(\frac{1}{h_1}\frac{\partial U_1}{\partial x_1} - \frac{U_1}{2h_1}\frac{\partial \ln g^2}{\partial x_1} + U_1k_2\right)FG'' - \frac{U_1^2}{U_2}k_1F'^2 - \left(\frac{U_1}{h_1}\frac{\partial \ln U_2}{\partial x_1} + \frac{1}{h_2}\frac{\partial U_2}{\partial x_2} + U_1k_2 - \frac{U_1^2}{U_2}k_1\right) = 0 \quad \ldots [10]$$

Equations [9] and [10] will be termed the "transformed equations" and the principal problem that we shall be concerned with is to find the necessary and sufficient conditions for reducing the transformed equations to a system of ordinary differential equations. Before this step is undertaken, however, we will determine the transformed equations for the case when one of the main stream velocity components is identically zero.

Transformed Equations for One Main Stream Velocity Component Identically Zero. We now consider the case $U_2 \equiv 0$ and define u_1 and u_2 by Equations [6a] and [6b]. Again, the boundary-layer velocity component v can be obtained. The form for v will be identical to that given in Equation [8] with U_2 replaced by U_2^*.

Substitution of the expressions for u_1, u_2, and v into Equations [1a] and [1b], respectively, then gives

$$\frac{1}{h_1}\frac{\partial U_1}{\partial x_1}F'^2 - \left(\frac{1}{h_1}\frac{\partial U_1}{\partial x_1} + U_1k_2 - \frac{U_1}{2h_1}\frac{\partial \ln g^2}{\partial x_1}\right)FF'' - g^2F''' + \left(\frac{U_2^*}{h_2}\frac{\partial \ln U_1}{\partial x_2} + U_2^*k_1\right)G'F' - \left(\frac{1}{h_2}\frac{\partial U_2^*}{\partial x_2} - \frac{U_1}{2h_2}\frac{\partial \ln g^2}{\partial x_2} + U_2^*k_1\right)GF'' - \frac{U_2^{*2}}{U_1}k_2G' - \frac{1}{h_1}\frac{\partial U_1}{\partial x_1} = 0 \quad \ldots [11]$$

$$\frac{1}{h_2}\frac{\partial U_2^*}{\partial x_2}G'^2 - \left(\frac{1}{h_2}\frac{\partial U_2^*}{\partial x_2} + U_2^*k_1 - \frac{U_2^*}{2h_2}\frac{\partial \ln g^2}{\partial x_2}\right)GG'' - g^2G'' + \left(\frac{U_1}{h_2}\frac{\partial \ln U_2}{\partial x_1} + U_1k_2\right)G'F' - \left(\frac{1}{h_1}\frac{\partial U_1}{\partial x_1} - \frac{U_1}{2h_1}\frac{\partial \ln g^2}{\partial x_1} + U_1k_2\right)FG'' - \frac{U_1^2}{U_2^*}k_1F'^2 - \frac{U_1^2}{U_2^*}k_1 = 0 \quad \ldots [12]$$

We see that Equations [11] and [12] are of exactly the same form as Equations [9] and [10] except for the final terms which are not coefficients of terms involving F, G, or their derivatives. This fact will be important in determining the general conditions necessary for reducing the transformed equations to ordinary differential equations.

It should be stated that the boundary conditions for $G'(\eta)$ for this case are given by

$$G'(0) = 0$$

$$\lim_{\eta \to \infty} G'(\eta) = 0$$

The boundary conditions on $F'(\eta)$ are the same as for the previous case.

Necessary Conditions for Obtaining Similarity Solutions. An analysis presented in reference (15) shows that a necessary condition for obtaining similarity solutions for a system of equations like Equations [9] and [10], and the system of Equations [11] and [12] is that the various terms which serve as coefficients of F, G and their derivatives in these equations be proportional. Let us first examine the implications of this result relative to Equations [9] and [10]. As the function g^2 serves as a coefficient in both equations, we have the general requirement

$$g^2 = a_1\frac{1}{h_1}\frac{\partial U_1}{\partial x_1} = a_2\left(\frac{1}{h_1}\frac{\partial U_1}{\partial x_1} - \frac{U_1}{2h_1}\frac{\partial \ln g^2}{\partial x_1} + U_1k_2\right) = a_3\left(\frac{U_2}{h_2}\frac{\partial \ln U_1}{\partial x_2} + U_2k_1\right) = a_4\left(\frac{1}{h_2}\frac{\partial U_2}{\partial x_2} - \frac{U_2}{2h_2}\frac{\partial \ln g^2}{\partial x_2} + U_2k_1\right) = a_5\frac{U_2^2}{U_1}k_2 = a_6\left(\frac{1}{h_1}\frac{\partial U_1}{\partial x_1} + \frac{U_2}{h_2}\frac{\partial \ln U_1}{\partial x_2} + U_2k_1 - \frac{U_2^2}{U_1}k_2\right) = a_7\frac{1}{h_2}\frac{\partial U_2}{\partial x_2} = a_8\left(\frac{U_1}{h_2}\frac{\partial \ln U_2}{\partial x_1} + U_1k_2\right) = a_9\frac{U_1^2}{U_2}k_1 = a_{10}\left(\frac{U_1}{h_1}\frac{\partial \ln U_2}{\partial x_1} + \frac{1}{h_2}\frac{\partial U_2}{\partial x_2} + U_1k_2 - \frac{U_1^2}{U_2}k_1\right) \quad \ldots [13]$$

We now make the following observations: First of all, g^2 cannot be identically zero (see Equation [5]). Therefore, if the individual terms

$$\frac{1}{h_1}\frac{\partial U_1}{\partial x_1}, \frac{U_2}{h_2}\frac{\partial \ln U_1}{\partial x_2} + U_2k_1, \text{ and } \frac{U_2^2}{U_1}k_2$$

are each proportional to g^2 (or identically zero), the term

$$\left(\frac{1}{h_1}\frac{\partial U_1}{\partial x_1} + \frac{U_2}{h_2}\frac{\partial \ln U_1}{\partial x_2} + U_2k_1 - \frac{U_2^2}{U_1}k_2\right)$$

will be proportional to g^2 (or identically zero). Similarly, if

$$\left(\frac{U_1}{h_2}\frac{\partial \ln U_2}{\partial x_1} + U_1k_2\right), \left(\frac{1}{h_2}\frac{\partial U_2}{\partial x_2}\right), \text{ and } \frac{U_1^2}{U_2}k_1$$

are each proportional to g^2 (or identically zero), the term

$$\left(\frac{U_1}{h_2}\frac{\partial \ln U_2}{\partial x_1} + \frac{1}{h_2}\frac{\partial U_2}{\partial x_2} + U_1k_2 - \frac{U_1^2}{U_2}k_1\right)$$

will be proportional to g^2 (or identically zero). The requirement given by Equation [13] therefore reduces to the requirement that nine coefficients be proportional. Furthermore, various terms in certain of these coefficients can be deleted when the terms are required to be individually proportional to g^2. This leaves the

following list of nine terms which must be mutually proportional (or identically zero) if similarity solutions of Equations [9] and [10] are to be obtained

1 $\quad \dfrac{1}{h_1}\dfrac{\partial U_1}{\partial x_1}$

2 $\quad U_1 k_2 - \dfrac{U_1}{2h_1}\dfrac{\partial \ln g^2}{\partial x_1}$

3 $\quad g^2$

4 $\quad \dfrac{U_2}{h_2}\dfrac{\partial \ln U_1}{\partial x_2} + U_2 k_1$

5 $\quad U_2 k_1 - \dfrac{U_2}{2h_2}\dfrac{\partial \ln g^2}{\partial x_2}$

6 $\quad \dfrac{U_2^2}{U_1} k_2$

7 $\quad \dfrac{1}{h_2}\dfrac{\partial U_2}{\partial x_2}$

8 $\quad \dfrac{U_1}{h_1}\dfrac{\partial \ln U_2}{\partial x_1} + U_1 k_2$

9 $\quad \dfrac{U_1^2}{U_2} k_1$

Proportionality between the foregoing terms is equivalent to specifying a system of partial differential equations. Solutions of the equations determine main stream velocity components U_1 and U_2, and the components h_1 and h_2 of the metric tensor associated with the orthogonal co-ordinate system. As solutions of these equations will result in Equations [9] and [10] being reduced to ordinary differential equations, a stated proportionality between any two terms will be called "an ordinary differential equation condition" and will be abbreviated "o.d.e. condition." A similar set of conditions appears in reference (15).

If we proceed to set up o.d.e. conditions for Equations [11] and [12], it will follow that these conditions will be exactly the same as those given for Equations [9] and [10] except for the replacement of U_2 by U_2^*. Hence solutions for various functions in one case will correspond exactly to those in the other case. In stating the equations for the o.d.e. conditions, $\bar{U}_2$ will be used to denote either U_2 or U_2^*.

A general solution of the system of o.d.e. conditions would give all requirements on U_1, $\bar{U}_2$, g^2, h_1, and h_2 for the existence of possible similarity solutions of the boundary-layer equations relative to an orthogonal co-ordinate system. At present the complications which arise in attempting to treat the general case make it desirable to impose certain simplifying assumptions. Such additional assumptions were made in references (13–16). A discussion of these assumptions and a summary of the results obtained in these references will now follow.

Specific Solutions of the O.D.E. Conditions

The investigations presented in references (13, 14, 16) will first be reviewed. In reference (16) two separate assumptions are made. The first of these is that the surface over which the flow takes place is developable. This assumption is also basic to references (13, 14).

Analysis for Flow Over Developable Surfaces. An important property of surfaces is the so-called Gaussian or total curvature. The total curvature K is related to h_1, h_2, k_1, and k_2 by the following formula

$$K = -\left(\frac{1}{h_1}\frac{\partial k_2}{\partial x_1} + \frac{1}{h_2}\frac{\partial k_1}{\partial x_2}\right) - (k_1^2 + k_2^2)$$

(see reference 17). Now it is known from differential geometry that a necessary and sufficient condition for a surface to be developable is that $K \equiv 0$. Hence for developable surfaces

$$k_1^2 + k_2^2 = -\left(\frac{1}{h_1}\frac{\partial k_2}{\partial x_1} + \frac{1}{h_2}\frac{\partial k_1}{\partial x_2}\right)$$

This provides an additional equation beyond those already given by the o.d.e. conditions. Before the system of equations can be solved, however, it is necessary to make certain additional assumptions which influence the vanishing or nonvanishing of specific terms which comprise the o.d.e. conditions. Three subcases are considered in reference (16). These are (i) $k_1 \not\equiv 0$, $k_2 \not\equiv 0$, (ii) either $k_1 \equiv 0$ or $k_2 \equiv 0$ but both are not identically zero, and (iii) $k_1 \equiv 0$ and $k_2 \equiv 0$.

The analysis presented in reference (16) then yields the following major results for these three cases:

1 If $k_1 \not\equiv 0$ and $k_2 \not\equiv 0$ then necessary and sufficient conditions for Equations [9] to [12] to possess similarity solutions is that

(*a*) $k_1 = (\text{const})\, k_2$

(*b*) $U_1 = (\text{const})\, U_2$

(*c*) U_1, U_2, g^2, h_1, and h_2 must be expressible as

$h_1 = ax_2$, $h_2 = bx_1$	$(a \neq 0, b \neq 0)$
$g^2 = cx_1^{n-1}x_2^{m-1}$	$c \neq 0$
$U_1 = dx_1^n x_2^m$	$d \neq 0$
$\bar{U} = ex_1^n x_2^m$	$e \neq 0$

Equations [9] and [10] become, respectively

$$A_1F_1^2 - A_2FF'' - A_3F''' + A_4G'F' - A_5GF'' - A_6G'^2 - (A_1 + A_4 - A_6) = 0$$

$$B_1G'^2 - A_5GG'' - A_3G''' + B_2G'F' - A_2FG'' - B_3F'^2 - (B_1 + B_2 + B_3) = 0$$

where

$$A_1 = dn/a \qquad A_6 = e^2/da$$

$$A_2 = \frac{(n+3)d}{2a} \qquad B_1 = em/b$$

$$A_3 = c \qquad B_2 = \frac{d(n+1)}{a}$$

$$A_4 = \frac{e}{b}(m+1) \qquad B_3 = d^2/be$$

$$A_5 = \frac{e}{2b}(m+3)$$

Equations [11] and [12] have, respectively, the same form as those given in the foregoing except that the first equation has only A_6 as a constant term and the second has only B_3 as a constant term.

(*d*) The co-ordinate system for the surface can be uniquely determined in this case. The system is a "logarithmic spiral" co-ordinate system; that is, if the surface considered were a plane, the system would have the form shown in Fig. 2.

(*e*) The permissible main flow streamlines relative to this system on a plane turn out to be either logarithmic spirals, concentric circles, or radial lines.

2 If $k_1 \equiv 0$ and $k_2 \not\equiv 0$ (or vice versa) the analysis reduces to

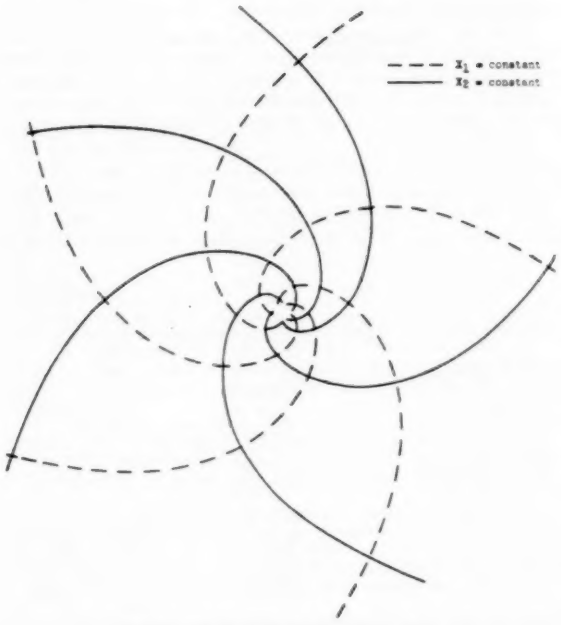

Fig. 2 System of spiral co-ordinates

the one presented in reference (14) with the exception that a developable surface instead of a flat plane is permissible. Some of the principal results here are the following:

(*a*) $U_1 = (\text{const})\ \bar{U}_2$ except in the case of radial flow in which no secondary flow takes place.

(*b*) The system of co-ordinates is a "polar-type" system; that is, if the flow were over a plane, the co-ordinate system would be the usual polar co-ordinate system.

(*c*) As in the previous case, the main flow streamlines are required to be either spirals, concentric circles, or radial lines.

The specific forms for U_1, U_2, h_1, h_2, and g^2 for this case and for all other cases which follow will be presented in tabular form in the next section.

3 If $k_1 \equiv 0$ and $k_2 \equiv 0$, the co-ordinate system is a "rectangular type," that is, on the surfaces in question, the co-ordinate lines are geodesics. The analysis principally reduces to the one presented in reference (13). One of the interesting results of this case is that it leads to solutions of flow problems where the boundary layer develops from a sharp leading edge. Particular cases are solved in references (1–3).

Solutions of O.D.E. Conditions for Flows with $U_1 = (Const)\ \bar{U}_2$. A second assumption considered in reference (16) is that $U_1 = (\text{const})\ \bar{U}_2$. This added restriction on the o.d.e. conditions makes it possible for the system to be solved quite readily. At first, such an assumption appears highly restrictive. However, past analyses have indicated that such a relation generally arises in determining the conditions for similarity solutions. To date, the author knows of no explicit expressions for the main stream velocity components in a similarity analysis employing nonrectangular co-ordinates which has not had this correspondence between U_1 and $\bar{U}_2$. Geis in reference (15) illustrates a case in which $U_1/\bar{U}_2 \not\equiv$ const when the flow is referred to a co-ordinate system in which the members of one set of co-ordinate lines have zero geodesic curvature. However, U_1 and $\bar{U}_2$ are defined implicitly in terms of a function which must satisfy a nonlinear differential equation. No solution of this equation is presented.

With the basic assumption that U_1 and $\bar{U}_2$ are proportional, it is no longer necessary to restrict the flow surface only to the developable type. However, with $K \not\equiv 0$, it is much more difficult to determine the nature of the co-ordinate system on a given surface. (If $K \equiv 0$ or if $K \equiv$ const, certain theorems from differential geometry make it possible to determine the nature of the system.)

The forms for U_1, $\bar{U}_2$, h_1, h_2, and g^2 are presented in reference (16) and, as mentioned previously, will be outlined in a following section. In using these results for a specific problem one might assume a surface and then imbed a particular co-ordinate system (x_1, x_2). The functions h_1 and h_2 could then be calculated and compared with the permissible values obtained from the analysis. If agreement was lacking a new co-ordinate system might be assumed and the process repeated. Probably, the first assumption would be that one set of co-ordinate lines were geodesics of the surface; i.e., the geodesic curvature of such lines would be identically zero. The form of the other set of co-ordinates then might be determined and checked. For any other set of co-ordinate lines assumed, the analysis shows that k_1 and k_2 would have to be proportional.

In reference (7) a solution is obtained for a nondevelopable surface. A surface of revolution is assumed and one set of co-ordinate lines are geodesics.

Solutions of the O.D.E. Conditions for Irrotational Mainstream Flow. The basic assumption made in reference (15) in addition to the o.d.e. conditions for a nonconstant rectangular system is that the main stream flow is irrotational. The functions U_1 and $\bar{U}_2$ must therefore satisfy the equation

$$\frac{\partial}{\partial x_1}(h_2\bar{U}_2) - \frac{\partial}{\partial x_2}(h_1U_1) = 0$$

For nonrectangular systems it develops that $U_1 = (\text{const})\ U_2$ except for two cases. The first is that

$$\bar{U}_2 = a(U_1^2 + b)^{1/2}\ (a, b, \text{constants})$$

and $U_1 = \varphi(x_1)$ where $\varphi(x_1)$ is nonconstant solution of the differential equation

$$(\varphi^2 + b)\varphi'' + \left(\frac{1}{2}\varphi^2 - c\varphi^2 + \frac{1}{2}b\varphi - ac\right)\varphi'^2 = 0\ (c = \text{const})$$

The second case is

$$U_1 = 1$$

$$U_2 = \frac{A}{(1 - \varphi')^{1/2}}$$

where $\varphi(x_1)$ is a solution of

$$\varphi'\varphi'' + (\varphi' - 1)^2 = 0$$

While the assumption of irrotationality is employed in a number of cases investigated in reference (15), solutions are given which hold for rotational flows as well. It should be pointed out that results similar to those obtained in references (13, 14) also are presented.

Although forms for h_1 and h_2 are determined in this analysis, a description of co-ordinate systems is generally omitted. Here again a problem exists if the total curvature of the surface is a nonconstant function of x_1 and x_2. Specific reference is made, however, to the case of flow over a surface revolution referred to earlier (7).

Summary of Requirements for Similarity Solutions

In Table 1 are presented the permissible forms for U_1, $\bar{U}_2$, h_1,

Table 1 Permissible forms for U_1, U_2, g^2, h_1, and h_2

U_1	U_2	g^2	h_1	h_2	Developable surface	Irrotational flow	References
$c_1x_1^nx_2^m$	c_2U_1	$c_3x_1^{n-1}x_2^{m-1}$	x_2	x_1	√	$(m+1) = c_2(n+1)$ for $U_2 \neq 0$ or $m = -1$, $U_2 = 0$	16, 15
$c_1x_1^ne^{mx_2}$	c_2U_1	$c_3x_1^{n-1}e^{mx_2}$	1	x_1	√	$m = c_2(n+1)$ for $U_2 \neq 0$	14, 15
						$c_1m = 0$ for $U_2 = 0$	16
$c_1e^{nx_1}$	$c_2e^{mx_2}$	$c_3e^{nx_1}$	1	1	√	$c_2m = 0$	13, 15
$c_1e^{nx_2}$	$c_2e^{mx_2}$	$c_3e^{mx_2}$	1	1	√	$c_1n = 0$	13, 15
$c_1e^{nx_1}e^{mx_2}$	$c_2e^{nx_1}e^{mx_2}$	$c_3e^{nx_1}e^{mx_2}$	1	1	√	$c_1m = c_2n$	13, 15
$c_1x_1^n$	$c_2x_1^m$	$c_3x_1^{n-1}$	1	1	√	$c_2m = 0$	13, 15
$c_1x_2^n$	$c_2x_2^m$	$c_3x_2^{m-1}$	1	1	√	$c_1n = 0$	13, 15
$c_1(ax_1 + bx_2)^n$	c_2U_2	$c_3(ax_1 + bx_2)^{n-1}$	1	1	√	$bc_1 = ac_2$	13, 15
$c_1e^{nx_1}x_2^{m-1}$	$c_2e^{nx_1}x_2^m$	$c_3e^{nx_1}x_2^{m-1}$	1	1	√	$c_1(m-1) = c_2n = 0$	13, 15
$c_1x_1^ne^{mx_2}$	$c_2x_1^{n-1}e^{mx_2}$	$c_3x_1^{n-1}e^{mx_2}$	1	1	√	$c_1m = c_2(n-1) = 0$	13, 15
$c_1x_1^nx_2^{m-1}$	$c_2x_1^{n-1}x_2^m$	$c_3x_1^{n-1}x_2^{m-1}$	1	1	√	$c_1(m-1) = c_2(n-1) = 0$	13, 15
c_1	c_2U_1	$c_3(ax_1 + bx_2 + c)^{-(n+1)}$	$(ax_1 + bx_2 + c)^n$	$(ax_1 + bx_2 + c)^n$		$c_2a = b$ $(U_2 \neq 0)$	16
c_1	c_2U_1	$c_3e^{-(ax_1+bx_2+c)}$	$e^{(ax_1+bx_2+c)}$	$e^{(ax_1+bx_2+c)}$		$c_2a = b$ $(U_2 \neq 0)$	16
$c_1e^{nx_1}$	c_2U_1	$c_3U_1e^{-(ax_1+bx_2+c)}$	$e^{(ax_1+bx_2+c)}$	$e^{(ax_1+bx_2+c)}$		$b = (n+a)$	16
$c_1e^{n(ax_1+bx_2+c)}$	c_2U_1	$c_3U_1e^{-(ax_1+bx_2+c)}$	$e^{(ax_1+bx_2+c)}$	$e^{(ax_1+bx_2+c)}$		$b = c_2a$	16
$c_1e^{n(ax_1+bx_2+c)}$	c_2U_1	$c_3U_1(ax_1 + bx_2 + c)^{-(n+1)}$	$(ax_1 + bx_2 + c)^n$	$(ax_1 + bx_2 + c)^n$		$b = c_2a$	16
$c_1e^{nx_1}e^{mx_2}$	c_2U_1	$c_3U_1e^{-(ax_1+bx_2+c)}$	$e^{(ax_1+bx_2+c)}$	$e^{(ax_1+bx_2+c)}$		$m + b = c_2(n+a)$	16
$c_1x_1^n$	c_2U_1	$c_3x_1^{m-1}$	1	x_1^n		$m = -n$	15, 16
$c_1e^{nx_1}$	c_2U_1	$c_3e^{nx_1}$	1	e^{nx_1}		$m = -n$	15, 16
c_1	c_2	c_3	1	e^{nx_1}		$U_2 = 0$	16
c_1	c_2	c_3/x_1	1	x_1^n		$U_2 = 0$	16

NOTE: The corresponding forms for the ordinary differential equations can be obtained by substituting these expressions into Equations [9] and [10] or [11] and [12].

h_2, and g^2 which when used in Equations [9] to [12] reduce the equations to ordinary differential equations. Solution of the final equations is a problem in its own right and, in general, requires the application of numerical techniques. Approximate solutions of one class of equations is discussed in reference (16).

It is of interest to note that in certain cases the differential equations which result are "uncoupled." By this we mean that one equation contains either $F(\eta)$ and its derivatives or $G(\eta)$ and its derivatives alone. The foregoing could result when either (*a*) the co-ordinate system employed is rectangular or (*b*) a point source flow is referred to polar-type co-ordinates (13, 14).

Practical Applications of Theory

From a practical standpoint, similarity solutions might be applied to the study of boundary-layer flows over such aerodynamic configurations as wings, missiles, fuselage forms, or channel flows. From the standpoint of analyzing flows over wings or in channels, the only type of analysis that seems promising is the one employing rectangular co-ordinates. The principal reason is that in such configurations the boundary layer generally develops along a line on the surface (leading edge, for example). As pointed out in references (13, 14), this physical case can only be approximated when an analysis allows a boundary layer of zero thickness to exist along such a line. Apparently this only can come about in a rectangular type co-ordinate system analysis. On the other hand, nonrectangular co-ordinate systems have particular application to flow over such configurations as missiles where three-dimensional boundary-layer flow develops from a point (nose of the missile, for example).

In most attempted applications, however, it should be kept in mind that a similarity analysis probably will predict only qualitative behavior of the flow. The restrictions imposed on the main flow velocity components, in general, will be too severe to conform to a specified flow configuration and at best an approximation to this flow can be constructed (1). Nevertheless, experimental verification of certain aspects of flow behavior predicted by theory has been very encouraging in at least one instance. The investigation presented in reference (1) showed that limiting-flow deflection on a channel surface could be predicted accurately.

The calculation of boundary-layer velocity profiles and various flow parameters from a similarity analysis also can serve as a guide in setting up approximate analysis of boundary-layer flows using momentum-integral methods. For example, one approach requires an *a priori* specification of the velocity profile shapes, which are then approximated by an analytical expression. From the standpoint of applications, momentum-integral methods seem to be most promising.

Problems Remaining for Investigation

The following problems pertaining to the analysis of similarity solutions seem worth while for continued investigation:

1 A general analysis for all possible types of similarity solutions has not yet been evolved. In investigations to date (13–16) certain assumptions have been made in addition to the o.d.e. conditions. The general solution involves solving the o.d.e. conditions without any such restrictions.

2 Although requirements are known for reducing the partial differential equations of the boundary-layer equations to ordinary differential equations, little work has been done on solving these equations. Most solutions are for systems in which one equation contains either $F(\eta)$ alone or $G(\eta)$ alone (references 1 to 3, for example). Hence further work on "mixed systems" would be of interest. Use of present-day high-speed computing machines should make it possible to obtain a wide range of solutions quite readily.

3 Further work might be carried out on the differential geometric properties of surfaces and co-ordinate systems associated with similarity analysis. For example: What types of surfaces might be permissible in a study of this type, and what is the nature of permissible co-ordinate systems imbedded in such surfaces?

4 Extension of the present theory for incompressible, laminar, boundary-layer flow to compressible, laminar, boundary-layer flow would be of interest. An investigation of similarity requirements for a two-dimensional compressible flow is given in reference (11). A particular solution of a three-dimensional compressible problem is given in reference (18). However, a general analysis for similarity solutions of the compressible-flow equations has not been developed.

5 The present analysis has been restricted to "stationary" coordinate systems. In problems where a surface is in motion, it is often desirable to employ a rotating system. The extension of analyses to include these cases should be straightforward.

Bibliography

1 "Cross Flows in Laminar Incompressible Boundary Layers," by A. G. Hansen and H. Z. Herzig, NACA TN 3651, 1956.

2 "A Simple Laminar Boundary Layer With Secondary Flow," by H. G. Loos, *Journal of the Aeronautical Sciences*, vol. 22, no. 1, 1955, pp. 35–40.

3 "Secondary Flow in a Boundary Layer," by L. Sowerby, British R.A.E., Report No. AERO 2512, March, 1954.

4 "Die Drehstromung über festens Grunde," by U. T. Bodewadt, *Zeitschrift für angewandte Mathematik und Mechanik*, Bd. 20, Heft 5, October, 1950, pp. 241–253.

5 "The Boundary Layer in Three Dimensional Flow. II—The Flow Near a Stagnation Point," by L. Howarth, *Philosophical Magazine*, series 7, vol. 42, 1951, pp. 1433–1440.

6 "Three-Dimensional Laminar Boundary Layer With Small Crossflow," by A. Mager, *Journal of the Aeronautical Sciences*, vol. 21, 1954, pp. 835–845.

7 "Ahnliche Grenzschichten an Rotationskorpen," by Th. Geis, Festschrift "50 Jahre Grenzschichtforschung," Verlag F. Vieweg, Braunschweig, Germany, 1955.

8 "Die ahnlichen Losungen der Prandtlschen Grenzschichtgleichungen," by Werner Mangler, *Zeitschrift für angewandte Mathematik und Mechanik*, Bd. 23, Heft 5, October, 1943, pp. 241–251.

9 "A Note on the Boundary-Layer Equations," by S. Goldstein, Proceedings of the Cambridge Philosophical Society, vol. 35, 1939, pp. 338–340.

10 "Similar Solutions of Compressible Boundary-Layer Equations," by Ting-Y Li and H. T. Nagamatsu, *Journal of the Aeronautical Sciences*, vol. 22, 1955, pp. 607–616.

11 "Similar Solutions of Compressible Laminar Boundary-Layer Equations," by C. B. Cohen, *Journal of the Aeronautical Sciences*, vol. 21, 1954, pp. 281–282.

12 "Similar Solutions for the Compressible Laminar Boundary Layer With Heat Transfer and Pressure Gradient," by C. B. Cohen and Eli Reshotko, NACA TN 3325, 1955.

13 "On Possible Similarity Solutions for Three-Dimensional Incompressible Laminar Boundary Layers. I—Similarity With Respect to Stationary Rectangular Co-Ordinates," by A. G. Hansen and H. Z. Herzig, NACA TN 3768, October, 1956.

14 "On Possible Similarity Solutions for Three-Dimensional Incompressible Laminar Boundary Layers. II—Similarity With Respect to Stationary Polar Co-Ordinates," by H. Z. Herzig and A. G. Hansen, NACA TN 3832, November, 1956.

15 "Ahnliche dreidimensional Grenzschichten," by Th. Geis, *Journal of Rational Mech., Anal.*, vol. 5, no. 4, 1956.

16 "Similarity Solutions of the Laminar, Incompressible, Three-Dimensional Boundary-Layer Equations," by A. G. Hansen, PhD thesis, Case Institute of Technology, 1957.

17 "Tensor Analysis," by I. S. Sokolnikoff, John Wiley & Sons, Inc., New York, N. Y., 1951.

18 "Compressible Laminar Boundary Layer Over a Yawed Infinite Cylinder With Heat Transfer and Arbitrary Prandtl Number," by Eli Reshotko and I. E. Beckwith, NACA TN 3986, June, 1957.

Discussion

A. J. A. Morgan.[4] The paper is of particular interest to the writer since it provides an interesting opportunity for the application of a general theory for obtaining similarity solutions of partial differential equations developed by the writer[5] and generalized by A. D. Michal.[6] The purpose of this note is to illustrate the application of this general theory to the basic partial differential equations of, and to make some observations on the results obtained in, the paper.

For convenience in the formulation of the boundary conditions, let

$$u_1 = \frac{u_1'}{U_1} \quad \text{and} \quad u_2 = \frac{u_2'}{U_2} \qquad \ldots\ldots [14]$$

where the u_1' and u_2' correspond to the author's u_1 and u_2. Under the transformations [14] of this discussion, Equations [1*a*], [1*b*] and [1*c*] of the paper (for the case $U_1, U_2 \not\equiv 0$) assume the form

$$\frac{U_1u_1}{h_1}\frac{\partial u_1}{\partial x_1} + \frac{U_2u_2}{h_2}\frac{\partial u_1}{\partial x_2} + \frac{v}{\sqrt{\nu}}\frac{\partial u_1}{\partial y} - \frac{\partial^2 u_1}{\partial y^2} + \frac{1}{h_1}\frac{\partial U_1}{\partial x_1}(u_1^2 - 1) + \left[k_1U_2 + \frac{1}{h_2}\frac{U_2}{U_1}\frac{\partial U_1}{\partial x_2}\right](u_1u_2 - 1) - k_2\frac{U_2^2}{U_1}(u_2^2 - 1) = 0 \ldots\ldots [15a]$$

$$\frac{U_1u_1}{h_1}\frac{\partial u_2}{\partial x_1} + \frac{U_2u_2}{h_2}\frac{\partial u_2}{\partial x_2} + \frac{v}{\sqrt{\nu}}\frac{\partial u_2}{\partial y} - \frac{\partial^2 u_2}{\partial y^2} - k_1\frac{U_1^2}{U_2}(u_1^2 - 1) + \left[k_2U_1 + \frac{1}{h_1}\frac{U_1}{U_2}\frac{\partial U_2}{\partial x_1}\right](u_1u_2 - 1) + \frac{1}{h_2}\frac{\partial U_2}{\partial x_2}(u_2^2 - 1) = 0 \ldots\ldots [15b]$$

and

$$\left[k_2U_1 + \frac{1}{h_1}\frac{\partial U_1}{\partial x_1}\right]u_1 + \left[k_1U_2 + \frac{1}{h_2}\frac{\partial U_2}{\partial x_2}\right]u_2 + \frac{U_1}{h_1}\frac{\partial u_1}{\partial x_1} + \frac{U_2}{h_2}\frac{\partial u_2}{\partial x_2} + \frac{1}{\sqrt{\nu}}\frac{\partial v}{\partial y} = 0 \ldots\ldots [15c]$$

where the notation is defined in the paper.

To seek similarity solutions of the system of Equations [15*a*]–[15*c*] is equivalent to determining the invariant solutions of these equations under a particular continuous one-parameter group of transformations.[5,7] To illustrate the application of this theory,[5] there will be determined the set of invariant solutions of Equations [15*a*]–[15*c*] under the continuous one-parameter group which is a generalization of the group of uniform expansions. This group (Γ_1) is given by the set of transformations

$$\left.\begin{aligned} \bar{x}_1 &= a^{\alpha_1}x_1, \quad \bar{x}_2 = a^{\alpha_2}x_2, \quad \bar{y} = a^{\alpha_3}y \\ \bar{u}_1 &= a^{\alpha_4}u_1, \quad \bar{u}_2 = a^{\alpha_5}u_2, \quad \bar{v} = a^{\alpha_6}v \\ \bar{U}_1 &= a^{\alpha_7}U_1, \quad \bar{U}_2 = a^{\alpha_8}U_2 \\ \bar{h}_1 &= a^{\alpha_9}h_1, \quad \bar{h}_2 = a^{\alpha_{10}}h_2 \\ \bar{k}_1 &= a^{\alpha_{11}}k_1, \quad \bar{k}_2 = a^{\alpha_{12}}k_2 \end{aligned}\right\} \ldots\ldots [16]$$

where $a(\neq 0)$ is the parameter and $\alpha_1, \ldots, \alpha_{12}$ are arbitrary real numbers whose interrelationship will be determined by the subsequent analysis. The functionally independent set of absolute in-

[4] President, AER, Inc., Pasadena, Calif. Mem. ASME.

[5] A. J. A. Morgan, "The Reduction by One of the Number of Independent Variables in Some Systems of Partial Differential Equations," *Quarterly Journal of Mathematics*, Oxford Second Series, vol. 3, December, 1952, pp. 250–259.

[6] A. D. Michal, "Differential Invariants and Invariant Partial Differential Equations Under Continuous Transformation Groups in Normed Linear Spaces," *Proceedings of the National Academy of Sciences*, vol. 37, September, 1952, pp. 623–627.

[7] A continuous r-parameter group of transformations ($r \geq 1$) will sometimes be referred to as, simply, "a group."

variants of the group [16] play a central role in the theory; one such set is given by

$$\left.\begin{aligned} &\eta_1 = yx_1^{-(\alpha_1/\alpha_1)}, \quad \eta_2 = x_1^{-(\alpha_2/\alpha_1)}x_2, \\ g_1 = y^{-(\alpha_1/\alpha_1)}u_1, \quad &g_2 = y^{-(\alpha_2/\alpha_1)}u_2, \quad g_3 = x_1^{-(\alpha_3/\alpha_1)}v, \\ &g_4 = x_1^{-(\alpha_7/\alpha_1)}U_1, \quad g_5 = x_1^{-(\alpha_8/\alpha_1)}U_2, \\ &g_6 = x_1^{-(\alpha_9/\alpha_1)}h_1, \quad g_7 = x_1^{-(\alpha_{10}/\alpha_1)}h_2, \\ &g_8 = x_1^{-(\alpha_{11}/\alpha_1)}k_1, \quad g_9 = x_1^{-(\alpha_{12}/\alpha_1)}k_2. \end{aligned}\right\} \quad \ldots [17]$$

Now, by Theorem [3],[8] Equations [15a]–[15c] will admit a set of invariant (similarity) solutions if they are constant conformally invariant[9] under the group [16]. Upon substitution of the transformations [16] in Equations [15a]–[15c] it is found that this condition is satisfied when

$$\left.\begin{aligned} &\frac{\alpha_2}{\alpha_1} = A_1, \quad \frac{\alpha_3}{\alpha_1} = A_2, \quad \frac{\alpha_4}{\alpha_3} = \frac{\alpha_5}{\alpha_2} = 0, \quad \frac{\alpha_6}{\alpha_1} = -A_2 \\ &\frac{\alpha_7}{\alpha_2} = \frac{\alpha_8}{\alpha_1} = A_1 + A_2 - 2A_3, \quad \frac{\alpha_9}{\alpha_1} = A_1 + A_2 - 1, \\ &\frac{\alpha_{10}}{\alpha_1} = A_2, \quad \frac{\alpha_{11}}{\alpha_1} = \frac{\alpha_{12}}{\alpha_1} = -(A_1 + A_2) \end{aligned}\right\} \quad \ldots [18]$$

where A_1, A_2, and A_3 are arbitrary constants.

Hence on using Equations [18] in Equations [17] and the writer's theory (Theorem 3),[8] Equations [15a]–[15c] will be reduced to a system of partial differential equations in two independent variables by the following set of substitutions:

$$\left.\begin{aligned} &\eta_1 = yx_1^{-A_3}, \quad \eta_2 = x_1^{-A_1}x_2, \\ u_1 = F_1(\eta_1, \eta_2), \quad &u_2 = F_2(\eta_1, \eta_2), \quad v = x_1^{-A_3}F_3(\eta_1, \eta_2), \\ U_1 = x_1^{A_1+A_2-2A_3}&U_3(\eta_1, \eta_2), \\ &U_2 = x_1^{A_1+A_2-2A_3}U_4(\eta_1, \eta_2), \\ h_1 = x_1^{A_1+A_2-1}&h_3(\eta_1, \eta_2), \quad h_2 = x_1^{A_2}h_4(\eta_1, \eta_2), \\ k_1 = x_1^{-(A_1+A_2)}&k_3(\eta_1, \eta_2), \quad k_2 = x_1^{-(A_1+A_2)}k_4(\eta_1, \eta_2), \end{aligned}\right\} \quad \ldots [19]$$

where, even though U_1, U_2, h_1, h_2, k_1, and k_2 are restricted to be functions of x_1 and x_2 a dependence on η_1 has been introduced for reasons which will be apparent later. On using the relations [19] in Equations [15a]–[15c] the resulting set of partial differential equations is

$$\left.\begin{aligned} &-\frac{U_3}{h_3}\left[A_3\eta_1\frac{\partial F_1}{\partial\eta_1} + A_1\eta_2\frac{\partial F_1}{\partial\eta_2}\right]F_1 + \frac{U_4}{h_4}\frac{\partial F_1}{\partial\eta_2}F_2 \\ &+ \frac{1}{\sqrt{\nu}}\frac{\partial F_1}{\partial\eta_1}F_2 - \frac{\partial^2 F_1}{\partial\eta_1^2} - k_4\frac{U_4^2}{U_3}(F_2^2 - 1) \\ &+ \frac{1}{h_3}\left[(A_1 + A_2 - 2A_3)U_3 - A_3\eta_1\frac{\partial U_3}{\partial\eta_1}\right. \\ &\left. - A_1\eta_2\frac{\partial U_3}{\partial\eta_2}\right](F_1^2 - 1) + \left[k_3U_4\right. \\ &\left. + \frac{1}{h_4}\frac{U_4}{U_3}\frac{\partial U_3}{\partial\eta_2}\right](F_1F_2 - 1) = 0 \end{aligned}\right\} \quad \ldots [20a]$$

$$\left.\begin{aligned} &-\frac{U_3}{h_3}\left[A_3\eta_1\frac{\partial F_2}{\partial\eta_1} + A_1\eta_2\frac{\partial F_2}{\partial\eta_2}\right]F_1 + \frac{U_4}{h_4}\frac{\partial F_2}{\partial\eta_2}F_2 \\ &+ \frac{1}{\sqrt{\nu}}\frac{\partial F_2}{\partial\eta_1}F_2 - \frac{\partial^2 F_2}{\partial\eta_1^2} + \frac{1}{h_4}\frac{\partial U_4}{\partial\eta_2}(F_2^2 - 1) \\ &- k_3\frac{U_3^2}{U_4}(F_1^2 - 1) + \left\{k_4U_3 + \frac{1}{h_3}\frac{U_3}{U_4}\right. \\ &\left[(A_1 + A_2 - 2A_3)U_4 - A_3\eta_1\frac{\partial U_4}{\partial\eta_1}\right. \\ &\left.\left. - A_1\eta_2\frac{\partial U_4}{\partial\eta_2}\right]\right\}(F_1F_2 - 1) = 0 \end{aligned}\right\} \quad \ldots [20b]$$

and

$$\left.\begin{aligned} &\left\{k_4U_3 + \frac{1}{h_3}\left[(A_1 + A_2 - 2A_3)U_3 - A_3\eta_1\frac{\partial U_3}{\partial\eta_1}\right.\right. \\ &\left.\left. - A_1\eta_2\frac{\partial U_3}{\partial\eta_2}\right]\right\}F_1 + k_3U_4 + \frac{1}{h_4}\frac{\partial U_4}{\partial\eta_2}F_2 \\ &- \frac{U_3}{h_3}\left[A_3\eta_1\frac{\partial F_1}{\partial\eta_1} + A_1\eta_2\frac{\partial F_1}{\partial\eta_2}\right] + \frac{U_4}{h_4}\frac{\partial F_2}{\partial\eta_2} \\ &+ \frac{1}{\sqrt{\nu}}\frac{\partial F_3}{\partial\eta_1} = 0 \end{aligned}\right\} \quad \ldots [20c]$$

It is worthwhile to note several features of Equations [20a]–[20c]. If the analysis were to be stopped at this stage, then U_3, U_4, h_3, h_4, k_3, and k_4 would be made independent of η_1. This, in turn, would imply that, on redefining F_1 and F_2 to be the partial derivatives with respect to η_1 of two new functions and setting $A_3 = 0$, Equation [20c] can be immediately solved for $F_3(\eta_1, \eta_2)$ on integrating it once with respect to η_1. In fact, the restriction $A_3 = 0$ arises when Equations [15a]–[15c] are required to be absolutely invariant under the group [16]. The boundary conditions for Equations [20a]–[20c], then assume the form

$$\left.\begin{aligned} &\text{at } \eta_1 = 0 \\ &F_1(0, \eta_2) = F_2(0, \eta_2) = F_3(0, \eta_2) = 0 \\ &\text{and} \quad \lim_{\eta_1\to\infty} F_1(\eta_1, \eta_2) = 1, \quad \lim_{\eta_1\to\infty} F_2(\eta_1, \eta_2) = 1 \end{aligned}\right\} \quad \ldots [21]$$

To proceed further, it is necessary to inquire as to the existence of a set of invariant solutions of Equations [20a]–[20c] under the group (Γ_2)

$$\left.\begin{aligned} &\bar\eta_1 = b^{\beta_1}\eta_1, \quad \bar\eta_2 = b^{\beta_2}\eta_2, \\ \bar F_1 = b^{\beta_3}F_1, \quad &\bar F_2 = b^{\beta_4}F_2, \quad \bar F_3 = b^{\beta_5}F_3, \\ &\bar U_3 = b^{\beta_6}U_3, \quad \bar U_4 = b^{\beta_7}U_4, \\ &\bar h_3 = b^{\beta_8}h_3, \quad \bar h_4 = b^{\beta_9}h_4, \\ &\bar k_3 = b^{\beta_{10}}k_3, \quad \bar k_4 = b^{\beta_{11}}k_4, \end{aligned}\right\} \quad \ldots [22]$$

where $b(\neq a \neq 0)$ is the parameter of the group and $\beta_1, \ldots, \beta_{11}$ are arbitrary real numbers to be determined in the previously indicated manner. One set of functionally independent absolute invariants of the group [21] is

$$\left.\begin{aligned} &\eta = \eta_1^{-(\beta_2/\beta_1)}\eta_2, \\ \bar g_1 = \eta_1^{-(\beta_3/\beta_1)}F_1, \quad &\bar g_2 = \eta_1^{-(\beta_4/\beta_1)}F_2, \\ &\bar g_3 = \eta_1^{-(\beta_5/\beta_1)}F_3, \\ \bar g_4 = \eta_1^{-(\beta_6/\beta_1)}U_3, \quad &\bar g_5 = \eta_1^{-(\beta_7/\beta_1)}U_4, \\ \bar g_6 = \eta_1^{-(\beta_8/\beta_1)}h_3, \quad &\bar g_7 = \eta_1^{-(\beta_9/\beta_1)}h_4, \\ \bar g_8 = \eta_1^{-(\beta_{10}/\beta_1)}k_3, \quad &\bar g_9 = \eta_1^{-(\beta_{11}/\beta_1)}k_4. \end{aligned}\right\} \quad \ldots [23]$$

[8] A set of functions $\Phi_\delta(x_1, \ldots, x_n)$, abbreviated $\Phi_\delta(x_i)$, is said to be "conformally invariant" under a group $\bar x_i \to x_i$, with numerical parameter a, if $\Phi_\delta(x_i) = f_\delta(\bar x_i;\ a)\,\Phi_\delta(\bar x_i)$, $i = 1, \ldots, n$, $\delta = 1, \ldots, m$ where the $\Phi_\delta(\bar x_i)$ are exactly the same functions of the $\bar x_i$ as the Φ_δ are of the x_i. These functions will be said to be "constant conformally invariant" under the group if the $f_\delta(\bar x_i;\ a)$ are independent of the $\bar x_i$, and "absolutely invariant" if $f_\delta(\bar x_i;\ a) \equiv 1$, $\delta = 1, \ldots, m$.

Equations [20a]–[20c] will be constant conformally invariant under the group [22] if

$$\left.\begin{aligned} &\frac{\beta_2}{\beta_1} = B_1, \quad \frac{\beta_3}{\beta_1} = \frac{\beta_4}{\beta_1} = 0, \quad \frac{\beta_5}{\beta_1} = -1, \\ &\frac{\beta_6}{\beta_1} = \frac{\beta_7}{\beta_1} = B_2, \quad \frac{\beta_8}{\beta_1} = B_2 + 2 \\ &\frac{\beta_9}{\beta_1} = B_2 - B_1 + 2, \quad \frac{\beta_{10}}{\beta_1} = \frac{\beta_{11}}{\beta_1} = -(B_2 + 2) \end{aligned}\right\} \quad \ldots [24]$$

where B_1 and B_2 are arbitrary real numbers.

Again, on using Equations [24] in [23] and invoking Theorem [3][5] Equations [20a]–[20c] will be reduced to a system of "ordinary" differential equations by the following set of substitutions:

$$\left.\begin{aligned} &\eta = \eta_1^{-B_1}\eta_2 \\ &F_1 = G_1(\eta), \quad F_2 = G_2(\eta), \quad F_3 = \eta_1^{-1}G_3(\eta), \\ &U_3 = \eta_1^{B_3}U_5(\eta), \qquad U_4 = \eta_1^{B_3}U_6(\eta), \\ &h_2 = \eta_1^{B_2+2}h_5(\eta), \qquad h_4 = \eta_1^{B_2-B_1+2}h_6(\eta), \\ &k_2 = \eta_1^{-(B_2+2)}k_5(\eta), \quad k_4 = \eta_1^{-(B_2+2)}k_6(\eta). \end{aligned}\right\} \quad \ldots [25]$$

On using the relations [25] in Equations [20a]–[20c] the resulting set of ordinary differential equations is found to be

$$\begin{aligned} &-(A_1\eta - A_3B_1)\frac{U_5}{h_5}\frac{dG_1}{d\eta}G_1 + \frac{U_6}{h_6}\frac{dG_1}{d\eta}G_2 \\ &\quad - \frac{B_1}{\sqrt{\nu}}\eta\frac{dG_1}{d\eta}G_3 - B_1\eta\left[(1+B_1)\frac{dG_1}{d\eta} + B_1\eta\frac{d^2G_1}{d\eta^2}\right] \\ &\quad + \frac{1}{h_5}\left[(A_1 + A_2 - 2A_3 - A_3B_2)U_5 + (A_3B_1 - A_1)\eta\frac{dU_5}{d\eta}\right] \\ &\qquad (G_1^2 - 1) + \left[k_5U_6 + \frac{1}{h_6}\frac{U_6}{U_5}\frac{dU_5}{d\eta}\right](G_1G_2 - 1) \\ &\qquad\quad - k_6\frac{U_6^2}{U_5}(G_2^2 - 1) = 0 \quad \ldots [26a] \end{aligned}$$

$$\begin{aligned} &-(A_1\eta - A_3B_1)\frac{U_5}{h_5}\frac{dG_2}{d\eta}G_1 + \frac{U_6}{h_6}\frac{dG_2}{d\eta}G_2 \\ &\quad - \frac{B_1}{\sqrt{\nu}}\eta\frac{dG_2}{d\eta}G_3 - B_1\eta\left[(1+B_1)\frac{dG_2}{d\eta} + B_1\eta\frac{d^2G_2}{d\eta^2}\right] \\ &\qquad - k_5\frac{U_5^2}{U_6}(G_1^2 - 1) + \left\{k_6U_5 + \frac{1}{h_5}\frac{U_5}{U_6}\right. \\ &\qquad \left.\left[(A_1 + A_2 - 2A_3 - A_3B_2)U_6 + (A_3B_1 - A_1)\eta\frac{dU_6}{d\eta}\right]\right\} \\ &\qquad\quad (G_1G_2 - 1) + \frac{1}{h_6}\frac{dU_6}{d\eta}(G_2^2 - 1) = 0 \quad \ldots [26b] \end{aligned}$$

and

$$\begin{aligned} &\left\{k_6U_5 + \frac{1}{h_5}\left[(A_1 + A_2 - 2A_3 - A_3B_2)U_5\right.\right. \\ &\quad \left.\left. + (A_3B_1 - A_1)\eta\frac{dU_5}{d\eta}\right]\right\}G_1 + \left\{k_5U_6 + \frac{1}{h_6}\frac{dU_6}{d\eta}\right\}G_2 \\ &\quad - (A_1\eta - A_3B_1)\frac{U_5}{h_5}\frac{dG_1}{d\eta} + \frac{U_6}{h_6}\frac{dG_2}{d\eta} \\ &\qquad - \frac{1}{\sqrt{\nu}}\left[G_2 + B_1\eta\frac{dG_2}{d\eta}\right] = 0 \quad \ldots [26c] \end{aligned}$$

On combining Equations [19] and [25], it is seen that, in terms of the original variables, the substitutions which tranform Equations [15a]–[15c] into a system of ordinary differential equations are

$$\left.\begin{aligned} &\eta = y^{-B_1x_1 - (A_1 - A_3B_1)x_2} \\ &u_1 = G_1(\eta), \quad u_2 = G_2(\eta), \quad v = y^{-1}G_3(\eta), \\ &U_1 = y^{B_2x_1}{}^{(A_1 + A_2 - 2A_3 - A_3B_2)}U_5(\eta), \\ &\qquad U_2 = y^{B_2x_1}{}^{(A_1 + A_2 - 2A_3 - A_3B_2)}U_6(\eta), \\ &h_1 = y^{B_2+2_{x_1}(A_1 + A_2 - 2A_3 - A_3B_2 - 1)}h_5(\eta), \\ &\qquad h_2 = y^{B_2 - B_1 + 2_{x_1}[A_3 - A_3(B_2 - B_1 + 2)]}h_6(\eta), \\ &k_1 = y^{-(B_2+2)x_1 - (A_1 + A_2 - 2A_3 - A_3B_2)}k_5(\eta), \\ &\qquad k_2 = y^{-(B_2+2)x_1 - (A_1 + A_2 - 2A_3 - A_3B_2)}k_6(\eta), \end{aligned}\right\} \quad \ldots [27]$$

which, aside from a trivial transformation of independent variable, subsumes several of the cases given in Table 1 of the paper. The restrictions which must be imposed on U_5, U_6, h_5, h_6, k_5, and k_6 so that U_1, U_2, h_1, h_2, k_1, and k_2 are independent of y can now be clearly seen; that is

$$U_5(\eta) = C_1\eta^{(B_2/B_1)}, \quad U_6(\eta) = C_2\eta^{(B_2/B_1)} \quad \ldots [28a]$$

$$h_5(\eta) = C_3\eta^{(B_2+2)/B_1}, \quad h_6(\eta) = C_4\eta^{(B_2 - B_1 + 2)/B_1} \quad \ldots [28b]$$

$$k_5(\eta) = C_5\eta^{-(B_2+2)/B_1}, \quad k_6(\eta) = C_6\eta^{-(B_2+2)/B_1} \quad \ldots [28c]$$

where $C_1, \ldots, C_6$ are arbitrary constants. Furthermore, the relations $k_1 = \dfrac{1}{h_1h_2}\dfrac{\partial h_1}{\partial x_2}$ and $k_2 = \dfrac{1}{h_1h_2}\dfrac{\partial h_2}{\partial x_1}$ impose the additional restrictions

$$C_5 = \frac{1}{C_4}\frac{B_2 + 2}{B_1},$$

$$C_6 = \frac{1}{C_3}\left[A_2 - \frac{A_1}{B_1}(B_2 - B_1 + 2)\right] \quad \ldots [28d]$$

Under Equations [28], Equations [27] imply that $U_2/U_1 = \text{const}$. If, however, $U_1 = \text{const}$ and $U_2 = U_2(x_1, x_2)$, then the appropriate similarity variables can be found in a similar manner by altering Equations [15] accordingly and investigating their invariance properties under the groups Γ_1 and Γ_2 with U_1 suppressed therefrom.

With the preceding results at hand, it is now possible to remark upon those obtained in the paper in greater detail. The following observations can be made:

1 Although otherwise implied in the paper, a completely general theory for determining the *form* of the "similarity" solutions of systems of partial differential equations does exist. It is given in references cited.[5,6]

2 In view of the preceding development it is clear that in order for similarity solutions of Equations [15] to exist it *is not* necessary to:

(i) assume the form of the similarity variables beforehand (as was done in Equation [5] of the paper)

(ii) restrict the coefficient functions in Equations [9 and 10] of the paper to be mutually proportional, and

(iii) impose the "o.d.e. conditions" of the paper. In fact, the existence or nonexistence of invariant (similarity) solutions for a system of partial differential equations is determined solely by their invariance properties under a particular one (or more) parameter continuous group of transformations.

3 However, as indicated by Equations [27], and [28], in order for invariant (similarity) solutions to exist under the groups [16] *and* [22] certain restrictions must be imposed on the functional

form of the external velocity components and the geometrical properties of the surface over which the boundary layer flow occurs.

4 The functionally independent sets of absolute invariants [17] and [23] of the groups Γ_1 and Γ_2 respectively represent, in each instance, only one of many possible such sets. Clearly, other sets could have been used in the determination of the form of the invariant (similarity) solutions of Equations [15a]–[15c].

It should be noted that the groups Γ_1 and Γ_2 need not have been taken as generalizations of group of uniform expansions. To mention another possibility, one could have been chosen to work with the spiral group

$$\bar{x}_1 = e^a x_1, \quad \bar{x}_2 = x_2 + \gamma_2 a, \quad \bar{x}_3 = x_3 + \gamma_3 a,$$
$$\bar{Y}_\delta = Y_\delta + \gamma_\delta a, \quad \delta = 4, \ldots, n \ldots\ldots\ldots [29]$$

where the x_i ($i = 1, \ldots, 3$) and the Y_δ are, respectively, the independent and dependent variables (and/or coefficient functions) in the partial differential equations. In the group [29], a is the parameter, the γ_δ ($\delta = 2, \ldots, n$) are arbitrary numerical constants, and one set of its absolute invariants is given by

$$\eta_i = x_i - \gamma_i \ln x_1, \quad g_\delta = Y_\delta - \gamma_\delta \ln x_1,$$
$$i = 2, 3, \qquad \delta = 4, \ldots, n \ldots\ldots [30]$$

Thus invariant (similarity) solutions of Equations [15a]–[15c] could have been determined under Γ_1 = group [16] and Γ_2 = group [29], or Γ_1 = group [29] and Γ_2 = group [27], and Γ_1 = group [29] with parameter a and Γ_2 = group [29] with parameter b ($\neq a$). In fact, an investigation of these possibilities in the case of Equations [15a]–[15c] will show that they yield the remaining cases listed in Table 1 of the paper.

Finally, it should be remarked that the analysis given in this discussion could have been performed with greater sophistication by investigating the invariance properties of Equations [15a]–[15c] under two-parameter continuous groups of transformations and applying the theory developed by Michal.[8] The intermediate steps, culminating in Equations [19] and [20], were given to illustrate the ease with which invariant (similarity) solutions can be found and because, due to their less restrictive character, Equations [20a]–[20c] may prove to be of interest in the further analysis of three dimensional boundary layers.

Author's Closure

The author expresses his appreciation to Dr. Morgan for a very worth-while contribution to study of similar solutions of the boundary layer equations. The author fully agrees with Dr. Morgan's observation that the analysis leading to Equations [20a] [20c] may prove of interest in boundary layer theory and might well receive further study.

In reading the conclusions 1–4 given in the discussion, it became evident that certain facts in the paper needed clarification. First, let it be stated that the author's remark "a completely general analysis of possible similarity solutions does not exist at present. . ." was perhaps misunderstood by Dr. Morgan. The intent of the remark was that a complete determination of all possible similarity "solutions" has not as yet been obtained for (*a*) equations initially expressed in arbitrary orthogonal co-ordinates (*b*) an analysis based on the "classical" similarity transformations $\eta = yg(x_1, x_2)$; $u_1/U_1 = F'(\eta)$; $u_2/U_2 = G'(\eta)$. This problem has been solved, for example, for equations expressed in rectangular co-ordinates. While Dr. Morgan's analysis illustrates an approach to solving similarity problems it is still not clear that the method will readily answer certain questions associated with the original paper. One question, for example, is whether or not similarity solutions exist for $k_1 \not\equiv 0$, $k_2 \not\equiv 0$, and $U_1 \not\equiv$ (constant) U_2.

The statement by Dr. Morgan that the form of the similarity parameter need not be assumed initially is certainly true in light of his analysis. It should be pointed out, however, that the form chosen for η appears quite reasonable. In NACA TN 3768 (ref. 13) the author and H. Herzig applied the one-parameter group method to a study of the boundary layer equations in rectangular co-ordinates. (This method is outlined in G. Birkhoff's "Hydrodynamics"). The analysis showed that η was expressible as a product of a function of y and a function of x_1, x_2 for the transformations used. It seemed reasonable then, to assume a priori such a form for η and set up conditions for similarity. At present, this a priori specification of $\eta = yg(x_1, x_2)$ continues to appear reasonable in light of Dr. Morgan's contribution. It is not evident that other forms for η can be obtained which are not reducible by a scale transformation to the form used in the paper.

In defense of the "o.d.e. conditions," one can refer to T. Geis (ref. 15) who established that the conditions were necessary and sufficient for establishment of similarity conditions for the complete boundary value problem. Again, this is based on η being expressed as given. While the use of o.d.e. conditions may lack the generality of Dr. Morgan's approach, it has a minor advantage in giving only one specific set of requirements to work with at the outset. The one-parameter group method requires first choosing suitable groups and then separately investigating combinations of these groups in an analysis.

A remark might be inserted here about the proportionality of U_1 and U_2. It is shown in the discussion that, under the groups Γ_1 and Γ_2, $U_1/U_2 \equiv$ constant. It is then suggested that the case $U_1 =$ constant, $U_2 = U_2(x_1, x_2)$ be investigated. If this problem is analyzed using the o.d.e. conditions under the assumption $k_1 \not\equiv 0$, $k_2 \not\equiv 0$, it follows at once from ④ and ⑨ that $U_2 =$ constant. Hence, one might expect success only in the case where either k_1 or k_2 were identically zero.

In conclusion, the author would like to point out that one o the problems left unsolved in the paper has since been analyzed. This was the problem of determining the differential-geometric properties of the surfaces associated with the various solutions and the nature of corresponding co-ordinate systems. The analysis is given in NACA TN 4322. It is also shown that the solutions listed in the paper can be grouped into four basic categories which cover all cases.

One-Way Surge Tanks for Pumping Plants

By JOHN PARMAKIAN,[1] DENVER, COLO.

One-way low-level surge tanks may be used for the control of water hammer at pumping plants where water-column separation occurs in the discharge line subsequent to a power failure at the pump motors. This paper describes the characteristics of these tanks and also includes a typical graphical water-hammer solution of the problem.

Nomenclature

The following nomenclature is used in the paper:

- A = cross-sectional area of pipe, sq ft
- a = velocity of pressure wave, fps
- α = ratio of pump speed at any time to rated pump speed, $\alpha = N/N_R$
- β = ratio of pump input torque for any given speed to pump input torque at rated speed and head, $\beta = M/M_R$
- D = inside diameter of conduit, in.
- e = thickness of pipe wall, in.
- g = acceleration due to gravity, fps per sec
- H_0 = pumping head for initial steady pumping conditions, ft
- H_R = rated pumping head, ft
- H = pressure head for surge conditions measured above pump-intake water-surface elevation, ft
- H_a = barometric pressure, ft
- H_v = vapor pressure of water, ft
- h = ratio of pressure head for surge conditions to rated pumping head, $h = H/H_R$
- K_1 = defined by Equation [2], sec^{-1}
- L = length of pipe, ft
- L/a = wave travel time of discharge line, sec
- M = pump-input torque corresponding to a given speed and head, lb-ft
- M_R = pump-input torque at rated speed and head, lb-ft
- N = pump speed at any time, rpm
- N_R = rated pump speed, rpm
- η_R = pump efficiency at rated speed and head
- Q = pump discharge at any time, cfs
- Q_0 = pump discharge for initial pumping conditions, cfs
- Q_R = pump discharge at rated speed and head, cfs
- ρ = a pipeline constant as defined by Equation [5]
- t = time at instant under consideration during variable-flow conditions; time $t = 0$ is taken at the instant of power failure, sec
- V = velocity of water in discharge line for surge conditions at any time t, fps
- V_0 = velocity of water in discharge line for initial steady conditions, fps
- v = ratio of velocity of water for surge conditions to that for initial steady conditions, $v = V/V_0 = Q/Q_0$
- w = specific weight of water, pcf
- WR^2 = flywheel effect, or moment of inertia in terms of weight of rotating parts of motor, pump, and entrained water, pfs

[1] Head, Technical Engineering Analysis Section, Division of Design, Bureau of Reclamation, U. S. Department of the Interior. Mem. ASME.

Contributed by the Hydraulic Division and presented at the Annual Meeting, New York, N. Y., December 1–6, 1957, of THE AMERICAN SOCIETY OF MECHANICAL ENGINEERS.

 Manuscript received at ASME Headquarters, June 5, 1957. Paper No. 57—A-25.

Introduction

The graphical method of water-hammer analysis for pump-discharge lines has been well established. In order to determine the transient hydraulic conditions at the pump and discharge line subsequent to a power failure at the pump motor, three effects must be considered; namely, the pump and motor inertia, the pump characteristics, and the water-hammer wave phenomena in the discharge line.

The effect of the pump and motor inertia is obtained from the following inertia equation[2]

$$\alpha_1 - \alpha_2 = K_1(\beta_1 + \beta_1)\Delta t \quad \ldots\ldots\ldots\ldots [1]$$

where

$$K_1 = \frac{450\, gwH_RQ_R}{\pi^2 WR^2 \eta_R N^2_R} \quad \ldots\ldots\ldots\ldots [2]$$

This equation defines the relation between the pump speed and torque at a given instant of time in terms of the kinetic energy of the rotating system.

The pump-performance data usually supplied by the pump manufacturer include the head, brake-horsepower, and efficiency curves plotted against the discharge. By utilizing the laws of homologous pump operation these data can be converted to a family of torque and speed curves on an h-v diagram as shown in Fig. 1. When a power failure occurs at the pump motor, these pump characteristics are adequate for determining the minimum transient pressures at all points in the discharge line and for determining the likelihood of water-column separation. However, if a control valve is not present on the discharge side of the pump,

[2] See reference (5).

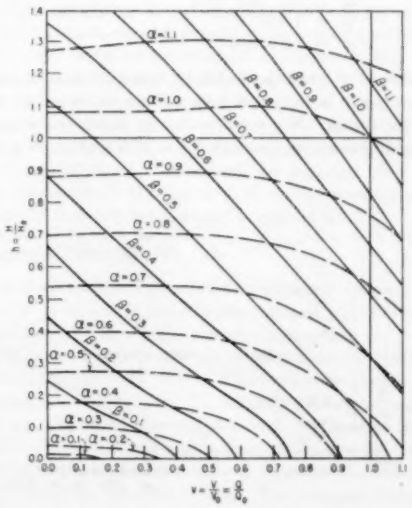

Fig. 1 Speed and torque curves. Zone of normal pump operation.

the flow reverses through the pump and additional pump characteristics are required to determine the transient conditions for the zone of energy dissipation in which the pump is running in the forward direction with the flow through the pump in reverse, and for the zone of turbine operation in which the flow through the pump and the pump rotation are both in reverse.

Finally, the water-hammer effects are obtained from the following conjugate water-hammer equations

$$h_{B_1t_1} - h_{C_1t_2} = -2\rho(v_{B_1t_1} - v_{C_1t_2}) \quad [3]$$

$$h_{C_2t_3} - h_{B_2t_4} = +2\rho(v_{C_2t_3} - v_{B_2t_4}) \quad [4]$$

where

$$2\rho = \frac{aV_0}{gH_0} \quad [5]$$

which is the pipeline constant. These equations define the relations between the head and flow in the discharge line during the transient-flow conditions under the action of the water-hammer waves. In the first equation, $(t_2 - t_1)$ is the wave travel time between two points on the pipeline B_1 and C_1 for a pressure wave which originates at the pump and moves in the direction of normal pump flow. In the second equation, $(t_4 - t_3)$ is the wave travel time between C_2 and B_2 for a pressure wave which originates at the upper basin and moves opposite to the direction of normal pump flow.

Water-Hammer Analysis Without Water-Column Separation

Consider the pump-discharge-line profile shown in Fig. 2. The basic data for this pumping plant are as follows:

D	=	$32^5/_8$ in.
A	=	5.81 sq ft
e	=	3/16 in.
a	=	2820 fps
Q_0	=	33.7 cps (for 3-pump operation)
V_0	=	5.81 fps (for 3-pump operation)
H_0	=	220 ft
L	=	3940 ft
Motor rating	=	400 hp for each pump motor
WR^2	=	384.9 lb-ft² for each pump and motor
N_R	=	1760 rpm
η_R	=	84.7 per cent
ρ	=	1.155
L/a	=	1.397 sec

In order to shorten the water-hammer solution, it is assumed that each pump is equipped with a check valve on the discharge side of the pump. For a power failure which occurs simultaneously at all three pump motors, $2\rho = 2.31$ and $K_1 = 0.224$. If a

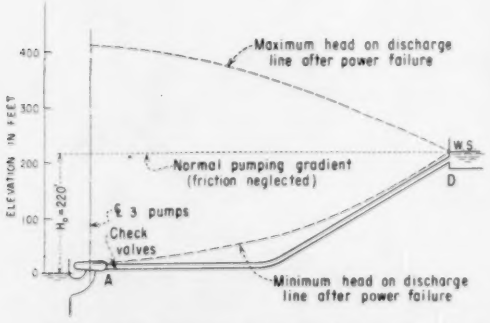

Fig. 2 Pipeline profile—with transient gradients

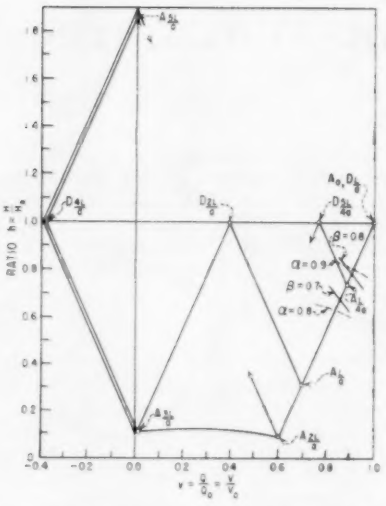

Fig. 3 Graphical water-hammer solution—no water-column separation

time interval of $\Delta t = L/4a = 0.349$ sec is selected for the computations

$$\alpha_1 - \alpha_2 = K_1\Delta t(\beta_1 + \beta_2) = 0.0782(\beta_1 + \beta_2) \quad [6]$$

The simultaneous solution of the water-hammer equations and the inertia equation on the pump characteristics diagram by graphical methods is shown in Fig. 3. Pipeline friction effects are negligible in this problem and have been neglected in the analysis. The starting point in the solution corresponding to A_0 is located on the h-v diagram at the co-ordinates $h = 1$, $v = 1$. $A_L/4a$ is then located on the line of slope $2\rho = +2.31$ which passes through A_0 in the following manner: The location of $A_L/4a$ is first estimated. Values of α_2 and β_2 are then read from the pump-characteristics curves. This value of β_2 is used in Equation [6] to compute α_2. If the computed value of α_2 does not agree with the value of α_2 on the curves, the point for $A_L/4a$ is shifted up or down on the sloping line $2\rho = +2.31$ until these values of α_2 agree. This particular point is found to be located at a value of $\beta = 0.760$ and $\alpha = 0.863$. Other points for subsequent time intervals are determined in a similar manner. The basic graphical water-hammer solution is shown in Fig. 3. The limiting values of head are as follows:

Maximum drop in head at pump = $0.92\,H_0$ = 202 ft

Maximum drop in head at mid-length = $0.69\,H_0$ = 152 ft

Maximum head rise at pump = $0.90\,H_0$ = 198 ft

Water-Column Separation

The maximum positive and negative pressure changes obtained from the water-hammer solution are plotted on the discharge-line profile in Fig. 2 to show the limiting pressure for which the discharge line should be designed. When the minimum pressure at any point along the pump-discharge line reaches the vapor pressure of water, the water-hammer solution shown in Fig. 3 is no longer valid. If this subatmospheric pressure condition inside the pipe persists for a sufficient period, the liquid water column parts and is separated by a section of vapor. This phenomenon is known as water-column separation. Water-column separation sometimes occurs upon power failure at the pump motors during

the initial negative surge waves on long pump-discharge lines at high points which are near the hydraulic gradient. Whenever economically possible, this condition should be avoided by using either a surge tank, an air chamber, or larger motor WR^2 because of the high pressures created when the two liquid water columns rejoin. When water-column separation cannot be avoided, special means are usually taken to minimize the violence of impact resulting from the rejoining of the water columns. This can be accomplished by positioning special control valves or other protective devices in the discharge line, which will either reduce the reverse velocity of the upper water column, or increase the reverse velocity of the lower water column prior to the rejoining of the two columns.

Water-Hammer Analysis With Water-Column Separation

In order to illustrate the effect of the water-column separation phenomena, consider the pipeline shown in Fig. 4. With the exception of the change in the pipeline profile and the sharp crest at B this installation is assumed to have the same characteristics as those shown in Fig. 2. The graphical water-hammer solution for this installation upon a power failure at the pump motors is shown in Fig. 6. The solution starts off in the same manner as

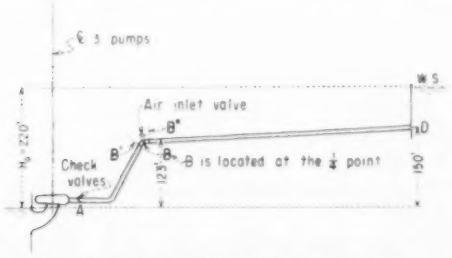

Fig. 4 Pipeline profile—with air inlet valve

that described previously for Fig. 3. However, at $t = 3L/4a$ sec the pressure at the crest B has reduced to atmospheric pressure at a value of $h = 0.56$. Air then begins to enter the pipe through the air-inlet valve and the water columns part. Let B' designate the extremity of the lower water column AB' and B'' designate the extremity of the upper water column $B''D$. It is assumed that the air valve is of sufficient size to maintain atmospheric pressure at B until the columns reunite. It is further assumed that the break at the extremities of the water column at B is complete and therefore complete wave reflections occur at the separated points B' and B'' in the two water columns. From a consideration of the wave travel time in the two water columns, the point $B'_{3L/4a}$ in addition to representing the condition at B' at $t = 3L/4a$ sec, also represents the condition at B'' from $t = 3L/4a$ to $7L/4a$ sec. In other words, the head and velocity at B'' remain constant during this time interval until the initial pressure wave reflected at D arrives at B'' at $t = 2L/a$ sec.

To complete the solution it is necessary to maintain a record of the movement of the two water columns at B' and B'' in order to ascertain the instant when the columns rejoin. A plot of the movement of the water columns from data obtained from the graphical solution is shown in Fig. 7. The separation of the water columns based on these movements is shown in Fig. 8, from which it is seen that the maximum separation is about 8.7 ft and that the water columns rejoin at $t = 29L/4a$ sec. At this instant of time and thereafter, the points B' and B'' are synonymous and are designated as B. It is assumed that the air admitted to the pipe is released prior to the rejoining of the water columns. The maximum head rise at the check valve as read from the graphical solution is 3.10 H_0 or about 682 ft.

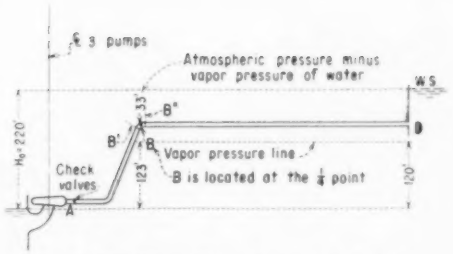

Fig. 5 Pipeline profile—with no air inlet valve

The graphical water-hammer solution shown in Fig. 6 is also applicable to the pipeline profile shown in Fig. 5 without an air-inlet valve. In the latter case the minimum pressure at B drops down to the vapor pressure of water and the question of air admission or release at the point of separation is not pertinent.

Water-Hammer Analysis With One-Way Surge Tank

A one-way low-level surge tank may be used effectively to eliminate the large water-hammer pressures resulting from the water-column separation phenomena just described. The basic construction of one of these tanks is shown in Fig. 9. The primary purpose of the tank is to supply water to the discharge line at the point of separation whenever the head in the line drops below that corresponding to the level of water in the tank, thus preventing the formation of a void. When the flow in the discharge line at the tank reverses, the check valve at the surge tank closes.

To illustrate the effect on water hammer for an installation with a one-way surge tank consider the pumping-plant installation shown in Fig. 10. Aside from replacing the air-inlet valve with a one-way surge tank this installation is assumed to be identical to that shown in Fig. 4. In order that a direct comparison may be obtained, the minimum level in the one-way surge tank is assumed to be constant during the transient and is taken so that the head at B is maintained at the same value as in the preceding section with water-column separation, that is, at $h = 0.56$. The graphical water-hammer solution for the pump-discharge line with the one-way surge tank is shown in Fig. 11. The first part of the solution is identical with that shown in Figs. 6 and 7 until $t = 4L/a$ sec. At this time the check valve at the surge tank closes momentarily and then closes finally at $t = 5L/a$ sec. This is due to the saw-tooth nature of the velocity curve for the point B' on the lower water columns as shown in Fig. 7. The graphical solution is then completed as shown. The maximum head rise at the check valves at the pumps is 0.44 H_0 or 97 ft. It is noted that since the maximum separation of the water columns was about 8.7 ft the volume of water supplied by the tank was only 51 cu ft. This could be supplied by a tank of the same dimensions as the pipe with the initial water level in the tank about 10 ft above the assumed minimum level.

Miscellaneous Features

From a study of the water-hammer solutions described in the foregoing, it is seen that the economy gained by the use of the one-way surge tank in pump-discharge lines where water-column separation occurs lies primarily in the fact that the initial water level in the tank does not have to reach the normal pumping hydraulic gradient. Moreover, the required volume of water supplied by the tank to fill the void due to the separation is usually very small. The locations where these tanks can be used most effectively and the optimum height of water in the tank depend somewhat upon the pipeline profile. For example, referring to

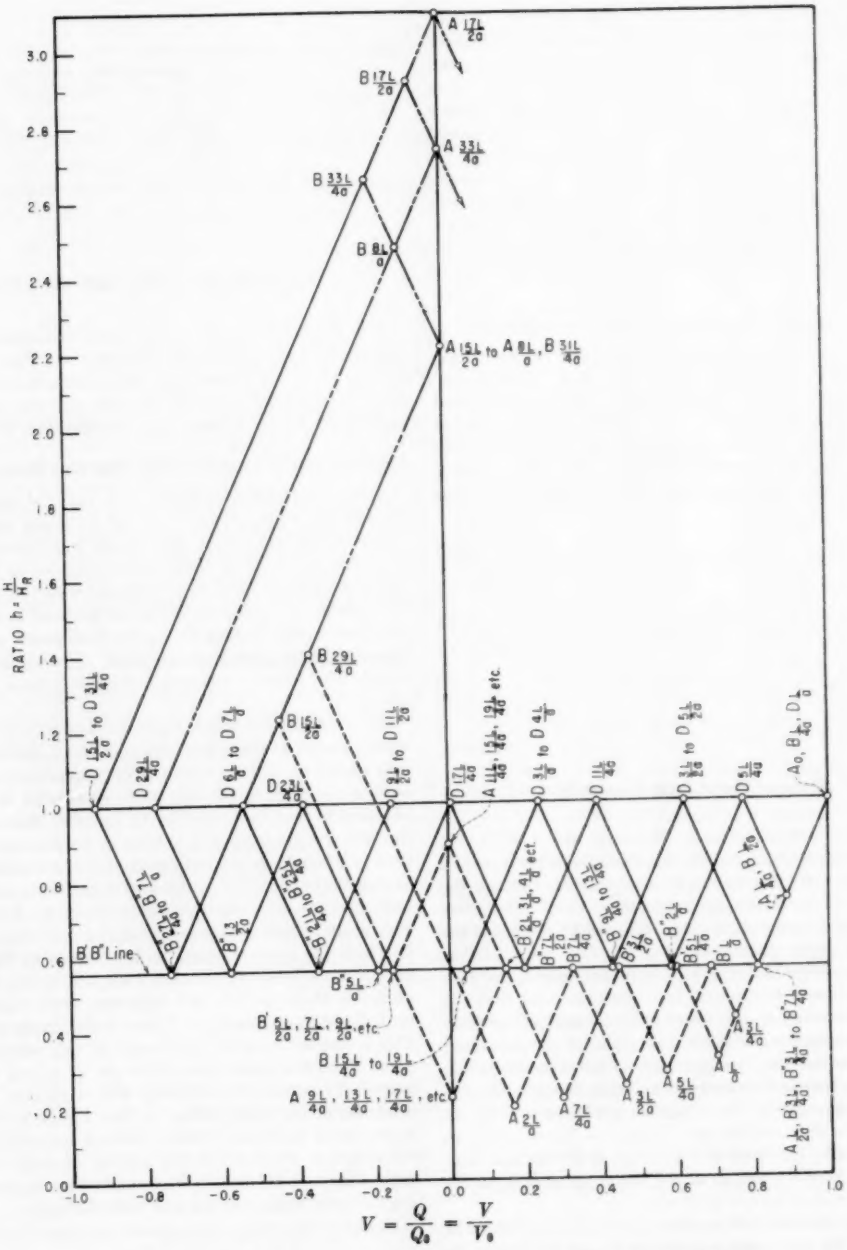

Fig. 6 Graphical water-hammer solution—with water-column separation

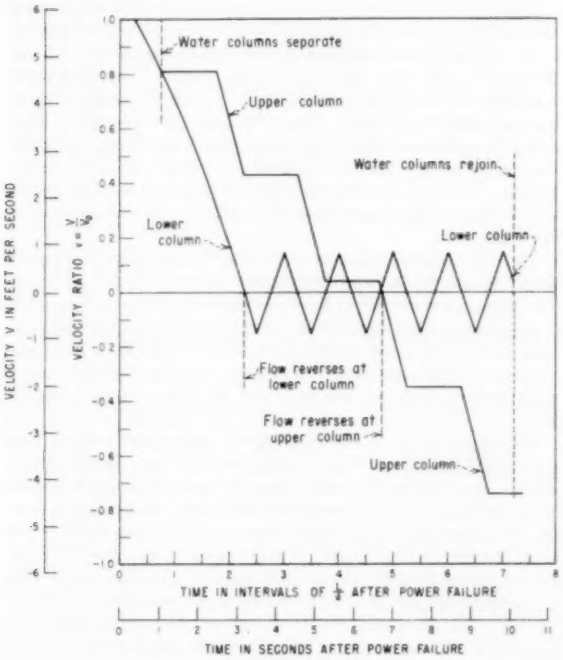

Fig. 7 Movement of water columns

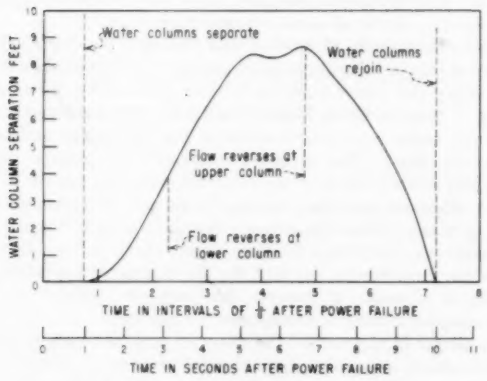

Fig. 8 Water-column separation

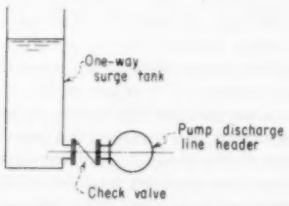

Fig. 9 Basic construction of one-way surge tank

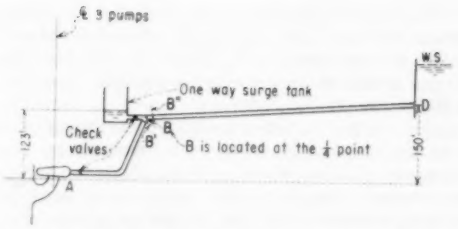

Fig. 10 Pipeline profile—with one-way surge tank

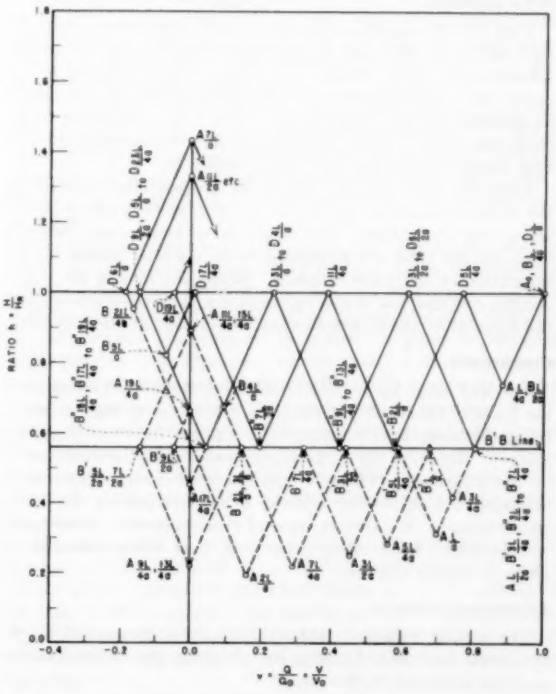

Fig. 11 Graphical water-hammer solution—with one-way surge tank

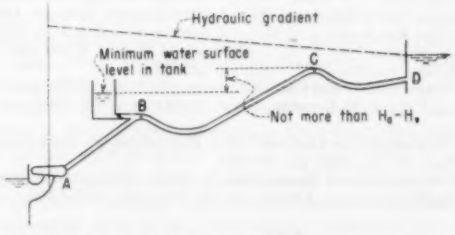

Fig. 12 Pipeline profile—two crests—with one-way surge tank

Fig. 12, the height of water in one tank which would be required to protect the entire line against the effects of water-column separation at both crests B and C should be such that the minimum water level in the tank during the transient is not less than about 30 ft below the high point at C.

The effect of pipeline friction and head losses through the check valve at the tank can be approximated easily in the graphical water-hammer solution whenever these effects are substantial. In the example just given these effects were negligible. A graphical water-hammer solution for this installation also could be performed if the check valves at the pumps were omitted or replaced by other types of control valves whose time cycle was specified.

Field Experience

Each of the one-way surge tanks which have been built and field tested to date has been equipped with a pair of smaller nonslam-type check valves. The tanks were connected to the pump-discharge line adjacent to the location where water-column separation was most likely to occur first. The initial level in the surge tank was established either manually or automatically with float control valves depending on accessibility.

Upon power failure the head in the discharge line adjacent to the surge tank drops rapidly to a value corresponding to the water level in the tank. The check valves at the tank then pop open and the tank starts draining to fill the void formed by the separation of the water columns. When the flow in the upper column reverses, the check valves at the tank close quietly and the harmful effects of water-column separation are thus avoided.

Conclusions

One-way surge tanks offer an effective method for eliminating the harmful effects of water-column separation at high points in pump-discharge lines subsequent to a power failure at the pump motors. Basically, the tank supplies water to fill the void formed by the separation. This prevents the upper water column from attaining a high reverse velocity prior to rejoining the lower water column. For certain types of pipeline profiles, these tanks will be found to be more economical than other conventional pressure-control devices.

Acknowledgments

The author wishes to acknowledge the assistance of C. W. Lundgren and Ben Donsky for checking the water-hammer analyses presented in this paper.

References

1 "Water Hammer in Pipes, Including Those Supplied by Centrifugal Pumps: Graphical Treatment," by R. W. Angus, University of Toronto Press, Bulletin No. 152, 1938.

2 "Du Coup de Bélier en Hydraulique au Coup de Foudre en Electricité," by L. Bergeron, Dunod, Paris, France, 1950, pp. 129–133.

3 "The Break-Away of Water Columns as a Result of Negative Pressure Shocks," by P. de Haller and A. Bedue, *Water and Water Engineering*, vol. 56, June, 1952, pp. 220–224.

4 "Experiments and Calculations on the Resurge Phase of Water Hammer," by J. N. Leconte, Trans. ASME, vol. 59, 1937, pp. 691–694.

5 "Waterhammer Analysis," by J. Parmakian, Prentice-Hall, Inc., New York, N. Y., 1955, pp. 74–100.

6 "Water-Column Separation in Pump-Discharge Lines," by R. T. Richards, Trans. ASME, vol. 78, 1956, pp. 1297–1306.

Discussion

Benjamin Donsky.[3] In his interesting paper, the author has demonstrated that a small one-way tank can be a valuable method of preventing water-column separation.

[3] Engineer, Technical Engineering Analysis Section, Bureau of Reclamation, Denver, Colo.

Although the one-way tank has the valuable feature of being low in height, it does not operate as simply as an ordinary surge tank. Its operation depends on the proper choice and adjustments of a refill float valve and check valve. Therefore some consideration should be given to the size, rate of closure or opening, and possible leakage. The refill float valve should be large enough to refill the tank to the proper level in a reasonable time, thus preparing the tank for the next interruption of power to the pumps. The refill valve should also be adjusted to close gradually so that a large head rise is not produced on each refilling of the tank.

The check valve of the one-way tank should open and supply water quickly to the line after power interruption to the pump. The inertia of the water in the tank-outflow line should be kept to a minimum. Also, because of the initial low water level in the tank, the loss in head on flow from the tank should be kept to a minimum. This ordinarily will require that the tank be located close to the discharge line and that the valve be of adequate size.

The check valve at the tank should close quickly when flow starts back into the one-way tank. A slight delay in the closure of the valve may cause a head rise at the pumps which is greater than that computed for instant valve closure. In the author's example, there was a momentary closure of the check valve at the tank at time interval $4L/a$. The check valve was open again at time interval $17L/4a$ (about 0.349 sec later) and remained open until time interval $5L/a$ when it closed permanently. With this operation of the valve, the head rise at the pumps was 97 ft. Now if we assume a delay of about 0.35 sec or greater in the movement of the valve so that there is no momentary closure at time interval $4L/a$, the computed head rise at the pumps will be 172 ft. This is a special case peculiar to this example and should perhaps be considered as an emergency condition.

This phenomenon of opening and closing of the valve which occurred only once in the author's example occurred about 5 times in a study this writer made on Ventura Avenue No. 1 Pumping Plant of Ventura River Project, Calif. For this discharge line, 2 one-way tanks were used because of the bad profile and large hydraulic head. The repeated openings and closings, which occurred at the tank near the reservoir, were due mainly to the wave reflections from the tank near the pumps. The opening and closing of the valve in the author's example was caused mainly by the reflected waves from the closed pump check valves. In both cases the head rises at the tank due to the repeated opening and closing were small. If, however, this head rise is large, it may be decreased by a dashpot arrangement on the valve.

As shown in the article, the one-way tank not only prevents water-column separation, but also may reduce the head rise at the pumps. With no tank and no water-column separation, the head rise for the author's example was about 198 ft, as compared to 97 ft with the one-way tank. If a plain surge tank had been used in place of the one-way tank, the head rise would have been 128 ft. As a further comparison, a graphical solution with no check valves at the pumps gave head rises at both the pumps and one-way tank of about 37 ft as seen in Fig. 13; and as seen in Fig. 14, there was no intermediate instant of valve closure. In this case, with no pump check valves, the plain surge tank gave 40 ft of head rise at the pumps. With no tank and no water-column separation, the computed head rise is 92 ft. This would seem to indicate that the one-way tank was as effective as the plain surge tank in reducing pressure rises at the pump. However, for some pumping systems the head rises at the pump may be greater when using a one-way tank than when using a simple surge tank. Also, the one-way tank provides no relief when starting the pumps because the check valves at the tank are closed. It is, therefore, necessary to consider the shutoff head of the

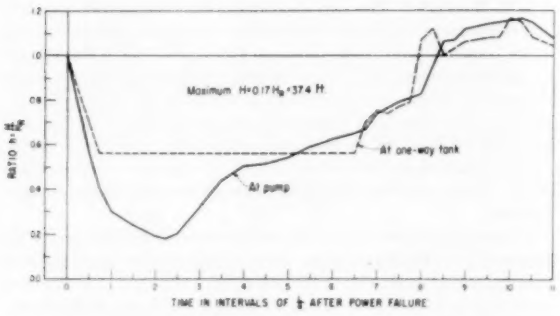

Fig. 13 Hydraulic transient for Fig. 10—with no check valves at pumps

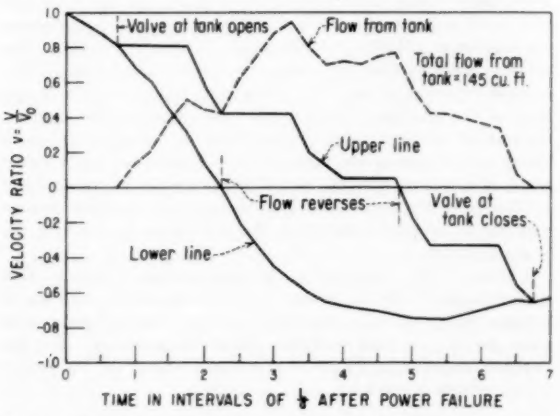

Fig. 14 Flow in pipeline of Fig. 10—with no check valves at pumps

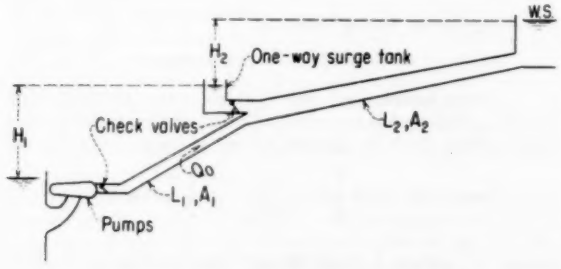

Fig. 15 Pipeline—with one-way surge tank

pumps in the design of the discharge line or start the pumps against slow-opening valves.

Since the main purpose of the one-way tank is to supply water to the discharge line during downsurge, it is necessary that there be an adequate amount of water in the tank. This amount determines the minimum size of the tank, and can be calculated by the following approximate method. Assume a pumping system as shown in Fig. 15, where H_1 and H_2 are differences in head before power failure to the pumps. The starting-up times of the lower and upper pipelines, respectively, are t_1 and t_2 where $t_1 = \frac{L_1 Q_0}{A_1 g H_1}$ and $t_2 = \frac{L_2 Q_0}{A_2 g H_2}$. During time t_1 the flow in the lower line changes from Q_0 to zero, so that the average flow toward the tank is about $Q_0/2$. Also, the average flow away from the tank during t_2 is about $Q_0/2$. Therefore the quantity of flow from the tank during the transient is approximately $Q_0/2\,(t_2 - t_1)$. Because of friction, inertia of the pumps, and a drop in the water-surface elevation of the tank during the transient, this method will give conservative values of tank size. For the author's example, it gives 68 cu ft of tank. For Brewster Flat Pumping Plant of Chief Joseph Dam Project, Washington State, this method gave 150 cu ft versus 140 cu ft from the graphical solution.

E. E. Elliott.[4] A large-scale industrial application of the principles and analyses covered by this paper was put into service late last year at the Tidewater Delaware Refinery. The refinery's cooling-water system handles enough water for a metropolitan area the size of Greater Philadelphia. Its pumping station and distribution headers are protected against water hammer by two large one-way surge tanks.

The Water System. The pumping station lifts some 275,000 gpm of water from the Delaware River and circulates it through the refinery and the adjacent Delaware Power and Light Company steam power plant. The water flows through two parallel piping systems, each designed to supply half of the cooling-water demand.

The station's nine pumps are among the largest ever used for such service. Each is driven by a 2000-hp motor. The pumps are of vertical, centrifugal design—rated at 34,400 gpm each, at a discharge pressure of 80 psig. Four pumps discharge into each header system. The ninth pump, a spare, is piped to discharge into either or both headers. An automatic butterfly valve on each pump discharge operates under hydraulic control to control the discharge and to protect the pump against backflow.

The two main headers are 78-in-diam concrete cylinder pipe at the pumping station. They gradually reduce in size to 16-in-diam at the most distant points of use. The most distant user is the power station, some 7000 ft along the pipeline from the pumping station.

Surge Protection. The author's water-hammer analysis for the over-all system indicated that, without surge tanks, a power failure at the pump motors would cause the water column to separate at several points in the pipeline profile. To forestall such separation and the damage that could be caused by the subsequent rejoining of the column, the surge facilities were designed and installed.

A one-way surge tank guards each header system against water hammer. Fig. 16 shows the completed installation. The two tanks, located next to the pumping station, are 20 ft in diam and 80 ft high, with their tops about 100 ft below the normal hydraulic-gradient line.

The tanks, which were built to API Spec. 12-C, rest on concrete pads supported by piling. As shown diagrammatically in Fig. 17, each tank, when necessary, can discharge into its 78-in-diam header through two 54-in-diam tilting-disk check valves. The tanks can be filled manually through an 8-in-diam line. Any overflow is carried away through a 10-in-diam line inside the tank and drained to a sewer.

Testing the System. Upon completion of the system, in August, 1956, the author and the writer's company conducted a series of water-hammer tests at the river-water pumping station. They simulated power failure at the pumps on each header system, and measured the effectiveness of water-hammer control devices. The test conditions were more severe than those existing during operation of the refinery, when a considerable part of the flow is taken off the line at refinery units close to the pumping station.

[4] Project Engineer, C. F. Braun & Company, Alhambra, Calif.

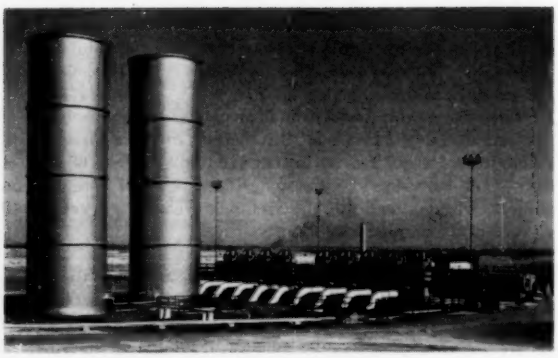

Fig. 16 Photograph of the surge tank installation, with pumping station in the background

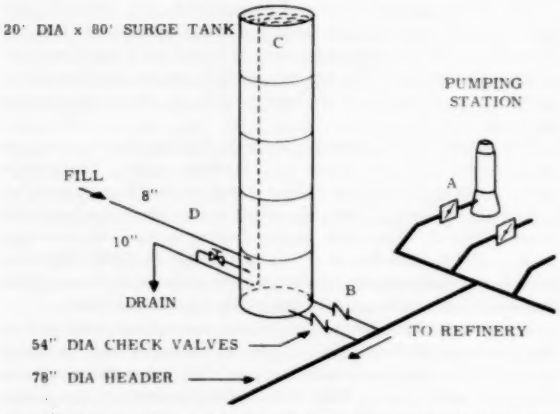

Fig. 17 Line drawing of the surge tank installation, showing how the tanks are connected to the main headers

The hydraulically operated butterfly valves on the pump discharges were adjusted to close 10 to 12 sec after power failure. The surge tanks were filled to a level about 76 ft above the pipeline. One header was tested with three pumps operating at the time of simulated power failure. The other header was tested with four pumps on the line. Oscillographs recorded the pressure changes in the header, next to the pumps, and the change in water level in the surge tank.

When the power was shut off, the pressure in the discharge line dropped rapidly to a value corresponding to the head in the surge tank. At this point the check valves at the surge tank opened and water from the tank began to flow into the header. This effectively prevented water-column separation at all points in the pipeline and the subsequent pressure rise that would have resulted from rejoining of the water columns.

The surge tank continued to drain slowly until the pressure in the header corresponded to the water level in the tank. Then the check valves at the tank closed smoothly.

Under test, the protection facilities operated in a manner that agreed very closely with predictions. For this large pumping station, one-way surge tanks provided an effective and economical solution to the problem of water-column separation.

All of the facilities described were designed and installed by the present discusser's company who engineered and built the refinery and power station.

J. T. Kephart.[5] The one-way surge tank is a simple, reliable, and economical way to eliminate water-column separation and the surge pressure due to rejoinder of water columns. Though air chambers or other devices may be used to eliminate water-column separation or reduce the effect of a rejoinder of water columns, the one-way surge tank stands out as a device which can be used without reliance on mechanical equipment (air compressors, valve actuators, and so forth) or without the direct introduction of air into a pipeline, which is undesirable under some circumstances.

In many locations, it would be desirable to provide freeze-up protection for the check valve and piping between the surge tank and the main pipeline by providing a small bypass line around the check valve and allowing the tank to overflow during cold seasons.

To provide an additional measure of protection with the one-way surge tank, multiple check valves may be used. Maximum check-valve size is developed from the assumption that one check valve fails to close immediately upon flow reversal, and does not close until water flowing from the pipeline into the tank reaches the maximum velocity possible under the head available. The valve is sized so that the pressure surge resulting from instantaneous stoppage of the reverse flow does not exceed the design head of the pipeline. Using check valves sized in this manner, the number of check valves is established by assuming one check valve fails to open when required. The number of check valves required is one more than the number necessary to permit water to flow from the surge tank into the pipeline at a low enough velocity to prevent pressure in the pipeline from reaching the vapor pressure.

Unless energy contained in the pump-motor system is large when compared with the energy in the flowing water, rigid water-column theory yields a sufficiently accurate result of surge pressures for certain water-column-separation problems. For the example depicted in Fig. 5 of this paper, energy in the pump-motor system is given by

$$E_R = 1/2\,\frac{WR^2\omega^2}{g} = 1/2\,\frac{WR^2}{g}\left(\frac{2\pi N}{60}\right)^2 = 609{,}000 \text{ ft-lb}$$

and energy in the flowing water by

$$E_W = 1/2MV^2 = 710{,}000 \text{ ft-lb}$$

For a system having check valves at the pumps and neglecting friction, a formula has been derived based on rigid water-column theory which yields the maximum head at the pump as follows:

$$h_{max} = 2k_2 + 2\rho\left[1 - \frac{k_1(1-k_2)}{k_2(1-k_1)}\right]^{1/2};\ 2\rho \geq 1.0 \ldots [7]$$

with $k_1 = \dfrac{L_1}{L}$, where L_1 is the distance from the pump to the high point and L is the length of pipeline; and $k_2 = \dfrac{H_1}{H_0}$, where H_1 is the elevation difference between the water supply and the high point and H_0 is the elevation difference between the water supply and the free surface at the discharge point.

For either of the cases illustrated in Figs. 4 and 5 of the paper

$$k_1 = 0.25$$

$$k_2 = \frac{123}{220} = 0.56$$

[5] Power Engineer, Engineering Department, E. I. du Pont de Nemours & Company, Wilmington, Del. Mem. ASME.

$$\text{and } h_{max} = 2(0.56) + 2.31\left[1 - \frac{0.25(1 - 0.56)}{0.56(1 - 0.25)}\right]^{1/2}$$

$$h_{max} = 3.10$$

It is evident that this result is identical to the graphical solution obtained in the paper.

Using a similar approach, the solution with the one-way surge tank is given by

$$h_{max} = k_2 + 2(1 - k_2) \text{ for } k_2 \leq 0.667,\ 2\rho \geq 1.0 \quad [8]$$

or

$$h_{max} = 2k_2 \text{ for } k_2 \geq 0.667,\ 2\rho \geq 1.0 \quad [9]$$

which for the example in Figs. 10 and 11 is

$$h_{max} = 0.56 + 2(1 - 0.56)$$

$$h_{max} = 1.44$$

This is in near agreement with the graphical solution in the paper.

The same pipeline without the surge tank was solved by both the graphical method and Equation [7] using L as 1970 ft rather than 3940 ft, resulting in the same value of h_{max} as before using Equation [7] and a value of $h_{max} = 2.28$ using the graphical method. This illustrates the effect of high energy in the pumping system compared with the flowing water.

Analysis of Equation [7] shows the surge pressure due to water-column separation and subsequent rejoinder increases as values of k_2 and 2ρ increase, and as values of k_1 decrease. The case of $k_1 = 0$ is a common one for pumping installations using vertical pumps where the pump discharge is essentially at pump-house-deck elevation, and the deck is located above flood level.

C. E. Withers.[6] The first one-way surge tank designed and built by the Bureau of Reclamation was for a pump-discharge line for one of the pumping plants of the Brewster Irrigation District near the town of Brewster, Wash.

There are three interconnected pumping plants in this system. The first is the River Pumping Plant which consists of four deep-well-type pumps rated at 11.7 cfs each at 190 ft of head. Each pump has a separate discharge line which connects directly to the suction side of the four pumps in the second or Booster Pumping Plant. The pumps in the River Plant are automatically controlled by pressure switches on the suction side of the pumps in the Booster Pumping Plant. The River Pumping Plant discharge lines are 16 in. in diam, approximately 360 ft long, and, due to a very favorable profile, they present no transient hydraulic problems.

The Booster Pumping Plant consists of four centrifugal pumps rated at 11.7 cfs at 350 ft of head. Reverse operation of the pump and motors and draining of the pump-discharge line are prevented by check valves ahead of each pump. Gate valves are installed ahead of each check valve for maintenance purposes. The four pumps are connected to a single 36-in-diam pump-discharge line approximately 7400 ft long. The water from these pumps is discharged into a 500,000-gal storage tank in which are float controls which automatically operate the four pumps in the Booster Pumping Plant.

The third or Relift Plant is located at, and receives water from, the 500,000-gal storage tank. This plant consists of three centrifugal pumps rated at 13 cfs at 150 ft of head. Check valves and gate valves are installed ahead of each pump in the same manner as the Booster Pumping Plant. These three pumps are connected to a single pump-discharge line made up of 5100 ft of 36-in. line and 1500 ft of 18-in. line. The water from these pumps discharges into a 300,000-gal storage tank in which are located the float controls which automatically operate the three pumps in the Relift Pumping Plant. The profile of this discharge line is very favorable and presents no transient hydraulic problems.

The water being pumped is for a sprinkler irrigation system and there will be no winter operation. It is essential to have automatic operation of the pumping plants so that only one operator is required to be on duty at a time. The two storage tanks are in a populated area and precautions have to be taken to prevent overflow of these tanks.

The investigations into the transient hydraulic conditions in the Booster Pumping Plant discharge line disclosed that water-column separation would occur upon power failure and that the pressure rise upon the rejoining of these columns would be so high that to design for this condition would be impractical.

The first remedy considered was the use of butterfly valves which had a variable speed of opening and closing in place of the check valves. This required that for a short interval of time the pumps in the Booster Plant would have to run in reverse, and it would raise the pressure in the suction line where the pressure switch was located which automatically operated the pumps in the River Pumping Plant. This item alone ruled out this type of control.

Consideration was given to increasing the rotating moment of inertia of the pumping unit to control the transient hydraulic conditions; however, this increase proved to be too great to be practical. An attempt to find a more favorable profile failed.

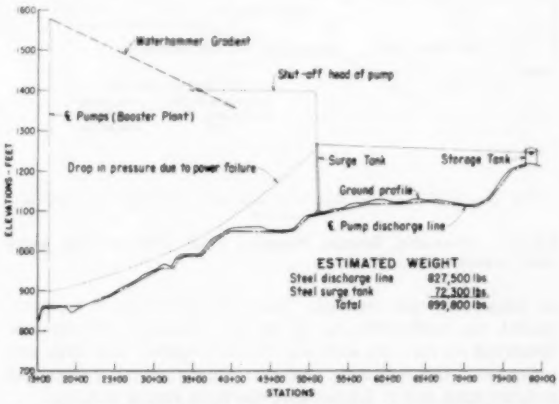

Fig. 18 Schematic, Booster Pumping Plant with surge tank, Brewster Flats, Wash.

The next method investigated was the use of a conventional surge tank, Fig. 18. In order to prevent water-column separation between the surge tank and the pumps, the surge tank was located at Station 51 + 00. This necessitated a tank which, with ample freeboard, would be about 200 ft high. The pressure rise in the pump-discharge line was quite high and required plates as heavy as $^5/_8$ in. thick. Due to the height of the surge tank and the high cost of this installation, this solution was not adopted.

The use of an air chamber was then investigated, Fig. 19. The size and controls of this air chamber were such that the pressure rise in the system was approximately that of the design-shutoff head of the pump, and the drop in pressure in the pump-discharge line upon power failure of the pump motors was not in excess of a half an atmosphere at any point in the discharge line. This produced the most economical arrangement possible, as far as the transient hydraulic conditions in the pump-discharge line were concerned. However, there were other complications. The control system at the air chamber was quite complicated and a small

[6] Engineer, Mechanical Branch, Design Division, Bureau of Reclamation, Denver, Colo.

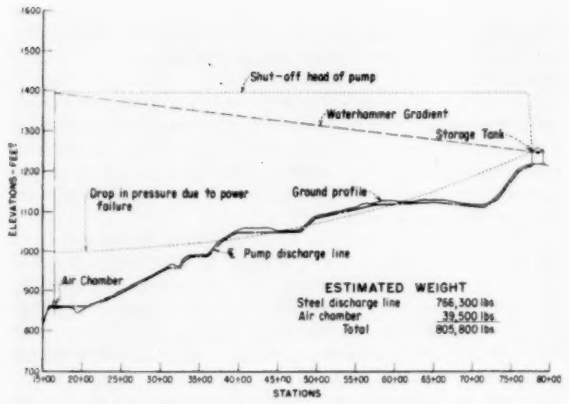

Fig. 19 Schematic, Booster Pumping Plant with air chamber, Brewster Flats, Wash.

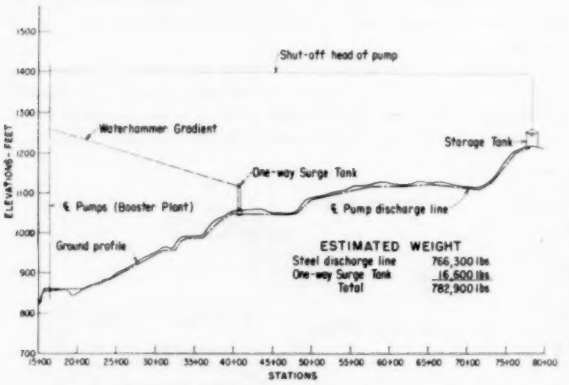

Fig. 20 Schematic, Booster Pumping Plant with one-way surge tank, Brewster Flats, Wash.

air compressor was required. Since this plant was to be unattended, the malfunctioning of the air chamber could produce disastrous results. In addition, the air chamber was large and expensive. Any savings in cost over the surge-tank system was problematical and it did not give the same degree of safety.

One-way surge tanks had previously been used by the author but had never been considered for a Bureau project. This problem was not responding in an agreeable manner to the normal remedies, so that a new approach was indicated. Fig. 20 shows schematically the results of these investigations. The one-way surge tank was located at Station 41 + 00 where good foundation and drainage conditions were present. The pressure rise in the discharge line was less than the design shutoff head of the pump and there was no possibility of water-column separation. A safe, simple, economical method was thus provided to handle the transient hydraulic conditions in the pump-discharge line.

Fig. 21 is a sketch of the one-way surge tank. When the head in the system becomes sufficient, the water flows through the float control valve to fill the one-way surge tank. When the water in the tank reaches the proper elevation, the float closes the valve. This valve closure is controlled by the rate of speed that the water surface is rising in the tank and is so slow that no harmful effects can be produced by this valve closure. An overflow is provided to take care of any leakage in any of the valves. Two 12-in. check valves are provided to allow the water to run from the tank into the pump-discharge line upon power failure of the pump motors.

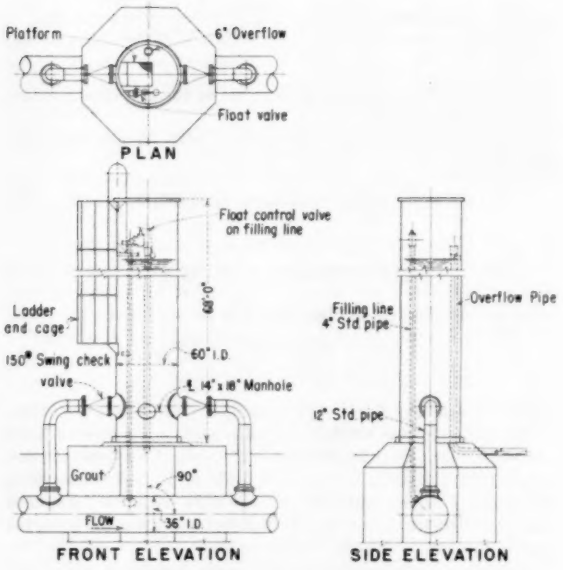

Fig. 21 One-way surge tank

One of these valves could supply sufficient water to protect the discharge line; however, in the interests of safety two were installed. No gate valves were provided ahead of these check valves and none were provided in the filling line ahead of the float valve.

Summarizing the results of these studies shows the following:

(*a*) For the conventional surge-tank system	
Weight of discharge line	827,500 lb
Weight of surge tank	72,300 lb
Total	899,800 lb
Additional equipment required	
none	
(*b*) For the air chamber system	
Weight of discharge line	766,300 lb
Weight of air chamber	39,500 lb
Total	805,800 lb
Additional equipment required	
Air compressor and motor	
Automatic control system	
(*c*) For one-way surge-tank system	
Weight of discharge line	766,300 lb
Weight of one-way surge tank	16,600 lb
Total	782,900 lb
Additional equipment required	
Two check valves	
One float-operated gate valve	

Thus it is quite evident that, in this particular instance, the system developed in the subject paper provided a control over the transient hydraulic conditions in the pump-discharge line that fulfilled all the requirements of economy in installation and maintenance, simplicity in operation, and control and safety to equipment and personnel, should any part of the system fail to function properly.

Author's Closure

The author wishes to thank Messrs. Donsky, Elliott, Kephart, and Withers for their excellent discussions. These have added

materially to the value of the paper. Mr. Donsky's and Mr. Kephart's discussions include some useful concepts in connection with determining the appropriate size of the check valves and filling lines to be used with these tanks. Mr. Donsky's approximate formula for computing the flow out of the tank should be found useful for estimating purposes. Mr. Kephart's analysis of one-way surge tanks, based on the rigid water column theory, is a valuable contribution and should also be found useful for estimating purposes. Mr. Elliott's description of the design and operation of a large pumping plant installation where one-way surge tanks were used should give confidence in the use of this device. Mr. Wither's description of the design of the one-way surge tank for the Brewster Booster Pumping Plant and the savings produced with its use are very informative. A recent field test of this installation also shows satisfactory operation of the one-way surge tank.

Contribution to the Stability Theory of Systems of Surge Tanks

By CHARLES JAEGER,[1] RUGBY, ENGLAND

The paper develops and discusses the theory of stability for two surge tanks in series on the same tunnel. The number of free parameters involved in the analysis is reduced to the point where a general discussion becomes possible. The effect of relative tank locations, diameters, and periods is discussed, and the importance of friction losses on the over-all stability.

Nomenclature

The following nomenclature is used in the paper:

H = gross head
H_0 = head available at downstream surge tank, in steady state
A_T = cross-sectional area of tunnel
L_1, L_2 = tunnel lengths
A_s = horizontal area of cross section of surge tank
A_{Th} = "Thoma" cross-sectional area of surge tank
V = velocity of flow in tunnel
Q_0 = flow required by turbines at full load, in steady state
$\pm FV^2$ = head loss in tunnel, positive when $V > 0$
FV_0^2 = head loss in tunnel at steady state
z = water level in surge tank above reservoir level
x = water level in surge tank above running level
t = time
$T = 2\pi \left(\frac{LA_s}{gA_T}\right)^{1/2}$ = period of mass oscillation neglecting friction
$Z_* = V_0 \left(\frac{LA_T}{gA_s}\right)^{1/2}$ = amplitude of oscillation at sudden stoppage of flow to turbines neglecting friction

Introduction

Some modern hydropower stations incorporate several interconnected surge tanks working in series on the hydraulic-pressure system. For simplicity, the case of two interconnected surge tanks will be considered here. The surges in the tanks are then the result of a complex superposition of basic oscillations (2, 6, 10).[2] Unstable oscillations may occur (1, 2, 3, 5, 8). Such hydraulic systems are becoming more common and it is felt that a detailed surge-stability theory is becoming indispensable.

It was shown in 1943 (1) that the stability theory of a system of surge tanks leads to a differential equation of the fourth order. Later publications (3, 8, 8a) brought some additional information on the complexity of the equation to be solved which contains not less than ten free parameters. Hitherto hydraulic engineers have failed to reduce the equations to a type which can be used for a general discussion and for representation on simple diagrams. The present paper is a contribution to the general theory of stability of systems of surge tanks.

In the case of a single surge tank and a turbine provided with a proper governor, the surge equation can be written, Fig. 1

$$\frac{d^2z}{dt^2} + 2a\frac{dz}{dt} + bz = 0$$

For small oscillations, a and b are shown to be constant. For $a = 0$, the oscillations are sine curves; for $a > 0$, they are damped, and forced for $a < 0$. The condition $a = 0$ is called the stability condition, and when a is being expressed in terms of the parameters Q_0, L, A_T, H, FV_0^2, shown in Fig. 1, it leads to the so-called

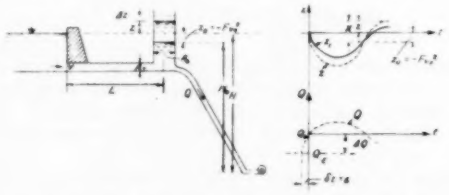

Fig. 1 Diagram showing stability conditions for a single surge tank when governing with constant output $N = \gamma Q(H + Z)$

"Thoma formula." This formula determines the minimum value A_{Th} to be given to the surge-tank area A_s for stable oscillations

$$A_{Th} = \frac{Q_0^2}{2gA_T^2} \frac{LA_T}{FV_0^2(H - FV_0^2)}$$

It is convenient to write

$$A_s = nA_{Th}$$

It has been shown (2) that the general discussion of the stability conditions for a single surge tank is simplified if all the parameters are referred to this variable n. In the case of the equation of the fourth order ruling a double-tank system, the coefficients are far more complicated. However, it can be shown that a similar approach leads to substantial simplification of the formulas and a reduction in the number of free parameters.

Referring to Figs. 2 and 3, the following parameters can be defined

Q_0 = steady discharge through pressure tunnels
L_1, L_2 = tunnel lengths
A_{T1}, A_{T2} = areas of tunnel cross sections
A_1, A_2 = horizontal areas of surge tanks
$F_1V_{10}^2$, $F_2V_{20}^2$ = pressure losses in two tunnels for $Q = Q_0$ (steady flow conditions)
H = gross head

It can be shown that the general stability problem for two interconnected surge tanks depends on these ten free parameters. In addition

---

[1] Consulting Civil Engineer, Water Turbine Department, English Electric Company Limited.

[2] Numbers in parentheses refer to the Bibliography at the end of the paper.

Contributed by the Hydraulic Division and presented at the Annual Meeting, New York, N. Y., December 1–6, 1957, of The American Society of Mechanical Engineers.

Note: Statements and opinions advanced in papers are to be understood as individual expressions of their authors and not those of the Society. Manuscript received at ASME Headquarters, July 26, 1957. Paper No. 57—A-65.

Q = variable discharge through pressure pipeline at time t

$V_1 = Q_1/A_{T1}$, $V_2 = Q_2/A_{T2}$ = velocities in tunnels

Z_1, Z_2 = surges above static level

The suffix 1 refers to the upstream tank and the suffix 2 to the other.

Fig. 2 refers to the case where surge tank 1 is on the upstream side of a reaction turbine and a surge tank 2 is on the downstream side. This case has been dealt with in a series of recent papers (1, 3, 4, 5, 8). The arrangement as shown in Fig. 3 applies to any turbine of the reaction or impulse type. The present paper deals with this second arrangement only.

It has been shown (4, 5) that, in the case of Fig. 2, it is convenient to introduce two parameters—the "Thoma-areas" A_{Th1} for the upstream tank 1, and A_{Th2} for the tank 2.

If (Fig. 2)

$$H_0 = H - F_1V_{10}^2 - F_2V_{20}^2$$

then, supposing each of the tanks to be working alone

$$A_{Th1} = \frac{1}{2g}\left(\frac{Q_0}{A_{T1}}\right)^2 \frac{L_1A_{T1}}{H_0F_1V_{10}^2}$$

and

$$A_{Th2} = \frac{1}{2g}\left(\frac{Q_0}{A_{T2}}\right)^2 \frac{L_2A_{T2}}{H_0F_2V_{20}^2}$$

By referring all quantities to these two basic values, the number of free parameters can be reduced to the two unknown quantities n_1 and n_2, respectively, defined by

$$n_1 = \frac{A_1}{A_{Th1}} \quad \text{and} \quad n_2 = \frac{A_2}{A_{Th2}}$$

and to three free parameters, the ratio of the periods of surge tanks and the losses in the tunnels L_1 and L_2 (5). A general discussion of the problem is then possible, the results of which can be summarized readily in a single diagram, Fig. 4.

The object of the present paper is to show that the same general method of approach can be used for the discussion of the case represented in Fig. 3.

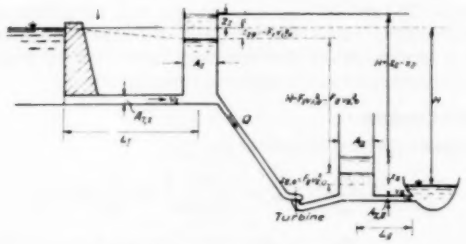

Fig. 2 Stability conditions for case 1

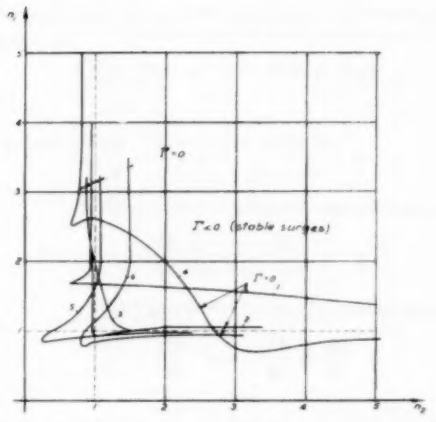

Curves 1 and 2: $\bar{m}^* = 0.2$, $F_{r1}' = F_{r2}' = 0.1$ and 0.3
Curves 3 and 4: $\bar{m}^* = 1$, $F_{r1}' = F_{r2}' = 0.1$ and 0.3
Curves 5 and 6: $\bar{m}^* = 5$, $F_{r1}' = F_{r2}' = 0.1$ and 0.3

Fig. 4 Diagram showing limits for stable governing ($\Gamma \leq 0$) for case 1 for varying values of $\bar{m}^*$, F_{r1}', and F_{r2}'

General Equations

The continuity equations for the case represented in Fig. 3 are

$$A_{T1}V_1 = A_1\frac{dZ_1}{dt} + A_{T2}V_2 \quad \ldots\ldots [1]$$

$$A_{T2}V_2 = A_2\frac{dZ_2}{dt} + Q \quad \ldots\ldots [2]$$

The corresponding two dynamic equations are

$$\frac{L_1}{g}\frac{dV_1}{dt} + Z_1 + F_1V_1^2 = 0 \quad \ldots\ldots [3]$$

$$\frac{L_2}{g}\frac{dV_2}{dt} + Z_2 - Z_1 + F_2V_2^2 = 0 \quad \ldots\ldots [4]$$

The net head is

$$H_0 = H - F_1V_{10}^2 - F_2V_{20}^2$$

Referring to Fig. 3, we can write

$$X_1 = Z_1 + F_1V_{10}^2$$

$$X_2 = Z_2 + F_1V_{10}^2 + F_2V_{20}^2$$

$$X_2 - X_1 = Z_2 - Z_1 + F_2V_{20}^2$$

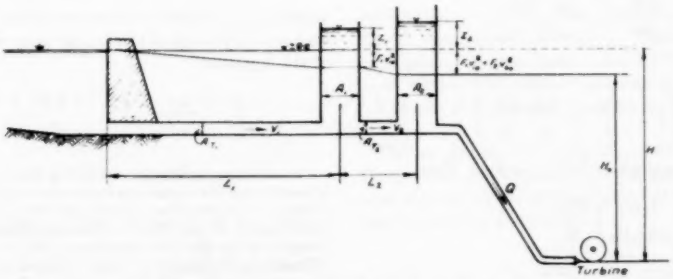

Fig. 3 Stability conditions for case 2

When governing at constant output, the governing equation can be written (for constant turbine efficiency)

$$Q_0 H_0 = Q(H + Z_2) = Q(H_0 + X_2)$$

and

$$Q = \frac{Q_0 H_0}{H_0 + X_2} \simeq Q_0 \left(1 - \frac{X_2}{H_0}\right)$$

for small oscillations. This last equation gives also

$$\frac{dQ}{dt} = -\frac{Q_0}{H_0} \frac{dX_2}{dt}$$

From Equations [1] and [2], observing that

$$\frac{dZ_1}{dt} = \frac{dX_1}{dt} \quad \text{and} \quad \frac{dZ_2}{dt} = \frac{dX_2}{dt}$$

we get

$$V_1 = \frac{A_1}{A_{T1}} \frac{dX_1}{dt} + \frac{A_2}{A_{T1}} \frac{dX_2}{dt} + \frac{Q_0}{A_{T1}} \left(1 - \frac{X_2}{H_0}\right)$$

$$\frac{dV_1}{dt} = \frac{A_1}{A_{T1}} \frac{d^2X_1}{dt^2} + \frac{A_2}{A_{T1}} \frac{d^2X_2}{dt^2} - \frac{Q_0}{A_{T1}H_0} \frac{dX_2}{dt}$$

The losses in the tunnel can be calculated as

$$F_1 V_1^2 = F_1 \left[\frac{A_1}{A_{T1}} \frac{dX_1}{dt} + \frac{A_2}{A_{T1}} \frac{dX_2}{dt} + \frac{Q_0}{A_{T1}} \left(1 - \frac{X_2}{H_0}\right)\right]^2$$

$$= \frac{F_1 Q_0^2}{A_{T1}^2} \left[1 - \frac{X_2}{H_0} + \frac{A_1}{Q_0} \frac{dX_1}{dt} + \frac{A_2}{Q_0} \frac{dX_2}{dt}\right]^2$$

Assuming again small oscillations, and writing

$$\frac{F_1 Q_0^2}{A_{T1}^2} = F_1 V_{10}^2 = F_{10}$$

we get

$$F_1 V_1^2 \simeq F_{10} \left[1 - \frac{2X_2}{H_0} + \frac{2A_1}{Q_0} \frac{dX_1}{dt} + \frac{2A_2}{Q_0} \frac{dX_2}{dt}\right]$$

Introducing these values of $(dV_1)/(dt)$ and $F_1 V_1^2$, Equation [3] yields

$$\frac{L_1}{g} \frac{A_1}{A_{T1}} \frac{d^2X_1}{dt^2} + \frac{2F_{10}A_1}{Q_0} \frac{dX_1}{dt} + X_1 = -\frac{L_1 A_2}{gA_{T1}} \frac{d^2X_2}{dt^2}$$

$$- \left(\frac{2F_{10}A_2}{Q_0} - \frac{L_1 Q_0}{gA_{T1}H_0}\right) \frac{dX_2}{dt} + \frac{2F_{10}}{H_0} X_2 \ldots\ldots [3a]$$

Equation [4] can be dealt with on similar lines, when

$$V_2 = \frac{A_2}{A_{T2}} \frac{dX_2}{dt} + \frac{Q_0}{A_{T2}} \left(1 - \frac{X_2}{H_0}\right)$$

$$\frac{dV_2}{dt} = \frac{A_2}{A_{T2}} \frac{d^2X_2}{dt^2} - \frac{Q_0}{A_{T2}H_0} \frac{dX_2}{dt}$$

and

$$F_2 V_2^2 \simeq F_{20} \left[1 - \frac{2X_2}{H_0} + \frac{2A_2}{Q_0} \frac{dX_2}{dt}\right]$$

for small oscillations only, and when $F_2 V_{20}^2 = F_{20}$. Then

$$\frac{L_2}{g} \frac{A_2}{A_{T2}} \frac{d^2X_2}{dt^2} + \left(\frac{2F_{20}A_2}{Q_0} - \frac{L_2 Q_0}{gA_{T2}H_0}\right) \frac{dX_2}{dt}$$

$$+ X_2 - \frac{2F_{20}}{H_0} X_2 = X_1 \ldots\ldots [4a]$$

Introduction of "Relative Values"

Let now the relative values of Calame and Gaden (11) be introduced. If x_1, x_2, F_{r1}, h_{10}, F_{r2}, h_{20} are relative values, we obtain the well-known relations (5)

$$Z_{*1} = Q_0 \left(\frac{L_1}{gA_{T1}A_1}\right)^{1/2}; \quad Z_{*2} = Q_0 \left(\frac{L_2}{gA_{T2}A_2}\right)^{1/2}$$

$$T_1 = 2\pi \left(\frac{L_1 A_1}{gA_{T1}}\right)^{1/2} = \frac{2\pi Z_{*1} A_1}{Q_0}; \quad T_2 = \frac{2\pi Z_{*2} A_2}{Q_0}$$

$$X_1 = x_1 Z_{*1}, \quad X_2 = x_2 Z_{*2}, \quad h_{10} = \frac{H_0}{Z_{*1}}$$

$$h_{20} = \frac{H_0}{Z_{*2}}, \quad F_{r1} = \frac{F_{10}}{Z_{*1}}, \quad F_{r2} = \frac{F_{20}}{Z_{*2}}$$

Equation [3a] then becomes

$$\frac{d^2x_1}{dt^2} + \frac{2\pi}{T_1} 2F_{r1} \frac{dx_1}{dt} + \frac{4\pi^2}{T_1^2} x_1 = -m^* \frac{d^2x_2}{dt^2}$$

$$- \frac{2\pi}{T_1} \left(2F_{r1}m^* - \frac{1}{h_{20}}\right) \frac{dx_2}{dt} + \frac{4\pi^2}{T_1^2} \frac{2F_{r1}}{h_{20}} x_2 \ldots\ldots [3b]$$

where

$$m^* = \frac{T_2}{T_1} = \left(\frac{L_2 A_2 A_{T1}}{L_1 A_1 A_{T2}}\right)^{1/2}$$

is the ratio of the periods of the two surge tanks, supposing they were alone. Similarly, Equation [4a] can be transformed and becomes

$$\frac{d^2x_2}{dt^2} + \frac{2\pi}{T_2} \left(2F_{r2} - \frac{1}{h_{20}}\right) \frac{dx_2}{dt} + \frac{4\pi^2}{T_2^2} \left(1 - \frac{2F_{r2}}{h_{20}}\right) x_2$$

$$= \frac{4\pi^2}{T_2^2} \frac{Z_{*1}}{Z_{*2}} x_1 = \frac{4\pi^2}{T_2^2} \frac{1}{m} x_1 \ldots\ldots [4b]$$

where

$$m = \frac{Z_{*2}}{Z_{*1}} = \left(\frac{L_2 A_1 A_{T1}}{L_1 A_2 A_{T2}}\right)^{1/2}$$

Equations [3b] and [4b] can be compared with the similar equations obtained for case 1 (Fig. 1) (3, 5).[3] The perfect symmetry of case 1 is no more observed in this case 2 and it is to be expected that the calculations will be somewhat more laborious.

Stability Conditions

Equations [3b] and [4b] are of the type

$$\frac{d^2x_1}{dt^2} + a_1 \frac{dx_1}{dt} + b_1 x_1 = A_1 \frac{d^2x_2}{dt^2} + B_1 \frac{dx_2}{dt} + C_1 x_2$$

$$\frac{d^2x_2}{dt^2} + a_2 \frac{dx_2}{dt} + b_2 x_2 = C_2 x_1$$

which are well-known equations ruling stability problems. They lead to an equation of the fourth order which is linked to the roots of the equation

$$\begin{vmatrix} p^2 + a_1 p + b_1 & -(A_1 p^2 + B_1 p + C_1) \\ -C_2 & p^2 + a_2 p + b_2 \end{vmatrix} = 0$$

[3] Another approach for obtaining Equations [3b] and [4b] would be to start from the equations in relative values, as given by Calame and Gaden. This was the method used by L. Escande and R. Houron in their paper of *La Houille Blanche*, October, 1953. The quickest method is to use the equations [88] to [99], p. 48 of A. Gardel, "Chambres d'Equilibre," and to adapt these equations to the case of two surge tanks. All three methods finally yield Equations [3b] and [4b].

or

$$(p^2 + a_1p + b_1)(p^2 + a_2p + b_2) - (-C_2)(-A_1p^2 - B_1p - C_1) = 0$$

which can be put into the form

$$p^4 + \alpha_1p^3 + \alpha_2p^2 + \alpha_3p + \alpha_4 = 0 \quad \ldots\ldots\ldots [5]$$

where

$$\left.\begin{aligned} \alpha_1 &= a_1 + a_2 \\ \alpha_2 &= b_1 + a_1a_2 + b_2 - A_1C_2 \\ \alpha_3 &= a_1b_2 + a_2b_1 - B_1C_2 \\ \alpha_4 &= b_1b_2 - C_1C_2 \end{aligned}\right\} \quad \ldots\ldots\ldots [6]$$

Equation [5] represents stable oscillations when

$$\alpha_1 > 0, \quad \alpha_2 > 0, \quad \alpha_3 > 0, \quad \alpha_4 > 0$$

and

$$\Gamma = \alpha_3^2 - \alpha_1(\alpha_2\alpha_3 - \alpha_1\alpha_4) < 0 \quad \ldots\ldots\ldots [7]$$

The problem consists now in calculating $\alpha_1, \alpha_2, \alpha_3, \alpha_4$, and Γ and discussing the Equations [7].

Equations [3*b*] and [4*b*] still contain eight apparent parameters: F_{r1}, F_{r2}, h_{10}, h_{20}, T_1, T_2, m^*, and m. These parameters all implicitly depend on Z_{*1}, Z_{*2}, A_1, A_2, and Q. A general discussion is not likely to be successful unless new parameters are introduced. These will be the same as those used for the discussion of case 1 (2, 4, 5).

Accordingly, the fundamental values

$$A_{Th1} = \frac{1}{2g}\left(\frac{Q_0}{A_{T1}}\right)^2 \frac{L_1A_{T1}}{F_{10}H_0} \quad \text{and} \quad A_{Th2} = \frac{1}{2g}\left(\frac{Q_0}{A_{T2}}\right)^2 \frac{L_2A_{T2}}{F_{20}H_0}$$

are introduced. These are the Thoma areas for the surge tanks 1 and 2, Fig. 3, supposed to work alone, each of them characterized by the parameters L_1, A_{T1}, F_{10}, H_0, and Q_0 for the upstream tank and L_2, A_{T2}, F_{20}, H_0, and Q_0 for the downstream tank.

The true areas of the surge tanks are then

$$A_1 = n_1A_{Th1} \text{ and } A_2 = n_2A_{Th2}$$

n_1 and n_2 are the main variables to be used for further discussion.

Let all the parameters be now defined as functions of

$$Z_{*1}' = Q_0\left(\frac{L_1}{gA_{Th1}A_{T1}}\right)^{1/2} = \sqrt{(n_1)}Z_{*1}$$

and

$$Z_{*2}' = Q_0\left(\frac{L_2}{gA_{Th2}A_{T2}}\right)^{1/2} = \sqrt{(n_2)}Z_{*2}$$

so that

$$h_{10}' = \frac{H_0}{Z_{*1}'} \quad \text{and} \quad h_{10} = \sqrt{(n_1)}h_{10}'$$

$$h_{20}' = \frac{H_0}{Z_{*2}'} \quad \text{and} \quad h_{20} = \sqrt{(n_2)}h_{20}'$$

$$F_{r1}' = \frac{F_{10}}{Z_{*1}'} \quad \text{and} \quad F_{r1} = \sqrt{(n_1)}F_{r1}'$$

$$F_{r2}' = \frac{F_{20}}{Z_{*2}'} \quad \text{and} \quad F_{r2} = \sqrt{(n_2)}F_{r2}'$$

It can be shown that, because of the definition of the Thoma areas F_{Th1} and F_{Th2}

$$\frac{1}{h_{10}'} = 2F_{r1}' \quad \text{and} \quad \frac{1}{h_{20}'} = 2F_{r2}'$$

This remark brings substantial simplifications of the equations. In addition, let

$$T_1' = 2\pi\left(\frac{L_1A_{Th1}}{gA_{T1}}\right)^{1/2} \quad \text{and} \quad T_2' = 2\pi\left(\frac{L_2A_{Th2}}{gA_{T2}}\right)^{1/2}$$

the periods of the two Thoma surge tanks, and

$$m^* = \frac{T_2}{T_1} = \left(\frac{L_2A_2A_{T1}}{L_1A_1A_{T2}}\right)^{1/2}$$

$$\overline{m}^* = \frac{T_2'}{T_1'} = \left(\frac{L_2A_{Th2}A_{T1}}{L_1A_{Th1}A_{T2}}\right)^{1/2} = m^*\sqrt{\frac{n_1}{n_2}}$$

$$m = \frac{Z_{*2}}{Z_{*1}} = \overline{m}^*\left(\frac{n_1}{n_2}\right)^{1/2}\frac{1}{\lambda'} = m^*\frac{n_1}{n_2}\frac{1}{\lambda'}$$

where

$$\lambda' = \frac{A_{Th2}}{A_{Th1}}$$

With these new parameters, α_1, α_2, α_3, and α_4 now become

$$\alpha_1 = \frac{2\pi}{T_2}\left[\sqrt{n_2}(2F_{r1}'\overline{m}^* + 2F_{r2}') - \frac{2F_{r2}'}{\sqrt{n_2}}\right]$$

$$\alpha_2 = \frac{4\pi^2}{T_2^2}\left[1 + \frac{n_2}{n_1}(\overline{m}^{*2} + \lambda') - (2F_{r2}')^2 - \overline{m}^*(2F_{r1}')(2F_{r2}')(1 - n_2)\right]$$

$$\alpha_3 = \frac{8\pi^3}{T_2^3}\left[\overline{m}^{*2}\frac{n_2}{n_1}\left(\sqrt{n_2} - \frac{1}{\sqrt{n_2}}\right)2F_{r2}' + \overline{m}^*\sqrt{n_2}2F_{r1}'(1 - [2F_{r2}']^2) + \frac{n_2}{n_1}\lambda'\left(2F_{r1}'\overline{m}^*\sqrt{n_2} - \frac{2F_{r2}'}{\sqrt{n_2}}\right)\right]$$

$$\alpha_4 = \frac{16\pi^4}{T_2^4}\frac{n_2}{n_1}\left[\overline{m}^{*2}\left\{1 - (2F_{r2}')^2\right\} - \overline{m}^*(2F_{r1}')(2F_{r2}')\lambda'\right] \quad [8]$$

Furthermore

$$\Gamma = \alpha_3^2 - \alpha_1(\alpha_2\alpha_3 - \alpha_1\alpha_4)$$

Discussion of Stability Conditions

All the terms of $\Gamma = 0$ contain the factor $64\pi^6/T_2^6$ which is always positive and therefore can be ignored. The coefficients α_1, α_2, α_3, and α_4, and the function Γ depend now only on n_1 and n_2 which we choose as independent variables for the discussion and on the free parameters $\overline{m}^*$, F_{r1}', F_{r2}', and λ'. These all depend on A_{Th1} and A_{Th2} (and not on A_1 or A_2) and can all be calculated beforehand, thus making a general discussion possible.

Similarly, when discussing case 1, it was found that the problem depends only on n_1, n_2 and on $\overline{m}^*$, F_{r1}', and F_{r2}'. It is well worth while to show here Fig. 4 on which some characteristic curves $\Gamma = 0$ have been drawn for case 1. They clearly show when and in what proportion the basic values of Thoma A_{Th1} and A_{Th2} have to be increased if stable regulation is required (4, 5).

The aim of this discussion is to establish similar curves for case 2.

The parameter $\lambda' = A_{Th2}/A_{Th1}$ has first to be dealt with. The Thoma area A_{Th} depends only on the tunnel diameter D, on the head H_0, and on the friction factor of Manning. It is well known that A_{Th} can be written (2)

$$A_{Th} = \frac{CD^{\frac{10}{3}}}{k_s^2H_0}$$

where

k_s = Manning friction factor
C = const

A_{Th} does not depend on the tunnel length L nor on the discharge Q_0. If the two tunnels L_1 and L_2 have the same diameter D and the same friction factor k_s, which is likely to be the case, then $\lambda' = 1$ and $A_{Th1} \doteq A_{Th2} \doteq A_{Th}$.

All numerical calculations will be done for $\lambda' = 1$, so that the number of free parameters for case 2 is now reduced to five, as it was for case 1.

The parameters α_1, α_2, α_3, and α_4 and the function Γ have been calculated for three typical sets of parameters.

(1) $\overline{m}^* = 0.3$, $F_{r1}' = 0.3$, $F_{r2}' = 0.1$
(2) $\overline{m}^* = 1$, $F_{r1}' = F_{r2}' = 0.2$
(3) $\overline{m}^* = 3$, $F_{r1}' = 0.03$, $F_{r2}' = 0.3$

The first case corresponds to a system where $L_1/L_2 \doteq 11$, the two surge tanks being near the end of the long tunnel L_1. The second case corresponds to $L_1 \doteq L_2$, the upstream surge tank being located about half way down the pressure tunnel. The third case corresponds to the upstream tank near the reservoir.

The curves $\alpha_1 = 0$, $\alpha_3 = 0$, and $\Gamma = 0$, the only curves of interest for the discussion, are represented in Fig. 5 for both cases 1 and 2.

The curves show that for values $n_2 < 1$ the factor n_1 lies between two curves, representing the two roots of equation $\Gamma = 0$ for varying values of n_2. They also show that for $n_2 < 1$, the sum $n_1 + n_2 > 1$. Nothing can be gained by reducing the area of surge tank 2 below the value of Thoma. In exceptional cases, the limiting value of n is given by the condition $\alpha_3 > 0$, the curve $\alpha_3 = 0$ cutting the curve $\Gamma = 0$.

It is of great interest to notice the position of the points B_1, B_2 . . . in Fig. 5. These points correspond to the condition $\alpha_1 = 0$ or

$$n_2 = \frac{F_{r2}'}{\overline{m}^* F_{r1}' + F_{r2}'} \quad \ldots\ldots\ldots\ldots\ldots\ldots [9]$$

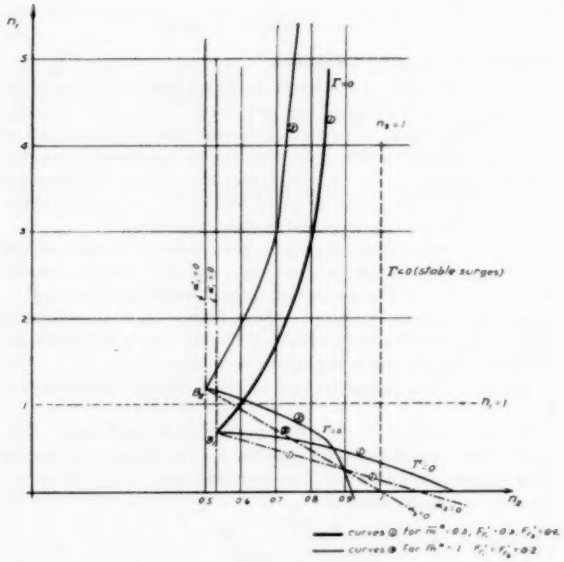

Fig. 5 Diagram showing the limits for stable surges ($\Gamma \leq 0$) for case 2 for varying values of $\overline{m}^*$, F_{r1}', and F_{r2}'

The additional condition $\alpha_2 = 0$ or

$$\frac{n_2}{n_1}(\overline{m}^{*2}\, 2F_{r2}' + \lambda'\overline{m}^* 2F_{r1}) - \frac{2F_{r2}'}{n_1}(\overline{m}^{*2} + \lambda') + \overline{m}^* 2F_{r1}'[1 - (2F_{r2}')^2] = 0 \quad \ldots\ldots [10]$$

yields the value n_1 for which $\Gamma = 0$. Point B therefore corresponds to the simultaneous conditions $\alpha_1 = 0$, $\alpha_2 = 0$, and $\Gamma = \alpha_2^2 = 0$ which obviously is a double root.

The shape of the curves $\alpha_2 = 0$ and $\Gamma = 0$ obviously depends on the position of point B. To illustrate this analysis, the following cases have been calculated ($\lambda' = 1$)

(1) $\overline{m}^* = 0.3$, $F_{r1}' = 0.3$, $F_{r2}' = 0.1$, $n_2 = 0.526$, $n_1 = 0.66$

(1a) $\overline{m}^* = 0.3$, $F_{r1}' = 0.3$, $F_{r2}' = 0.03$, $n_2 = 0.25$, $n_1 = 0.106$

(2) $\overline{m}^* = 1$, $F_{r1}' = 0.2$, $F_{r2}' = 0.2$, $n_2 = 0.5$, $n_1 = 1.19$

(3) $\overline{m}^* = 3$, $F_{r1}' = 0.03$, $F_{r2}' = 0.3$, $n_2 = 0.77$, $n_1 = 14.9$

Fig. 6 shows how point B moves on the diagram (n_1, n_2) when m^*, F_{r1}', and F_{r2}' vary. Even a small variation of the friction losses F_{r2}' from 0.1 to 0.03 causes the point B to move from B_1 to B_{1a}.

The value $\overline{m}^* = 3$ corresponds to a short tunnel L_1 and to a system where the upstream surge tank is near the reservoir ($L_1/L_2 \doteq 0.09$). Point B_3 ($n_2 = 0.77$ and $n_1 = 14.9$) falls outside the diagram Fig. 5 and is shown only in Fig. 6. Further numerical analysis shows that for $n_2 = 1$, n_1 must be larger than 12 ($n_1 > 12$). The dimensions of the upstream tank must be fairly large. [This curve (3) could not be drawn in Fig. 5.] When $\overline{m}^*$ is > 1 or 2, the numerical value of Γ depends mainly on $\alpha_4 = C(n_2/n_1)$ (where C = const). In this particular case, the ratio of n_2/n_1 is of major importance.

This short analysis shows there is, in most cases, little or nothing to be gained by choosing a narrow downstream tank ($n_2 < 1$). For practical reasons, the surge tanks nearest to the pressure pipe should be equal to or larger than A_{Th}. For a wide range of values stability nevertheless can be achieved when $n_2 < 1$ provided n_1 has the required minimum value for Γ to be negative ($\Gamma < 0$); in most cases this requires a greater volume for the upstream tank

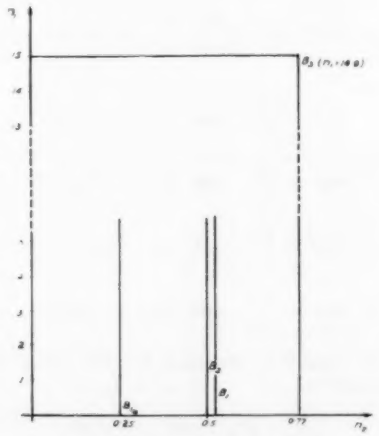

Fig. 6 Position of point B for varying values of $\overline{m}^*$, F_{r1}', F_{r2}'

which more than counterbalances the economy in the downstream shaft.

Case (1*a*) with $\bar{m}^* = 0.3$, $F_{r1}' = 0.3$, $F_{r2}' = 0.03$ is a possible exception to this general remark.

For many years, designers who used shafts for introducing secondary water streams into the main pressure stream adhered to the rule of thumb that the shaft nearest to the pressure pipeline was the real surge tank and had to be designed according to the old formula of Thoma. The present analysis shows that this is a correct approach.

Another type of tank comes into this category—the Innertkirchen type of tank which has been repeated for many other power systems (e.g., the surge tanks of the three power stations of the Maggia Development). These are systems of tanks where L_2/L_1 is very small. They all have been designed with $n_2 > 1$.

For large values of $\bar{m}^*$, the stability conditions, as shown by the analysis of the function $\Gamma = 0$, change considerably. The example calculated here, with $\bar{m}^* = 3$ and $L_1/L_2 \simeq 1/11$, shows that the area of the upstream surge tank 1 must be quite considerable, as compared with F_{Th1} even if $n_2 \geqslant 1$, if stability is to be achieved.

A problem of this type may occur when a sand eliminator, designed as a tank with free surface, is to be built inside the pressure tunnel near the intake.

According to Gardel (9), who studied surge-tank systems with small upstream reservoirs, stability of oscillations could be achieved when the reservoir is provided with an overflow. In some cases, this could be a way out of the difficulty when designing a system where the ratio L_1/L_2 is small ($L_1/L_2 < 1/5$).

An alternative solution is to keep everything under pressure, including the sand eliminator. This is the solution used at Wassen power station in Switzerland.

It is not recommended that a secondary water stream be introduced into the main pressure tunnel by using a vertical shaft if the shaft is located near the intake. In such a case the correct solution would be to divert the water towards the reservoir, eliminating the dangerous shaft.

The values n_1 and n_2 given by diagram Fig. 5 correspond to the limit of stability ($\Gamma = 0$). For the oscillations to be damped ($\Gamma < 0$), values larger than the one calculated here have to be chosen.

A detailed theory of the damping of surges has been developed for case 1 (2, 5, 7). There is no need to repeat it here.

The practical importance of the theory developed in paper (5) and in this contribution can be stressed now. Some examples of multiple surge tanks according to case 2 have been mentioned. Case 1 is of greater importance, especially for underground power stations. The Kiewa surge tank and the Chute des Passes surge tank have been mentioned in paper (5). But there are many other tank systems of the same type, of very large dimensions, now under construction or consideration, to which the theory applies.

The results of this general investigation have been summarized in Figs. 4, 5, and 6. They show that the whole problem depends mainly on the ratios of the tank periods m^* or $\bar{m}^*$, the importance of which was stressed in the 1943 paper and now appears to be the key of both problems (case 1 and case 2). The importance of the friction losses, expressed in relative values (F_{r1}' and F_{r2}') had been somewhat overlooked in previous researches. The friction losses are more critical than were expected and cause the curves $\Gamma = 0$ to vary considerably over the (n_1, n_2) diagrams, Figs. 4 and 5. To have these ratios F_{r1}' and F_{r2}' included in the present analysis considerably adds to the interest of the results.

To complete the over-all picture, the results obtained by Zienkiewicz on "parallel-branch" and "differential" surge tanks should be mentioned here.

The cautious approach to these problems shown in the past by many designers is justified by this more detailed analysis.

Bibliography

1 "De la Stabilité des Chambres d'Equilibre et des Systèmes de Chambres d'Equilibre," by Charles Jaeger, *Schweizerische Bauzeitung*, vol. 122, nos. 21, 24, 25, 26, November/December, 1943.

2 "Engineering Fluid Mechanics," by Charles Jaeger, Blackie & Son, Glasgow, Scotland, 1956, and New York, N. Y., 1957.

3 "Stability of Two Surge Tanks Built Respectively on the Head-Race and Tail-Race Tunnels," by L. Escande and R. Houron, *La Houille Blanche*, October, 1953, pp. 647–654, and *Water Power*, vol. 5, no. 9, 1953, p. 338.

4 "Sur la Stabilité des Systèmes de Chambres d'Equilibre.', by Charles Jaeger, *Comptes Rendus Académie des Sciences*, Tome 244, no. 5, January 28, 1957, pp. 562–564.

5 "The Double Surge Tank System. General Discussion of the Stability Problem," by Charles Jaeger, *Water Power*, vol. 9, no. 7/8, July, 1957, pp. 253–258; August, 1957, pp. 301–305.

6 "L'Agrandissement des Usines Hydro-Électriques," by Charles Jaeger, *La Technique Moderne*, vol. 30, no. 2, January 15, 1938, pp. 33–38.

7 "Present Trends in Surge Design," by Charles Jaeger, *Proceedings of The Institution of Mechanical Engineers*, vol. 168, no. 2, 1954, pp. 91–124.

8 "Conditions Analogous to Those of Thoma in the Case of a Hydro-Electric Installation Having One Surge Tank Above the Turbines and Another Below Them," by R. Meyer, *La Houille Blanche*, October, 1955, pp. 640–646.

8a "Some Remarks" by R. Meyer, concerning the article "Present Trends in Surge Tank Design," *Proceedings of The Institution of Mechanical Engineers*, vol. 168, no. 2, 1954; see also *La Houille Blanche*, No. 4, 1952.

9 "Chambres d'Equilibre," by A. Gardel, Rouge, Lausanne, Switzerland, 1956.

10 "Alcune considerazioni sulle oscillazioni nei systemi a due pozzi piezometrici," by F. Ramponi, *Technica Italiana*, vol. 3, no. 3, 1948.

11 "Théorie des Chambres d'Equilibre," by J. Calame and D. Gaden, Gauthier-Villars, Paris, France, and Lausanne, Switzerland, 1926.

12 "Stability of Parallel-Branch and Differential Surge Tanks," by O. C. Zienkiewicz, *Proceedings of The Institution of Mechanical Engineers*, vol. 170, no. 7, 1956, pp. 265–280.

13 "Stabilité de Deux Chambres d'Equilibre dans le Cas d'une Liaison entre Galeries d'Amenée," by Geza Bata, *Comptes Rendus Académie des Sciences*, vol. 239, August 9, 1954, pp. 476–478.

14 "Die Stabilität der Schwingungen in zwei hintereinander liegenden Wasserschlössern," by W. Jureka, *Oesterreichisches Ingenieur-Archiv*, vol. 5, no. 3, 1951.

Discussion

C. G. Smallridge[4] and K. J. Gray.[5] In order to appreciate fully the significance of the author's contribution, we should first consider when a surge-tank system can be used in practice.

Multiple tanks on the upstream side of the units can be used under the following circumstances:

1 A long headrace tunnel with subsidiary water being supplied through shafts.

2 A long headrace tunnel for which a downstream tank becomes excessively large and costly to construct.

3 When an existing scheme is extended and the surge-tank capacity has to be increased.

4 To obtain better stability for an existing tank for which operating conditions have changed.

5 When a vertical or slope shaft can be used to decrease the size of the main surge tank.

The design engineer, with the aid of the analysis presented by the author, can conclude more quickly what influence the introduction of an additional shaft would have on the stability of the

[4] Hydraulic Engineer, The Shawinigan Engineering Company, Limited, Montreal, Canada. Mem. ASME.

[5] Project Engineer, The Shawinigan Engineering Company, Limited.

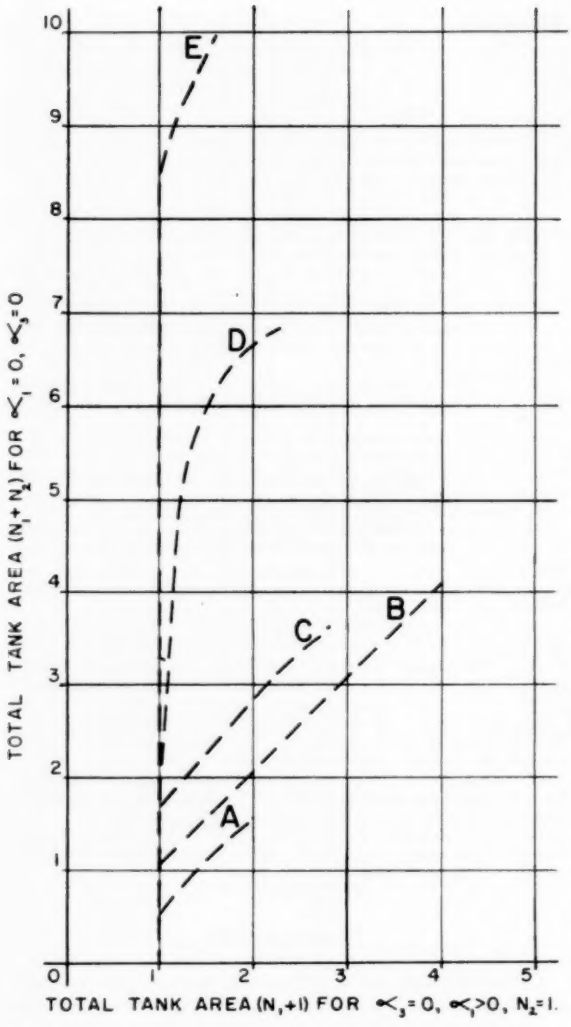

Curve	$\overline{M}^*$	Fr_1'	Fr_2'	Physical arrangement
A	0.2	0.3	varies	Tanks close together at
B	0.3	0.3	varies	downstream end
C	1.0	varies	0.2	Upstream tank near mid-
D	1.0	0.2	varies	way point of tunnel
E	3.0	varies	0.2	Upstream tank near reservoir

Fig. 7 Diagram showing saving in total area by making downstream tank equal to Thoma area

system, and is able to define the limiting stability range as a guide to preliminary selection of tank sizes and locations.

Now that this tool is available, an appreciation of the influence of the location of the second tank relative to the first tank is readily obtainable by making a few mathematical calculations.

The theory does not size the tanks but readily shows whether the tanks are stable; in other words, a stable region can be established within which the designer knows that stability will be attained.

Carrying the investigation a step further, the writers have shown that, as the location of the upstream tank varies, there is a decided advantage in retaining the area of the downstream tank as the theoretical Thoma area. This results in a saving on the combined area of the two tanks and, therefore, the over-all cost of the main tank system. This becomes particularly evident as the upstream tank moves upstream from the half-way point towards the intake end.

Referring to Equation [9] the criterion for $\alpha_1 = 0$, n_2 is always <1 for the limiting stability points.

By making $\mu = (Fr_2'/(Fr_1')$

$$N_1 = \frac{\mu - \overline{m}^*}{\overline{m}^*(1 - 4Fr_2^2)}$$

where N_1 = value of n_1 when $n_2 = 1$.

Fig. 7 indicates the effect of making the area of the downstream tank as near as possible to the Thoma area even though stability can be achieved for smaller values.

The author is to be congratulated on this valuable contribution to the understanding of complex surge-tank problems.

H. M. Paynter.[6] The author is to be heartily commended for his notable contributions to the field of surge-tank performance and stability. This paper manifests again his concerted effort to reduce an inherently large number of parameters to a sufficiently small group for practical general studies of multiple-tank stability. Since analytical results based upon a linearized set of equations, assuming constant hydraulic power, should never be used for more than preliminary sizing, these efforts of the author will reduce greatly the task of final sizing and design. This latter phase necessarily will require detailed calculations which are currently based largely upon "hand" numerical and graphical studies, but which are ever more commonly being performed on analog and digital computing machines.

The writer has long been actively interested in questions concerning surge-tank performance. He is convinced that there is ample need for additional reliable and logically consistent preliminary design data. To this end he has taken the liberty of using the opportunity of this discussion to add to the results and simplifications of the author.

An extremely practical simplification results in Case 2 by pursuing a little further the author's remark concerning the near equality of Thoma areas if both sections of the tunnel may be assumed to have the same diameter. By substituting a Darcy-Weisbach friction-loss term in the Thoma equation, there results the following simple expression for the Thoma area:

$$A_{Th}/A_T = D_T/fH_0 \quad \ldots\ldots [11]$$

where f is the Darcy friction factor ($\leqq 0.015$) and the remaining terms are as defined by the author.

Thus in Case 2, if the tunnels can be assumed to have the same diameter

$$D_{T1} = D_{T2} = D_T \quad \ldots\ldots [12]$$

then it is reasonable to expect that

$$f_1 \approx f_2 \approx f \quad \ldots\ldots [13]$$

and, therefore

$$A_{Th1} \approx A_{Th2} \approx A_{Th} \quad \ldots\ldots [14]$$

These results were noted by the author. However, under these

[6] Assistant Professor of Mechanical Engineering, Massachusetts Institute of Technology, Cambridge, Mass. President, Pi-Square Engineering Company, Inc., Boston, Mass. Mem. ASME.

same conditions, the rated friction losses, F_{10} and F_{20}, may be assumed to vary in direct proportion to the ratio of tunnel lengths L_1 and L_2, thus

$$F_{10}/F_{20} = L_1/L_2 \quad \ldots\ldots [15]$$

This simplification and specialization of Case 2 thus reduces the general study to a systematic exploration of only four parameters:

$$n_1 = A_1/A_{Th}; \qquad n_2 = A_2/A_{Th}$$
$$\rho = L_1/(L_1 + L_2); \qquad h = 2(F_{10} + F_{20})/H_0$$

as indicated in Fig. 8 of this discussion.

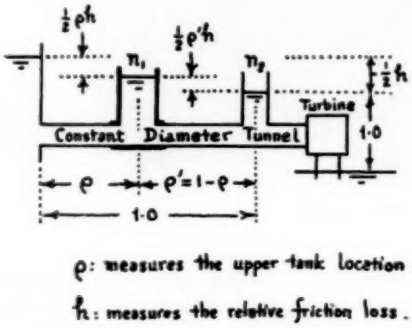

Fig. 8 Definition sketch for new parameters

In terms of the new parameters ρ and h, the author's parameters for Equation [8] can be expressed as follows:

$$\left.\begin{aligned} \bar{m}^* &= (\rho'/\rho)^{1/3} = [(1-\rho)/\rho]^{1/3} \\ 2F_{r1}' &= (\rho h)^{1/3} \\ 2F_{r2}' &= (\rho' h)^{1/3} = [(1-\rho)h]^{1/3} \end{aligned}\right\} \quad \ldots\ldots [16]$$

Then the characteristic equation and its coefficients, Equation [8], may be expressed as follows

$$p^4 + \alpha_1' p^3 + \alpha_2' p^2 + \alpha_3' \rho' + \alpha_4' = 0$$

$$\left.\begin{aligned} \alpha_1' &= 2n_2 - 1 \\ \alpha_2' &= n_2 + (1 - 2\rho' h)\rho n_1 + \rho\rho' n_1 n_2 h \\ \alpha_3' &= \rho n_1 n_2 (1 - \rho' h) + n_2(n_2 - 1) \\ \alpha_4' &= \rho\rho' n_1 n_2 (1 - h) \end{aligned}\right\} \quad \ldots\ldots [17]$$

For typical hydroelectric stations, the friction parameter h will vary in the range

$$0 < h \leqslant 0.2 \quad \ldots\ldots [18]$$

unless the tunnel conduit is sized upon other than economic factors.

From its definition, the spacing parameter ρ must lie in the range

$$0 \leq \rho \leq 1 \quad \ldots\ldots [19]$$

Fig. 9 of this discussion presents stability plots determined from analog-computer studies of the system equations as given in the paper and indicated in Fig. 10 of this discussion. This machine is indicated in Figs. 11 and 12 of this discussion and is one of the standard facilities of the American Center for Analog Computing in Boston but represents a novel form of computing equipment.

In the present application each unit as indicated in Fig. 13 performs the following operation

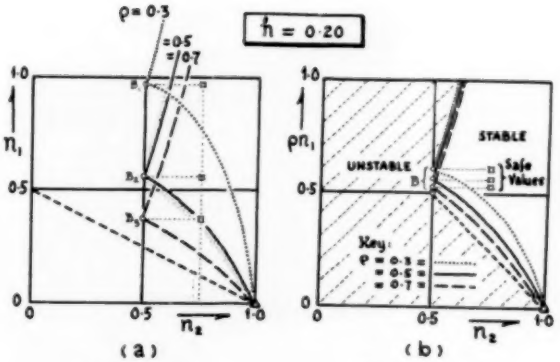

(a) n_1 versus n_2 (b) n_1 versus n_2

Fig. 9 Stability plots

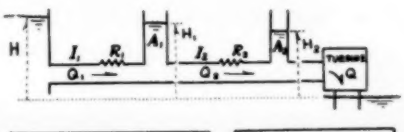

EQUATIONS
$H - H_1 = I_1 \frac{dQ_1}{dt} + R_1 Q_1$
$Q_1 - Q_2 = A_1 \frac{dH_1}{dt}$
$H_1 - H_2 = I_2 \frac{dQ_2}{dt} + R_2 Q_2$
$Q_2 - Q = A_2 \frac{dH_2}{dt}$
$Q = -S\sqrt{H_2}$

PARAMETERS		
	Physical	Normalized
I_1	L_1/gA_{T1}	$\rho' h$
R_1	$2F_{10}/Q_0$	ρh
A_1	A_1	n_1
I_2	L_2/gA_{T2}	$\rho' h$
R_2	$2F_{20}/Q_0$	$\rho' h$
A_2	A_2	n_2
S	Q_0/H_0	1

Fig. 10 Equations and parameters for Case 2

$$y = Y + 10^m \int \sum_{i=1}^{4} a_i x_i dt \quad \ldots\ldots [20]$$

where

y = output variable
x_1, x_2, x_3, x_4 = any four input variables
Y = static level
m = 0, 1, 2, 3
a_i = adjustable constant from 0 to ±11.10

This machine is unique in that all parameter settings and interconnections are executed by switches alone. The setup sheet for Case 2 with the parameters indicated is shown in Fig. 13. Only four K5-U elements were required.

Returning to the results of Fig. 9, as the author has shown, Γ will vanish identically whenever α_1' and α_3' vanish simultaneously. Let us call the values of n_1 and n_2 for which this is true n_1^* and n_2^*. These values fix the points B_k in Fig. 10 and are readily found to be the following:

$$\left.\begin{aligned} n_1^* &= \frac{0.500/\rho}{1 - (1-\rho)h} \\ n_2^* &= 0.500 \end{aligned}\right\} \quad \begin{matrix} \text{Critical values} \\ \text{at} \\ \text{point B} \end{matrix} \quad \ldots\ldots [21]$$

In order to apply these results in practice it is necessary to employ values of n_1 and n_2 greater than the critical values for any

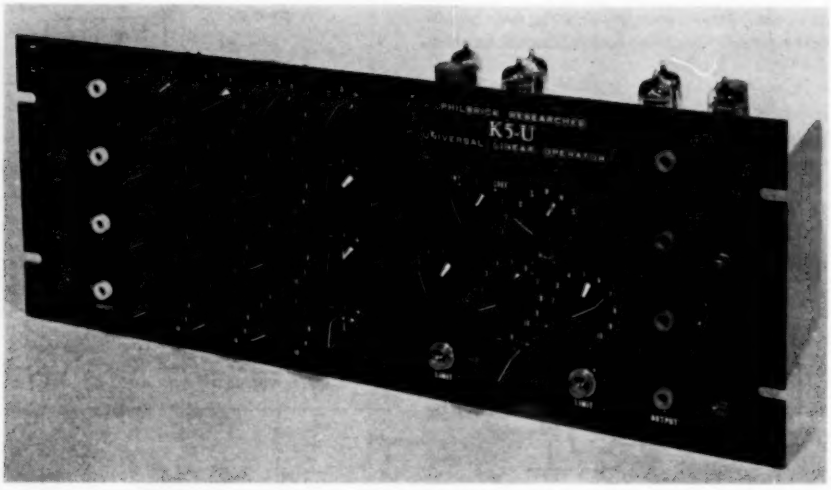

Fig. 11 Electronic-analog universal linear operator

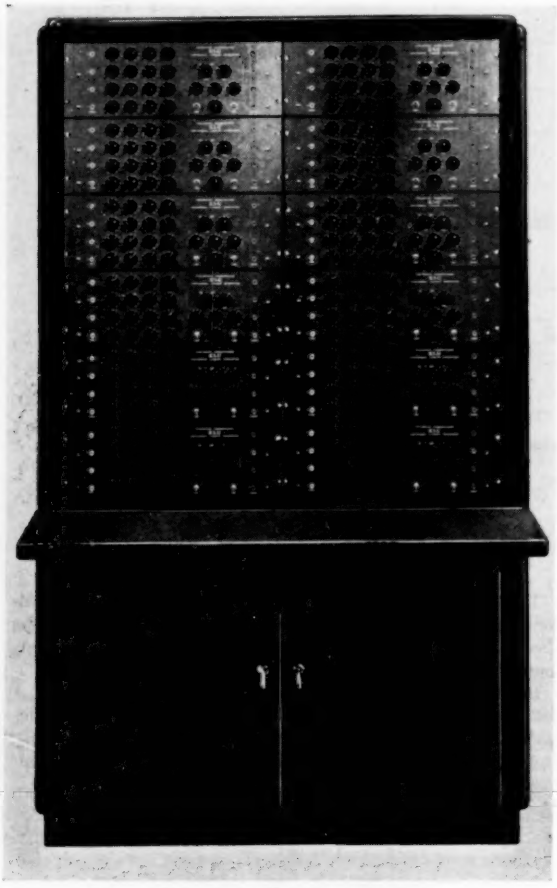

Fig. 12 Electronic-analog computer console

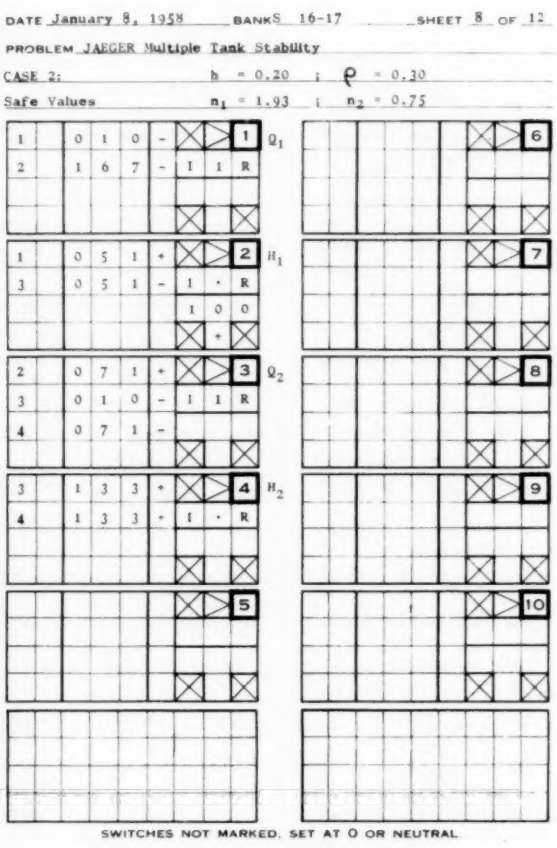

Fig. 13 K5-U setup diagram for Case 2

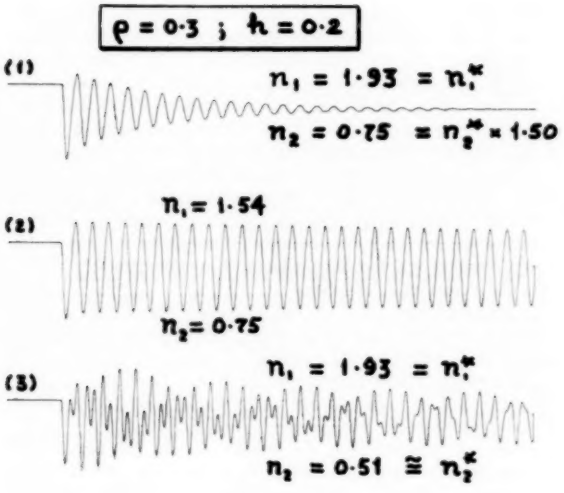

Fig. 14(*a*)

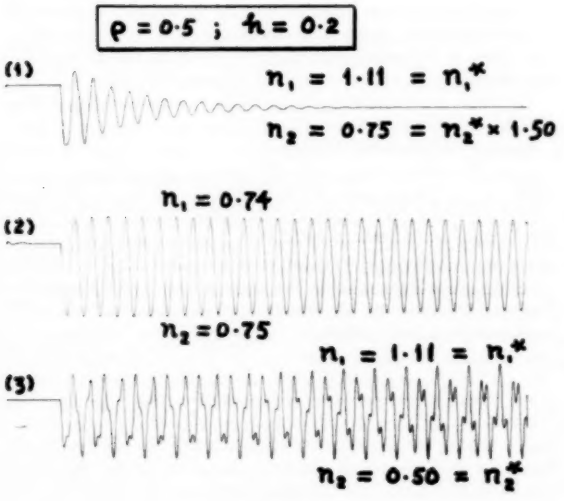

Fig. 14(*b*)

given values of ρ and h. A possible set of safe values for preliminary use would be the following:

$$\left.\begin{aligned} n_1 &= n_1^* = \frac{0.500/\rho}{1-(1-\rho)h} \\ n_2 &= 1.5n_2^* = 0.750 \end{aligned}\right\} \quad \begin{matrix}\text{Safe values} \\ \text{for} \\ \text{preliminary design}\end{matrix} \quad \ldots [22]$$

The relative stability margin is indicated in Figs. 14(*a*, *b*, *c*). These depict analog solutions for the values of n_1 and n_2 corresponding to Equation [22], for the indicated values of ρ and h, together with the effect of reducing n_1 and n_2, separately, to their critical values.

A fuller discussion of these results as well as comparable developments for Case 1 and other cases, developing working charts for the Jaeger stability conditions, using analog computers, is shortly to be presented in a paper by the writer and his colleagues.

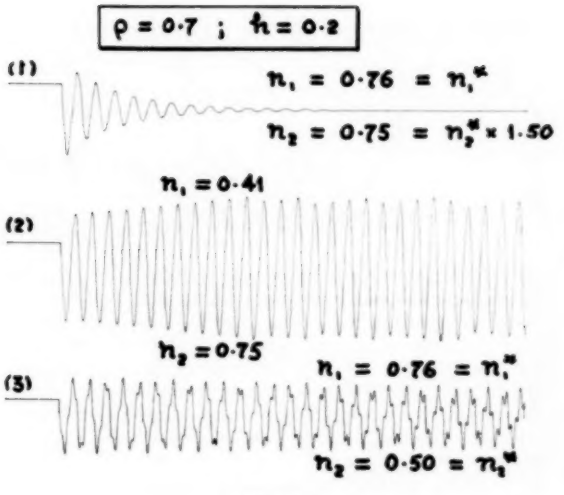

Fig. 14(*c*)

Fig. 14(*a*, *b*, *c*) Computer results for Case 2 downstream levels versus time

1 Safe values of n_1 and n_2
2 n_1 reduced to stability limit
3 n_2 reduced to stability limit

C. C. Crawford.[7] Another important chapter has been added to the book on surge tank stability. The author has again earned the thanks of the engineering profession.

Had this solution been available, the writer could have applied it during the stability analyses of the proposed surge-tank systems for T-1 Power-plant, Australia. As shown in Fig. 15, T-1 has a system of three surge tanks to be considered for stability; two upstream and one downstream from the turbines. The sizes of these tanks were fixed by other considerations and then were checked for stability.

Stability of the system was considered to be satisfactory if small oscillations were damped with the plant developing maximum out-

[7] Engineer, Technical Engineering Analysis Section, Bureau of Reclamation, Denver, Col.

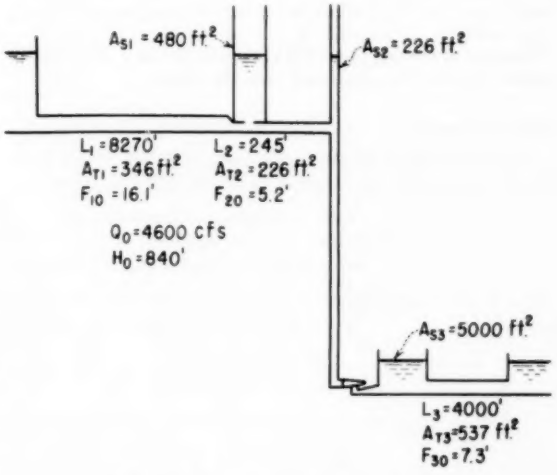

Fig. 15 T-1 power-plant waterways system

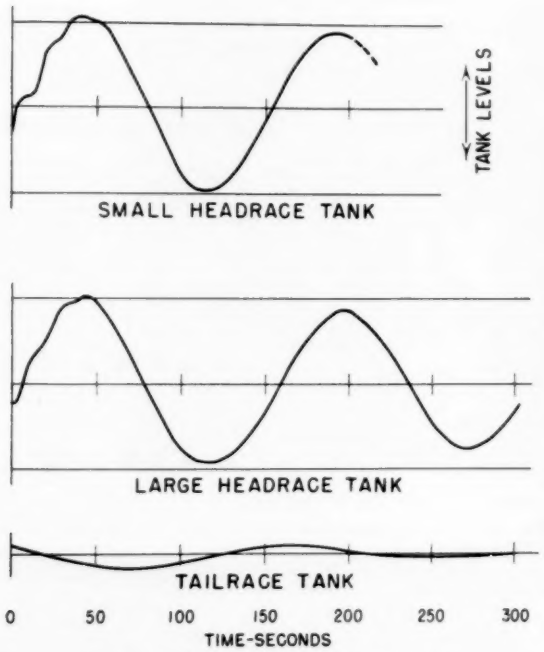

Fig. 16 T-1 power-plant stability study

put at minimum head, regulating to constant power output at constant efficiency.

From analytical studies of the system it was concluded:

1 The tailrace surge tank and tunnel would have very little effect on the stability of the system.

2 There would be no instability between the two upstream tanks.

3 The small headrace tank would "synchronize" quickly with the large headrace tank.

4 The whole system would be stable for the operating conditions just given.

Application of the author's solution, assuming the tailrace system to have no effect, shows the system of headrace surge tanks to be stable.

Stability of the complete T-1 system is shown in Fig. 16, the results of a stepwise, graphical, stability solution.

Author's Closure

Two recent papers by the author and a third one by Mr. Zienkiewicz summarize the problem of the stability of systems of surge tanks. The particular case dealt with in the paper submitted to the ASME concerns surge tanks on the upstream side of the turbine. In their comments Messrs. C. G. Smallridge and K. J. Gray enumerate five cases when multiple tanks on the upstream side of the turbines can be used, and Mr. C. C. Crawford describes in his contribution a most interesting surge tank system designed by the Snowy Mountains Authority in conjunction with the Bureau of Reclamation for Snowy T-1 Power Plant in Australia. The author's solution shows this system to be stable.

The importance of surge tanks has further been stressed by a recent article by the same author on "Economics of Large Surge Tanks"[3] where it is said that some modern surge tanks may cost over one or two million dollars.

In his contribution Prof. H. M. Paynter makes a further most valuable suggestion regarding friction losses, which can be taken proportional to the tunnel lengths L_1 and L_2. This reduces the number of free parameters to two [$\rho = L_1/(L_1 + L_2)$ and $h = 2(F_{10} + F_{20})/H_0$] instead of three ($m^*$, F_{10}, F_{20}) used by the author. The two variables remain as before n_1 and n_2.

After such simplification the problem can be put on an electronic-analog computer for rapid analysis. The curves shown by Professor Paynter, Figs. 9(a and b), confirm diagram Fig. 5 by the author.

Messrs. Smallridge and Gray have suggested to calculate the sum $(n_1 + n_2)$ for $n_2 = 1$ and for varying values $n_2 < 1$, the total surge tank volume being proportional to $(n_1 + n_2)$. They show that there is a decided advantage in retaining the area of the downstream tank as the theoretical Thoma area ($n_2 = 1$).

The same problem can easily be tackled using Professor Paynter's simplified assumptions:

For $n_2 = 1$, equations [17] become:

$$\alpha_1' = 1 \qquad \alpha_2' = 1 + \rho n_1(1 - \rho' h)$$

$$\alpha_3' = \rho n_1(1 - \rho' h) \qquad \alpha_4' = \rho\rho' n_1(1 - h)$$

and $\Gamma = \alpha_2^2 - \alpha_1(\alpha_2\alpha_3 - \alpha_1\alpha_4) = 0$

yields the conditions $n_1 \equiv 0$ and $n_1 + n_2 = -1$.

The critical values at point B are given (assumptions made by Professor Paynter) by Equations [21] and for this particular point (see Figs. 5, 6, and 9):

$$n_1^* + n_2^* = 0.5 + \frac{0.5/\rho}{1 - (1 - \rho)h}$$

The inequality $n_1^* + n_2^* \geq 1$ becomes $-\rho^2 h - (1 - h)\rho + 1 \geq 0$. The roots of this equation are $\rho = 1$ and $\rho = -1/h$. As ρ must always be $0 < \rho < 1$, the inequality $n_1^* + n_2^* > 1$ is always fulfilled for point B. For $\rho < 0.5$, $n_1^* + n_2^*$ rapidly increases to values substantially larger than 1.5.

This confirms by another method the conclusions of Messrs. Smallridge and Gray.

[3] "The Economics of Large Surge Tanks," by Charles Jaeger, *Water Power*, vol. 10, no. 5, 1958.

Water Hammer in Nonuniform Pipes as an Example of Wave Propagation in Gradually Varying Media

By H. M. PAYNTER[1] and F. D. EZEKIEL,[2] CAMBRIDGE, MASS.

Wave disturbances propagate down a fluid pipe, whose characteristics vary only gradually over a single wavelength, in nearly the same manner as a uniform pipe of the same total transmission time. However, the variations in pressure and flow along the pipe are modified directly and inversely, respectively, with the square root of the change in characteristic impedance level. This generally useful "Green's Law" approximation is checked against exact solutions and other methods of approximation.

Statement of General Problem

The phenomenon of pressure-wave propagation in fluid pipelines known as water hammer has now become well understood. However, nearly all solutions and solution methods are based on the assumption of one or more sections of pipe and enclosed fluid having uniform properties throughout the length. Indeed, the very mathematical existence of wave-like behavior is premised on the constancy of the transmission parameters.

Yet it is readily appreciated that such strict constancy is altogether lacking in practical structures in which such phenomena are known *physically* to exist. One need only consider the numerous occurrences of bends, joints, stiffeners, anchors, and the like, in actual pipes to realize that some variation in at least the elastic properties of a fluid pipeline is inevitable. Thus the interesting question arises as to how much variation in properties can occur before the distortions in wave forms become of such practical significance and importance as to be taken into account in design and operation. A closely related problem arises in pipes whose thickness is varied to take into account variations in static and dynamic pressures. Since the latter themselves depend on the local thickness, it is easy to see that a "vicious circle" could arise in the design problem unless the order of magnitude of these variations is well understood.

Another manifestation of variation occurs in the use of some of the standard approximate formulas which replace an actual composite pipe by an assumed equivalent uniform pipe. However, the strength and weakness of such approximations are not well known.

It is the purpose of this paper to point out that the answers to these and other questions follow directly from a number of researches on propagation in variable media which have stemmed from both the early studies of George Green in 1837 (1),[3] concerning the classic "Green's Law" of gravity waves in shallow channels and also an entirely independent and more recent development in electrical engineering and electromagnetic theory culminating in papers of Schelkunoff (2), and Barthold (3). Some of the history behind this evolution has been recounted in a discussion by one of the authors (4).

Since nearly all these researches have arisen *outside* the province of conventional water-hammer studies, it would seem appropriate to present herewith a short "dictionary" of equivalent terms in generalized dynamics to aid and encourage interested readers both in going back to the original sources and in keeping current with extremely pertinent work in these closely analogous fields. Such an analog glossary is given in Table 1.

Inspection of this table makes clear the setting into which this paper is cast; namely, that water hammer in nonuniform pipes is merely a special case of the broad general field of wave propagation in varying and stratified media. Thus it should be no surprise that this problem is closely related to: (*a*) Transients in tapered electric transmission lines (column 2 of Table 1), (*b*) seismic waves in the ground (column 3), (*c*) vibrations in turbine shafts (column 4), (*d*) tidal waves in river estuaries (column 5), (*e*) acoustic propagation in horns (column 6), as well as many other fields. The authors could achieve no better purpose in this paper than to press the point that even on a probability basis, alone, important new developments in water-hammer theory are more likely to arise in these related fields than in the narrow context of water-hammer problems.

Use of Canonical Variables

The classical water-hammer equations (neglecting pipe friction) can be written in the form

$$-\frac{\partial H}{\partial s} = \frac{1}{gA}\cdot\frac{\partial Q}{\partial t} \quad \ldots\ldots [1]$$

$$-\frac{\partial Q}{\partial s} = \frac{gA}{a^2}\cdot\frac{\partial H}{\partial t} \quad \ldots\ldots [2]$$

where

$H = H(s, t)$ total head, ft
$Q = Q(s, t)$ flow, cu ft/sec
s = distance along pipe, ft
t = time, sec
g = gravitational acceleration, ft/sec^2
$A = A(s)$ = local pipe sectional area, sq ft
$a = a(s)$ = local speed of sound, ft/sec

Using the generalized concepts of local inertance, per ft, and local capacitance, per ft, (13), defined as

$$I = I(s) \equiv 1/gA(s)$$
$$C = C(s) \equiv gA(s)/a^2(s)$$

Equations [1] and [2] may be rewritten in the form

$$-\frac{\partial H}{\partial s} = I(s)\cdot\frac{\partial Q}{\partial t} \quad \ldots\ldots [3]$$

---

[1] Assistant Professor of Mechanical Engineering, Massachusetts Institute of Technology. Mem. ASME.

[2] Assistant Professor of Mechanical Engineering, Massachusetts Institute of Technology. Assoc. Mem. ASME.

[3] Numbers in parentheses refer to the Bibliography at the end of the paper.

Contributed by the Hydraulic Division and presented at the Annual Meeting, New York, N. Y., December 1–6, 1957, of The American Society of Mechanical Engineers.

Note: Statements and opinions advanced in papers are to be understood as individual expressions of their authors and not those of the Society. Manuscript received at ASME Headquarters, August 1, 1957. Paper No. 57—A-107.

Table 1 Analogous quantities in wave media

	Medium				
		Mechanical		Fluid	
Generalized term	Electrical	Linear	Rotary	Liquid	Gas
Effort e	voltage E	force F	torque M	head H	pressure P
Flow f	current I	velocity V	speed ω	flow Q	flow W
Power $\boldsymbol{P} = e \cdot f$	$\boldsymbol{P} = E \cdot I$	$\boldsymbol{P} = F \cdot V$	$\boldsymbol{P} = M \cdot \omega$	$\boldsymbol{P} = \gamma H \cdot Q$	$\boldsymbol{P} = \frac{1}{\gamma} P \cdot W$
Impulse $p = \int e dt$	flux $\psi = \int E dt$	impulse $P = \int F dt$	impulse $\mathfrak{M} = \int M dt$	impulse $p = \int H dt$	impulse $p = \int P dt$
Displacement $q = \int f dt$	charge $Q = \int I dt$	distance $X = \int V dt$	angle $\theta = \int \omega dt$	volume $V = \int Q dt$	weight $S = \int W dt$
Inertance $I = \Delta p / \Delta f$	inductance $L = \Delta \psi / \Delta I$	mass $M = \Delta p / \Delta V$	inertia $I = \Delta M / \Delta \omega$	inertance $I = \Delta p / \Delta Q$	inertance $I = \Delta p / \Delta W$
Capacitance $C = \Delta q / \Delta e$	capacitance $C = \Delta Q / \Delta E$	compliance $1/K = \Delta X / \Delta F$	compliance $1/K = \Delta \theta / \Delta M$	capacitance $C = \Delta V / \Delta H$	capacitance $C = \Delta S / \Delta P$
Surge impedance $Z = (I/C)^{1/2}$	$Z = (L/C)^{1/2}$	$Z = (MK)^{1/2}$	$Z = (IK)^{1/2}$	$Z = (I/C)^{1/2}$	$Z = (I/C)^{1/2}$
Wave time $T = (IC)^{1/2}$	$T = (LC)^{1/2}$	$T = (M/K)^{1/2}$	$T = (I/K)^{1/2}$	$T = (IC)^{1/2}$	$T = (IC)^{1/2}$

$$-\frac{\partial Q}{\partial s} = C(s) \cdot \frac{\partial H}{\partial t} \quad \ldots\ldots [4]$$

In a practical pipe, it is clear that variations in diameter, thickness, material, and constraints will cause the local inertance and capacitance to vary from section to section. The computation of these parameters is sufficiently well detailed in readily available literature (5, 6, 7, 8, 9, 10) to obviate inclusion here.

Following suggestive leads from the original work of Green (1), Evangelisti (11, 12) developed a transformation of variables which greatly reduces the variability in wave form due to variations in properties and parameters. This scheme has been used in an earlier paper of the authors (13). By the entirely independent route noted here, Schelkunoff (2) has arrived at the identical transformations which he appropriately denotes as a "reduction to canonical form." These redefinitions of variables are as follows

(A) Distance Transformation

$$\tau \equiv \int_0^s \gamma(s) \cdot ds, \quad \text{seconds} \quad \ldots\ldots [5]$$

or

$$d\tau \equiv \gamma ds$$

(B) Head (or "Effort") Transformation

$$\mathbf{U} \equiv \frac{1}{\epsilon(s)} \cdot H, \quad \text{ft}^2/\text{sec}^{1/2} \quad \ldots\ldots [6]$$

(C) Flow (or "Flow") Transformation

$$\mathbf{V} \equiv \epsilon(s) \cdot Q, \quad \text{ft}^2/\text{sec}^{1/2} \quad \ldots\ldots [7]$$

(D) Transforming Parameters

$$\gamma(s) \equiv [I(s) \cdot C(s)]^{1/2}, \quad \text{sec/ft} \quad \ldots\ldots [8]$$

$$= \text{reciprocal wave speed}$$

$$\epsilon(s) \equiv [I(s)/C(s)]^{1/2}, \quad \text{sec}^{1/2}/\text{ft} \quad \ldots\ldots [9]$$

$$= \text{root surge impedance}$$

For a fluid pipeline the transforming parameters become

$$\gamma(s) = 1/a(s)$$

$$\epsilon(s) = [a(s)/gA(s)]^{1/2}$$

Moreover we should note that the local fluid power is measured by

$$H \cdot Q = \mathbf{U} \cdot \mathbf{V}$$

As shown in Appendix 1, use of these canonical variables, τ, $\mathbf{U}$, and $\mathbf{V}$, reduces the first-order equations [1] and [2], (or [3] and [4]) to the canonical pair

$$-\frac{\partial \mathbf{U}}{\partial \tau} = \frac{\partial \mathbf{V}}{\partial t} + \nu \mathbf{U} \quad \ldots\ldots [10]$$

$$-\frac{\partial \mathbf{V}}{\partial \tau} = \frac{\partial \mathbf{U}}{\partial t} - \nu \mathbf{V} \quad \ldots\ldots [11]$$

where

$$\nu \equiv \frac{\partial}{\partial \tau} (\ln \epsilon) = \frac{1}{\gamma(s)} \cdot \frac{\partial}{\partial s} [\ln \epsilon(s)] \quad \ldots\ldots [12]$$

For a fluid pipe $\nu = \nu(s)$ can be written

$$\nu(s) = \frac{a(s)}{[a(s)/gA(s)]^{1/2}} \frac{\partial}{\partial s} [a(s)/gA(s)]^{1/2}$$

$$= (aA)^{1/2} \frac{\partial}{\partial s} \cdot \left(\frac{a}{A}\right)^{1/2}$$

or

$$\nu(s) = \frac{A(s)}{2} \frac{\partial}{\partial s} \left(\frac{a(s)}{A(s)}\right) \quad \ldots\ldots [13]$$

In terms of an arbitrary reference level for characteristic impedance namely, a_0/gA_0, we can deal with the relative changes Z where

$$Z = Z(s) = \frac{a(s)/gA(s)}{a_0/gA_0} = \frac{a(s)}{a_0} \frac{A_0}{A(s)}, \quad \text{per unit}$$

In these terms, the parameter ν becomes

$$\nu(s) = \frac{a(s)}{2Z} \frac{\partial Z(s)}{\partial s}, \quad \text{sec}^{-1} \quad \ldots\ldots [14]$$

Thus if Z varies by as much as 1 per cent per foot, and a was approximately 4000 ft per sec, ν would have the value

$$\nu = \frac{4000}{2} (0.01) = \pm 20 \text{ sec}^{-1}$$

However, this would represent an enormous variation if sustained over the length of, say, 1000 ft of pipe since ΔZ would be 1000 per cent or a tenfold increase (or decrease) in surge impedance.

For a gradually and more or less uniformly tapered pipe, such as frequently encountered in hydro plants and pumping stations, the value of ν would be much less. For example consider a variation in pipe thickness (and possibly diameter) such that

$$Z = 1 \text{ at one end}$$

$$Z = 2 \text{ at opposite end}$$

of a 2000-ft pipe with average a of 3000 ft/sec. This would yield the value

$$|\nu| \cong \frac{3000}{2} \cdot \frac{1}{2000} = 0.75 \text{ sec}^{-1}$$

which represents a more typical situation in practice.

Derivation of General Wave Equation

Corresponding to the canonical pair of first-order equations [10] and [11], we may simply derive general wave equations. These have been established in Appendix 2 as the following pair

$$\frac{\partial^2 \mathbf{U}}{\partial \tau^2} = \frac{\partial^2 \mathbf{U}}{\partial t^2} + \left(\nu^2 - \frac{\partial \nu}{\partial \tau}\right)\mathbf{U} \quad \ldots\ldots\ldots [15]$$

$$\frac{\partial^2 \mathbf{V}}{\partial \tau^2} = \frac{\partial^2 \mathbf{V}}{\partial t^2} + \left(\nu^2 + \frac{\partial \nu}{\partial \tau}\right)\mathbf{V} \quad \ldots\ldots\ldots [16]$$

It is now directly evident that if ν is everywhere zero along the pipe $\left(\nu \equiv 0;\ \frac{\partial \nu}{\partial \tau} \equiv 0\right)$ the foregoing equations reduce identically to the classical wave equations. Moreover, it is also evident that small and gradual changes in characteristics produce materially different behavior from large and abrupt changes. In the first instance ν^2 and $d\nu/d\tau$ may be sufficiently small as to be neglected, while in the latter case this is not usually possible.

Consider an assumed wave form

$$\mathbf{U} = K \sin [\omega(t + \tau)] \quad \ldots\ldots\ldots [17]$$

This corresponds to an *exact* solution for the classical wave case ($\nu \equiv 0$), as can be seen by differentiation

$$\frac{\partial^2 \mathbf{U}}{\partial t^2} = -K\omega^2 \sin [\omega(t + \tau)] = \frac{d^2 \mathbf{U}}{d\tau^2} \quad \ldots\ldots\ldots [18]$$

If this result is taken as a first approximation, we may evaluate the relative magnitudes of the two terms on the right side of Equation [15]

$$F = \frac{\partial^2 \mathbf{U}}{\partial t^2} = -K\omega^2 \sin [\omega(t + \tau)]$$

$$G = \left(\nu^2 - \frac{\partial \nu}{\partial \tau}\right)\mathbf{U} = \left(\nu^2 - \frac{\partial \nu}{\partial \tau}\right) K \sin [\omega(t + \tau)]$$

The ratio of these terms is therefore given by

$$|F/G| \sim \omega^2 \Big/ \left(\nu^2 - \frac{\partial \nu}{\partial \tau}\right)$$

Thus as the frequency ω increases, the effect of any *gradual* variation $\left(\nu,\ \frac{\partial \nu}{\partial \tau}\right.$ finite and small$\left.\right)$ will become less and less significant. By contrast, any *abrupt* variation in properties $\left(\nu,\right.$ $\left.\frac{\partial \nu}{\partial \tau}\right.$ infinite$\left.\right)$ may produce measurable effects at *many frequencies*. Indeed, ν and $\frac{\partial \nu}{\partial \tau}$ play the role of "structural frequencies," which will perturb only those portions of the solution in the corresponding range of temporal frequencies (20).

Effects of Abrupt and Gradual Nonuniformities

A general variable-section conduit can always be considered as a finite or infinite sequence of small elements, as indicated in Fig. 1. Each small section may be considered as two small lengths of uniform pipe, each having equal transmission time. The properties and corresponding surge impedance of one half-section are

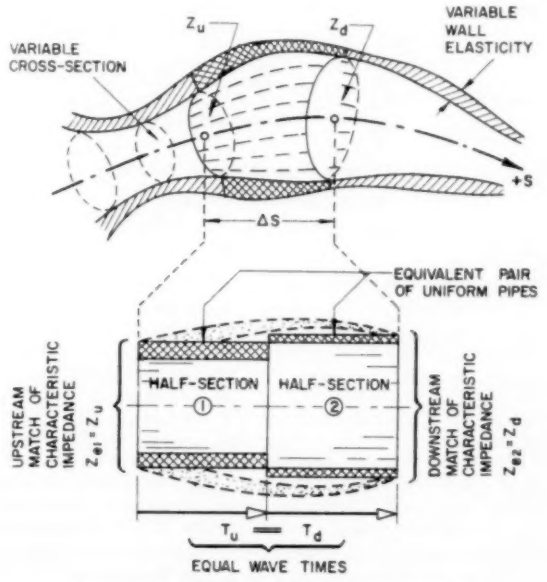

Fig. 1 Fluid pipe of gradually varying properties

taken as that at the *beginning* of the physical element, while the parameters of the other half-section are those corresponding to the *end* of the physical element. It is then clear to see that as the lengths and corresponding transmission times shrink to zero, this "model" of the physical case will approach exactitude. What is not immediately evident is the fact that often only one or very few sections are required to accurately represent typical pipelines for design and operating purposes. The validity of this approximation can be examined on the basis of the previous formulation.

Some Expository Examples

In order to make some of these points clear, let us consider two contrasting cases with the following data, as indicated in Fig. 2. In each case, the physical geometry has been taken as two lengths of uniform pipe with equal transmission lines.

Case 1

Upstream pipe	Downstream pipe
$A_u = 100$ ft^2	$A_d = 50$ ft^2
$a_u = 3220$ ft/sec	$a_d = 3220$ ft/sec
$L_u = 805$ ft	$L_d = 805$ ft
$I_u = L_u/gA_u$ = 0.25 sec^2/ft^2	$I_d = L_d/gA_d$ = 0.5 sec^2/ft^2
$Z_u = a_u/gA_u$ = 1 sec/ft^2	$Z_d = a_d/gA_d$ = 2 sec/ft^2
$T_u = I_u/Z_u = L_u/a_u$ = 0.25 sec	$T_d = I_d/Z_d = L_d/a_d$ = 0.25 sec

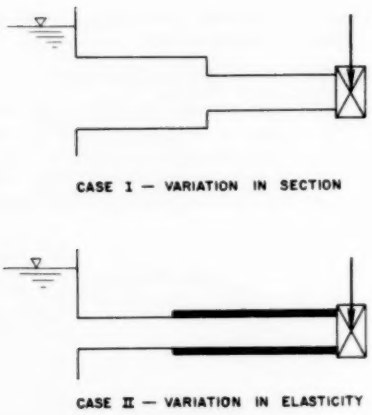

Fig. 2 Expository examples

Case 2

Upstream pipe	Downstream pipe
$A_u = 50$ ft²	$A_d = 50$ ft²
$a_u = 1660$ ft/sec	$a_d = 3220$ ft/sec
$L_u = 403$ ft	$L_d = 805$ ft
$I_u = 0.25$ sec²/ft²	$I_d = 0.50$ sec²/ft²
$Z_u = 1$ sec/ft²	$Z_d = 2$ sec/ft²
$T_u = 0.25$ sec	$T_d = 0.25$ sec

Thus it should be noted that in each case the wave parameters are identical but for different reasons. In the first case, the change in surge impedance, Z, is due to a *section* change while in the latter case it is due to a change in *wall elasticity*. Fig. 3 demonstrates the approximate nature of the pressure gradient during a *uniform deceleration* of flow in each case. Note that the head rise ΔH_m at the junction M is the same in both cases and is equal to $^1/_2$ the rise in downstream head ΔH_d. If the deceleration were truly uniform the results would be identical whether computed *inelastically* (using I_u and I_d) or *elastically* (using Z_u and Z_d).

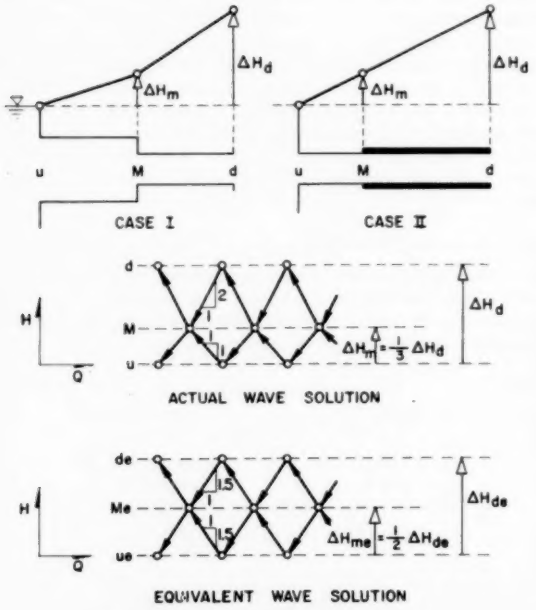

Fig. 3 Solution for uniform deceleration

While these results are well-established and widely employed in water-hammer practice, what is perhaps surprising is that essentially the same results would be obtained using the approximations of the previous paragraph, following the procedures of Evangelisti (11, 12).

Essentially this method would be to replace the composite pipe by an equivalent *single uniform pipe* with the following characteristics

$$Z_e = \frac{1}{2}(Z_u + Z_d) = 1.5 \text{ sec/ft}^2$$

$$T_e = T_u + T_d = 0.5 \text{ sec}$$

It now makes no difference whether we carry out an elastic wave solution in H-Q variables (graphically on the H-Q plane) or in **U-V** variables (graphically on a **U-V** plane). In either case, we would arrive at the following conclusion in terms of the *actual* head and flow at the junction M

$$\Delta H_m(t) \cong (Z_u/Z_d)^{1/3} \cdot \Delta H_{me}(t) \quad [19]$$

$$\Delta Q_m(t) \cong (Z_d/Z_u)^{1/3} \cdot \Delta Q_{me}(t) \quad [20]$$

These *generalized Green's Law* relations follow directly from the scaling transformations [6] and [7]. The head ΔH_{me} and flow ΔQ_{me} are those determined in the elastic solution for the equivalent pipe at the *temporal midlength*, which is, of course, the actual midlength of the *equivalent* uniform pipe.

For the uniform deceleration case of Fig. 3, we now can indicate graphically the nature of the elastic solution for this equivalent uniform pipe. We observe that the head ΔH_{me} at the midlength of the equivalent pipe is now, of course, exactly one-half that at the downstream end ΔH_{de}. Let us presume that flow has been decelerated at a rate such that

$$\Delta H_{de} \equiv \Delta H_d \quad [21]$$

Then

$$\Delta H_{me} = \frac{1}{2}\Delta H_{de} = \frac{1}{2}\Delta H_d$$

and applying Equation [19] we find

$$\Delta H_m \cong (Z_u/Z_d)^{1/3} \cdot \Delta H_{me} = 0.707 \times \frac{1}{2}\Delta H_d$$

or

$$\Delta H_m \cong 0.35 \Delta H_d \quad [22]$$

This compares with

$$\Delta H_m = 0.33 \Delta H_d \quad [23]$$

for the exact solution.

However, this technique of approximate solution has several distinct advantages: (*a*) It will improve in accuracy as the frequency of the disturbance increases. (*b*) It will improve in accuracy as the variation in Z with length decreases. (*c*) It will give a sequence of better and better approximations to the *actual continuous instantaneous gradelines* for the practical cases of continuous variation in Z with length, so long as enough sections of uniform pipe are taken.

It is this last point which is perhaps most significant, since the currently used methods of approximation do not specify how the *continuous* gradelines are to be drawn, especially for fast changes in pressure.

Approximation by One Equivalent Uniform Line

Let us presume that in a conduit of arbitrary shape as indicated in Fig. 1, we now subdivide it into a multiplicity of n sections of equal transmission time where

$$T_k = L_k/a_k = \text{const} = T_n \quad [24]$$

then for every such section

$$I_k/Z_k = T_k = \text{const} = T_n \quad [25]$$

and the *section inertance* I_k is thus directly proportional to the *section surge impedance* Z_k.

For the whole pipe, it is evident that

$$T_p = \sum_{k=1}^{n} T_k = nT_n \quad [26]$$

$$I_p = \sum_{k=1}^{n} I_k \quad [27]$$

where the summation is taken over the n sections of uniform pipe. If the number of sections n were permitted to become infinite it is evident that both of these sums would give way to the integrals

$$T_p = \int_0^L \frac{ds}{a(s)} \quad [28]$$

$$I_p = \frac{1}{g} \int_0^L \frac{ds}{A(s)} \quad [29]$$

where L is the total length of pipe. All these relations are familiar and are merely restated here for convenience.

It is natural to introduce an equivalent *mean surge impedance*, Z_p *defined* by the equation

$$Z_p \equiv \frac{I_p}{T_p} = \frac{\Sigma I_k}{\Sigma T_k} = \frac{1}{g} \frac{\int \frac{ds}{A}}{\int \frac{ds}{a}} \quad [30]$$

For the expository cases considered, the value of Z_p would be given by

$$Z_p = \frac{I_u + I_d}{T_u + T_d} = \frac{0.25 + 0.50}{0.25 + 0.25} = 1.5 = \frac{1}{2}(Z_u + Z_d) \quad [31]$$

The fact that Z_p is merely the arithmetic average of Z_k follows from using sections with equal transmission times.

We are now in the position to state the following general proposition concerning the variation in *effective* surge impedance, Z_e, as the frequency of disturbance increases:

For a nonuniform pipe connected at one end of a constant pressure reservoir and at the opposite end to a regulating valve, the effective surge impedance Z_e will vary from Z_p at sufficiently low frequencies to Z_d at sufficiently high frequencies, where Z_d is the local characteristic impedance at the valve end.

This result is well known to communication engineers (14) and acoustical engineers (15, 16).

This raises the natural question as to the precise value of Z_e to use for any particular case. Two limiting conditions, however, are obvious:

a For very slow changes in valve position the head rise is predominantly due to inertial effects. In this case $Z_e = Z_p$ will usually give the best approximation.

b For sudden valve closures and other shock problems, the head rise is predominantly due to elastic effects. In this case, $Z_e = Z_d$ will usually give the best approximation.

In intermediate cases, which arise rather frequently, the error in any approximation can be measured by the relative variation in Z; namely, ΔZ, where

$$|\Delta Z| = |Z_d - Z_p|/Z_p$$

If this number, as a percentage, is large compared with the accuracy desired, it will be necessary to break the pipe into more sections (if the variation in Z is continuous) or to use an approximation more nearly identical with the prototype (if the variation in Z is discontinuous).

Relation to Characteristic Curves

If we add and subtract Equations [10] and [11] we can obtain the following pair of equations

$$\frac{\partial}{\partial t}(\mathbf{U} + \mathbf{V}) + \frac{\partial}{\partial \tau}(\mathbf{U} + \mathbf{V}) = -\nu(\mathbf{U} - \mathbf{V}) \quad [32]$$

$$\frac{\partial}{\partial t}(\mathbf{U} - \mathbf{V}) - \frac{\partial}{\partial \tau}(\mathbf{U} - \mathbf{V}) = +\nu(\mathbf{U} + \mathbf{V}) \quad [33]$$

Let us then consider the parametric co-ordinates, α and β, where

$$\alpha = t + \tau \quad [34]$$

$$\beta = t - \tau \quad [35]$$

As shown in Appendix 3, these wave co-ordinates permit the preceding equations to be written in the form of *characteristics*, namely

$$2\frac{\partial}{\partial \alpha}(\mathbf{U} + \mathbf{V}) = -\nu(\mathbf{U} - \mathbf{V}) \quad [36]$$

$$2\frac{\partial}{\partial \beta}(\mathbf{U} - \mathbf{V}) = +\nu(\mathbf{U} + \mathbf{V}) \quad [37]$$

In the case of a uniform pipe ($\nu \equiv 0$) the right-hand side vanishes and these give the familiar characteristic equations

$$\mathbf{U} + \mathbf{V} = \text{const, along } \beta = t - \tau = \text{const} \quad [38]$$

$$\mathbf{U} - \mathbf{V} = \text{const, along } \alpha = t + \tau = \text{const} \quad [39]$$

or in conventional water-hammer terms

$$\Delta H = -\frac{a}{gA}\Delta Q, \text{ along } s = +at \quad [40]$$

$$\Delta H = +\frac{a}{gA}\Delta Q, \text{ along } s = -at \quad [41]$$

These equations, of course, directly establish the basis of the well-known graphical method of Schnyder, Bergeron, and Angus (17, 18, 19).

If, on the other hand, ν is not zero but small, the characteristic equations will be modified to curved paths as indicated in Fig. 4.

Moreover, it is not mandatory to deal in the $\mathbf{U}$ versus $\mathbf{V}$ space to see the relationship to characteristic curves and the graphical methods of solution. For example, Fig. 5(*a*) indicates a sketch solution for a typical tapered pipe which has been approximated by three sections of uniform pipe with equal transmission times. Fig. 5(*b*) indicates the corresponding *exact* solution, with *continuous curves* replacing the *line segments*. Again the error of approximation is measured by the ratio

$$|\Delta Z| = \frac{|Z_{k+1} - Z_k|}{Z_{k+1} + Z_k}$$

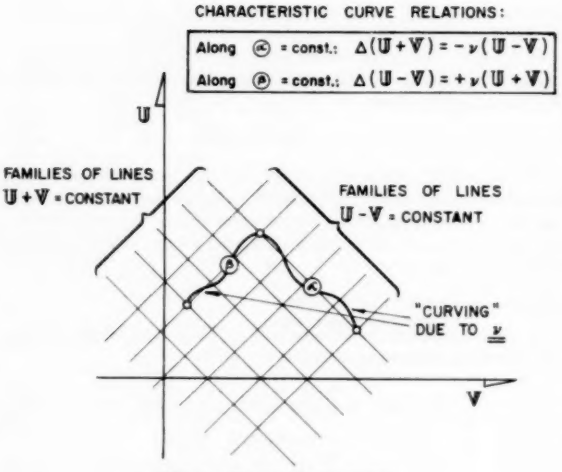

Fig. 4 Characteristic curves

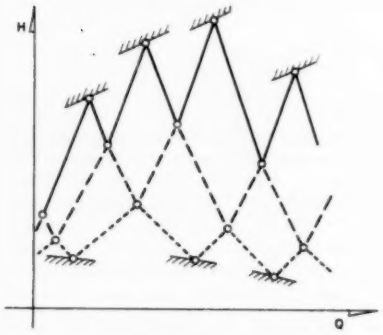

(a) APPROXIMATE SOLUTION

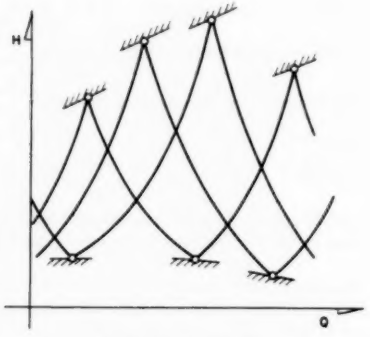

(b) EXACT SOLUTION

Fig. 5 Tapered pipeline

which is manifested by the angle between adjacent segments in Fig. 5(*a*).

Conclusions

From the foregoing analyses and remarks, we may generally conclude that pipes of gradually varying properties may always be approximated by a sequence of uniform pipes of equal transmission times but unequal characteristic impedances. While friction was neglected in the analysis, it is evident that it may always be lumped at the joints between these sections.

Even if only a single such section is taken, continuous gradelines may still be drawn, accounting for the local variations in Z, by correcting the local head variations by the square root of the local impedance ratio.

Bibliography

1 "On the Motion of Waves in a Variable Canal of Small Depth and Width," by G. Green, *Trans., Cambridge Philosophical Society*, vol. 6, 1837.

2 "Remarks Concerning Wave Propagation in Stratified Media," by S. A. Schelkunoff, Symposium on the Theory of Electromagnetic Waves, Interscience Publishers, Inc., New York, N. Y., 1951.

3 "An Approximate Transient Solution of the Tapered Transmission Line," by L. O. Barthold, AIEE Paper No. DP57-548, 1957.

4 Discussion by H. M. Paynter of a paper entitled "On Application of Impedance Method to Continuous Systems," by P. F. Chenea, *Journal of Applied Mechanics*, TRANS. ASME, vol. 75, 1953, p. 571.

5 "Hydraulic Transients," by G. R. Rich, McGraw-Hill Book Company, Inc., New York, N. Y., 1951.

6 "Waterhammer Analysis," by J. Parmakian, Prentice-Hall, Inc., New York, N. Y., 1955.

7 "Engineering Fluid Mechanics," by C. Jaeger, Blackie & Sons, London, England, 1956.

8 "Engineering Hydraulics," by H. Rouse, John Wiley & Sons, Inc., New York, N. Y.

9 "Handbook of Applied Hydraulics," by C. V. Davis, McGraw-Hill Book Company, Inc., New York, N. Y., 1952.

10 "Hydroelectric Handbook," by W. P. Creager and J. D. Justin, John Wiley & Sons, Inc., New York, N. Y., 1950.

11 "Sul calcolo del colpo d'ariete nelle condotte forzate a caratteristoche variabili," by G. Evangelisti, *L'Energia Elettrica*, vol. 16, December, 1939.

12 "Veröffentlichungen zur Erforschung der Druckstoss Probleme in Wasserkraftanlagen und Rohrleitungen," by F. Tölke, Springer Verlag, Berlin, Germany, 1949.

13 "Computer Representations of Engineering Systems Involving Fluid Transients," by F. D. Ezekiel and H. M. Paynter, TRANS. ASME, vol. 79, 1957, pp. 1840–1850.

14 "The Exponential Transmission Line," by C. R. Burrows, *Bell System Technical Journal*, vol. 17, 1938, pp. 555–573.

15 "Elements of Acoustical Engineering," by H. F. Olson, D. Van Nostrand Company, Inc., New York, N. Y., 1947.

16 "Acoustics," by L. L. Beranek, McGraw-Hill Book Company, Inc., New York, N. Y., 1954.

17 "Druckstösse in Pumpensteigleitungen," by O. Schnyder, *Schweizerische Bauzeitung*, vol. 94, nos. 22 and 23, 1929.

18 "Methode graphique générale de calcul des propagations d'ondes planes," by L. Bergeron, *Mémoires de la Société des Ingénieurs Civils de France*, 1937.

19 "Water Hammer in Pipes, Including Those Supplied by Centrifugal Pumps," by R. W. Angus, *Proceedings of the Institution of Mechanical Engineers*, vol. 136, 1937, p. 245.

20 "Wave Propagation in Periodic Structures," by L. Brillouin, Dover Publications, New York, N. Y., 1953.

Appendix 1 Derivation of the Canonical Equations

Consider the pair of equations

$$-\frac{\partial e}{\partial s} = I(s)\frac{\partial f}{\partial t} \quad \ldots\ldots [42]$$

$$-\frac{\partial f}{\partial s} = C(s)\frac{\partial e}{\partial t} \quad \ldots\ldots [43]$$

It will prove convenient to use the abbreviated notation

$$(\ )_x = \partial(\ )/\partial x$$

Thus the preceding equations may be rewritten

$$e_s + If_t = 0 \quad \ldots\ldots [44]$$

$$f_s + Ce_t = 0 \quad \ldots\ldots [45]$$

We can also usefully define *local* values of the following quantities:
Surge impedance

$$Z = Z(s) = [I(s)/C(s)]^{1/2} \quad [46]$$

Propagation constant

$$\gamma = \gamma(s) = [I(s) \cdot C(s)]^{1/2} \quad [47]$$

Note that γ is the reciprocal of the local wave speed c where
Wave speed

$$c = c(s) = 1/\gamma(s) \quad [48]$$

The equations [44] and [45] may best be examined in a form employing variables of homogeneous dimensions. We can accomplish this *normalization* by the following scaling transformations:

(*a*) Distance transformation

$$d\tau \equiv \gamma \, ds \quad [49]$$

(*b*) Effort transformation

$$\mathbf{U} \equiv \frac{1}{\sqrt{z}} e = \epsilon^{-1} e \quad [50]$$

(*c*) Flow transformation

$$\mathbf{V} \equiv (\sqrt{Z}) f = \epsilon f \quad [51]$$

In these terms, $\mathbf{U}$ and $\mathbf{V}$ have the same dimensions and yet they are complementary quantities with the instantaneous local power still given by

$$P = \mathbf{UV} = \epsilon^{-1} e \epsilon f = ef \quad [52]$$

The distance variable s has been converted to a time measure τ. The derivative of any variable with respect to s can then be simply related to the derivative with respect to τ, namely

$$(\quad)_s \equiv s_\tau (\quad)_\tau = \gamma^{-1} (\quad)_\tau \quad [53]$$

Substituting the transformed variables $\mathbf{U}$ and $\mathbf{V}$ into Equations [44] and [45] gives

$$(\epsilon \mathbf{U})_s + I(\epsilon^{-1}\mathbf{V})_t = 0 \quad [54]$$

$$(\epsilon^{-1}\mathbf{V})_s + C(\epsilon \mathbf{U})_t = 0 \quad [55]$$

or

$$\epsilon_s \mathbf{U} + \epsilon \mathbf{U}_s + I\epsilon^{-1}\mathbf{V}_t = 0 \quad [56]$$

$$\epsilon_s^{-1}\mathbf{V} + \epsilon^{-1}\mathbf{V}_s + C\epsilon \mathbf{U}_t = 0 \quad [57]$$

Using [53] these become

$$\gamma^{-1}\epsilon_\tau \mathbf{U} + \epsilon\gamma^{-1}\mathbf{U}_\tau + I\epsilon^{-1}\mathbf{V}_t = 0 \quad [58]$$

$$\gamma^{-1}\epsilon_\tau^{-1}\mathbf{V} + \epsilon^{-1}\gamma^{-1}\mathbf{V}_\tau + C\epsilon \mathbf{U}_t = 0 \quad [59]$$

Multiplying Equation [58] through by $\gamma\epsilon^{-1} = \epsilon I^{-1}$, and Equation [59] by $\gamma\epsilon = C^{-1}\epsilon^{-1}$ gives

$$\epsilon^{-1}\epsilon_\tau \mathbf{U} + \mathbf{U}_\tau + \mathbf{V}_t = 0 \quad [60]$$

$$\epsilon\, \epsilon_\tau^{-1}\mathbf{V} + \mathbf{V}_\tau + \mathbf{U}_t = 0 \quad [61]$$

If we then define the quantity ν as

$$\nu \equiv (\ln \epsilon)_\tau = \epsilon^{-1}\epsilon_\tau = -\epsilon\, \epsilon_\tau^{-1} \quad [62]$$

the preceding expressions may be rearranged in the *canonical form*

$$\mathbf{U}_\tau + \mathbf{V}_t = -\nu \mathbf{U} \quad [63]$$

$$\mathbf{V}_\tau + \mathbf{U}_t = +\nu \mathbf{V} \quad [64]$$

Appendix 2 Derivation of the Generalized Wave Equation

Given the canonical pair

$$\mathbf{U}_\tau + \mathbf{V}_t = -\nu \mathbf{U} \quad [65]$$

$$\mathbf{V}_\tau + \mathbf{U}_t = +\nu \mathbf{V} \quad [66]$$

Differentiate the first by τ and the second by t, giving

$$\mathbf{U}_{\tau\tau} + \mathbf{V}_{t\tau} = -\nu_\tau \mathbf{U} - \nu \mathbf{U}_\tau \quad [67]$$

$$\mathbf{V}_{\tau t} + \mathbf{U}_{tt} = +\nu \mathbf{V}_t \quad [68]$$

Subtract the first of these from the second, leaving

$$\mathbf{U}_{tt} - \mathbf{U}_{\tau\tau} = \nu \mathbf{V}_t + \nu_\tau \mathbf{U} + \nu \mathbf{U}_\tau \quad [69]$$

But from Equation [65] we know

$$\nu \mathbf{V}_t = -\nu^2 \mathbf{U} - \nu \mathbf{U}_\tau \quad [70]$$

Substituting this in [69] gives

$$\begin{aligned} \mathbf{U}_{tt} - \mathbf{U}_{\tau\tau} &= -\nu^2 \mathbf{U} - \nu \mathbf{U}_\tau + \nu_\tau \mathbf{U} + \nu \mathbf{U}_\tau \\ &= -\nu^2 \mathbf{U} + \nu_\tau \mathbf{U} \\ &= (\nu_\tau - \nu^2)\mathbf{U} \end{aligned} \quad [71]$$

This last may then be written in the standard form

$$\mathbf{U}_{\tau\tau} = \mathbf{U}_{tt} + (\nu^2 - \nu_\tau)\mathbf{U} \quad [72]$$

In a directly similar fashion we may obtain an expression for $\mathbf{V}$ in the form

$$\mathbf{V}_{\tau\tau} = \mathbf{V}_{tt} + (\nu^2 + \nu_\tau)\mathbf{V} \quad [73]$$

We should note that these equations both reduce to the classical wave equations for the uniform case where ν is identically zero everywhere, namely

$$\mathbf{U}_{\tau\tau} = \mathbf{U}_{tt} \quad [74]$$

$$\mathbf{V}_{\tau\tau} = \mathbf{V}_{tt} \quad [75]$$

It is perhaps easiest to set the effect of $\nu(\tau)$ for the case of a monotonically and exponentially tapered transmitter where

$$\epsilon = \epsilon_0 e^{k\tau} \quad [76]$$

we find

$$\begin{aligned} \ln \epsilon &= \ln \epsilon_0 + k\tau \\ \nu &= (\ln \epsilon)_\tau = k \\ \nu^2 &= k^2 \\ \nu_\tau &= 0 \end{aligned}$$

Thus we may make the following identification of the parameters ν and ν_τ

$$\begin{aligned} \nu &= \text{log taper structural frequency} \\ \sqrt{|\nu_\tau|} &= \text{deviational structural frequency} \\ \nu^2 \pm \nu_\tau &= \text{local structural squared frequency} \end{aligned}$$

The practical significance of these parameters is evident when considering the large number of possible cases with low structural frequencies, or

$$|\nu^2 \pm \nu_\tau| \cong 0 \quad \text{for all } \tau$$

For these cases we may then state that $\mathbf{U}$ and $\mathbf{V}$ approximately satisfy the wave equations [74] and [75]. Then from the scale constants given by equations [50] and [51], we may express a generalized form of Green's Law, namely

$$|e/e_0| = (z/z_0)^{1/2} = \left[\frac{I(s) \cdot C_0}{I_0 \cdot C(s)}\right]^{1/4} \quad [77]$$

$$|f/f_0| = (z_0/z)^{1/3} = \left[\frac{I_0C(s)}{I(s)C_0}\right]^{1/4} \quad [78]$$

from the fact that

$$|\mathbf{U}| = |\mathbf{U}_0| = |\mathbf{V}| = |\mathbf{V}_0| \quad [79]$$

for the transformed waves. This result can represent an enormous simplification in many practical situations.

Appendix 3 Derivation of the Characteristic Equations

Given the canonical pair

$$\mathbf{U}_\tau + \mathbf{V}_t = -\nu\mathbf{U} \quad [80]$$

$$\mathbf{V}_\tau + \mathbf{U}_t = +\nu\mathbf{V} \quad [81]$$

By adding and subtracting we can obtain the pair

$$\mathbf{U}_\tau + \mathbf{V}_\tau + \mathbf{U}_t + \mathbf{V}_t = -\nu\mathbf{U} + \nu\mathbf{V} \quad [82]$$

$$\mathbf{U}_\tau - \mathbf{V}_\tau + \mathbf{V}_t - \mathbf{U}_t = -\nu\mathbf{U} - \nu\mathbf{V} \quad [83]$$

These may be simplified to the form

$$(\mathbf{U} + \mathbf{V})_\tau + (\mathbf{U} + \mathbf{V})_t = -\nu(\mathbf{U} - \mathbf{V}) \quad [84]$$

$$(\mathbf{U} - \mathbf{V})_\tau - (\mathbf{U} - \mathbf{V})_t = -\nu(\mathbf{U} + \mathbf{V}) \quad [85]$$

Let us transform co-ordinates to the characteristic co-ordinates or *wave co-ordinates*, α and β, where

$$\alpha \equiv t + \tau \quad [86]$$

$$\beta \equiv t - \tau \quad [87]$$

Note that given (α, β) we can always uniquely determine (t, τ) since

$$t = \frac{1}{2}(\alpha + \beta), \qquad \tau = \frac{1}{2}(\alpha - \beta)$$

Thus we are merely *mapping* the (t, τ) plane onto a (conformal) equivalent (α, β) plane.

Let us now perform the operations

$$(\mathbf{U} + \mathbf{V})_\alpha = \frac{\partial(\mathbf{U} + \mathbf{V})}{\partial\alpha} = \frac{\partial(\mathbf{U} + \mathbf{V})}{\partial t}\frac{\partial t}{\partial\alpha} + \frac{\partial(\mathbf{U} + \mathbf{V})}{\partial\tau}\frac{\partial\tau}{\partial\alpha} \quad [88]$$

$$(\mathbf{U} - \mathbf{V})_\beta = \frac{\partial(\mathbf{U} - \mathbf{V})}{\partial\beta} = \frac{\partial(\mathbf{U} - \mathbf{V})}{\partial t}\frac{\partial t}{\partial\beta} + \frac{\partial(\mathbf{U} - \mathbf{V})}{\partial\tau}\frac{\partial\tau}{\partial\beta} \quad [89]$$

We can directly determine the results as

$$2(\mathbf{U} + \mathbf{V})_\alpha = (\mathbf{U} + \mathbf{V})_t(1) + (\mathbf{U} + \mathbf{V})_\tau(1) \quad [90]$$

$$2(\mathbf{U} - \mathbf{V})_\beta = (\mathbf{U} - \mathbf{V})_t(1) + (\mathbf{U} - \mathbf{V})_\tau(-1) \quad [91]$$

Employing these results in [84] and [85] yields the simplification

$$2(\mathbf{U} + \mathbf{V})_\alpha = -\nu(\mathbf{U} - \mathbf{V}) \quad [92]$$

$$2(\mathbf{U} - \mathbf{V})_\beta = +\nu(\mathbf{U} + \mathbf{V}) \quad [93]$$

By defining new *characteristic variables*, $\mathbf{P}$ and $\mathbf{Q}$, where

$$\mathbf{P} \equiv \mathbf{U} + \mathbf{V} \quad [94]$$

$$\mathbf{Q} \equiv \mathbf{U} - \mathbf{V} \quad [95]$$

the preceding expressions may be further reduced to

$$2\mathbf{P}_\alpha = -\nu\mathbf{Q} \quad [96]$$

$$2\mathbf{Q}_\beta = +\nu\mathbf{P} \quad [97]$$

In the case of *uniform transmitters*, where ν vanishes identically, these yield the classical results

$$\mathbf{P}_\alpha \equiv 0; \quad \mathbf{P} \text{ constant, along } \beta = \text{constant} \quad [98]$$

$$\mathbf{Q}_\beta \equiv 0; \quad \mathbf{Q} \text{ constant, along } \alpha = \text{constant} \quad [99]$$

Thus where ν is small as in a smoothly nonuniform transmitter, the principal effect of variable properties is to produce a *curvature* in the characteristic curves. The change in $\mathbf{P}$ and $\mathbf{Q}$ along the respective characteristics is then given by

$$2\Delta\mathbf{P} = \int_{\alpha_1}^{\alpha_2}(-\nu\mathbf{Q})d\alpha$$

$$2\Delta\mathbf{Q} = \int_{\beta_1}^{\beta_2}(\nu\mathbf{P})d\beta$$

Since these integrals may be indicated in terms of *mean values* along the characteristics we find

$$2\Delta\mathbf{P} \cong -\bar{\nu}\bar{\mathbf{Q}}\Delta\alpha$$

$$2\Delta\mathbf{Q} \cong +\bar{\nu}\bar{\mathbf{P}}\Delta\beta$$

In many cases involving small nonuniformities scattered along the transmitter, $\bar{\nu} \cong 0$, since every region of positive values must be balanced by a region of negative values. In such cases, the behavior is clearly approximated by Equations [98] and [99].

Discussion

J. Parmakian.[4] As noted by the authors, most pipelines which are encountered in practice do not have uniform properties throughout the length. From practical considerations it then becomes necessary to make certain approximations in order to reduce the water-hammer computational work. To that end the authors have provided a useful method for estimating the error due to approximating the actual pipeline with a small number of equivalent uniform pipe lengths. If available, some typical examples for actual rather than hypothetical pipelines would be instructive.

E. B. Strowger.[5] The writer has had occasion to compute the probable water-hammer pressure developed in the penstock of a small Pelton-wheel installation where a spherically shaped rock about 4 in. in diam suddenly blocked a 3-in. nozzle supplying the wheel. Of course, water hammer, which could be characterized as instantaneous, developed and the penstock burst at a point about 8.3 ft upstream from the point of stoppage, the point of bursting being just upstream from a gate valve and at the small end of a section of conical pipe. For the computation, Allievi's equations III and IV were used under the assumption of a theoretically instantaneous closure. Most of the pipe between the nozzle and the point of failure was of varying diameter, and was either built of heavy cast-steel pipe or was concreted in. The problem involved wave propagation in a pipe of changing diameter but with the velocity of the pressure wave approximately constant and not far from its maximum value of 4675 fps.

---

[4] Head, Technical Engineering Analysis Section, Bureau of Reclamation, Denver, Colo. Mem. ASME.

[5] System Project Engineer, Hydro Stations, Niagara Mohawk Power Corporation, Buffalo, N. Y. Mem. ASME.

The basic equation used for the pressure rise was

$$\Delta p \text{ in psi} = \frac{Q\,\frac{L}{a}}{\int_{s=0}^{s=L} A\left(\frac{1}{k}+\frac{d}{Ee}\right)ds} \quad \ldots\ldots [100]$$

where

Q = cfs
L = length of pipe from point of shutoff to point of pressure rise computation
a = velocity of pressure wave, fps
A = area of pipe, sq ft
k = voluminal modulus of elasticity of water in compression (taken at 294,000 psi)
E = modulus of elasticity of the material of the pipe walls, psi
e = thickness of pipe walls, in in.
s = distance along pipe from shutoff to any point

By approximating the real values of a by a constant (4000 fps), the computation of pressure rise in the nonuniform pipe for the upstream travel of the wave was greatly simplified and the method of arithmetic integration was used. Fig. 6 shows a similar installation and Fig. 7 shows the total pressure developed in the pipe as computed.

It may be of interest to consider this problem in its simplest form and to compare its solution by using Allievi's equations with that using the Green's-law adjustment. Fig. 8 shows a taper section of pipe of length L varying in diameter from d_1 at one end to d_2 at the other end. Let us assume that the pipe is concreted in and that, therefore, the value of a is 4675 fps[6]

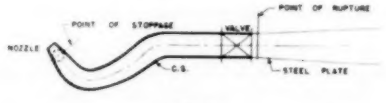

Fig. 6

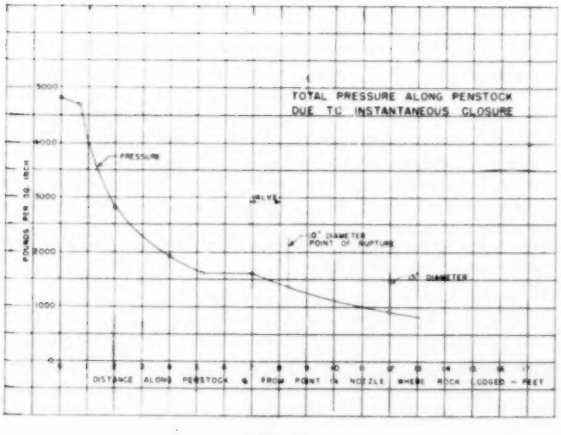

Fig. 7

Fig. 8 A taper section of pipe of length L, varying in diameter from d_1 at one end to d_2 at the other

Allievi's equation IV[7] is

$$\frac{\partial v}{\partial t} = g\,\frac{\partial H}{\partial s} \quad \ldots\ldots [101]$$

$$\frac{\partial v}{\partial s} = \frac{g}{a^2}\,\frac{\partial H}{\partial t} \quad \ldots\ldots [102]$$

Equation [102] may be written

$$\frac{\partial Q}{\partial s} = \frac{gA}{a^2}\,\frac{\partial H}{\partial t} \quad \ldots\ldots [103]$$

or

$$\partial H = \frac{a^2}{gA}\,\frac{\partial Q}{\partial s}\,\partial t \quad \ldots\ldots [104]$$

If all of the flow is stopped instantaneously ∂Q becomes Q and

$$\partial H = \frac{a^2 Q \partial t}{gA\,\partial s} \quad \ldots\ldots [105]$$

From Allievi's equation III

$$a = \frac{1}{\left[\frac{w}{g}\left(\frac{1}{k}+\frac{d}{Ee}\right)\right]^{1/2}} \quad \ldots\ldots [106]$$

From this equation

$$\frac{a^2}{g} = \frac{1}{w\left(\frac{1}{k}+\frac{d}{Ee}\right)} \quad \ldots\ldots [107]$$

Substituting this value of a^2/g in Equation [104]

$$\partial H = \frac{Q dt}{w\left(\frac{1}{k}+\frac{d}{Ee}\right)A\,ds} \quad \ldots\ldots [108]$$

The rise at a point L feet from the nozzle would be

$$\Delta H \text{ (in feet)} = \frac{Q\int_0^T dt}{\int_{s=0}^{s=L} w\left(\frac{1}{k}+\frac{d}{Ee}\right)A\,ds} = \frac{QT}{\int_{s=0}^{s=L} w\left(\frac{1}{k}+\frac{d}{Ee}\right)A\,ds}$$

but if a is constant, $T = L/a$ so that

$$\Delta p(\text{in psi}) = w\Delta H = \frac{Q\,\frac{L}{a}}{\int_{s=0}^{s=L} A\left(\frac{1}{k}+\frac{d}{Ee}\right)ds} \quad \ldots [100]$$

[6] Chapter on "Water Hammer" in "Hydroelectric Handbook" by W. P. Creager and J. D. Justin, John Wiley & Sons, Inc., New York, N. Y., 2nd edition, 1950, p. 711; and "American Civil Engineering Practice," edited by Robert W. Abbett, McGraw-Hill Book Company, New York, N. Y., 1956, pp. 16–38.

[7] Discussion no. 5 by E. B. Strowger, "Symposium on Water Hammer," The American Society of Mechanical Engineers, June, 1933, pp. 133–139.

With the pipe concreted in, d/Ee is negligible and so in our example

$$\Delta p = \frac{QT}{\frac{1}{k}\int_{s=0}^{s=L} A\, ds} = \frac{QTk}{V'} \quad \text{[109]}$$

where V' = volume of taper pipe. This is an exact solution for pressure rise assuming infinite frequency of the water-hammer wave. For the following example, the pressure rise is 2313 psi as shown

$Q = 7.5$ cfs $\quad L = 3$ ft
$d_1 = 4$ in. $\quad a = 4675$ fps
$d_2 = 8$ in.

$$V' = \frac{1}{3}\frac{\pi}{4}\,3\left[\left(\frac{1}{3}\right)^2 + \left(\frac{3}{4}\right)^2 + \frac{1}{3}\times\frac{3}{4}\right] = 0.611 \text{ cf}$$

$$T = \frac{L}{a} = \frac{3}{4675} = 0.000641 \text{ sec}$$

$$\Delta p = \frac{7.5 \times 0.000641 \times 294{,}000}{0.611} = 2313 \text{ psi}$$

Now going to Equations [9] and [46] of the authors' paper, we may write

$$Z^{1/2} = \left[\frac{I(s)}{C(s)}\right]^{1/4} = \epsilon(s)$$

But

$$\epsilon(s) = \left[\frac{a(s)}{gA(s)}\right]^{1/2}$$

so that

$$Z = \frac{a(s)}{gA(s)}$$

But g is constant and in our case $a(s)$ is a constant, so that

$$Z \cong \frac{1}{A} \quad \text{or} \quad Z \cong \frac{1}{d^2}$$

and

$$\epsilon \cong \sqrt{Z} = \frac{1}{d}$$

This means that

$$U \cong dH$$

But since we are dealing with the transmission of a pressure wave upstream which would be of a constant value if the pipe were uniform, H would vary with $\frac{1}{d}$. The Green's-law adjustment would, therefore, give

$$\frac{P_s}{P_0} \cong \frac{d_0}{d_s}$$

Applying this to the example given

$$\text{Initial velocity at nozzle} = \frac{7.5}{0.7854 \times \left(\frac{1}{3}\right)^2} = 85.95 \text{ fps}$$

Instantaneous pressure rise at nozzle

$$= \frac{4675 \times 85.95}{32.2} = 12470 \text{ ft or } 5410 \text{ psi}$$

Pressure rise at end of taper section

$$= \frac{4}{8} \times 5410 = 2705 \text{ psi}$$

Actually the true pressure rise is somewhere between 2313 psi and 2705 psi but in this case with such a steep wave front the value of 2313 is probably closer to the correct result.

The authors have made a useful contribution to the subject of water hammer involving nonuniform pipes and are to be congratulated for presenting a classical treatise.

Authors' Closure

The authors are very appreciative of the kind remarks of Messrs. Parmakian and Strowger. These gentlemen have both made many noteworthy contributions to this field, far too briefly indicated by references (6) and (10) of the paper.

With regard to the request by Mr. Parmakian for some specific examples and practical applications, we are particularly happy to acknowledge our debt to Mr. Strowger in submitting so pertinent an example for treatment by these various methods. Let us trust that this will serve sufficiently for the present purpose.

Mr. Strowger's example, then, can be used to demonstrate in more detail the specific use of Green's Law for engineering estimates and the associated probable errors. Here one is concerned with the pressure surge resulting from a complete sudden shutoff at the small end of a tapered pipe.

Mr. Strowger has compared an estimate of pressure rise at various points in such a pipe by two approximate methods:

(I) Using a mean surge admittance: $\Delta H \cong Q/Y_p$
(II) Using a Green's Law correction: $\Delta H \sim 1/d$

We may further rationalize his use of a mean surge admittance Y_p by analogy to Equations [25] through [31] of the paper.

For every section of the n-section pipe of Fig. 1 we may say that:

$$C_k/Y_k = T_k = \text{constant} = T_n \quad \text{[110]}$$

Moreover for the whole pipe:

$$C_p = \sum_{k=1}^{n} C_k \quad \text{[111]}$$

and if n becomes infinite with T_n going to zero, then:

$$C_p = g\int_0^L \frac{A}{a^2}\, ds \quad \text{[112]}$$

By analogy to Equation [30] we may finally define a *mean surge admittance* by the relation:

$$Y_p \equiv \frac{C_p}{T_p} = \frac{\Sigma C_k}{\Sigma T_k} = g\,\frac{\int (A/a^2)ds}{\int ds/a} \quad \text{[113]}$$

We should most particularly note that, in general

$$Y_p \neq 1/Z_p$$

except for the special case of the uniform pipe. This may be seen immediately in terms of the product Z_pY_p, namely:

$$Z_pY_p = \frac{[\int ds/A]\cdot[\int (A/a^2)ds]}{[\int ds/a]^2} \quad \text{[114]}$$

If $A = A_0 =$ constant, and $a = a_0 =$ constant, then:

$$Z_pY_p = \frac{[L/A_0]\cdot[A_0L/a_0^2]}{[L/a_0]^2} \equiv 1 \quad \text{[115]}$$

Further, if only $a = a_0 = \text{constant}$, then

$$Z_p Y_p = \frac{1}{L^2}\left[\int_0^L ds/A\right]\cdot\left[\int_0^L A\,ds\right] \neq 1 \quad [116]$$

If, in this last case,

$$A = A_0(1 + \alpha)$$
$$1/A = (1/A_0)(1 + \alpha)^{-1} = (1/A_0)(1 - \alpha + \alpha^2 - \ldots)$$

then, for small values of α:

$$Z_p \cong (a_0/gA_0)(1 - \bar{\alpha}) \quad [117]$$

$$Y_p \cong (gA_0/a_0)(1 + \bar{\alpha}) \quad [118]$$

$$Z_p Y_p \cong 1 - \bar{\alpha}^2 \quad [119]$$

where

$$\bar{\alpha} \equiv \frac{1}{L}\int_0^L \alpha\,ds \quad [120]$$

Thus Mr. Strowger's Equation [109] becomes

$$(I)\text{: Rise in feet: } \Delta H \cong Q/Y_p \cong (QLa)\Big/\left(g\int_0^L A\,ds\right) \quad [121]$$

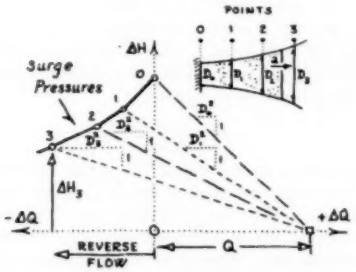

Fig. 9 Graphical solution for pressure surges in a tapered pipe

That this equation cannot be exact is indicated in the graphical solution portrayed in Fig. 9. Particularly important to note is the fact that there will be substantial *reverse surge flows* at all points upstream of any such pipe, with an increasing section moving upstream.

Mr. Strowger has further specialized his results to the simple case of a pipe with *linear flare* or taper in diameter. Table 2 compares the exact results calculated (according to a characteristics analysis similar to Fig. 9) with the approximations obtained by methods I and II.

It is readily seen that for this case both methods give results of comparable accuracy and that Mr. Strowger is quite correct in his supposition that the true answer lies somewhere between these estimates. However, the Green's Law approximation is vastly simpler to apply, particularly for pipes with more complicated tapers. It is clearly of interest to determine the probable errors in a Green's Law estimate for other than a linear case, and to this end, we submit the results of Fig. 10. For all the cases shown, the maximum error in surge pressure is less than 8 per cent, using the Green's Law estimate:

$$\Delta H = (a_0 Q/gA_0)(D_0/D(s)) \quad [122]$$

Such results would seem to indicate much practical engineering value in this method of approximation.

In closing, we would like to draw attention to a number of points of general interest.

What we have referred to as "structural frequencies" are, for

Table 2 Relative surge pressures in a tapered pipe. Abrupt flow stoppage, linear flare in diameter.

		Calculated relative head rise		
			Approximate	
Station	Relative diameter Dk	Exact wave equation	Method I[a] mean admittance	Method II[b] Green's Law
0	1.00	1.00	1.00	1.00
1	1.20	0.82	0.82	0.83
2	1.40	0.69	0.69	0.71
3	1.60	0.60	0.58	0.63
4	1.80	0.53	0.48	0.56
5	2.00	0.47	0.43	0.50

[a] $\Delta H \sim 3/[1 + D_k + D_k^2]$.
[b] $\Delta H \sim 1/D_k$.

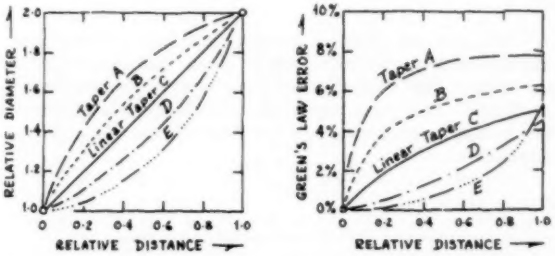

Fig. 10 Green's Law errors for sudden flow stoppage in tapered pipes

the special case of acoustical horns, called the *flare cutoff frequencies* (15, 16) and determine the transition between a low-frequency (long period) band in which the horn (or transmitter) behaves as a single, lumped equivalent, and a high-frequency (short period) band in which only local properties are of importance. We hope that our paper will serve to draw attention to interesting practical and analytical problems concerning the effects of the structural frequencies in more general situations.

It is also of interest to note that the general variable lossless transmitter may be viewed as an finite (or infinite) order *four-terminal matrix* (4, 20) of the form:

$$\mathbf{M} = \prod_{k=1}^{n}\left[\begin{array}{c|c} 1+\Delta_k & 0 \\ \hline 0 & 1+\Delta_k' \end{array}\right]\cdot\left[\begin{array}{c|c} \cosh TD & \sinh TD \\ \hline \sinh TD & \cosh TD \end{array}\right] = \prod_k (\mathbf{E}_k \cdot \mathbf{T}) = \mathbf{E}_1\cdot\mathbf{T}\cdot\mathbf{E}_2\cdot\mathbf{T}\cdot\mathbf{E}_3\cdot\ldots\cdot\mathbf{E}_n\cdot\mathbf{T} \quad [123]$$

The **E**-matrices are nothing but *ideal transformers* with

$$1 + \Delta_k \equiv \frac{\overline{[\epsilon(s)]_k}}{\epsilon_0} \equiv \frac{1}{1 + \Delta_k'} \quad [124]$$

measuring the *mean transformation ratio* from section to section. If Δ is everywhere near zero, corresponding to $\nu \to 0$, then:

$$\mathbf{M} \cong \left[\prod_k \mathbf{E}_k\right]\cdot\mathbf{T}^n \cong \mathbf{T}^n\cdot\left[\prod_k \mathbf{E}_k\right] \quad [125]$$

This last relation may be used as a justification for the single equivalent transmitter concept. More analytical details, based on the use of *spinors*, *quaternions*, and *unimodular transformations* can be found in reference (21).

Reference

21 W. T. Payne: "Spinor Theory of Four-Terminal Networks," *Journal of Mathematics and Physics*, vol. 32, no. 1, April, 1953, pp. 19–33.

Technical Briefs

Effective and Local Surface Coefficients in Fin Systems

By G. M. DUSINBERRE,[1] UNIVERSITY PARK, PA.

When tests are made on systems containing extended heat-transfer surface, the direct result is an "effective" surface coefficient. The desired result is a "local" or true surface coefficient. This paper shows how, on reasonable assumptions, the one can be calculated from the other without trial-and-error procedures.

Nomenclature

A_b = area of base metal not covered by fins or pins
A_f = surface area of fins or pins
A_s = section area of a pin
A = total heat-transfer area, $A = A_b + A_f$
B = ratio, A_b/A
C = function of fin geometry and material, Equations (9), (12), (13), (14)
h = "local" surface coefficient of heat transfer, $h = dQ/\theta dA$
h' = "effective" surface coefficient, Equation (1)
k = conductivity of fin metal
L = height of fin
n = ratio defined by Equation (6)
P = perimeter of a pin
Q_b = heat flow to base metal
Q_f = heat flow to fin or pin
Q = total heat flow, $Q = Q_b + Q_f$
r_b = radius at base of a circumferential fin
r_t = radius at tip of a circumferential fin
y_0 = half-thickness of a fin at its base
θ = temperature difference
θ_b = temperature difference, ambient to base metal
ϕ = fin efficiency, defined by Equation (2)

Definitions and Assumptions

By a "fin system" we mean a practical assembly such as a finned tube or finned plate in which part of the heat-transfer area is extended surface and part is "base metal" not covered by the fins (or pins). Tests on such surfaces are described in numerous papers,[2] and the use of test data in design is outlined in many works.[3]

In this paper we make the usual assumptions of one-dimensional fin theory.[4] We make the additional assumption that the local surface coefficient is the same for the base metal as for the extended surface. To do otherwise would require much more test instrumentation than is usually practicable.

Derivation

When tests are made on fin systems, the directly measured quantities will be the heat flux, Q, Btu/hr, the total heat-transfer area, A, ft², and the temperature-difference, θ_b, deg F, between the fluid and the base metal. The temperature-difference may be some appropriate mean value. From these, an "effective" surface coefficient can be computed:

$$h' = Q/A\theta_b \tag{1}$$

We are interested in expressing the surface coefficient, via a Nusselt or Stanton number, as a function of the Reynolds and Prandtl numbers. But the coefficient found by Equation (1) is a function also of the fin efficiency which is itself a function of the surface coefficient. Therefore we need to find the true or "local" surface coefficient.

On the usual assumptions, the fin efficiency is defined as:

$$\phi = \frac{Q_f}{hA_f\theta_b} \tag{2}$$

On our additional assumption, the heat flux is:

$$\begin{aligned} Q &= Q_b + Q_f = hA_b\theta_b + \phi hA_f\theta_b \\ &= h'A\theta_b \end{aligned} \tag{3}$$

whence:

$$h' = h\left(\frac{A_b}{A} + \frac{\phi A_f}{A}\right) = h[B + \phi\,(1 - B)] \tag{4}$$

Note that B is a function only of the geometry of the system. But we need ϕ as a function of h.

Considering for the present only longitudinal fins of rectangular profile (the most common type), the fin efficiency is given by the equation:

$$\phi = \frac{\tanh n}{n} \tag{5}$$

where:

$$n = L\sqrt{h/ky_0} \tag{6}$$

Using these relations, Equations (4) can be solved for h in terms of h' by a trial-and-error procedure. But this is awkward, and a simpler relation can be reached.

---

[1] Department of Mechanical Engineering, The Pennsylvania State University, University Park, Pa. Fellow, ASME.

[2] For example, W. M. Kays and A. L. London, "Heat-Transfer and Flow-Friction Characteristics of Some Compact Heat-Exchanger Surfaces," TRANS. ASME, vol. 72, 1950.

[3] For example, W. M. Kays and A. L. London, "Compact Heat Exchangers," The National Press, Palo Alto, Calif., 1955.

Contributed by the Heat Transfer Division for publication in the Technical Briefs section of TRANSACTIONS.

NOTE: Statements and opinions advanced in papers are to be understood as individual expressions of their authors and not those of the Society. Manuscript received at ASME Headquarters, January 15, 1958.

[4] See, for example, K. A. Gardner, "Efficiency of Extended Surface," TRANS. ASME, vol. 67, 1945, pp. 621–631.

A series expansion of Equation (5) is as follows:[5]

$$\phi = \frac{1}{1 + \frac{n^2}{3} - \frac{n^4}{45} + \frac{2n^6}{945} - \ldots .} \tag{7}$$

Let us curtail this after the term in n^2 and find the error for $n = 1$. Then Equation (7) gives $\phi = 0.75$, while Equation (5) gives $\phi = 0.7616$, an error of 1.55 per cent. This is better than the usual accuracy of measurement of the surface coefficient, and for $n < 1$ the error is still less.

But what about $n > 1$? This says that $\phi < 0.75$ and, practically speaking, this means that the fin is ill-suited to the given operating conditions, will probably be uneconomical, and we had better revise the design. Of course, we can still fall back on Equation (5) if necessary.

Equation (7), as modified, can be put in a more useful form. Let:

$$\phi = \frac{1}{1 + n^2/3} = \frac{1}{1 + Ch} \tag{8}$$

then:

$$C = \frac{n^2}{3h} = \frac{L^2h/ky_0}{3h} = \frac{L^2}{3ky_0} \tag{9}$$

for the rectangular longitudinal fin. Note that C is a function only of the *fin* geometry and material. With this simplification, Equation (4) becomes:

$$h' = h\left[B + \frac{1 + B}{1 + Ch}\right] = h\left[\frac{1 - BCh}{1 + Ch}\right] \tag{10}$$

whence: $$h = \frac{\sqrt{(1 - Ch')^2 + 4BCh'} - (1 - Ch')}{2BC} \tag{11}$$

Thus, within the limitation on ϕ, we replace the trial-and-error procedure by the solution of a simple quadratic form.

Equations (8), (10), and (11) are useful for other fin shapes if we use the appropriate value[6] of C: For a cylindrical pin:

$$C = \frac{L^2P}{3kA_c} \tag{12}$$

For a longitudinal fin of triangular section:

$$C = \frac{L^2}{2ky_0} \tag{13}$$

For a circumferential fin of rectangular section:

$$C = \frac{L^2\sqrt{r_t/r_b}}{3ky_0} \tag{14}$$

For a conical spine:

$$C = \frac{0.15L^2P}{kA_c} \tag{15}$$

In Equation (15), P and A_c refer to the base of the spine.

In all these equations the limitation, $\phi > 0.75$, applies.

From Equation (11) we can write:

$$\frac{h'}{h} = \frac{2B\,(Ch')}{\sqrt{(1 - Ch')^2 + 4B\,(Ch')} - (1 - Ch')} \tag{16}$$

The ratio h'/h as a function of B and Ch' is shown in Fig. 1, which will do for rough work.

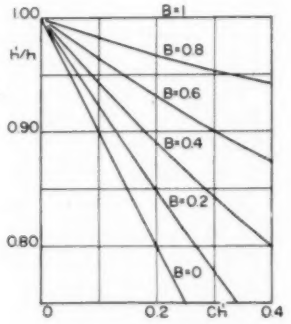

Fig. 1 Fin characteristic ratios

[5] See, for example, O. W. Eschbach, "Handbook of Engineering Fundamentals," p. 2-84.

[6] See G. M. Dusinberre, "Fin Efficiency," *Mechanical Engineering*, vol. 78, 1956, p. 570.